UNIVERSIDAD NACIONAL AUTÓNOMA DE MÉXICO

PROGRAMA DE MAESTRÍA Y DOCTORADO EN INGENIERÍA

CENTRO DE INVESTIGACIÓN EN ENERGÍA

NEW DISCRIMINATION AND CLASSIFICATION DIAGRAMS FOR IGNEOUS ROCKS AND APPLICATION TO GEOTHERMAL FIELDS

PROPUESTA DE T E S I S

QUE PARA OPTAR POR EL GRADO DE

DOCTOR EN INGENIERÍA

P R E S E N T A

SANJEET KUMAR VERMA

TUTOR

DR. SURENDRA P. VERMA

TEMIXCO, MORELOS

2012

APPROVED THESIS COMMITTEE:

President: Dr. Eduardo González Partida

Secretary: Dr. Surendra Pal Verma

Vocal: Dr. Edgar Rolando Santoyo Gutiérrez

1st Supplement: Dr. Pandarinath Kailasa

2nd Supplement: Dr. Fernando Velasco Tapia

Centro de Investigación en Energía
Universidad Nacional Autónoma de México
(CIE-UNAM)

Advisor of Thesis

Dr. Surendra Pal Verma

Acknowledgments

Three years for a Ph.D. appeared to me as a long period when I was at the beginning.
As the first questions started to be answer, new ones, more complicated arose and the time went faster and faster. Suddenly, I found myself at the end of these three years. I had very nice and fun times in México, but I didn't avoid the difficult ones, when I was full of questions and doubts. But during all the time I had people around me with whom I shared the happy moments and who supported me when the times were hard. Today, I would like to say THANK YOU to all of these people.

First of all, I would like to thank my advisor (Prof. Surendra Pal Verma) and committee members, (Dr. Edgar R. Santoyo Gutiérrez, Dr. Pandarinath Kailasa, Dr. Eduardo González Partida and Dr. Fernando Velasco Tapia) for providing me the opportunity to work on interesting projects, for scientific discussions, enthusiastic moral support and motivation.

I would like to thank my parents (Munni Lal Verma and Geeta Verma), brother Sanjay Verma, sister in-law Geeta Verma, and my nephews Deepti Verma and Shubham Verma, my closest friends Dinesh Chandar Pant, Ranjeet Prasad Singh, Dr. Pankaj Mehta and Suman Kushwaha. Although they were very far from Mexico, they always supported me and gave me the courage and strength never to give up.

I would like to thank Secretaría de Relaciones Exteriores, SRE (Mexico) and Ministry of Human Resource Development, MHRD (India) for my doctoral fellowship.

I would like to thank Mirna Guevara for her academic supports.

I am grateful to Alfredo Quiroz Ruiz, for his valuable support in computational programming and software maintenance.

I would like to thank my formerly assistant of doctorate students “Christian Brito” for her valuable support in official documentation work in posgrado, CIE-UNAM.

These last three years were not only about work but also for enjoying life in Mexico with great friends around me. Thank you, Sarika, Viresh, Ashutosh, Richa, Bassam, Amina, Maya, Alejandra, Daniel, Efraín, Christian, María Abdelaly, Mario Barrera, Tereca Luice, Andrés Alanís, Manuel Alejandro Ramirez, Dalia Alejandra, Enue Barrios, Rebeca Maricela Aragón who were always ready for celebrating whatever was the occasion. Thank you Dr. Manoj and Dr. Reshmi chechi and Bharat it was always challenging to climb with you and it helped keeping the body and mind in a good health.

I met many nice people and I cannot put all the names in this short paragraph, but I think about everybody who influenced my stay here, in Mexico.

Last but not least, the most important person, who gave me her love and understanding. I would like to express my heartfelt thanks to my wife, Renu Verma. Without her I would be a very different person today, and it would have been certainly much harder to finish a PhD. Still today, learning to love her and to receive her love makes me a better person. Special thanks to her also for helping me with the figures and epigraph of this PhD work.

I finish with a final silence of gratitude for my life.

Sanjeet Kumar Verma

DEDICATIONS

My Parents

This thesis is dedicated to my parents Munni Lal Verma and Geeta Verma, who have supported me all the way since beginning of my life and studies.

My Lovely Wife

Also, this thesis is dedicated to my lovely wife Renu Verma, who has been a great source of motivation and inspiration.

My brother, sister-in-law and sisters

Finally, this thesis is dedicated to my brother, sister-in-law and all sisters for their love and great moral support.

Contents

List of Figures

List of Figures in Chapter 1

tholeiite (IAB+WPT; region C), and overlap region of normal type island arc basalt and mid-ocean ridge basalt (IAB+N-MORB; region D).

10. The La/10-Nb/8-Y/15 ternary diagram (Cabanis and Lecolle 1989) assumed to discriminated arc basalt (IAB) field A, continental basalt (CRB) field B and ocean floor basalt (OIB+N-MORB+E-MORB) filed.

11. The Score1-Score2 diagram (Butler and Woronow 1986) for arc (IAB), within-plate (WPB), and mid-ocean ridge (MORB).

12. The F1-F2 discriminant function diagram (Pearce 1976) for low-potassium tholeiite and calc-alkali basalt (LKT+CRB; assumed as arc –IAB- setting), within-plate (WPB), shoshonite (SHO; not assumed to belong to any of the four setting), ocean floor basalt (OFB; assumed as mid-ocean ridge basalt –MORB- setting).

13. The F1-F2 discriminant function diagram (Pearce 1976) for low-potassium tholeiite (LKT), calc-alkali basalt (CRB), shoshonite (SHO), ocean floor basalt (OFB; assumed as mid-ocean ridge basalt –MORB- setting).

14. The chemical classification and nomenclature of volcanic rocks using the total alkali versus silica diagrams of Le Bas *et al.* (1986).

15. Co-Th, (Hastie *et al.* 2007) classification diagram for altered igneous rocks. The rock type abbreviations in Co-Th diagram are: B-basalt; BA/A-basaltic andesite/andesite; D/R*-dacite/rhyolite/latite/trachyte; IAT-island arc tholeiite; CA-calc-alkaline; and H-K and SHO-high-K and shoshonite.

List of Figures in Chapter 4

1. The set of five new discriminant-function multi-dimensional diagrams for the discrimination of intermediate rocks from island arc (IA) or continental arc (CA), continental rift (CR), ocean-island (OI), and collision (Col) tectonic settings, showing samples from the training set.

2. The set of five new discriminant-function multi-dimensional diagrams based on natural logarithm-transformed ratios of major elements for the discrimination of intermediate rocks, showing samples from the thirteen case studies. The solid red lines represent discrimination boundaries. A: IA+CA–CR+OI–Col (1+2–3+4–5) diagram; B: IA+CA–CR–OI (1+2–3–4) diagram; C: IA+CA–CR–Col (1+2–3–5) diagram; D: IA+CA–OI–Col (1+2–4–5) diagram; and E: CR–OI–Col (3–4–5) diagram.

List of Figures in Chapter 5

List of Figures in Chapter 6

List of Tables

LIST OF TABLES IN CHAPTER 4

10. APPLICATION OF THE SET OF FIVE DISCRIMINANT FUNCTION MULTI-DIMENSIONAL DIAGRAMS FOR BASIC AND ULTRABASIC MAGMAS (VERMA *ET AL*. 2006).

11. APPLICATION OF THE SET OF FIVE DISCRIMINANT FUNCTION MULTI-DIMENSIONAL DIAGRAMS FOR ACID MAGMAS (VERMA *ET AL*. 2011).

LIST OF TABLES IN CHAPTER 5

1. TOTAL NUMBER OF SAMPLES AND ROCKS TYPE IN DATABASE.

2. MEAN AND STANDARD DEVIATION OF $(SiO_2)_{adj}$ AND LOG-TRANSFORMED RATIO VARIABLES FOR THE THREE ROCKS TYPE (BASIC+ULTRABASIC, INTERMEDIATE, AND ACID) SAMPLES OF THE DATABASE.

3. TEST OF EQUALITY OF GROUP MEANS FOR TEN LOG-TRANSFORMED RATIO VARIABLES IN THE GROUP SAMPLES.

4. DISCRIMINANT-FUNCTION EQUATIONS FOR THE NEW MULTI-DIMENSIONAL CLASSIFICATION DIAGRAM.

LIST OF TABLES IN CHAPTER 6

1. APPLICATION OF TAS DIAGRAM FOR FRESH ROCKS FROM LOS AZUFRES, AMEALCO, HUICHAPAN, LOS HUMEROS, AND SIERRA LA PRIMAVERA FOR THE EVALUATION OF DISCRIMINANT-FUNCTION-BASED CLASSIFICATION DIAGRAM.

2. APPLICATION OF DISCRIMINANT-FUNCTION-BASED CLASSIFICATION DIAGRAM FOR ALTERED ROCKS FROM LOS AZUFRES AND LOS HUMEROS FOR THE EVALUATION OF TAS DIAGRAM.

3. APPLICATION OF THE SET OF FIVE DISCRIMINANT FUNCTION MULTI-DIMENSIONAL DIAGRAMS FOR INTERMEDIATE MAGMAS (CHAPTER 4).

4. APPLICATION OF THE SET OF FIVE DISCRIMINANT FUNCTION MULTI-DIMENSIONAL DIAGRAMS FOR ACID MAGMAS (VERMA *ET AL*. 2012).

Abstract

This thesis consists of the Introduction and seven chapters followed by a reference section and six annexures.

The **Introduction** provides the main reasons for developing new discrimination and classification diagrams, including the importance of this work in energy research. It also briefly states the objectives set forth for the thesis.

Chapter 1 outlines the previous work on discrimination as well as classification diagrams.

Chapter 2 describes the evaluation of the four tectonic discrimination diagrams of Pearce *et al.* (1984) [Journal of Petrology, v. 25, p. 956-983; a highly cited paper] for granitic rocks, along with the proposal of a set of five new discriminant-function-based multi-dimensional diagrams for acid magma from four tectonic settings (island arc, continental arc, continental rift, and collision), published by Verma *et al.* (2012) [International Geology Review, v. 54, p. 325-347; **Annexure I**]. The very similar tectonic settings of island and continental arcs are discriminated for the first time. The success rates obtained from the testing set were about 60%-90%. These diagrams are based on statistically correct handling of compositional data as documented by Verma *et al.* (2010) [Advances in Geosciences, v. 26, p. 11-22; **Annexure II**], which requires log-ratio transformation, whereas the multivariate technique of linear discriminant analysis (LDA) assumes a normal distribution of the transformed variables. These diagrams were applied to data for acid rock samples of Cretaceous to Quaternary age from all over the world.

Chapter 3 illustrates the application example of discriminant-function-based multi-dimensional discrimination diagrams for basic and ultrabasic rocks (four sets of new diagrams published by Agrawal *et al.* 2004, 2006; Verma *et al.* 2006; Verma and Agrawal 2011, proposed through Indo-Mexican collaboration) to tectonically complex area of southern Mexico (Mexican Volcanic Belt, Los Tuxtlas volcanic field, and Eastern Alkaline Province) and continental arc area of Central America (Central American Volcanic Arc); the results were documented by Verma *et al.* (2011) [Pure and Applied Geophysics, v. 168, p. 1501-1525; **Annexure III**]. Success rates of 51.0%-94.4% and 89.3%-98.7% were obtained for the Mexican Volcanic Belt and Los Tuxtlas, respectively. The inferred tectonic settings are presented in this publication. The success rate for Central America Volcanic arc as an arc setting were also high (76.5%-80.7%). Similarly, for the application to northern Mexico (Baja California, Baja California Sur and Sonora, including the Gulf of California), the paper by Pandarinath and Verma (2012) [Journal of Iberian Geology, in press; **Annexure IV**] is presented. The success rates were shown as follows. For on-land basic rocks of <13 Ma age, success rates of 71%-93% and 58%-90% were obtained for major-element and trace-element based diagrams, respectively. For the on-land basic rocks of >13 Ma age, major-element based diagrams indicated a rift setting (high success rates of 62-92%). However, the trace-element based discrimination diagrams of Agrawal *et al.* (2008) indicated a transition from arc to rift setting. A single sample from Comondú arc of an age >13 Ma consistently showed an arc setting in all diagrams of Verma and Agrawal (2011) based on immobile elements. All the four sets of discrimination diagrams indicated a MORB setting (very high success rates 90%-98% and 100% for major-element and trace-element based diagrams, respectively) for off-shore rocks (dominantly from DSDP drilled sites in the Gulf of California and some dredged rock samples from the Gulf of California).

Chapter 4 documents a set of five multi-dimensional discrimination diagrams obtained from the correct statistical methodology of log-ratio transformation and linear discriminant analysis of discordant outlier-free normally distributed major element log-ratio variables in 2595 intermediate rock samples from five tectonic settings. From

these diagrams with probability-based tectonic field boundaries, high success rates (60%-95%) were obtained for tectonic discrimination of thirteen case studies of Archean to highly altered Quaternary rocks. The results are submitted by Verma and Verma (2012) [Turkish Journal of Earth Science, in press; **Annexure V**] of arc, rift, ocean island, and collision settings for eight, one, one, and three case studies, respectively, were supported by probability estimates and were generally consistent with those of the multi-dimensional diagrams for basic and acid magmas from the same regions.

Chapter 5 presents one discriminant-function-based classification diagram for altered igneous rocks. For its proposal an extensive database for 23768 analyses of Miocene to Recent fresh rocks was used. This classification diagram can provide the name of magma type as basic and ultrabasic, intermediate, or acid. This diagram is based on discriminant-function of log-transformed ratio variables and probability based boundaries and gave success rates of 81%-96%. The utility of this diagram resides in the proper selection of discrimination diagrams for basic and ultrabasic, intermediate or acid rock varieties.

Chapter 6 elaborates the application examples of classification and discrimination diagrams from five case studies (three geothermal fields and two calderas of Mexico). The success rates were showed as follows for different case studies: in the Sierra La Primavera a rift setting was shown with very high success rates 86%-100% for acid rocks; for Los Azufres geothermal field, both the intermediate and acid rocks consistently showed a collision setting with high success rates of 71%-76% and 56%-68%, respectively; the intermediate rocks from the Amealco caldera showed a collision setting because very high (81%-94%) success rates were shown of this tectonic field, although the acid rocks showed an arc setting with less success rates of 48%-81%; the intermediate and acid rocks from the Huichapan caldera showed a collision setting because relatively high success rates (48%-68% for intermediate rocks and 48%-52% for acid rocks) were shown of this field; and finally the Los Humeros geothermal field or caldera seems to be characterized by a collision setting because relatively high

success rates (49%-75% for intermediate rocks and 52%-76% for acid rocks) were shown for this field. These results were supported by probability estimates. For most cases, the multi-dimensional diagrams for intermediate and acid magmas provided mutually consistent results for the inferred tectonic setting.

Chapter 7 presents the application example of Archean rocks from five case studies (Australia, South Africa, Brazil, Canada, and India). The tectonic settings were showed as follows for different case studies: For the eastern part of the Pilbara craton (Australia), a Paleoarchean (3570-3450 Ma) and Mesoarchean (2900 Ma) continental arc setting apparently evolved to a collision setting during the Neoarchean (2600 Ma). Infer an island arc environment for Kambalda (Australia) during the Neoarchean (2700 Ma). For the Barberton belt (South Africa), transition from a mid-ocean ridge regime during the older part of the Paleoarchean (3470 Ma) to an island arc setting during the younger part (3300-3260 Ma) is likely. An arc environment were indicated for the São Francisco craton (Brazil) and the Rio Maria terrane (Brazil) during the Mesoarchean (3085-2983 Ma and 2870 Ma, respectively), whereas a within-plate setting is clearly indicated for the Carajás metallogenic province (Brazil) during the Neoarchean (2740-2700 Ma). Also recognize an island arc regime for the Mesoarchean (3000 Ma) North Caribou and Neoarchean (2700 Ma) Abitibi greenstone belts (Canada), and for the Gadwal greenstone belt (India) during the Neoarchean (2700-2500 Ma). A collision setting was inferred for the Archean sanukitoid suite (Canada) and the Kolar suture zone (India) during the Neoarchean (2700-2660 Ma and 2630-2520 Ma, respectively. This work has been accepted by [International Geology Review, in press, DOI: 10.1080/00206814.2012.693246, ISSN 0020-6814 print/ISSN 1938-2839 online; **Annexure VI**].

The references cited in this thesis are listed in a separate section after Chapter 7. This is followed by six annexures, which include the six papers (three published two in press and one submitted) in international journals, in which the author of this thesis actively participated.

Resumen

Esta tesis consiste en la introducción y siete capítulos seguidos de una sección de referencia y seis anexos.

La introducción proporciona las razones principales para el desarrollo de una nueva clasificación de diagramas de discriminación, incluida la importancia de este trabajo en la investigación energética. También se describen brevemente los objetivos establecidos para la tesis.

En el **Capítulo 1** se exponen los trabajos anteriores sobre la discriminación, así como los diagramas de clasificación.

En el **capítulo 2** se describe la evaluación de los cuatro diagramas de discriminación tectónica de Pearce *et al.* (1984) [Journal of Petrology, v. 25, p. 956-983; un artículo muy citado] para rocas graníticas, junto con la propuesta de un conjunto de cinco nuevos diagramas multi-dimensionales basados en las funciones discriminantes para magma ácido de cuatro ambientes tectónicos (arco de isla, arco continental, rift continental, y colisión), publicado por Verma *et al.* (2012) [International Geology Review, v. 54, p. 325-347; **Anexo I**]. Las configuraciones tectónicas muy similares de arco de isla y arco continental han sido discriminadas por primera vez. Los porcentajes de éxito obtenidos a partir del conjunto de pruebas fueron alrededor de 60%-90%. Estos diagramas se basan en el manejo estadísticamente correcto de los datos de composición como fue documentado por Verma *et al.* (2010) [Advances in Geosciences, v. 26, p. 11-22; **Anexo II**], lo cual requiere transformación logarítmica de relaciones de las concentraciones de dos elementos, mientras que la técnica multivariada del análisis discriminante lineal (LDA) supone una distribución normal de las variables transformadas. Estos diagramas se aplicaron a los datos de muestras de roca ácida del Cretácico al Cuaternario de todo el mundo.

En el **Capítulo 3** se ilustra el ejemplo de aplicación de diagramas multi-dimensionales basados en las funciones discriminantes para las rocas básicas y ultrabásicas (cuatro conjuntos de diagramas publicado por Agrawal *et al.* 2004, 2006; Verma et al. 2006;

Verma y Agrawal 2011, que fueron propuestas a través de la colaboración indo-mexicana) provenientes de la zona tectónicamente compleja del sur de México (Cinturón Volcánico Mexicano, campo volcánico de Los Tuxtlas, y la Provincia Oriental Alcalinas) y el área del Arco Continental de América Central; los resultados fueron documentados por Verma *et al.* (2011) [Pure and Applied Geophysics, v. 168, p. 1501-1525; **Anexo III**]. La tasa de éxito del 51.0%-94.4% y 89.3%-98.7% fue obtenida para el Cinturón Volcánico Mexicano y Los Tuxtlas, respectivamente. Los ambientes tectónicos inferidos se presentan en esta publicación. La tasa de éxito para el Arco Volcánico de Centroamérica como el ambiente de un arco también fue elevada (76.5%-80.7%). Del mismo modo, para la aplicación del norte de México (Baja California, Baja California Sur y Sonora, incluyendo el Golfo de California), se presenta el trabajo de Pandarinath y Verma (2012) [Journal of Iberian Geology, en prensa; **Anexo IV**]. Las tasas de éxito se muestran de la siguiente manera. Para las rocas básicas de la tierra firme con la edad <13 Ma, se obtuvo una tasa de éxito de 71%-93% y 58%-90% para los diagramas basados en los elementos mayores y traza, respectivamente. Para las rocas básicas de la tierra firme con la edad >13 Ma, los diagramas basados en elementos mayores indicaron un ambiente de rift continental (altas tasas de éxito del 62-92%). Sin embargo, los diagramas basados en elementos traza (Agrawal *et al.* 2008) indicaron una transición del ambiente de arco a rift continental. Una sola muestra proveniente del arco de Comondú consistentemente fue discriminada como del arco en todos los diagramas de elementos inmóviles propuestos por Verma y Agrawal (2011). Todos los cuatro tipos de diagramas de discriminación indicaron ajuste MORB (las tasas de éxito muy altas del 90%-98% y 100% para los diagramas de elementos mayores y trazas de elementos basados, respectivamente) para las rocas off-shore (predominantemente de DSDP sitios de perforación en el Golfo de California y algunas muestras de rocas de dragado del Golfo de California).

En el **capítulo 4** se documenta una serie de cinco diagramas de discriminación multi-dimensionales obtenidos a partir de la metodología estadística correcta de la transformación logarítmica de relaciones de dos elementos y el análisis discriminante lineal de datos libres de valores discordantes de los variables de interés en 2595 muestras de rocas intermedias de cinco ambientes tectónicos. Uso de estos diagramas, en los cuales los límites del campo tectónicos se basan en la probabilidad, nos dio las tasas de éxito altas (60%-95%) para la discriminación tectónica de trece casos de

aplicación en rocas desde el Arcaico hasta el Cuaternario; para este último se probaron rocas muy alteradas. Los resultados son enviadas por Verma y Verma (2012) [Turkish Journal of Earth Science, en prensa; **Anexo V**] de ambientes de arco, rift, islas oceánicas y colisión para ocho, uno, uno, y tres estudios, respectivamente, fueron apoyados en las estimaciones de probabilidad y fueron, en general, consistentes con los de los esquemas multi-dimensionales para los magmas básicos y ácidos de las mismas regiones.

En el **capítulo 5** presenta un diagrama multi-dimensional basado en las funciones discriminantes para la clasificación de las rocas ígneas alteradas. Para su propuesta, una amplia base de datos de 23768 análisis de las rocas frescas del Mioceno al Reciente fue usada. Este esquema de clasificación puede proporcionar el nombre del tipo de magma básico y ultrabásico, intermedio o ácido. Este diagrama se basa en funciones discriminantes de las variables log-transformadas, en el cual los límites de los ambientes tectónicos fueron obtenidos por estimaciones de la probabilidad; este diagrama tuvo la tasa de éxito del 81%-96%. La utilidad de este esquema radica en la adecuada selección de los diagramas de discriminación para las variedades de rocas básicas y ultrabásicas, intermedio o ácido.

En el **capítulo 6** se desarrolla los ejemplos de aplicación de la clasificación y los diagramas de discriminación para cinco estudios (tres campos geotérmicos y dos calderas de México). Las tasas de éxito se muestran de la siguiente manera para los diferentes estudios: Sierra La Primavera se muestra una configuración de ruptura (rift continental) con las tasas de éxito de 86%-100% para las rocas ácidas; para el campo geotérmico de Los Azufres, tanto las rocas intermedias como las ácidas mostraron consistentemente un escenario de colisión con las tasas de éxito muy elevadas de 71%-76% y 56%-68%, respectivamente; las rocas intermedias de la caldera de Amealco mostraron un escenario de colisión debido a las tasas de éxito muy altas (81%-94%), aunque las rocas ácidas mostraron un ambiente del arco con tasas de éxito menores 48%-81%; las rocas intermedias y el ácido de la caldera de Huichapan mostraron un escenario de colisión debido a tasas de éxito relativamente altas (48%-68% para las rocas intermedias y 48%-52% para las rocas ácidas); y, finalmente, el campo geotérmico de Los Humeros parece estar caracterizado por un entorno de colisión debido a las tasas de éxito relativamente altas (49%-75% para las rocas intermedias y

el 52%-76% de rocas ácidas) mostradas para este campo. Estos resultados fueron apoyados por las estimaciones de probabilidad. Para la mayoría de los casos, los esquemas multi-dimensionales para los magmas intermedios y ácidos proporcionaron resultados coherentes entre sí de los ambientes tectónicos inferidos.

El **capítulo 7** presenta el ejemplo de aplicación de las rocas Arcaicas de los cinco estudios de caso (Australia, Sudáfrica, Brasil, Canadá y la India). El ambiente tectónico se mostró de la siguiente manera para los estudios de casos diferentes: Para la parte oriental del Cratón de Pilbara (Australia), un Paleoarchean (3570-3450 Ma) y Mesoarchean (2900 Ma) ajuste de arco continental aparentemente evolucionó a un ajuste de colisión durante el Neoarchean (2600 Ma). Inferir un ambiente de arco de islas para el Kambalda (Australia) durante el Neoarchean (2700 Ma). Por el cinturón de Barberton (Sudáfrica), la transición de un régimen de dorsales oceánicas durante la parte más antigua de la Paleoarchean (3470 Ma), a un ajuste de arco de islas en el parte más joven (3300-3260 Ma) es probable. Un ambiente de arco se indica para el São Francisco cratón (Brasil) y el Río María terreno (Brasil) durante el Mesoarchean (3085-2983 Ma y 2870 Ma, respectivamente), mientras que un ajuste dentro de la placa es claramente indicado para la provincia de Carajás metalogénico (Brasil) durante el Neoarchean (2740 – 2700 Ma). Reconocemos asimismo un régimen de arco de islas para la Mesoarchean (3000 Ma), del Norte Caribou y Neoarchean (2700 Ma), cinturones de Abitibi piedraverde (Canadá), y para el Gadwal Cinturón de piedraverde (India) durante el Neoarchean (2700-2500 Ma). Una colisión ajuste se dedujo para el conjunto de sanukitoid Arcaico (Canadá) y la sutura Kolar zona (India) durante el Neoarchean (2700-2660 Ma y 2630-2520 Ma, respectivamente. Este trabajo ha sido aceptado por Verma y Verma (2012) [International Geology Review, en prensa, DOI: 10.1080/00206814.2012.693246, ISSN 0020-6814 print/ISSN 1938-2839 en línea; **Anexo VI**].

Las referencias citadas en esta tesis se presentan en una sección aparte después del Capítulo 7. Esto es seguido por seis anexos, que incluyen los seis documentos (tres publicados, dos en prensa, uno entregado) en revistas internacionales, en los cuales el autor de esta tesis ha participado activamente.

Introduction

Igneous rocks, thermal springs, and geothermal systems in a given area are associated to each other, particularly when the former are young (ages < 1 Ma). Many geothermal systems contain extrusive igneous rocks. In Mexico, for example, three geothermal fields under exploitation (Los Azufres, Los Humeros, and Las Tres Vírgenes) are associated with igneous rocks and the most important one (Cerro Prieto) probably owes its origin to extensional tectonics (Demant 1981; Verma 1984; Dobson and Mahood 1985; Ferriz and Mahood 1987; Cathelineau *et al.* 1987; Pradal and Robin 1994; Silva and Mora 1998; Torres-Alvarados and Satir 1998; Verma 2000a; Torres-Alvarados 2002; Verma *et al.* 2005, 2006; Pandarinath *et al.* 2008; Verma *et al.* 2011). However, surrounding this geothermal field too, there are igneous rocks whose study could throw light on the deeper part of this field. On the other hand, high temperature geothermal systems are mostly located along or near the boundaries of the lithospheric plates that make up the brittle outermost rind of the earth. Even though these plate boundary zones comprise less than 10% of the earth surface, their potential to contribute to world energy supply is substantial and widespread. The "Ring of Fire" that surrounds the Pacific Ocean basin, mostly as subduction zones and related volcanic arcs, is replete with high temperature geothermal resources; these make significant and growing contribution to the energy demand of many circum pacific countries. Thus, igneous activity, regional tectonics and hydrothermal alteration play important role in the study of geothermal fields.

Contemporaneously with the development of plate tectonics and the recognition of specific tectonic settings such as island arc, continental rift, oceanisland, and mid-ocean ridge, the idea that magmas from different tectonic settings might be distinguishable in their chemistry was pioneered by Pearce and Cann (1971, 1973). Since then, numerous bivariate and ternary tectonomagmatic diagrams have appeared in the literature (for more details see, e.g., Rollinson 1993; Verma 2000a, 2006). These

diagrams provide additional evidence, complementary to the field evidence, and suggest an affiliation rather than an unequivocal confirmation of the tectonic environment. From the statistical point of view, probably a major advance in the proposal and functioning of discrimination diagrams came with the introduction of discriminant analysis, in which a large number of variables are examined to isolate those that most effectively classify the samples in their predefined classes or groups. As early as 1965, Chayes and Velde (1965) used discriminant functions to distinguish between circum-oceanic and ocean-island basaltic lavas. Later, Pearce (1976) used 8 major-elements (SiO_2, TiO_2, Al_2O_3, FeO, MgO, CaO, Na_2O, and K_2O) in a total of 358 samples of basaltic rocks and 6 classes to propose new discriminant function diagrams. The linear field boundaries between the groups were, however, drawn by 'eye' (Pearce 1976, p. 22), instead of some objective procedure. Soon afterwards, Yellur and Nair (1978) used Pearce (1976) discriminant function and other diagrams to infer the tectonic environment of Chitradurga metabasalts in south India. The problem of 'eye-fitted boundaries' persisted in the proposal of most discrimination diagrams until Agrawal (1999) suggested how to replace these eye-fitted boundaries by probability-based surface boundaries. The other problem in the creation of such discrimination diagrams was the inadequacy of the dataset used to represent the population, i.e., the statistical sample probably was not representative of the population. For example, only 358 samples were used by Pearce (1976) to represent 6 classes; many other diagrams are based on similar or still smaller data sets (e.g., 507 samples from 5 settings by Mullen 1983; 35 mean values from about 300 analysis for 5 classes by Butler and Woronow 1986). The lack of representativeness as well as the use of 'eye-fitted' boundaries might be the reasons why Armstrong-Altrin and Verma (2005) found that many tectonic setting discrimination diagrams proposed and used for sedimentary rocks do not work properly. Both these shortcomings of discrimination diagrams (lack of representativeness of the database and use of 'eye-fitted' boundaries) were recently overcome by Agrawal *et al.* 2004, who used a total of 1159 samples of mostly basic rocks from 4 tectonic settings (island arc, continental rift, oceanisland, and mid-ocean ridge) and performed the discriminant analysis to propose 5 new discriminant function diagrams, in which the boundaries were probability-based surfaces (or lines in two

dimensions). Another problem attacked or addressed by none of the proposals of discrimination diagrams using linear discriminant analysis, as of today, is the 'closure' or 'constant sum' of compositional data including the major-elements in rocks (e.g., Chayes 1960; Skala 1977, 1979; Aitchison 1986; Reyment 1987; Woronow and Love 1990; Rollinson 1993; Reyment and Savazzi 1999). One of the rare exceptions is Butler and Woronow (1986) who used a small set of 35 TiO_2 , Zr, Y, and Sr average analyses (based on about 300 individual analyses) of basalts to perform principal component analysis (but not linear discriminant analysis) of log centred components. As is well known, the compositional data ideally sum to 1 (constant sum of parts) or 100% (the 'closure' problem persists even if the constituents of analysis do not sum exactly to 100%). This makes them statistically dependent of each other, for example, if we suppose that the rock composition is represented by 10 major-elements or oxides (SiO_2, TiO_2, Al_2O_3, Fe_2Ot_3, MnO, MgO, CaO, Na_2O, K_2O, and P_2O_5), all parts are mutually dependent because all of them sum up ideally to 1 or 100%. Now, if we assume that all parts are non-zero, and we fix one part (no matter which first part we choose, an essential property of the closure or constant sum is that this part has to be less than the whole, i.e., <1 or <100%), the second part (irrespective of which part we imagine to be the second), although not totally predictable, has to be < (1-first part) or < (100%-first part%) (i.e. partly predefined and dependent). The third and later parts will also be partly defined, but within consecutively smaller ranges. The final part will be totally predictable, defined, and dependent. These interdependences arising from the closure problem are an undesirable property for any statistical analysis, including the frequently used bivariate 'Harker-type' and ternary diagrams for the interpretation of igneous rock chemistry (for the latter, the situation is even worse because of the renormalization – to 100 – of the three parts used for constructing them; see Butler 1979). According to Aitchison (1986), the study of compositions is essentially concerned with the relative magnitudes of the parts rather than their absolute values, which leads to the conclusion that we should think in terms of ratios (e.g., Rollinson 1993) and perhaps some additional transformation of these ratio data in order to free the sample space. We must, however, be aware of the danger of spurious correlations between certain kind of ratios (e.g., Chayes 1978; Butler 1986). The ratios formed

from uncorrelated variables will be correlated (a so called spurious correlation) if both ratios have common denominator. I am giving here some geochemical ratios; which may show spurious correlation, e.g., [SiO2/TiO2] and [(MgO+FeO)/ TiO2] as pointed out by Butler (1986). However, this phenomenon will influence bivariate and ternary discrimination diagrams because variables are not multiplied by any factor but in multi-dimensional discrimination diagrams the variables (ten major elements) are multiplied by a factor prior to linear discriminant analysis (LDA) so there should not be a spurious correlation. Further, my aim is not looking for any correlation between variables in this thesis, may be there could be some correlation. Basically I am looking for group separation in variables (ten major elements) by LDA. For LDA, the variable should be normally distributed then log-transformed ratios between geochemical variables are an adequate solution.

Objective of thesis

My present thesis work is intended to address the issue of closure or constant sum, while complying with the other two aspects – the statistical sample representative of the population and an objective procedure for drawing probability based field boundaries, to arrive at a statistically sound or valid discriminant analysis of major-element data. I present a set of five highly successful, new discrimination-function based multi-dimensional discrimination diagrams (using linear discriminant analysis of log-transformation of major-element ratios). I performed discriminant analysis of actual major-element concentration data from the new extended database and compared the success rates with my research group earlier work with a smaller database, as well as with those obtained from the log-transformation of concentration ratios to show that the log-transformation is a recommended, statistically-correct procedure for handling compositional data. I also include some specific application examples for illustration purposes.

Furthermore, for identifying magmas types according to the IUGS Subcommission on the Systematics of Igneous Rocks (Le Bas *et al.* 1986), the volcanic rock classification and TAS diagram should be prepared on an anhydrous 100% adjusted

basis after a proper Fe-adjustment of the major-element data, i.e., using both Fe_2O_3 and FeO varieties and not simply total Fe as Fe_2O_{t3} or FeO_t. The Subcommission recommended that either actually-analyzed Fe_2O_3 and FeO concentrations be used before the adjustment to 100%, or when only total Fe is available, Le Maitre (1976) method for Fe_2O_3 and FeO calculations should be used. However, the use of actually measured Fe_2O_3 and FeO concentrations in igneous rocks for rock classification may not be appropriate, in spite of the Subcommission's recommendations, because inevitable, extensive post-eruptive changes in their values take place, according to Middlemost (1989) who, in fact, evaluated the different ways for estimating the Fe_2O_3/FeO ratio and proposed rock-type based values for the division of total Fe into the Fe_2O_3 and FeO varieties. And this subdivision is a difficult task without using a suitable computer program, such as SINCLAS – standard igneous norm and volcanic rock classification system (Verma *et al.* 2002). All data should be, therefore, processed using SINCLAS computer program under the option of Middlemost (1989) for iron-oxidation ratio calculations and 100% adjustment on an anhydrous basis (Verma *et al.* 2002); this computer program provides highly accurate and consistent results as documented by Verma *et al.* (2003). The data processing by SINCLAS is thus a required step because I wish to separate the total Fe into its two types – the Fe_2O_3 and FeO varieties, and to choose the appropriate samples with $(SiO_2)_{adj}$ value.

Energy engineering related importance of the work

The importance of the work is as follows.

1. Although some geothermal fields such as in Central America (González Partida *et al.* 1997; Agostini *et al.* 2006) are located in a well known tectonic setting of subduction (arc setting), the Mexican geothermal fields such as Los Azufres (Dobson and Mahood 1985; Cathelineau *et al.* 1987; Pradal and Robin 1994; Silva and Mora 1998; Verma *et al.* 2005; Pandarinath *et al.* 2008), Los Humeros (Demant 1981; Ferriz and Mahood 1987; Verma 2000), or La Primavera (Demant 1981; Mahood 1981), are housed in the Mexican Volcanic Belt (MVB), which is shown to be a very complex tectonic area (e.g. Márquez *et al.* 1999; Verma 2002, Velasco-Tapia and Verma 2012). Thus, the

MVB is interpreted classically as a continental arc (Robin 1982) but also as the trace of a mantle plume (Márquez *et al.* 1999) as well as a continental rift (Verma 2009). When two or more types of tectonic settings are involved in a given area, the thermal regime will reflect all these tectonic mechanisms. In an arc setting, the primary magmas are likely to be originated at relatively lower temperatures due to the presence of subduction fluids, whereas in a rift setting, the mantle is likely to come closer to the upper crust and magmas may be generated at higher temperature. Besides, the mantle, being the primary heat source, is likely to underlie a thinner crust. In a dual or transitional tectonic setting, the thermal regime will thus be controlled by multiple processes. Therefore, it is important to understand the tectonic setting of geothermal areas.

2. To decipher tectonic setting one of the widely techniques involves the use of discrimination diagrams. Therefore, it is necessary to develop new more efficient tools for this purpose.

3. Geothermal fields are also known in several other countries, some of them may have a simpler tectonic history, such as Japan, whereas others, such as Turkey, are likely to show a more complex tectonic evolution. Tectonic setting is more complex in Turkey because on a regional scale, many different plate tectonic processes have taken place throughout the Cenozoic. These include: subduction, collision, and rifting (e.g., Evans *et al.* 1985; Keskin 2003; Collins *et al.* 2008). On the other hand, in Japan only the subduction process has taken place during all of Cenozoic e.g., Shuto *et al.* (2006). Therefore, the discrimination diagrams will be able to clarify the tectonic setting of fields in other countries as well.

4. Thermal modelling has proved to be an important tool to understand the evolution of geothermal fields at a local scale and the present subsurface temperature contours in such areas (Verma and Andaverde 2007). In such models, one of the input variables is the rock type. Thermal properties and emplacement temperatures of rocks depend on their type, whether ultrabasic, basic, intermediate, or acid. For example, basic and ultrabasic magmas are emplaced at higher temperatures than the intermediate and acid varieties. Therefore, it is mandatory to precisely know the rock or magma types present in a geothermal area. However, the conventional diagrams to infer the magma types

depend on mobile elements (Le Bas *et al.* 1986). Therefore, new diagrams for classification of magma types are required. Besides, the correct application of discrimination diagrams also requires the identification of magma types.

5. The rocks from the geothermal fields may be altered due to hydrothermal processes, which may make it difficult to infer the original rock or magma type, or prevailing tectonic setting. Therefore, on one hand the diagrams should be able to identify the magma type and tectonic settling and on the other to know the implications of hydrothermal effects. If the samples plot coherently in a given tectonic field, these effects may not have been so severe, and the original magma type or the tectonic setting can be correctly inferred. Otherwise, if the samples show a wide scatter, this may be due to severe alteration effects. In that case, the diagrams may have to be improved.
6. Both discrimination and classification diagrams will be applicable to study the roots of geothermal systems, probably exposed in mines (which are the source of precious minerals or elements). This would constitute a very extensive application for a major part of the Earth´s crust. This kind of application will clarify us whether the present diagrams provide a satisfactory answer or more appropriate diagrams should be proposed in future from a suitable database.

Chapter 1

Chapter 1

Discrimination and Classification Diagrams

1.1 Theoretical approach

The idea of trying to fingerprint magma from different tectonic settings chemically is probably best attributed to Pearce and Cann (1971, 1973). In two very important papers these authors showed that it was possible to use geochemistry to distinguish between basalts produced in different, known tectonic settings. They produced what have become known as tectonomagmatic discrimination diagrams, geochemical variation diagrams on which magmas produced in different tectonic settings may be distinguished from one another on the basis of their chemistry. The relatively simple approach and the wide applicability of their results meant that the environment of eruption of both ancient and modern basalts could be defined by the analysis of a rock for just a few readily determined elements. This led quickly to a plethora of papers purporting to show the tectonic setting of ancient volcanic rocks whose state of preservation and poor exposure had previously precluded the identification of the palaeotectonic environment. More recently, however, geochemists have moved away from the 'cookbook' type of approach to tectonomagmatic discrimination diagrams to closer examination of the reason why different tectonic environments have variable geochemical signature.

The work pioneered by Pearce and Cann (1971, 1973) brought together three separate strands of thinking. These are the statistical technique of discriminant analysis, the rapid and accurate analysis of trace elements though to be normally

immobile under hydrothermal conditions and the identification of a number of distinct tectonic environments.

1.2 Tectonic environments

The number of tectonic environments recognized today is much greater than twenty years ago. This reflects the advances made in understanding both earth processes and the geochemistry of igneous rocks. Pearce and Cann (1971, 1973) originally identified the geochemical signature of rocks from volcanic arc, from the ocean floor and from within plates. Today the chemical discrimination of tectonic environments has expanded to include granitic rocks and sediments.

A summary of the main tectonic environments discussed in this thesis is given below:

Tectonic environments recognizable using geochemical criteria

Arc setting
Island arc
Continental arc

Rift setting
Continental rift

Island setting
Ocean island

Ridge setting
Mid-ocean ridge

Collision setting
Collision

It is not possible to develop discrimination diagrams that can work for all these six tectonic setting at a time. In other words, no single discrimination diagram or a set of diagrams can successfully identify six tectonic settings for several reasons. First, basis rocks are present in all tectonic settings (island arc, continental arc, continental rift,

ocean-island, mid-ocean-ridge) except collision, whereas acid rocks are scarce at least in ocean-island and mid-ocean-ridge settings. Further, ocean ridge are best distinguished using basalt chemistry, whereas discrimination between the different types of collision zone is better done using granite geochemistry. The second reason might be related to the more complicated petrogenetic history of granites affected by processes such as crystal fractional and accumulation, extensive involvement of continental crust, magma mixing, and redistribution and loss of elements by volatile fluxing (e.g. Rollinson 1993), which can make the chemical composition of such evolved acid magmas more difficult to interpret than of basic magmas. These complexities may also significantly reduce the chemical differences of acid magma from different tectonic settings with the consequence that meaningful tectonic discrimination diagrams may not be easily proposed. There are also statistical difficulties if one wishes to discriminate all six tectonic settings at a time, which will not be elaborated in this thesis.

1.3 Discrimination diagrams

Discrimination diagrams have been in use for nearly four decades since the advent of the plate tectonics theory. Discrimination of fresh igneous rocks into distinct tectonic varieties solely based on field occurrence in different tectonic environments (island arc, continental rift, ocean-island, mid-ocean ridge and collision) has gained wide acceptance amongst geologists (e.g., Wilson 1989). Further, based on the assumption that physical parameters and chemical environments of magma generation in various tectonic settings are distinct, numerous attempts have been made to identify differences in the chemical composition of the magmas generated in different tectonic environments.

Secondly, using a discrimination diagram constructed from modern volcanic rocks to postulate an Archaean tectonic setting is likely to produce equivocal results. Furthermore, discrimination diagrams were never intended to be use for single samples, but rather with a suite of samples. This simple precaution will eliminate the

occasional spurious results and highlight data sets from mixed or multiple environments.

Since the early seventies, a plethora of tectonomagmatic discrimination diagrams have been proposed (e.g., Wang and Golver III 1992; Rollinson 1993; Verma1996, 1997, 2000b, 2006; Gorton and Schandl 2000; Agrawal *et al*. 2004, 2008; Vasconcelos-F *et al*. 2004, 2008; Verma *et al.* 2006; Verma and Agrawal 2011). These diagrams were mostly meant for use with basic igneous rocks. Very few diagrams exist for granitic rocks or felsic rocks (Pearce *et al*. 1984; Verma *et al*. 2012) and with exception of bivariate diagrams by Bailey (1981) for refined tectonic setting of only orogenic andesite, almost none are available for intermediate rocks. Such a scarcity of tectonic diagrams for intermediate rocks led us to fill this gap in the literature, the new multi-dimensional discrimination diagrams were proposed by Verma and Verma (2012). Tectonic settings have also been discriminated by Arai et al. (2011) using chromian spinel chemistry. A meaningful approach to the problem of tectonics and basalt geochemistry can be through careful stratigraphic geochemical studies which document important temporal and spatial variations in melt compositions (Myers and Breitkopf 1989). Multi-dimensional discrimination technique is also based on Bayesian probability theory (Shragge and Snow 2006).

Discrimination diagrams are widely used for sedimentary rocks as well (e.g., Bhatia 1983; Roser and korsch 1986), which were evaluated by Armstrong-Altrin and Verma (2005), using published data from Miocene to Recent sand and sand stone from all around the world.

1.3.1 Examples of different discrimination diagrams

There are large number of discrimination diagrams are available to basalt and basaltic andesites which use trace elements, major and minor elements. Further these are divided into different subheadings.

a) Four bivariate diagrams

All bivariate diagrams are based on the so-called immobile or high field strength elements

Ti, Zr, Na, Y and V (Rollinson 1993), which seems to be an advantage for application to altered samples, especially those from older terrains. Nevertheless, the problems common to all diagrams in this category are incorrect statistical handling of compositional data (Aitchison 1981, 1986; Vermeesch 2006; Verma *et al*. 2006; Agrawal and Verma 2007) and use of boundaries subjectively drawn by eye (Agrawal 1999). The lack of a representative sample database may be also included in these criteria.

1) Ti/Y-Zr/Y of Pearce and Gale (1977)

Pearce and Gale (1977) proposed a discrimination diagram which based upon Ti/Y and Zr/Y variations to discriminate between within-plate basalts and other types of basalt, collectively termed 'plate margin basalts' (Figure 1). This diagram makes use of the enrichment in Ti and Zr but not Y in within-plate basalt.

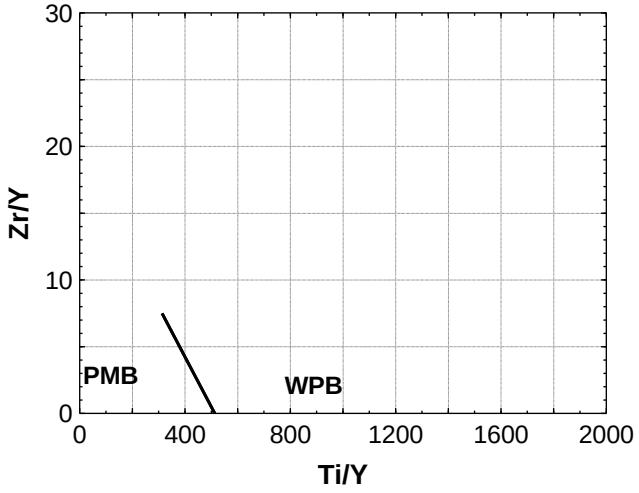

Figure 1. The Ti/Y-Zr/Y (Pearce and Cann 1977) discrimination diagram for basalts showing the fields of plate margin basalts (PMB) and within-plate basalts (WPG). PMB is assumed to include both arc and mid-ocean ridge (MOR) setting, whereas WPB would include both continental rift and ocean-island setting.

2) Zr-Zr/Y of Pearce and Norry (1979)

Pearce and Norry (1979) found that the fractional index Zr plotted against the ratio Zr/Y proved an effective discriminant between basalts from ocean-island arc, MORB and within- plate basalts (Figure 2). Arc basalts plot in filed A and D, MORB in field B, D and E and within-plate basalts in field C and E. Pearce (1980) contoured the MORB field of this diagram for spreading rate.

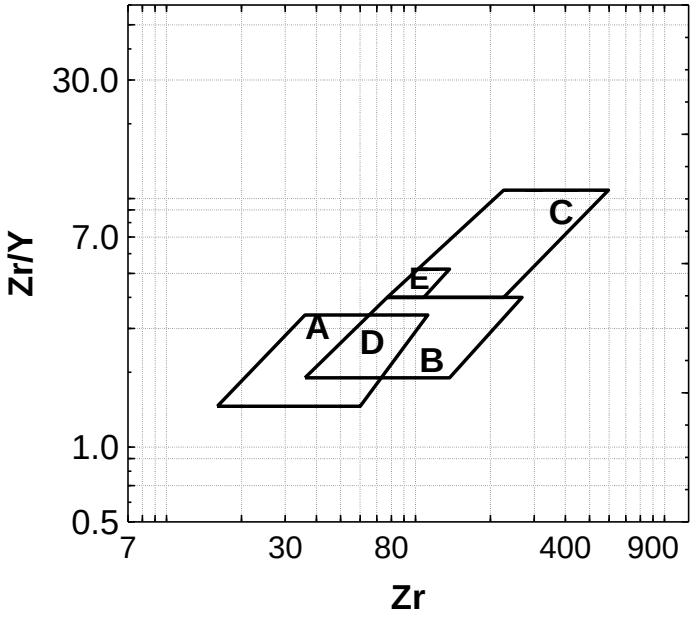

Figure 2. The Zr-Zr/Y bivariate diagram (base 10 log-log scales; Pearce and Norry 1979) for island arc basalt (IAB; field A), within-plate basalt (WPB; field C), mid-ocean ridge basalt (MORB; field B), overlape region of IAB and MORB (IAB+MORB; field D), and WPB and MORB (WPB+MORB; field E).

3) Ti/1000-Vof Shervais (1982)

Ti and V are adjacent members of the first transitional series in the periodic table and yet silicate system they behave in different ways. This is basis of the discrimination diagram of Shrivais (1982), which is used to distinguish between volcanic-arc tholeiites, MORB and alkali basalts.

The different basalt fields are subdivided according to Ti/1000-V ratio (Figure 3). MORB plots between Ti/1000-V ratio of 20 and 50, although there is considerable overlap with the fields of continental flood basalt and back-arc basin basalts. Ocean-island and alkali basalts plot between Ti/1000-V ratio of 50 and 100. Island-arc thoeiites plot between Ti/1000-V ratio of 10 and 20 with a small overlap onto the field of MORB.

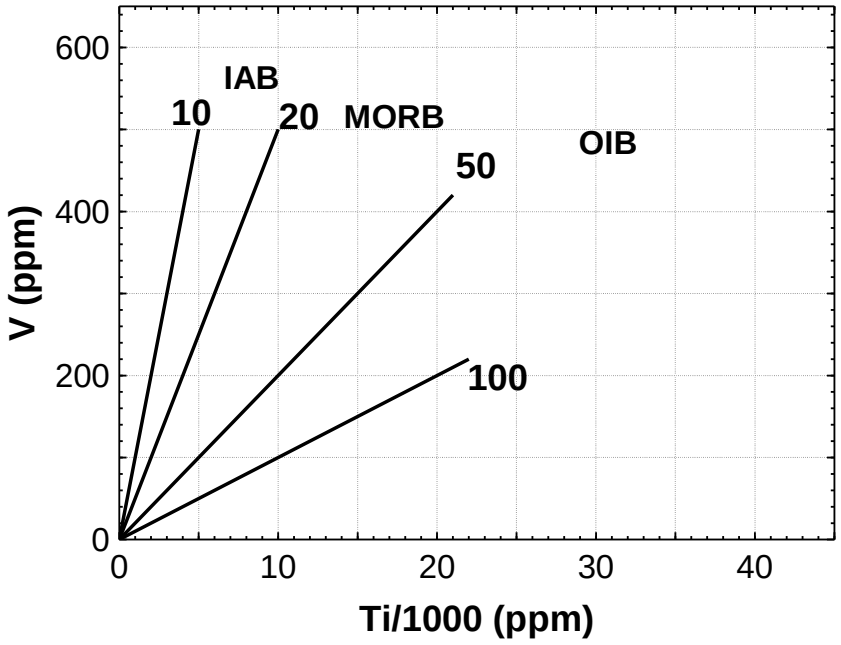

Figure 3. The Ti/1000-V bivariate diagram (Shervais 1982) for island arc basalt (IAB; Ti/1000-V equi value of 10-20), ocean-island basalt (OIB; Ti/1000-V equi value of 50-100), and mid-cean ridge basalt (MORB; equi value of 20-50).

4) Nb/Y-Ti/Y of Pearce (1982)

This diagram, shown in Figure 4, successfully separates the within-plate basalt group from MORB and volcanic-arc basalts, which overlap extensively on this plot. Within-plate basalts have higher Nb/Y and Ti/Y than the other types of basalt, difference which are thought to reflect an enrich mantle source relative to the source of MORB and volcanic-arc basalts. Differences in Nb/Y allow the within-plate basalt group to be further subdivided into tholeiitic, transitional and alkaline types.

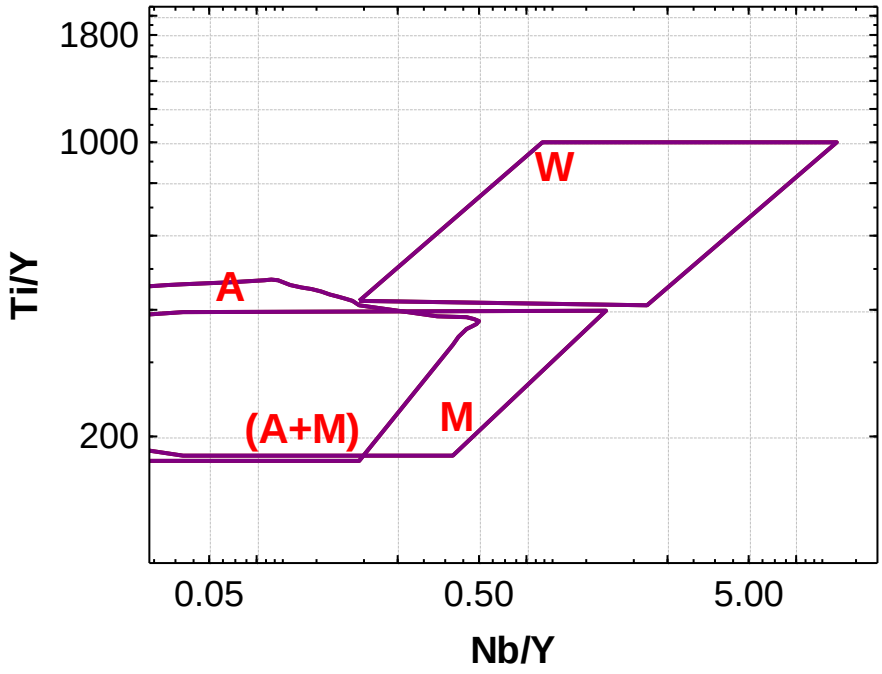

Figure 4. The Nb/Y-Ti/Y bivariate diagram (Pearce 1982) for island arc basalt (IAB; field A), within-plate basalt (WPB; field W), mid-ocean ridge basalt (MORB; field M), overlap region of IAB and MORB (IAB+MORB; field A+M).

b) Six Ternary Diagrams

As like bivariate diagrams, the six ternary diagrams are as described below.

1) Zr-3Y-Ti/100 Ternary Diagram of Pearce and Cann (1973)

The diagram in Figure 5, most effectively discriminates between within-plate basalts, i.e. ocean-island or continental flood basalts (field D) and other basalt types. Island-arc tholeiites plot in field A and calc-alkaline basalts in field C. MORB, island-arc tholeiites and calc-alkaline basalts all plot in field B. Data points are calculated

according to their assigned weightings [Zr (ppm), 3Y (ppm), Ti/100 (ppm)], recast to 100%, and plotted on the triangular diagram.

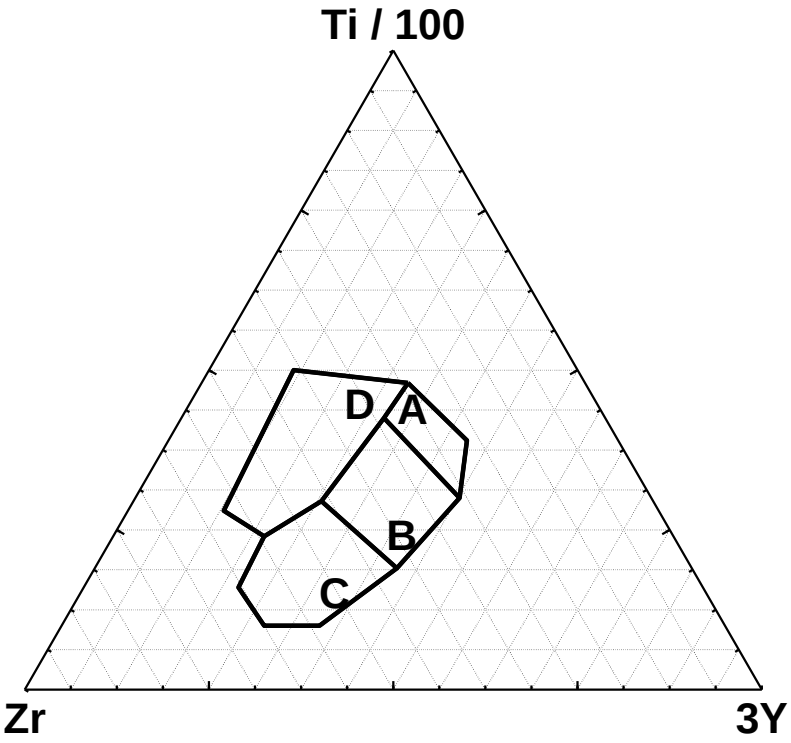

Figure 5. The Zr-3Y-Ti/100 ternary diagram (Pearce and Cann 1973) for island arc tholeiite (IAT; field A), mid-ocean ridge (MORB; field B), calc-alkaline basalts (CAB; field C), and within-plate basalts (WPB; field D).

2) Mgo-Al_2O_3-FeO^t of Pearce et al. (1977)

Pearce *et al*. (1977) used a data file of 8400 analyses of recent volcanic rocks to discriminate between basalt from different tectonic environments on the basis of their major element chemistry. This diagram is different from most others described in this chapter because it applies to rock in the silica range 51-56 wt % (Analyses recalculated dry), i.e. for subalkaline basalts and basaltic andesites. Pearce *et al*. (1977) found that the oxides MgO, Al_2O_3 and FeO (Total Fe recalculated as FeO) were able to discriminate between the following tectonic environments: ocean-island and floor basalts (MORB); ocean-island basalts; continental basalts; volcanic arc and active continental margin basalts (orogenic basalts in terminology of Pearce *et al*. (1977);

spreading centre island basalt (e.g. Iceland, Galapagos). The boundaries between the different fields are shown in Figure 6.

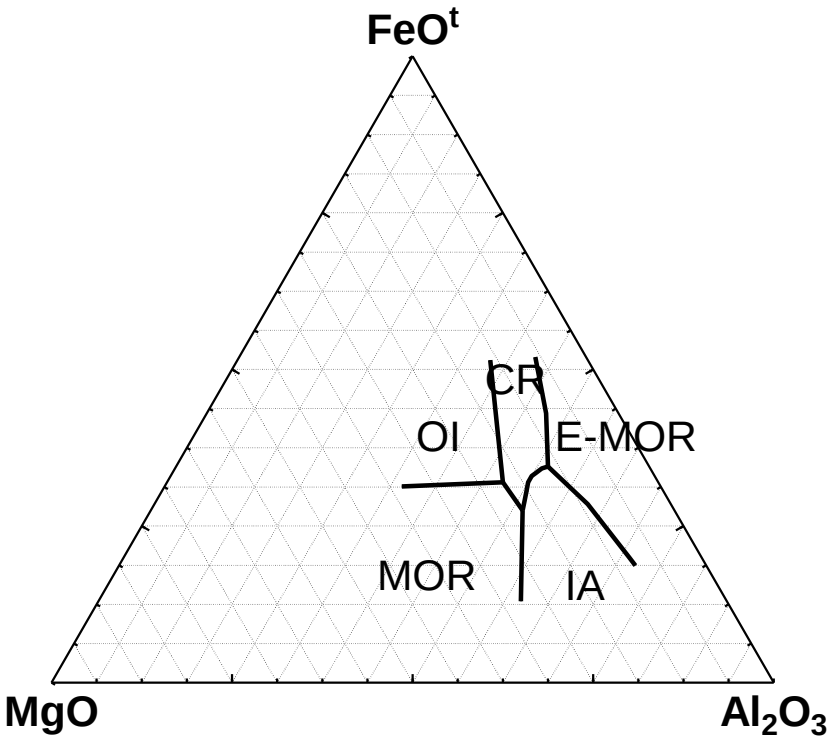

Figure 6. The Mgo-Al_2O_3-FeO^t ternary diagram (Pearce *et al*. 1977) for island and continental arc (IA+CA shown as IA), mid-ocean ridge and ocean floor (termed as MOR), continental rift (CR), ocean-island (OI), and spreading centre island (termed as E-MOR).

3) Th-Ta-Hf/3 of Wood (1980)

A discrimination diagram based upon immobile HFS (High Field Strength) elements Th-Ta-Hf was proposed by Wood (1980). In order to expand and centre the fields of basalt types, concentrations are plotted (in ppm) as Th, Ta and Hf/3. The elements Th, Ta and Hf are present in very low concentration in basalt and cannot be accurately determined by XRF analysis and so must be determined by INAA. In cases where reliable Hf and Ta analyses are not given but Zr and Nb concentration have been Figure 7 shows the filed for different magma type. N-type MPRB plot in field A whilst

E-type MORB and tholeiitic within-plate basalts both plot in field B. Within-plate alkali basalts plot on the Th-Ta-Hf diagram in filed C and volcanic-arc basalts in filed D. Field D may be subdivided into island-arc tholeiites (primitive arc tholeiites) - lavas with an Hf/Th ratio greater than 3- and calc-alkaline with an Hf/Th ratio less than 3.

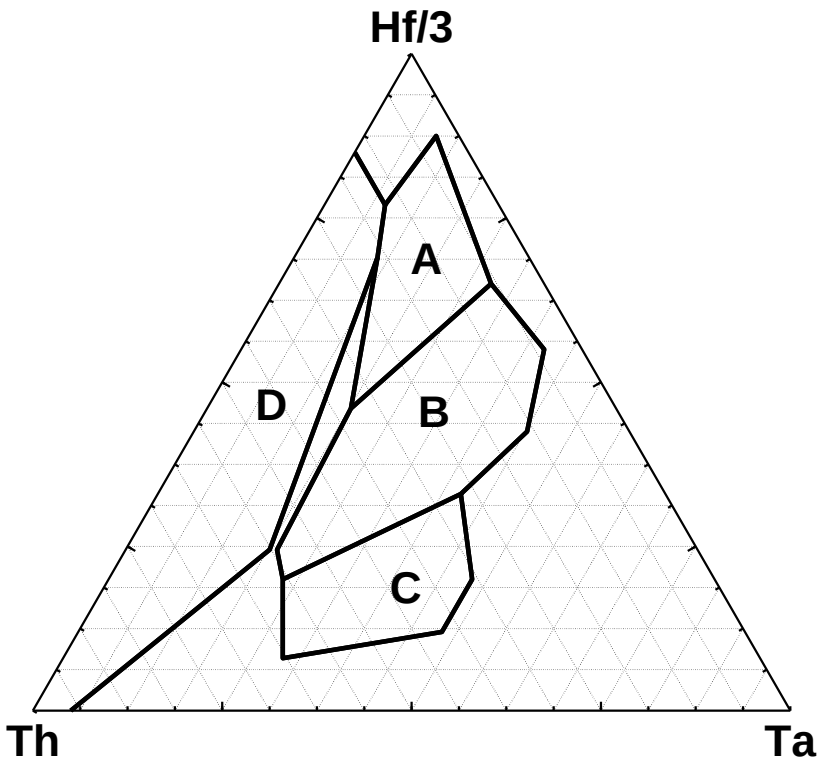

Figure 7. The Th-Ta-Hf/3 ternary diagram (Wood 1980) for island arc basalt (IAB; field D), within-plate basalt (WPB; field C), normal type mid-ocean ridge basalt (N-MORB; field A), and enriched type mid-ocean ridge basalt (E-MORB; filed B).

4) 10MnO-15P_2O_5-TiO_2 of Mullen (1983)

Basalts and basaltic andesites in the silica range 45-54 wt % SiO_2 can be subdivided on the basis of their MnO_2, TiO_2 and P_2O_5 concentrations into the following types: MORB; ocean-island tholeiites, ocean-island alkali basalts; island-arc tholeiites; calc-alkali basalts (Mullen 1983). The boundaries defined in Figure 8 are based upon an empirical study. MnO and P_2O_5 values are multiplied by 10 in order to expand the plotted fields and although this also amplifies the analytical errors for MnO and P_2O_5,

the enhanced errors still do not exceed the width of the fields. It should be noted, however, that the composition ranges for these elements are small- the mean values for all basalt types are in the range MnO 0.16-0.24 wt %, P_2O_5 0.14-0.74 wt % and TiO_2 0.81-3.07 wt % - and require accuracy of measurement.

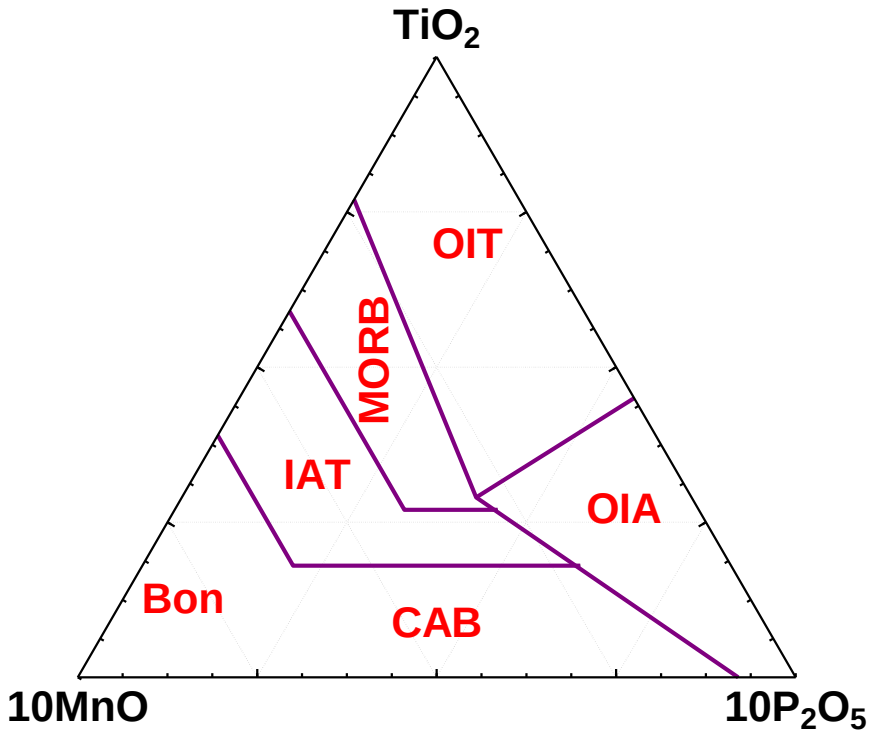

Figure 8. The 10MnO-15P_2O_5-TiO_2 ternary diagram (Mullen 1983) for island arc tholeiite (IAT), calc-alkaline basalt (CAB), boninite (Bon), ocean-island tholeiite (OIT), ocean-island basalt (OIA), and mid-ocean ridge basalt (MORB).

5) Zr/4-Y-2Nb of Meschede (1986)

The oceanic basalt chemistry has expanded over the past 20 years, it has become apparent that there is more than one type of MORB or 'ocean-floor basalt' as it was called by Pearce and Cann (1973). Meschede (1986) suggested that the immobile trace element Nb can be used to separate the different type of ocean-floor basalt and recognized two type of MORB. These are N-type MORB, basalt from a 'normal' mid-ocean ridge environment depleted in incompatible trace elements, and E-type MORB

(also known as P-type MORB) - ocean floor basalt from plume-influenced regions such as Iceland which are generally enriched in incompatible trace elements. On the triangular plot of Zr/4, Y and 2Nb, Figure 9 showed that four main basalt field can be identified.

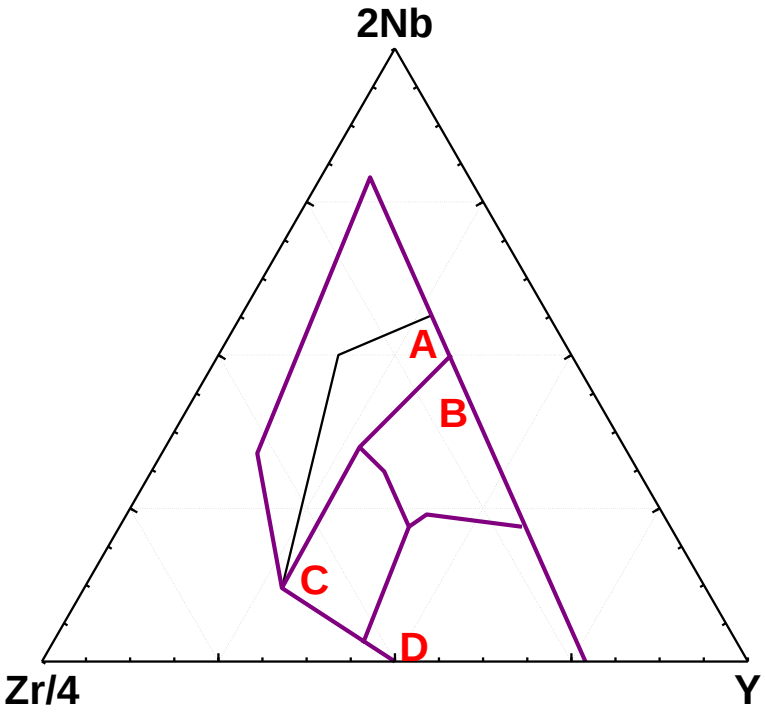

Figure 9. The Zr/4-Y-Nb ternary diagram (Meschede 1986) for within-plate alkali basalts and tholeiite (WPB; region A), enriched type mid-ocean ridge basalt and within-plate tholeiite (IAB+WPT; region C), and overlap region of normal type island arc basalt and mid-ocean ridge basalt (IAB+N-MORB; region D).

6) La/10-Nb/8-Y/15 of Cabanis and Lecolle (1989)

Using a comparatively small number of samples, Cabanis and Lecolle (1989) constructed

a triangular diagram based on La-Nb-Y concentration which discriminate between volcanic-arc basalts, continental basalts and oceanic basalts. Elemental concentrations

are plotted in ppm as La/10, Nb/8 and Y/15 and the three main fields are further subdivided. Volcanic-arc basalts plot in (field A), continental basalt (field B), and oceanic basalt (field C). Figure 10 is represented all these fields.

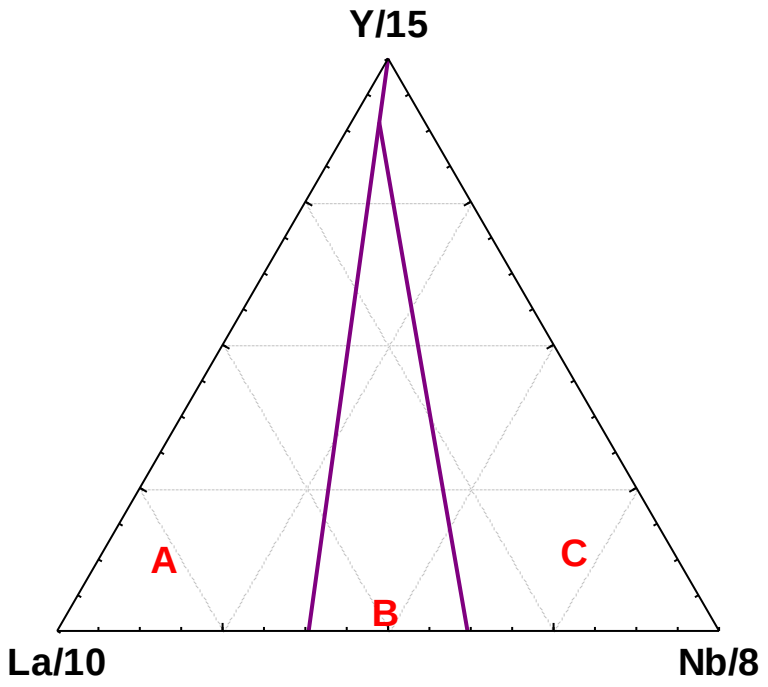

Figure 10. The La/10-Nb/8-Y/15 ternary diagram (Cabanis and Lecolle 1989) assumed to discriminated arc basalt (IAB) field A, continental basalt (CRB) field B and ocean floor basalt (OIB+N-MORB+E-MORB) filed.

c) Four discriminant function based diagrams

As like bivariate and ternary diagrams, the four discriminant function based diagrams are as described below.

1) $Score_1$-$Score_2$ diagram of Butler and Woronow (1986)

The $Score_1$-$Score_2$ diagram is much less used probably because of the complicated calculations involved, which are more difficult than those for the simple bivariate and ternary diagrams.

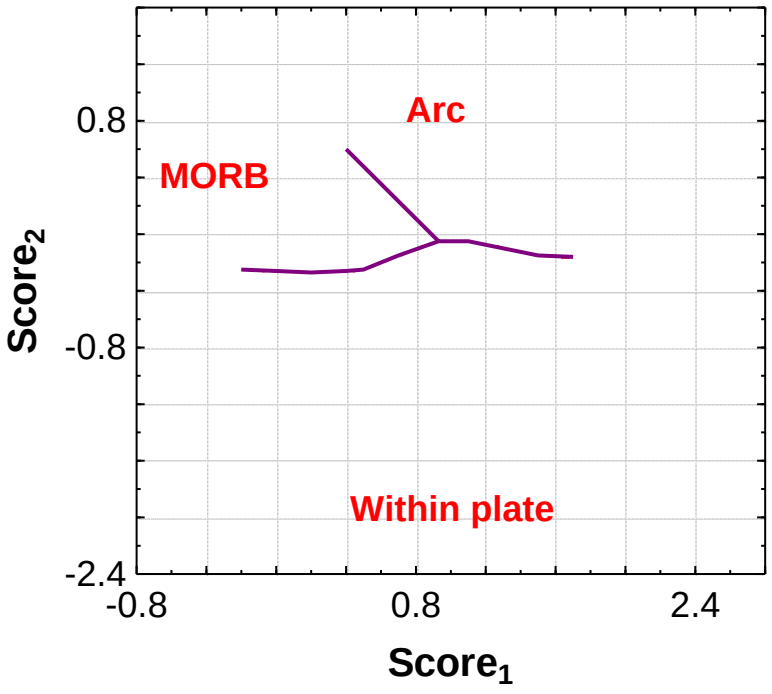

Figure 11. The $Score_1$-$Score_2$ diagram (Butler and Woronow 1986) for arc (IAB), within-plate (WPB), and mid-ocean ridge (MORB).

2) F_1-F_2 diagram of Pearce (1976)

Pearce (1976) calculated discriminant functions based upon the eight major element oxides SiO_2, TiO_2, Al_2O_3, FeO (recalculated from total Fe), MgO, CaO, Na_2O, K_2O

and presented discriminant diagrams to identify MORB, within-plate basalts (ocean-island/continental basalts), calc-alkaline basalt, island arc tholeiites and shoshonite. The boundaries of discriminant diagrams were based upon fresh modern basalt (samples with $FeO/Fe_2O_{3<}$ 0.5 were rejected) in the compositional range 20 wt %> CaO+MgO>12 wt%, with sum (including H_2O) between 99 and 101%, figure 12 and 13.

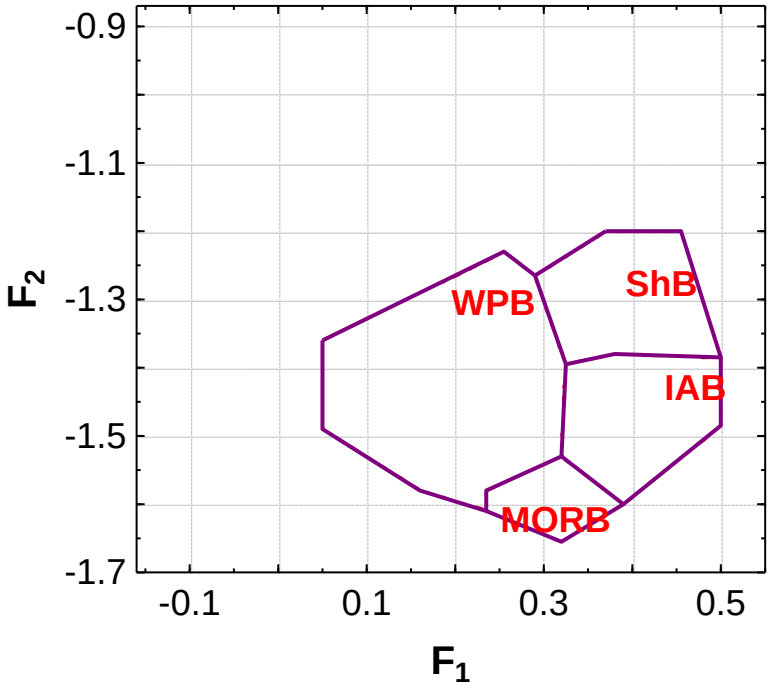

Figure 12. The F_1-F_2 discriminant function diagram (Pearce 1976) for low-potassium tholeiite and calc-alkali basalt (LKT+CRB; assumed as arc –IAB- setting), within-plate (WPB), shoshonite (SHO; not assumed to belong to any of the four setting), ocean floor basalt (OFB; assumed as mid-ocean ridge basalt –MORB- setting).

3) *F2-F3 diagram of Pearce (1976)*

A plot of separates island-arc tholeiites, calc-alkaline basalts and shoshonite from each other from MORB.

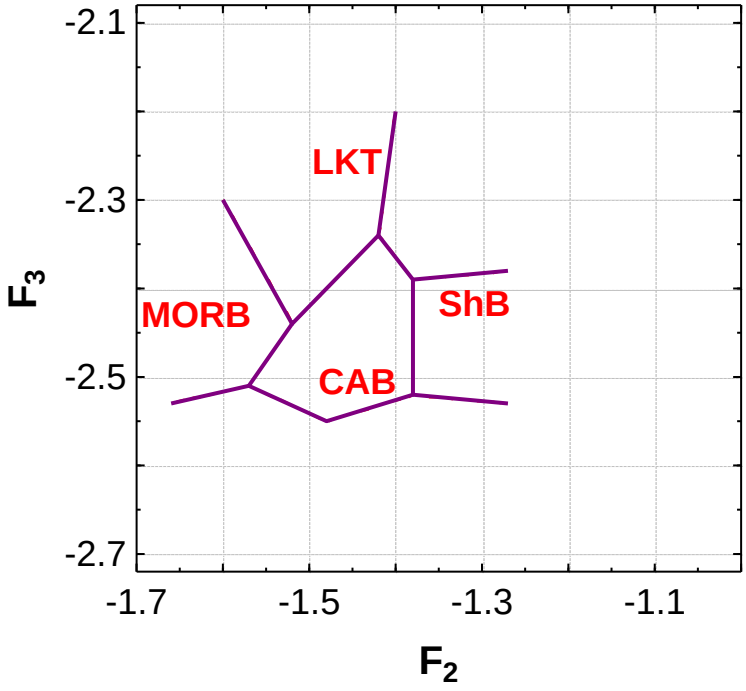

Figure 13. The F_1-F_2 discriminant function diagram (Pearce 1976) for low-potassium tholeiite (LKT), calc-alkali basalt (CRB), shoshonite (SHO), ocean floor basalt (OFB; assumed as mid-ocean ridge basalt –MORB- setting).

4) *Set of five diagrams based on major elements (Agrawal et al. 2004, Verma et al. 2006)*

Examples of these multi-dimensional discriminant-function based discrimination diagrams were already presented in Annexure II, III and IV along with chapter 4. See Annexures II, III, IV and chapter 4.

1.4 Classification diagrams

Rock classification and nomenclature is widely used in igneous petrology but is also useful for some sedimentary rocks. With advent of automated XRF analysis, most geochemical investigations produce a large number of major elements data. Thus, increasingly it is both useful and in some cases necessary to attempt to classify rocks on the basis of their chemical composition. It is reviews the classification schemes in current use and outlines the rock types for which they may be specifically suited. The criteria employed in the evaluation of a classification scheme are that it should be easy to use and widely applicable; its logical basis should be readily understood and that as far as possible it accurately should reflect the existing nomenclature, based upon mineralogical criteria. The summary of chemical classification schemes are described below in box.

Summary of chemical classification schemes

Igneous rocks

The total alkalis-silica diagram (TAS) is:

1. For volcanic rocks

1.4.1 Examples of different classification diagrams

There is several classification diagrams are proposed by different researcher but I am going to present here only two diagrams, rest are Ne-Di-Ol-Hy-Q diagram of Thompson (1984) for basaltic classification, Ab-An-Or diagram of O' Connor (1965)

for granite classification, The Q(F)-ANOR diagram of Streckeisen and Le Maitre (1979), The R1-R2 diagram of De la Roche *et al.* (1980).

1) The total alkalis-silica diagram (TAS) of Le Bas et al. (1986)

The total alkali-silica diagram is one of the most useful classification schemes available for volcanic rocks. Chemical data - the sum of the Na_2O and K_2O content (total alkalis, TA) and the SiO_2 content (S) are taken directly from a rock analysis as wt % oxides and plotted onto the classification diagrams.

The usefulness of the TAS diagram was demonstrated by Cox *et al.* (1979), who showed that there are sound theoretical reasons for choosing SiO_2 and $Na_2O+ K_2O$ as a basis for the classification of volcanic rocks. This diagram was constructed from a data-set of 24000 analyses of fresh volcanic rocks carrying the names used in their original classification. The field boundaries are defined according to current usage with the minimum of overlap between adjoining fields, Figure 11.

The TAS diagram divides rocks into ultrabasic, basic, intermediate and acid on the basis of their silica content (following the usage of Peccerillo and Taylor 1976). The TAS classification scheme is intended for the more common, fresh volcanic rocks. It is inappropriate for potash-rich rocks and highly magnesian rocks and should not be normally used with weathered, altered or metamorphosed volcanic rocks because the alkalis are likely to be mobilized. Rocks showing obvious signs of crystal fractionation should also be avoided. Analysis should be recalculated to 100% on an H_2O- and CO_2-free basis.

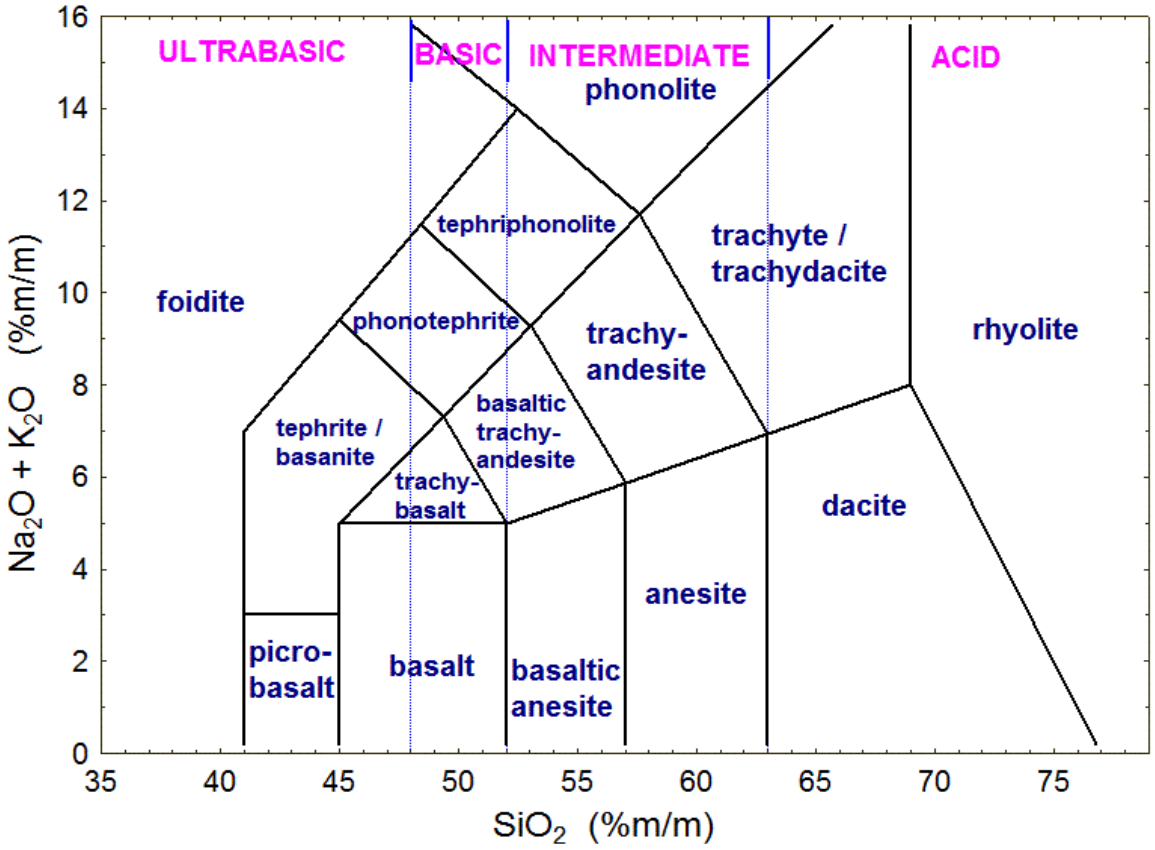

Figure 14. The chemical classification and nomenclature of volcanic rocks using the total alkali versus silica diagrams of Le Bas *et al.* (1986).

2) Co-Th diagram of Hastie et al. (2007)

Recently, Hastie *et al.* (2007) proposed classification diagrams for altered igneous rocks. He recognised from an altogether different approach (analysis of the chemical effect of alternation) that there is need for a reliable way to classify rocks from the geological records´. They state that none of the frequently used SiO_2-K_2O (Peccerillo

and Taylor 1976) and the IUGS recommended TAS (Le Bas *et al.* 1986) diagrams are appropriate. They also argued that although Winchester and Floyd (1977) developed immobile element proxies for the TAS diagram, the need still existed for the proxies of the SiO_2-K_2O diagram. Hastie *et al.* (2007) proposed the use of two proxy elements –Co for SiO_2 and Th for K_2O- in a new Co-Th bivariate diagram.

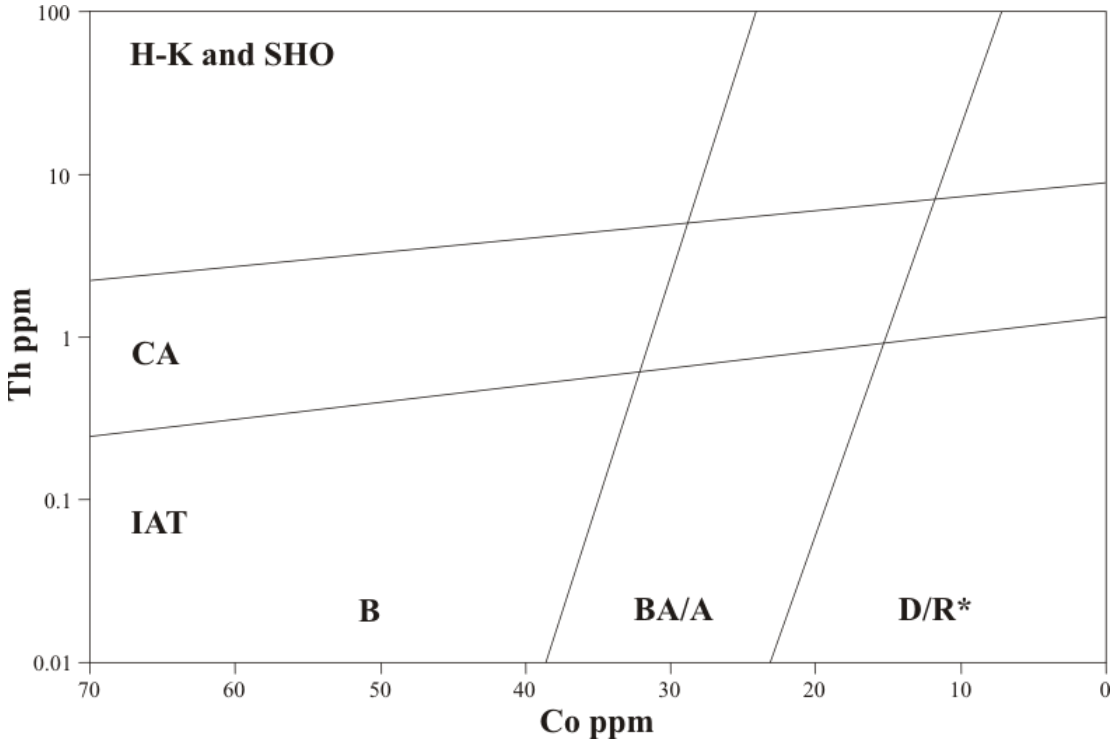

Figure 15. Co-Th, (Hastie *et al.* 2007) classification diagram for altered igneous rocks. The rock type abbreviations in Co-Th diagram are: B-basalt; BA/A-basaltic andesite/andesite; D/R*-dacite/rhyolite/latite/trachyte; IA-T-island arc tholeiite; CA-calc-alkaline; and H-K and SHO-high-K and shoshonite.

Chapter 2

Chapter 2

Statistical evaluation of existing discrimination diagrams for granitic rocks and proposal of new discriminant-function-based multi-dimensional diagrams for acid rocks

2.1 Antecedents

This chapter is based on the following two publications, in which the author of this thesis actively participated. Both are listed in the Science Citation Index (the first as a journal and the second as a book).

Appendix I:

Verma S.K., Pandarinath, K., Verma, S.P. (2012) Statistical evaluation of tectonomagmatic discrimination diagrams for granitic rocks and proposal of new discriminant-function-based multi-dimensional diagrams for acid rocks. **International Geology Review** 54 (3): 325-347.

My contribution involved in this work can be summarized as follows.

1) Compilation of the databases.
2) Statistical evaluation of old discrimination diagrams with compiled new databases.
3) Computation of discriminant-function equations.
4) Calculation of probability based boundaries in discrimination diagrams.
5) Proposal of the new discriminant-function-based multi-dimensional diagrams.

Appendix II:

Verma S.P., Pandarinath, K., Verma, S.K. (2010) Statistically correct methodology for compositional data in new discriminant function tectonomagmatic diagrams and application to ophiolite origin. **Advance in Geosciences,** A 6-Volume Set (Set Editor-in-chief: Kenji Satake), Solid Earth, v. 26, p. 11-22, world Scientific Publishing Company.

My contribution in this work was as follows.

1) Compilation of databases.
2) Preparation of discriminant-function diagrams.

2.2 Introduction

There are several inherent discrimination diagrams proposed for basic igneous rocks (e.g. see Rollinson 1993; Verma 2010), but only a few diagrams are available for tectonic discrimination of acid magmas or granitic rocks (see Appendix I). The main reasons to explain the existence of very few diagrams for discriminating tectonic setting of acid rocks are probably many. First, basic rocks are present in all tectonic settings (island arc, continental arc, continental rift, ocean-island, mid-ocean ridge, and flood basalt province), whereas acid rocks are scarce at least in the ocean-island and mid-ocean ridge settings (Appendix I). The second reason might be related to the more complicated petrogenetic history of granites affected by processes such as crystal fractionation or accumulation, extensive involvement of continental crust, magma mixing, and redistribution and loss of elements by volatile fluxing (e.g., Hanson 1978; Rollinson 1993), which can make the chemical composition of such evolved acid magmas more difficult to interpret than of basic magmas (Appendix I). That's why I proposed the new discriminant-function-based multi-dimensional diagrams for acid rocks.

2.3 Statistical evaluation and proposal of new discriminant-function-based multi-dimensional diagrams

I have evaluated the performance of the four discrimination diagrams Y-Nb, Yb-Ta, (Y+Nb)-Rb, and (Yb+Ta)-Rb) of Pearce et al. (1984), using a parameter called "success rate" (Appendix I). Success rate refers to the efficiency of a plot for a given tectonic setting, and is the ratio of the number of correctly discriminated samples to the total number of samples, expressed as percentage. The incorrect discrimination or mis-discrimination is the complement of the efficiency, which refers to the samples incorrectly plotted in a tectonic setting different from the expected or inferred one. To understand the quality of the diagrams proposed by Pearce et al. (1984) I used the original database of these authors (Appendix I). The first diagram (Y-Nb) cannot discriminate volcanic-arc and collision settings. Both Y-Nb and Yb-Ta diagrams have an overlapping field for within-plate and ocean-ridge granitoids. The remaining two diagrams (Y+Nb-Rb and Yb+Ta-Rb) use a mobile element (Rb) in their y-axis (Appendix I). Although these diagrams successfully discriminate volcanic-arc and within-plate granites, they perform less well for collision tectonics. Besides, felsic or acid rocks are scarce in ocean-ridge setting, which limits the usefulness of these diagrams for this geological environment. Therefore, using an extensive database, I proposed a set of five new discriminant-function-based multi-dimensional diagrams for acid magmas from four tectonic settings (island arc, continental arc, continental rift, and collision). The very similar tectonic settings of island and continental arcs are discriminated for the first time. The success rates of these diagrams as inferred from testing set are indicated in Appendix I. These diagrams are based on correct statistical treatment of compositional data (see Appendix II), objective probability based boundaries replacing those drawn by eye, natural logarithm transformation of major-element ratios and linear discriminant analysis (LDA) (e.g., Verma and Agrawal 2011).

2.4 Compositional data in discriminant-function-based multi-dimensional diagrams

Data expressed as part of whole (percentages or parts per million) are described as compositional data. A normal percentage array of major element data is described

by Chayes (1960) as a ‘closed’ space (see also Aitchison (1986) who uses the term ‘composition’ for such arrays). Chayes (1960) showed that both positive and negative (non-zero) correlations could be obtained in compositional data from

statistical considerations alone and thus drew attention of geoscientists to such false correlations (Appendix II). Therefore, caution is required if we were to interpret geochemical data in diagrams based on compositional data. However, statistical methods to handle variables under study assume an ‘‘open’’ space for them, i.e., theoretically, the variables can take any value up to infinity, which is not possible for compositional data. Thus, most diagrams used in geochemical work for interpreting compositional data violate the basic statistical assumption of open the space for all variables, although this violation may be of somewhat less concern for diagrams used for simply classification purposes (Appendix II). Therefore, log-ratio transformation of compositional variables suggested by Aitchison (1986) was opted to overcome these statistical problems (Appendices I and II).

Five new discriminant-function-based multi-dimensional discrimination diagrams were proposed from LDA of log-ratios of major elements (Appendix I).

2.5 Application of new discriminant-function-based multi-dimensional diagrams

Application of these new diagrams to five case studies is provided in Appendix I. The data from these case studies were not complied in the initial database used for constructing these diagrams. The inference from this application were as follows (Appendix I): a collision setting for the Himalayas at about 30 Ma; an island arc setting for Quaternary acid rocks from geothermal boreholes in El Salvador; an island- or continental-arc setting for northern Italy at 35-52 Ma; a continental arc setting for Italy-Austria border at about 30 Ma; either a rift or a collision setting for northern Nigeria at about 164 Ma; a collision setting for central Nigeria at about 144 Ma and for

the Cretaceous Masirah ophiolites of Oman; and an island arc setting for the Cretaceous Semail ophiolites of Oman.

2.6 Conclusions

A set of five new discrimination diagrams were successfully proposed (Appendix I). These diagrams provided high success rates in both training and testing sets. These multi-dimensional diagrams are based on natural log-ratio transformation of major-element ratios and application of discordant outlier tests prior to LDA. Thus, the combination of discordant outlier tests and LDA has provided a powerful and correct statistical treatment of compositional data. These diagrams have been used for several case studies, and in most cases, consistent results are obtained for the tectonic setting (Appendices I and II).

Chapter 3

Chapter 3

Application of tectonomagmatic discrimination diagrams in Southern and Northwest Mexico and Central America

3.1 Antecedents

This chapter is based on the following two publications, in which the author of this thesis actively participated. Both are listed in the Science Citation Index (both as a journal).

Appendix III:

Verma S.P., Verma, S.K., Pandarinath, K., Rivera-Gómez, M.A. (2011) Evaluation of recent tectonomagmatic discrimination diagrams and their application to the origin of basic magmas in southern Mexico and Central Americas. **Pure and Applied Geophysics** 168, 1501-1525.

My contribution involved in this work can be summarized as follows.

1) Compilation of the databases.
2) Simplified tectonic map of Southern Mexico and Central America.
3) Statistical evaluation of tectonomagmatic discrimination diagrams.

Appendix IV:

Pandarinath, K., Verma, S.K., (2012) Application of four sets of tectonomagmatic discriminant function based diagrams to basic rocks from northwest Mexico. **Journal of Iberian Geology (in press)**.

My contribution involved in this work can be summarized as follows.

1) Compilation of the databases.

3.2 Introduction

The main volcanic area of southern Mexico and Central America, constituting the Mexican Volcanic Belt (MVB), Los Tuxtla volcanic field (LTVF) and isolated centers, such as El Chichón volcano, which merge with the Central American Volcanic Arc (CAVA). Geochemical and radiogenic isotope data for volcanic rocks from Southern Mexico, mainly from the central to eastern parts of the MVB and LTVF were interpreted by Verma (2002, 2004) to demonstrate a lack of relationship with the subduction process, in spite of the ongoing subduction of the Cocos plate beneath the North American plate. Such a conclusion was also drawn by Verma (2006) for the LTVF. Verma (2002) also showed a text-book type case for volcanic centers of the CAVA, particularly from Guatemala to north-western Costa Rica (see Appendix III). Nevertheless, for the MVB and LTVF conventional subduction-related models (see appendix III) and other proposals such as plume-related origin also exist, which therefore make the tectonic setting of these provinces highly complex and controversial (Appendix III). More recently, Verma (2009) reviewed all the available geological, geochemical and geophysical evidence from the MVB, particularly for its central part, and concluded that this volcanic province should better be called Mexican Volcanic Rift, because all the available data are more consistent with a rift rather than an arc.

These are some of the reasons that motivated me to explore more constraints to elucidate this problem of the Mexican Pacific and on-land volcanism as well as to document the differences or similarities between the volcanism and tectonics of Southern Mexico and Central America (CAVA).

Northwest Mexico

The late Cenezoic tectonic framework of northwestern Mexico has been discussed in detail by several researchers (for example, Saunders *et al.* 1987; Luhr *et al.* 1995; Calmus *et al.* 2003) and hence, only a brief discussion is provided here. The west coast of northwestern Mexico has been a convergent plate boundary since mid-cretaceous. The eastward subduction of oceanic lithosphere beneath western North America continued from Cretaceous to about 29 Ma (Mammerickx and Klitgord 1982). Towards the west of northwestern Mexico, subduction related magmatism is represented by batholitic granitoids between 90 and 40 Ma (McDowell *et al.* 1997). Whereas, towards the east of the Baja California peninsula, a continuous subduction related magmatism during Eocene-Oligocene (between 38 and 23 Ma) has generated important inland magmatism along the Sierra Madre Occidental belt (McDowell and Keizer 1977; Stock and Lee 1994; Benoit *et al.* 2002). Afterwards, during the Lower Miocene, the volcanic front shifted towards the west, forming the magmatic arc (the Comondú arc) all along the Baja California Peninsula. This volcanic belt had a longer activity between 24 and 12 Ma in southern Baja California compared to northern Baja California where Miocene (21 to 16 Ma) volcanism consisted several volcanic fields. The subduction in this region ended at 12.9 Ma (Mammerickx and Klitgord 1982; Calmus *et al.* 2003). Afterwards, transform boundary is developed between Pacific and North America plates parallel to the Pacific margin of Baja California (Spencer and Normark, 1979). Consequently, the tectonic setting has changed from subduction to rifting along the western margin of North America in Late-Cenozoic time (see Appendix IV).

3.3 Databases for Application to Southern and Northwest Mexico and Central America

For the application of the new discrimination diagrams, four extensive databases of basic and ultrabasic rocks of (1) island arc (IAB); (2) continental rift (CRB); (3) ocean island (OIB); (4) mid-ocean ridge (MORB), were separated from the combined database of all rock type (Appendices III&IV)

3.4 Results of Application

3.4.1 Southern Mexico and Central America

The results of application of the four sets of new diagrams to basic rocks from Southern Mexico (Mexican Volcanic Belt (MVB), arbitrarily divided into four parts: W-western, WC-west-central, C-central and E-eastern) and Los Tuxtlas volcanic field (LTVF) and Central America (Appendix III). The success rates are calculated when the number of samples was at least 30 (an arbitrarily set limit), and the "inapplicable" results are also indicated. Although a total of 120 diagrams were prepared, I present only four sets of discrimination diagrams as follows: Agrawal *et al*. (2004) diagrams for W-MVB and WC-MVB; Verma *et al.* (2006) diagrams for C-MVB; Agrawal *et al.* (2008) diagrams for E-MVB; and Verma and Agrawal (2011) diagrams for LTVF and CAVA (Appendix III). I described in detail only one set of diagrams Agrawal *et al.* (2004) to illustrate their use for inferring the tectonic setting. I compiled W-MVB data plotted in diagram and calculate rates for four tectonic settings of IAB, CRB, OIB and MORB. The results show that for W-MVB the expected tectonic setting from the first four filed IAB, CRB, OIB and MORB is a continental rift setting (Appendix III).

For the LTVF, both set of major-element based diagrams Agrawal *et al*. (2004) and Verma *et al.* (2006) clearly indicated a rift setting very high success rate 82.7-89.3 and 89.3-98.7% (Appendix III). Simultaneously, For CAVA, both set of major-element based diagrams Agrawal *et al*. (2004) and Verma *et al.* (2006) clearly provide an arc setting, with high success rates 74.8-99.2% and 76.5-82.4% (Appendix III).

3.4.2 Northwest Mexico

The geochemical database of on-land and off-shore basic rocks of northwest Mexico is plotted in all four sets of new discrimination diagrams (Agrawal *et al.* 2004, 2008; Verma *et al.* 2006; Verma and Agrawal 2011) to infer the tectonomagmatic origin of these rocks. For each set of diagrams, five different plots were prepared,

which provides a total of 20 diagrams. The samples in different tectonic setting fields are counted and their percentage range in each tectonic setting was calculated (wherever number of samples >8) and reported in Appendix IV. I discuss below only the dominant tectonic settings inferred by these diagrams for each group of rocks. All the indicated dominant tectonic setting are statistically significant because they are >>33.3% (being the simple "by chance" probability).

For on-shore basic rocks of northwest Mexico, the major-element based discrimination diagrams of (Agrawal *et al.* 2004; Verma *et al.* 2006) and immobile-element based diagrams of (Agrawal *et al.* 2008; Verma and Agrawal 2011), indicated the tectonic setting of continental rift for on-land basic rocks of <13 Ma age and continental rift and island arc) setting for on-land basic rocks of >13 Ma age (Appendix IV).

For off-shore basic rocks of northwest Mexico, the major-element based discrimination diagrams of (Agrawal *et al.* 2004; Verma *et al.* 2006) and immobile-element based diagrams of Verma and Agrawal (2011) indicated MORB tectonic setting for these off-shore rocks (Appendix IV).

3.5 Conclusions

The four sets of new discrimination diagrams proposed during 2004-2011 were evaluated with high success rates from data from four tectonic settings of arc, rift, ocean-island, and mid-ocean ridge. They were then applied to decipher tectonic setting of MVB and LTVF in Southern Mexico and CAVA in Central America. The arc setting of the CAVA was confirmed from these diagrams, whereas for the MVB and LTVF the dominance of a rift setting was concluded (Appendix III). .

These diagrams (2004-2011) have also indicated with very high success rates in case of northern Mexico: the dominant continental rift setting for on-land basic rocks of <13 Ma age; the dual tectonic settings of continental rift and arc for on-land basic rocks of >13 Ma age; and MORB setting for offshore rocks (Appendix IV).

Chapter 4

Chapter 4

The first multi-dimensional tectonic discrimination diagrams for intermediate magmas

Antecedents

This chapter includes the result of investigation related to discrimination diagrams for the intermediate magma. Paper has been submitted in Turkish Journal of Earth Sciences.

Abstract

Although for ultrabasic and basic magmas a plethora of tectonomagmatic diagrams have been in use now for nearly forty years, with the exception of one bivariate diagram for refined tectonic setting of orogenic andesites, none is available for intermediate magma, which is highly abundant in the Earth´s crust. To fill this gap in the literature and allow tectonic discrimination of intermediate magmas, we present here the first set of five multi-dimensional discrimination diagrams obtained from the correct statistical methodology of log-ratio transformation and linear discriminant analysis of discordant outlier-free normally distributed major element log-ratio variables in 2595 intermediate rock samples from five tectonic settings. These diagrams with probability-based tectonic field boundaries and high success rates (60%-95%) were used for tectonic discrimination of thirteen case studies of Archean to highly altered Quaternary rocks; none of them was included in the original database for proposing the diagrams. The results of arc, rift, ocean island, and collision settings for eight (Wawa greenstone belt, Canada; South-central Sweden; Adola, Ethiopia; Western Tasmania, Australia; Bonin Islands, Japan; Guam, Marianas; Moyuta and Tecuamburro volcanoes, Guatemala; and Berlín and Ahuachapán, El Salvador), one (South-western Tibet), one (Malani, Rajasthan, India), and three (Nanded and Yeotmal disticts, Maharastra, India; Alps, France-Italy-Switzerland; and Central Anatolia,

Turkey) case studies, respectively, were supported by probability estimates and were consistent with those of the multi-dimensional diagrams for basic and acid magmas from the same regions.

4.1 Introduction

Magmas are subdivided in four main categories on the basis of anhydrous 100% adjusted SiO2 contents (Le Bas *et al.*1986)−ultrabasic (SiO2=35-45%); basic (45-52%); intermediate (52-63%); and acid (>63%), which may originate in different tectonic settings (island arc−IA; continental arc−CA; continental rift−CR; ocean-island−OI; collision−Col; and mid-ocean ridge−MOR). To reconstruct the geologic-tectonic history, especially in older or tectonically complex areas, it is mandatory to know the most likely tectonic setting that gave rise to magmas in a given region. This can be done by the so called tectonomagmatic discrimination diagrams (e.g. Rollinson 1993). Numerous such diagrams (bivariate−x-y, ternary−x-y-z and multi-dimensional−DF1-DF2) are available for ultrabasic, basic or acid magmas (e.g. Pearce and Cann 1971, 1973; Wood 1980; Shervais 1982; Meschede 1986; Verma 2010; Verma and Agrawal 2011; Verma *et al.* 2011) and only bivariate type Bailey (1981) for "fine-scale" discrimination of only one type of intermediate magma (orogenic or arc andesite).

Therefore, tectonic origin of intermediate magma (basaltic andesite, andesite, basaltic trachyandesite, trachyandesite, tephriphonolite, phonolite, and boninite) cannot be inferred from discrimination diagrams and new ones are very much required to innovate this widely used geochemical technique. I propose a set of five new multi-dimensional diagrams for intermediate magma, evaluate their success rates, and use them efficiently for thirteen case studies demonstrating thus their versatility.

4.2 Database and the statistically correct procedure

For constructing the new diagrams, a representative five-part database (IA, CA, CR, OI, and Col; MOR was not included due to the scarcity of intermediate magma) was established from Miocene to Recent rocks from different parts of the world (Table1) where tectonic setting is clearly and unambiguously known.

TABLE 1. LOCATIONS AND LITERATURE SOURCES FOR THE FIVE-PART DATABASE

Region	(References)
island arcs	
Aegean	(Zellmer *et al.*2000)
Alaska peninsula	(Hildreth *et al.*2004)
Aleutian	(Kay *et al.*1982; Myers *et al.*1985, 2002; Brophy 1986; Nye and Reid 1986; Romick *et al.*1990; Singer *et al.*1992a, 1992b; Kay and Kay 1994; Finney *et al.*2008)
Barren Islands	(Alam *et al.*2004; Luhr and Haldar 2006)
Burma	(Stephenson and Marshall 1984)
Izu-Bonin	(Tatsumi *et al.*1992; Taylor and Nesbitt 1998; Shukuno *et al.*2006; Tamura *et al.*2007)
Japan	(Sakuyama and Nesbitt 1986; Togashi *et al.*1992; Tamura 1994; Ujike and Stix 2000; Kita *et al.*2001; Sano *et al.*2001; Kimura *et al.*2002; Tamura *et al.*2003; Moriguti *et al.*2004; Shuto *et al.*2004, 2006; Hirotani and Ban 2006; Kimura and Yoshida 2006; Sato *et al.*2007; Ohba *et al.*2009),
Java	(Edwards *et al.*1994)
Kamchatka	(Kepezhinskas *et al.*1997; Dorendorf *et al.*2000; Ishikawa *et al.*2001; Churikova *et al.*2001; Izbekov *et al.*2004)
Kuril	(Zhuravlev *et al.*1987; Nakagawa *et al.*2002)
Lesser Antilles	(Brown *et al.*1977; Thirlwall and Graham 1984; Smith *et al.*1996; Turner *et al.*1996; Thirlwall *et al.*1997; Defant *et al.*2001; Zellmer *et al.*2003; Lindsay *et al.*2005)
Mariana	(Hole *et al.*1984; Woodhead 1988; Bloomer *et al.*1989; Elliott *et al.*1997; de Moor *et al.*2005; Nakada *et al.*2005; Pallister *et al.*2005; Wade *et al.*2005)
New Britain	(Woodhead and Johnson 1993)
New Hebrides	(Dupuy *et al.*1982; Monzier *et al.* 1997)
Papua New Guinea	(Hegner and Smith, 1992)
Philippines (Arayat,	(Defant *et al.*1989, 1991a; Bau and Knittel, 1993; Knittel *et al.*1997; Castillo and Newhall, 2004;
Bataan, Bicol,	McDermott *et al.*2005; DuFrane *et al.*2006)
Ryukyu	(Shinjo, 1998, 1999; Shinjo *et al.*2000)
Sangihe	(Tatsumi *et al.*1991)
South Shetland	(Smellie, 1983)
Sunda-Banda	(Foden and Varne, 1980; Wheller *et al.*1987; Stolz *et al.*1988, 1990; van Bergen *et al.*1992; Hoogewerff *et al.*1997; Turner and Foden, 2001; Turner *et al.*2003; Elburge and Kamenetsky, 2007; Sendjaja *et al.*2009)
Taupo	(Cole, 1981; Gamble *et al.*1993, Schmitz and Smith, 2004)
Tonga-Kermadec	(Bryan *et al.*1972; Ewart and Bryan, 1972; Ewart *et al.*1977; Gamble *et al.*1993, 1995; Haase *et al.*2002; Smith *et al.*2003; Wright *et al.*2006)
Vanuatu	(Barsdell, 1988; Barsdell and Berry, 1990; Eggins, 1993; Peate *et al.*1997)
continental arcs	
Argentina	(Déruelle, 1982, 1991; Sruoga *et al.*2005; Bruni *et al.*2008)
Bolivia	(Hoke and Lamb, 2007)
Chile	(Déruelle, 1982; Frey *et al.*1984; Hickey *et al.*1986, Hickey-Vargas *et al.*1989; Davidson *et al.*1988; Gerlach *et al.*1988; Kay *et al.*1987, 1988; de Silva, 1991; López-Escobar *et al.*1991, 1993; Tormey *et al.*1991; Kay and Gordillo, 1994; Trumbull *et al.*1999; Vergara *et al.*2004)
Costa Rica	(Reagan and Gill, 1989; Alvarado *et al.*2006; Chan *et al.*1999; Bolge *et al.*2006; Ryder *et al.*2006)
El Salvador	(Carr, 1984; González Partida *et al.*1997; Rotolo and Castorina, 1998; Chan *et al.*1999; Agostini *et al.*2006)
Guatemala	(Bardintzeff and Deniel, 1992; Duffield *et al.*1992; Chan *et al.*1999; Walker *et al.*2000; Cameron *et al.*2002)
Honduras	(Patino *et al.*1997; Walker *et al.*2000)
Nicaragua	(Sussman, 1985; Hazlett, 1987; Carr *et al.*1990; Chan *et al.*1999; Walker *et al.*2001; Pardo *et al.*2008)
Panama	(Defant *et al.*1991b, 1991c)

TABLE 1 (CONTD.). LOCATIONS AND LITERATURE SOURCES FOR THE FIVE-PART DATABASE

Region	(References)
continental rifts and break-up regions	
Afar	(Barberi *et al.*1975; Deniel *et al.*1994)
Antractica	(Hart *et al.*1995; Kelly *et al.*2008)
Australia	(Price *et al.*1997)
Beppu-Shimbara graben, Japan	(Kita *et al.*2001)
China	(Peng *et al.*1986; Zhi *et al.*1990; Basu *et al.*1991; Fan and Hooper, 1991; Liu *et al.*1994; Zhang *et al.*1995; Han *et al.*1999; Ho *et al.*2000; Hsu *et al.*2000; Zou *et al.*2000, 2003)
Ethiopia	(Hart *et al.*1989; Trua *et al.*1999; Peccerillo *et al.*2003, 2007; Rooney *et al.*2007; Ronga *et al.*2010)
France	(Chauvel and Jahn, 1984)
Germany	(Haase *et al.*2004)
Kenya	(Bell and Peterson, 1991; Kampunzu and Mohr, 1991; Macdonald *et al.*1995, 2008; Kabeto *et al.*2001; Le Roex *et al.*2001)
Mali and Morocco	(Bertrand, 1991)
Republic of Congo	(de Mulder *et al.*1986)
Ruanda	(Kampunzu and Mohr, 1991)
Saudi Arabia	(Camp *et al.*1991)
Spain	(Benito *et al.*1999)
Sudan	(Davidson and Wilson, 1989)
Taiwan	(Chung *et al.*1995)
Tanzania	(Kampunzu and Mohr, 1991; Paslick *et al.*1995)
Turkey	(Buket and Temel, 1998; Aldanmaz *et al.*2000)
Uganda	(Kampunzu and Mohr, 1991; Llyod *et al.*1991)
U.S.A- Henry basin	(Streck and Grunder, 1999)
U.S.A- Basin and Range	(Singer and Kudo, 1986; Moyer and Esperança, 1989; Perry *et al.*1990; Fitton *et al.*1991; Kempton *et al.*1991; Feuerbach *et al.*1993)
U.S.A- Rio Grande Rift	(Johnson and Lipman, 1988; Duncker *et al.*1991, Gibson *et al.*1992; McMillan *et al.*2000; Maldonado *et al.*2006)
Zaire	(Auchapt *et al.*1987)
ocean islands	
Cameroon line	(Déruelle *et al.*1991)
Canary islands	(Praegel and Holm, 2006)
Cape Verde	(Holm *et al.*2006)
Cook-Austral-Samoa islands	(Palacz and Saunders, 1986)
French Polynesia	(Cheng *et al.*1993)
Hawaiian islands	(Feigenson *et al.*1983; Spengler and Garcia, 1988; Chen *et al.*1990; Lipman *et al.*1990; West *et al.*1992; Frey *et al.*1994; Cousens *et al.*2003; Xu *et al.*2005, 2007)
Heard and McDonald	(Barling *et al.*1994)
Kerguelen	(Weis *et al.*1993)
Madeira	(Geldmacher and Hoernle, 2000)
Pitcairn	(Hekinian *et al.*2003)
San Miguel	(Beier *et al.*2006)
Socorro	(Bohrson and Reid, 1995)
Tenerife	Krochert and Buchner, 2009)
Tropic seamount	(Blum *et al.*1996)
Collision	
Azerbaijan	(Dilek *et al.*2010)
Himalayas	(Turner *et al.*1993; Mo *et al.*2007; Reichardt *et al.*2010)
Italy	(Dini *et al.*2002)
Turkey	(Pearce *et al.*1990; Keskin *et al.*1998; Aldanmaz *et al.*2000; Ekící *et al.*2009)

Importantly, the character of intermediate magma for each sample included in the database was confirmed from SINCLAS software Verma *et al.* (2002). Because compositional data represent a "closed" space with unit sum constraint and linear discriminant analysis (LDA) requires that variables be normally distributed, log-ratio transformation (Aitchison 1986; Agrawal and Verma 2007) was used to provide the "normal" or "Gaussian" variable space. Before applying LDA, the compiled data from each tectonic setting were processed through DODESSYS software Verma and Díaz-González (2011) for identifying and separating discordant outliers Barnett and Lewis (1994) in the ten variables of logarithms of element ratios (logarithms of the ratio of all major elements−TiO_2 to P_2O_5−with SiO2 as the common denominator). The samples with complete analyses and discordant outlier-free log-ratio data were used to propose the new diagrams from training set data and evaluate them independently from testing set data. Success rates (i.e. correct classification expressed as percentages) were calculated from counting the correctly discriminated samples. The probability-based boundaries and the probabilities for individual samples were computed from the method recently outlined Verma and Agrawal (2011). For applications, probabilities for individual samples of intermediate magma were used to infer the dominant tectonic setting.

4.3 New Diagrams

A total of 3032 rock samples with complete major-element analyses were available in our database for proposing new diagrams. The results of LDA performed on these samples (success rates) can be summarized as follows: 81.20% for IA+CA together, 74.93% for CR+OI together, and 73.90% for Col.

Discordant outlier-free 2731 complete major element analyses of intermediate rocks from the five tectonic settings were randomly divided (Table 2) in training (2595 analyses) and testing (136 analyses) sets. We purposely selected many more data for training set because our aim was to obtain "best-trained" diagrams for a more reliable application to different case studies. After all, the good functioning of the diagrams can also be demonstrated from application examples.

TABLE 2. NUMBER OF SAMPLES IN THE TRAINING AND TESTING SETS OF NORMALLY DISTRIBUTED DISCORDANT OUTLIER-FREE DATABASE

Tectonic setting *	Group number	Training set	Testing set	Total
IA	1	1254	65	1319
CA	2	583	30	613
CR	3	333	18	351
OI	4	245	13	258
Col	5	180	10	190
Sum	1–5	2595	136	2731

* IA = island arc; CA = continental arc; CR= continental rift; OI= ocean-island; Col = collision; the numbers 1–5 are group numbers discussed in the text and used in other Tables.

The log-ratio variables used in LDA are summarized in Table 3. Although IA and CA as well as CR and OI are somewhat similar, statistically significant differences inferred from statistical tests (Wilks´ lambda<<1 and F-ratio>>1) exist for element concentrations and, more importantly, in log-transformed ratios among the five tectonic groups at an extremely low significance level approaching zero for all variables (Table 4), i.e. very high confidence level approaching 100%. These differences were enhanced by the multivariate technique of LDA practiced here.

LDA was performed five times on 2595 samples of the training set, the first time being for all groups with IA+CA (arc samples were always kept together), CR+OI together and Col settings (Fig. 1A), and four times for all possible combinations of three groups at a time out of four groups–IA+CA, CR, OI, and Col (Fig. 1B-E). The equations for the DF1 and DF2 functions (x- and y-axes; Fig. 1A-E) are given in Table 5.

TABLE 3. MEAN AND STANDARD DEVIATION OF $(SiO_2)_{adj}$ AND LOG-TRANSFORMED RATIO VARIABLES FOR THE FIVE TECTONIC SETTINGS (IA, CA, CR, OI, AND Col) FOR DISCORDANT OUTLIER-FREE SAMPLES OF THE TRAINING SET

loge-transformed ratio variable	IA (1) (*n =1254*)		CA (2) (*n = 583*)		CR (3) (*n =333*)		OI (4) (*n =245*)		Col (5) (*n =180*)	
	$\bar{x}$	*s*	$\bar{x}$	*s*	$\bar{x}$	*s*	$\bar{x}$	*s*	$\bar{x}$	*s*
$(SiO_2)_{adj}$	56.28	3.22	55.63	2.84	55.40	2.98	54.95	2.91	58.50	2.71
$\ln(TiO_2/SiO_2)_{adj}$	-4.192	0.288	-4.181	0.328	-3.570	0.416	-3.57	0.63	-4.049	0.249
$\ln(Al_2O_3/SiO_2)_{adj}$	-1.166	0.109	-1.111	0.102	-1.257	0.108	-1.209	0.134	-1.220	0.085
$\ln(Fe_2O_3/SiO_2)_{adj}$	-3.367	0.189	-3.382	0.160	-3.239	0.225	-3.264	0.317	-3.576	0.223
$\ln(Feo/SiO_2)_{adj}$	-2.234	0.239	-2.232	0.205	-2.196	0.317	-2.25	0.49	-2.541	0.242
$\ln(MnO/SiO_2)_{adj}$	-5.829	0.202	-5.884	0.186	-5.911	0.357	-5.716	0.200	-6.299	0.330
$\ln(MgO/SiO_2)_{adj}$	-2.671	0.415	-2.660	0.376	-2.68	0.70	-3.02	1.09	-2.860	0.364
$\ln(CaO/SiO_2)_{adj}$	-1.948	0.256	-1.932	0.236	-2.136	0.425	-2.30	0.68	-2.178	0.217
$\ln(Na_2O/SiO_2)_{adj}$	-2.860	0.168	-2.798	0.133	-2.707	0.243	-2.553	0.418	-2.710	0.118
$\ln(K_2O/SiO_2)_{adj}$	-4.05	0.59	-4.08	0.50	-3.33	0.72	-3.63	1.11	-3.352	0.347
$\ln(P_2O_5/SiO_2)_{adj}$	-5.70	0.50	-5.534	0.340	-4.96	0.65	-5.10	0.76	-5.220	0.380

$\bar{x}$ –mean; *s*–standard deviation.

TABLE 4. TEST OF EQUALITY OF GROUP MEANS FOR TEN LOG-TRANSFORMED RATIO VARIABLES IN THE TRAINING SET (DISCORDANT OUTLIER-FREE SAMPLES)

Element	Wilks' lambda	F-ratio	Significance
$\ln(TiO_2/SiO_2)_{adj}$	0.37147	261.559	0.00000
$\ln(Al_2O_3/SiO_2)_{adj}$	0.27277	20.615	0.00000
$\ln(Fe_2O_3/SiO_2)_{adj}$	0.27381	23.154	0.00000
$\ln(FeO/SiO_2)_{adj}$	0.28204	43.254	0.00000
$\ln(MnO/SiO_2)_{adj}$	0.30620	102.218	0.00000
$\ln(MgO/SiO_2)_{adj}$	0.26872	10.738	0.00000
$\ln(CaO/SiO_2)_{adj}$	0.27771	32.673	0.00000
$\ln(Na_2O/SiO_2)_{adj}$	0.26997	13.778	0.00000
$\ln(K_2O/SiO_2)_{adj}$	0.28449	49.226	0.00000
$\ln(P_2O_5/SiO_2)_{adj}$	0.27422	24.146	0.00000

Wilks' lambda (U-statistic) and univariate F-ratio with degree of freedom, df1= $\nu 1$ = g-1 = 5-1 = 4 and df2 = $\nu 2$ = n-g = 2595-5 = 2590, where g is the number of groups and n is total number of samples.

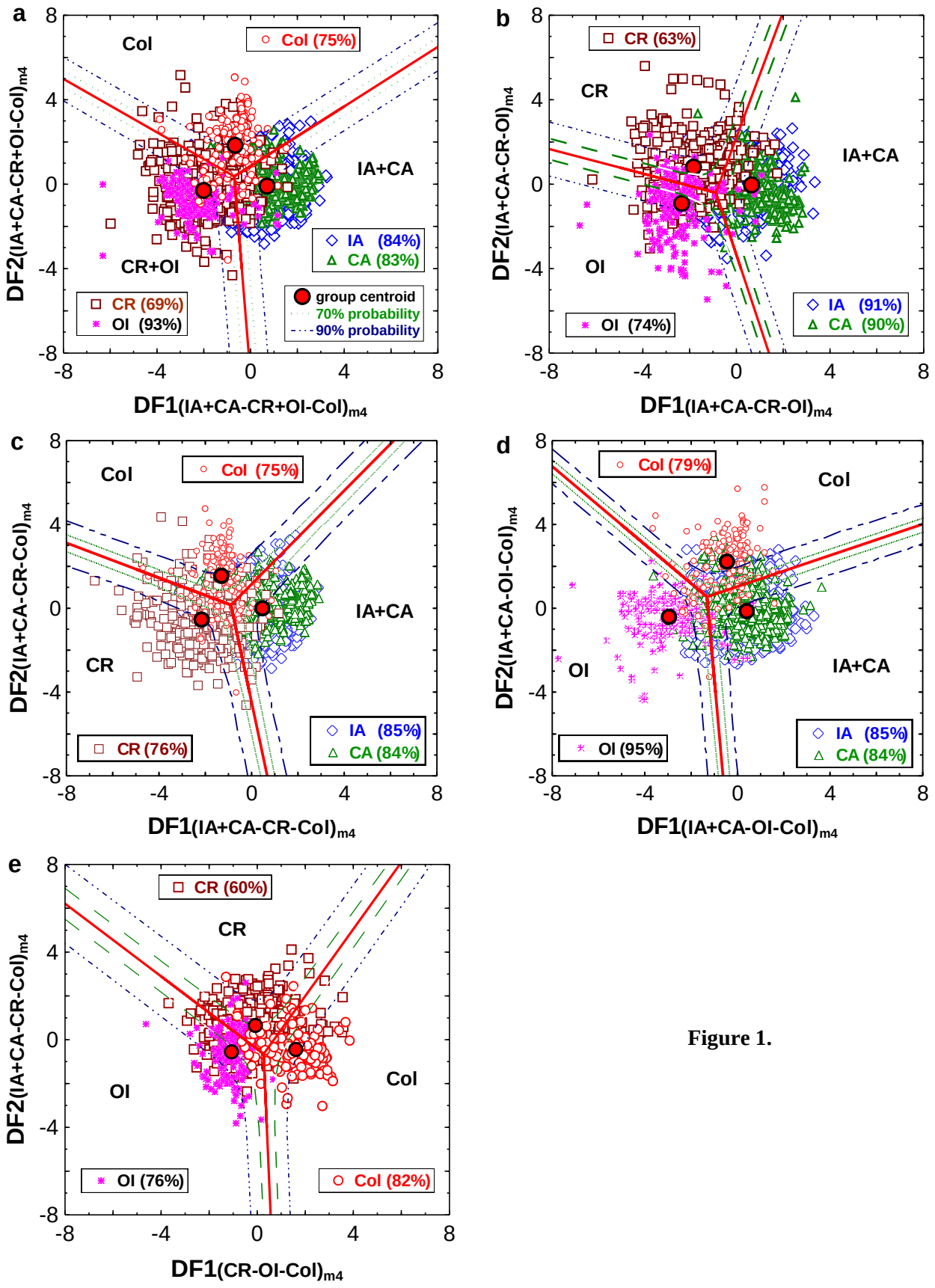
a
Col
Col (75%)
IA+CA
IA (84%)
CA (83%)
CR+OI
CR (69%)
OI (93%)
group centroid
70% probability
90% probability
DF2(IA+CA-CR+OI-Col)m4
DF1(IA+CA-CR+OI-Col)m4
b
CR (63%)
CR
IA+CA
OI
OI (74%)
IA (91%)
CA (90%)
DF2(IA+CA-CR-OI)m4
DF1(IA+CA-CR-OI)m4
c
Col
Col (75%)
IA+CA
CR
CR (76%)
IA (85%)
CA (84%)
DF2(IA+CA-CR-Col)m4
DF1(IA+CA-CR-Col)m4
d
Col (79%)
Col
OI
IA+CA
OI (95%)
IA (85%)
CA (84%)
DF2(IA+CA-OI-Col)m4
DF1(IA+CA-OI-Col)m4
e
CR (60%)
CR
OI
Col
OI (76%)
Col (82%)
DF2(IA+CA-CR-Col)m4
DF1(CR-OI-Col)m4

Figure 1.

Figure 1 The set of five new discriminant-function multi-dimensional diagrams for the discrimination of intermediate rocks from island arc (IA) or continental arc (CA), continental rift (CR), ocean-island (OI), and collision (Col) tectonic settings, showing samples from the training set. The symbols are explained as inset in Figure 1a. Although this is the first set of diagrams for intermediate magma, the subscript m4 in axis names refers to the fourth set of multi-dimensional diagrams based on log-transformed major element ratios. The percentages in each figure refer to correct discrimination for training and testing sets samples (see Table 6). The red lines represent discrimination boundaries, the green dotted curves are for 70% probability, and blue dashed curves represent 90% probability. a, IA+CA–CR+OI–Col (1+2–3+4–5) diagram, the coordinates of the field boundaries are (−0.08229, −8.0) and (−0.69747, 0.37221) for IA+CA–CR+OI; (8.0, 6.50811) and (−0.69747, 0.37221) for IA+CA–Col; and (−8.0, 4.98409) and (−0.69747, 0.37221) for CR+OI–Col; b, IA+CA–CR–OI (1+2–3–4) diagram, the coordinates of the field boundaries are (1.94467, 8.0) and (−0.88017, −0.40397) for IA+CA–CR; (1.39285, −8.0) and (−0.88017, −0.40397) for IA+CA–OI; and (−8.0, 1.66752) and (−0.88017, −0.40397) for CR–OI; c, IA+CA–CR–Col (1+2–3–5) diagram, the coordinates of the field boundaries are (0.67196, −8.0) and (−0.89178, 0.15656) for IA+CA–CR; (6.13605, 8.0) and (−0.89178, 0.15656) for IA+CA–Col; and (−8.0, 3.11951) and (−0.89178, 0.15656) for CR–Col; d, IA+CA–OI–Col (1+2–4–5) diagram, the coordinates of the field boundaries are (−0.62593, −8.0) and (−1.31519, 0.54604) for IA+CA–OI; (8.0, 4.01586) and (−1.31519, 0.54604) for IA+CA–Col; and (−8.0, 6.77499) and (−1.31519, 0.54604) for OI–Col; and e, CR–OI–Col (3–4–5) diagram, the coordinates of the field boundaries are (−8.0, 6.21312) and (0.26727, −0.65169) for CR–OI; (5.93160, 8.0) and (0.26727, −0.65169) for CR–Col; and (0.55856, −8.0) and (0.26727, −0.65169) for OI–Col.

TABLE 5. DISCRIMINANT-FUNCTION EQUATIONS FOR THE FIVE NEW MULTI-DIMENSIONAL DISCRIMINATION DIAGRAMS

Figure no.	Equations
Figure 1A (1+2-3+4-5)	$\mathbf{DF1_{(IA+CA-CR+OI-Col)_{m4}} = (-3.41369 \times \ln(TiO_2/SiO_2)_{adj}) + (0.24375 \times \ln(Al_2O_3/SiO_2)_{adj}) + (-3.95490 \times \ln(Fe_2O_3/SiO_2)_{adj}) + (5.14611 \times \ln(FeO/SiO_2)_{adj}) + (-0.099086 \times \ln(MnO/SiO_2)_{adj}) + (-0.674715 \times \ln(MgO/SiO_2)_{adj}) + (1.77544 \times \ln(CaO/SiO_2)_{adj}) + (-0.10447 \times \ln(Na_2O/SiO_2)_{adj}) + (0.083364 \times \ln(K_2O/SiO_2)_{adj}) + (0.24752 \times \ln(P_2O_5/SiO_2)_{adj}) - 12.6521102}$
	$\mathbf{DF2_{(IA+CA-CR+OI-Col)_{m4}} = (-0.34899 \times \ln(TiO_2/SiO_2)_{adj}) + (-0.51400 \times \ln(Al_2O_3/SiO_2)_{adj}) + (-1.22636 \times \ln(Fe_2O_3/SiO_2)_{adj}) + (-0.13289 \times \ln(FeO/SiO_2)_{adj}) + (-3.465298 \times \ln(MnO/SiO_2)_{adj}) + (-0.22304 \times \ln(MgO/SiO_2)_{adj}) + (0.946505 \times \ln(CaO/SiO_2)_{adj}) + (0.3491613 \times \ln(Na_2O/SiO_2)_{adj}) + (-0.02155 \times \ln(K_2O/SiO_2)_{adj}) + (0.544490 \times \ln(P_2O_5/SiO_2)_{adj}) - 21.6119757}$
Figure 1B (1+2-3-4)	$\mathbf{DF1_{(IA+CA-CR-OI)_{m4}} = (-3.45953 \times \ln(TiO_2/SiO_2)_{adj}) + (-0.062717 \times \ln(Al_2O_3/SiO_2)_{adj}) + (-4.36425 \times \ln(Fe_2O_3/SiO_2)_{adj}) + (5.55420 \times \ln(FeO/SiO_2)_{adj}) + (-0.565639 \times \ln(MnO/SiO_2)_{adj}) + (-0.65991 \times \ln(MgO/SiO_2)_{adj}) + (1.88951 \times \ln(CaO/SiO_2)_{adj}) + (-0.131752 \times \ln(Na_2O/SiO_2)_{adj}) + (0.226288 \times \ln(K_2O/SiO_2)_{adj}) + (0.27691 \times \ln(P_2O_5/SiO_2)_{adj}) - 15.515287}$
	$\mathbf{DF2_{(IA+CA-CR-OI)_{m4}} = (-0.89931 \times \ln(TiO_2/SiO_2)_{adj}) + (-1.71911 \times \ln(Al_2O_3/SiO_2)_{adj}) + (1.73385 \times \ln(Fe_2O_3/SiO_2)_{adj}) + (1.23288 \times \ln(FeO/SiO_2)_{adj}) + (-2.53190 \times \ln(MnO/SiO_2)_{adj}) + (0.26325 \times \ln(MgO/SiO_2)_{adj}) + (0.95076 \times \ln(CaO/SiO_2)_{adj}) + (-1.92768 \times \ln(Na_2O/SiO_2)_{adj}) + (1.590374 \times \ln(K_2O/SiO_2)_{adj}) + (0.052335 \times \ln(P_2O_5/SiO_2)_{adj}) - 8.14012524}$

Continues

TABLE 5 (CONTD.). DISCRIMINANT-FUNCTION EQUATIONS FOR THE FIVE NEW MULTI-DIMENSIONAL DISCRIMINATION DIAGRAMS

Figure no.	Equations
Figure 1C (1+2-3-5)	$\mathbf{DF1_{(IA+CA-CR-Col)_{m4}} = (-3.15331 \times \ln(TiO_2/SiO_2)_{adj}) + (0.65537 \times \ln(Al_2O_3/SiO_2)_{adj}) + (-3.93836 \times \ln(Fe_2O_3/SiO_2)_{adj}) + (5.06475 \times \ln(FeO/SiO_2)_{adj}) + (0.829539 \times \ln(MnO/SiO_2)_{adj}) + (-0.661201 \times \ln(MgO/SiO_2)_{adj}) + (0.865299 \times \ln(CaO/SiO_2)_{adj}) + (0.558129 \times \ln(Na_2O/SiO_2)_{adj}) + (-0.203319 \times \ln(K_2O/SiO_2)_{adj}) + (0.0254213 \times \ln(P_2O_5/SiO_2)_{adj}) - 8.2453098}$ $\mathbf{DF2_{(IA+CA-CR-Col)_{m4}} = (-0.69738 \times \ln(TiO_2/SiO_2)_{adj}) + (0.202068 \times \ln(Al_2O_3/SiO_2)_{adj}) + (-1.97925 \times \ln(Fe_2O_3/SiO_2)_{adj}) + (0.147678 \times \ln(FeO/SiO_2)_{adj}) + (-3.085997 \times \ln(MnO/SiO_2)_{adj}) + (-0.4668309 \times \ln(MgO/SiO_2)_{adj}) + (1.3204017 \times \ln(CaO/SiO_2)_{adj}) + (0.87092558 \times \ln(Na_2O/SiO_2)_{adj}) + (-0.203454 \times \ln(K_2O/SiO_2)_{adj}) + (0.4222721 \times \ln(P_2O_5/SiO_2)_{adj}) - 21.7732917}$
Figure 1D (1+2-4-5)	$\mathbf{DF1_{(IA+CA-OI-Col)_{m4}} = (-3.86046 \times \ln(TiO_2/SiO_2)_{adj}) + (-1.220169 \times \ln(Al_2O_3/SiO_2)_{adj}) + (-4.09366 \times \ln(Fe_2O_3/SiO_2)_{adj}) + (6.3396597 \times \ln(FeO/SiO_2)_{adj}) + (-1.3538459 \times \ln(MnO/SiO_2)_{adj}) + (-0.50564138 \times \ln(MgO/SiO_2)_{adj}) + (2.316068 \times \ln(CaO/SiO_2)_{adj}) + (-0.373064279 \times \ln(Na_2O/SiO_2)_{adj}) + (0.658549 \times \ln(K_2O/SiO_2)_{adj}) + (0.22007139 \times \ln(P_2O_5/SiO_2)_{adj}) - 18.6852137}$ $\mathbf{DF2_{(IA+CA-OI-Col)_{m4}} = (0.2793486 \times \ln(TiO_2/SiO_2)_{adj}) + (-0.500346 \times \ln(Al_2O_3/SiO_2)_{adj}) + (0.755699 \times \ln(Fe_2O_3/SiO_2)_{adj}) + (-1.463788 \times \ln(FeO/SiO_2)_{adj}) + (-4.1433447 \times \ln(MnO/SiO_2)_{adj}) + (0.0105235 \times \ln(MgO/SiO_2)_{adj}) + (0.876947 \times \ln(CaO/SiO_2)_{adj}) + (-0.2604276 \times \ln(Na_2O/SiO_2)_{adj}) + (0.28334509 \times \ln(K_2O/SiO_2)_{adj}) + (0.421289 \times \ln(P_2O_5/SiO_2)_{adj}) - 19.9901665}$

Continues

TABLE 5 (CONTD.). DISCRIMINANT-FUNCTION EQUATIONS FOR THE FIVE NEW MULTI-DIMENSIONAL DISCRIMINATION DIAGRAMS

Figure no.	Equations
Figure 1E (3-4-5)	$\mathbf{DF1_{(CR\text{-}OI\text{-}Col)_{m4}} = (-2.274018 \times \ln(TiO_2/SiO_2)_{adj}) + (-0.02205 \times \ln(Al_2O_3/SiO_2)_{adj}) + (-3.339376 \times \ln(Fe_2O_3/SiO_2)_{adj}) + (3.093479 \times \ln(FeO/SiO_2)_{adj}) + (-1.94631 \times \ln(MnO/SiO_2)_{adj}) + (-0.1064117 \times \ln(MgO/SiO_2)_{adj}) + (1.4126369 \times \ln(CaO/SiO_2)_{adj}) + (-0.4156048 \times \ln(Na_2O/SiO_2)_{adj}) + (0.658919 \times \ln(K_2O/SiO_2)_{adj}) + (0.639796 \times \ln(P_2O_5/SiO_2)_{adj}) - 16.7770813}$ $\mathbf{DF2_{(CR\text{-}OI\text{-}Col)_{m4}} = (0.069719 \times \ln(TiO_2/SiO_2)_{adj}) + (-1.65749 \times \ln(Al_2O_3/SiO_2)_{adj}) + (1.853310 \times \ln(Fe_2O_3/SiO_2)_{adj}) + (1.69862 \times \ln(FeO/SiO_2)_{adj}) + (-0.41540 \times \ln(MnO/SiO_2)_{adj}) + (0.89240 \times \ln(MgO/SiO_2)_{adj}) + (-0.178666 \times \ln(CaO/SiO_2)_{adj}) + (-0.86792 \times \ln(Na_2O/SiO_2)_{adj}) + (2.04786 \times \ln(K_2O/SiO_2)_{adj}) + (-0.950417 \times \ln(P_2O_5/SiO_2)_{adj}) + 7.85372358}$

The three boundaries dividing the fields in each diagram (Fig. 1A-E) were based on probability calculations expressed in percentages (Verma and Agrawal, 2011). Training and testing sets group centroid DF1-DF2 values required for these calculations are included in Fig. 1. Each boundary represents 50% probability for the two fields that it separates, and this probability decreases to 33.33% at the triple point. For all fields (Fig. 1), we also calculated the probability-based curves for 70% (dotted curves) and 90% (dashed curves). The probability to belong to a certain group increases very rapidly for transects from the discrimination boundaries (thick solid line) into a given field (dotted and dashed curves).

The correct and incorrect discriminations (Table 6) are reported separately for training and testing sets (Fig.1). For each tectonic setting, only four of the five diagrams (Fig. 1A-E) are applicable (the inapplicable diagram is indicated by an asterisk in Table 6). The success rates for IA and CA, discriminated as combined IA+CA setting, varied from 84% to 91% and 83% to 90% for training set and 82% to 86% and 67% to 80% for testing set, respectively.

TABLE 6. ASSESSMENT OF CORRECT DISCRIMINATION (SUCCESS RATE %) OF ISLAND ARC (GROUP 1–IA), CONTINENTAL ARC (GROUP 2–CA), CONTINENTAL RIFT (GROUP 3–CR), OCEAN ISLAND (GROUP 4–OI), AND COLLISION (GROUP 5–COL) TECTONIC SETTINGS IN THE SET OF FIVE DISCRIMINANT-FUNCTION-BASED MULTI-DIMENSIONAL DIAGRAMS

Actual affinity	Discrimination diagram	Total no. of samples [training or testing]	Predicted tectonic affinity and number of discriminated samples (%)				
			IA+CA (1+2)	CR+OI (3+4)	CR (3)	OI (4)	Col (5)
IA (1)	1+2-3+4-5	1254 [training]	***1057*** (84)	83 (7)	---	---	114 (9)
IA (1)	1+2-3-4	1254 [training]	***1142*** (91)	---	80 (6)	32 (3)	---
IA (1)	1+2-3-5	1254 [training]	***1071*** (85)	---	77 (6)	---	106 (9)
IA (1)	1+2-4-5	1254 [training]	***1071*** (85)	---	---	57 (5)	126 (10)
IA (1)	3-4-5 *	1254 [training]	---	---	263 (21)	198 (16)	793 (63)
IA (1)	1+2-3+4-5	65 [testing]	***53*** (82)	7	---	---	5
IA (1)	1+2-3-4	65 [testing]	***56*** (86)	---	8	1	---
IA (1)	1+2-3-5	65 [testing]	***53*** (82)	---	7	---	5
IA (1)	1+2-4-5	65 [testing]	***54*** (83)	---	---	2	9
CA (2)	1+2-3+4-5	583 [training]	***483*** (83)	40 (7)	---	---	60 (10)
CA (2)	1+2-3-4	583 [training]	***523*** (90)	---	34 (6)	25 (4)	---
CA (2)	1+2-3-5	583 [training]	***487*** (84)	---	41 (7)	---	55 (9)
CA (2)	1+2-4-5	583 [training]	***487*** (84)	---	---	38 (6)	58 (10)
CA (2)	3-4-5 *	583 [training]	---	---	76 (13)	46 (8)	461 (79)
CA (2)	1+2-3+4-5	30 [testing]	***20*** (67)	3	---	---	7
CA (2)	1+2-3-4	30 [testing]	***24*** (80)	---	5	1	---
CA (2)	1+2-3-5	30 [testing]	***20*** (67)	---	3	---	7
CA (2)	1+2-4-5	30 [testing]	***20*** (67)	---	---	3	7
CA (2)	3-4-5 *	30 [testing]	---	---	6	1	23 (77)
CR (3)	1+2-3+4-5	333 [training]	35 (11)	***231*** (69)	---	---	67 (20)
CR (3)	1+2-3-4	333 [training]	42 (13)	---	***211*** (63)	80 (24)	---
CR (3)	1+2-3-5	333 [training]	30 (9)	---	***253*** (76)	---	50 (15)
CR (3)	1+2-4-5 *	333 [training]	57 (17)	---	---	158 (48)	118 (35)
CR (3)	3-4-5	333 [training]	---	---	***198*** (60)	77 (23)	58 (17)
CR (3)	1+2-3+4-5	18 [testing]	1	***14*** (78)	---	---	3
CR (3)	1+2-3-4	18 [testing]	2	---	***9*** (50)	7	---
CR (3)	1+2-3-5	18 [testing]	2	---	***14*** (78)	---	2
CR (3)	1+2-4-5 *	18 [testing]	2	---	---	11 (61)	5
CR (3)	3-4-5	18 [testing]			***9*** (50)	6	3
OI (4)	1+2-3+4-5	245 [training]	16 (7)	***228*** (93)	---	---	1
OI (4)	1+2-3-4	245 [training]]	13 (5)	---	51 (21)	***181*** (74)	---
OI (4)	1+2-3-5 *	245 [training]	31 (13)	---	202 (82)	---	12 (5)
OI (4)	1+2-4-5	245 [training]	11 (4)	---	---	***233*** (95)	1
OI (4)	3-4-5	245 [training]	---	---	53 (22)	***187*** (76)	5
OI (4)	1+2-3+4-5	13 [testing]	2	***11*** (85)	---	---	0
OI (4)	1+2-3-4	13 [testing]	1	---	1	***11*** (85)	---
OI (4)	1+2-3-5 *	13 [testing]	3	---	10 (75)	---	0
OI (4)	1+2-4-5	13 [testing]	1	---	---	***12*** (92)	0
OI (4)	3-4-5	13 [testing]	---	---	2	***11*** (85)	0
Col (5)	1+2-3+4-5	180 [training]	18 (10)	27 (15)	---	---	***135*** (75)
Col (5)	1+2-3-4 *	180 [training]	108 (60)	---	66 (37)	6	---
Col (5)	1+2-3-5	180 [training]	15 (8)	---	31 (17)	---	***134*** (75)
Col (5)	1+2-4-5	180 [training]	21 (12)	---	---	16 (9)	***143*** (79)
Col (5)	3-4-5	180 [training]	---	---	27 (15)	6	***147*** (82)
Col (5)	1+2-3+4-5	10 [testing]	1	1	---	---	**8** (80)
Col (5)	1+2-3-4 *	10 [testing]	9	---	1	0	---
Col (5)	1+2-3-5	10 [testing]	1	---	1	---	***8*** (80)
Col (5)	1+2-4-5	10 [testing]	1	---	---	1	***8*** (80)
Col (5)	3-4-5	10 [testing]	---	---	1	0	***9*** (90)

The numbers in the parentheses "()" are the percentages of samples plotting in a given field: the correct discrimination can be seen in the column with italic boldface numbers. * inapplicable diagram.

The success rates for CR and OI were, respectively, 60%-76% and 74%-95% for training set and 50%-78% and 85%-92% for testing set. When the CR and OI settings were combined together (Fig. 1A), high success rates of about 69%-93% were obtained. The highest success rate of about 95% (correct discrimination) for OI was obtained in Fig. 1D, in which CR setting is absent. Finally, for Col samples we obtained high success rates of about 75%-82% and 80%-90% for training and testing sets, respectively.

4.4 Applications

I selected thirteen case studies with ages varying from Archean to Quaternary to illustrate the application and excellent functioning of the new multi-dimensional discrimination diagrams. The Archean to Proterozoic rocks were evaluated under the assumption of prevalence of plate tectonic processes and similar log-ratio geochemical variables for Archean to present-day tectonic regimes. The plotting of samples in diagrams (Fig. 2) can be fully replaced by probability calculations (Tables 7 and 8). In any discrimination diagram (Fig. Fig.2 A-E) a sample will have probability values for all tectonic fields being discriminated, which will add up to 1.0000, and the sample will be plot in the field for which the probability is the highest.

Importantly, besides the intermediate magma, contemporaneous ultrabasic, basic, and acid magmas may also be present in a given area. The inferences from the new diagrams should be considered more reliable when the multi-dimensional diagrams for other magma varieties (ultrabasic and basic by Verma *et al.* 2006 and Verma and Agrawal 2011; and acid by Verma *et al.* 2011) also provided consistent results.

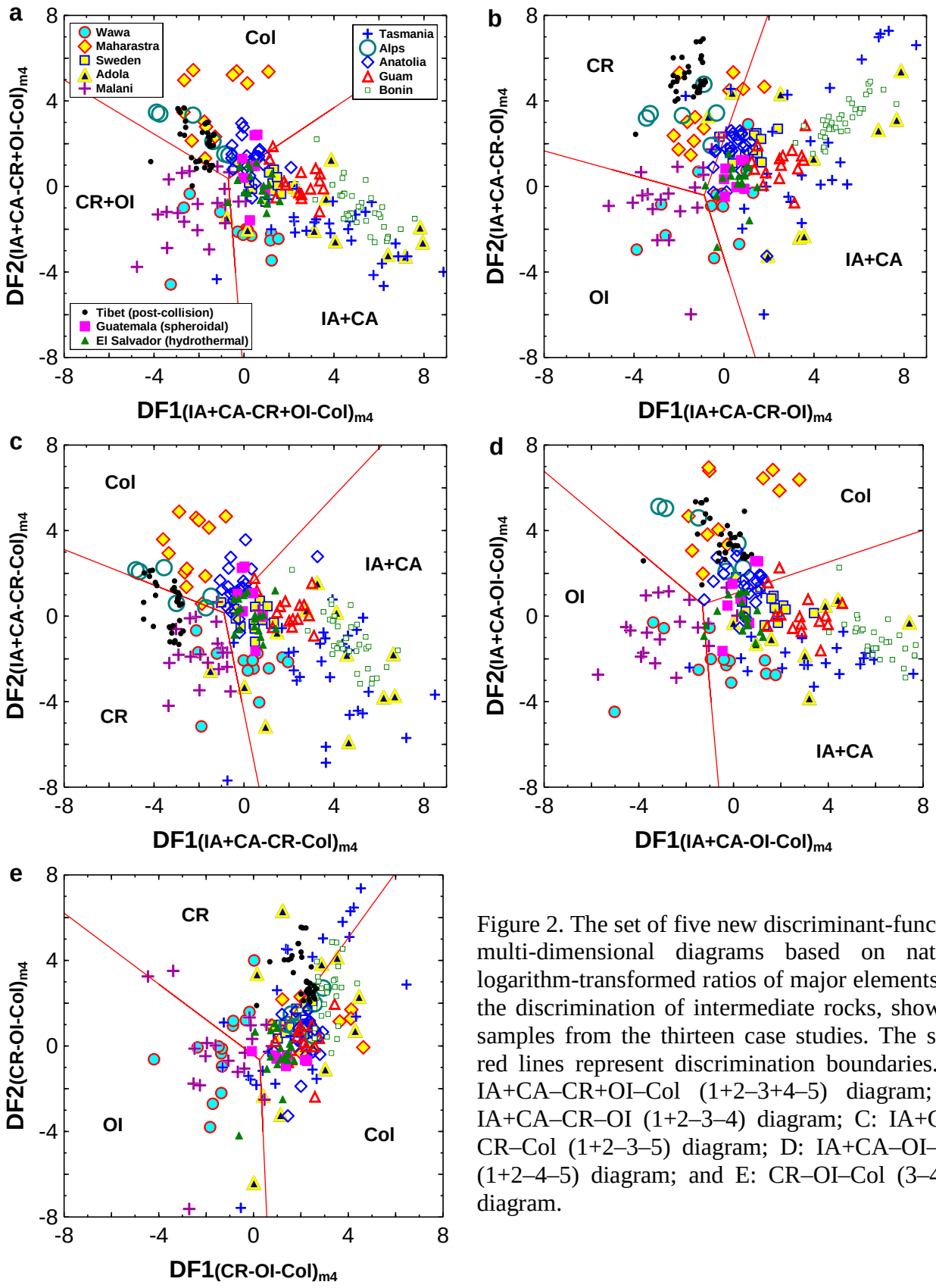

Figure 2. The set of five new discriminant-function multi-dimensional diagrams based on natural logarithm-transformed ratios of major elements for the discrimination of intermediate rocks, showing samples from the thirteen case studies. The solid red lines represent discrimination boundaries. A: IA+CA–CR+OI–Col (1+2–3+4–5) diagram; B: IA+CA–CR–OI (1+2–3–4) diagram; C: IA+CA–CR–Col (1+2–3–5) diagram; D: IA+CA–OI–Col (1+2–4–5) diagram; and E: CR–OI–Col (3–4–5) diagram.

TABLE 7. APPLICATION OF THE SET OF FIVE DISCRIMINANT FUNCTION MULTI-DIMENSIONAL DIAGRAMS FOR INTERMEDIATE MAGMAS

(case study no.) Locality (reference); age; inferred tectonic setting	Figure type §	Total number of samples	Number of discriminated samples				
			IA+CA (1+2) [p_{IA+CA}] Θ	Within-plate			Col (5) [p_{Col}] Θ
				CR+OI (3+4) [p_{CR+OI}] Θ	CR (3) [p_{CR}] Θ	OI (4) [p_{OI}] Θ	
(1) Wawa greenstone belt, Canada (Polat *et al.*1999); Late Archean, 2700 Ma; arc.	1+2-3+4-5	14	***10*** [0.6548-0.9955]	4 [0.7655-0.9996]	---	---	0
	1+2-3-4	14	***9*** [0.5078-0.9933]	---	1 [0.7290]	4 [0.7865-0.9971]	---
	1+2-3-5	14	***10*** [0.7597-0.9980]	---	4 [0.8445-0.9950]	---	0
	1+2-4-5	14	***10*** [0.6211-0.9999]	---	---	4 [0.7981-1.0000]	0
	3-4-5 *****	14	---	---	5 [0.6758-0.9914]	9 [0.7143-0.9947]	0

§ Figure type refers to the tectonic fields being discriminated where the tectonic group numbers are as follows: 1–IA, 2–CA, 3–CR, 4–OI, 5–Col;

***** Inapplicable results and diagrams;

Θ Probability estimates for different tectonic groups are summarized after the number of discriminated samples as follows: [p_{IA+CA}]–range of probability values estimated for IA+CA settings, [p_{CR+OI}]–for CR+OI, [p_{CR}]–for CR, [p_{OI}]–for OI and [p_{Col}]–for Col. Boldface italic font shows the expected or more probable tectonic setting;

For the Late Archean Wawa greenstone belt in Canada (Polat *et al.* 1999), the present diagrams for intermediate magma (14 samples) indicated a dominantly arc setting, because the probabilities for 9 or 10 samples were highest for arc (0.5078-0.9999), whereas for the remaining 5 or 4 samples the probabilities were highest (0.7290-1.0000) as continental rift or ocean island (Table 7; Fig. 2A-D, with Fig. 2E considered as the inapplicable diagram). An arc setting was also indicated from multi-dimensional diagrams based on immobile elements in ultrabasic and basic magmas (Verma and Agrawal 2011), because 36 to 41 samples (out of 50) were discriminated as arc (probabilities 0.3887-1.0000; Table 9). Similarly, in the other set of diagrams (Verma *et al.* 2006) also, 32 to 35 samples (out of 50) plotted in the arc field (Table 10).

TABLE 8. APPLICATION OF THE SET OF FIVE DISCRIMINANT FUNCTION MULTI-DIMENSIONAL DIAGRAMS FOR INTERMEDIATE MAGMAS

(case study no.) Locality (reference); age; inferred tectonic setting	Figure type	Total number of samples	Number of discriminated samples				
			IA+CA (1+2) [p_{IA+CA}]	Within-plate			Col (5) [p_{Col}]
				CR+OI (3+4) [p_{CR+OI}]	CR (3) [p_{CR}]	OI (4) [p_{OI}]	
(2) Maharastra (Nanded and Yeotmal disticts), India (Banerjee and Shivkumar, 2010); Early Proterozoic, 2385-2074 Ma; collision.	1+2-3+4-5	12	0	0	---	---	***12*** [0.6396-0.9999]
	1+2-3-4 *	12	2 [0.5281-0.9146]	---	10 [0.7952-0.9994]	0	---
	1+2-3-5	12	0	---	0	---	***12*** [0.4825-0.9997]
	1+2-4-5	12	0	---	---	0	***12*** [0.9498-1.0000]
	3-4-5	12	---	---	4 [0.5896-0.8149]	0	***8*** [0.5539-0.9987]
(3) South-central Sweden (Rutanen and Andersson, 2009); Early Proterozoic, 1870-1780 Ma); arc.	1+2-3+4-5	13	***12*** [0.5762-0.9904]	0	---	---	1 [0.6868]
	1+2-3-4	13	***12*** [0.7558-0.9961]	---	1 [0.6440]	0	---
	1+2-3-5	13	***12*** [0.5357-0.9867]	---	0	---	1 [0.5591]
	1+2-4-5	13	***12*** [0.5705-0.9943]	---	---	0	1 [0.8518]
	3-4-5 *	13	---	---	2 [0.5092, 0.5595]	0	11 [0.5071-0.8814]
(4) Adola, Ethiopia (Wolde *et al.*1996); Late Proterozoic, 885-765 Ma; arc.	1+2-3+4-5	12	***11*** [0.8617-1.0000]	1 [0.6287]	---	---	0
	1+2-3-4	12	***10*** [0.8239-1.0000]	---	2 [0.7276-0.9340]	0	---
	1+2-3-5	12	***11*** [0.6592-1.0000]	---	1 [0.9467]	---	0
	1+2-4-5	12	***12*** [0.9446-1.0000]	---	---	0	0
	3-4-5 *	12	---	---	4 [0.6429-0.9976]	1 [0.7848]	7 [0.5066-0.9945]
(5) Malani, Rajasthan, India (Maheshwari *et al.*1996; Bhushan and Chandrasekaran, 2002; Sharma, 2004; Singh and Vallinayagam, 2004); Late Proterozoic, 750 Ma; ocean island.	1+2-3+4-5	20	2 [0.7007, 0.8338]	***16*** [0.5356-0.9999]	---	---	2 [0.4771, 0.5681]
	1+2-3-4	20	0	---	8 [0.5085-0.8325]	***12*** [0.6437-0.9988]	---
	1+2-3-5 *	20	1 [0.9114]	---	*18* [0.6028-0.9998]	---	1 [0.5810]
	1+2-4-5	20	4 [0.5882-0.9444]	---	---	***15*** [0.6175-1.0000]	1 [0.7212]
	3-4-5	20	---	---	6 [0.5619-0.8364]	***12*** [0.5030-0.9998]	2 [0.4746, 0.5545]
(6) Western Tasmania, Australia (Brown and Jenner, 1989); Cambrian; arc.	1+2-3+4-5	29	***28*** [0.8212-1.0000]	1 [0.9097]	---	---	0
	1+2-3-4	29	***27*** [0.9486-1.0000]	---	2 [0.7709, 0.9968]	0	---
	1+2-3-5	29	***28*** [0.5948-1.0000]	---	1 [0.9711]	---	0
	1+2-4-5	29	***28*** [0.7246-1.0000]	---	---	1 [0.9330]	0
	3-4-5 *	29	---	---	10 [0.6378-0.9784]	6 [0.5538-0.9465]	13 [0.4495-0.9986]
(7) Alps, France-Italy-Switzerland (Debon and Lemmet, 1999); Late Carboniferous, 295 Ma; collision	1+2-3+4-5	6	0	0	---	---	***6*** [0.8188-0.9849]
	1+2-3-4 *	6	0	---	6 [0.7571-0.9951]	0	---
	1+2-3-5	6	0	---	2 [0.5088, 0.7089]	---	***4*** [0.6773-0.8881]
	1+2-4-5	6	0	---	---	0	***6*** [0.9279-0.9999]
	3-4-5 *	6	---	---	1 [0.5238]	0	***5*** [0.5198-0.9233]
(8) Central Anatolia, Turkey (Ilbeyli *et al.*2004); Late Cretaceous, 76 Ma; collision	1+2-3+4-5	22	8 [0.4792-0.9415]	0	---	---	***14*** [0.5285-0.9830]
	1+2-3-4 *	22	19 [0.5884-0.9966]	---	3 [0.5086-0.6194]	0	---
	1+2-3-5	22	5 [0.4934-0.9596]	---	0	---	***17*** [0.4060-0.9749]
	1+2-4-5	22	5 [0.6322-0.9760]	---	---	0	***17*** [0.4751-0.9914]
	3-4-5 *	22	---	---	1 [0.6721]	0	***21*** [0.5076-0.9803]

Continues

TABLE 8 (CONTD.). APPLICATION OF THE SET OF FIVE DISCRIMINANT FUNCTION MULTI-DIMENSIONAL DIAGRAMS FOR INTERMEDIATE MAGMAS

(case study no.) Locality (reference); age; inferred tectonic setting	Figure type	Total number of samples	Number of discriminated samples				
			IA+CA (1+2) [p_{IA+CA}]	CR+OI (3+4) [p_{CR+OI}]	CR (3) [p_{CR}]	OI (4) [p_{OI}]	Col (5) [p_{Col}]
(9) Bonin Islands, Japan (Taylor *et al.*1994); Eocene; arc.	1+2-3+4-5	35	***35*** [0.8574-1.0000]	0	---	---	0
	1+2-3-4	35	***35*** [0.9997-1.0000]	---	0	0	---
	1+2-3-5	35	***35*** [0.8984-1.0000]	---	0	---	0
	1+2-4-5	35	***35*** [0.7389-1.0000]	---	---	0	0
	3-4-5 *	35	---	---	7 [0.5006-0.7335]	0	28 [0.5264-0.9909]
(10) Guam, Marianas (Reagan and Meijer, 1984); Eocene-Oligocene, 43-32 Ma; arc.	1+2-3+4-5	15	***14*** [0.6601-0.9998]	0	---	---	1 [0.5649]
	1+2-3-4	15	***15*** [0.9788-1.0000]	---	0	0	---
	1+2-3-5	15	***14*** [0.7031-0.9998]	---	0	---	1 [0.5508]
	1+2-4-5	15	***13*** [0.9659-0.9999]	---	---	0	2 [0.5084, 0.7810]
	3-4-5 *	15	---	---	0	0	15 [0.4813-0.9944]
(11) South-western Tibet (Zhao *et al.*2009); Miocene, 11.5-17.7 Ma; continental rift (collision to continental rift transition).	1+2-3+4-5	35	0	8 [0.5017-0.9497]	---	---	***27*** [0.4971-0.9876]
	1+2-3-4	35	0	---	***35*** [0.9658-0.9998]	0	---
	1+2-3-5	35	0	---	***22*** [0.5919-0.9916]	---	13 [0.4985-0.7970]
	1+2-4-5	35	0	---	---	1 [0.6787]	***34*** [0.8312-1.0000]
	3-4-5	35	---	---	***24*** [0.5395-0.9846]	0	11 [0.5119-0.6863]
(12) Moyuta and Tecuamburro volcanoes, Guatemala (Patino *et al.*2003); Quaternary; arc.	1+2-3+4-5	7	***4*** [0.5975-0.9517]	0	---	---	3 [0.6874-0.9067]
	1+2-3-4	7	***7*** [0.7713-0.9808]	---	0	0	---
	1+2-3-5	7	***4*** [0.6845-0.9542]	---	0	---	3 [0.5490-0.8651]
	1+2-4-5	7	***4*** [0.6870-0.9776]	---	---	0	3 [0.7587-0.9455]
	3-4-5 *	7	---	---	1 [0.4496]	0	6 [0.6362-0.9635]
(13) Berlín and Ahuachapán, El Salvador Agostini *et al.*2006); Quaternary; arc	1+2-3+4-5	18	***15*** [0.5467-0.9918]	1 [0.5392]	---	---	2 [0.4980-0.5507]
	1+2-3-4	18	***16*** [0.6885-0.9952]	---	1 [0.4557]	1 [0.6128]	---
	1+2-3-5	18	***17*** [0.4915-0.9914]	---	0	---	1 [0.5099]
	1+2-4-5	18	***16*** [0.5213-0.9973]	---	---	1 [0.5390]	1 [0.5247]
	3-4-5 *	18	---	---	4 [0.5728-0.7058]	1 [0.9336]	13 [0.5370-0.9036]

For more explanation see footnote of Table 7.

Most samples of intermediate magma from Early Proterozoic intrusive rocks of the Nanded and Yeotmal districts, Maharastra, India (Banerjee and Shivkumar, 2010) plotted in the collision setting (Fig. 2A,C-E) and showed high probabilities (Table 8)

TABLE 9. APPLICATION OF THE SET OF FIVE DISCRIMINANT FUNCTION MULTI-DIMENSIONAL DIAGRAMS FOR BASIC MAGMAS (VERMA AND AGRAWAL 2011)

(case study no.) Locality; age; inferred tectonic setting	Figure type	Total number of samples	Number of discriminated samples				
			IAB (1) [p_{IAB}]	Within-plate			MORB (4) [p_{MORB}]
				CRB+OIB (2+3) [$p_{CRB+OIB}$]	CRB (2) [p_{CRB}]	OIB (3) [p_{OIB}]	
(1) Wawa greenstone belt, Canada; Late Archean, 2700 Ma; arc.	1-2+3-4	50	***36*** [0.3887-1.0000]	8 [0.6040-1.0000]	---	---	6 [0.5829-0.9605]
	1-2-3	50	***41*** [0.5783-1.0000]	---	1 [0.5017]	8 [0.6071-0.9888]	---
	1-2-4	50	***36*** [0.8620-1.0000]	---	5 [0.7905-0.9973]	---	9 [0.7315-0.9873]
	1-3-4	50	***36*** [0.9063-1.0000]	---	---	6 [0.7424-1.0000]	8 [0.7848-0.9331]
	2-3-4 *	50	---	---	3 [0.5456-0.6117]	9 [0.4944-0.9678]	38 [0.6935-0.9306]
(2) Maharastra (Nanded and Yeotmal districts), India; Early Proterozoic, 2385-2074 Ma.	1-2+3-4 1-2-3 1-2-4 1-3-4 2-3-4	Only 2 samples.	Collision setting was not included in these diagrams.				
(3) South-central Sweden; Early Proterozoic, 1870-1780 Ma); arc.	1-2+3-4	4	***3*** [0.9597-0.9980]	1 [0.6727]	---	---	0
	1-2-3	4	***3*** [0.9990-1.0000]	---	1 [0.5753]	0	---
	1-2-4	4	***3*** [0.9361-1.0000]	---	1 [0.5753]	---	1 [0.6254]
	1-3-4	4	***2*** [0.9909-1.0000]	---	---	1 [0.9243]	1 [0.9984]
	2-3-4 *	4	---	---	0	0	4 [0.4936-0.9894]
(4) Adola, Ethiopia; Late Proterozoic, 885-765 Ma; arc.	1-2+3-4	7	***5*** [0.9286-1.0000]	0	---	---	2 [0.6680, 0.8833]
	1-2-3	7	***6*** [0.9502-1.0000]	---	0	1 [0.9771]	---
	1-2-4	7	***6*** [0.5717-1.0000]	---	0	---	1 [1.0000]
	1-3-4	7	***5*** [0.9898-1.0000]	---	---	0	2 [0.7527, 1.0000]
	2-3-4 *	7	---	---	0	1 [0.7473]	6 [0.6330-0.9080]
(5) Malani, Rajasthan, India; Late Proterozoic, 750 Ma.	1-2+3-4 1-2-3 1-2-4 1-3-4 2-3-4	No samples with complete data.					
(6) Western Tasmania, Australia; Cambrian.	1-2+3-4 1-2-3 1-2-4 1-3-4 2-3-4	No samples with complete data.					
(7) Alps, France-Italy-Switzerland; Late Carboniferous, 295 Ma.	1-2+3-4 1-2-3 1-2-4 1-3-4 2-3-4	No samples with complete data.					
(8) Central Anatolia, Turkey; Late Cretaceous, 76 Ma.	1-2+3-4 1-2-3 1-2-4 1-3-4 2-3-4	Only 1 sample with complete data.	Collision setting was not included in these diagrams.				

TABLE 9 (CONTD.). APPLICATION OF THE SET OF FIVE DISCRIMINANT FUNCTION MULTI-DIMENSIONAL DIAGRAMS FOR BASIC MAGMAS (VERMA AND AGRAWAL, 2011)

(case study no.) Locality; age; inferred tectonic setting	Figure type	Total number of samples	Number of discriminated samples				
			IAB (1) [p_{IAB}]	CR+OI (2+3) [$p_{CRB+OIB}$]	CR (2) [p_{CRB}]	OI (3) [p_{OIB}]	MORB (4) [p_{MORB}]
(9) Bonin Islands, Japan; Eocene.	1-2+3-4 1-2-3 1-2-4 1-3-4 2-3-4	No samples with complete data.					
(10) Guam, Marianas; Eocene-Oligocene, 43-32 Ma.	1-2+3-4 1-2-3 1-2-4 1-3-4 2-3-4	No samples with complete data.					
(11) South-western Tibet; Miocene, 11.5-17.7 Ma.	1-2+3-4 1-2-3 1-2-4 1-3-4 2-3-4	5 samples.	Collision setting was not included in these diagrams.				
(12) Moyuta and Tecuamburro volcanoes, Guatemala; Plio-Pleistocene.	1-2+3-4 1-2-3 1-2-4 1-3-4 2-3-4	No samples with complete data.					
(13) Berlín and Ahuachapán, El Salvador; Quaternary.	1-2+3-4 1-2-3 1-2-4 1-3-4 2-3-4	No samples with complete data.					

Figure type refers to the tectonic fields being discriminated where the tectonic group numbers are as follows: 1–IAB, 2–CRB, 3–OIB, 4–MORB; *****–inapplicable results and diagrams; boldface italic font shows the expected or more probable tectonic setting; the probability estimates for the different tectonic groups are summarized after the number of discriminated samples as follows: [p_{IAB}]–range of probability values estimated for IAB settings, [$p_{CRB+OIB}$]–for CRB+OIB, [p_{CRB}]–for CRB, [p_{OI}]–for OIB, and [p_{MORB}]–for MORB.

The collision setting was confirmed from the diagrams for acid magmas because 32 to 44 (out of 50) samples plotted in this field (Table 11).

TABLE 10. APPLICATION OF THE SET OF FIVE DISCRIMINANT FUNCTION MULTI-DIMENSIONAL DIAGRAMS FOR BASIC AND ULTRABASIC MAGMAS (VERMA *ET AL.* 2006)

(case study no.) Locality; age; inferred tectonic setting	Figure type	Total number of samples	Number of discriminated samples			
			IAB (1)	Within-plate		MORB (4)
				CRB (2)	OIB (3)	
(1) Wawa greenstone belt, Canada; Late Archean, 2700 Ma; arc.	1-2-3-4	50	***34***	6	1	9
	1-2-3	50	***35***	2	13	---
	1-2-4	50	***32***	5	---	13
	1-3-4	50	***34***	---	10	6
	2-3-4 *	50	---	12	13	25
(2) Maharastra, Nanded and Yeotmal districts, India; Early Proterozoic, 2385-2074 Ma.	1-2-3-4 1-2-3 1-2-4 1-3-4 2-3-4	Only 2 samples.	Collision setting was not included in these diagrams.			
(3) South-central Sweden; Early Proterozoic, 1870-1780 Ma); arc.	1-2-3-4	5	***5***	0	0	0
	1-2-3	5	***5***	0	0	---
	1-2-4	5	***5***	0	---	0
	1-3-4	5	***5***	---	0	0
	2-3-4 *	5	---	4	0	1
(4) Adola, Ethiopia; Late Proterozoic, 885-765 Ma; arc.	1-2-3-4	10	***9***	0	0	1
	1-2-3	10	***9***	0	1	---
	1-2-4	10	***9***	0	---	1
	1-3-4	10	***9***	---	0	1
	2-3-4 *	10	---	7	0	3
(5) Malani, Rajasthan, India; Late Proterozoic, 750 Ma; continental rift.	1-2-3-4	19	2	***12***	3	2
	1-2-3	19	2	***15***	2	---
	1-2-4	19	2	***15***	---	2
	1-3-4*	19	4	---	13	2
	2-3-4	19	---	***14***	3	2
(6) Western Tasmania, Australia; Cambrian; arc.	1-2-3-4	6	***6***	0	0	0
	1-2-3	6	***6***	0	0	---
	1-2-4	6	***6***	0	---	0
	1-3-4	6	***6***	---	0	0
	2-3-4 *	6	---	6	0	0
(7) Alps, France-Italy-Switzerland; Late Carboniferous, 295 Ma.	1-2-3-4 1-2-3 1-2-4 1-3-4 2-3-4	No samples.	Collision setting was not included in these diagrams.			
(8) Central Anatolia, Turkey; Late Cretaceous, 76 Ma.	1-2-3-4 1-2-3 1-2-4 1-3-4 2-3-4	Only 1 sample.	Collision setting was not included in these diagrams.			

Continues

TABLE 10 (CONTD.). APPLICATION OF THE SET OF FIVE DISCRIMINANT FUNCTION MULTI-DIMENSIONAL DIAGRAMS FOR BASIC AND ULTRABASIC MAGMAS (VERMA *ET AL.* 2006)

(case study no.) Locality; age; inferred tectonic setting	Figure type	Total number of samples	Number of discriminated samples			
			IAB (1)	Within-plate		MORB (4)
				CRB (2)	OIB (3)	
(9) Bonin Islands, Japan; Eocene.	1-2-3-4 1-2-3 1-2-4 1-3-4 2-3-4	No samples.				
(10) Guam, Marianas; Eocene-Oligocene, 43-32 Ma; arc.	1-2-3-4	3	***3***	0	0	0
	1-2-3	3	***3***	0	0	---
	1-2-4	3	***3***	0	---	0
	1-3-4	3	***3***	---	0	0
	2-3-4 *	3	---	1	0	2
(11) South-western Tibet; Miocene, 11.5-17.7 Ma; continental rift (collision to continental rift transition).	1-2-3-4 1-2-3 1-2-4 1-3-4 2-3-4	5 samples.	Collision setting was not included in these diagrams.			
(12) Moyuta and Tecuamburro volcanoes, Guatemala; Plio-Pleistocene.	1-2-3-4 1-2-3 1-2-4 1-3-4 2-3-4	Only 2 samples (not plotted).				
(13) Berlín and Ahuachapán, El Salvador; Quaternary; arc	1-2-3-4	2	***2***	0	0	0
	1-2-3	2	***2***	0	0	---
	1-2-4	2	***2***	0	---	0
	1-3-4	2	***2***	---	0	0
	2-3-4 *	2	---	2	0	0

Figure type refers to the tectonic fields being discriminated where the tectonic group numbers are as follows: 1–IA, 2–CR, 3–OI, 4–MORB; *****–inapplicable results and diagrams; boldface italic font shows the expected tectonic setting.

For mafic intrusive rocks (1870-1780 Ma) from south-central Sweden (Rutanen and Andersson 2009), 12 out of 13 intermediate rock samples consistently showed an arc setting (Fig. 2A-D; Table 7). Additionally, three out of four and all five basic rock samples showed an arc setting (Tables 9 and 10, respectively).

Ten to all twelve Late Proterozoic intermediate rock samples from Adola (Wolde *et al.* 1996) showed high probabilities for arc (IA+CA) tectonic setting (Table 8; Fig. 2A-D). In agreement with this, ten samples of ultrabasic and basic magmas from the same area

also indicated an arc setting because nine of them plotted in this tectonic field (Table 10). Seven of these samples had complete data for immobile-element-based diagrams; five or six of them also showed very high probabilities for the arc field (Table 9). Finally, nine samples of acid magma confirmed the arc setting (high probabilities for 4 to 6 samples for the arc field; Table 11).

Twenty samples of Late Proterozoic intermediate magma from Malani igneous complex, Rajasthan, India (Maheshwari *et al.* 1996; Bhushan and Chandrasekaran, 2002; Sharma, 2004; Singh and Vallinayagam, 2004), showed an ocean island or continental rift setting (Fig. 2). Twelve to fifteen samples were discriminated as ocean island, whereas six to eighteen samples as continental rift (Table 8). The nineteen ultrabasic and basic rock samples from Malani indicated a continental rift setting (12 to 15 samples in this field; Table 10). Similarly, thirty samples of acid magma from Malani also indicated a continental rift setting (Table 11; ocean island setting was not included in these diagrams). This case study highlights the difficulty in discriminating very similar continental rift and ocean island settings.

Twenty-nine samples of Cambrian intermediate magma from western Tasmania, Australia (Brown and Jenner 1989), were discriminated as an arc setting (Fig. 2), because most (27 to 28 out of 29) samples showed high probabilities (Table 8) for the IA+CA field. The six basic rock samples fully confirmed the arc setting (Table 10).

Six samples of intermediate rocks of about 295 Ma from the Alps (France-Italy-Switzerland; Debon and Lemmet 1999) clearly showed a collision setting during the Late Carboniferous, because most (four to all six) samples plotted in this field with high probabilities (Fig. 2; Table 8). This result was fully consistent with the 11 samples of acid magma, most (9 to 10) of which plotted in the collision field (Table 11).

Twenty-two samples of Late Cretaceous intermediate magma from central Anatolia, Turkey (Ilbeyli *et al.* 2004), showed a collision setting because most (14 to 21) samples

TABLE 11. APPLICATION OF THE SET OF FIVE DISCRIMINANT FUNCTION MULTI-DIMENSIONAL DIAGRAMS FOR ACID MAGMAS (VERMA *ET AL.* 2011)

(case study no.) Locality; age; inferred tectonic setting	Figure type	Total number of samples	Number of discriminated samples				
			IA+CA (1+2) [p_{IA+CA}]	IA (1) [p_{IA}]	CA (2) [p_{CA}]	CR (3) [p_{CR}]	Col (4) [p_{Col}]
(1) Wawa greenstone belt, Canada; Late Archean, 2700 Ma.	1+2-3-4	No samples.					
	1-2-3						
	1-2-4						
	1-3-4						
	2-3-4						
(2) Nanded and Yeotmal, Maharastra, India; Early Proterozoic, 2385-2074 Ma; collision.	1+2-3-4	50	1 [0.4987, 0.6026]	11 [0.4615-0.9625]	---	---	***37*** [0.4181, 0.9947]
	1-2-3 *	50	1 [0.5857]	---	46 [0.5803-0.9343]	43 [0.4975- 0.9973]	---
	1-2-4	50	2 [0.5863, 0.6678]	---	4 [0.4941-0.8015]	---	***44*** [0.4159- 0.9998]
	1-3-4	50	4 [0.5411-0.9311]	---	---	14 [0.5024-0.9106]	***32*** [0.5289-0.9879]
	2-3-4	50	---	---	4 [0.4280-0.8763]	12 [0.4792-0.9445]	***34*** [0.4155, 0.9834]
(3) South-central Sweden; Early Proterozoic, 1870-1780 Ma).	1+2-3-4	No Samples.					
	1-2-3						
	1-2-4						
	1-3-4						
	2-3-4						
(4) Adola, Ethiopia; Late Proterozoic, 885-765 Ma; arc.	1+2-3-4	9	***6*** [0.3727-1.0000]	2 [0.5185, 0.7216]	---	---	1 [0.6740]
	1-2-3	9	***5*** [0.5414-1.0000]	---	1 [0.3648]	3 [0.8045-0.9856]	---
	1-2-4	9	***4*** [0.6117-1.0000]	---	0	---	5 [0.5326-0.9789]
	1-3-4	9	***5*** [0.4570-1.0000]	---	---	2 [0.4427, 0.7516]	1 [0.8622]
	2-3-4 *	9	---	---	7 [0.4597-1.0000]	2 [0.4441, 0.6419]	0
(5) Malani, Rajasthan, India; Late Proterozoic, 750 Ma; continental rift.	1+2-3-4	30	1 [0.6448]	***16*** [0.0.7085-1.0000]	---	---	13 [0.4741-0.9947]
	1-2-3	30	0	---	3 [0.3921-0.7299]	***27*** [0.5065-1.0000]	---
	1-2-4 *	30	2 [0.4328, 0.5072]	---	7 [0.3703-0.6580]	---	21 [0.5720-1.0000]
	1-3-4	30	1 [0.5690]	---	---	***16*** [0.6921-1.0000]	13 [0.5029-0.9966]
	2-3-4	30	---	---	3 [0.3975-0.6989]	***15*** [0.5576-1.0000]	12 [0.5059-0.9645]
(6) Western Tasmania, Australia; Cambrian; arc.	1+2-3-4	No Samples.					
	1-2-3						
	1-2-4						
	1-3-4						
	2-3-4						
(7) Alps, France-Italy-Switzerland; Late Carboniferous, 295 Ma; collision	1+2-3-4	11	0	1 [0.6925]	---	---	***10*** [0.3997-0.9859]
	1-2-3 *	11	0	---	2 [0.6198, 0.9150]	8 [0.4330-0.9941]	---
	1-2-4	11	0	---	2 [0.6316, 0.7949]	---	***9*** [0.6094-0.9956]
	1-3-4	11	0	---	---	2 [0.5104, 0.8442]	***9*** [0.6170-0.9793]
	2-3-4	11	---	---	0	2 [0.4933, 0.7594]	***9*** [0.5354-0.9699]
(8) Central Anatolia, Turkey; Late Cretaceous, 76 Ma; collision	1+2-3-4	13	2 [0.5779, 0.6053]	1 [0.4402]	---	---	***10*** [0.3793-0.9719]
	1-2-3 *	13	0	---	11 [0.5000-0.9469]	2 [0.6300, 0.7672]	---
	1-2-4	13	0	---	*7* [0.5952-0.7964]	---	***6*** [0.6411-0.9936]
	1-3-4	13	0	---	---	3 [0.5157-0.5473]	***9*** [0.5387-0.9759]
	2-3-4	13	---	---	1 [0.4520]	1 [0.4771]	***11*** [0.4789-0.9480]

TABLE 11 (CONTD.). APPLICATION OF THE SET OF FIVE DISCRIMINANT FUNCTION MULTI-DIMENSIONAL DIAGRAMS FOR ACID MAGMAS (VERMA *ET AL.* 2011)

(case study no.) Locality; age; inferred tectonic setting	Figure type	Total number of samples	Number of discriminated samples				
			IA+CA (1+2) [p_{IA+CA}]	IA (1) [p_{IA}]	CA (2) [p_{CA}]	CR (3) [p_{CR}]	Col (4) [p_{Col}]
(9) Bonin Islands, Japan; Eocene; arc.	1+2-3-4	7	***7*** [0.7530-0.9905]	0	---	---	0
	1-2-3	7	***7*** [0.8119-0.9860]	---	0	0	---
	1-2-4	7	***7*** [0.8467-0.9902]	---	0	---	0
	1-3-4	7	***7*** [0.9814-0.9999]	---	---	0	0
	2-3-4 *	7	---	---	***7*** [0.9939-0.9999]	0	0
(10) Guam, Marianas; Eocene-Oligocene, 43-32 Ma.	1+2-3-4	No samples.					
	1-2-3						
	1-2-4						
	1-3-4						
	2-3-4						
(11) South-western Tibet; Miocene, 11.5-17.7 Ma.	1+2-3-4	No samples.					
	1-2-3						
	1-2-4						
	1-3-4						
	2-3-4						
(12) Moyuta and Tecuamburro volcanoes, Guatemala; Plio-Pleistocene.	1+2-3-4	No samples.					
	1-2-3						
	1-2-4						
	1-3-4						
	2-3-4						
(13) Berlín and Ahuachapán, El Salvador; Quaternary; arc	1+2-3-4	4	***4*** [0.8506-0.9526]	0	---	---	0
	1-2-3	4	***4*** [0.8314-0.9955]	---	0	0	---
	1-2-4	4	***4*** [0.8936-0.9899]	---	0	---	0
	1-3-4	4	***4*** [0.9682-0.9997]	---	---	0	0
	2-3-4 *	4	---	---	4 [0.9926-1.0000]	0	0

Figure type refers to the tectonic fields being discriminated where the tectonic group numbers are as follows: 1–IA, 2–CA, 3–CR, 4–Col; *****–inapplicable results and diagrams; boldface italic font shows the expected or more probable tectonic setting; the probability estimates for the different tectonic groups are summarized after the number of discriminated samples as follows: [p_{IA+CA}]–range of probability values estimated for IA+CA settings, [p_{IA}]–for IA, [p_{CA}]–for CA, [p_{CR}]–for CR and [p_{Col}]–for Col.

plotted in this field (Fig. 2; Table 8). Thirteen samples of acid magma confirmed these results (Table 11).

The Bonin Archipelago represents an uplifted fore-arc area exposing the products of Eocene supra-subduction zone magmatism, with Chichijima being the type locality for boninite rocks (Taylor *et al.* 1994). An arc setting was fully confirmed for the Bonin Archipelago during the Eocene because all 35 intermediate rock samples plotted in the arc field with very high probabilities (Table 8). Interestingly, the arc setting was also inferred from seven samples of acid magma, all of which plotted in this field (Table 11).

In spite of the alteration in Eocene-Oligocene volcanic rocks from Guam, Marianas fore-arc area (Reagan and Meijer 1984), 15 samples of intermediate rocks clearly showed an arc setting with 13 to 15 samples having high probabilities (Table 8) for the IA+CA field. The major element data for three samples of basic rocks confirmed the arc setting (Table 10).

Thirty-five samples of ultrapotassic intermediate post-collision Miocene rocks from south-western Tibet (Zhao *et al.* 2009) showed a transition from collision to rift setting (Table 8). In two diagrams (Fig. 2A,C), 27 and 34 samples plotted in the collision field, whereas in the remaining three (Fig. 2B,D,E), 22 to 35 samples did so in the continental rift field (Table 8).

Seven samples of intermediate magma of corestone-shell complexes from Moyuta and Tecuamburro volcanoes of Guatemala (a part of the Central American Volcanic Arc–CAVA; Patino *et al.* 2003) were used to evaluate the effects of spheroidal weathering in our new multi-dimensional diagrams (Table 8). An arc setting was still inferred for these highly altered rocks because most of them (4 to all 7 samples) plotted in the IA+CA field (Fig. 2) and showed high probabilities for this field (Table 8). Although these authors did not report analyses of fresh rocks from these volcanoes, which might have helped in better understanding of the alteration effects in our multi-dimensional diagrams, we may hypothesize that these effects probably rendered some samples to plot in the collision field, with relatively high probabilities (Table 8).

Eighteen samples of hydrothermally altered (zeolite alteration) intermediate volcanic rocks from boreholes in Berlín and Ahuachapán geothermal areas of El Salvador (CAVA; Agostini *et al.* 2006) clearly showed an arc setting, because, in spite of the alteration effects, most of them (15 to 17 samples) plotted in the arc (IA+CA;

Fig. 2) field (Table 8). Major element data for two samples of basic (Table 10) and four of acid magmas confirmed the arc setting (Table 11).

4.5 Conclusions

A The new set of five diagrams with high success rates for intermediate magma, put forth in this work from correct statistical treatment of log-ratio transformation, discordant outlier-free database, multivariate technique of LDA, probability-based boundaries and associated sample probability calculations as a replacement for plotting samples, are shown to work well for relatively fresh to highly altered rocks of almost all ages from several areas around the world, and are therefore recommended to be used to decipher the tectonic settings of old or tectonically complex areas.

Chapter 5

Chapter 5

Proposal of first multi-dimensional classification diagram for magma type of altered igneous rocks

Antecedents

In this chapter, I am presenting the progress proposal report of the classification diagram. In future, this work may be published in international journal.

Abstract

The International Union of Geological Sciences (IUGS) has proposed recommendations for the classification of relatively fresh rocks. The total alkali versus silica (TAS) diagram has been in use for the classification of fresh rocks now for over thirty years. I present here the new multi-dimensional classification diagram obtained from correct statistical methodology of log-ratio transformation and linear discriminant analysis, major element log-ratio variables in 23764 rock samples from four rock or magma types (Basic+Ultrabasic, Intermediate and Acid). This diagram with probability-based field boundaries and high success rates (80.47%-96.89%) was used for class discrimination. This classification diagram consistent with the IUGS nomenclature for fresh rocks can be used for altered rocks as well.

5.1 Introduction

The most widely used classification diagrams for fresh volcanic rocks are the total alkali-silica (TAS) diagrams (Le Bas *et al.* 1986, 1992). The total alkali (Na_2O+K_2O) axis mainly distinguishes alkaline from sub-alkaline rock type, whereas the silica axis mainly distinguishes primitive from evolved rock types. This diagram does, however, have limited application to volcanic arc lavas, the vast majority of which simply classify as sub-alkaline instead of the subdivision into calc-alkaline and tholeiitic rock types.

In the published literature, some diagrams (alternative to the TAS diagram) have long been proposed, using the so-called immobile elements (Floyd and Winchester 1975, 1978; Winchester and Floyd 1976, 1977) with hundreds of citations. More recently, classification diagrams for altered rocks are proposed by Hastie *et al.* (2007) who state that the existing diagrams did not work well for arc rocks and proposed, more specifically, the use of Co-Th diagrams for the classification of altered rocks from volcanic arcs.

According to the original authors, these diagrams (Floyd and Winchester 1975, 1978; Winchester and Floyd 1976, 1977) and more recent (Hastie *et al.* 2007) diagrams "correctly" classified altered rocks. Verma *et al.* (2010) presented the following reasoning before evaluating these diagrams. The question was: Do the diagrams work well for altered rocks? We cannot precisely answer this question by studying altered rocks, because we do not know how much their chemical composition was modified by alteration processes in the field. We could, of course, resort to experimental laboratory-controlled work to answer it, which could also be costly, time consuming and difficult due to multivariate nature of this problem. Verma *et al.* (2010) thus concluded that the above mentioned old as well as the newer diagrams do not work well, making it clear that new classification diagrams are still needed.

Therefore, I proposed a new multi-dimensional classification diagram based on all ten major element oxides, instead of a few selective elements used in the earlier diagrams, for altered igneous rocks, using the philosophy of International Union of

Geological Sciences (IUGS) classification scheme (contribution of TAS diagram and CIPW norms Le Maitre *et al.* 2002; Verma *et al.* 2002). The main purpose was to correctly classify the magma type as one of the three varieties: (i) ultrabasic or basic, (ii) intermediate, and (iii) acid. This could help me to correctly choose the suitable discrimination diagrams.

5.2 Databases

In order to propose the classification diagram, an updated version of database was prepared with new analyses (about 9492 samples) and the combined data for 23764 samples were used for this work. The existing database was used earlier by Verma *et al.* (2011, 2012); for more information see Annexure I & III as well as chapter 4 which already presents the information of number of samples, their tectonic setting and magma type and location coordinates, and literature references. Therefore, to avoid repetition and reduce the thesis space, these details are omitted from this chapter.

The important aspects of this database are as follows.

- Rocks type: Fresh igneous rocks
- Age: Young (Miocene to Recent)
- Location: All over the world (oceans and continents)

I assigned a proper rock name and magma type (basic, ultrabasic, intermediate and acid) to each compiled rock sample following the IUGS volcanic rock classification scheme (Le Bas *et al.* 1986, Le Bas 2000) using computer program SINCLAS (Verma *et al.* 2002, 2003) under the Middlemost (1989) option for Fe-oxidation adjustment. This implicitly requires that complete chemical analysis involving all 10 major oxides be available for a rock sample.

The samples with complete analyses and log-ratio data were used to propose the new classification diagram from complete data set. Success rates (i.e. correct classification expressed as percentages) were calculated from counting the correctly discriminated samples. The probability-based boundaries and the probabilities for

individual samples were computed from the method recently outlined Verma and Agrawal (2011).

5.3 New Classification Diagram

A total of 23764 rock samples with complete major-element analyses were available in my database for proposing new diagram. The results of linear discriminant analysis (LDA) performed on these samples (success rates) can be summarized as follows: 86.22% for basic+ultrabasic rock together, 96.89% for intermediate rock, and 80.47% for acid rock.

The complete major element analyses of classification diagram are divided into their magma types (Table 1).

TABLE 1. TOTAL NUMBER OF SAMPLES AND ROCKS TYPE IN DATABASE

Rocks Type *	Group number	Total Samples
Basic+Ultrabasic	1+2	10435
Intermediate	3	8465
Acid	4	4864
Sum	1–4	23764

The synthesis of log-ratio variables used in LDA is summarized in Table 2. In which the mean and standard deviation values for all samples are included.

TABLE 2. MEAN AND STANDARD DEVIATION OF $(SiO_2)_{adj}$ AND LOG-TRANSFORMED RATIO VARIABLES FOR THE THREE ROCKS TYPE (BASIC+ULTRABASIC, INTERMEDIATE, AND ACID) SAMPLES OF THE DATABASE

loge-transformed ratio variable	Basic+Ultrabasic (1+2) (*n =10435*)		Intermediate (3) (*n = 8465*)		Acid (4) (*n =4865*)	
	x	*S*	*x*	*S*	*x*	*s*
$(SiO_2)_{adj}$	48.42	2.70	57.06	3.29	69.43	5.00
$\ln(TiO_2/SiO_2)_{adj}$	-3.287	0.572	-4.122	0.488	-5.194	0.799
$\ln(Al_2O_3/SiO_2)_{adj}$	-1.163	0.157	-1.211	0.138	-1.554	0.310
$\ln(Fe_2O_3/SiO_2)_{adj}$	-3.238	0.243	-3.465	0.265	-4.300	0.657
$\ln(Feo/SiO_2)_{adj}$	-1.718	0.231	-2.402	0.338	-3.513	0.710
$\ln(MnO/SiO_2)_{adj}$	-5.590	0.394	-6.034	0.486	-6.877	0.804
$\ln(MgO/SiO_2)_{adj}$	-1.880	0.481	-2.764	0.731	-4.816	1.619
$\ln(CaO/SiO_2)_{adj}$	-1.547	0.301	-2.153	0.449	-3.607	1.167
$\ln(Na_2O/SiO_2)_{adj}$	-2.837	0.372	-2.764	0.317	-2.868	0.459
$\ln(K_2O/SiO_2)_{adj}$	-4.300	1.198	-3.615	0.780	-3.164	0.620
$\ln(P_2O_5/SiO_2)_{adj}$	-5.041	0.971	-5.474	0.753	-6.792	1.417

x –mean; *s*–standard deviation.

All log-transformed ratios are negative, because I have chosen the most abundant major element $(SiO_2)_{adj}$ as denominator. Although there is progressive, unwanted increase of mean value of $(SiO_2)_{adj}$ from basic+ultrabasic rock to acid (Table 2), there are differences in mean value of most log-transformed ratio as well.

To understand if these differences are statistically significant, Table 3 gives the results of equality of these elements and their ratio. Both tests (Wilks´ lambda<<1 and F-ratio>>1) indicate that significant differences exist for element concentrations and, more importantly, in log-transformed ratios among the four groups at an extremely low

significance level approaching zero for all variables except $\ln(P_2O_5/SiO_2)_{adj}$ (Table 3), i.e. very high confidence level approaching 100%.

TABLE 3. TEST OF EQUALITY OF GROUP MEANS FOR TEN LOG-TRANSFORMED RATIO VARIABLES IN THE GROUP SAMPLES

Element	Wilks' lambda	F-ratio	Significance
$\ln(TiO_2/SiO_2)_{adj}$	0.11928	364.334	0.00000
$\ln(Al_2O_3/SiO_2)_{adj}$	0.12135	559.399	0.00000
$\ln(Fe_2O_3/SiO_2)_{adj}$	0.20716	9351.693	0.00000
$\ln(FeO/SiO_2)_{adj}$	0.20840	9479.668	0.00000
$\ln(MnO/SiO_2)_{adj}$	0.11724	137.644	0.00000
$\ln(MgO/SiO_2)_{adj}$	0.11855	271.541	0.00000
$\ln(CaO/SiO_2)_{adj}$	0.11701	114.602	0.00000
$\ln(Na_2O/SiO_2)_{adj}$	0.11711	124.812	0.00000
$\ln(K_2O/SiO_2)_{adj}$	0.11921	339.343	0.00000
$\ln(P_2O_5/SiO_2)_{adj}$	0.11592	2.967	0.05146

Wilks' lambda (U-statistic) and univariate F-ratio with degree of freedom, df1= $\nu 1$ = g-1 = 4-1 = 3 and df2 = $\nu 2$ = n-g = 23764-4 = 23760, where g is the number of groups and n is total number of samples.

Furthermore, these differences among groups can be enhanced by the multivariate technique of LDA to achieve acceptable separation of groups in multi-dimensional classification diagram.

5.4 Probability-based field boundaries

I carried out LDA on 23764 samples of data set. In total, the discriminant analysis was carried out only one time because only three groups had to be separated.

Table 4 contains the equation of DF1 and DF2 functions (x-and y-axes; Fig. 1). In these equations, the log-transformed ratios of major elements are multiplied by corresponding coefficients or the multiplication factors obtained from LDA (called

'raw coefficients' of canonical analysis in *Statistica* software). The last factor in each equation is a constant term for that equation.

Because in LDA I used three groups at a time, even in the first diagram, two functions (DF1 and DF2) together would define the total (100%) variance (Fig.1), with two discriminant functions is sufficient to fully visualize the samples from three groups being discriminated at a given time. Furthermore, we call this diagram as multi-dimensional, because each of two DF1 and DF2 functions contains 10 log-ratio variables. Thus, we are able to visualize 10-dimentional data in two dimensions. This is the major advantage of discriminant-function-based diagram.

TABLE 4. DISCRIMINANT-FUNCTION EQUATIONS FOR THE NEW MULTI-DIMENSIONAL CLASSIFICATION DIAGRAM

Figure no.	Equations
Figure 1 (1+2-3-4)	$DF1_{(B+Ub\text{-}Int\text{-}Acid)} = (0.381852 \times \ln(TiO_2/SiO_2)_{adj}) + (0.789856 \times \ln(Al_2O_3/SiO_2)_{adj}) + (-5.26887 \times \ln(Fe_2O_3/SiO_2)_{adj}) + (5.64354 \times \ln(FeO/SiO_2)_{adj}) + (0.228959 \times \ln(MnO/SiO_2)_{adj}) + (0.020858 \times \ln(MgO/SiO_2)_{adj}) + (-0.0003908 \times \ln(CaO/SiO_2)_{adj}) + (0.056826 \times \ln(Na_2O/SiO_2)_{adj}) + (0.252379 \times \ln(K_2O/SiO_2)_{adj}) + (0.026725 \times \ln(P_2O_5/SiO_2)_{adj}) - 0.26660076874502$
	$DF2_{(B+Ub\text{-}Int\text{-}Acid)} = (-0.526167 \times \ln(TiO_2/SiO_2)_{adj}) + (2.19843 \times \ln(Al_2O_3/SiO_2)_{adj}) + (5.97823 \times \ln(Fe_2O_3/SiO_2)_{adj}) + (-4.65921 \times \ln(FeO/SiO_2)_{adj}) + (0.216275 \times \ln(MnO/SiO_2)_{adj}) + (0.438321 \times \ln(MgO/SiO_2)_{adj}) + (0.430037 \times \ln(CaO/SiO_2)_{adj}) + (-0.632727 \times \ln(Na_2O/SiO_2)_{adj}) + (-0.178113 \times \ln(K_2O/SiO_2)_{adj}) + (-0.0055025 \times \ln(P_2O_5/SiO_2)_{adj}) + 11.93836316452$

As an example, for drawing the boundary the discriminates Basic+Ultrabasic and Intermediate fields in Figure 1, I first calculated the probabilities all along the top horizontal line (DF1 top axis) of the diagram, i.e., the line connecting (-8, 18) and (18, -8), and tried to obtain the coordinates of the point with equal probability for Basic+Ultrabasic and Intermediate fields, which were observed to be (8, 17.5347). Similarly, I obtained the coordinates of the Intermediate-Acid boundary along the DF2 axis (the line joining 8, -8 and 18, -8) as (–8, 9.29077) and those for the Basic+Ultrbasic-Acid along the DF1 axis (the line joining -8, -8 and 18, -8) as (-0.0007636, -8.00). The next step was to locate additional equal probability points along two horizontal or vertical lines well within the diagram, e.g., for Figure 1, I located equal probability points along two lines, one horizontal joining (8, 4) to (-8, 9) and the other vertical joining (-4, -8) and (-4, 8). These equal probability inner coordinates were (4.00, 8.03245) for the Basic+Ultrabasic–Intermediate boundary and (-0.3341, -4.00) for the Basic+Ultrabasic–Acid boundary. Then, I obtained two equations, one joining two points (4, 8.03245) and (8, 17.5370) to obtain Basic+Ultrabasic–Intermediate boundary and the other connecting (-0.3341, -4.00) and (-0.0007636, -8) for the Basic+Ultrabasic–Acid boundary. The point of intersection of these two equations was obtained to be (-0.454898, -2.5504358). The third boundary (Intermediate–Acid) from (–8.00, 9.29077) will automatically pass through this point (-0.454898, -2.5504358). Because all three boundaries meet at this point, it can be called triple point for this diagram. I assured that the probability for this triple point was about 0.3333, or 33.33%, for each of the three tectonic fields (Figure 1), because in LDA we had assumed equal probability for all groups being discriminated, irrespective of the sample sizes.

The major advantage of LDA is that the tectonic boundaries can be based on probability estimates (Agrawal 1999). The posterior probability calculations for individual samples are similar to those describe recently by Verma and Agrawal (2011). Therefore instead of elaborating on these probability calculations, I briefly present the method to obtain the probability-based field boundaries.

The boundary coordinates for all diagrams are reported in the explanation of Figure 1.

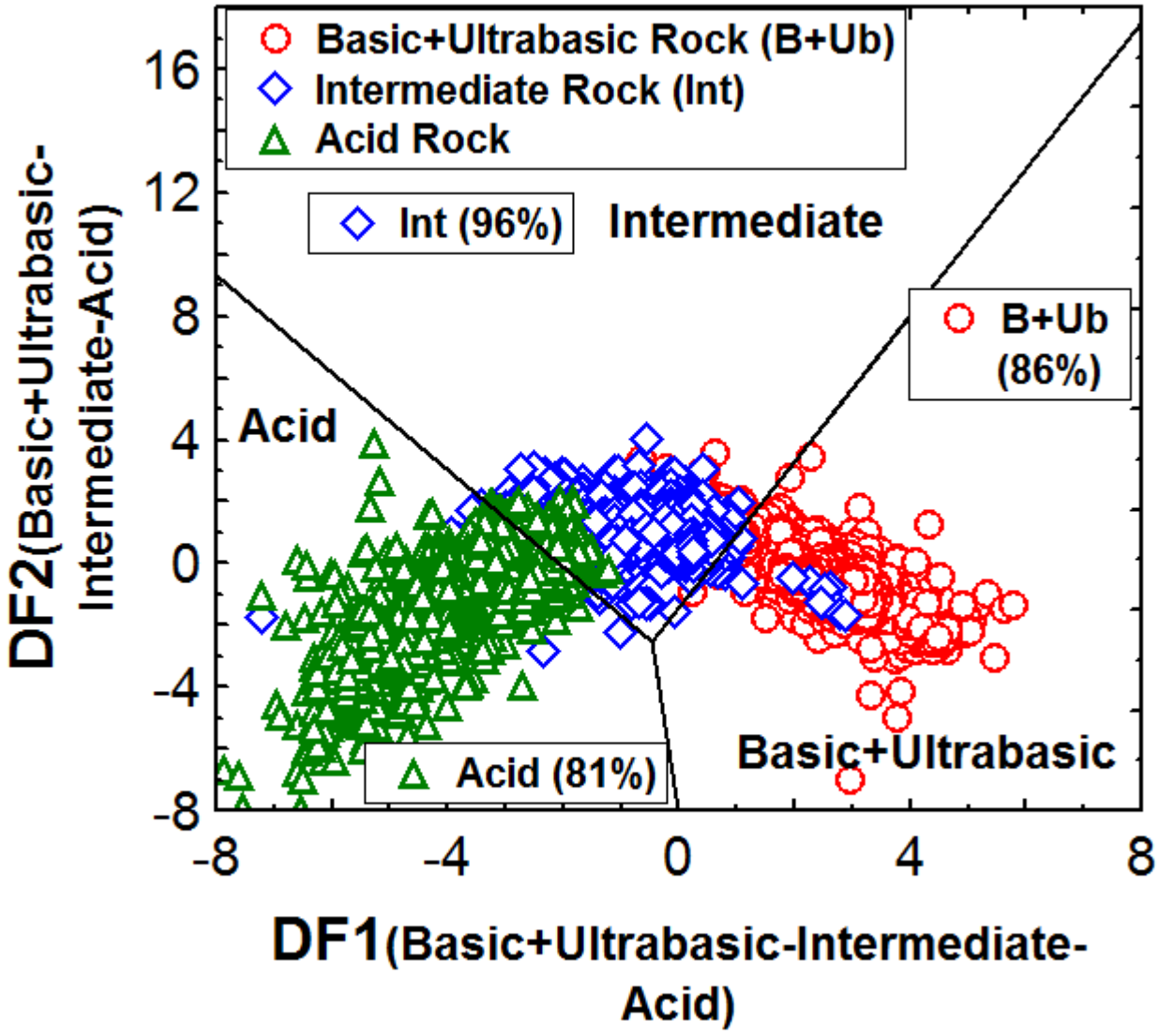

Figure 1 New discriminant-function based multi-dimensional diagrams for the classification of igneous rocks from basic+ultrabasic (B+Ub), intermediate (Int), and acid rocks, showing samples from the data set.

The symbols are explained as inset in Figure 1. The black lines represent discrimination boundaries, Basic+Ultrabasic-Intermediate-Acid (1+2–3–4) diagram, the coordinates of the field boundaries are (8, 17.5347) and (-0.454898, -2.5504358)

for Basic+Ultrabasic-Intermediate; (−8.0, 9.29077) and (-0.454898, -2.5504358) for Intermediate-Acid; and (−0.0007636, -8) and (-0.454898, -2.5504358) for Basic+Ultrabasic-Acid.

5.5 Result of success rate

Using the complete data set samples (23764) I obtained the success rates, for which the samples were plotted in new discriminant-function-based multi-dimensional classification diagram (Figure 1).

In Figure 1, about 86% samples are plotted in basic+ultrabasic field. For the intermediate field I obtained the success rate of about 96%. The success rate for Acid filed is achieved 81%.

5.6 Conclusions

The new classification diagram with high success rates for basic+ultrabasic, intermediate and acid magmas is successfully proposed. This multi-dimensional diagram is based on correct statistical treatment of log-ratio transformation, multivariate technique of LDA, probability-based boundaries and associated sample probability calculations as a replacement for plotting samples, are shown to work well for relatively fresh as well as altered rocks. This multi-dimensional diagram is consistent with the IUGS nomenclature.

Chapter 6

Application of Classification and Discrimination diagrams

6.1 Application of the classification diagram

I selected five case studies, with Neogene ages, to illustrate the application of the new classification diagram. None of the samples from these case studies had been included in the database used for constructing this diagram (chapter 5). Therefore, these case studies provide an unbiased application result of new classification diagram for fresh as well as altered rocks.

Further, I divided these case studies samples in two parts.

1. Case studies based on fresh rocks (Table 1)
2. Case studies based on altered rocks (Table 2)

1. Case studies based on fresh rocks

For fresh rocks, I compiled the samples from five areas (Caldera Los Azufres, Caldera Amealco, Caldera Huichapan, and Caldera Los Humeros, Sierra la Primavera) around the Mexico, age and references are given in Tables 3 and 4. Then, I plotted these samples in Total Alkali versus Silica diagram (Fig. 1a) as well as in new discriminant-function-based classification diagram (Fig 1b) to compare the result efficiency of new discriminant-function-based classification diagram. Here, I considered TAS diagram as a reference for new discriminant-function-based classification diagram and the results are summarized in Table 1.

6.2 Location map

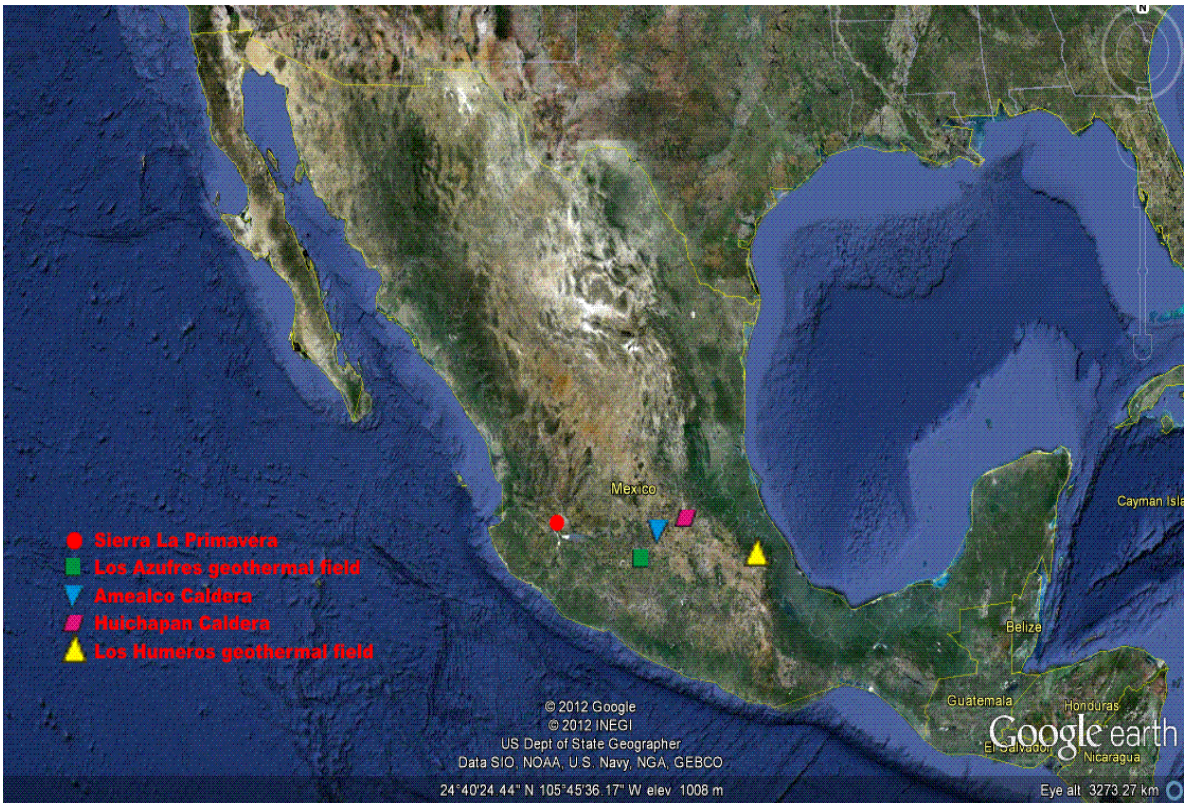

Location map of Sierra La Primavera, Los Azufres geothermal field, Amealco Caldera, Huichapan Caldera and Los Humeros geothermal field in Mexico. The symbols are indicated on the above map.

First, using TAS diagram Le Bas *et al.* (1986), I classified the samples into basic magma (14 samples), intermediate magma (193 samples) and acid magma (215 samples) for (Fig. 1a and Table 1).

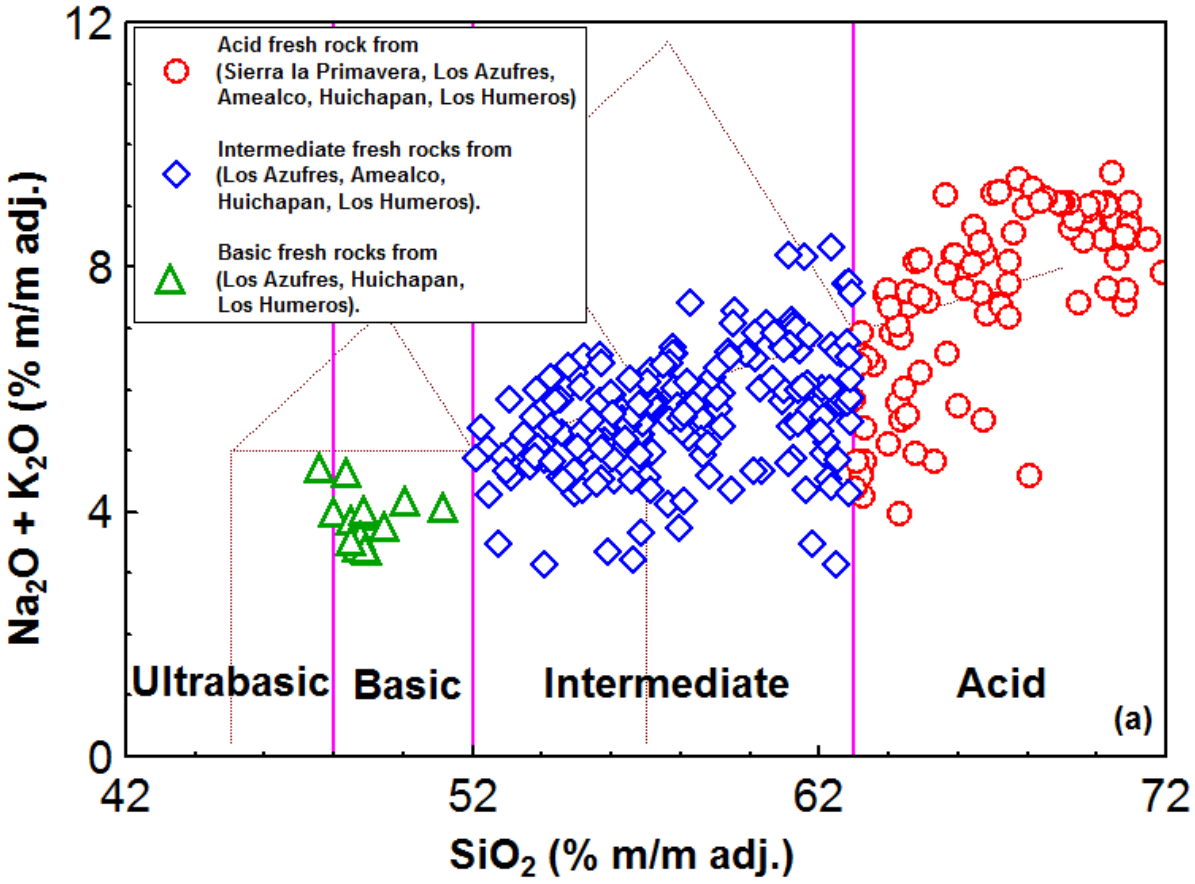

Figure 1a. Total Alkali versus Silica (TAS) classification diagram for fresh rocks, showing samples from the five case studies. The solid pink lines represent field boundaries for ULTRABASIC–BASIC–INTERMEDIATE–ACID (1+2–3–4) fields.

The same samples 14 for basic magma, 193 samples for intermediate magma and 215 samples for acid magma were plotted in Figure 1b, for evaluation of the new discriminant-function-based classification diagram. The results are summarized in Table 1). For the basic rocks samples, (14 out of 14) plot in basic field while intermediate and acid rocks were mis-classified with (3 out of 193) and (6 out of

215 samples) in acid and intermediate fields, respectively (Fig. 1b; Table 1). So over all I obtained very high (97%-100%) success rate for the new discriminant-function-based classification diagram.

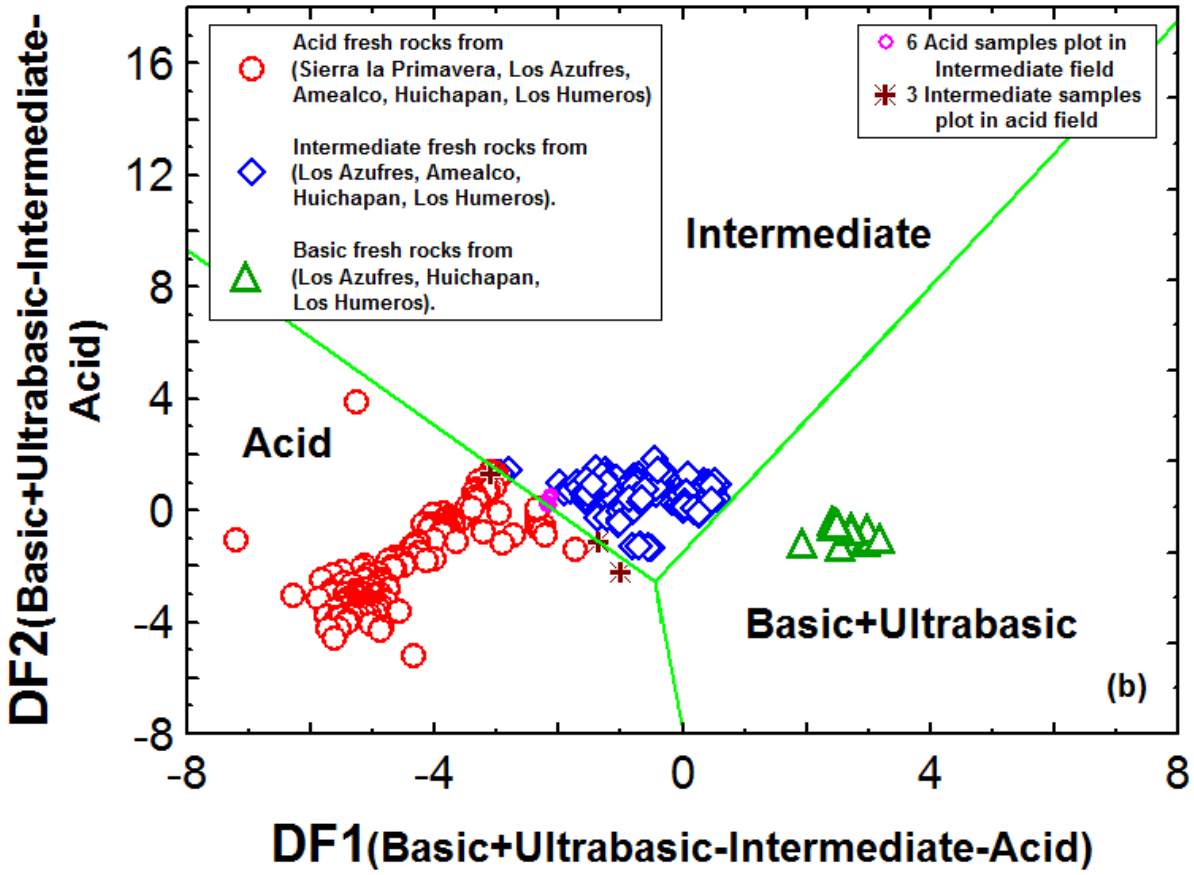

Figure 1b. The new discriminant-function, multi-dimensional diagram based on natural logarithm-transformed ratios of major elements for the classification of fresh rocks, showing samples from the five case studies. The solid green lines represent discrimination boundaries for BASIC+ULTRABASIC–INTERMEDIATE–ACID (1+2–3–4) fields.

Thus, it is justified that new discriminant-function-based classification diagram can be use for fresh volcanic rocks, as well TAS diagram because in both diagrams, I obtained significant result.

TABLE 1. APPLICATION OF TAS DIAGRAM FOR FRESH ROCKS FROM LOS AZUFRES, AMEALCO, HUICHAPAN, LOS HUMEROS, AND SIERRA LA PRIMAVERA FOR THE EVALUATION OF DISCRIMINANT-FUNCTION-BASED CLASSIFICATION DIAGRAM.

Rocks Type	Total Number of samples in TAS diagram*	Rock Type in Discriminant-function-based classification diagram [Total Number of samples (%)]		
		Basic	Intermediate	Acid
Basic	14 (100)	14 (100)	0	0
Intermediate	193 (100)	0	190 (98)	3 (2)
Acid	215 (100)	0	6 (3)	209 (97)

* TAS diagram is reference for the discriminant-function-based classification diagram

We also see (Table 1) that more samples of intermediate and acid rocks than basic rocks have been analyzed, which may reflect the actual abundance of these magma types in these geothermal fields. Further, in TAS diagram (Fig. 1a) numerous rock samples plot close to the boundaries (fixed following the accepted nomenclature), some of them are mis-discriminated in the new multi-dimensional diagram (Fig. 1b).

2. Case studies based on altered rocks

For altered rocks, I also compiled geochemical data, age and references (Tables 3 and 4) samples from two areas (Caldera Los Azufres, and Caldera Los Humeros; for the rest of the areas, no geochemical data are available for altered rocks.

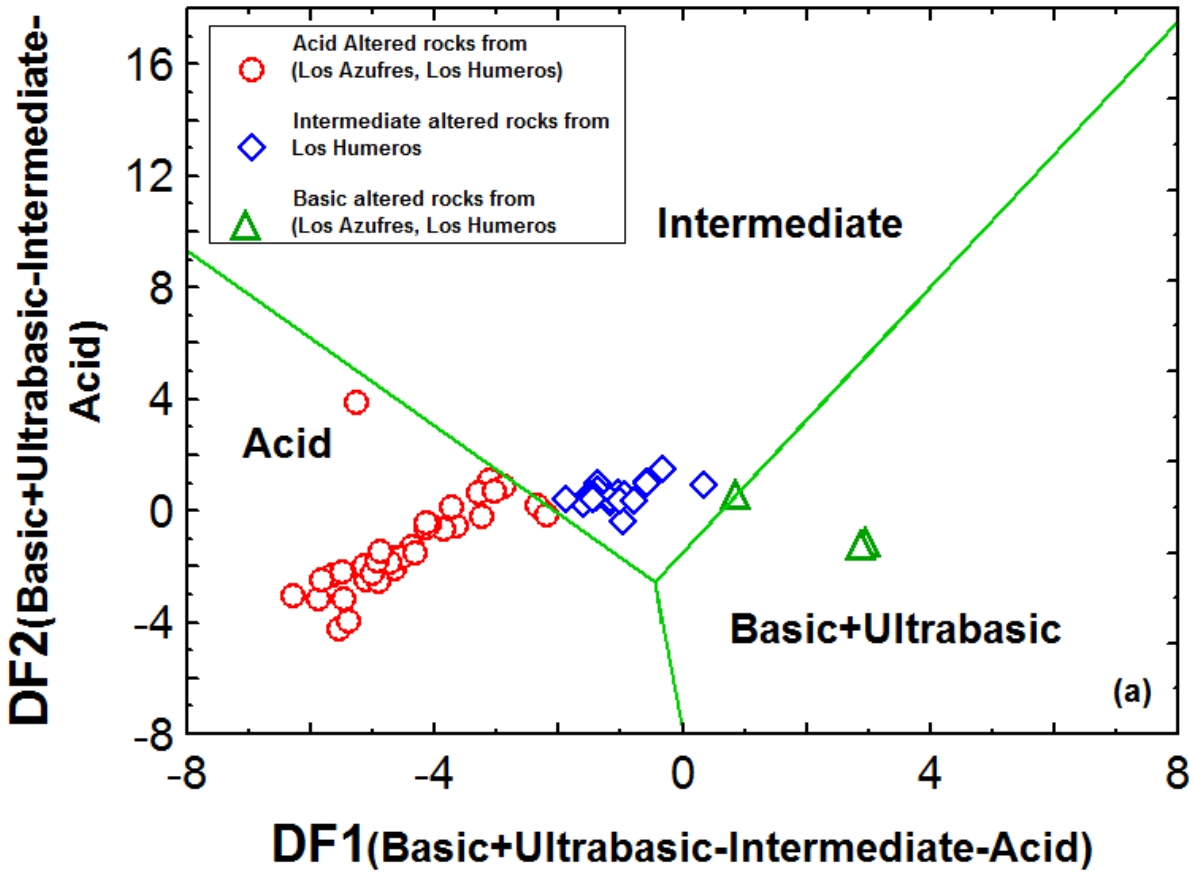

Figure 2a. The new discriminant-function, multi-dimensional diagram based on natural logarithm-transformed ratios of major elements for the classification of altered rocks, showing samples from the five case studies. The solid green lines represent discrimination boundaries for BASIC+ULTRABASIC–INTERMEDIATE–ACID (1+2–3–4) fields.

For the application of altered rocks, I classified, compile samples into basic magma (3 samples), intermediate magma (19 samples) and acid magma (34 samples) from new discriminant-function-based classification diagram in Figure 2a.

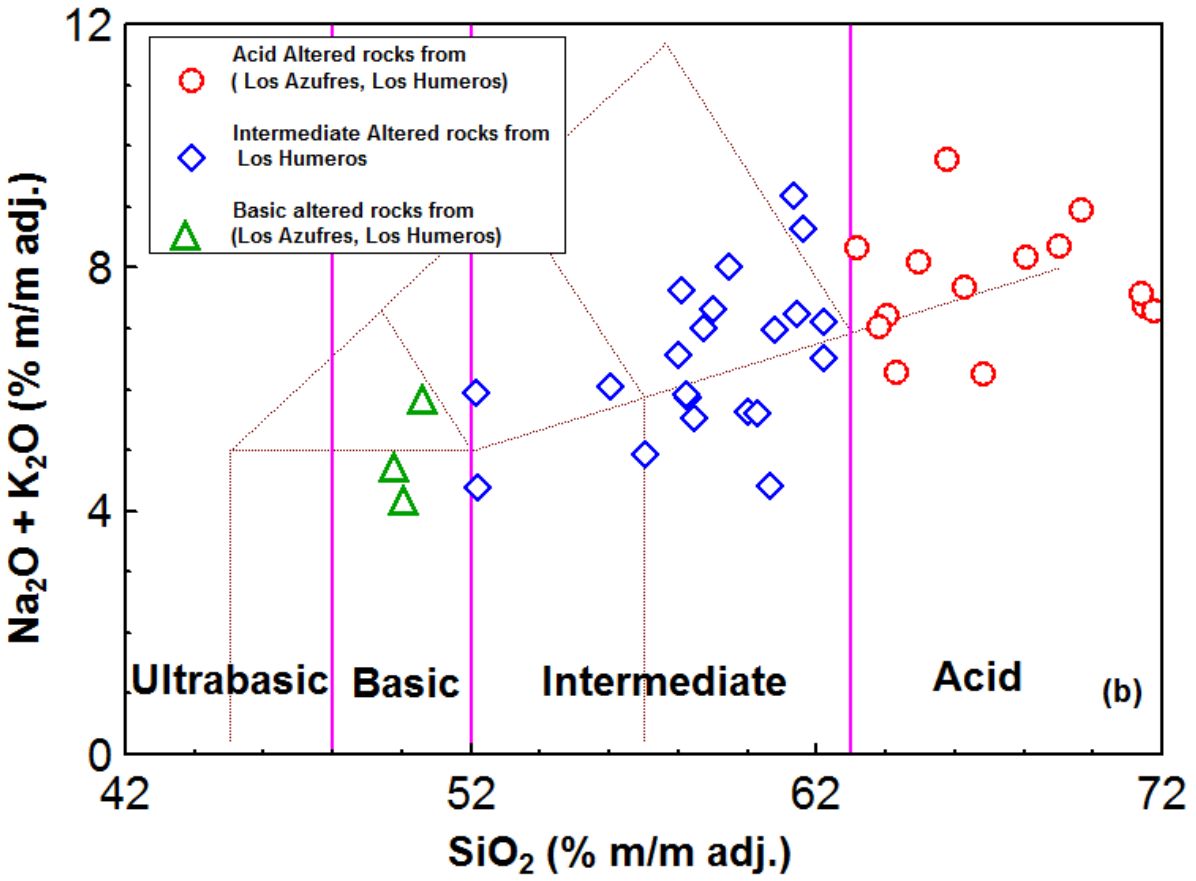

Figure 2b. Total Alkali versus Silica (TAS) classification diagram for altered rocks, showing samples from the five case studies. The solid pink lines represent field boundaries for ULTRABASIC–BASIC–INTERMEDIATE–ACID (1+2–3–4) fields.

Further, I plotted these samples in TAS diagram. For the basic magma, (3 out of 3 samples), plot in basic field (Fig. 2b; Table 2). For intermediate magmas (19 out of 19 samples) plot in intermediate filed. The same pattern is also repeated for acid magma (34 out of 34 samples) plot in acid field (Fig 2b; Table 2). For the TAS diagram, I obtained 100% success rate for all cases. Here, I used new discriminant-function-based multi-dimensional diagrams as a reference material for the TAS diagram.

Furthermore, I can say safely that the new discriminant-function-based multi-dimensional diagrams can be use for the fresh as well as altered rocks.

TABLE 2. APPLICATION OF DISCRIMINANT-FUNCTION-BASED CLASSIFICATION DIAGRAM FOR ALTERED ROCKS FROM LOS AZUFRES AND LOS HUMEROS FOR THE EVALUATION OF TAS DIAGRAM

Rocks Type	Total Number of samples in (Discriminant-function-based classification diagram*)	Rock Type in (TAS) diagram [Total Number of samples (%)]		
		Basic	Intermediate	Acid
Basic	3 (100)	3 (100)	0	0
Intermediate	19 (100)	0	19 (100)	0
Acid	34 (100)	0	0	34 (100)

* Discriminant-function-based classification diagram is reference material for the TAS diagram

For altered rocks, the number of samples is much more limited than for fresh rocks (Compare Tables 1 and 2) and most of them plot in the TAS diagram (Fig. 2b) well within the assumed fields of magma types. This may be the reason why all samples are equally well classified in both the new classification and TAS diagrams (Table 2). In order to better evaluate the functioning of the TAS diagram for altered rocks, we need to establish a world database having a much larger number of samples than Table 2. For the Mexican fresh and altered rocks compiled in this chapter, both diagrams seem to work well.

Finally, newer classification diagrams based on immobile elements should also be proposed in future.

6.3 Application of discrimination diagrams

For application of discrimination diagrams, I selected the same five case studies of Neogene rocks to illustrate the application and excellent functioning of the new multi-dimensional discrimination diagrams. The rocks were evaluated under the assumption of prevalence of plate tectonic processes and similar log-ratio geochemical variables for Neogene tectonic regimes. The plotting of samples in intermediate and acid diagrams (Fig. 3 and 4) can be fully replaced by probability calculations (Tables 3 and 4). In any discrimination diagram (Fig. 3a-e and Fig.4a-e) a sample will have probability values for all tectonic fields being discriminated, which will add up to 1.0000, and the sample will be plot in the field for which the probability is the highest. I also note that very few basic rock samples with complete data were available for this work. These samples were, therefore, not used for the evaluation of tectonic setting. Further, the basic rock samples from the Mexican Volcanic Belt were also extensively used and discussed in Chapter 3.

Importantly, besides the intermediate magma, contemporaneous acid magmas may also be present in a given area. In terms of the inferences based exclusively on discrimination diagrams, the inferences from the intermediate diagrams (Chapter 4) should be considered more reliable when the multi-dimensional diagrams for other magma varieties (acid by Verma *et al.* 2012) also provided consistent results.

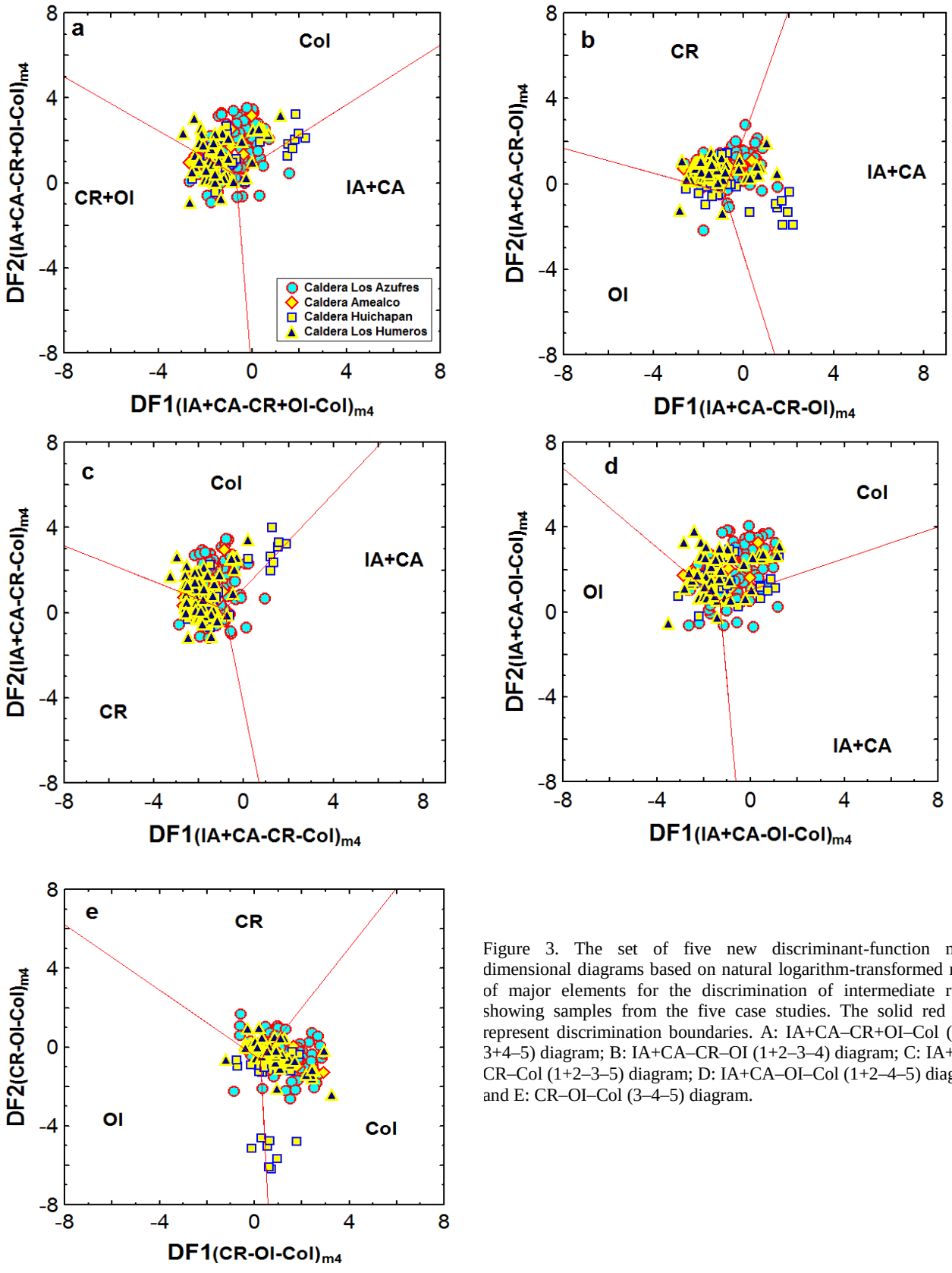

Figure 3. The set of five new discriminant-function multi-dimensional diagrams based on natural logarithm-transformed ratios of major elements for the discrimination of intermediate rocks, showing samples from the five case studies. The solid red lines represent discrimination boundaries. A: IA+CA–CR+OI–Col (1+2–3+4–5) diagram; B: IA+CA–CR–OI (1+2–3–4) diagram; C: IA+CA–CR–Col (1+2–3–5) diagram; D: IA+CA–OI–Col (1+2–4–5) diagram; and E: CR–OI–Col (3–4–5) diagram.

TABLE 3. APPLICATION OF THE SET OF FIVE DISCRIMINANT FUNCTION MULTI-DIMENSIONAL DIAGRAMS FOR INTERMEDIATE MAGMAS

(Case study no.) Locality (reference); age; inferred tectonic setting	Figure type§	Total number of samples	Number of discriminated samples				
			IA+CA (1+2) (%) [p_{IA+CA}] Θ	Within-plate			Col (5) (%) [p_{Col}] Θ
				CR+OI (3+4) (%)[p_{CR+OI}] Θ	CR (3) (%) [p_{CR}] Θ	OI (4) (%) [p_{OI}] Θ	
(1) Los Azufres geothermal field, Mexico (Dobson and Mahood 1985, Cathelineau *et al.* 1987, Pradal and Robin1994, Silva and Mora 1998, Verma *et al*. 2005, Pandarinath *et al.* 2008); Neogene; collision.	1+2-3+4-5	91 (100)	6 (6%) [0.4871, 0.9503]	16 (18%) [0.3653-0.9586]	---	---	***69*** (76%) [0.3649-0.9956]
	1+2-3-4*****	91 (100)	40 (44%) [0.4172-0.9960]	---	47 (52%) [0.4583-0.9208]	4 (4%) [0.4984,0.9569]	---
	1+2-3-5	91 (100)	9 (8%) [0.3632,0.9120]	---	18 (20%) [0.4401-0.9566]	---	***64*** (71%) [0.4158-0.9923]
	1+2-4-5	91 (100)	11 (12%) [0.4339-0.9749]	---	---	8 (9%) [0.6828,0.9895]	***72*** (79%) [0.4228-0.9994]
	3-4-5	91 (100)	---	---	20 (22%) [0.4091-0.8653]	4 (4%) [0.3986,0.9168]	***67*** (74%) [0.4565-0.9927]
(2) Amealco caldera, Mexico (Verma *et al*. 1991, Aguirre-Díaz and McDowell 2000, Aguirre-Díaz *et al.* 2002); Neogene; collision	1+2-3+4-5	16 (100)	0 (0%)	3 (19%) [0.5765,0.8060]	---	---	***13*** (81%) [0.5619-0.9977]
	1+2-3-4*****	16 (100)	2 (12%) [0.6534,0.8498]	---	14 (88%) [0.4547-0.7641]	0 (0%)	---
	1+2-3-5	16 (100)	0 (0%)	---	3 (19%) [0.5945,0.7677]	---	***13*** (81%) [0.5277-0.9842]
	1+2-4-5	16 (100)	0 (0%)	---	---	1 (6%) [0.6686]	***15*** (94%) [0.6665-0.9934]
	3-4-5	16 (100)	---	---	2 (13%) [0.4189-0.4270]	1 (6%) [0.4604]	***13*** (81%) [0.3819-0.9936]
(3) Huichapan caldera, Mexico (Verma 1991, Aguirre-Díaz and López-Martínez 2009); Neogene; collision	1+2-3+4-5	31(100)	6 (20%) [0.5514, 0.7796]	10 (32%) [0.4393,0.9412]	---	---	***15*** (48%) [0.4867- 0.9805]
	1+2-3-4*****	31(100)	10 (32%) [0.5047-0.9994]	---	16 (52%) [0.4043-0.8142]	5 (16%) [0.5703,0.7695]	---
	1+2-3-5	31(100)	4 (13%) [0.5116-0.6827]	---	9 (29%) [0.4413-0.9046]	---	***18*** (58%) [0.4950-0.9663]
	1+2-4-5	31(100)	5 (16%) [0.5182-0.7852]	---	---	5 (16%) [0.5047-0.9756]	***21*** (68%) [0.5153-0.9946]
	3-4-5	31(100)	---	---	3 (9) [0.3941-0.5453]	8 (26%) [0.3808-0.8165]	***20*** (65%) [0.4212-0.9738]
(4) Los Humeros geothermal field, Mexico (Demant 1981, Ferriz and Mahood 1987, Verma 2000); Neogene; collision	1+2-3+4-5	55	1 (2%) [0.5762]	25 (45%) [0.4460-9909]	---	---	***29*** (53%) [0.5201-0.9664]
	1+2-3-4*****	55	10 (18%) [0.6067-0.9934]	---	43 (78%) [0.4670- 0.9053]	2 (4%) [0.6437,0.9147]	---
	1+2-3-5	55	1 (2%) [0.4402]	---	22 (40%) [0.4833-0.9750]	---	***32*** (58%) [0.5008-0.9664]
	1+2-4-5	55	3 (5%) [0.5049-0.6681]	---	---	11 (20%) [0.3734-0.9993]	***41*** (75%) [0.4161-0.9977]
	3-4-5	55	---	---	25 (45%) [0.3796-0.7719]	3 (6%) [0.3898,0.7943]	***27*** (49%) [0.4090-0.9987]

§ Figure type refers to the tectonic fields being discriminated where the tectonic group numbers are as follows: 1–IA, 2–CA, 3–CR, 4–OI, 5–Col;

***** Inapplicable results and diagrams;

Θ Probability estimates for different tectonic groups are summarized after the number of discriminated samples as follows: [p_{IA+CA}]–range of probability values estimated for IA+CA settings, [p_{CR+OI}]–for CR+OI, [p_{CR}]–for CR, [p_{OI}]–for OI and [p_{Col}]–for Col. Boldface italic font shows the expected or more probable tectonic setting.

For the Sierra La Primavera in Mexico (Demant 1981; Mahood 1981), the present diagrams for acid magma (40 samples) indicated a rift setting, because the probabilities for 35 to 40 samples were highest for rift (0.4470-0.9950), whereas for the remaining 2 to 5 samples the probabilities were highest (0.4569-0.8657) as collision (Table 4; Fig. 4a, b, d, e,). Note that Figure 4c should be considered as the inapplicable diagram because the inferred tectonic setting of continental rift is missing from this diagram. There are no samples of intermediate rocks from this area. In summary, the acid rocks from the Sierra La Primavera show a continental rift setting because very high (86%-100%) success rates were shown for this field.

Most samples of intermediate magma for Neogene extrusive rocks of the Los Azufres geothermal field, Mexico (Dobson and Mahood 1985; Cathelineau *et al.* 1987; Pradal and Robin 1994; Silva and Mora 1998; Verma *et al.* 2005; Pandarinath *et al.* 2008) plotted in the collision setting (Fig. 3a,c-e) and showed high probabilities (0.3649-0.9994; Table 3) The collision setting was confirmed from the diagrams for acid magmas, because 43 to 52 (out of 77) samples plotted in this field (probabilities 0.4287-1.0000; Table 4; Fig. 4a, c-e). In summary, the intermediate and acid rocks from the Caldera de Los Azufres show a collision setting, because very high (71%-79%; Table 3) and (56%-68%; Table 4) success rates were shown of this field. This is an example where both sets of diagrams (intermediate and acid) provide consistent result.

Sixteen samples of Neogene intermediate magma from the Amealco caldera, Mexico (Verma *et al.* 1991, Aguirre-Díaz and McDowell 2000, Aguirre-Díaz *et al.* 2002), showed a collision setting (Fig. 3a, c-e). Thirteen to fifteen samples (81%-94%; Table 3) were discriminated as collision with high probabilities of 0.3819-0.9977, whereas two to three samples as continental rift. Out of 21 samples of acid magma from Amealco (Table 4), 10 to 17 samples (48%-81%) plotted in the continental arc field (probabilities 0.4465-0.9256), 4 to 9 samples (19%-43%; probabilities 0.3884-0.9214) in the continental rift field, and 4 to 7 samples (19%-33%; probabilities 0.4954-0.9577) in the collision setting.

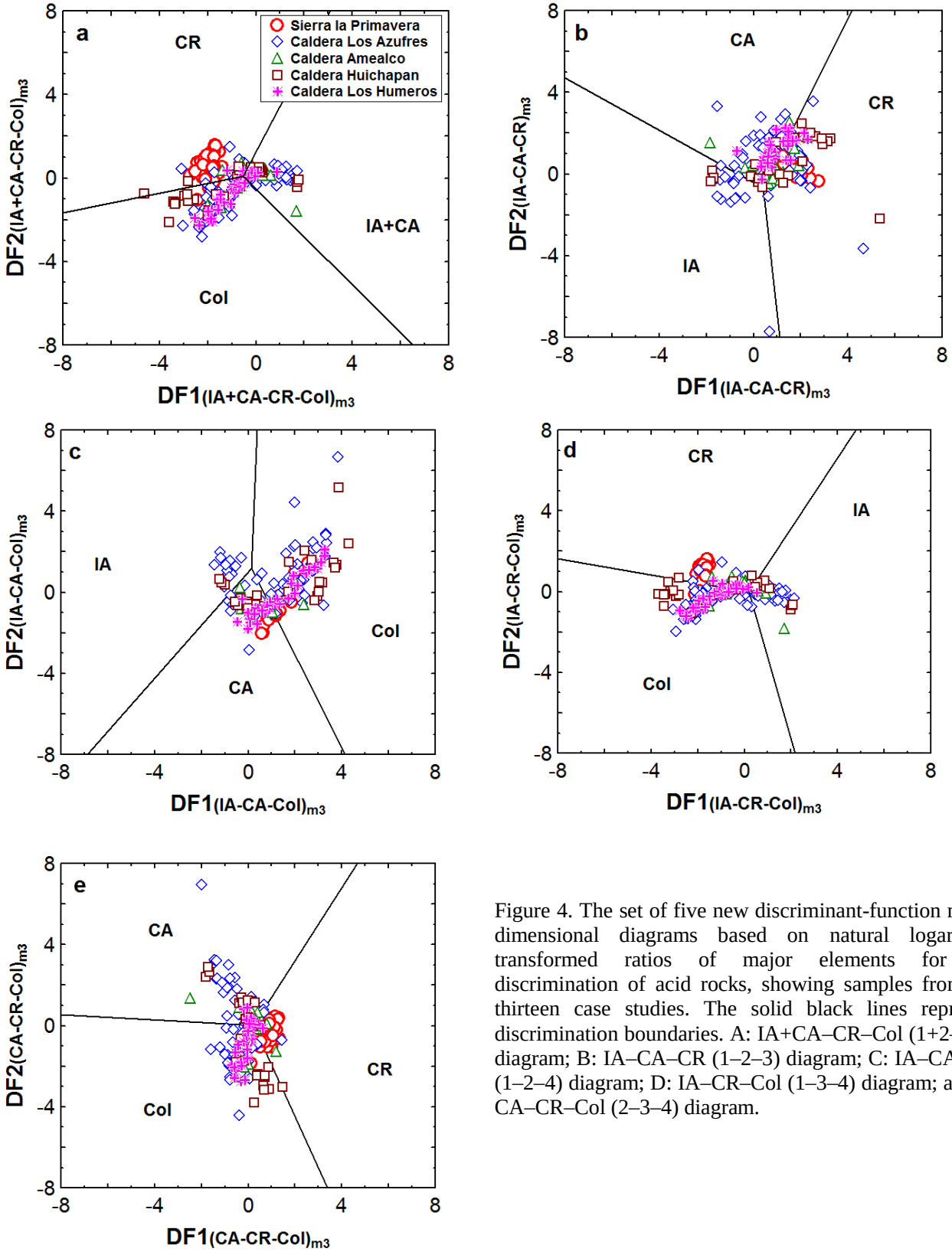

Figure 4. The set of five new discriminant-function multi-dimensional diagrams based on natural logarithm-transformed ratios of major elements for the discrimination of acid rocks, showing samples from the thirteen case studies. The solid black lines represent discrimination boundaries. A: IA+CA–CR–Col (1+2–3–4) diagram; B: IA–CA–CR (1–2–3) diagram; C: IA–CA–Col (1–2–4) diagram; D: IA–CR–Col (1–3–4) diagram; and E: CA–CR–Col (2–3–4) diagram.

Thus, even without considering Figure 4d, from which the continental arc setting is missing and in which the samples mostly plot in continental rift and collision settings, the number of samples plotting in these two (rift and collision) settings are significant (4 to 11; Table 4).In summary, the intermediate rocks from the Amealco show a more consistent result of a collision setting (Table 3). The acid rocks, on the other hand, show an arc setting but with much less success rate (48%-81% for acid rocks in Table 4 versus 81%-94% for intermediate rocks in Table 3).

Fifteen to twenty-one out of thirty-one samples of Neogene intermediate rock samples (48%-68%) from the Huichapan caldera, Mexico (Verma 1991; Aguirre-Díaz and López-Martínez 2009) showed high probabilities (0.4212-0.9946) for a collision tectonic setting (Table 3; Fig. 3a, c-e). Similarly, twenty-seven samples of acid magma confirmed the collision setting (high probabilities 0.4094-1.0000 for 13 or 14 samples (48%-52%) for the collision field; Table 4; Fig. 4a, c-e). In summary, the intermediate and acid rocks from the Huichapan caldera show a collision setting, because relatively high (48%-68%) and (48%-52%) success rates were shown for this field.

TABLE 4. APPLICATION OF THE SET OF FIVE DISCRIMINANT FUNCTION MULTI-DIMENSIONAL DIAGRAMS FOR ACID MAGMAS (VERMA *ET AL*. 2012)

(Case study no.) Locality; age; inferred tectonic setting	Figure type	Total number of samples	Number of discriminated samples				
			IA+CA (1+2) (%) [p_{IA+CA}]	IA (1) (%) [p_{IA}]	CA (2) (%) [p_{CA}]	CR (3) (%) [p_{CR}]	Col (4) (%) [p_{Col}]
(1) Sierra La Primavera, Mexico (Demant 1981; Mahood 1981); Neogene, 0.032-0.096 Ma; continental rift.	1+2-3-4	40 (100)	0 (0%)	---	---	***38*** (95%) [0.4948-0.9825]	2 (5%) [0.6531, 0.8657]
	1-2-3	40 (100)	---	0 (0%)	0 (0%)	***40*** (100%) [0.5353-0.9950]	---
	1-2-4*****	40 (100)	---	0 (0%)	13(33%) [0.4973-0.8449]	---	27 (67%) [0.4955- 0.9925]
	1-3-4	40 (100)	---	0 (0%)	---	***36*** (90%) [0.5081-0.9625]	4 (10%) [0.5242,0.8123]
	2-3-4	40 (100)	---	---	0 (0%)	***35*** (86%) [0.4470-0.8493]	5 (14%) [0.4569, 0.8651]
(2) Los Azufres geothermal field, Mexico (Dobson and Mahood 1985,Cathelineau *et al.* 1987, Pradal and Robin1994, Silva and Mora 1998, Verma *et al*. 2005, Pandarinath *et al.* 2008); Neogene; collision.	1+2-3-4	77 (100)	24 (31%) [0.5015-0.9845]	---	---	6 (8%) [0.4849,0.9384]	***47*** (61%) [0.4766-0.9986]
	1-2-3*****	77 (100)	---	16 (21%) [0.5237-0.9092]	37 (48%) [0.5177-0.9757]	24 (31%) [0.5602-1.0000]	---
	1-2-4	77 (100)	---	13 (17%) [0.6257-0.9122]	17 (22%) [0.4205-0.9536]	---	***47*** (61%) [0.5232-1.0000]
	1-3-4	77 (100)	---	20 (26%) [0.5506-0.9963]	---	5 (6%) [0.5285, 0.9540]	***52*** (68%) [0.4287-0.9985]
	2-3-4	77 (100)	---	---	30 (39%) [0.4325-1.0000]	4 (5%) [0.4110, 0.8776]	***43*** (56%) [0.4587-0.9959]
(3) Amealco Caldera, Mexico (Verma et al. 1991, Aguirre-Díaz and McDowell 2000, Aguirre-Díaz *et al.* 2002); Neogene; arc-rift	1+2-3-4	21(100)	***10*** (48%) [0.4343-0.8536]	---	---	4 (19%) [0.3884,0.7343]	7 (33%) [0.5972-0.9577]
	1-2-3	21(100)	---	0 (0%)	***12*** (57%) [0.4519-0.7371]	9 (43%) [0.4594,0.9214]	---
	1-2-4	21(100)	---	0 (0%)	***17*** (81%) [0.5096-0.8165]	---	4 (19%) [0.4954,0.9566]
	1-3-4*****	21(100)	---	4 (19%) [0.6160,0.9754]	---	10 (48%) [0.5473-0.8025]	7 (33%) [0.6632,0.9341]
	2-3-4	21(100)	---	---	***10*** (48%) [0.4465-0.9256]	4 (19%) [0.4144,0.7379]	7 (33%) [0.5487,0.9341]
(4) Huichapan caldera, Mexico (Verma 1991, Aguirre-Díaz and López-Martínez 2009); Neogene; collision	1+2-3-4	27 (100)	9 (33%) [0.5105, 0.9793]	---	---	5 (19%) [0.4006-0.6838]	***13*** (48%) [0.4094-0.9838]
	1-2-3 *****	27 (100)	---	3 (11%) [0.6797, 0.8185]	8 (30%) [0.4425, 0.7119]	15 (59%) [0.6385-1.0000]	---
	1-2-4	27 (100)	---	3 (11%) [0.6417, 0.7613]	10 (37%) [0.5901- 0.7628]	---	***14***(52%) [0.8810-1.0000]
	1-3-4	27 (100)	---	9 (33%) [0.4980, 0.9966]	---	4 (15%) [0.5331,0.7076]	***14***(52%) [0.4747-0.9786]
	2-3-4	27 (100)	---	---	12 (45%) [0.4167- 0.9968]	2 (7%) [0.4962,0.5242]	***13*** (48%) [0.5900-0.9683]
(5) Los Humeros geothermal field, Mexico (Demant 1981, Ferriz and Mahood 1987, Verma 2000); Neogene; collision	1+2-3-4	50 (100)	10 (20%) [0.3890-0.9160]	---	---	2 (4%) [0.4160,0.6689]	***38*** (76%) [0.3777-0.9947]
	1-2-3 *****	50 (100)	---	0 (0%)	37 (74%) [0.4526- 0.8221]	13 (26%) [0.5261-0.8927]	---
	1-2-4	50 (100)	---	0 (0%)	24 (48%) [0.4924- 0.8902]	---	***26*** (52%) [0.5005-1.0000]
	1-3-4	50 (100)	---	0 (0%)	---	12 (24%) [0.4526-0.6553]	***38*** (76%) [0.4856-0.9896]
	2-3-4	50 (100)	---	---	10 (24%) [0.3366- 0.7456]	2 (10%) [0.4489,0.5682]	***38*** (76%) [0.3902-0.9827]

Figure type refers to the tectonic fields being discriminated where the tectonic group numbers are as follows: 1–IA, 2–CA, 3–CR, 4–Col; *–inapplicable results and diagrams; boldface italic font shows the expected or more probable tectonic setting; the probability estimates for the different tectonic groups are summarized after the number of discriminated samples as follows: [pIA+CA]–range of probability values estimated for IA+CA settings, [pIA]–for IA, [pCA]–for CA, [pCR]–for CR and [pCol]–for Col.

For the Neogene magma of the Los Humeros caldera or geothermal field, Mexico (Demant 1981; Ferriz and Mahood 1987; Verma 2000), the present diagrams for intermediate magma indicated a collision setting, because the probabilities for 27 to 41 (out of 55; 53%-75%) samples were highest for collision (0.4090-0.9977), whereas for the remaining 22 to 25 samples (40%-45%) the probabilities were highest (0.3796-0.9756) for continental rift (Table 3; Fig. 3a, c-e, with Fig. 3b considered as the inapplicable diagram). A collision setting was also indicated from multi-dimensional diagrams based on major elements in acid magmas (Verma *et al.* 2012), because 26 to 38 samples (out of 50; 52%-76%) were discriminated as collision (probabilities 0.3777-1.0000; Table 4; Fig. 4a, c-e). In summary, the intermediate and acid rocks from the Los Humeros caldera show a collision setting because high (49%-75%) and (52%-76%) success rates were shown of this field.

6.4 Conclusions

A new classification diagram has been used for five case studies; consistent results were obtained for these applications. Furthermore, probability-based boundaries and associated sample probability calculations (as a replacement for plotting samples), are shown to work well for relatively fresh rocks of Neogene age from several areas of Mexico. They can be similarly used to decipher tectonic settings of geothermally altered rocks as well as old or tectonically complex areas.

Chapter 7

Application of multi-dimensional discrimination diagrams for Archean rocks

7.1 Antecedents

This chapter is based on the following publication, in which the author of this thesis actively participated. This paper is listed in the Science Citation Index (as a journal).

Appendix VI:

Verma, S K and Verma, S.P. (2012). Identification of plate tectonic processes in the Archean from multi-dimensional discrimination diagrams and probability calculations. **International Geology Review**. DOI: 10.1080/00206814.2012.693246, ISSN 0020-6814 print/ISSN 1938-2839 online.

7.2 Introduction

Once the application of the discrimination and classification diagrams has been well documented for energy research, it will be a good idea to explore other applications to older rocks as well. Numerous mineral resources are housed in such old

rocks. Therefore, I present application of all multi-dimensional diagrams to Archean rocks from different areas of the world.

With the renewed interest in how far back in time we can track modern-style plate tectonics, we might ask where we should go from here. Such a challenge bringing about renewed efforts to understand if and how the Archean differs from later time in the Earth's history. A wealth of geological, geochemical, structural, volcanologic, and geodynamic evidence seems to demand the operation of plate tectonics in the late Archean (e.g., Condie and Pease 2008; Ernst 2009; Van Kranendonk 2010). There are some similarities of the Archean with modern-style plate tectonics. However, the new multi-dimensional discrimination diagrams proposed during 2006-2012 by the Geoenergy group of Centro de Investigación en Energía (UNAM) have been seldom used for Archean rocks. For more information, see Appendices VI. Therefore, I decided to estimate the usefulness of these diagrams for Archean rocks from different cratons.

7.3 Databases for application to Archean rocks from different parts of world

For the application of the new multi-dimensional discrimination diagrams, I compiled age and geochemical data for Archean rocks from Australia, South Africa, Brazil, Canada, and India (Appendices VI). For the subdivision of the Archean, I followed the scheme proposed by the International Commission on Stratigraphy (Gradstein et al. 2004) (Appendix VI).

7.4 Results of Application

For the eastern part of the Pilbara craton (Australia), a Paleoarchean (3570-3450 Ma) and Mesoarchean (2900 Ma) continental arc setting apparently evolved to a collision setting during the Neoarchean (2600 Ma). I infer an island arc environment for Kambalda (Australia) during the Neoarchean (2700 Ma). For the Barberton belt (South Africa), transition from a mid-ocean ridge regime during the older part of the

Paleoarchean (3470 Ma) to an island arc setting during the younger part (3300-3260 Ma) is likely. I inferred an arc environment for the São Francisco craton (Brazil) and the Rio Maria terrane (Brazil) during the Mesoarchean (3085-2983 Ma and 2870 Ma, respectively), whereas a within-plate setting is clearly indicated for the Carajás metallogenic province (Brazil) during the Neoarchean (2740-2700 Ma). I also recognize an island arc regime for the Mesoarchean (3000 Ma) North Caribou and Neoarchean (2700 Ma) Abitibi greenstone belts (Canada), and for the Gadwal greenstone belt (India) during the Neoarchean (2700-2500 Ma). A collision setting was inferred for the Archean sanukitoid suite (Canada) and the Kolar suture zone (India) during the Neoarchean (2700-2660 Ma and 2630-2520 Ma, respectively (Appendix VI).

7.5 Conclusions

The Applications of new multi-dimensional diagrams (proposed by our group during 2006-2012), based on natural logarithms of element ratios and linear discriminant analysis, to Archean igneous rocks from Australia, South Africa, Brazil, Canada and India have been successfully documented. Probability calculations have been shown to successfully replace the newer diagrams proposed during 2011-2012. Therefore, such probability-based methods, proposed and used by Verma (2012) and also practiced in this work, are likely to open new ways of interpreting geochemical data (Appendix VI).

References

References

Agostini, S., Corti, G., Doglioni, C., Carminati, E., Innocenti, F., Tonarini, S., Manetti, P., Di Vincenzo, G., Montanari, D., 2006. Tectonic and magmatic evolution of the active volcanic front in El Salvador: insight into the Berlín and Ahuachapán geothermal areas: Geothermics, v. 35, p. 368-408.

Agrawal, S., 1999. Geochemical discrimination diagrams: a simple way of replacing eye-fitted boundaries with probability based classifier surfaces: Journal of the Geological Society of India, v. 54, p. 335-346.

Agrawal, S., Guevara, M., Verma, S.P., 2004. Discriminant analysis applied to establish major-element field boundaries for tectonic varieties of basic rocks: International Geology Review, v. 46, p. 575-594.

Agrawal, S., Guevara, M., Verma, S.P., 2008. Tectonic discrimination of basic and ultrabasic rocks through log-transformed ratios of immobile trace elements: International Geology Review, v. 50, p. 1057-1079.

Agrawal, S., Verma, S.P., 2007, Comment on "Tectonic classification of basalts with classification trees" by Pieter Vermeesch (2006): Geochimica et Cosmochimica Acta, v. 71, p. 3388-3390.

Aguirre-Díaz, G. J. López-Martínez, M., 2009. Geologic evolution of the Donguinyó-Huichapan caldera complex, central Mexican Volcanic Belt, Mexico: Journal of Volcanology and Geothermal Research, v. 179, p. 133-148.

Aguirre-Díaz, G. J. McDowell, F. W., 2000. Volcanic evolution of the Amealco caldera, Central Mexico. Cenozoic tectonics and volcanism of Mexico: H. Delgado-Granados, G. Aguirre-Díaz and J. M. Stock: GSA. Special paper, v.334, p. 179-193.

Aguirre-Díaz, G. J., Dubois M., Lozano-SantaCruz, R., López-Martínez, M., 2002. Nature and P-T conditions of the crust beneath the central Mexican Volcanic Belt based on a Precambrian crustal xenoliths: International Geology Review, v. 44, p. 222-242.

Aitchison, J., 1981. A new approach to null correlations of proportions: Mathematical Geology v. 13, p. 175-189.

Aitchison, J., 1986. The statistical analysis of compositional data: London, Chapman and Hall, 416 p.

Alam, M.A., Chandrasekharam, D., Vaselli, O., Capaccioni, B., Manetti, P., Santo, P.B., 2004, Petrology of the prehistoric lavas and dyke of the Barren island, Andaman sea, Indian ocean: Proceedings of the Indian Academy of Sciences (Earth and Planetary Sciences), v. 113, p. 715-722.

Aldanmaz, E., Pearce, J.A., Thirlwall, M.F., Mitchell, J.G., 2000, Petrogenetic evolution of late Cenozoic, post-collision volcanism in western Anatolia, Turkey: Journal of Volcanology and Geothermal Research, v. 102, p. 67-95.

Alvarado, G.E., Soto, G.J., Schmincke, H.-U., Bolge, L.L., Sumita, M., 2006. The 1968 andesitic lateral blast eruption at Arenal volcano, Costa Rica: Journal of Volcanology and Geothermal Research, v. 157, p. 9-33.

Arai, S., Okamura, H., Kadoshima, K., Tanaka, Ch., Suzuki, K., Ishimaru, S., 2011. Chemical characteristics of chromian spinel in plutonic rocks: implications for deep magma processes and discrimination of tectonic setting: Island Arc, v. 20, p. 125-137.

Armstrong-Altrin, J. S., Verma., S. P., 2005. Critical evaluation of six tectonic setting discrimination diagrams using geochemical data of Neogene sediments from known tectonic settings: Sedimentary Geology, v. 177, p. 115-129.

Auchapt, A., Dupuy, C., Dostal, J., Kanika, M., 1987. Geochemistry and petrogenesis of rift-related volcanic rocks from South Kivi (Zaire): Journal of Volcanology and Geothermal Research, v. 31, p. 33-46.

Bailey, J.C., 1981. Geochemical criteria for a refined tectonic discrimination of orogenic andesites: Chemical Geology, v. 32, p. 139-154.

Banerjee, R., Shivkumar, K., 2010. Geochemistry and petrogenesis of radioactive Palaeoproterozoic granitoids of Kinwat crystalline inlier, Nanded and Yeotmal districts, Maharashtra: Journal of the Geological Society of India, v. 75, p. 596-617.

Barberi, F., Ferrara, G., Santacroce, R., Treuil, M., Varet, J., 1975. A transitional basalt-pantellerite sequence of fractional crystallization, the Boina centre (Afar rift, Ethiopia): Journal of Petrology, v. 16, p. 22-56.

Bardintzeff, J.M., Deniel, C., 1992. Magmatic evolution of Pacaya and Cerro Chiquito volcanological complex, Guatemala: Bulletin of Volcanology, v. 54, p. 267-283.

Barling, J., Goldstein, S.L., Nicholls, I.A., 1994. Geochemistry of Heard Island (Southern Indian Ocean): characterization of an enriched mantle component and implication for enrichment of the Sub-Indian ocean mantle: Journal of Petrology, v. 35, p. 1017-1053.

Barnett, V., Lewis, T., 1994. Outliers in statistical data: Chichester, John Wiley, and Sons, 584 p.

Barsdell, M., 1988. Petrology and petrogenesis of clinopyroxene-rich tholeiitic lavas, Merelava volcano, Vanuatu: Journal of Petrology, v. 29, p. 927-964.

Barsdell, M., Berry, R.F., 1990. Origin and evolution of primitive island arc ankaramites from western Epi, Vanuatu: Journal of Petrology, v. 31, p. 747-777.

Basu, A.R., Junwen, W., Wankang, H., Guanghong, X., Tatsumoto, M., 1991. Major element, REE, and Pb, Nd and Sr isotopic geochemistry of Cenozoic volcanic rocks of eastern China: implications for their origin from suboceanic-type mantle reservoirs: Earth and Planetary Science Letters, v. 105, p. 149-169.

Bau, M., Knittel, U., 1993. Significance of slab-derived partial melts and aqueous fluids for the genesis of tholeiitic and calc-alkaline island-arc basalts: evidence from Mt. Arayat, Philippines: Chemical Geology, v. 105, p. 233-251.

Beier, C., Haase, K.M., Hansteen, T.H., 2006. Magma Evolution of the Sete Cidades Volcano, São Miguel, Azores: Journal of Petrology, v. 47, p. 1375-1411.

Bell, K., Peterson, T., 1991. Nd and Sr isotopic systematics of Shombole volcano, East Africa, and the links between nephelinites, phonolites, and carbonatites: Geology, v. 19, p. 582-585.

Benito, R., López-Ruiz, J., Cebriá, J.M., Hertogen, J., Doblas, M., Oyarzum, R., Demaiffe, D., 1999. Sr and O isotope constraints on source and crustal contamination in the high-K calc-alkaline and shoshonitic Neogene volcanic rocks of SE Spain: Lithos, v. 46, p. 773-802.

Benoit, M., Robles, A.A., Calmus, T., Maury, R.C., Bellon , H., Cotten, J., J., B., Michaud, F., 2002. Geochemical Diversity of Late Miocene Volcanism in Southern Baja California, México: Implication of Mantle and Crustal Sources during the Opening of an Asthenospheric Window: Journal of Geology, v. 110, p. 627-648.

Bertrand, H., 1991. The Mesozoic tholeiitic province of northwest Africa: a volcano-tectonic record of the early opening of Central Atlantic. In: A.B. Kampunzu and R.T. Lubala (Editors), Magmatism in extensional structural settings. Springer Verlag, Berlin, Germany, pp. 147-188.

Bhatia, M. R., 1983. Plate tectonics and geochemical composition of sandstones: Journal of Geology, v. 91, p. 611-627.

Bhushan, S. K., Chandrasekaran, V., 2002. Geology and geochemistry of the magmatic rocks of the Malani igneous suite and Tertiary volcanic province of western Rajasthan: Memoirs of Geological Survey of India, v. 126, p. 1-180.

Bloomer, S.H., Stern, R.J., Fisk, E., Geschwind, C.H., 1989. Shoshonitic volcanism in the northern Mariana arc. 1. Mineralogic and major and trace element characteristics: Journal of Geophysical Research, v. 94, p. 4469-4496.

Blum, N., Halbach, P., Münch, U., 1996. Geochemistry and mineralogy of alkali basalts from Tropic Seamount, central Atlantic Ocean: Marine Geology, v. 136, p. 1-19.

Bohrson, W.A., Reid, M.R., 1995. Petrogenesis of alkaline basalts from Socorro Island, Mexico: Trace element evidence for contamination of ocean island basalt in the shallow ocean crust. Journal of Geophysical Research, v. 100, p. 24555-24576.

Bolge, L.L., Carr, M.J., Feigenson, M.D., Alvarado, G.E., 2006. Geochemical stratigraphy and magmatic evolution at Arenal volcano, Costa Rica: Journal of Volcanology and Geothermal Research, v. 157 34-48.

Brophy, J.G., 1986. The Cold Bay volcanic center, Aleutian volcanic arc. I. Implications for the origin of hi-alumina arc basalt: Contributions to Mineralogy and Petrology, v. 93, p. 368-380.

Brown, A.V., Jenner, G.A., 1989, Geological setting, petrology and chemistry of Cambrian boninite and low-Ti tholeiite lavas in western Tasmania, in Crawford, A.J., Boninites: London, Unwin Hyman, p. 233-263.

Brown, G.M., Holland, J.G., Sigurdsson, H., Tomblin, J.F., Arculus, R.J., 1977. Geochemistry of the Lesser Antilles volcanic island arc: Geochimica et Cosmochimica Acta, v. 41, p. 785-801.

Bruni, S., D'Orazio, M., Haller, M.J., Innocenti, F., Manetti, P., Pécskay, Z., Tonarini, S., 2008. Time-evolution of magma sources in a continental back-arc setting: the Cenozoic basalts from Sierra de San bernardo (Patagonia, Chubut, Argentina): Geological Magazine, v. 145, p. 714-732.

Bryan, W.B., Stice, G.D., Ewart, A., 1972. Geology, petrography, and geochemistry of the volcanic islands of Tonga: Journal of Geophysical Research, v. 77, p. 1566-1585.

Buket, E., Temel, A., 1998. Major-element, trace-element, and Sr-Nd isotopic geochemistry and genesis of Varto (Mus) volcanic rocks, Eastern Turkey: Journal of Volcanology and Geothermal Research, v. 85, p. 405-422.

Butler, J. C. Woronow, A., 1986. Discrimination among tectonic settings using trace element abundances of basalts: Journal of Geophysical Research, v. 91, p. 10289-10300.

Butler, J. C., 1979. Trends in ternary petrologic variation diagrams - fact or fantasy?: American Mineralogist, v. 64, p. 1115-1121.

Butler, J. C., 1986. The role of spurius correlation in the development of a komatiite alteration model: Journal of Geophysical Research, v. 91, p. 275-E280.

Butler, J.C., Woronow, A., 1986. Discrimination among tectonic settings using trace element abundances of basalts: Journal of Geophysical Research, v. 91, p. B10289-B10300.

Butler., 1986. The role of spurious correlation in the development of a komatiite alteration model: Journal of Geophysical Research, v. 91, p. E275-E280.

Cabanis, B., Lecolle, M., 1989. Le diagramme La/10-Y/15-Nb/8: un outil pour la discrimination des séries volcaniques et la mise en évidence des processus de mélange et/ou de contamination crustale: C.R. Acad. Sci. Paris, v. 309, p. 2023-2029.

Calmus, T., Aguillón-Robles, A., Maury, R.C., Bellon , H., Benoit, M., Cotten, J., Bourgois, J., Michaud, F., 2003. Spatial and temporal evolution of basalts and magnesian andesites ("Bajaites") from Baja California, Mexico: the role of slab melts: Lithos, v. 66, p. 77-105.

Cameron, B.I., Walker, J.A., Carr, M.J., Patino, L.C., Matías, O., Feigenson, M.D., 2002. Flux versus decompression melting at stratovolcanoes in southestern Guatemala: Journal of Volcanology and Geothermal Research, v. 119, p. 21-50.

Camp, V.E., Roobol, M.J., Hooper, P.R., 1991. The Arabian continental alkali basalt province: part II. Evolution of Harrats Khaybar, Ithnayn, and Kura, Kingdom of Saudi Arabia. Geological Society of America Bulletin, v. 103, p. 363-391.

Carr, M.J., 1984. Symmetrical and segmented variation of physical and geochemical characteristics of the Central American volcanic front: Journal of Volcanology and Geothermal Research, v. 20: 231-252.

Carr, M.J., Feigenson, M.D., Bennett, E.A., 1990. Incompatible element and isotopic evidence for tectonic control of source mixing and melt extraction along the Central American arc: Contributions to Mineralogy and Petrology, v. 105, p. 369-380.

Castillo, P.R., Newhall, C.G., 2004. Geochemical constraints on possible subduction components in lavas of Mayon and Taal volcanoes, southern Luzon, Philippines: Journal of Petrology, v. 45, p. 1089-1108.

Cathelineau, M., R. Oliver., Nieva, D., 1987. Geochemistry of volcanic series of the Los Azufres geothermal field (Mexico): Geofísica Internacional, v. 26, p. 273-290.

Chan, L.H., Leeman, W.P., You, C.-F., 1999. Lithium isotopic composition of Central American Volcanic Arc lavas: implications for modification of subarc mantle by slab-derived fluids: Chemical Geology, v. 160, p. 255-280.

Chauvel, C., Jahn, B.-M., 1984. Nd-Sr isotope and REE geochemistry of alkali basalts from the Massif Central, France: Geochimica et Cosmochimica Acta, v. 48, p. 93-110.

Chayes, F., 1960. On correlation between variables of constant sum: Journal of Geophysical Research, v. 65, p. 4185-4193.

Chayes, F., 1978. Ratio correlation. A manual for students of petrology and geochemistry: Chicago and London, The University of Chicago Press.

Chayes, F., Velde, D., 1965. On distinguishing basaltic lavas of circumoceanic and oceanic-island type by means of discriminant functions: American Journal of Science, v. 263, p 206-222.

Chen, C.-Y., Frey, F.A., Garcia, M.O., 1990. Evolution of alkalic lavas at Heleakala volcano, east Maui, Hawaii: Contributions to Mineralogy and Petrology, v. 105, p. 197-218.

Cheng, Q.C., Macdougall, J.D., Lugmair, G.W., 1993. Geochemical studies of Tahiti, Teahitia and Mahetia, Society Island Chain: Journal of Volcanology and Geothermal Research, v. 55, p. 155-184.

Chung, S.L., Jahn, B.M., Chen, S.J., Lee, T., Chen, C. H., 1995. Miocene basalts in northwestern Taiwan: Evidence for EM-type mantle sources in the continental lithosphere: Geochimica et Cosmochimica Acta, v. 59, p. 549-555.

Churikova, T., Dorendorf, F., Wörner, G., 2001. Sources and fluids in the mantle wedge below Kamchatka, evidence from across-arc geochemical variation: Journal of Petrology, v. 42: 1567-1593.

Cole, J.W., 1981. Genesis of lavas of the Taupo volcanic zone, North Island, New Zealand: Journal of Volcanology and Geothermal Research, v. 10, p. 317-337.

Collins, P. E. F., Rust, D. J., Bayraktutan, M. S., 2008.Geomorphological evidence for a changing tectonic regime, Pasinler Basin, Turkey: Journal of the Geological Society, London, v. 165, p. 849-857.

Condie, K.C., and Pease, V., 2008, Preface, in Condie, K.C., and Pease, V., eds., When did plate tectonics begin on planet Earth?: Boulder, Colorado, Geological Society of America Special Paper, v. 440, p. v-viii.

Cousens, B.L., Clague A., D., Sharp, W.D., 2003. Chronology, chemistry and origin of trachytes from Hualalai Volcano, Hawaii: Geochemistry Geophysics Geosystems, v. 4: 1078, doi: 10.1029/2003GC000560.

Cox, K. G., Bell, J. D., Pankhurst, R. J., 1979. The interpretation of igneous rocks: London, George Allen & Unwin, 450 p.

Davidson, J.P., Ferguson, K.M., Colucci, M.T., Dungan, M.A., 1988. The origin and evolution of magmas from the San Pedro-Pellado volcanic complex, S. Chile: multicomponent sources and open system evolution: Contributions of Mineralogy and Petrology, v. 100, p. 429-445.

Davidson, J.P., Wilson, I.R., 1989. Evolution of an alkali basalt-trachyte suite from Jebel Marra volcano, Sudan, through assimilation and fractional crystallization: Earth and Planetary Science Letters, v. 95, p. 141-160.

De la Roche H., Leterrier, J., Grande Claude, P., Marchal, M., 1980. A classification of volcanic and plutonic rocks using R1-R2 diagrams and major element analyses-its relationships and current nomenclature. Chemical Geology, v. 29, p. 183-210.

de Moor, J.M., Fischer, T.P., Hilton, D.R., Hauri, E., Jaffe, L.A., Camacho, J.T., 2005. Degassing at Anathan volcano during the May 2003 eruption: implications from petrology, ash leachates, and SiO2 emissions: Journal of Volcanology and Geothermal Research, v. 146, p. 117-138.

de Mulder, M., Hertogen, J., Deutsch, S., André, L., 1986. The role of crustal contamination in the potassic suite of the Karisimbi volcano (Virunga, African Rift Valley): Chemical Geology, v. 57: 117-136.

De Silva, S.L., 1991. Styles of zoning in central Andean ignimbrites: insights into magma chamber processes: Geological Society of America Special Paper 265, p. 217-232.

Debon, F., Lemmet, M., 1999, Evolution of Mg/Fe ratios in Late Variscan plutonic rocks from the External Crystalline Massifs of the Alps (France, Italy, Switzerland): Journal of Petrology, v. 40, p. 1151-1185.

Defant, M.J., Clark, L.F., Stewart, R.H., Drummond, M.S., De Boer, J.Z., Maury, R.C., Bellon, H., Jackson, T.E., Restrepo, J.F., 1991b. Andesite and dacite genesis via contrasting processes: the geology and geochemistry of El Valle Volcano, Panama: Contributions to Mineralogy and Petrology, v. 106, p. 309-324.

Defant, M.J., Jacques, D., Maury, R.C., De Boer, J., Joron, J. L., 1989. Geochemistry and tectonic setting of the Luzon arc, Philippines: Geological Society of America Bulletin, v. 101, p. 663-672.

Defant, M.J., Maury, R.C., Ripley, E.M., Feigenson, M.D., Jacques, D., 1991a. An example of island-arc petrogenesis: goechemistry and petrology of the southern Luzon arc, Philippines: Journal of Petrology, v. 32, p. 455-500.

Defant, M.J., Richerson, P.M., De Boer, J.Z., Stewart, R.H., Maury, R.C., Bellon, H., Drummond, M.S., Feigenson, M.D., Jackson, T.E., 1991c. Dacite genesis via both slab melting and differentiation: petrogenesis of La Yeguada volcanic complex, Panama: Journal of Petrology, v. 32, p. 1101-1142.

Defant, M.J., Sherman, S., Maury, R.C., Bellon, H., de Boer, J., Davidson, J., Kepezhinskas, P., 2001. The geology, petrology, and petrogenesis of Saba Island, Lesser Antilles: Journal of Volcanology and Geothermal Research, v. 107, p. 87-111.

Demant, A., 1981. L'axe néo-volcanique transmexicain, étude volcanologique et pétrographique, signification géodynamique: Faculté des Sciences et Techniques de St. Jérome, Université de Droit, d'Economie et des Sciences d'Aix-Marseille.

Deniel, C., Vidal, P., Coulon, C., Vellutini, P., Piguet, P., 1994. Temporal evolution of mantle sources during continental rifting: The volcanism of Djibouti (Afar): Journal of Geophysical Research, v. 99, p. 2853-2869.

Déruelle, B., 1982. Petrology of the Plio-Quaternary volcanism of the south-central and meridional Andes: Journal of Volcanology and Geothermal Research, v. 14, p. 77-124.

Déruelle, B., 1991. Petrology of Quaternary shoshonitic lavas of northwestern Argentina: Geological Society of America Special Paper 265: 201-216.

Déruelle, B., Moreau, C., Nkoumbou, C., Kambou, R., Lissom, J., Njonfang, E., Ghogomu, R.T., Nono, A., 1991. The Cameron line: a review. In: A.B. Kampunzu and R.T. Lubala (Editors), Magmatism in extensional structural settings. Springer Verlag, Berlin, Germany: p. 274-327.

Dilek, Y., Imamverdiyev, N., Altunkaynak, S., 2010. Geochemistry and tectonics of Cenozoic volcanism in the Lesser Caucasus (Azerbaijan) and the peri-Arabian region: collision-induced mantle dynamics and its magmatic fingerprint: International Geology Review, v. 52, p. 536-578.

Dini, A., Innocenti, F., Rocchi, S., Tonarini, S., Westerman, D.S., 2002. The magmatic evolution of the late Miocene laccolith-pluton-dyke granitic complex of Elba Island, Italy: Geological Magazine, v. 139, p. 257-279.

Dobson, P. F. Mahood, G. A., 1985. Volcanic stratigraphy of the Los Azufres geothermal area, Mexico: Journal of Volcanology and Geothermal Research, v. 25, p. 273-287.

Dorendorf, F., Churikova, T., Koloskov, A., Wörner, G., 2000. Late Pliocene to Holocene activity at Bakening volcano and surrounding monogenetic centers (Kamchatka): volcanic geology and geochemical evolution: Journal of Volcanology and Geothermal Research, v. 104, p. 131-151.

Duffield, W.A., Heiken, G.H., Wohletz, K.H., Maassen, L.W., Dengo, G., McKee, E.H., Castañeda, O., 1992. Geology and geothermal potential of the Tecuamburro volcano area, Guatemala: Geothermics, v. 21, p. 425-446.

DuFrane, S.A., Asmerom, Y., Mukasa, S.B., Morris, J.D., Dreyer, B.M., 2006. Subduction and melting processes inferred from U- series, Sr- Nd- Pb isotope, and trace element data, Bicol and Bataan arcs, Philippines: Geochimica et Cosmochimica Acta, v. 70, p. 3401-3420.

Duncker, K.E., Wolff, J.A., Harmon, R.S., Leat, P.T., Dickin, A.P., Thompson, R.N., 1991. Diverse mantle and crustal components in lavas of the NW Cerros del Rio volcanic field, Rio Grande Rift, New Mexico: Contributions to Mineralogy and Petrology, v. 108, p. 331-345.

Dupuy, C., Dostal, J., Marcelot, G., Bougault, H., Joron, J.L., Treuil, M., 1982. Geochemistry of basalts from central and southern New Hebrides arc: implication for their source rock composition: Earth and Planetary Science Letters, v. 60, p. 207-225.

Edwards, C.M.H., Menzies, M.A., Thirlwall, M.F., Morris, J.D., Leeman, W.P., Harmon, R.S., 1994. The transition to potassic alkaline volcanism in island arcs: The Ringgit-Beser complex, east Java, Indonesia: Journal of Petrology, v. 35: 1557-1595.

Eggins, S.M., 1993. Origin and differentiation of picritic arc magmas, Ambae (Aoba), Vanuatu: Contributions to Mineralogy and Petrology, v. 114, p. 79-100.

Ekící, T., Alpaslan, M., Parlak, O., Uçurum, A., 2009. Geochemistry of Middle Miocene Collision-related Yamadagi (Eastern Anatolia) calc-alkaline volcanics, Turkey: Turkish Journal of Earth Sciences, v. 18, p. 511-528.

Elburg, M.A., Kamenetsky, V.S., 2007. The origin of medium-K ankaramitic arc magmas from Lombok (Sunda arc, Indonesia): mineral and melt inclusion evidence: Chemical Geology, v. 240, p. 260-279.

Elliott, T., Plank, T., Zindler, A., White, W.M., Bourdon, B., 1997. Element transport from slab to volcanic front at the Mariana arc: Journal of Geophysical Research, v. 102, p. 14991-15019.

Ernst, W.G., 2009, Archean plate tectonics, rise of Proterozoic supercontinentality and onset of regional, episodic stagnant-lid behavior: Gondwana Research, v. 15, p. 243-253.

Evans, R., Asudeh, I., Crampin, S., Balamir Üçer, S., 1985. Tectonics of the Marmara Sea region of Turkey: new evidence from microearthquake fault plane solutions: Geophysical Journal of Geophysical Journal of the Royal Astronomical Society, v. 83, p. 47-60.

Ewart, A., Brothers, R.N., Mateen, A., 1977. An outline of the geology and geochemistry, and the possible petrogenetic evolution of the volcanic rocks of the Tonga-Kermadec-New Zealand island arc: Journal of Volcanology and Geothermal Research, v. 2, p. 205-270.

Ewart, A., Bryan, W.B., 1972. Petrography and geochemistry of the igneous rocks from EUA, Tongan islands: Geological Society of America Bulletin, v. 83, p. 3281-3298.

Fan, Q., Hooper, P.R., 1991. The Cenozoic basaltic rocks of eastern China: petrology and chemical composition: Journal of Petrology, v. 32, p. 765-810.

Feigenson, M.D., Hofmann, A.W., Spera, F.J., 1983. Case studies on the origin of basalt. II. The transition from tholeiitic to alkalic volcanism on Kohala volcano, Hawaii: Contributions to Mineralogy and Petrology, v. 84, p. 390-405.

Ferriz, H., Mahood, G. A., 1987. Strong compositional zonation in a silicic magmatic system: Los Humeros, Mexican Neovolcanic Belt: Journal of Petrology, v. 28, p. 171-209.

Feuerbach, D.L., Smith, E.I., Walker, J.D., Tangeman, J.A., 1993. The role of the mantle during crustal extension: constraints from geochemistry of volcanic rocks in the Lake Mead area, Nevada and Arizona: Geological Society of America Bulletin, v. 105, p. 1561-1575.

Finney, B., Turner, S., Hawkesworth, C., Larsen, J., Nye, C., George, R., Bindeman, I., Eichelberger, J., 2008. Magmatic differentiation at an Island-arc Caldera: Okmok Volcano, Aleutian Islands, Alaska: Journal of Petrology, v. 49, p. 857-884.

Fitton, J.G., James, D., Leeman, W.P., 1991. Basic magmatism associated with Late Cenozoic extension in the western United States: compositional variations in space and time: Journal of Geophysical Research, v. 96, p. 13693-13711.

Floyd, P. A., Winchester, J. A.., 1975. Magma type and tectonic setting discrimination using immobile elements: Earth and Planetary Science Letters, v. 27, p. 211-218.

Floyd, P. A., Winchester, J. A.., 1978. Identification and discrimination of altered and metamorphosed volcanic rocks using immobile elements: Chemical Geology, v. 21, p. 291-306.

Foden, J.D., Varne, R., 1980. The petrology and tectonic setting of Quaternary-Recent volcanic centres of Lombok and Sumbawa, Sunda arc: Chemical Geology, v. 30, p. 201-226.

Frey, F.A., Garcia, M.O., Roden, M.F., 1994. Geochemical characteristics of Koolau volcano: implications of intershield geochemical differences among Hawaiian volcanoes: Geochimica et Cosmochimica Acta, v. 58, p. 1441-1462.

Frey, F.A., Gerlach, D.C., Hickey, R.L., Lopez-Escobar, L., Munizaga-Villavicencio, F., 1984. Petrogenesis of the Laguna del Maule volcanic complex, Chile (36°S): Contributions to Mineralogy and Petrology, v. 88, p. 133-149.

Gamble, J.A., Smith, I.E.M., McCulloch, M.T., Graham, I.J., Kokelaar, B.P., 1993. The geochemistry and petrogenesis of basalts from the Taupo volcanic zone and Kermadec Island arc, S.W. Pacific: Journal of Volcanology and Geothermal Research, v. 54, p. 265-290.

Gamble, J.A., Wright, I.C., Woodhead, J.D., McCulloch, M.T., 1995. Arc and back-arc geochemistry in the southern Kermadec arc-Ngatoro basin and offshore Taupo volcanic zone, SW Pacific. In: J.L. Smellie (Editor), Volcanism associated with extension at consuming plate margins. Geological Society Special Publication: p. 193-212.

Geldmacher, J., Hoernle, K., 2000. The 72 Ma geochemical evolution of the Medeira hotspot (eastern North Atlantic): recycling of Paleozoic (≤ 500 Ma) oceanic lithosphere: Earth and Planetary Science Letters, v. 183, p. 73-92.

Gerlach, D.C., Frey, F.A., Moreno-Roa, H., Lopez-Escobar, L., 1988. Recent volcanism in the Puyehue-Cordon Caulle region, southern Andes, Chile (40.5°S): petrogenesis of evolved lavas: Journal of Petrology, v. 29, p. 333-382.

Gibson, S.A., Thompson, R.N., Leat, P.T., Dickin, A.P., Morrison, M.A., Hendry, G.L., Mitchell, J.G., 1992. Asthenosphere-derived magmatism in the Rio Grande rift, western USA: implications for continental break-up. In: B.C. Storey, T. Alabaster and R.J. Pankhurst (Editors), Magmatism and the causes of continental break-up. Geological Society Special Publication: p. 61-89.

González Partida, E., Torres Rodriguez, V., Birkle, P., 1997. Plio-Pleistocene volcanic history of the Ahuachapan geothermal system, El Salvador: The Concepción de Ataco caldera: Geothermics, v. 26, p. 555-575.

Gorton, M. P., Schandl, E. S., 2000. From continents to island arcs: a geochemical index of tectonic setting for arc-related and within-plate felsic to intermediate volcanic rocks: The Canadian Mineralogist, v. 38, p. 1065-1073.

Gradstein, F.M., Ogg, J.G., Smith, A.G., Bleeker, W., and Lourens, L.J., 2004, A new Geologic Time Scale, with special reference to Precambrian and Neogene: Episodes, v. 27, p. 84-100.

Haase, K.M., Goldschmidt, B., Garbe-Schönberg, C.-D., 2004. Petrogenesis of Tertiary continental intra-plate lavas from the Westerwald region, Germany: Journal of Petrology, v. 45, p. 883-905.

Haase, K.M., Worthington, T.J., Stoffers, P., Garbe-Schönberg, D., Wright, I., 2002. Mantle dynamics, element recycling, and magma genesis beneath the Kermadec arc-Havre Trough: Geochemistry Geophysics Geosystems, v. 3: 1071, doi:10.1029/2002GC00035.

Han, B.-F., Wang, S.-G., Kagami, H., 1999. Trace element and Nd-Sr isotope constraints on origin of the Chifeng flood basalts, North China: Chemical Geology, v. 155, p. 187-199.

Hanson, G. N., 1978. The application of trace elements to the petrogenesis of igneous rocks of granitic composition: Earth and Planetary Science Letters, v. 38, p. 26-43.

Hart, S.R., Blusztajn, J., Craddock, C., 1995. Cenozoic volcanism in Antarctica: Jones mountains and Peter I island: Geochimica et Cosmochimica Acta, v. 59, p. 3379-3388.

Hart, W.K., WoldeGabriel, G., Walter, R.C., Mertzman, S.A., 1989. Basaltic volcanism in Ethiopia: constraints on continental rifting and mantle interactions: Journal of Geophysical Research, v. 94, p. 7731-7748.

Hastie, A. R., Kerr, A. C., Pearce, J.A., Mitchell, S.F., 2007. Classification of altered volcanic island rocks using immobile trace elements: development of the Th-Co discrimination diagram: Journal of Petrology, v. 48, p. 2341-2357.

Hazlett, R.W., 1987. Geology of San Cristobal volcanic complex, Nicaragua: Journal of Volcanology and Geothermal Research, v. 33, p. 223-230.

Hegner, E., Smith, I.E.M., 1992. Isotopic compositions of late Cenozoic volcanics from southeast Papua New Guinea: evidence for multi-component sources in arc and rift environments: Chemical Geology, v. 97, p. 233-249.

Hekinian, R., Cheminée, J.L., Dubois, J., Stoffers, P., Scott, S., Guivel, C., Garbe-Schönberg, D., Devey, C., Bourdon, B., Lackschewitz, K., McMurtry, G., Le Drezen, E., 2003. The Pitcairn hotspot in the South Pacific: distribution and composition of submarine volcanic sequences: Journal of Volcanology and Geothermal Research, v. 121, p. 219-245.

Hickey, R.L., Frey, F.A., Gerlach, D.C., Lopez-Escobar, L., 1986. Multiple sources for basaltic arc rocks from the southern volcanic zone of the Andes (34°-41°S): trace element and isotopic evidence for contributions from subducted oceanic crust, mantle, and continental crust: Journal of Geophysical Research, v. 91, p. 5963-5983.

Hickey-Vargas, R., Moreno Roa, H., Lopez Escobar, L., Frey, F.A., 1989. Geochemical variations in Andean basaltic and silicic lavas from the Villarrica-Lanin volcanic chain (39.5oS): an evaluation of source heterogeneity, fractional crystallization and crustal assimilation: Contributions to Mineralogy and Petrology, v. 103, p. 361-386.

Hildreth, W., Fierstein, J., Siems, D.F., Budahn, J.R., Ruíz, J., 2004. Rear-arc vs. arc-front volcanoes in the Katmai reach of the alaska peninsula: a critical appraisal of across-arc compositional variation: Contributions to Mineralogy and Petrology, v. 147, p. 243-275.

Hirotani, S., Ban, M., 2006. Origin of silicic magma and magma feeding system of the Shirataka volcano, NE Japan: Journal of Volcanology and Geothermal Research, v. 156, p. 229-251.

Ho, K.-S., Chen, J.-C., Juang, W.-S., 2000. Geochronology and geochemistry of late Cenozoic basalts from Leiqiong area, southern China: Journal of Asian Earth Sciences, v. 18, p. 307-324.

Hoke, L., Lamb, S., 2007. Cenozoic behind arc volcanism in the Bolivian Andes, South America: implications for mantle melt generation and lithoshperic structure: Journal of Geological Society London, v. 164, p. 795 - 814.

Hole, M.J., Saunders, A.D., Marriner, G.F., Tarney, J., 1984. Subduction of pelagic sediments: implications for the origin of Ce-anomalous basalts from the Marianas Islands: Journal of the Geological Society of London, v. 141, p. 453-472.

Holm, P.M., Wilson, J.R., Christensen, B.P., Hansen, L., Hansen, S.L., Hein, K.M., Mortensen, A.K., Pedersen, R.B., Plesner, S., Runge, M.K., 2006. Sampling of Cape Verde mantle plume: evolution of melt compositions on Santo Antao, Cape Verde Islands: Journal of Petrology, v. 47, p. 145-189.

Hoogewerff, J.A., van Bergen, M.J., Vroon, P.Z., Hertogen, J., Wordel, R., Sneyers, A., Nasution, A., Varekamp, J.C., Moens, H.L.E., Mouchel, D., 1997. U-series, Sr-Nd-Pb isotope and trace-element systematics across an active island arc-continent collision zone: implications for element transfer at the slab-wedge interface: Geochimica et Cosmochimica Acta, v. 61, p. 1057-1072.

Hsu, C.-N., Chen, J.-C., Ho, K.-S., 2000. Geochemistry of Cenozoic volcanic rocks from Kirin Province, northeast China: Geochemical Journal, v. 34, p. 33-58.

Ilbeyli, N., Pearce, J.A., Thirlwall, M.F., Mitchell, J.G., 2004, Petrogenesis of collision-related plutonics in central Anatolia, Turkey: Lithos, v. 72, p. 163-182.

Ishikawa, T., Tera, F., Nakazawa, T., 2001. Boron isotope and trace element systematics of the three volcanic zones in the Kamchatka arc: Geochimica et Cosmochimica Acta, v. 65, p. 4523-4537.

Izbekov, P.E., Eichelberger, J.C., Ivanov, B.V., 2004. The 1996 eruption of Karymsky volcano, Kamchatka: historical record of basaltic replenishment of an andesite reservoir: Journal of Petrology, v. 45, p. 2325-2345.

Johnson, C.M., Lipman, P.W., 1988. Origin of metaluminous and alkaline volcanic rocks of the Latir volcanic field, northern Rio Grande rift, New Mexico: Contributions to Mineralogy and Petrology, v. 100, p. 107-128.

Kabeto, K., Sawada, Y., Iizumi, S., Wakatsuki, T., 2001. Mantle sources and magma-crust interactions in volcanic rocks from northern Kenya rift: geochemical evidence: Lithos, v. 56, p. 111-136.

Kampunzu, A.B., Mohr, P., 1991. Magmatic evolution and petrogenesis in the East African rift system. In: A.B. Kampunzu and R.T. Lubala (Editors), Magmatism in extensional structural settings: Springer Verlag, Berlin, Germany, p. 85-136.

Kay, S.M., Gordillo, C.E., 1994. Pocho volcanic rocks and the melting of depleted continental lithosphere above a shallowly dipping subduction zone in the central Andes. Contributions to Mineralogy and Petrology, v. 117, p. 25-44.

Kay, S.M., Kay, R.W., 1994. Aleutian magmas in space and time. In: G. Plafker and H.C. Berg (Editors), The Geology of North America: Geological Society of America, USA, p. 687-722.

Kay, S.M., Kay, R.W., Citron, G.P., 1982. Tectonic controls on tholeiitic and calc-alkaline magmatism in the Aleutian arc: Journal of Geophysical Research, v. 87, p. 4051-4072.

Kay, S.M., Maksaev, V., Moscoso, R., Mpodozis, C., Nasi, C., 1987. Probing the evolving Andean lithosphere: mid-late Tertiary magmatism in Chile (29°-30°30'S) over the modern zone of subhorizontal subduction: Journal of Geophysical Research, v. 92, p. 6173-6189.

Kay, S.M., Maksaev, V., Moscoso, R., Mpodozis, C., Nasi, C., Gordillo, C.E., 1988. Tertiary Andean magmatism in Chile and Argentina between 28°S and 33°S: correlation of magmatic chemistry with a changing Benioff zone: Journal of South American Earth Sciences, v. 1, p. 21-38.

Kelly, P.J., Kyle, P.R., Dunbar, N.W., Sims, K.W.W., 2008. Geochemistry and mineralogy of the phonolite lava lake, Erebus volcano, Antarctica: 1972-2004 and comparison with older lavas: Journal of Volcanology and Geothermal Research, v. 177, p. 589-605.

Kempton, P.D., Fitton, J.G., Hawkesworth, C.J., Ormerod, D.S., 1991. Isotopic and trace element constraints on the composition and evolution of the lithosphere beneath the Southwestern United States: Journal of Geophysical Research, v. 96, p. 13713-13735.

Kepezhinskas, P., McDermott, F., Defant, M.J., Hochstaedter, A., Drummond, M.S., Hawkesworth, C.J., Koloskov, A., Maury, R.C., Bellon, H., 1997. Trace element and Sr-Nd-Pb isotopic constraints on a three-component model of Kamchatka arc petrogenesis: Geochimica et Cosmochimica Acta, v. 61, p. 577-600.

Keskin, M., 2003. Magma generation by slab steepening and breakoff beneath a subduction-accretion complex: An alternative model for collision-related volcanism in Eastern Anatolia, Turkey: Geophysical Research Letters, v. 30, p. 8046.

Keskin, M., Pearce, J.A., Mitchell, J.G., 1998. Volcano-stratigraphy and geochemistry of collision-related volcanism on the Erzurum-Kars Plateau, northeastern Turkey: Journal of Volcanology and Geothermal Research, v. 85, p. 355-404.

Kim,Y. H., Clayton, R. W., Keppie, Fraser., 2011. Evidence of a collision between the Yucatán Block and Mexico in the Miocene: Geophysical Journal International, v.187, p. 989-1000.

Kimura, J.-I., Manton, W.I., Sun, C.-H., Iizumi, S., Yoshida, T., Stern, R.J., 2002. Chemical diversity of the Ueno basalts, Central Japan: identification of mantle and crustal contributions to arc basalts: Journal of Petrology, v. 43, p. 1923-1946.

Kimura, J.-I., Yoshida, T., 2006. Contributions of slab fluid, mantle wedge and crust to the origin of Quaternary lavas in the NE Japan arc: Journal of Petrology, v. 47, p. 2185-2232.

Kita, I., Yamamoto, M., Asakawa, Y., Nakagawa, M., Taguchi, S., Hasegawa, H., 2001. Contemporaneous ascent of within-plate type and island-arc type magmas in the Beppu-Shimabara graben system, Kyushu island, Japan: Journal of Volcanology and Geothermal Research, v. 111, p. 99-109.

Knittel, U., Hegner, E., Bau, M., Satir, M., 1997. Enrichment processes in the sub-arc mantle: a Sr-Nd-Pb isotopic and REE study of primitive arc basalts from the Philippines: The Canadian Mineralogist, v. 35, p. 327-346.

Krochert, J., Buchner, E., 2009. Age distribution of cinder cones within the Bandas del Sur Formation, southern Tenerife, Canary Islands: Geological Magazine, v. 146, p. 161-172.

Le Bas, M.J., Le Maitre, R.W., Streckeisen, A., Zanettin, B., 1986, A chemical classification of volcanic rocks based on the total alkali-silica diagram: Journal of Petrology, v. 27, p. 745-750.

Le Bas,M. J., 2000.IUGS reclassification of the high-Mg and picritic volcanic rocks: Journal of Petrology, v. 27, p.745-750

Le Bas,M. J., LeMaitre, R.W. and Woolley, A. R., 1992.The construction of the total alkali-silica chemical classification of volcanic rocks: Mineralogy and Petrology, v. 46, p.1-22.

Le Maitre, R. W., 1976. A new approach to the classification of igneous rocks using the basalt-andesite-dacite-rhyolite suite as an example: Contributions to Mineralogy and Petrology, v. 56, p. 191-203.

Le Maitre, R. W., Streckeisen, A., Zanettin, B., Le Bas, M.J., Bonin, B., Bateman, P., Bellieni, G., Dudek, A., Schmid, R., Sorensen, H., Woolley, A.R., 2002. Igneous rocks. A classification and glossary of terms: recommendations of the International Union of Geological Sciences Subcommission of the Systematics of Igneous Rocks: Cambridge, Cambridge University Press.

Le Roex, A.P., Späth, A., Zartman, R.E., 2001. Lithospheric thickness beneath the southern Kenya rift: implications from basalt geochemistry: Contributions to Mineralogy and Petrology, v. 142, p. 89-106.

Lindsay, J.M., Trumbull, R.B., Siebel, W., 2005. Geochemistry and petrogenesis of late Pleistocene to Recent volcanismo in Southern Dominica, Lesser Antilles: Journal of Volcanology and Geothermal Research, v. 148, p. 253-394.

Lipman, P.W., Rhodes, R.M., Dalrymple, G.B., 1990. The Ninole Basalt - Implications for the structural evolution of Mauna Loa volcano, Hawaii: Bulletin of Volcanology, v. 53, p. 1-19.

Liu, C.-Q., Masuda, A., Xie, G.-H., 1994. Major- and trace-element compositions of Cenozoic basalts in eastern China: petrogenesis and mantle source: Chemical Geology, v. 114, p. 19-42.

Lloyd, F.E., Huntingdon, A.T., Davies, G.R., Nixon, P.H., 1991. Phanerozoic volcanism of southern Uganda: a case for regional K and LILE enrichment of the lithosphere beneath a domed and rifted continental plate. In: A.B. Kampunzu and R.T. Lubala (Editors), Magmatism in extensional structural settings. Springer Verlag, Berlin, Germany, p. 23-72.

López-Escobar, L., Kilian, R., Kempton, P.D., Tagiri, M., 1993. Petrography and geochemistry of Quaternary rocks from the southern volcanic zone of the Andes between 41°30´and 46°00´S, Chile: Revista Geológica de Chile, v. 20, p. 33-35.

López-Escobar, L., Tagiri, M., Vergara, M., 1991. Geochemical features of southern Andes Quaternary volcanics between 41º5' and 43º00'S. Geological Society of America Special Paper 265, p. 45-56.

Luhr, J.F., Aranda-Gómez, J.J., Housh, T.B., 1995. San Quintín volcanic field, Baja California Norte, México: geology, petrology, and geochemistry: Journal of Geophysical Research, v. 100, p. 10353-10380.

Luhr, J.F., Haldar, D., 2006. Barren island volcano (NE Indian ocean): island-arc high-alumina basalts produced by troctolite contamination: Journal of Volcanology and Geothermal Research, v. 149, p. 177-212.

Macdonald, R., Belkin, H.E., Fitton, J.G., Rogers, N.W., Nejbert, K., Tindle, A.G., Marshall, A.S., 2008. The role of fractional crystallization, magma mixing, crystal mush remobilization and volatile-melt interactions in the genesis of young basalt-peralkaline rhyolite suite, the Greater Olkaria Volcanic Complex, Kenya Rift Valley: Journal of Petrology, v. 49, p. 1515-1547.

Macdonald, R., Davies, G.R., Upton, B.G.J., Denkley, P.N., Smith, M., Leat, P.T., 1995. Petrogenesis of Silali volcano, Gregory rift, Kenya: Journal of the Geological Society of London, v. 152, p. 703-720.

Maheshwari, A., Coltorti, M., Sial, A.N., Mariano, G., 1996, Crustal influences in the petrogenesis of the Malani rhyolites, southwestern Rajasthan: combined trace element and oxygen isotope constraints: Journal of the Geological Society of India, v. 47, p. 611-619.

Mahood, G. A., 1981. Chemical evolution of a Pleistocene rhyolitic center: Sierra La Primavera, Jalisco, México: Contributions to Mineralogy and Petrology, v. 77, p. 129-149.

Maldonado, F., Budahn, J.R., Peters, L., Unruh, D.M., 2006. Geology, geochronology, and geochemistry of basaltic flows of the Cat Hills, Cat Mesa, Wind Mesa, Cerro Verde, and Mesita Negra central New Mexico: Canadian Journal of Earth Sciences, v. 43, p. 1251-1268.

Mammerickx, J., Klitgord, K.D., 1982. Northern East Pacific Rise: evolution from 25 m.y. B.P. to the Present: Journal of Geophysical Research, v. 87, p. 6751-6759.

Márquez, A., R. Oyarzun, Verma, S. P., 1999. Alkalic (ocean-island basalt type) and calc-alkalic volcanism in the Mexican Volcanic Belt: a case for plume-related magmatism and propagating rifting at an active margin?: Geology, v. 27, p. 51-54.

Martínez Serrano, R. G., Alibert, C., 1994. Características geoquímicas de las rocas volcánicas del sistema geotérmico Los Humeros, Puebla y su relación con la mineralogía de alteración: Geofísica Internacional, v. 33, p. 585-605.

McDermott, F., Delfin Jr, F.G., Defant, M.J., Turner, S., Maury, R., 2005. The petrogenesis of volcanics from Mt. Bulusan and Mt. Mayon in the Bicol arc, the Philippines: Contributions to Mineralogy and Petrology, v. 150, p. 652-670.

McDowell, F.W., Keizer, R.P., 1977. Timing of mid-tertiary volcanism in the Sierra Madre Occidental between Durango City and Mazatlan, Mexico: Geological Society of America Bulletin, v. 88, p. 1479-1487

McDowell, F.W., Roldán-Q., J., Amaya-M., R., 1997. Interrelationship of sedimentary and volcanic deposits associated with Tertiary extension in Sonora, Mexico: Geological Society of America Bulletin, v.109, p. 1349-1360.

McMillan, N.J., Dickin, A.P., Haag, D., 2000. Evolution of magma source regions in the Rio Grande rift, southern New Mexico: Geological Society of America Bulletin, v. 112, p. 1582-1593.

Meschede, M., 1986, A method of discriminating between different types of mid-ocean ridge basalts and continental tholeiites with the Nb-Zr-Y diagram: Chemical Geology, v. 56, p. 207-218.

Meschede, M., 1986. A method of discriminating between different types of mid-ocean ridge basalts and continental tholeiites with the Nb-Zr-Y diagram: Chemical Geology, v. 56, p. 207-218.

Middlemost, E. A. K., 1989. Iron oxidation ratios, norms and the classification of volcanic rocks: Chemical Geology, v. 77, p. 19-26.

Mo, X., Hou, Z., Niu, Y., Dong, G., Qu, X., Zhao, Z., Yang, Z., 2007. Mantle contributions to crustal thickening during continental collision: Evidence from Cenozoic igneous rocks in southern Tibet: Lithos, v. 96, p. 225-242.

Monzier, M., Robin, C., Eissen, J.-P., Cotten, J., 1997. Geochemistry vs. seismo-tectonics along the volcanic New Hebrides Central Chain (Southwest Pacific) : Journal of Volcanology and Geothermal Research, v. 78, p. 1-29.

Moriguti, T., Shibata, T., Nakamura, E., 2004. Lithium, boron and lead isotope and trace element systematics of Quaternary basaltic volcanic rocks in northeastern Japan: mineralogical controls on slab-derived fluid composition: Chemical Geology, v. 212, p. 81-100.

Moyer, T.C., Esperança, S., 1989. Geochemical and isotopic variations in a bimodal magma system: the Kaiser Spring volcanic field, Arizona: Journal of Geophysical Research, v. 94, p. 7841-8759.

Mullen, E. D., 1983. $MnO/TiO_2/P_2O_5$: a minor element discrimination for basaltic rocks of oceanic environments and its implications for petrogenesis: Earth and Planetary Science Letters, v. 62, p. 53-62.

Myers, J.D., Marsh, B.D., Frost, C.D., Linton, J.A., 2002. Petrologic constraints on the spatial distribution of crustal magma chambers, Atka volcanic center, central Aleutian arc: Contributions to Mineralogy and Petrology, v. 143, p. 567-586.

Myers, J.D., Marsh, B.D., Sinha, A.K., 1985. Strontium isotopic and selected trace element variations between two Aleutian volcanic centers (Adak and Atka): implications for the development of arc volcanic plumbing systems: Contributions to Mineralogy and Petrology, v. 91, p. 221-234.

Myers, R.E., Breitkopf, J.H., 1989. Basalt geochemistry and tectonic setting: A new approach to relate tectonic and magmatic processes: Lithos, v. 23, p. 53-62.

Nakada, S., Matsushima, T., Yoshimoto, M., Sugimoto, T., Kato, T., Watanabe, T., Chong, R., Camacho, J.T., 2005. Geological aspects of the 2003-2004 eruptions of Anathan volcano, northern Mariana Islands: Journal of Volcanology and Geothermal Research, v. 146, p. 226-240.

Nakagawa, M., Ishizuka, Y., Kudo, T., Yoshimoto, M., Hirose, W., Ishizaki, Y., Gouchi, N., Katsui, Y., Solovyow, A.W., Steinberg, G.S., Abdurakhmanov, A.I., 2002. Tyatya volcano, southwestern Kuril arc: recent eruptive activity inferred from widespread tephra: The Island Arc, v. 11, p. 236-254.

Nye, C.J., Reid, M.R., 1986. Geochemistry of primary and least fractionated lavas from Okmok volcano, central Aleutians: implications for arc magma genesis: Journal of Geophysical Research, v. 91, p. 10271-10287.

O' Connor, J. T., 1965. A classification for quartz-rich igneous rocks based on feldspar ratio: U.S Geological Survey Professional Paper, 525B, p. B79-B84.

Ohba, T., Matsuoka, K., Kimura, Y., Ishikawa, H., Fujimaki, H., 2009. Deep crystallization differentiation of arc tholeiite basalt magmas from Northern Honshu Arc, Japan: Journal of Petrology, v. 50, p. 1025-1046.

Palacz, Z.A., Saunders, A.D., 1986. Coupled trace element and isotope enrichment in the Cook-Austral-Samoa islands, southwest Pacific: Earth and Planetary Science Letters, v. 79, p. 270-280.

Pallister, J.S., Truesdell, F.A., Brownfield, I.K., Siems, D.F., Budahn, J.R., Sutley, S.F., 2005. The 2003 phreatomagmatic eruptions of Anathan volcano- textural and petrological features of deposits at an emergent island volcano: Journal of Volcanology and Geothermal Research, v. 146, p. 208-225.

Pandarinath, K., P. Dulski, Torres-Alvarado, I.S., Verma, S.P., 2008. Element mobility during hydrothermal alteration of rhyolitic rocks of the Los Azufres geothermal field, Mexico: Geothermics, v.37, p.53-72.

Pandarinath, K., Verma, S.K., 2012. Application of four sets of tectonomagmatic discriminant function based diagrams to basic rocks from northwest Mexico: Journal of Iberian Geology, in press.

Pardo, N., Avellán, D.R., Macías, J.L., Scolamacchia, T., Rodríguez, D., 2008. The 1245 yr BP Asososca maar: new advances on recent volcanic stratigraphy of Managua (Nicaragua) and hazard implications: Journal of Volcanology and Geothermal Research, v. 176, p. 493-512.

Paslick, C., Halliday, a., James, D., Dawson, J.B., 1995. Enrichment of the continental lithosphere by OIB melts: isotopic evidence from the volcanic province of northern Tanzania: Earth and Planetary Science Letters, v. 130, p. 109-126.

Patino, L.C., Carr, M.J., Feigenson, M.D., 1997. Cross-arc geochemical variations in volcanic fields in Honduras C.A.: progressive changes in source with distance from the volcanic front: Contributions to Mineralogy and Petrology, v. 129, p. 341-351.

Patino, L.C., Velbel, M.A., Price, J.R., Wade, J.A., 2003, Trace element mobility during spheroidal weathering of basalts and andesites in Hawaii and Guatemala: Chemical Geology, v. 202, p. 343-364.

Pearce, J. A. Cann, J. R., 1973. Tectonic setting of basic volcanic rocks determined using trace element analyses: Earth and Planetary Science Letters, v. 19, p. 290-300.

Pearce, J. A. Gale, G. H., 1977. Identification of ore-deposition environment from trace-element geochemistry of associated igneous host rocks: Geological Society of London Special Publication, v. 7, p. 14-24.

Pearce, J. A. Norry, M. J., 1979. Petrogenetic implications of Ti, Zr, Y, and Nb variations in volcanic rocks: Contributions to Mineralogy and Petrology, v. 69, p. 33-47.

Pearce, J. A., 1976. Statistical analysis of major element patterns in basalts: Journal of Petrology, v. 17, p. 15-43.

Pearce, J. A., 1982. Trace element characteristics of lavas from destructive plate boundaries. Andesites. R. S. Thorpe. Chichester, John Wiley & Sons: p. 525-548.

Pearce, J.A., 1976. Statistical analysis of major element patterns in basalts: Journal of Petrology, v. 17, p. 15-43.

Pearce, J.A., Bender, J.F., Long, S.E.D., Kidd, W.S.F., Low, P.J., Guner, Y., Saroglu, F., Yilmaz, Y., Moorbath, S., Mitchell, J.G., 1990. Genesis of collision volcanism in Eastern Anatolia, Turkey: Journal of Volcanology and Geothermal Research, v. 44, p. 189-229.

Pearce, J.A., Cann, J.R., 1971. Ophiolite origin investigated by discriminant analysis using Ti, Zr and Y: Earth and Planetary Science Letters, v. 12, p. 339-349.

Pearce, J.A., Cann, J.R., 1973. Tectonic setting of basic volcanic rocks determined using trace element analyses: Earth and Planetary Science Letters, v. 19, p. 290-300.

Pearce, J.A., Harries, N.B.W., Tindle, A.G., 1984. Trace element discrimination diagrams for the tectonic interpretation of granitic rocks: Journal of Petrology, v. 25, p. 956-983.

Pearce, T. H., Gorman, B. E., Birkett, T.C., 1977. The relationship between major element chemistry and tectonic environment of basic and intermediate volcanic rocks: Earth and Planetary Science Letters, v. 36, p. 121-132.

Peate, D.W., Pearce, J.A., Hawkesworth, C.J., Colley, H., Edwards, C.M.H., Hirose, K., 1997. Geochemical variations in Vanuatu arc lavas: the role of subducted material and a variable mantle wedge composition: Journal of Petrology, v. 38, p. 1331-1358.

Peccerillo, A., Barberio, M.R., Yirgu, G., Ayalew, D., Barbieri, M., Wu, T.W., 2003. Relationships between mafic and peralkaline silicic magmatism in continental rift settings: a petrological, geochemical and isotopic study of the Gedemsa volcano, central Ethiopian rift: Journal of Petrology, v. 44, p. 2003-2032.

Peccerillo, A., Donati, C., Santo, A.P., Orlando, A., Yirgu, G., Ayalew, D., 2007. Petrogenesis of silicic peralkaline rocks in the Ethiopian Rift: geochemical evidence and volcanological implications: Journal of African Earth Sciences, v. 48, p. 161-173.

Peccerillo, A., Taylor, S. R., 1976. Geochemistry of Eocene calc-alkaline volcanic rocks from the Kastamonu area, Northern Turkey: Contributions to Mineralogy and Petrology, v. 58, p. 63-81.

Peng, Z.C., Zartman, R.E., Futa, K., Chen, D.G., 1986. Pb-, Sr- and Nd-isotopic systematics and chemical characteristics of Cenozoic basalts, eastern China: Chemical Geology, v. 59, p. 3-33.

Perry, F.V., Baldridge, W.S., DePaolo, D.J., Shafiqullah, M., 1990. Evolution of a magmatic system during continental extension: the mount Taylor volcanic field, New Mexico: Journal of Geophysical Research, v. 95, p. 19327-19348.

Polat, A., Kerrich, R., Wyman, D.A., 1999, Geochemical diversity in oceanic komatiites and basalts from the late Archean Wawa greenstone belts, Superior Province, Canada: trace element and Nd isotope evidence for a heterogeneous mantle: Precambrian Research, v. 94, p. 139-173.

Pradal, E., Robin, C., 1994. Long-lived magmatic phases at Los Azufres volcanic center, Mexico: Journal of Volcanology and Geothermal Research, v.63, p. 201-215.

Praegel, N.-O., Holm, P.M., 2006. Lithosphere contributions to high-MgO basanites from the Cumbre Vieja volcano, La Palma, Canary Islands and evidence for temporal variation in plume influence: Journal of Volcanology and Geothermal Research, v. 149, p. 213-239.

Price, R.C., Gray, C.M., Frey, F.A., 1997. Strontium isotopic and trace element heterogeneity in the plains basalts of the Newer Volcanic Province, Victoria, Australia: Geochimica et Cosmochimica Acta, v. 61, p. 171-192.

Reagan, M.K., Gill, J.B., 1989. Coexisting calcalkaline and high-niobium basalts from Turrialba volcano, Costa Rica: implications for residual titanates in arc magma sources: Journal of Geophysical Research, v. 94, p. 4619-4633.

Reagan, M.K., Meijer, A., 1984, Geology and geochemistry of early arc-volcanic rocks from Guam: Geological Society of America Bulletin, v. 95, p. 701-713.

Reichardt, H., Weinberg, R.F., Andersen, U.B., Fanning, C.M., 2010. Hybridization of granitic magmas in the source: The origin of the Karakoram Batholith, Ladakh, NW India: Lithos, v. 116, p. 249-272.

Reyment, R. A., 1987. Multivariate analysis in Geoscience: fads, fallacies and the future: Chemometrics and Intelligent Laboratory Systems, v. 2, p. 79-91.

Reyment, R. A., Savazzi, E., 1999. Aspects of multivariate statistical analysis in geology: Amsterdam, Elsevier.

Robin, C., 1982. Relations volcanologie-magmatologie-géodynamique: application au passage entre volcanismes alcalin et andésitique dans le sud Mexicain (Axe Trans-mexicain et Province Alcaline Orientale): Annales Scientifiques de l´Universite de Clermont-Ferrand II 31 v. 70, 503 p.

Rollinson, H.R., 1993, Using geochemical data: evaluation, presentation, interpretation: Essex, Longman Scientific Technical, 344 p.

Romick, J.D., Perfit, M.R., Swanson, S.E., Shuster, R.D., 1990. Magmatism in the eastern Aleutian arc: temporal characteristic of igneous activity on Akutan Island: Contributions to Mineralogy and Petrology, v. 104, p. 700-721.

Ronga, F., Lustrino, M., Marzoli, A., Melluso, L., 2010. Petrogenesis of a basalt-comendite-pantellerite rock suite: the Boseti Volcanic Complex (Main Ethiopian Rift): Mineralogy and Petrology, v. 98, p. 227-243.

Rooney, T., Furman, T., Bastow, I., Ayalew, D., Yirgu, G., 2007. Lithospheric modification during crustal extension in the Main Ethiopian Rift: Journal of Geophysical Research, v. 112, p. B10201, doi:1029/2006JB004916.

Roser, B.P., Korsch, R.J., 1986. Determination of tectonic setting of sandstone-mudstone suites using SiO2 content and K2O/Na2O ratio: Journal of Geology, v. 94, p. 635-650.

Rotolo, S.G., Castorina, F., 1998. Transition from midly-tholeiitic to calc-alkaline suite: the case of Chicontepec volcanic centre, El Salvador, Central America: Journal of Volcanology and Geothermal Research, v. 86, p. 117-136.

Rutanen, H., Andersson, U.B., 2009, Mafic plutonic rocks in a continental-arc setting: geochemistry of 1.87-1.78 Ga rocks from south-central Sweden and models of their palaeotectonic setting: Geological Journal, v. 44, p. 241-279.

Ryder, C.H., Gill, J.B., Tepley III, F., Ramos, F., Reagan, M., 2006. Closed- to open-system differentiation at Arenal volcano (1968-2003): Journal of Volcanology and Geothermal Research, v. 157, p. 75-93.

Sakuyama, M., Nesbitt, R.W., 1986. Geochemistry of the Quaternary volcanic rocks of the Northeast Japan arc: Journal of Volcanology and Geothermal Research, v. 29, p. 413-450.

Sano, T., Hasenaka, T., Shimaoka, A., Yonesawa, C., Fukuoka, T., 2001. Boron contents of Japan trench sediments and Iwate basaltic lavas, northeastern Japan arc: estimation of sediment-derived fluid contribution in mantle wedge: Earth and Planetary Science Letters, v. 186, p. 187-198.

Sato, M., Shuto, K., Yagi, M., 2007. Mixing of asthenospheric and lithospheric mantle-derived basalt magmas as shown by along-arc variation in Sr and Nd isotopic compositions of Early Miocene basalts from back-arc margin of the NE Japan arc: Lithos, v. 96, p. 453-474.

Saunders, A.D., Rogers, G., Marriner, G.F., Terrell, D.J., Verma, S.P., 1987. Geochemistry of Cenozoic volcanic rocks, Baja California, Mexico: implications for the petrogenesis of post-subduction magmas: Journal of Volcanology and Geothermal Research, v. 32, p. 223-245.

Schmitz, M.D., Smith, I.E.M., 2004. The petrology of the Rotoiti eruption sequence, Taupo Volcanic Zone: an example of fractionation and mixing in a rhyolitic system: Journal of Petrology, v. 45, p. 2045-2066.

Sendjaja, Y.A., Kimura, J., Sunardi, E., 2009. Across-arc geochemical variation of Quaternary lavas in west Java, Indonesia: mass-balance elucidation using arc basalt simulator model: Island Arc, v. 18, p. 201-224.

Sharma, K.K., 2004, The Neoproterozoic Malani magmatism of the northwestern Indian shield: implications for crust-building processes: Proceedings of Indian Academy of Sciences (Earth and Planetary Sciences), v. 113, p. 795-807.

Shervais, J. W., 1982. Ti-V plots and the petrogenesis of modern and ophiolitic lavas: Earth and Planetary Science Letters, v. 59, p. 101-118.

Shervais, J.W., 1982, Ti-V plots and the petrogenesis of modern and ophiolitic lavas: Earth and Planetary Science Letters, v. 59, p. 101-118.

Shinjo, R., 1998. Petrochemistry and tectonic significance of the emerged late Cenozoic basalts behind the Okinawa Trough Ryukyu arc system: Journal of Volcanology and Geothermal Research, v. 80, p. 39-53.

Shinjo, R., 1999. Geochemistry of high Mg andesites and the tectonic evolution of the Okinawa Trough-Ryukyu arc system: Chemical Geology, v. 157, p. 69-88.

Shinjo, R., Woodhead, J.D., Hergt, J.M., 2000. Geochemical variation within the northern Ryukyu: magma source compositions and geodynamic implications. Contributions to Mineralogy and Petrology, v. 140, p. 263-282.

Shragge, J., Snow, C. A., 2006. Bayesian geochemical discrimination of mafic volcanic rocks: American Journal of Science, v. 306, p. 191-209.

Shukuno, H., Tamura, Y., Tani, K., Chang, Q., Suzuki, T., Fiske, R.S., 2006. Origin of silicic magmas and the compositional gap at Sumisu submarine caldera, Izu-Bonin arc, Japan: Journal of Volcanology and Geothermal Research, v. 156, p. 187-216.

Shuto, K., Hirahara, Y., Ishimoto, H., Aoki, A., Jinbo, A., Goto, Y., 2004. Sr and Nd isotopic compositions of the magma source beneath north Hokkaido, Japan: comparison with the back-arc side in the NE Japan arc: Journal of Volcanology and Geothermal Research, v. 134, p. 57-75.

Shuto, K., Ishimoto, H., Hirahara, Y., Sato, M., Matsui, K., Fujibayashi, N., Takazawa, E., Yabuki, K., Sekine, M., kato, M., Rezanov, A.I., 2006. Geochemical secular variation of magma source during Early to Middle Miocene time in the Niigata area, NE Japan: asthenospheric mantle upwelling during back-arc basin opening: Lithos, v. 86, p. 1-33.

Shuto, K., Ishimotob, H., Hiraharab, Y., Satob, M., Matsuic, k., Fujibayashid, N., Takazawaa, E., Yabukie, K., Sekinef, M., Katob, M., Rezanovg, A, I., 2006. Geochemical secular variation of magma source during Early to Middle Miocene time in the Niigata area, NE Japan: Asthenospheric mantle upwelling during back-arc basin opening: Lithos, v. 86, p. 1-33.

Silva Mora, L. 1988. Algunos aspectos de los basaltos y andesitas cuaternarias de Michoacán Oriental: Revista del Instituto de Geología, UNAM, v. 7, p. 89-96.

Singer, B.S., Kudo, A.M., 1986. Assimilation-fractional crystallization of Polvadera Group rocks in the northwestern Jemez volcanic field, New Mexico: Contributions to Mineralogy and Petrology, v. 94, p. 374-386.

Singer, B.S., Myers, J.D., Frost, C.D., 1992a. Mid-Pleistocene lavas from the Seguam volcanic center, central Aleutian arc: closed-system fractional crystallization of a basalt to rhyodacite eruptive suite: Contributions to Mineralogy and Petrology, v. 110, p. 87-112.

Singer, B.S., Myers, J.D., Frost, C.D., 1992b. Mid-Pleistocene basalt from the Seguam volcanic center, central Aleutian arc, Alaska: local lithospheric structures and source variability in the Aleutian arc: Journal of Geophysical Research, v. 97: 4561-4578.

Singh, K.A., Vallinayagam, G., 2004, Geochemistry and petrogenesis of anorogenic basic volcanic-plutonic rocks of the Kundal area, Malani igneous suite, western Rajasthan, India: Proceedings of Indian Academy of Sciences (Earth and Planetary Sciences), v. 113, p. 667-681.

Skala, W., 1977. A mathematical model to investigative distortions of correlation coefficients in closed arrays: Mathematical Geology, v. 9, p. 519-528.

Skala, W., 1979. Some aspects of the constant-sum problem in geochemistry: Chemical Geology, v. 27, p. 1-9.

Smellie, J.L., 1983. A geochemical overview of subduction-related igneous activity in the South Shetland islands, Lesser Antarctica. In: R.L. Oliver, P.R. James and J.B. Jago (Editors), Antarctic Earth Science: Australian Academy of Sciences and Cambridge University Press, p. 352-356.

Smith, I.E.M., Stewart, R.B., Price, R.C., 2003. The petrology of a large intra-oceanic silicic eruption: the Sandy Bay tephra, Kermadec arc, southwest Pacific. Journal of Volcanology and Geothermal Research, v. 124, p. 173-194.

Smith, T.E., Thirlwall, M.F., MacPherson, C., 1996. Trace element and isotope geochemistry of the volcanic rocks of Bequia, Grenadine Islands, Lesser Antilles Arc: a study of subduction enrichment and intra-crustal contamination: Journal of Petrology, v. 37, p. 117-143.

Spencer, J.E., Normark, R., 1979. Tosco-Abreojos fault zone: A Neogene transform plate boundary within the Pacific margin of southern Baja California, Mexico: Geology, v. 7, p. 554-557.

Spengler, S.R., Garcia, M.O., 1988. Geochemistry of the Hawi lavas, Kohala Volcano, Hawaii: Contributions to Mineralogy and Petrology, v. 99, p. 90-104.

Sruoga, P., Llambías, E.J., Fauqué, L., Schonwandt, D., Repol, D.G., 2005. Volcanological and geochemical evolution of the Diamante caldera-Maipo volcano complex in the southern Andes of Argentina (34°10'S): Journal of South American Earth Sciences, v. 19, p. 399-414.

Stephenson, D., Marshall, T.R., 1984. The petrology and mineralogy of Mt. Popa volcano and the nature of the late-Cenozoic Burma volcanic arc: Journal of the Geological Society of London, v. 141, p. 747-762.

Stock, J.M., Lee, J., 1994. Do microplates in subduction zones leave a geological record?: Tectonics, v. 13, p. 1472-1487.

Stolz, A.J., Varne, R., Davies, G.R., Wheller, G.E., Fodon, J.D., 1990. Magma source components in an arc-continent collision zone: the Flores-Lembata sector, Sunda arc, Indonesia: Contributions to Mineralogy and Petrology, v. 105, p. 585-601.

Stolz, A.J., Varne, R., Wheller, G.E., Foden, J.D., Abbott, M.J., 1988. The geochemistry and petrogenesis of K-rich alkaline volcanics from the Batu Tara volcano, eastern Sunda arc: Contributions to Mineralogy and Petrology 98: 374-389.

Streck, M.J., Grunder, A.L., 1999. Enrichment of basalt and mixing of dacite in the rootzone of a large rhyolite chamber: inclusions and pumices from the Rattelsnake tuff, Oregon: Contributions to Mineralogy and Petrology, v. 136, p. 193-212.

Streckeisen, A., Le Maitre, R. W., 1979. A chemical approximation to the modal QAPF classification of igneous rocks. Neues Jahrbuch für Mineralogie Abhandlungen, v. 136, p. 169-206.

Sussman, D., 1985. Apoyo caldera, Nicaragua: a major Quaternary silicic eruptive center: Journal of Volcanology and Geothermal Research, v. 24, p. 249-282.

Tamura, Y., 1994. Genesis of island arc magmas by mantle derived bimodal magmatism: evidence from the Shiraham group, Japan: Journal of Petrology, v. 35, p. 619-645.

Tamura, Y., Tani, K., Chang, Q., Shukuno, H., Kawabata, H., Ishizuka, O., Fiske, R.S., 2007. Wet and dry basalt magma evolution at Torishima Volcano, Izu-Bonin Arc, Japan: the possible role of phengite in the downgoing slab: Journal of Petrology, v. 48, p. 1999-2031.

Tamura, Y., Yuhara, M., Ishii, T., Irino, N., Shukuno, H., 2003. Andesites and dacites from Daisen volcano, Japan: partial-to-total remelting of an andesite magma body: Journal of Petrology, v. 44, p. 2243-2260.

Tatsumi, Y., Murasaki, M., Arsadi, E.M., Nohda, S., 1991. Geochemistry of Quaternary lavas from NE Sulawesi: transfer of subduction components into the mantle wedge: Contributions to Mineralogy and Petrology, v. 107, p. 137-149.

Tatsumi, Y., Murasaki, M., Nohda, S., 1992. Across-arc variation of lava chemistry in the Izu-Bonin arc: identification of subduction components: Journal of Volcanology and Geothermal Research, v. 49, p. 179-190.

Taylor, R.N., Nesbitt, R.W., 1998. Isotopic characteristics of subduction fluids in an intra-oceanic setting, Izu-Bonin Arc, Japan: Earth and Planetary Science Letters, v. 164, p. 79-98.

Taylor, R.N., Nesbitt, R.W., Vidal, P., Harmon, R.S., Auvray, B., Croudace, I.W., 1994, Mineralogy, chemistry, and genesis of the boninite series volcanics, Chichijima, Bonin Islands, Japan: Journal of Petrology, v. 35, p. 577-617.

Thirlwall, M.F., Graham , A.M., Arculus, R.J., Harmon, R.S., Macpherson, C.G., 1997. Resolution of the effects of crustal assimilation, sediment subduction, and fluid transport in island arc magmas: Pb-Sr-Nd-O isotope geochemistry of Grenada, Lesser Antilles: Geochimica et Cosmochimica Acta, v. 60, p. 4785-4810.

Thirlwall, M.F., Graham, A.M., 1984. Evolution of high-Ca, high-Sr C-series basalts from Grenada, Lesser Antilles: the effects of intra-crustal contamination: Journal of the Geological Society of London, v. 141, p. 427-445.

Thompson, R. N., 1984. Dispatches from the basalt front. 1. Experiments: Proceedings of the Geologists' Association, v. 95, p. 249-262.

Togashi, S., Tanaka, T., Yoshida, T., Ishikawa, K.-I., Fujinawa, A., Kurasawa, H., 1992. Trace elements and Nd-Sr isotopes of island arc tholeiites from frontal arc of northeast Japan: Geochemical Journal, v. 26, p. 261-277.

Tormey, D.R., Hickey-Vargas, R., Frey, F.A., López-Escobar, L., 1991. Recent lavas from the Andean volcanic front (33 to 42°S); interpretations of along-arc compositional variations. In: R.S. Harmon and C.W. Rapela (Editors), Andean magmatism and its tectonic setting, Geological Society of America Special Paper. Geological Society of America, Boulder, Colorado, p. 57-77.

Torres-Alvarado, I. S., 2002. Chemical equilibrium in hydrothermal systems: the case of Los Azufres geothermal field, Mexico: International Geology Review, v. 44, p. 639-652.

Torres-Alvarado, I. S., K. Pandarinath., Verma, S.P., Dulski, P., 2007. Mineralogical and geochemical effects due to hydrothermal alteration in the Los Azufres geothermal field, Mexico: Revista Mexicana de Ciencias Geológicas, v. 24, p. 15-24.

Torres-Alvarado, I. S., Satir, M., 1998. Geochemistry of hydrothermally altered rocks from Los Azufres geothermal field, Mexico: Geofísica Internacional, v. 37, p. 201-213.

Trua, T., Deniel, C., Mazzuoli, R., 1999. Crustal control in the genesis of Plio-Quaternary bimodal magmatism of the Main Ethiopian Rift (MER): geochemical and isotopic (Sr, Nd, Pb) evidence: Chemical Geology, v. 155, p. 201-231.

Trumbull, R.B., Wittenbrink, R., Hahne, K., Emmermann, R., Büsch, W., Gerstenberger, H., Siebel, W., 1999. Evidence for Late Miocene to Recent contamination of arc andesites by crustal melts in the Chilean Andes (25-26°S) and its geodynamic implications: Journal of South American Earth Sciences, v. 12, p. 135-155.

Turner, S., Foden, J., 2001. U, Th and Ra disequilibria, Sr, Nd and Pb isotope and trace element variations in Sunda arc lavas: predominance of a subducted sediment component: Contributions to Mineralogy and Petrology, v. 142, p. 43-57.

Turner, S., Foden, J., George, R., Evans, P., Varne, R., Elburg, M., Jenner, G., 2003. Rates and processes of potassic magma evolution beneath Sangeang Api volcano, East Sunda arc, Indonesia: Journal of Petrology, v. 44, p. 491-515.

Turner, S., Hawkesworth, C., Liu, J., Rogers, N., Kelley, S., Calsteren, P.V., 1993. Timing of Tibetan uplift constrained by analysis of volcanic rocks: Nature, v. 364, p. 50-54.

Turner, S., Hawkesworth, C.J., Calsteren, P.V., Heath, E., Macdonald, R., Black, S., 1996. U-series isotopes and destructive plate margin magma genesis in the Lesser Antilles: Earth and Planetary Science Letters, v. 142, p. 191-207.

Ujike, O., Stix, J., 2000. Geochemistry and origins of Ueno and On-take basaltic to andesitic rocks (<3 Ma) produced by distinct contributions of subduction components, central Japan: Journal of Volcanology and Geothermal Research, v. 95, p. 49-64.

van Bergen, M.J., Vroon, P.Z., Varekamp, J.C., Poorter, R.P.E., 1992. The origin of the potassic rock suite from Batu Tara volano (East Sunda Arc, Indonesia): Lithos, v. 28, p. 261-282.

Van Kranendonk, M.J., 2010, Two types of Archean continental crust: plume and plate tectonics on early earth: American Journal of Science, v. 310, p. 1187-1209.

Vasconcelos-F., M., Verma, S.P., Rodriguez-G., J.F., 1998. Discriminacion tectonica: Nuevo diagrama Nb-Ba para arcos continentales, arcos insulares, "rifts" e islas oceanicas en rocas maficas (Tectonic discrimination: new Nb-Ba diagram for mafic magmas from continental arcs, island arcs, rifts and ocean-islands): Boletin de la Sociedad Espanola de Mineralogia, v.21, p. 129-146.

Velasco-Tapia, F., Verma, S. P., 2012. Magmatic processes at the Volcanic Front of Central Mexican Volcanic Belt: Sierra de Chichinautzin Volcanic Field (Mexico): Turkish Journal of Earth Sciences, v. 21, p. 1-58.

Vergara, M., López-Escobar, L., Palma, J.L., Hickey-Vargas, R., Roeschmann, C., 2004. Late Tertiary volcanic episodes in the area of the city of Santiago de Chile: new geochronological and geochemical data: Journal of South American Earth Sciences, v. 17, p. 227-238.

Verma S.P., Pandarinath, K., Verma, S.K., 2010. Statistically correct methodology for compositional data in new discriminant function tectonomagmatic diagrams and application to ophiolite origin: Advance in Geosciences, A 6-Volume Set (Set Editor-in-chief: Kenji Satake), Solid Earth, v. 26, p. 11-22, world Scientific Publishing Company.

Verma, S. P. 2001. Geochemical and Sr-Nd-Pb isotopic evidence for a combined assimilation and fractional crystallisation process for volcanic rocks from the Huichapan caldera, Hidalgo, Mexico: Lithos, v. 56, p. 141-164.

Verma, S. P., 1996. Uso y abuso de los diagramas de discriminación: Actas INAGEQ, v.2, p. 17-22.

Verma, S. P., 1997. Sixteen statistical tests for outlier detection and rejection in evaluation of International Geochemical Reference Materials: example of microgabbro PM-S. Geostandards Newslette: The Journal of Geostandards and Geoanalysis, v. 21, p. 59-75.

Verma, S. P., 2000b. Geochemistry of the subducting Cocos plate and the origin of subduction-unrelated mafic volcanism at the volcanic front of the central Mexican Volcanic Belt. Cenozoic tectonics and volcanism of Mexico: H. Delgado-Granados, G. Aguirre-Díaz and J. M. Stock: Geological Society of America Special paper, v. 334, p. 195-222.

Verma, S. P., 2002. Absence of Cocos plate subduction-related basic volcanism in southern Mexico: a unique case on Earth?: Geology, v. 30, p. 1095-1098.

Verma, S. P., 2004. Solely extension-related origin of the eastern to west-central Mexican Volcanic Belt (Mexico) from partial melting inversion model: Current Science, v. 86, p. 713-719.

Verma, S. P., 2006. Extension related origin of magmas from a garnet-bearing source in the Los Tuxtlas volcanic field, Mexico: International Journal of Earth Sciences, v. 95, p. 871-901.

Verma, S. P., 2009. Continental rift setting for the central part of the Mexican Volcanic Belt: A statistical approach: Open Geology Journal, v. 3, p. 8-29.

Verma, S. P., 2010. Statistical evaluation of bivariate, ternary and discriminant function tectonomagmatic discrimination diagrams: Turkish Journal of Earth Sciences, v. 19, p. 185-238.

Verma, S. P., Andaverde, J., 2007. Coupling of thermal and chemical simulations in a 3-D integrated magma chamber-reservoir model: a new geothermal energy research frontier. Geothermal Energy Research Trends: H. I. Ueckermann. New York, Nova Science Publishers, Inc.: p. 149-189.

Verma, S. P., Carrasco-Núñez, G., Milán, M., 1991. Geology and geochemistry of Amealco caldera, Qro., Mexico: Journal of Volcanology and Geothermal Research, v. 47, p. 105-127.

Verma, S. P., I. S. Torres-Alvarado., Satir, M., Dobson, P.F., 2005. Hydrothermal alteration effects in geochemistry and Sr, Nd, Pb, and O isotopes of magmas from the Los Azufres geothermal field (Mexico): a statistical approach: Geochemical Journal, v. 39, p. 141-163.

Verma, S. P., I. S. Torres-Alvarado., Sotelo-Rodríguez, Z.T., 2002. SINCLAS: standard igneous norm and volcanic rock classification system: Computers & Geosciences, v. 28, p. 711-715.

Verma, S. P., I. S. Torres-Alvarado., Velasco-Tapia, F., 2003. A revised CIPW norm: Schweizerische Mineralogische und Petrographische Mitteilungen, v. 83, p. 197-216.

Verma, S., Pandarinath, P. K., Santoyo, E., González-Partida, E., Torres-Alvarado, I., Tello-Hinojosa, E., 2006. Fluid chemistry and temperature prior to exploitation at the Las Tres Vírgenes geothermal field, Mexico: Geothermics, v. 35, p. 156-180.

Verma, S.K., Pandarinath, K., Verma, S.P., 2012, Statistical evaluation of tectonomagmatic discrimination diagrams for granitic rocks and proposal of new discriminant-function-based multi-dimensional diagrams for acid rocks: International Geology Review, v. 54, p. 325-347

Verma, S.P., 1984. Alkali and alkaline earth element geochemistry of Los Humeros caldera, Puebla: Journal of Volcanology and Geothermal Research, v. 20, p. 21-40.

Verma, S.P., 2000a. Geochemical evidence for a lithospheric source for magmas from Los Humeros: Chemical Geology, v. 164, p. 35-60.

Verma, S.P., 2012, Application of multi-dimensional discrimination diagrams and probability calculations to acid rocks from Portugal and Spain: Comunicações Geológicas, v. 99, in press.

Verma, S.P., Agrawal, S., 2011. New tectonic discrimination diagrams for basic and ultrabasic volcanic rocks through log-transformed ratios of high field strength elements and implications for petrogenetic processes: Revista Mexicana de Ciencias Geológicas, v. 28, p. 24-44.

Verma, S.P., Díaz-González, L., 2011. Application of the discordant outlier detection and separation system in the geosciences: International Geology Review (in press) DOI: 10.1080/00206814.2011.569402.

Verma, S.P., Gómez-Arias, E., Andaverde, J., 2011. Thermal sensitivity analysis of emplacement of the magma chamber in Los Humeros caldera, Puebla, Mexico: International Geology Review, v. 53, p. 905-925.

Verma, S.P., Guevara, M., Agrawal, S., 2006. Discriminating four tectonic settings: five new geochemical diagrams for basic and ultrabasic volcanic rocks based on log-ratio transformation of major-element data: Journal of Earth System Science, v. 115, p. 485-528.

Verma, S.P., Lopez, M.M., 1982. Geochemistry of Los Humeros caldera, Puebla, Mexico: Bulletin Volcanologique, 45, p. 63-79.

Verma, S.P., Torres-Alvarado, I.S., Sotelo-Rodríguez, Z.T., 2002. SINCLAS: standard igneous norm and volcanic rock classification system: Computers and Geosciences, v. 28, p. 711-715.

Vermeesch, P., 2006. Tectonic discrimination diagrams revisited: Geochemistry Geophysics Geosystems, v. 7, Q06017.

Wade, J.A., Plank, T., Stern, R.J., Tollstrup, D.L., Gill, J.B., O'Leary, J.C., Eiler, J.M., Moore, R.B., Woodhead, J.D., Trusdell, F., Fischer, T.P., Hilton, D.R., 2005. The May 2003 eruption of Anatahan volcano, Mariana islands: geochemical evolution of a silicic island-arc volcano: Journal of Volcanology and Geothermal Research, v. 146, p. 139-170.

Walker, J.A., Patino, L.C., Cameron, B.I., Carr, M.J., 2000. Petrogenetic insights provided by compositional transects across the Central American arc: southeastern Guatemala and Honduras: Journal of Geophysical Research, v. 105, p. 18949-18963.

Walker, J.A., Patino, L.C., Carr, M.J., Feigenson, M.D., 2001. Slab control over HFSE depletions in central Nicaragua: Earth and Planetary Science Letters, v. 192, p. 533-543.

Wang, P. and Glover, L. III., 1992. A tectonics test of the most commonly used geochemical discriminant diagrams and patterns: Earth-Science Reviews, v. 33, p. 111-131.

Weis, D., Frey, F.A., Leyrit, H., Gautier, I., 1993. Kerguelen archipelago revisited: geochemical and isotopic study of the southeast province lavas: Earth and Planetary Science Letters, v. 118, p. 101-119.

West, H.B., Garcia, M.O., Gerlach, D.C., Romero, J., 1992. Geochemistry of tholeiites from Lanai, Hawaii: Contributions to Mineralogy and Petrology, v. 112, p. 520-542.

Wheller, G.E., Varne, R., Foden, J.D., Abbott, M.J., 1987. Geochemistry of Quaternary volcanism in the Sunda-Banda arc, Indonesia, and three-component genesis of island-arc basaltic magmas: Journal of Volcanology and Geothermal Research, v. 32, p. 137-160.

Wilson, M. 1989. Igneous petrogenesis. A global tectonic approach: London, Harper Collins Academic, 456 p.

Winchester, J. A., Floyd, P. A., 1976. Geochemical magma type discrimination: application to altered and metamorphosed basic igneous rocks: Earth and Planetary Science Letters, v. 28, p. 459-469.

Winchester, J. A., Floyd, P. A., 1977. Geochemical discrimination of different magma series and their differentiation products using immobile elements: Chemical Geology, v. 20, p. 325-343.

Wolde, B., Asres, Z., Desta, Z., Gonzalez, J.J., 1996, Neoproterozoic zirconium-depleted boninite and tholeiitic series rocks from Adola, southern Ethiopia: Precambrian Research, v. 80, p. 261-279.

Wood, D. A., 1990. The application of a Th-Hf-Ta diagram to problems of tectonomagmatic classification and to establishing the nature of crustal contamination of basaltic lava of the British tertiary volcanic province: Earth and Planetary Science Letters, v. 50, p. 11-30.

Wood, D.A., 1980. The application of a Th-Hf-Ta diagram to problems of tectonomagmatic classification and to establishing the nature of crustal contamination of basaltic lavas of the British Tertiary volcanic province: Earth and Planetary Science Letters, v. 50, p. 11-30.

Woodhead, J.D., 1988. The origin of geochemical variations in Mariana lavas: a general model for petrogenesis in intra-oceanic island arcs: Journal of Petrology, v. 29, p. 805-830.

Woodhead, J.D., Johnson, R.W., 1993. Isotopic and trace-element profiles across the New Britain island arc, Papua New Guinea: Contributions to Mineralogy and Petrology, v. 113, p. 479-491.

Woronow, A., Love, K. M., 1990. Quantifying and testing differences among means of compositional data suites: Mathematical Geology, v. 22, p. 837-852.

Wright, I.C., Worthington, T.J., Gamble, J.A., 2006. New multibeam and geochemistry of the 30°-35°S sector, and overview of southern Kermadec arc volcanism: Journal of Volcanology and Geothermal Research, v. 149, p. 263-296.

Xu, G., Frey, F.A., Clague, D.A., Abouchami, W., Blichert-Toft, J., Cousens, B., Weisler, M., 2007. Geochemical characteristics of West Molokai shield- and postshield-stage lavas: Constraints on Hawaiian plume models: Geochemistry Geophysics Geosystems, v. 8, p. 1-40.

Xu, G., Frey, F.A., Clague, D.A., Weis, D., Beeson, M.H., 2005. East Molokai and other Kea-trend volcanoes: magmatic processes and sources as they migrate away from the Hawaiian hot spot: Geochemistry Geophysics Geosystems, v. 6: Q05008, doi: 10.1029/2004GC000830.

Yellur, D. D., Nair, R. S., 1978. Assigning a magmatically defined tectonic environment to Chitradurga metabasalts, India, by geochemical methods: Precambrian Research, v. 7, p. 259-281.

Zellmer, G., Turner, S., Hawkesworth, C., 2000. Timescales of destructive plate margin magmatism: new insights from Santorini, Aegean volcanic arc: Earth and Planetary Science Letters, v. 174, p. 265-281.

Zellmer, G.F., Hawkesworth, C.J., Sparks, R.S.J., Thomas, L.E., Harford, C.L., Brewer, T.S., Loughlin, S.C., 2003. Geochemical evolution of the Soufrière Hills volcano, Montserrat, Lesser Antilles volcanic arc: Journal of Petrology, v. 44, p. 1349-1374.

Zhang, M., Suddaby, P., Thompson, R.N., Thirlwall, M.F., Menzies, M.A., 1995. Potassic volcanic rocks in NE China: geochemical constraints on mantle source and magma genesis: Journal of Petrology, v. 36, p. 1275-1303.

Zhao, Z., Mo, X., Dilek, Y., Niu, Y., DePaolo, D.J., Robinson, P., Zhu, D., Sun, C., Dong, G., Zhou, S., Luo, Z., Hou, Z., 2009, Geochemical and Sr-Nd-O isotopic compositions of the post-collisional ultrapotassic magmatism in SW Tibet: petrogenesis and implications for India intra-continental subduction beneath southern Tibet: Lithos, v. 113, p. 190-212.

Zhi, X., Song, Y., Frey, F.A., Feng, J., Zhai, M., 1990. Geochemistry of Hannuoba basalts, eastern China: constraints on the origin of continental alkalic and tholeiitic basalt: Chemical Geology, v. 88, p. 1-33.

Zhuravlev, D.Z., Tsvetkov, A.A., Zhuravlev, A.Z., Gladkov, N.G., Chernysheva, I.V., 1987. 143Nd/144Nd and 87Sr/86Sr ratios in recent magmatic rocks of the Kurile Island Arc: Chemical Geology, v. 66, p. 227-243.

Zou, H., Reid, M.R., Liu, Y., Yao, Y., Xu, X., Fan, Q., 2003. Constraints on the origin of historic potassic basalts from northeast China by U-Th disequilibrium data: Chemical Geology, v. 200, p. 189-201.

Zou, H., Zindler, A., Xisheng, X., Qi, Q., 2000. Major, trace element, and Nd, Sr and Pb isotope studies of Cenozoic basalts in SE China: mantle sources, regional variations and tectonic significance: Chemical Geology, v. 171, p. 33-47.

Annexures

ANNEXURE I (Page 149-172)

Verma S.K., Pandarinath, K., Verma, S.P., 2012. Statistical evaluation of tectonomagmatic discrimination diagrams for granitic rocks and proposal of new discriminant-function-based multi-dimensional diagrams for acid rocks: **International Geology Review,** v. 54, p. 325-347.

International Geology Review
Publication details, including instructions for authors and subscription information:
http://www.tandfonline.com/loi/tigr20

Statistical evaluation of tectonomagmatic discrimination diagrams for granitic rocks and proposal of new discriminant-function-based multi-dimensional diagrams for acid rocks

Sanjeet K. Verma [a] , Kailasa Pandarinath [b] & Surendra P. Verma [b]

[a] Posgrado en Ingeniería, Centro de Investigación en Energía, Universidad Nacional Autónoma de México, Priv. Xochicalco s/no., Col Centro, Apartado Postal 34, Temixco, 62580, Mexico

[b] Departamento de Sistemas Energéticos, Centro de Investigación en Energía, Universidad Nacional Autónoma de México, Priv. Xochicalco s/no., Col Centro, Apartado Postal 34, Temixco, 62580, Mexico

Available online: 07 Jul 2011

To cite this article: Sanjeet K. Verma, Kailasa Pandarinath & Surendra P. Verma (2012): Statistical evaluation of tectonomagmatic discrimination diagrams for granitic rocks and proposal of new discriminant-function-based multi-dimensional diagrams for acid rocks, International Geology Review, 54:3, 325-347

To link to this article: http://dx.doi.org/10.1080/00206814.2010.543784

International Geology Review
Vol. 54, No. 3, February 2012, 325–347

Taylor & Francis
Taylor & Francis Group

Statistical evaluation of tectonomagmatic discrimination diagrams for granitic rocks and proposal of new discriminant-function-based multi-dimensional diagrams for acid rocks

Sanjeet K. Verma[a], Kailasa Pandarinath[b] and Surendra P. Verma[b]*

[a]*Posgrado en Ingeniería, Centro de Investigación en Energía, Universidad Nacional Autónoma de México, Priv. Xochicalco s/no., Col Centro, Apartado Postal 34, Temixco 62580, Mexico;* [b]*Departamento de Sistemas Energéticos, Centro de Investigación en Energía, Universidad Nacional Autónoma de México, Priv. Xochicalco s/no., Col Centro, Apartado Postal 34, Temixco 62580, Mexico*

(*Accepted 29 September 2010*)

The four tectonic discrimination diagrams of Pearce *et al*. [Journal of Petrology, v. 25, p. 956–983] for granitic rocks were first evaluated using the literature cited by these authors as well as from our new database. The first diagram (Y−Nb) cannot discriminate volcanic-arc and collision settings. Both Y−Nb and Yb−Ta diagrams have an overlapping field for within-plate and ocean-ridge granitoids. The remaining two diagrams (Y+Nb−Rb and Yb+Ta−Rb) use a mobile element (Rb) in their *y*-axis. Although these diagrams successfully discriminate volcanic-arc and within-plate granites, they perform less well for collision tectonics. Besides, felsic or acid rocks are scarce in ocean-ridge settings, which limits the usefulness of these diagrams for this geological environment. Therefore, using an extensive database, we proposed a set of five new discriminant-function-based multi-dimensional diagrams for acid magmas from four tectonic settings (island arc, continental arc, continental rift, and collision). The very similar tectonic settings of island and continental arcs are discriminated for the first time. These diagrams are based on correct statistical treatment of compositional data, because they use natural logarithm transformation of major-element ratios and linear discriminant analysis (LDA). The use of discordant outlier-free samples prior to LDA improved the success rates by about 3–5%. Success rates of these diagrams as inferred from a testing set were between 76% and 88% for island arc, 60% and 92% for continental arc, and 72% and 84% for both continental rift and collision settings. Finally, application of these new diagrams to case studies not compiled in our initial database used for constructing these diagrams provided the following results: a collision setting for the Himalayas at about 30 Ma; an island arc setting for Quaternary acid rocks from geothermal boreholes in El Salvador; an island- or continental-arc setting for northern Italy at 35–52 Ma; a continental-arc setting for the Italy–Austria border at about 30 Ma; either a rift or a collision setting for northern Nigeria at about 164 Ma; a collision setting for central Nigeria at about 144 Ma and for the Cretaceous Masirah ophiolites of Oman; and an island arc setting for the Cretaceous Semail ophiolites of Oman. In spite of the relative mobility of major elements, these applications suggest utility of the new discrimination diagrams for all four tectonic settings.

Keywords: major-element; tectonic settings; acid rocks; felsic rocks; discordant outliers; log-ratio transformation; tectonomagmatic discrimination

Introduction

The development of geochemical discrimination diagrams for plate tectonic environments was pioneered by Pearce and Cann (1971, 1973). Discrimination diagrams have been developed on the basis of the geochemical characteristics of volcanic or plutonic rocks from known tectonic environments. These diagrams are frequently applied to rocks of different ages from areas where the tectonic regime prevailing at the time of formation of those rocks is not well understood. In recent years, there has been renewed interest in the subject of tectonomagmatic discrimination diagrams (e.g. Wang and Glover III 1992; Rollinson 1993; Verma 2000, 2010; Agrawal *et al*. 2004, 2008; Verma *et al.* 2006; Verma and Agrawal 2011).

Following the International Union of Geological Sciences (IUGS) nomenclature (Le Bas *et al.* 1986), we will use the geochemical term 'acid' for those rocks that have $(SiO_2)_{adj} > 63\%$ (the subscript adj refers to the major-element data adjusted to 100% on an anhydrous basis and after Fe-oxidation ratio adjustment; Verma *et al.* 2002). Therefore, the mineralogical term 'felsic' will not be used.

Numerous discrimination diagrams have been proposed for basic igneous rocks with $(SiO_2)_{adj} < 52\%$ (e.g. Rollinson 1993; Verma 2010), but only a few diagrams are available for tectonic discrimination of acid magmas or granitic rocks. The most widely used diagrams for granitic rocks were proposed by Pearce *et al.* (1984; with more than 2100 citations in international journals as documented in the Science Citation Index). We hypothesize two main reasons to explain the existence of very few diagrams for discriminating tectonic setting of acid rocks. First, basic rocks are present in all tectonic settings (island

*Corresponding author. Email: spv@cie.unam.mx

ISSN 0020-6814 print/ISSN 1938-2839 online

http://dx.doi.org/10.1080/00206814.2010.543784
http://www.tandfonline.com

arc, continental arc, continental rift, ocean-island, mid-ocean-ridge, and flood basalt province), whereas acid rocks are scarce at least in the ocean-island and mid-ocean-ridge settings. The second reason might be related to the more complicated petrogenetic history of granites affected by processes such as crystal fractionation or accumulation, extensive involvement of continental crust, magma mixing, and redistribution and loss of elements by volatile fluxing (e.g. Hanson 1978; Rollinson 1993), which can make the chemical composition of such evolved acid magmas more difficult to interpret than of basic magmas. These complexities may also significantly reduce the chemical differences of acid magmas from different tectonic settings with the consequence that meaningful tectonic discrimination diagrams may not be easily proposed.

In this work, we have evaluated the performance of the four discrimination diagrams [Y−Nb, Yb−Ta, (Y+Nb)−Rb, and (Yb+Ta)−Rb] of Pearce *et al.* (1984), using a parameter called 'success rate'. Success rate refers to the efficiency of a plot for a given tectonic setting and is the ratio of the number of correctly discriminated samples to the total number of samples, expressed as percentage (Verma *et al.* 2006; Agrawal *et al.* 2008; Verma 2010). The incorrect discrimination or mis-discrimination is the complement of the efficiency, which refers to the samples incorrectly plotted in a tectonic setting different from the expected or inferred one. To understand the quality of the diagrams proposed by Pearce *et al.* (1984), we used the original database of these authors, because they had not reported success rates or correct discrimination of their diagrams. Additionally, a new database was necessary to achieve an unbiased evaluation of the overall performance of these diagrams.

Three of these diagrams [Yb−Ta, (Y+Nb)−Rb, and (Yb+Ta)−Rb] can discriminate acid magmas from four main tectonic settings: volcanic-arc granites (VAG), ocean-ridge granites (ORG), collision granites (syn-COLG), and within-plate granites (WPG), whereas the Y−Nb diagram can do so for three settings only, because VAG and syn-COLG represent a combined overlapping field (VAG+syn-COLG). Our conclusion is that the diagrams proposed by Pearce *et al.* (1984) might be useful for VAG and WPG, but they cannot successfully discriminate syn-COLG samples; besides, they are not likely to be useful for ORG.

Nevertheless, as documented by Verma (2010), all bivariate or ternary tectonomagmatic diagrams are characterized by statistically wrong treatment of compositional data (Aitchison 1986), eye-drawn subjective boundaries for different tectonic fields (Agrawal 1999), and lack of representation of the entire statistical population (Agrawal and Verma 2007). Pearce *et al*. (1984) diagrams are no exceptions to these criticisms. Therefore, new diagrams for acid magmas are required, which should be based on correct statistical treatment involving log-ratio transformation of chemical variables (Aitchison 1986; Agrawal and Verma 2007). We propose new discriminant-function-based multi-dimensional diagrams for acid rocks using log-ratios of major elements. These diagrams enable us to discriminate island arc, continental arc, continental rift, and collision settings.

Methodology

The methodology used to provide an unbiased evaluation of Pearce *et al.* (1984) diagrams and to propose new diagrams consists of the following steps: (1) establish a representative database from different tectonic settings from all over the world; (2) plot the samples in various diagrams (Pearce *et al.* 1984), obtain statistical information from each diagram, and report the utility of these diagrams based on this evaluation; (3) ascertain that the samples represent acid magmas; (4) apply linear discriminant analysis (LDA) to discordant outlier-free, normally distributed, log-ratio transformed major-element data of a training set for proposing new diagrams and evaluate the overall functioning of these diagrams from a testing set; and (5) apply these diagrams to case studies and thus illustrate and evaluate their usefulness.

(1) We compiled three data sets. The first data set or database was established from the literature that Pearce *et al*. (1984) had compiled, although we were unable to obtain all the references cited by them. The second data set consisted of published data on both plutonic and volcanic rocks from collision tectonic setting, which were not included in Pearce *et al.* (1984) paper. For the third data set, we compiled chemical data for mainly fresh, acid volcanic rock samples from the areas with a known, uncontroversial tectonic setting. The sample locations are shown schematically in Figure 1 and their longitude and latitude values are presented in Table S1 (see online supplementary material at www.informaworld.com/tigr).

The literature sources for the first database were as follows: for syn-COLG, Abbotts (1978), Alderton *et al*. (1980), Dietrich and Gansser (1981), Dupuy *et al*. (1982), and Vidal *et al.* (1982); for VAG, Bateman and Chappell (1979), López-Escobar *et al*. (1979), Saunders *et al*. (1979, 1980), and Alabaster *et al*. (1982); for WPG, Walsh *et al*. (1979), Imeokparia (1982, 1983), and Harris *et al*. (1983); and for ORG, Engel and Fisher (1975) and Aldiss (1981).

For constructing the new database (second and third sets), we applied the same age restrictions (Miocene or younger) as imposed by Agrawal *et al.* (2004, 2008), Verma *et al.* (2006), Verma (2010), and Verma and Agrawal (2011), to their

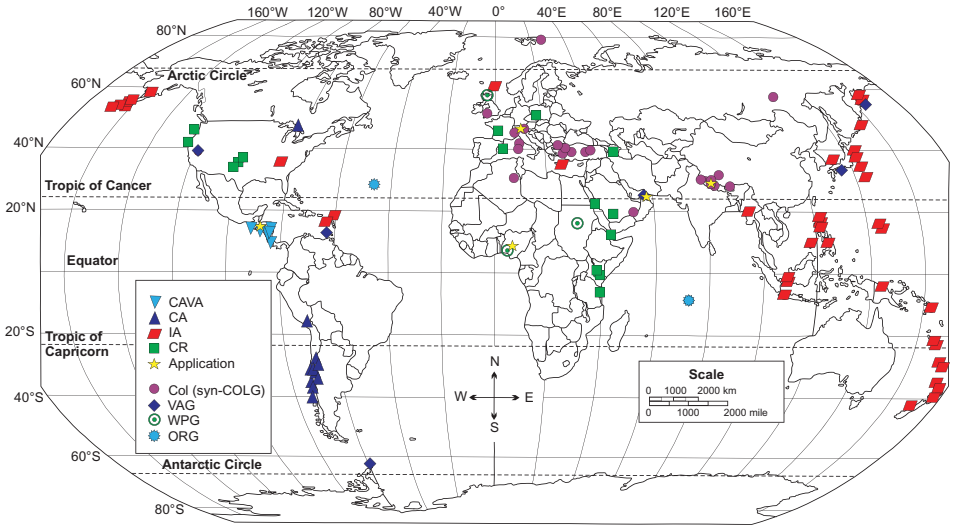

Figure 1. Sample localities on a world map (modified from an unpublished map kindly provided by J.S. Armstrong-Altrin). The abbreviations are as follows: CAVA, Central American Volcanic Arc; CA, continental arc of the Andes; IA, island arc; CR, continental rift; Col, collision; syn-COLG, syn-collision granites (as used by Pearce *et al.* 1984); VAG, volcanic-arc granite; WPG, within-plate granite; and ORG, ocean-ridge granite. Star symbols indicate the locations of application examples. Approximate longitude and latitude values of sample locations are presented in Table S1. The symbols are shown as inset.

databases, except that the data for acid rather than basic magmas were compiled. The literature sources for the second data set (collision setting only) were as follows: Castelli and Lombardo (1988), Pearce *et al*. (1990), Scaillet *et al*. (1990), Morra *et al*. (1994), Guillot and Fort (1995), Ayres and Harris (1997), Grigoriev and Pshenichny (1998), Liégeois *et al*. (1998), Debon and Lemmet (1999), Aldanmaz *et al*. (2000), Delaloye and Bingol (2000), Dini *et al*. (2002), Visona and Lombardo (2002), Ilbeyli *et al*. (2004), Koprubasi and Aldanmaz (2004), Cherneva and Georgieva (2005), Hasozbek *et al*. (2011), and Reichardt *et al*. (2010).

The literature sources for the third data set are listed below for arc and rift settings. For island arc setting, we compiled data from several island arcs, whereas for continental-arc setting, the data from the Central American Volcanic Arc (CAVA) and the Andes of South America were compiled. The corresponding references were as follows: Bryan *et al*. (1972), Ewart and Bryan (1972), Brown *et al*. (1977), Ewart *et al*. (1977), Foden and Varne (1980), Cole (1981), Deruelle (1982), Smellie (1983), Frey *et al*. (1984), Stephenson and Marshall (1984), Myers *et al*. (1985), Kay *et al*. (1987), Wheller *et al*. (1987), Zhuravlev *et al*. (1987), Davidson *et al*. (1988), Gerlach *et al*. (1988), Woodhead (1988), Bloomer and Hawkins (1989), Hickey-Vargas *et al*. (1989), Barsdell and Berry (1990), Romick *et al*. (1990), Stolz *et al*. (1990), Defant *et al*. (1991), de Silva (1991), López-Escobar *et al*. (1991), Walker *et al*. (1991), Bardintzeff and Deniel (1992), Hegner and Smith (1992), Singer *et al*. (1992), Togashi *et al*. (1992), Tamura (1994), Gamble *et al*. (1995), Turner *et al*. (1996), Gonzalez-Partida *et al*. (1997), Kepezhinskas *et al*. (1997), Monzier *et al*. (1997), Patino *et al*. (1997), Rotolo and Castorina (1998), Taylor and Nesbitt (1998), Trumbull *et al*. (1999), Dorendorf *et al*. (2000), Ujike and Stix (2000), Zellmer *et al*. (2000, 2003), Churikova *et al*. (2001), Ishikawa *et al*. (2001), Turner and Foden (2001), Cameron *et al*. (2002), Haase *et al*. (2002), Smith *et al*. (2003), Tamura *et al*. (2003), Hildreth *et al*. (2004), Izbekov *et al*. (2004), Schmitz and Smith (2004), Vergara *et al*. (2004), Lindsay *et al*. (2005), McDermott *et al*. (2005), Sruoga *et al*. (2005), Wade *et al*. (2005), Agostini *et al*. (2006), DuFrane *et al*. (2006), Hirotani and Ban (2006), Kimura and Yoshida (2006), Lebti *et al*. (2006), Shukuno *et al*. (2006), Shuto *et al*. (2006), Wright *et al*. (2006), Finney *et al*. (2008), Sendjaja *et al*. (2009), and Schuth *et al*. (2009).

To represent the within-plate tectonic setting, we complied data from continental rifts and continental extension areas from the following sources: Barberi *et al*. (1975), Chauvel and Jahn (1984), Singer and Kudo (1986), Johnson and Lipman (1988), Davidson and Wilson (1989), Moyer and Esperança (1989), Perry *et al*. (1990), Basu *et al*. (1991), Camp *et al*. (1991), Duncker *et al*. (1991), Kampunzu and Mohr (1991), Feuerbach *et al*. (1993), Deniel *et al*. (1994), MacDonald *et al*. (1995), Buket and Temel (1998), Benito *et al*. (1999), Streck and Grunder (1999), Trua *et al*.

(1999), Hsu *et al*. (2000), McMillan *et al*. (2000), Kabeto *et al*. (2001), Le Roex *et al*. (2001), Streck (2002), Peccerillo *et al*. (2003, 2007), Haase *et al*. (2004), Ayalew *et al*. (2006), and Ronga *et al*. (2010). Unfortunately, acid magmas from the ocean-island setting are rather scarce; therefore, this setting could not be adequately represented in our database. In any case, this setting is already covered by discriminant-function-based diagrams for basic magmas (Agrawal *et al.* 2004, 2008; Verma *et al.* 2006; Verma and Agrawal 2011).

The first database was used to calculate the success rates of all four diagrams of Pearce *et al*. (1984). The new database (second and third data sets), consisting of new and more recent compositional data from collision, volcanic-arc, and continental rift tectonic settings, were also used to evaluate the four diagrams of Pearce *et al*. (1984). This procedure provided an unbiased evaluation of these diagrams.

Finally, we combined the second and third data sets for proposing new discrimination diagrams. The first database was not used for this purpose, because most of these samples were older than Miocene. The age constraint of Miocene or younger has been one of the main characteristics of the databases for proposing new diagrams (Agrawal *et al.* 2004, 2008; Verma *et al.* 2006; Verma 2010; Verma and Agrawal 2011). This ensures that the assigned tectonic setting is largely based on direct evidence, without resorting to plate reconstruction models. Nevertheless, we used selected papers from the first database for application purposes.

(2) The data for compiled samples were plotted in Pearce *et al.* (1984) diagrams and success rates were calculated. In this article, we use the term 'success rate' to refer to the correct or inferred tectonic setting. Success rate provides an objective and quantitative way to evaluate and compare the performance of discrimination diagrams. We will not resort to the discussion of mis-discrimination of samples, which was central to the topic of statistical evaluation of classification diagrams (Verma *et al.* 2010a).

(3) For determining the magma types we used the SINCLAS computer program (Verma *et al.* 2002), under the Middlemost (1989) option for Fe-oxidation adjustment. This program requires that complete chemical analyses involving 10 major elements (with total Fe as Fe_2O_3 or FeO) be available for the rock samples to qualify for inclusion in our database. Irrespective of whether the two Fe-oxidation varieties were reported for a given sample, the Fe concentrations were automatically subdivided by SINCLAS into Fe_2O_3 and FeO (Middlemost 1989; Verma *et al.* 2002). Thus, 11 major elements were obtained for all samples. The major-element composition after SINCLAS processing is recognized by the subscript adj added to each major-oxide name. This ensures that all analyses are treated in exactly the same way. Only acid magmas having $(SiO_2)_{adj} > 63\%$ (Le Bas *et al.* 1986) as inferred from SINCLAS, were used in this study.

(4) Correct statistical treatment of compositional data prior to LDA was applied for 10 natural log-transformed ratios of 11 major elements as follows: $\ln(TiO_2/SiO_2)_{adj}$, $\ln(Al_2O_3/SiO_2)_{adj}$, $\ln(Fe_2O_3/SiO_2)_{adj}$, $\ln(FeO/SiO_2)_{adj}$, $\ln(MnO/SiO_2)_{adj}$, $\ln(MgO/SiO_2)_{adj}$, $\ln(CaO/SiO_2)_{adj}$, $\ln(Na_2O/SiO_2)_{adj}$, $\ln(K_2O/SiO_2)_{adj}$, and $\ln(P_2O_5/SiO_2)_{adj}$, in which $(SiO_2)_{adj}$ was used as the common denominator. For simplicity, we use notations such as $\ln(TiO_2/SiO_2)_{adj}$ instead of $\ln[(TiO_2)_{adj}/(SiO_2)_{adj}]$. Because LDA requires that the variables should be normally distributed, to comply with this requirement we used all single-outlier discordancy tests (Barnett and Lewis 1994; Verma 1997; unpublished computer program DODESSYS by S.P. Verma and L. Díaz-González) on the above 11 log-ratio parameters for samples from each tectonic group.

Our database used for proposing new diagrams consisted of samples from island arc (IA), continental arc (CAVA and the Andes), continental rift (CR), and collision (Col) tectonic settings. To acquire an unbiased estimation of the performance of LDA, we divided the data set into two parts called training and testing sets. To create a testing set for a given tectonic setting, 25 samples were randomly drawn from each tectonic setting. The remaining samples (total number of samples – 25) in each group constituted the training set. The random number sequence of a normal distribution $N(0,1)$ generated by Verma and Quiroz-Ruiz (2006) from two different streams of identically and independently distributed numbers from a uniform distribution $U(0,1)$ was used to objectively achieve this subdivision.

A total of five diagrams should be proposed to fully discriminate four tectonic settings (IA, CA, CR, and Col). The first diagram discriminates all fields although IA and CA represent a combined setting (IA+CA), whereas the other four remaining diagrams discriminate three fields at a time.

The training set was used for LDA ('canonical analysis' option in the Advanced 'discriminant analysis-multivariate exploratory techniques' module of *Statistica* software) to obtain discriminant

functions for diagrams for three tectonic settings at a time. The testing set enabled us to estimate success rates for different settings in a given discrimination diagram.

(5) For the use of our new diagrams for a case study, the samples, after ascertaining from SINCLAS their magma character as acid, were plotted in each of the five diagrams and counted for each tectonic field. The first diagram, which contains all four tectonic settings, provides indications of the expected tectonic setting for the samples under study. Thus, the field with the highest number of samples, that is the highest success rate, is identified. If this field is CR or Col, we should then identify the diagram (out of the remaining four diagrams) from which this tectonic field is missing. That particular diagram should be considered as the inapplicable diagram for this case study. If, on the other hand, in the first diagram the field with the highest success rate is the combined field of IA+CA, we must evaluate the samples for these two fields in the second diagram. This diagram should generally indicate either IA or CA with the highest success rate. In this case, one of the remaining three diagrams from which IA or CA is missing will be the inapplicable diagram. If all four applicable diagrams give consistent results, that is one particular field is indicated with the highest success rate in all of them, this tectonic setting can be concluded as the valid or inferred setting for this application. Sometimes, it may not be possible to unequivocally identify the inapplicable diagram, in which case it will be difficult to decide on a unique tectonic setting.

Evaluation of existing diagrams

Evaluation of Pearce et al. (1984) diagrams with the first database

The first database was used to statistically evaluate the efficiency or success rate of a plot for a given tectonic setting (syn-COLG, VAG, WPG, or ORG). The plots are shown in Figure 2A–D whereas the success rates are summarized in Table 1. Success rates were not calculated when the number of samples from a given tectonic setting was low (arbitrarily assumed as <10).

The first diagram (Y−Nb; Figure 2A; Table 1) of Pearce *et al*. (1984), which discriminates only three tectonic settings of VAG+syn-COLG, WPG, and ORG, shows that syn-COLG and VAG cannot be objectively evaluated, because there is no overlap-free field for these two settings. We also envisage difficulty in using this diagram (Figure 2A) for WPG and ORG samples, because Pearce *et al.* (1984) proposed an additional boundary (see dotted line in Figure 2A) within the field of WPG to better discriminate ORG exposed in anomalous ridge segments. The following question arises. What conclusion about the success rate can be drawn when samples from a given area plot in the region bounded by these two lines (WPG–ORG boundary represented by a solid line and the dashed line within the WPG field), as is the case of numerous presumably WPG and ORG samples in Figure 2A? If we ignore this question, the success rate for WPG was 100%, and for ORG all five samples plotted within the ORG field defined by the dashed boundary (Table 1; Figure 2A), that is in the WPG–ORG overlapping field.

The second diagram (Yb−Ta; Figure 2B; Table 1) of Pearce *et al*. (1984) shows high success rates for syn-COLG and VAG (75% and 89%, respectively, Table 1), and if we ignore the above question, the WPG and ORG samples were also correctly discriminated.

The third and fourth diagrams [Figure 2C of (Y+Nb)−Rb and Figure 2D of (Yb+Ta)−Rb] of Pearce *et al*. (1984) showed, respectively, unacceptably low success rates of about 20% and 37% for syn-COLG, although both of them seemed to work well for VAG and WPG (Table 1).

Evaluation of Pearce et al. (1984) diagrams with the new database

To achieve an unbiased evaluation of these diagrams, we used our second data set for testing the collision tectonic setting and the third data set for arc and within-plate settings. The plots are shown in Figure 3 for collision and Figure 4 for arc and continental rift samples. The results are summarized in Table 2.

The first diagram (Figure 3A) shows that 78.9% of the collision samples plotted in the combined field of VAG+syn-COLG, with most of the remaining samples (about 16.6%) plotting in the overlapping field of WPG and ORG (region between the dashed and solid lines of WPG–ORG). Similarly, 74.0% of the volcanic-arc samples plotted in the combined VAG+syn-COLG field. Obviously, because an overlap-free region for arc and collision settings does not exist in this diagram, we cannot talk of success rates for these two tectonic settings. This diagram simply cannot discriminate them. The continental rift samples largely plotted in the within-plate field (71.4%) in this diagram.

In the second diagram, unacceptably low success rates were obtained for collision as Syn-COLG (27.9%; Figure 3B, Table 2), but high success rates were shown for arc and continental rift settings (76.6% as VAG and 74.2% as WPG, respectively, Figure 4B, Table 2).

The third and fourth diagrams (Figure 3C and 3D) also showed, respectively, low success rates of about 16.1% and 37.5% for syn-COLG (Table 2). On the other hand, the samples from volcanic-arc and within-plate settings gave high success rates (Table 2) of 83.0% and

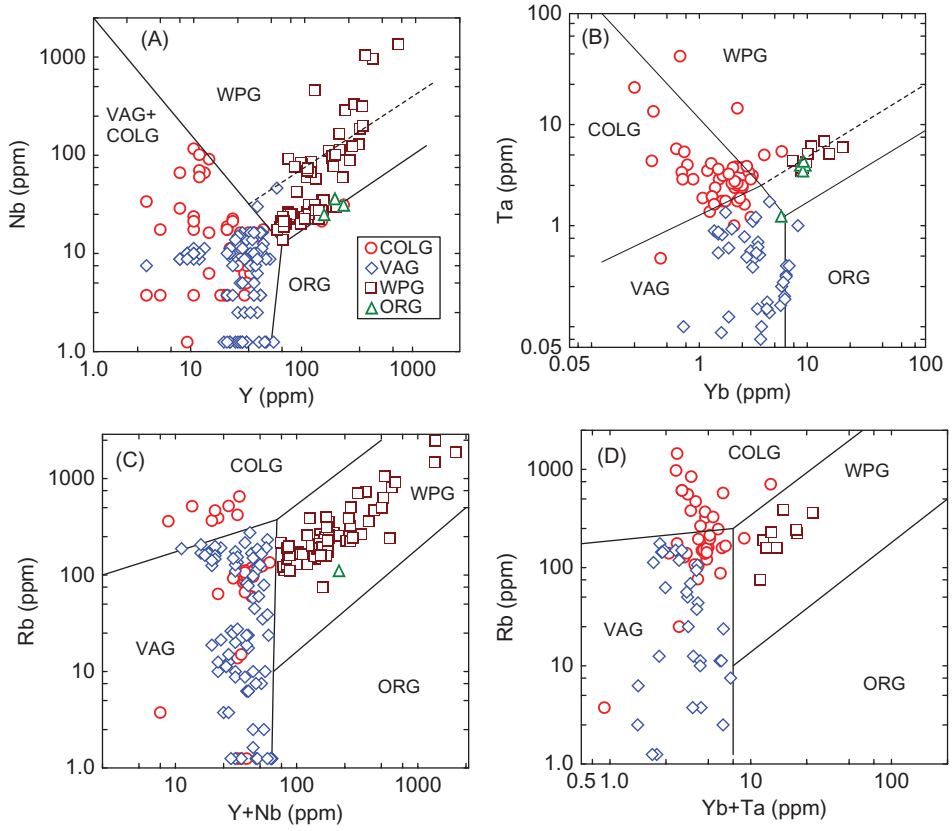

Figure 2. Evaluation of Pearce *et al.* (1984) discrimination diagrams for syn-collision granites (syn-COLG), volcanic-arc granites (VAG), within-plate granites (WPG), and ocean-ridge granites (ORG), using the original authors' database. The dashed line in Figure 2A and 2B represents the upper compositional boundary for ORG from anomalous ridge segments. For simplicity in diagrams we have written only COLG instead of syn-COLG. (A) Y−Nb diagram, in which the coordinates for the field boundaries are (1,2000) to (50,10) for VAG+syn-COLG–WPG; (40,1) to (50,10) for VAG+syn-COLG–ORG; (50,10) to (1000,100) for WPG–ORG solid line; and (25,25) to (1000,400) for the upper WPG–ORG dashed line. (B) Yb−Ta diagram, the field boundaries are (0.1,100) to (3,2) for syn-COLG–WPG; (0.1,0.35) to (3,2) for VAG–syn-COLG; (3,2) to (5,1) for VAG–WPG; (5,0.05) to (5,1) for VAG–ORG; (5,1) to (100,7) for WPG–ORG solid line; and (3,2) to (100,20) for WPG–ORG dashed line (the syn-COLG–WPG coordinates reported by Pearce *et al.* (1984) have been corrected). (C) (Y+Nb)−Rb diagram, the field boundaries are (2,80) to (55,300) for VAG–syn-COLG; (55,300) to (400,2000) for syn-COLG–WPG; (55,300) to (51.5,8) for VAG–WPG; (51.5,8) to (50,1) for VAG–ORG; and (51.5,8) to (2000,400) for WPG–ORG. (D) (Yb+Ta)−Rb diagram, the field boundaries are (0.5,140) to (6,200) for syn-COLG–VAG; (6,200) to (50,2000) for syn-COLG–WPG; (6,200) to (6,8) for VAG–WPG; (6,8) to (6,1) for VAG–ORG; (6,8) to (200,400) WPG–ORG (the VAG–syn-COLG coordinates reported by Pearce *et al.* (1984) have been corrected).

83.2%, respectively, in Figure 4C and 70.5% and 88.2%, respectively in Figure 4D.

From the above evaluation, it is clear that none of the four diagrams provides satisfactory discrimination for collision tectonics (syn-COLG). The first diagram (Y−Nb) cannot discriminate between arc and collision settings. Both the first and second diagrams (Y−Nb and Yb−Ta) show an overlapping region of WPG and ORG settings. In the third (Y+Nb−Rb) and fourth (Yb+Ta−Rb) diagrams, the *y*-axis is represented by Rb, being a mobile element as documented by several workers (e.g. Verma, 1981; Sturchio *et al*. 1986; Jochum and Verma 1996; Cole *et al*. 2006; Koszowska *et al*. 2007; Morishita *et al*. 2009). Because these diagrams are based on simple chemical parameters without any transformation, the alteration effects on Rb might be more pronounced in such diagrams than in the multi-dimensional diagrams based on log-ratios and linear combinations of transformed variables, although detailed analysis of such error propagation has still to be carried out. Fortunately, such analysis can be objectively achieved through Monte Carlo simulation (Espinosa-Paredes *et al.* 2010; Verma 2011) and is currently under progress. Furthermore, ocean-ridge setting considered by Pearce *et al.* (1984) may not be well represented by granitic rocks, because such felsic rocks are scarce in mid-ocean-ridges and their manifestations on land. Finally, all these diagrams proposed by Pearce *et al.* (1984) have the common problem of inadequate treatment of the compositional data (e.g. Aitchison 1986; Agrawal and Verma 2007).

Table 1. Statistical evaluation information for four trace-element-based discrimination diagrams (Pearce *et al.* 1984) for syn-collision granites (syn-COLG), volcanic-arc granites (VAG), within-plate granites (WPG), and ocean-ridge granites (ORG) using the first database.

			Number of discriminated samples (%)					
Tectonic setting	Figure number (type)	Total number of samples (%)	VAG+syn-COLG	syn-COLG	VAG	WPG	ORG	Overlap (WPG+ORG)
syn-COLG	2A (Y−Nb)	46 (100)	44 (95.6)	–	–	0 (0.0)	2 (4.3)	0 (0.0)
VAG		46 (100)	44 (95.6)	–	–	0 (0.0)	0 (0.0)	2 (4.3)
WPG		89 (100)	0 (0.0)	–	–	73 (82.0)	0 (0.0)	16 (17.9)
ORG		5	0	–	–	0	1	4
syn-COLG	2B (Yb−Ta)	49 (100)	–	37 (75.5)	7 (14.2)	5 (10.2)	0 (0.0)	0 (0.0)
VAG		45 (100)	–	0 (0.0)	40 (88.9)	0 (0.0)	5 (11.1)	0 (0.0)
WPG		9	–	0	0	4	0	5
ORG		5	–	0	1	0	0	4
syn-COLG	2C [(Y+Nb)−Rb]	41 (100)	–	8 (19.5)	25 (61.0)	7 (17.1)	1 (2.4)	–
VAG		81 (100)	–	0 (0.0)	81 (100)	0 (0.0)	0 (0.0)	–
WPG		89 (100)	–	0 (0.0)	0 (0.0)	89 (100)	0 (0.0)	–
ORG		1	–	0	0	1	0	–
syn-COLG	2D [(Yb+Ta)−Rb]	38 (100)	–	14 (36.8)	23 (60.5)	1 (2.6)	0 (0.0)	–
VAG		32 (100)	–	0 (0.0)	32 (100)	0 (0.0)	0 (0.0)	–
WPG		9	–	0	0	9	0	–
ORG		–	–	–	–	–	–	–

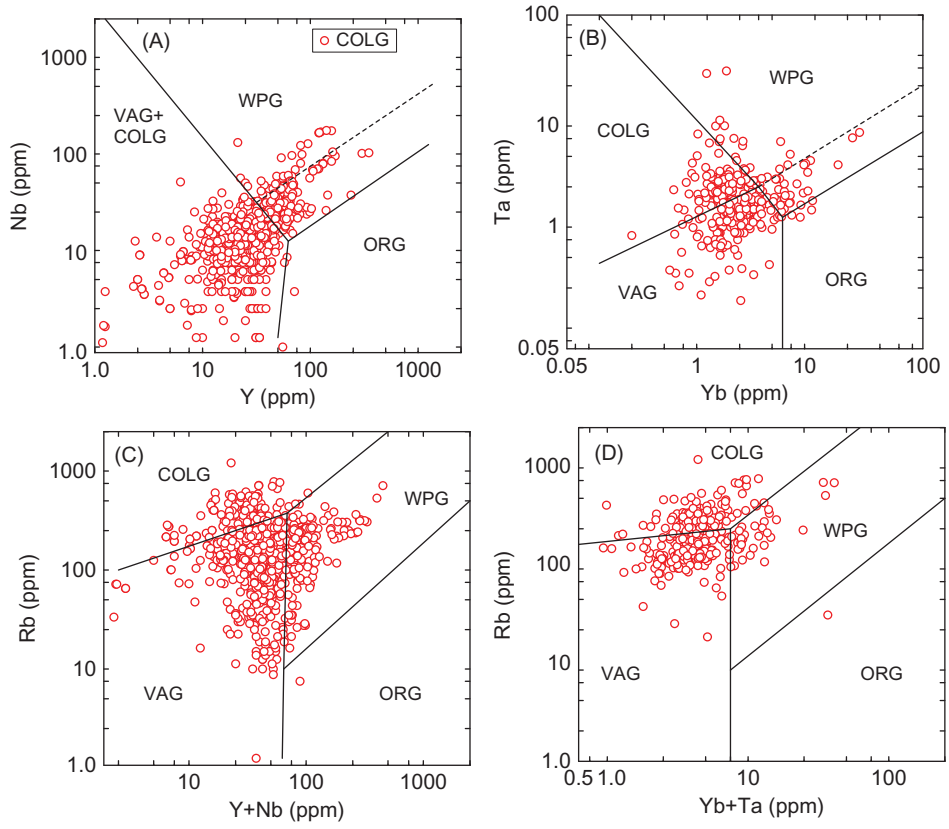

Figure 3. Evaluation of Pearce *et al.* (1984) discrimination diagrams for syn-collision granites (syn-COLG, simply COLG is used here), volcanic-arc granites (VAG), within-plate granites (WPG), and ocean-ridge granites (ORG), using new database for collision tectonics. The symbols are explained as inset in Figure 3A; A–D are the same as in Figure 2.

Proposal of new discrimination diagrams using linear discriminant analysis

The advantage of log-ratio transformation with correct statistical treatment in comparison with the use of raw compositional data (incorrect statistical treatment; Aitchison 1986; Agrawal and Verma 2007) has already been reported by Verma *et al.* (2006). Therefore, we adopted this transformation to incorporate the correct statistical treatment (Aitchison 1986) in the proposal of new diagrams. Furthermore for the first time, we tried to discriminate two very similar tectonic settings of IA and CA in our diagrams.

Advantages of normally distributed variables for use in LDA

A total of 1253 samples with complete major-element analyses [all 11 oxides $(SiO_2)_{adj}$ to $(P_2O_5)_{adj}$, with Fe-oxidation varieties provided by SINCLAS] were separated from the new database (second and third data sets) for proposing new diagrams. The tectonic settings were grouped as follows: group 1 – island arc; group 2 – continental arc (CAVA and the Andes); group 3 – continental rift; and group 4 – collision zone.

When LDA was performed on log-transformed major-element ratios of 1253 rock samples (complete database), the success rates were as follows (results obtained from the *Statistica* software): 80.12% for groups 1 and 2 together (IA+CA), 71.21% for group 3 (CR), and 72.16% for group 4 (Col). Further, application of single-outlier discordancy tests (Barnett and Lewis 1994; Verma 1997) to log-transformed major-element ratios of our complete database (1253 rock samples) resulted in the new database of 1132 rock samples and discordant outlier database of 121 samples (amounting to about 9.7% of samples). Again, LDA performed on the new database (1132 analyses) provided success rates of 85.47% for groups 1 and 2 together (IA+CA), 74.18% for group 3 (CR), and 76.50% for group 4 (Col). Therefore, when the basic requirement of normally distributed log-transformed ratio variables (discordant outlier-free data) was fulfilled before LDA, the success rates increased by about 5.4%, 3.0%, and 4.3% for IA+CA, CR, and Col, respectively.

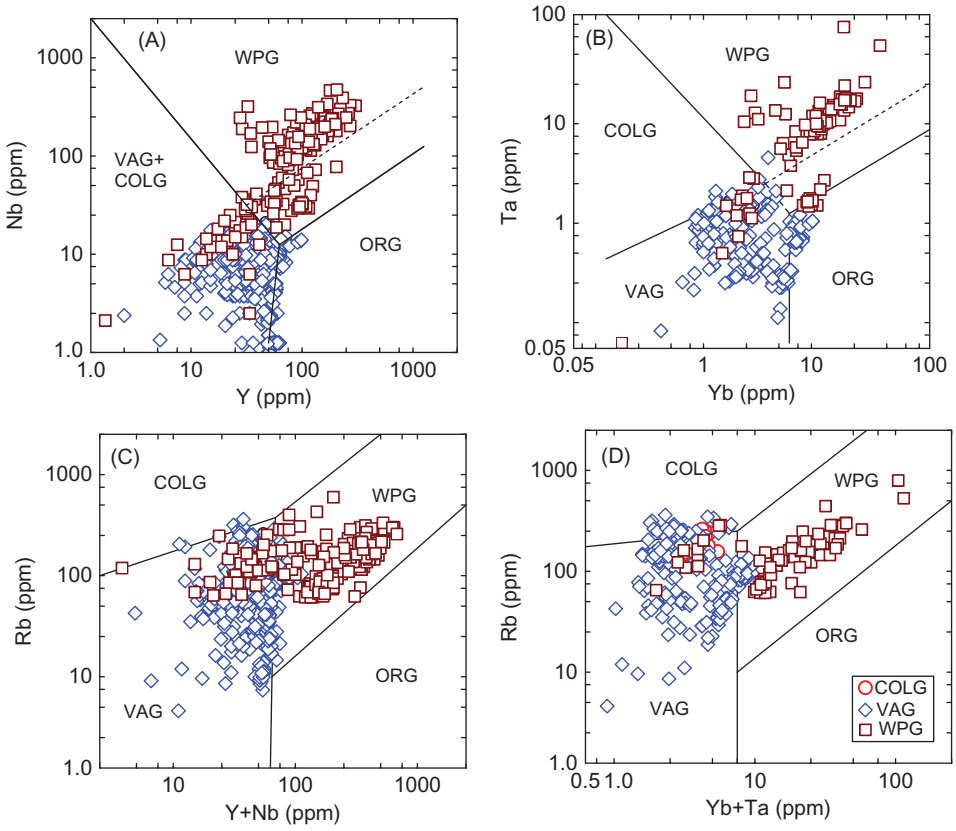

Figure 4. Evaluation of Pearce *et al.* (1984) discrimination diagrams for syn-collision granites (syn-COLG, simply COLG is used here), volcanic-arc granites (VAG), within-plate granites (WPG), and ocean-ridge granites (ORG), using new database for island and continental arcs and continental rifts. The symbols are explained as inset in Figure 4D; A–D are the same as in Figure 2.

Division of the database in training and testing sets and their statistical characteristics

The database (1132 samples) containing normally distributed log-ratio variables, that is without discordant outliers, was randomly divided in training and testing sets (1032 samples in the training set and 100 in the testing set; Table S2). Synthesis of the variables used in LDA is presented in Table S3, in which the mean and standard deviation values for all samples of the training set are included. All log-transformed ratios are negative, because we have chosen the most abundant major element $(SiO_2)_{adj}$ as the denominator. Although there is a progressive, unwanted increase of mean values of $(SiO_2)_{adj}$ from IA to Col (Table S3), there are differences in mean values of most log-transformed ratios as well. To understand if these differences are statistically significant, Table S4 gives the results of equality of these elements and their ratios. Both tests (Wilks' lambda $<<$ 1 and F-ratio $>>$ 1) show that there are statistically significant differences for most parameters among the four tectonic groups at low significance level (Table S4). Furthermore, these differences among groups can be enhanced by the multivariate technique of LDA to achieve acceptable separation of groups in multi-dimensional discrimination diagrams.

New discrimination diagrams from LDA and probability-based tectonic field boundaries

We carried out LDA on 1032 samples of the training set. In total, the discriminant analysis was carried out five times, the first time being for all groups with IA and CA combined together and four times for all possible combinations of three groups at a time.

Table 3 contains the equations for DF1 and DF2 functions (x- and y-axes) of Figure 5A–E. In these equations, the log-transformed ratios of major elements are multiplied by corresponding coefficients or the multiplication factors obtained from LDA (called 'raw coefficients' of canonical analysis in *Statistica* software). The last factor in each equation is a constant term for that equation. Because in LDA we used three groups at a time even in the first diagram, two functions (DF1 and DF2) together would define the total (100%) variance, that is

Table 2. Statistical evaluation information of four trace-element-based discrimination diagrams (Pearce *et al.* 1984) for syn-collision granites (syn-COLG), volcanic-arc granites (VAG), within-plate granites (WPG), and ocean-ridge granites (ORG), using our new databases.

Tectonic setting	Figure number (type)	Total number of samples (%)	Number of discriminated samples (%)					
			VAG+syn-COLG	syn-COLG	VAG	WPG	ORG	Overlap (WPG+ORG)
Collision	3A (Y−Nb)	721 (100)	569 (78.9)	–	–	32 (4.4)	1 (0.1)	119 (16.6)
Arc	4A (Y−Nb)	374 (100)	277 (74.0)	–	–	1 (0.3)	86 (23.0)	10 (2.7)
Continental rift	4A (Y−Nb)	220 (100)	31 (14.0)	–	–	157 (71.4)	0 (0.0)	32 (14.6)
Collision	3B (Yb−Ta)	301 (100)	–	84 (27.9)	156 (51.8)	24 (8.0)	4 (1.3)	33 (11.0)
Arc	4B (Yb−Ta)	193 (100)	–	11 (5.7)	148 (76.6)	1 (0.6)	32 (16.5)	1 (0.6)
Continental rift	4B (Yb−Ta)	93 (100)	–	2 (2.2)	9 (9.7)	69 (74.2)	6 (6.4)	7 (7.5)
Collision	3C [Y+Nb)−Rb]	721 (100)	–	116 (16.1)	457 (63.4)	147 (20.4)	1 (0.1)	–
Arc	4C [Y+Nb)−Rb]	370 (100)	–	2 (0.5)	307 (83.0)	61 (16.4)	0 (0.0)	–
Continental rift	4C [Y+Nb)−Rb]	220 (100)	–	0 (0.0)	37 (16.8)	183 (83.2)	0 (0.0)	–
Collision	3D [Yb+Ta)−Rb]	301 (100)	–	113 (37.5)	156 (51.8)	31 (10.4)	1 (0.3)	–
Arc	4D [Yb+Ta)−Rb]	180 (100)	–	26 (14.5)	127 (70.5)	27 (15)	0 (0.0)	–
Continental rift	4D [Yb+Ta)−Rb]	93 (100)	–	2 (2.1)	8 (8.6)	82 (88.2)	1 (1.1)	–

Table 3. Discriminant-function equations for the five new multi-dimensional discrimination diagrams.

Figure number	Equations
Figure 3A (1+2–3–4)	$DF1_{(IA+CA-CR-Col)_{m3}} = (0.36077 \times \ln(TiO_2/SiO_2)_{adj}) + (0.95693 \times \ln(Al_2O_3/SiO_2)_{adj}) + (-2.09239 \times \ln(Fe_2O_3/SiO_2)_{adj}) + (0.93391 \times \ln(FeO/SiO_2)_{adj}) + (0.42703 \times \ln(MnO/SiO_2)_{adj}) + (0.18732 \times \ln(MgO/SiO_2)_{adj}) + (0.45615 \times \ln(CaO/SiO_2)_{adj}) + (0.56098 \times \ln(Na_2O/SiO_2)_{adj}) + (-1.65167 \times \ln(K_2O/SiO_2)_{adj}) + (-0.15580 \times \ln(P_2O_5/SiO_2)_{adj}) - 1.58259$
	$DF2_{(IA+CA-CR-Col)_{m3}} = (0.472353 \times \ln(TiO_2/SiO_2)_{adj}) + (-0.954629 \times \ln(Al_2O_3/SiO_2)_{adj}) + (0.109516 \times \ln(Fe_2O_3/SiO_2)_{adj}) + (0.699238 \times \ln(FeO/SiO_2)_{adj}) + (0.739533 \times \ln(MnO/SiO_2)_{adj}) + (-0.027717 \times \ln(MgO/SiO_2)_{adj}) + (-0.244687 \times \ln(CaO/SiO_2)_{adj}) + (0.231677 \times \ln(Na_2O/SiO_2)_{adj}) + (0.173552 \times \ln(K_2O/SiO_2)_{adj}) + (-0.353797 \times \ln(P_2O_5/SiO_2)_{adj}) + 6.691035$
Figure 3B (1–2–3)	$DF1_{(IA-CA-CR)_{m3}} = (-0.4786 \times \ln(TiO_2/SiO_2)_{adj}) + (-0.0871 \times \ln(Al_2O_3/SiO_2)_{adj}) + (2.7433 \times \ln(Fe_2O_3/SiO_2)_{adj}) + (-1.0663 \times \ln(FeO/SiO_2)_{adj}) + (-0.1389 \times \ln(MnO/SiO_2)_{adj}) + (-0.1907 \times \ln(MgO/SiO_2)_{adj}) + (-0.8516 \times \ln(CaO/SiO_2)_{adj}) + (-0.7139 \times \ln(Na_2O/SiO_2)_{adj}) + (1.7166 \times \ln(K_2O/SiO_2)_{adj}) + (0.3386 \times \ln(P_2O_5/SiO_2)_{adj}) + 6.2573$
	$DF2_{(IA-CA-CR)_{m3}} = (-0.3204 \times \ln(TiO_2/SiO_2)_{adj}) + (-1.7585 \times \ln(Al_2O_3/SiO_2)_{adj}) + (-3.2046 \times \ln(Fe_2O_3/SiO_2)_{adj}) + (1.1210 \times \ln(FeO/SiO_2)_{adj}) + (0.2170 \times \ln(MnO/SiO_2)_{adj}) + (-0.0745 \times \ln(MgO/SiO_2)_{adj}) + (1.2505 \times \ln(CaO/SiO_2)_{adj}) + (1.3142 \times \ln(Na_2O/SiO_2)_{adj}) + (1.6616 \times \ln(K_2O/SiO_2)_{adj}) + (0.0186 \times \ln(P_2O_5/SiO_2)_{adj}) + 0.9984$
Figure 3C (1–2–4)	$DF1_{(IA-CA-Col)_{m3}} = (-0.3620 \times \ln(TiO_2/SiO_2)_{adj}) + (-0.0342 \times \ln(Al_2O_3/SiO_2)_{adj}) + (0.5198 \times \ln(Fe_2O_3/SiO_2)_{adj}) + (-0.4980 \times \ln(FeO/SiO_2)_{adj}) + (-0.7223 \times \ln(MnO/SiO_2)_{adj}) + (-0.1229 \times \ln(MgO/SiO_2)_{adj}) + (-0.1388 \times \ln(CaO/SiO_2)_{adj}) + (-0.8174 \times \ln(Na_2O/SiO_2)_{adj}) + (1.5074 \times \ln(K_2O/SiO_2)_{adj}) + (0.2684 \times \ln(P_2O_5/SiO_2)_{adj}) - 3.0829$
	$DF2_{(IA-CA-Col)_{m3}} = (-0.142 \times \ln(TiO_2/SiO_2)_{adj}) + (1.984 \times \ln(Al_2O_3/SiO_2)_{adj}) + (1.747 \times \ln(Fe_2O_3/SiO_2)_{adj}) + (-0.735 \times \ln(FeO/SiO_2)_{adj}) + (-1.226 \times \ln(MnO/SiO_2)_{adj}) + (0.062 \times \ln(MgO/SiO_2)_{adj}) + (-1.152 \times \ln(CaO/SiO_2)_{adj}) + (-3.189 \times \ln(Na_2O/SiO_2)_{adj}) + (-2.339 \times \ln(K_2O/SiO_2)_{adj}) + (0.495 \times \ln(P_2O_5/SiO_2)_{adj}) - 18.190$

(*Continued*)

Table 3. (*Continued*)

Figure number	Equations
Figure 3D (1–3–4)	$DF1_{(IA-CR-Col)_{m3}} = (0.0226 \times \ln(TiO_2/SiO_2)_{adj}) + (1.2877 \times \ln(Al_2O_3/SiO_2)_{adj}) + (-2.6406 \times \ln(Fe_2O_3/SiO_2)_{adj}) + (2.9494 \times \ln(FeO/SiO_2)_{adj}) + (0.1970 \times \ln(MnO/SiO_2)_{adj}) + (0.0673 \times \ln(MgO/SiO_2)_{adj}) + (0.0620 \times \ln(CaO/SiO_2)_{adj}) + (0.6219 \times \ln(Na_2O/SiO_2)_{adj}) + (-2.0579 \times \ln(K_2O/SiO_2)_{adj}) + (-0.0751 \times \ln(P_2O_5/SiO_2)_{adj}) - 2.1790$
	$DF2_{(IA-CR-Col)_{m3}} = (0.2786 \times \ln(TiO_2/SiO_2)_{adj}) + (-1.0544 \times \ln(Al_2O_3/SiO_2)_{adj}) + (0.8267 \times \ln(Fe_2O_3/SiO_2)_{adj}) + (0.3032 \times \ln(FeO/SiO_2)_{adj}) + (0.4084 \times \ln(MnO/SiO_2)_{adj}) + (-0.0905 \times \ln(MgO/SiO_2)_{adj}) + (-0.3260 \times \ln(CaO/SiO_2)_{adj}) + (0.1518 \times \ln(Na_2O/SiO_2)_{adj}) + (0.6698 \times \ln(K_2O/SiO_2)_{adj}) + (-0.2261 \times \ln(P_2O_5/SiO_2)_{adj}) + 6.5170$
Figure 3E (2–3–4)	$DF1_{(CA-CR-Col)_{m3}} = (0.0645 \times \ln(TiO_2/SiO_2)_{adj}) + (-1.7943 \times \ln(Al_2O_3/SiO_2)_{adj}) + (0.5264 \times \ln(Fe_2O_3/SiO_2)_{adj}) + (0.6385 \times \ln(FeO/SiO_2)_{adj}) + (0.3407 \times \ln(MnO/SiO_2)_{adj}) + (-0.0720 \times \ln(MgO/SiO_2)_{adj}) + (-0.3265 \times \ln(CaO/SiO_2)_{adj}) + (0.1063 \times \ln(Na_2O/SiO_2)_{adj}) + (1.8098 \times \ln(K_2O/SiO_2)_{adj}) + (-0.0338 \times \ln(P_2O_5/SiO_2)_{adj}) + 8.2616$
	$DF2_{(CA-CR-Col)_{m3}} = (0.8760 \times \ln(TiO_2/SiO_2)_{adj}) + (0.8018 \times \ln(Al_2O_3/SiO_2)_{adj}) + (0.2472 \times \ln(Fe_2O_3/SiO_2)_{adj}) + (-0.8796 \times \ln(FeO/SiO_2)_{adj}) + (0.7540 \times \ln(MnO/SiO_2)_{adj}) + (-0.0006 \times \ln(MgO/SiO_2)_{adj}) + (-0.0624 \times \ln(CaO/SiO_2)_{adj}) + (-0.2052 \times \ln(Na_2O/SiO_2)_{adj}) + (-3.3091 \times \ln(K_2O/SiO_2)_{adj}) + (-0.3526 \times \ln(P_2O_5/SiO_2)_{adj}) - 3.8959$

each DF1–DF2 type diagram (Figure 5A–E) with two discriminant functions is sufficient to fully visualize the samples from the three groups being discriminated at a given time. Furthermore, we describe these diagrams as multi-dimensional, because each of the two DF1 and DF2 functions contains 10 log-ratio variables. Thus, we are able to visualize 10-dimensional data in 2 dimensions. This is the major advantage of discriminant-function-based diagrams over the conventional bivariate or ternary diagrams.

The major advantage of LDA is that the tectonic boundaries can be based on probability estimates (Agrawal 1999). The posterior probability calculations for individual samples are similar to those described recently by Verma and Agrawal (2011). Therefore, instead of elaborating on these probability calculations, we briefly present the method to obtain the probability-based field boundaries.

As an example, for drawing the boundary that discriminates IA+CA and CR fields in Figure 5A, we first calculated the probabilities all along the top horizontal line (DF1 top axis) of the diagram, that is the line connecting (−8, 8) and (8, 8), and tried to obtain the coordinates of the point with equal probability for IA+CA and CR fields, which were observed to be (3.0914, 8.00). Similarly, we obtained the coordinates of the CR–Col boundary along the DF2 axis (the line joining −8, −8 and −8, 8) as (−8.00, −1.6511) and those for the IA+CA–Col along the DF1 axis (the line joining −8, −8 and 8, −8) as (6.5177, −8.00). The next step was to locate additional equal probability points along two horizontal or vertical

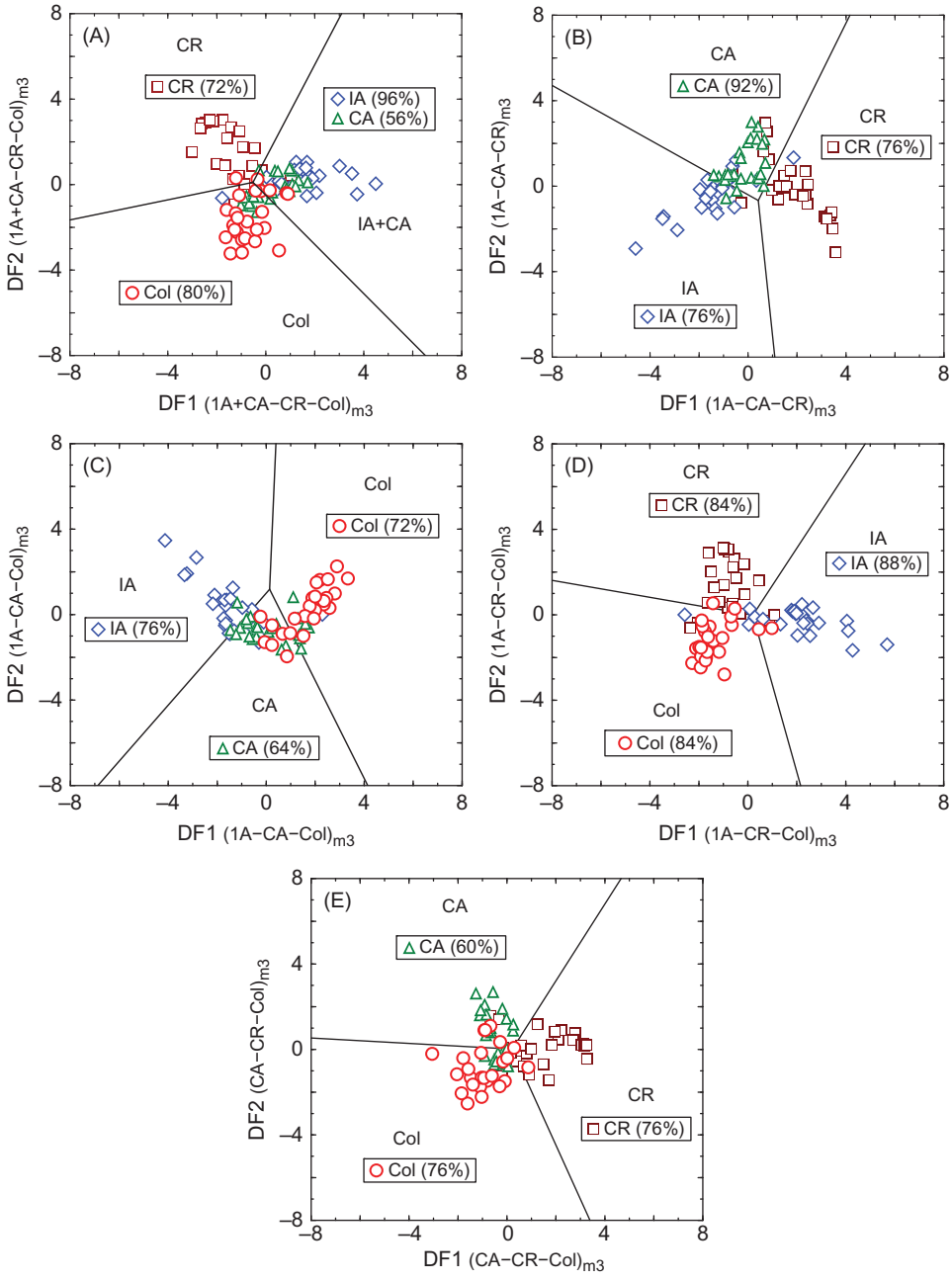

Figure 5. The set of five new discriminant-function diagrams based on natural log-transformed ratios of major elements for the discrimination of island arc (IA, group no. 1), continental arc (CA, group no. 2), continental rift (CR, group no. 3), and collision (COL, group no. 4) tectonic settings, showing samples from the testing set. In the first diagram, four groups are represented as three groups by combining IA and CA together. The other four diagrams are three groups at a time. The symbols are explained as inset in Figure 5A. The subscript m3 is used here to distinguish these diagrams from the previous two sets of major-element-based diagrams proposed by Agrawal *et al*. (2004) and Verma *et al*. (2006). (A) IA+CA–CR–Col (1–2+3–4) diagram, the coordinates DF1(IA+CA–CR–Col)m3 and DF2(IA+CA–CR–Col)m3, of the field boundaries are (3.0914, 8.00) and (−0.52237, 0.105108) for IA+CA–CR; (6.5177, −8.00) and (−0.52237, 0.105108) for IA+CA–Col; and (−8.00, −1.6511) and (−0.52237, 0.105108) for CR–Col; the percentages shown in this figure (both IA 96% and CA 60% for IA+CA field, CR 72%, and Col 80%) refer to correct discrimination for testing set samples (see Table 4); (B) IA–CA–CR (1–2–3) diagram, the coordinates of the field boundaries are (−8.00, 4.7147) and (0.41929, −0.66705) for IA–CA; (1.0939, −8.00) and (0.41929, −0.66705) for IA–CR; and (4.1608, 8.00) and (0.41929, −0.66705) for CA–CR; the correct discrimination is IA 76%, CA 92%, and CR 76%; (C) IA–CA–Col (1–2–4) diagram, the coordinates of the field boundaries are (−6.8768, −8.00) and (0.13893, 1.18829) for IA–CA; (0.39469, 8.00) and (0.13893, 1.18829) for IA–Col; and (4.1472, −8.00) and (0.13893, 1.18829) for CA–Col; the correct discrimination is IA 76%, CA 64%, and Col 72%; (D) IA–CR–Col (1–3–4) diagram, the coordinates of the field boundaries are (4.7956, 8.00) and (0.20518, −0.01689) for IA–CR; (2.1584, −8.00) and (0.20518, −0.01689) for IA–Col; and (−8.00, 1.61186) and (0.20518, −0.01689) for CR–Col; the correct discrimination is IA 88%, CR 84%, and Col 84%; (E) CA–CR–Col (2–3–4) diagram, the coordinates of the field boundaries are (4.6620, 8.00) and (0.22442, 0.015552) for CA–CR; (−8.00, 0.53675) and (0.22442, 0.015552) for CA–Col; and (3.3907, −8.00) and (0.22442, 0.015552) for CR–Col; the correct discrimination is CA 60%, CR 76%, and Col 76%.

lines well within the diagram, for example for Figure 5A, we located equal probability points along two lines, one horizontal joining (−8, 1) and (8, 1) and the other vertical joining (5, −8) and (5, 8). These equal probability inner coordinates were (−0.11275, 1) for the IA+CA–CR boundary and (5, −6.2527) for the IA+CA–Col boundary. Then, we obtained two equations, one joining two points (3.0914, 8.00) and (−0.11275, 1) to obtain the IA+CA–CR boundary and the other connecting (6.5177, −8.00) and (5, −6.2527) for the IA+CA–Col boundary. The point of intersection of these two equations was obtained to be (−0.52237, 0.105108). The third boundary (CR–Col) from (−8.00, −1.6511) will automatically pass through this point (−0.52237, 0.105108). Because all three boundaries meet at this point, it can be called the triple point for this diagram. We assured that the probability for this triple point was about 0.3333, or 33.33%, for each of the three tectonic fields (Figure 5A), because in LDA we had assumed equal probability for all groups being discriminated, irrespective of the sample sizes.

Finally, this process was repeated to obtain probability-based field boundaries in all other diagrams (Figure 5B–E). The boundary coordinates for all diagrams are reported in the explanation of Figure 5.

Success rates for training and testing sets

Using the testing set samples (100 samples) we obtained an unbiased estimate of success rates, for which the samples were plotted in our new discriminant-function-based multi-dimensional diagrams (Figure 5A–E; Table 4). For each tectonic setting, only four of the five diagrams are applicable. For example, for IA, the applicable diagrams are Figure 5A–D; Figure 5E would be the inapplicable diagram, because the IA field is missing from it.

In Figure 5A, about 96% of IA and 56% of CA samples plotted in the combined IA+CA field (Table 4). In other applicable diagrams (Figure 5B–D; Table 4), the success rates for IA varied from 76% to 88%. The success rate of 88% (correct discrimination) for IA was obtained for Figure 5D, in which CA setting is absent (see Table 4). For CA, the correct discrimination was 60–92% (Figure 5B, 5C, and 5E; Table 4). The highest value of 92% for CA was shown in Figure 5B, in which although IA is present, Col is absent. For both CR and Col settings, the success rates for correct discrimination varied from 72% to 84% (Figure 5A, 5B, 5D, and 5E for CR and Figure 5A and 5C–E for Col; Table 4).

For the training set samples (1032 samples not plotted in Figure 5A–E and success rates not shown in these diagrams), the initial analysis from LDA provided success rates of about 86.2%, 73.1%, and 77.7%, respectively, for IA+CA, CR, and Col settings (Figure 5A); 78.0%, 79.1%, and 80.4%, respectively, for IA, CA, and CR settings (Figure 5B); 74.0%, 69.8%, and 78.1%, respectively, for IA, CA, and Col settings (Figure 5C); 91.3%, 76.3%, and 82.4%, respectively, for IA, CR, and Col settings (Figure 5D); and 79.5%, 74.9%, and 77.3%, respectively, for CA, CR, and Col settings (Figure 5E). In spite of the considerably smaller number of samples in the testing set (100 vs. 1032), the success rates shown in Figure 5A–E were generally similar to those for the training set.

Application of new discriminant-function-based multi-dimensional diagrams

Five case studies were selected to illustrate the application of new diagrams. None of the samples from these case studies had been included in the database used for constructing our new diagrams (Figure 5A–E). Therefore, similar to the testing set samples, these case studies also provide an unbiased evaluation or functioning of our new diagrams.

These five case studies were as follows: (1) granitic rocks (about 30 Ma) from the Himalayas, India (Dietrich and Gansser 1981; Le Fort 1981); (2) acid rocks (Quaternary) from geothermal boreholes in El Salvador, Central America (Agostini *et al.* 2006); (3) granitic rocks from Adamello Massif, northern Italy (Dupuy *et al*. 1982; 35–52 Ma, Cortecci *et al.* 1979) and Vedrette di Ries Massif (about 30 Ma; from Italy–Austria border; Bellieni *et al.* 1981); (4) granitic rocks from Amo younger granitic complex of about 164 Ma from northern Nigeria (Imeokparia 1983) and 144 Ma from central Nigeria (Imeokparia 1982); and (5) ophiolitic rocks (of Cretaceous age) from Oman (Masirah from Abbotts 1978; and Semail from Alabaster *et al.* 1982).

We note that, for a correct application of our diagrams to case studies, it is important to use SINCLAS (Verma *et al*. 2002) for ascertaining that the samples used for plotting in discrimination diagrams are actually acid magmas. Furthermore, assuring normally distributed samples (using DODESSYS, unpublished program by S.P. Verma and L. Díaz-González) is also recommended.

Himalayan leucogranites

For the first application, we plotted discriminant-function scores (DF1–DF2) calculated from the equations in Table 3 for each of the 26 samples in the multi-dimensional space of our new diagrams. The first diagram (Figure S1A; Table 5) indicated Col tectonic setting for these samples, because all of them (100%) plotted in this field. From the second diagram (Figure S1B), the Col setting is missing, and therefore, this diagram should be considered inapplicable for this case study. In the third, fourth, and fifth diagrams (Figure S1C–E) all samples (100%) plotted in the field of Col tectonic setting. This clearly establishes the collision tectonic setting for the Himalayan leucogranites at about 30 Ma.

Table 4. Assessment of correct discrimination (success rate %) of IA, CA, CR, and Col tectonic settings in the set of five discriminant-function-based multi-dimensional diagrams.[a]

Actual affinity	Discriminant-function discrimination diagram	Total number of samples (testing)	Predicted tectonic affinity [number of samples (%)]				
			IA+CA (1+2)	IA (1)	CA (2)	CR (3)	Col (4)
IA (1)	1 + 2 − 3 − 4	25	24 (96)	–	–	0 (0)	1 (4)
IA (1)	1 − 2 − 3	25	–	19 (76)	5 (20)	1 (4)	–
IA (1)	1 − 2 − 4	25	–	19 (76)	4 (16.0)	–	1 (4)
IA (1)	1 − 3 − 4	25	–	22 (88)	–	1 (4)	2 (8)
CA (2)	1 + 2 − 3 − 4	25	14 (56)	–	–	1 (4)	10 (40)
CA (2)	1 − 2 − 3	25	–	2 (8)	23 (92)	0 (0)	–
CA (2)	1 − 2 − 4	25	–	2 (8)	16 (64)	–	7 (28)
CA (2)	2 − 3 − 4	25	–	–	15 (60)	0 (0)	10 (40)
CR (3)	1 + 2 − 3 − 4	25	4 (16)	–	–	18 (72)	3 (12)
CR (3)	1 − 2 − 3	25	–	1 (4)	5 (20)	19 (76)	–
CR (3)	1 − 3 − 4	25	–	2 (8)	–	21 (84)	2 (8)
CR (3)	2 − 3 − 4	25	–	–	3 (12)	19 (76)	3 (12)
Col (4)	1 + 2 − 3 − 4	25	4 (16)	–	–	1 (4)	20 (80)
Col (4)	1 − 2 − 4	25	–	0 (0)	7 (28)	–	18 (72)
Col (4)	1 − 3 − 4	25	–	2 (8)	–	2 (8)	21 (84)
Col (4)	2 − 3 − 4	25	–	–	4 (16)	2 (8)	19 (76)

[a]Tectonic groups are as follows: (1) – IA, (2) – CA, (3) – CR, and (4) – Col.

Acidic volcanic rocks from El Salvador

For the application of our new multi-dimensional tectonomagmatic discrimination diagrams, we compiled four samples of acid volcanic rocks from geothermal boreholes in Ahuachapán, El Salvador (Agostini *et al*. 2006). In the first diagram (Figure S2A; Table 5) all four samples plotted in the combined field of IA+CA. The second, third, and fourth diagrams (Figure S2B–D; Table 5) indicated IA tectonic setting, because all four samples plotted in this field. In this application, the fifth diagram (Figure S2E), from which IA setting is missing, can be considered as the inapplicable diagram. Thus, the borehole samples with zeolite alteration consistently indicated IA setting, although only a small number of four samples of acid magmas were available for this application.

Intrusive rocks from Adamello Massif (northern Italy) and Vedrette di Ries Massif (Italy and Austria)

Intrusive rocks of acid magma composition from Adamello Massif show an arc setting (Figure S3A, Table 5), although it is difficult to decide between island- and continental-arc settings (Figure S3A–E). When both IA and CA settings are present in a given diagram, the success rates for IA and CA were, respectively, 45% and 55% with CR as the third setting (Figure S3B) and 55% and 45% with Col as the third setting (Figure S3C). These similar success rates for IA and CA were further confirmed in the remaining two diagrams, in which only one of these two settings is present (IA 100% in Figure S3D and CA 100% in Figure S3E). Therefore, none of the diagrams can be declared inapplicable. In this context, we note that island- and continental-arc settings are very similar and consequently, it is sometimes difficult to discriminate them even with our new diagrams (see Agrawal *et al.* 2004; Verma *et al.* 2010b, for discussion of this similarity). Discrimination of these very similar IA and CA settings for this area might probably be obtained in future through the use of immobile major and trace elements in discriminant-function-based multi-dimensional diagrams, currently under preparation.

Probably because these 'old' (>35 Ma) rocks are located in Southern Alps (Dupuy *et al*. 1982), Pearce *et al.* (1984) used them as part of the database of collision tectonic setting for proposing their tectonomagmatic diagrams. Our new diagrams indicate that during about 52–35 Ma, the tectonic setting of these samples from northern Italy was likely an island or continental arc. At that time in the past, that is >35 Ma, the collision setting might not be present in this area.

The intrusive rocks of acid composition from the Vedrette di Ries Massif located on a transect along the Italy–Austria border (Bellieni *et al.* 1981) show on most diagrams (Figure S3A, C–E) transition between arc and collision settings (note linear trends in most diagrams), with CA as the inferred setting (success rates of 67–100%; Figure S3A–C, E; Table 5). Therefore, at about 30 Ma, this area began to show transition from subduction to incipient collision tectonics, although the subduction process might have still continued. Probably, only during the more recent times (<<30 Ma) the shift to collision tectonics should have been fully achieved. The study of Miocene or younger acid rocks, if present in this or surrounding area, should provide the necessary evidence to test this hypothesis.

In this context, we note that all 10 samples of acid rocks from the external crystalline massifs of the Alps (about 295 Ma; France, Italy, and Switzerland; Debon and Lemmet 1999) consistently plotted in the collision field in our new diagrams (plots not shown). Thus, age-dependent multiple tectonic settings may be inferred in a given geographical region.

Granitic rocks from Amo complex, northern and central Nigeria

Our diagrams, when applied to older rocks (about 164 Ma) from northern Nigeria, cannot fully discriminate between continental rift and collision settings (Figure S4A, C–E; Table 5). However, the somewhat younger (about 144 Ma) granitic rocks from central Nigeria are more consistent with a collision setting. Once again, time-dependent tectonic settings may be obtained from the application of these new diagrams.

Ophiolitic rocks of Oman

We plotted (Figure S5A–E) nine samples of the Masirah ophiolite from an island located along the southeast coast of Oman (Cretaceous age; Abbotts 1978). Most samples plotted in the field of collision tectonic setting (Figure S5A, C–E; Table 5; Figure S5B is the inapplicable diagram in this case). However, seven samples of the Semail ophiolite of Oman from on-land northerly locations (also of Cretaceous age; Alabaster *et al.* 1982) were more consistent with an island arc setting (Figure S5A–D; Table 5; Figure S5E is the inapplicable diagram in this case). More refined age constraints are required to better interpret our results, particularly to determine if there was a time-dependent change of the tectonic setting in this area.

Final remarks

We point out that the application results of the five case studies indicate that in spite of the relative mobility of major elements, our new discriminant-function-based multi-dimensional diagrams provide a better framework for tectonomagmatic discrimination as compared to the widely used Pearce *et al.* (1984) diagrams. We therefore recommend that these new diagrams be used to infer tectonic

Table 5. Application of the set of five discriminant-function-based multi-dimensional discrimination diagrams to granitic or acid rocks.[a]

Actual affinity	Discriminant-function discrimination diagram	Total number of samples (testing)	Predicted tectonic affinity [number of samples (%)]				
			IA+CA (1+2)	IA (1)	CA (2)	CR (3)	Col (4)
Himalayas	1 + 2 − 3 − 4	26	0 (0)	–	–	0 (0)	26 (100)
Himalayas	1 − 2 − 3	26	–	0 (0)	23 (88)	3 (12)	–
Himalayas	1 − 2 − 4	26	–	0 (0)	0 (0)	–	26 (100)
Himalayas	1 − 3 − 4	26	–	0 (0)	–	0 (0)	26 (100)
Himalayas	2 − 3 − 4	26	–	–	0 (0)	0 (0)	26 (100)
El Salvador (boreholes)	1 + 2 − 3 − 4	4	4	–	–	0 (0)	0 (0)
El Salvador (boreholes)	1 − 2 − 3	4	–	–	4	0	0
El Salvador (boreholes)	1 − 2 − 4	4	–	4	0	0	–
El Salvador (boreholes)	1 − 3 − 4	4	–	4	0	–	0
El Salvador (boreholes)	2 − 3 − 4	4	–	4	–	0	0
Northern Italy	1 + 2 − 3 − 4	11	11 (100)	–	–	0 (0)	0 (0)
Northern Italy	1 − 2 − 3	11	–	5 (45)	6 (55)	0 (0)	–
Northern Italy	1 − 2 − 4	11	–	6 (55)	5 (45)	–	0 (0)
Northern Italy	1 − 3 − 4	11	–	11 (100)(100)	–	0 (0)	0 (0)
Northern Italy	2 − 3 − 4	11	–	–	11 (100)(100)	0 (0.0)	0 (0.0)
Italy−Austria border	1 + 2 − 3 − 4	18	13 (72)	–	–	0 (0)	5 (28)
Italy−Austria border	1 − 2 − 3	18	–	0 (0)	18 (100)	0 (0)	–
Italy−Austria border	1 − 2 − 4	18	–	0 (0)	13 (72)	–	5 (28)
Italy−Austria border	1 − 3 − 4	18	–	8 (44)	–	0 (0)	10 (56)
Italy−Austria border	2 − 3 − 4	18	–	–	12 (67)	0 (0.0)	6 (33)
Northern Nigeria	1 + 2 − 3 − −4	11	0 (0)	–	–	5 (45)	6 (55)
Northern Nigeria	1 − 2 − 3	11	–	0 (0)	1 (9)	10 (91)	–
Northern Nigeria	1 − 2 − 4	11	–	0 (0)	3 (27)	–	8 (73)
Northern Nigeria	1 − 3 − 4	11	–	0 (0)	–	6 (55)	5 (45)
Northern Nigeria	2 − 3 − 4	11	–	–	0 (0)	5 (45)0(0.0)	6 (55)
Central Nigeria	1 + 2 − 3 − 4	8	0	–	–	0	8
Central Nigeria	1 − 2 − 3	8	–	0	3	5	–
Central Nigeria	1 − 2 − 4	8	–	0	0	–	8
Central Nigeria	1 − 3 − 4	8	–	0	–	0	8
Central Nigeria	2 − 3 − 4	8	–	–	0	0	8
Masirah ophiolite (Oman)	1 + 2 − 3 − 4	9	0	–	–	0	9
Masirah ophiolite (Oman)	1 − 2 − 3	9	–	0	9	0	–
Masirah ophiolite (Oman)	1 − 2 − 4	9	–	0	1	–	8
Masirah ophiolite (Oman)	1 − 3 − 4	9	–	0	–	0	9
Masirah ophiolite (Oman)	2 − 3 − 4	9	–	–	1	0 0 (0.0)	8
Semail ophiolite (Oman)	1 + 2 − 3 − −4	7	7	–	–	0	0
Semail ophiolite (Oman)	1 − 2 − 3	7	–	7	0	0	–
Semail ophiolite (Oman)	1 − 2 − 4	7	–	7	0	–	0
Semail ophiolite (Oman)	1 − 3 − 4	7	–	7	–	0	0
Semail ophiolite (Oman)	2 − 3 − 4	7	–	–	7	0	0

[a]Tectonic groups are as follows: (1) − IA, (2) − CA, (3) − CR, and (4) − Col.

regime of acid volcanic or plutonic rocks. However, we note that the data should first be processed by SINCLAS and DODESSYS and then the discriminant-functions must be computed before the use of our diagrams. Therefore, we have prepared a *Statistica* template for using these diagrams and would be willing to process the data and provide the set of five diagrams along with their interpretation to scientists interested in employing our diagrams.

Conclusions

Pearce *et al.* (1984) diagrams, although widely used, in some cases do not provide reliable discrimination of granitic rocks from different tectonic settings. We have successfully developed a set of the five new discrimination diagrams for acid rocks from four tectonic settings (IA, CA, CR, and Col). These multi-dimensional diagrams show relatively high success rates as judged from both the training and testing sets and are based on natural log-ratio transformation of major-element ratios and application of discordant outlier tests prior to LDA. Thus, the combination of discordant outlier tests and LDA provided a powerful and correct statistical treatment of the compositional data. Finally, before using our diagrams for any particular area, we strongly recommend that the samples be processed in SINCLAS software to ascertain the acid character of the rocks, and only such rocks be utilized for inferring tectonic setting. Our diagrams have been used for five case studies; consistent results were obtained for most applications, although island- and continental-arc settings can be difficult to discriminate.

Acknowledgements

The first author (SKV) is grateful to Secretaría de Relaciones Exteriores (Mexico) for his doctorate fellowship. We thank John S. Armstrong-Altrin for providing us Figure 1 in Corel, which was modified in our present article.

Supplementary Material

Tables S1–S4 and Figures S1–S5 can be found in the online version of this article at www.informaworld.com/tigr.

References

Abbotts, I.L., 1978, High-potassium granites in the Masirah ophiolite of Oman: Geological Magazine, v. 6, p. 415–425.

Agostini, S., Corti, G., Doglioni, C., Carminati, E., Innocenti, F., Tonarini, S., Manetti, P., Di Vincenzo, G., and Montanari, D., 2006, Tectonic and magmatic evolution of the active volcanic front in El Salvador: Insight into the Berlín and Ahuachapán geothermal areas: Geothermics, v. 35, p. 368–408.

Agrawal, S., 1999, Geochemical discrimination diagrams: A simple way of replacing eye-fitted boundaries with probability based classifier surfaces: Journal of the Geological Society of India, v. 54, p. 335–346.

Agrawal, S., Guevara, M., and Verma, S.P., 2004, Discriminant analysis applied to establish major-element field boundaries for tectonic varieties of basic rocks: International Geology Review, v. 46, p. 575–594.

Agrawal, S., Guevara, M., and Verma, S.P., 2008, Tectonic discrimination of basic and ultrabasic rocks through log-transformed ratios of immobile trace elements: International Geology Review, v. 50, p. 1057–1079.

Agrawal, S., and Verma, S.P., 2007, Comment on 'Tectonic classification of basalts with classification trees' by Pieter Vermeesch (2006): Geochimica et Cosmochimica Acta, v. 71, p. 3388–3390.

Aitchison, J., 1986, The statistical analysis of compositional data, The statistical analysis of compositional data: London, New York, Chapman and Hall, p. 416.

Alabaster, T., Pearce, J.A., and Malpas, J., 1982, The volcanic stratigraphy and petrogenesis of the Oman ophiolite complex: Contributions to Mineralogy and Petrology, v. 81, p. 168–183.

Aldanmaz, E., Pearce, J.A., Thirlwall, M.F., and Mitchell, J.G., 2000, Petrogenetic evolution of late Cenozoic, post-collision volcanism in western Anatolia, Turkey: Journal of Volcanology and Geothermal Research, v. 102, p. 67–95.

Alderton, D.H.M., Pearce, J.A., and Potts, P.J., 1980, Rare earth element mobility during granite alteration: Evidence from southwest England: Earth and Planetary Science Letters, v. 49, p. 149–165.

Aldiss, D.T., 1981, Plagiogranites from the ocean crust and ophiolites: Nature, v. 289, p. 577–578.

Ayalew, D., Ebinger, C., Bourdon, E., Wolfenden, E., Yirgu, G., and Grassingeau, N., 2006, Temporal compositional variation of syn-rift rhyolites along the western margin of the southern Red Sea and northern Main Ethiopian Rift, *in* Yirgu, G., Ebinger, C., and Maguire, P.K.H., eds., The Afar volcanic province within the East African Rift system: London, Geological Society of London Special Publications, p. 121–130.

Ayres, M., and Harris, N., 1997, REE fractionation and Nd-isotope disequilibrium during crustal anatexis: Constraints from Himalayan leucogranites: Chemical Geology, v. 139, p. 249–269.

Barberi, F., Santacroce, R., and Varet, J., 1975, Silicic peralkaline volcanic rocks of the Afar depression (Ethiopia): Bulletin Volcanologique, v. 38, p. 755–790.

Bardintzeff, J.M., and Deniel, C., 1992, Magmatic evolution of Pacaya and Cerro Chiquito volcanological complex, Guatemala: Bulletin of Volcanology, v. 54, p. 267–283.

Barnett, V., and Lewis, T., 1994, Outliers in statistical data: Chichester, John Wiley & Sons, 584 p.

Barsdell, M., and Berry, R.F., 1990, Origin and evolution of primitive island arc ankaramites from western Epi, Vanuatu: Journal of Petrology, v. 31, p. 747–777.

Basu, A.R., Junwen, W., Wankang, H., Guanghong, X., and Tatsumoto, M., 1991, Major element, REE, and Pb, Nd and Sr isotopic geochemistry of Cenozoic volcanic rocks of eastern China: Implications for their origin from suboceanic-type mantle reservoirs: Earth and Planetary Science Letters, v. 105, p. 149–169.

Bateman, P.C., and Chappell, B.W., 1979, Crystallization, fractionation, and solidification of the Tuolumne Intrusive Series, Yosemite National Park, California: Geological Society of America Bulletin, v. 90, p. 465–482.

Bellieni, G., Peccerillo, A., and Poli, G., 1981, The Vedrette di Ries (Rieserferner) plutonic complex: Petrological and geochemical data bearing on its genesis: Contributions to Mineralogy and Petrology, v. 78, p. 145–156.

Benito, R., López-Ruiz, J., Cebriá, J.M., Hertogen, J., Doblas, M., Oyarzum, R., and Demaiffe, D., 1999, Sr and O isotope constraints on source and crustal contamination in the high-K calc-alkaline and shoshonitic Neogene volcanic rocks of SE Spain: Lithos, v. 46, p. 773–802.

Bloomer, S.H., and Hawkins, J.W., 1989, Petrology and geochemistry of boninite series volcanic rocks from the Mariana trench: Contributions to Mineralogy and Petrology, v. 97, p.361–377.

Brown, G.M., Holland, J.G., Sigurdsson, H., Tomblin, J.F., and Arculus, R.J., 1977, Geochemistry of the Lesser Antilles volcanic island arc: Geochimica et Cosmochimica Acta, v. 41, p. 785–801.

Bryan, W.B., Stice, G.D., and Ewart, A., 1972, Geology, petrography, and geochemistry of the volcanic islands of Tonga: Journal of Geophysical Research, v. 77, p. 1566–1585.

Buket, E., and Temel, A., 1998, Major-element, trace-element, and Sr-Nd isotopic geochemistry and genesis of Varto (Mus) volcanic rocks, Eastern Turkey: Journal of Volcanology and Geothermal Research, v. 85, p. 405–422.

Cameron, B.I., Walker, J.A., Carr, M.J., Patino, L.C., Matías, O., and Feigenson, M.D., 2002, Flux versus decompression melting at stratovolcanoes in southeastern Guatemala: Journal of Volcanology and Geothermal Research, v. 119, p. 21–50.

Camp, V.E., Roobol, M.J., and Hooper, P.R., 1991, The Arabian continental alkali basalt province: Part II. Evolution of Harrats Khaybar, Ithnayn, and Kura, Kingdom of Saudi Arabia: Geological Society of America Bulletin, v. 103, p. 363–391.

Castelli, D., and Lombard, B., 1988, The Gophu La and Western Lunana granites: Miocene muscovite leucogranites of the Bhutan Himalaya: Lithos, v. 21, p. 211–225.

Chauvel, C., and Jahn, B.-M., 1984, Nd-Sr isotope and REE geochemistry of alkali basalts from the Massif Central, France: Geochimica et Cosmochimica Acta, v. 48, p. 93–110.

Cherneva, Z., and Georgieva, M., 2005, Metamorphozed Hercynian granitoids in the Alpine structures of the Central Rhodope, Bulgaria: Geotectonic position and geochemistry: Lithos, v. 82, p. 149–168.

Churikova, T., Dorendorf, F., and Wörner, G., 2001, Sources and fluids in the mantle wedge below Kamchatka, evidence from across-arc geochemical variation: Journal of Petrology, v. 42, p. 1567–1593.

Cole, J.W., 1981, Genesis of lavas of the Taupo volcanic zone, North Island, New Zealand: Journal of Volcanology and Geothermal Research, v. 10, p. 317–337.

Cole, R.B., Nelson, S.W., Layer, P.W., and Oswald, P.J., 2006, Eocene volcanism above a depleted mantle slab window in southern Alaska: Bulletin of the Geological Society of America, v. 118, p. 140–158.

Cortecci, G., Del Moro, A., Leone, G., and Pardini, G.C., 1979, Correlation between strontium and oxygen isotopic compositions of rocks from the Adamello massif (northern Italy): Contributions to Mineralogy and Petrology, v. 68, p.421–427.

Davidson, J.P., Ferguson, K.M., Colucci, M.T., and Dungan, M.A., 1988, The origin and evolution of magmas from the San Pedro-Pellado volcanic complex, S. Chile: Multicomponent sources and open system evolution: Contributions of Mineralogy and Petrology, v. 100, p. 429–445.

Davidson, J.P., and Wilson, I.R., 1989, Evolution of an alkali basalt-trachyte suite from Jebel Marra volcano, Sudan, through assimilation and fractional crystallization: Earth and Planetary Science Letters, v. 95, p. 141–160.

Debon, F., and Lemmet, M., 1999, Evolution of Mg/Fe ratios in late variscan plutonic rocks from the External Crystalline Massifs of the Alps (France, Italy, Switzerland): Journal of Petrology, v. 40, p. 1151–1185.

Defant, M.J., Clark, L.F., Stewart, R.H., Drummond, M.S., De Boer, J.Z., Maury, R.C., Bellon, H., Jackson, T.E., and Restrepo, J.F., 1991, Andesite and dacite genesis via contrasting processes: The geology and geochemistry of El Valle Volcano, Panama: Contributions to Mineralogy and Petrology, v. 106, p. 309–324.

Delaloye, M., and Bingol, E., 2000, Granitoids from western and northwestern Anatolia: Geochemistry and modeling of geodynamic evolution: International Geology Review, v. 42, p. 241–268.

Deniel, C., Vidal, P., Coulon, C., Vellutini, P., and Piguet, P., 1994, Temporal evolution of mantle sources during continental rifting: The volcanism of Djibouti (Afar): Journal of Geophysical Research, v. 99, p. 2853–2869.

Deruelle, B., 1982, Petrology of the Plio-Quaternary volcanism of the south-central and meridional Andes: Journal of Volcanology and Geothermal Research, v. 14, p. 77–124.

de Silva, S.L., 1991, Styles of zoning in central Andean ignimbrites: Insights into magma chamber processes: Geological Society of America Special Paper, v. 265, p. 217–232.

Dietrich, V., and Gansser, A., 1981, The Leucogranites of Bhutan Himalaya (Crustal anatexis versus mantle melting): Schweizerische Mineralogische und Petrographische Mitteilungen, v. 61, p. 177–202.

Dini, A., Innocenti, F., Rocchi, S., Tonarini, S., and Westerman, D.S., 2002, The magmatic evolution of the late Miocene laccolith-pluton-dyke granitic complex of Elba Island, Italy: Geological Magazine, v. 139, p. 257–279.

Dorendorf, F., Churikova, T., Koloskov, A., and Wörner, G., 2000, Late Pliocene to Holocene activity at Bakening volcano and surrounding monogenetic centers (Kamchatka): Volcanic geology and geochemical evolution: Journal of Volcanology and Geothermal Research, v. 104, p. 131–151.

DuFrane, S.A., Asmerom, Y., Mukasa, S.B., Morris, J.D., and Dreyer, B.M., 2006, Subduction and melting processes inferred from U- series, Sr- Nd- Pb isotope, and trace element data, Bicol and Bataan arcs, Philippines: Geochimica et Cosmochimica Acta, v. 70, p. 3401–3420.

Duncker, K.E., Wolff, J.A., Harmon, R.S., Leat, P.T., Dickin, A.P., and Thompson, R.N., 1991, Diverse mantle and crustal components in lavas of the NW Cerros del Rio volcanic field, Rio Grande Rift, New Mexico: Contributions to Mineralogy and Petrology, v. 108, p. 331–345.

Dupuy, C., Dostal, J., and Fratta, M., 1982, Geochemical of the Adamello Massif (Northern Italy): Contributions to Mineralogy and Petrology, v. 80, p. 41–48.

Engel, C.G., and Fisher, R.L., 1975, Granitic to ultramafic rock complexes of the Indian Ocean ridge system, western Indian Ocean: Geological Society of America Bulletin, v. 86, p. 1553–1578.

Espinosa-Paredes, G., Verma, S.P., Vázquez-Rodríguez, A., and Núñez-Carrera, A., 2010, Mass flow rate sensitivity and uncertainty analysis in natural circulation boiling water reactor core from Monte Carlo simulations: Nuclear Engineering and Design, v. 240, p. 1050–1062.

Ewart, A., Brothers, R.N., and Mateen, A., 1977, An outline of the geology and geochemistry, and the possible petrogenetic evolution of the volcanic rocks of the Tonga-Kermadec-New

Zealand island arc: Journal of Volcanology and Geothermal Research, v. 2, p. 205–270.

Ewart, A., and Bryan, W.B., 1972, Petrography and geochemistry of the igneous rocks from EUA, Tongan islands: Geological Society of America Bulletin, v. 83, p. 3281–3298.

Feuerbach, D.L., Smith, E.I., Walker, J.D., and Tangeman, J.A., 1993, The role of the mantle during crustal extension: Constraints from geochemistry of volcanic rocks in the Lake Mead area, Nevada and Arizona: Geological Society of America Bulletin, v. 105, p. 1561–1575.

Finney, B., Turner, S., Hawkesworth, C., Larsen, J., Nye, C., George, R., Bindeman, I., and Eichelberger, J., 2008, Magmatic differentiation at an Island-arc Caldera: Okmok Volcano, Aleutian Islands, Alaska: Journal of Petrology, v. 49, p. 857–884.

Foden, J.D., and Varne, R., 1980, The petrology and tectonic setting of Quaternary-Recent volcanic centres of Lombok and Sumbawa, Sunda arc: Chemical Geology, v. 30, p. 201–226.

Frey, F.A., Gerlach, D.C., Hickey, R.L., Lopez-Escobar, L., and Munizaga-Villavicencio, F., 1984, Petrogenesis of the Laguna del Maule volcanic complex, Chile (36°S): Contributions to Mineralogy and Petrology, v. 88, p. 133–149.

Gamble, J.A., Wright, I.C., Woodhead, J.D., and McCulloch, M.T., 1995, Arc and back-arc geochemistry in the southern Kermadec arc-Ngatoro basin and offshore Taupo volcanic zone, SW Pacific, *in* Smellie, J.L., ed., Volcanism associated with extension at consuming plate margins, Geological Society Special Publication, p. 193–212.

Gerlach, D.C., Frey, F.A., Moreno-Roa, H., and Lopez-Escobar, L., 1988, Recent volcanism in the Puyehue-Cordon Caulle region, southern Andes, Chile (40.5°S): Petrogenesis of evolved lavas: Journal of Petrology, v. 29, p. 333–382.

González Partida, E., Torres Rodriguez, V., and Birkle, P., 1997, Plio-Pleistocene volcanic history of the Ahuachapan geothermal system, El Salvador: The Concepción de Ataco caldera: Geothermics, v. 26, p. 555–575.

Grigoriev, S.I., and Pshenichny, C.A., 1998, Late Mesozoic post-collisional intermediate to silicic magmatism in the Badjal area, Far East of Russia: Lithos, v. 45, p. 457–468.

Guillot, S., and Fort, P.L., 1995, Geochemical constraints on the bimodal origin of High Himalayan leucogranites: Lithos, v. 35, p. 221–234.

Haase, K.M., Goldschmidt, B., and Garbe-Schönberg, C.-D., 2004, Petrogenesis of Tertiary continental intra-plate lavas from the Westerwald region, Germany: Journal of petrology, v. 45, p. 883–905.

Haase, K.M., Worthington, T.J., Stoffers, P., Garbe-Schönberg, D., and Wright, I., 2002, Mantle dynamics, element recycling, and magma genesis beneath the Kermadec arc-Havre Trough: Geochemistry Geophysics Geosystems, v. 3, p. 1071, doi: 10.1029/2002GC00035.

Hanson, G.N., 1978, The application of trace elements to the petrogenesis of igneous rocks of granitic composition: Earth and Planetary Science Letters, v. 38, p. 26–43.

Harris, N.B.W., Duyverman, H.J., and Almond, D.C., 1983, The trace element and isotope geochemistry of the Sabaloka Igneous Complex, Sudan: Journal Geological Society London, v. 140, p. 245–256.

Hasözbek, A., Satır, M., Erdoğan, B., Akay, E., and Siebel, W., 2011, Early Miocene post-collisional magmatism in NW Turkey: geochemical and geochronological constraints: International Geology Review, v.53, doi: 10.1080/00206810903579302.

Hegner, E., and Smith, I.E.M., 1992, Isotopic compositions of late Cenozoic volcanics from southeast Papua New Guinea: Evidence for multi-component sources in arc and rift environments: Chemical Geology, v. 97, p. 233–249.

Hickey-Vargas, R., Moreno Roa, H., Lopez Escobar, L., and Frey, F.A., 1989, Geochemical variations in Andean basaltic and silicic lavas from the Villarrica-Lanin volcanic chain (39.5°S): An evaluation of source heterogeneity, fractional crystallization and crustal assimilation: Contributions to Mineralogy and Petrology, v. 103, p. 361–386.

Hildreth, W., Lanphere, M.A., Champion, D.E., and Fierstein, J., 2004, Rhyodacites of Kulshan caldera, North Cascades of Washington: Poscaldera lavas that span the Jaramillo: Journal of Volcanology and Geothermal Research, v. 130, p. 227–264.

Hirotani, S., and Ban, M., 2006, Origin of silicic magma and magma feeding system of the Shirataka volcano, NE Japan: Journal of Volcanology and Geothermal Research, v. 156, p. 229–251.

Hsu, C.-N., Chen, J.-C., and Ho, K.-S., 2000, Geochemistry of Cenozoic volcanic rocks from Kirin Province, northeast China: Geochemical Journal, v. 34, p. 33–58.

Ilbeyli, N., Pearce, J.A., Thirlwall, M.F., and Mitchell, J.G., 2004, Petrogenesis of collision-related plutonics in Central Anatolia, Turkey: Lithos, v. 72, p. 163–182.

Imeokparia, E.G., 1982, Geochemistry and relationships to mineralization of granitic rocks from the Afu Younger Granite Complex, Central Nigeria: Geological Magazine, v. 119, p. 39–56.

Imeokparia, E.G., 1983, Geochemical aspects of the evolution and mineralization of the Amo Younger Complex (Northern Nigeria): Chemical Geology, v. 40, p. 293–312.

Ishikawa, T., Tera, F., and Nakazawa, T., 2001, Boron isotope and trace element systematics of the three volcanic zones in the Kamchatka arc: Geochimica et Cosmochimica Acta, v. 65, p. 4523–4537.

Izbekov, P.E., Eichelberger, J.C., and Ivanov, B.V., 2004, The 1996 eruption of Karymsky volcano, Kamchatka: Historical record of basaltic replenishment of an andesite reservoir: Journal of Petrology, v. 45, p. 2325–2345.

Jochum, K.P., and Verma, S.P., 1996, Extreme enrichment of Sb, Tl and other trace elements in altered MORB: Chemical Geology, v. 130, p. 289–299.

Johnson, C.M., and Lipman, P.W., 1988, Origin of metaluminous and alkaline volcanic rocks of the Latir volcanic field, northern Rio Grande rift, New Mexico: Contributions to Mineralogy and Petrology, v. 100, p. 107–128.

Kabeto, K., Sawada, Y., Iizumi, S., and Wakatsuki, T., 2001, Mantle sources and magma-crust interactions in volcanic rocks from northern Kenya rift: Geochemical evidence: Lithos, v. 56, p. 111–136.

Kampunzu, A.B., and Mohr, P., 1991, Magmatic evolution and petrogenesis in the East African rift system, *in* Kampunzu, A.B., and Lubala R.T., eds., Magmatism in extensional structural settings: Berlin, Germany, Springer Verlag, p. 85–136.

Kay, S.M., Maksaev, V., Moscoso, R., Mpodozis, C., and Nasi, C., 1987, Probing the evolving Andean lithosphere: Mid-late Tertiary magmatism in Chile (29°–30°30′S) over the modern zone of subhorizontal subduction: Journal of Geophysical Research, v. 92, p. 6173–6189.

Kepezhinskas, P., McDermott, F., Defant, M.J., Hochstaedter, A., Drummond, M.S., Hawkesworth, C.J., Koloskov, A., Maury, R.C., and Bellon, H., 1997, Trace element and Sr-Nd-Pb isotopic constraints on a three-component model of Kamchatka arc petrogenesis: Geochimica et Cosmochimica Acta, v. 61, p. 577–600.

Kimura, J.-I., and Yoshida, T., 2006, Contributions of slab fluid, mantle wedge and crust to the origin of Quaternary lavas in the NE Japan arc: Journal of Petrology, v. 47, p. 2185–2232.

Koprubasi, N., and Aldanmaz, E., 2004, Geochemical constraints on the petrogenesis of Cenozoic I – type granitoids in Northwest Anatolia, Turkey: Evidence for magma generation by lithospheric delamination in a post – collision setting: International Geology Review, v. 46, p. 705–729.

Koszowska, E., Wolska, A., Zuchiewicz, W., Cuong, N.Q., and Pécskay, Z., 2007, Crustal contamination of Late Neogene basalts in the Dien Bien Phu Basin, NW Vietnam: Some insights from petrological and geochronological studies: Journal of Asian Earth Sciences, v. 29, p. 1–17.

Le Bas, M.J., Le Maitre, R.W., Streckeisen, A., and Zanettin, B., 1986, A chemical classification of volcanic rocks based on the total alkali-silica diagram: Journal of Petrology, v. 27, p. 745–750.

Lebti, P.P., Thouret., J.-C., Wörner, G., and Fornari, M., 2006, Neogene and Quaternary ignimbrites in the area of Arequipa, southern Peru: Stratigraphical and petrological correlations: Journal of Volcanology and Geothermal Research, v. 154, p. 251–275.

Le Fort, P., 1981, Manaslu leucogranite: A collision signature of the Himalaya. A model for its genesis and emplacement: Journal of Geophysical Research, v. 86, p. 10545–10568.

Le Roex, A.P., Späth, A., and Zartman, R.E., 2001, Lithospheric thickness beneath the southern Kenya rift: Implications from basalt geochemistry: Contributions to Mineralogy and Petrology, v. 142, p. 89–106.

Liégeois, J.P., Navez, J., Hertogen, J., and Black, R., 1998, Contrasting origin of post-collisional high-K calc-alkaline and shoshonitic versus alkaline and peralkaline granitoids. The use of sliding normalization: Lithos, v. 45, p. 1–28.

Lindsay, J.M., Trumbull, R.B., and Siebel, W., 2005, Geochemistry and petrogenesis of late Pleistocene to Recent volcanism in Southern Dominica, Lesser Antilles: Journal of Volcanology and Geothermal Research, v. 148, p. 253–394.

López-Escobar, L., Frey, F.A., and Oyarzún, J., 1979, Geochemical characteristics of central Chile (33°–34°S) granitoids: Contributions to Mineralogy and Petrology, v. 70, p. 439–450.

López-Escobar, L., Tagiri, M., and Vergara, M., 1991, Geochemical features of southern Andes Quaternary volcanics between 41°5′ and 43°00′S: Geological Society of America Special Paper, v. 265, p. 45–56.

Macdonald, R., Davies, G.R., Upton, B.G.J., Denkley, P.N., Smith, M., and Leat, P.T., 1995, Petrogenesis of Silali volcano, Gregory rift, Kenya: Journal of the Geological Society of London, v. 152, p. 703–720.

McDermott, F., Delfin, F.G., Jr., Defant, M.J., Turner, S., and Maury, R., 2005, The petrogenesis of volcanics from Mt. Bulusan and Mt. Mayon in the Bicol arc, the Philippines: Contributions to Mineralogy and Petrology, v. 150, p. 652–670.

McMillan, N.J., Dickin, A.P., and Haag, D., 2000, Evolution of magma source regions in the Rio Grande rift, southern New Mexico: Geological Society of America Bulletin, v. 112, p. 1582–1593.

Middlemost, E.A.K., 1989, Iron oxidation ratios, norms and the classification of volcanic rocks: Chemical Geology, v. 77, p. 19–26.

Monzier, M., Robin, C., Eissen, J.-P., and Cotten, J., 1997, Geochemistry vs. seismo-tectonics along the volcanic New Hebrides Central Chain (Southwest Pacific): Journal of Volcanology and Geothermal Research, v. 78, p. 1–29.

Morishita, T., Hara, K., Nakamura, K., Sawaguchi, T., Tamura, A., Arai, S., Okino, K., Takai, K., and Kumagai, H., 2009, Igneous, alteration and exhumation processes recorded in abyssal peridotites and related fault rocks from an oceanic core complex along the Central Indian Ridge: Journal of Petrology, v. 50, p. 1299–1325.

Morra, V., Secchi, F.A., and Assorgia, A., 1994, Petrogenetic significance of peralkaline rocks from Cenozoic calc – alkaline volcanism from SW Sardinia, Italy: Chemical Geology, v. 118, p. 109–142.

Moyer, T.C., and Esperança, S., 1989, Geochemical and isotopic variations in a bimodal magma system: The Kaiser Spring volcanic field, Arizona: Journal of Geophysical Research, v. 94, p. 7841–8759.

Myers, J.D., and Sinha, A.K., 1985, A detailed Pb isotopic study of crustal contamination/assimilation: The Edgecumbe volcanic field, SE Alaska: Geochimica et Cosmochimica Acta, v. 49, p. 1343–1355.

Patino, L.C., Carr, M.J., and Feigenson, M.D., 1997, Cross-arc geochemical variations in volcanic fields in Honduras C.A.: Progressive changes in source with distance from the volcanic front: Contributions to Mineralogy and Petrology, v. 129, p. 341–351.

Pearce, J.A., Bender, J.F., Long, S.E.D., Kidd, W.S.F., Low, P.J., Guner, Y., Saroglu, F., Yilmaz, Y., Moorbath, S., and Mitchell, J.G., 1990, Genesis of collision volcanism in Eastern Anatolia, Turkey: Journal of Volcanology and Geothermal Research, v. 44, p. 189–229.

Pearce, J.A., and Cann, J.R., 1971, Ophiolite origin investigated by discriminant analysis using Ti, Zr and Y: Earth and Planetary Science Letters, v. 12, p. 339–349.

Pearce, J.A., and Cann, J.R., 1973, Tectonic setting of basic volcanic rocks determined using trace element analyses: Earth and Planetary Science Letters, v. 19, p. 290–300.

Pearce, J.A., Harris, N.B.W., and Tindle, A.G., 1984, Trace element discrimination diagrams for the tectonic interpretation of granitic rocks: Journal of Petrology, v. 25, p. 956–983.

Peccerillo, A., Barberio, M.R., Yirgu, G., Ayalew, D., Barbieri, M., and Wu, T.W., 2003, Relationships between mafic and peralkaline silicic magmatism in continental rift settings: A petrological, geochemical and isotopic study of the Gedemsa volcano, central Ethiopian rift: Journal of Petrology, v. 44, p. 2003–2032.

Peccerillo, A., Donati, C., Santo, A.P., Orlando, A., Yirgu, G., and Ayalew, D., 2007, Petrogenesis of silicic peralkaline rocks in the Ethiopian Rift: Geochemical evidence and volcanological implications: Journal of African Earth Sciences, v. 48, p. 161–173.

Perry, F.V., Baldridge, W.S., DePaolo, D.J., and Shafiqullah, M., 1990, Evolution of a magmatic system during continental extension: The mount Taylor volcanic field, New Mexico: Journal of Geophysical Research, v. 95, p. 19327–19348.

Reichardt, H., Weinberg, R.F., Andersen, U.B., and Fanning, C.M., 2010, Hybridization of granitic magmas in the source: The origin of the Karakoram Batholith, Ladakh, NW India: Lithos, v.116, p. 249–272.

Rollinson, H.R., 1993, Discriminating between tectonic environments using geochemical data, *in* Rollinson, H.R., ed., Using geochemical data: Evaluation, presentation, interpretation: Essex, England, Longman Scientific & Technical, p. 171–214.

Romick, J.D., Perfit, M.R., Swanson, S.E., and Shuster, R.D., 1990, Magmatism in the eastern Aleutian arc: Temporal characteristic of igneous activity on Akutan Island: Contributions to Mineralogy and Petrology, v. 104, p. 700–721.

Ronga, F., Lustrino, M., Marzoli, A., and Melluso, L., 2010, Petrogenesis of a basalt-comendite-pantellerite rock suite: The Boseti Volcanic Complex (Main Ethiopian Rift): Mineralogy and Petrology, v. 98, p. 227–243, doi: 10.1007/s00710-009-0064-3.

Rotolo, S.G., and Castorina, F., 1998, Transition from midly-tholeiitic to calc-alkaline suite: The case of Chicontepec volcanic centre, El Salvador, Central America: Journal of Volcanology and Geothermal Research, v. 86, p. 117–136.

Saunders, A.D., Tarney, J., Stern, C.R., and Dalziel, I.W.D., 1979, Geochemistry of Mesozoic marginal basin floor igneous rocks from southern Chile: Geological Society of America Bulletin, v. 90, p. 237–258.

Saunders, A.D., Tarney, J., and Weaver, S.D., 1980, Transverse geochemical variations across the Antarctic Peninsula: Implications for the genesis of calc-alkaline magmas: Earth and Planetary Science Letters, v. 46, p. 344–360.

Scaillet, B., France-Lanord, C., and Fort, P.L., 1990, Badrinath-Gangotri plutons (Garhwal, India): Petrological and geochemical evidence for fractionation processes in a high Himalayan leucogranite: Journal of Volcanology and Geothermal Research, v. 44, p. 163–188.

Schmitz, M.D., and Smith, I.E.M., 2004, The petrology of the Rotoiti eruption sequence, Taupo Volcanic Zone: An example of fractionation and mixing in a rhyolitic system: Journal of Petrology, v. 45, p. 2045–2066.

Schuth, S., Munker, C., Konig, S., Qopoto, C., Basi, S., Schonberg, D.G., and Ballhaus, C., 2009, Petrogenesis of lavas along the Solomon island arc, SW Pacific: Coupling of compositional variations and subduction zone geometry: Journal of Petrology, v. 50, p. 781–811.

Sendjaja, Y.A., Kimura, J., and Sunardi, E., 2009, Across-arc geochemical variation of Quaternary lavas in west Java, Indonesia: Mass-balance elucidation using arc basalt simulator model: Island Arc, v. 18, p. 201–224.

Shukuno, H., Tamura, Y., Tani, K., Chang, Q., Suzuki, T., and Fiske, R.S., 2006, Origin of silicic magmas and the compositional gap at Sumisu submarine caldera, Izu-Bonin arc, Japan: Journal of Volcanology and Geothermal Research, v. 156, p. 187–216.

Shuto, K., Ishimoto, H., Hirahara, Y., Sato, M., Matsui, K., Fujibayashi, N., Takazawa, E., Yabuki, K., Sekine, M., kato, M., and Rezanov, A.I., 2006, Geochemical secular variation of magma source during Early to Middle Miocene time in the Niigata area, NE Japan: Asthenospheric mantle upwelling during back-arc basin opening: Lithos, v. 86, p. 1–33.

Singer, B.S., and Kudo, A.M., 1986, Assimilation-fractional crystallization of Polvadera Group rocks in the northwestern Jemez volcanic field, New Mexico: Contributions to Mineralogy and Petrology, v. 94, p. 374–386.

Singer, B.S., Myers, J.D., and Frost, C.D., 1992, Mid-Pleistocene basalt from the Seguam volcanic center, central Aleutian arc, Alaska: Local lithospheric structures and source variability in the Aleutian arc: Journal of Geophysical Research, v. 97, p. 4561–4578.

Smellie, J.L., 1983, A geochemical overview of subduction-related igneous activity in the South Shetland islands, Lesser Antarctica, *in* Oliver, R.L., James, P.R., and Jago, J.B., eds., Antarctic Earth Science, Australian Academy of Sciences and Cambridge University Press, p. 352–356.

Smith, I.E.M., Stewart, R.B., and Price, R.C., 2003, The petrology of a large intra-oceanic silicic eruption: The Sandy Bay tephra, Kermadec arc, southwest Pacific: Journal of Volcanology and Geothermal Research, v. 124, p. 173–194.

Sruoga, P., Llambías, E.J., Fauqué, L., Schonwandt, D., and Repol, D.G., 2005, Volcanological and geochemical evolution of the Diamante caldera-Maipo volcano complex in the southern Andes of Argentina (34°10′S): Journal of South American Earth Sciences, v. 19, p. 399–414.

Stephenson, D., and Marshall, T.R., 1984, The petrology and mineralogy of Mt. Popa volcano and the nature of the late-Cenozoic Burma volcanic arc: Journal of the Geological Society of London, v. 141, p. 747–762.

Stolz, A.J., Varne, R., Davies, G.R., Wheller, G.E., and Fodon, J.D., 1990, Magma source components in an arc-continent collision zone: The Flores-Lembata sector, Sunda arc, Indonesia: Contributions to Mineralogy and Petrology, v. 105, p. 585–601.

Streck, M.J., 2002, Partial melting to produce high-silica rhyolites of a young bimodal suite: Compositional constraints among rhyolites, basalts, and metamorphic xenoliths from the Harney Basin, Oregon: International Journal of Earth Sciences, v. 91, p. 583–593.

Streck, M.J., and Grunder, A.L., 1999, Enrichment of basalt and mixing of dacite in the rootzone of a large rhyolite chamber: Inclusions and pumices from the Rattelsnake tuff, Oregon: Contributions to Mineralogy and Petrology, v. 136, p. 193–212.

Sturchio, N.C., Muehlenbachs, K., and Seitz, M.G., 1986, Element redistribution during hydrothermal alteration of rhyolite in an active geothermal system: Yellowstone drill cores Y-7 and Y-8: Geochimica et Cosmochimica Acta, v. 50, p. 1619–1631.

Tamura, Y., 1994, Genesis of island arc magmas by mantle derived bimodal magmatism: Evidence from the Shiraham group, Japan: Journal of Petrology, v. 35, p. 619–645.

Tamura, Y., Yuhara, M., Ishii, T., Irino, N., and Shukuno, H., 2003, Andesites and dacites from Daisen volcano, Japan: Partial-to-total remelting of an andesite magma body: Journal of Petrology, v. 44, p. 2243–2260.

Taylor, R.N., and Nesbitt, R.W., 1998, Isotopic characteristics of subduction fluids in an intra-oceanic setting, Izu-Bonin Arc, Japan: Earth and Planetary Science Letters, v. 164, p. 79–98.

Togashi, S., Tanaka, T., Yoshida, T., Ishikawa, K.-I., Fujinawa, A., and Kurasawa, H., 1992, Trace elements and Nd-Sr isotopes of island arc tholeiites from frontal arc of northeast Japan: Geochemical Journal, v. 26, p. 261–277.

Trua, T., Deniel, C., and Mazzuoli, R., 1999, Crustal control in the genesis of Plio-Quaternary bimodal magmatism of the Main Ethiopian Rift (MER): Geochemical and isotopic (Sr, Nd, Pb) evidence: Chemical Geology, v. 155, p. 201–231.

Trumbull, R.B., Wittenbrink, R., Hahne, K., Emmermann, R., Büsch, W., Gerstenberger, H., and Siebel, W., 1999, Evidence for Late Miocene to Recent contamination of arc andesites by crustal melts in the Chilean Andes (25–26°S) and its geodynamic implications: Journal of South American Earth Sciences, v. 12, p. 135–155.

Turner, S., Arnaud, N., Liu, J., Roger, N., Hawkesworth, C., Harris, N., Kelley, S., Calsteren, P.V., and Deng, W., 1996, Post-collision, shoshonitic volcanism on the Tibet plateImplication for convective thinning of the lithosphere and the source of ocean island basalts: Journal of Petrology, v. 37, p. 45–71.

Turner, S., and Foden, J., 2001, U, Th and Ra disequilibria, Sr, Nd and Pb isotope and trace element variations in Sunda arc lavas: Predominance of a subducted sediment component: Contributions to Mineralogy and Petrology, v. 142, p.43–57.

Ujike, O., and Stix, J., 2000, Geochemistry and origins of Ueno and On-take basaltic to andesitic rocks (<3 Ma) produced by distinct contributions of subduction components, central Japan: Journal of Volcanology and Geothermal Research, v. 95, p. 49–64.

Vergara, M., López-Escobar, L., Palma, J.L., Hickey-Vargas, R., and Roeschmann, C., 2004, Late Tertiary volcanic episodes in

the area of the city of Santiago de Chile: New geochronological and geochemical data: Journal of South American Earth Sciences, v. 17, p. 227–238.

Verma, S.P., 1981, Seawater alteration effects on $^{87}Sr/^{86}Sr$, K, Rb, Cs, Ba and Sr in oceanic igneous rocks: Chemical Geology, v. 34, p. 81–89.

Verma, S.P., 1997, Sixteen statistical tests for outlier detection and rejection in evaluation of International Geochemical Reference Materials: Example of microgabbro PM-S: Geostandards Newsletter. The Journal of Geostandards and Geoanalysis, v. 21, p. 59–75.

Verma, S.P., 2000, Geochemistry of the subducting Cocos plate and the origin of subduction-unrelated mafic volcanism at the volcanic front of the central Mexican Volcanic Belt, *in* Delgado-Granados, H., Aguirre-Díaz, G., and Stock, J.M., eds., Cenozoic tectonics and volcanism of Mexico, Geological Society of America, p. 195–222.

Verma, S.P., 2010, Statistical evaluation of bivariate, ternary and discriminant function tectonomagmatic discrimination diagrams: Turkish Journal of Earth Sciences, v. 19, p. 185–238.

Verma, S.P., 2011, Geochemometrics: Revista Mexicana de Ciencias Geológicas (in press).

Verma, S.P., and Agrawal, S., 2011, Discriminant function discrimination diagrams for basic and ultrabasic volcanic rocks through log-transformed ratios of high field strength elements and implications for petrogenetic processes: Revista Mexicana de Ciencias Geológicas (in press).

Verma, S.P., Guevara, M., and Agrawal, S., 2006, Discriminating four tectonic settings: Five new geochemical diagrams for basic and ultrabasic volcanic rocks based on log-ratio transformation of major-element data: Journal of Earth System Science, v. 115, p. 485–528.

Verma, S.P., and Quiroz-Ruiz, A., 2006, Critical values for six Dixon tests for outliers in normal samples up to sizes 100, and applications in science and engineering: Revista Mexicana de Ciencias Geológicas, v. 23, p. 133–161.

Verma, S.P., Rodríguez-Ríos, R., and González-Ramírez, R., 2010a, Statistical evaluation of classification diagrams for altered igneous rocks: Turkish Journal of Earth Sciences, v. 19, p. 239–265.

Verma, S.P., Torres-Alvarado, I.S., and Sotelo-Rodríguez, Z.T., 2002, SINCLAS: Standard igneous norm and volcanic rock classification system: Computers & Geosciences, v. 28, p. 711–715.

Verma, S.P., Verma, S.K., Pandarinath, K., and Rivera-Gómez, M.A., 2010b, Evaluation of recent tectonomagmatic discrimination diagrams and their application to the origin of basic magmas in Southern Mexico and Central America: Pure and Applied Geophysics (in press), doi: 10.1007/s00024-010-0173–2.

Vidal, P., Cocherie, A., and Forte, P., 1982, Geochemical investigation of the origin of the Manaslu leucogranite (Himalaya, Nepal): Geochimica et Cosmochimica Acta, v. 46, p. 2279–2292.

Visona, D., and Lombard, B., 2002, Two-mica and tourmaline leucogranites from the Everest-Makalu region (Nepal-Tibet). Himalayan leucogranite genesis by isobaric heating: Lithos, v. 62, p. 125–150.

Wade, J.A., Plank, T., Stern, R.J., Tollstrup, D.L., Gill, J.B., O'Leary, J.C., Eiler, J.M., Moore, R.B., Woodhead, J.D., Trusdell, F., Fischer, T.P., and Hilton, D.R., 2005, The May 2003 eruption of Anatahan volcano, Mariana islands: Geochemical evolution of a silicic island-arc volcano: Journal of Volcanology and Geothermal Research, v. 146, p. 139–170.

Walker, J.A., Moulds, T.N., Zentilli, M., and Feigenson, M.D., 1991, Spatial and temporal variations in volcanics of the Andean Central volcanic zone (26 to 28°S): Geological Society of America Special Paper, v. 265, p. 139–156.

Walsh, J.N., Beckinsale, R.D., Skelhorn, R.R., and Thorpe, R.S., 1979, Geochemistry and petrogenesis of Tertiary granitic rocks from the Island of Mull, northwest Scotland: Contributions to Mineralogy and Petrology, v. 71, p. 99–116.

Wang, P., and Glover, L., III, 1992, A tectonics test of the most commonly used geochemical discriminant diagrams and patterns: Earth-Science Reviews, v. 33, p. 111–131.

Wheller, G.E., Varne, R., Foden, J.D., and Abbott, M.J., 1987, Geochemistry of Quaternary volcanism in the Sunda-Banda arc, Indonesia, and three-component genesis of island-arc basaltic magmas: Journal of Volcanology and Geothermal Research, v. 32, p. 137–160.

Woodhead, J.D., 1988, The origin of geochemical variations in Mariana lavas: A general model for petrogenesis in intra-oceanic island arcs: Journal of Petrology, v. 29, p. 805–830.

Wright, I.C., Worthington, T.J., and Gamble, J.A., 2006, New multibeam and geochemistry of the 30°-35°S sector, and overview of southern Kermadec arc volcanism: Journal of Volcanology and Geothermal Research, v. 149, p. 263–296.

Zellmer, G., Turner, S., and Hawkesworth, C., 2000, Timescales of destructive plate margin magmatism: New insights from Santorini, Aegean volcanic arc: Earth and Planetary Science Letters, v. 174, p. 265–281.

Zellmer, G.F., Hawkesworth, C.J., Sparks, R.S.J., Thomas, L.E., Harford, C.L., Brewer, T.S., and Loughlin, S.C., 2003, Geochemical evolution of the Soufrière Hills volcano, Montserrat, Lesser Antilles volcanic arc: Journal of Petrology, v. 44, p. 1349–1374.

Zhuravlev, D.Z., Tsvetkov, A.A., Zhuravlev, A.Z., Gladkov, N.G., and Chernyshev, I.V., 1987, $^{143}Nd/^{144}Nd$ and $^{87}Sr/^{86}Sr$ ratios in recent magmatic rocks of the Kurile island arc: Chemical Geology, v. 66, p. 227–243.

Annexure I

Verma *et al.* (2012) IGR_Supplementary file

Electronic Supplement

Statistical evaluation of existing tectonomagmatic discrimination diagrams for granitic rocks and proposal of new discriminant-function-based multi-dimensional diagrams for acid rocks

Sanjeet K. Verma[a], Kailasa Pandarinath[b], Surendra P. Verma[b*]

[a] *Posgrado en Ingeniería, Centro de Investigación en Energía, Universidad Nacional Autónoma de México,Priv. Xochicalco s/no., Col. Centro, Apartado Postal 34, Temixco, Mor. 62580, MEXICO;*

[b] *Departamento de Sistemas Energéticos, Centro de Investigación en Energía, Universidad Nacional Autónoma de México, Priv. Xochicalco s/no., Col. Centro, Apartado Postal 34, Temixco, Mor. 62580, MEXICO.*

* Corresponding author. Email: spv@cie.unam.mx

This supplement contains four Tables and five Figures.

Table S1. Longitude and latitude values of sample locations shown in the world map (Figure 1)*.

Serial No.	Longitude (E-W) (degree, minute, second)			Latitude (N-S) (degree, minute, second)			References
				Collision			
1	80	---	---	30	---	---	Ayres and Harris (1997)
2	90	9	56.61	28	3	2.24	Castelli and Lombardo (1988)
3	24	38	59.3	41	37	0.81	Cherneva and Georgieva (2005)
4	9	18	41.91	46	15	18.37	Debon and Lemmet (1999)
5	27	50	19.67	39	55	49.83	Delaloye and Bingol (2000)
6	10	11	34.16	42	46	42.74	Dini *et al*. (2002)
7	128	52	42.31	59	19	52	Grigoriev and Pshenichny (1998)
8	83	16	42.92	28	52	38.15	Guillot and Fort (1995)
9	29	2	46.83	39	59	46.64	Hasozbek *et al*. (2010)
10	34	47	19.81	39	49	15.89	Ilbeyli *et al*. (2004)
11	27	52	51.75	40	23	42.58	Koprubasi and Aldanmaz (2004)
12	6	46	57.48	30	56	42.02	Liégeois *et al*. (1998)
13	8	54	25.16	40	7	51.41	Morra *et al*. (1994)
14	39	1	26.22	38	29	5.1	Pearce *et al*. (1990)
15	78	13	39.4	34	4	10.5	Reichardt *et al*. (2010)
16	30	70	---	78	55	---	Scaillet *et al*. (1990)
17	86	57	35.61	27	53	41.19	Visona and Lombardo (2002)
				(i) syn-Collision granite (syn-COLG)			
1	58	48	55	20	28	20.76	Abbotts (1978)
2	4	34	6.84	50	17	23.89	Alderton *et al*. (1980)
3	91	1	34.05	29	44	47.6	Dietrich and Gansser (1981)
4	10	29	46.59	46	9	19.89	Dupuy *et al*. (1982)
5	84	30	37.83	28	31	40.37	Vidal *et al.* (1982)
				Volcanic-arc			
				(i) CAVA			
1	89	50	33.9	13	49	33.3	Agostini *et al*. (2006)
2	90	36	0.42	14	22	59.79	Bardintzeff and Deniel (1992)
3	90	33	24.68	14	38	1.58	Cameron *et al*. (2002)
4	89	50	35.55	13	55	6.51	Gonzalez-Partida *et al*. (1997)
5	86	14	30.88	15	12	11.62	Patino *et al*. (1997)
6	88	53	47.51	13	47	45.72	Rotolo and Castorina (1998)
				(ii) Continental arc (CA)			
1	70	53	15.87	35	57	34.05	Davidson *et al*. (1988)
2	68	54	1	33	29	18	de Silva (1991)
3	69	55	1.72	33	28	16.02	Deruelle (1982)
4	69	53	2	34	30	10	Gerlach *et al*. (1988)
5	69	55	3	39	29	17	Hickey-Vargas *et al*. (1989)
6	70	30	5	30	30	---	Kay *et al*. (1987)

Continues

Table S1 (Contd.). Longitude and latitude values of sample locations shown in the world map (Figure 1)*.

Serial No.	Longitude (E-W) (degree, minute, second)			Latitude (N-S) (degree, minute, second)			References
7	72	20	5.54	16	9	18.74	Lebti *et al*. (2006)
8	73	19	33.67	41	5	49.64	López-Escobar *et al*. (1991)
9	70	48	11.09	34	10	51.75	Sruoga *et al*. (2005)
10	69	44	25.77	25	16	55	Trumbull *et al*. (1999)
11	70	33	59.23	33	25	24.08	Vergara *et al*. (2004)
12	81	0	18.48	46	30	17.21	Walker *et al*. (1991)
				(iii) Volcanic-arc granite (VAG)			
1	56	41	58.58	24	1	2.06	Alabaster *et al*. (1982)
2	119	34	33.03	37	44	36.22	Bateman and Chappell (1979)
3	159	28	21.17	54	1	41	Izbekov *et al*. (2004)
4	71	37	22.67	33	37	1.28	López-Escobar *et al*. (1979)
5	58	5	1.89	63	44	5.25	Saunders *et al*. (1979, 1980)
6	133	30	1.83	35	30	42	Tamura *et al*. (2003)
				(iv) Island arc (IA)			
1	166	57	34.29	15	23	47.41	Barsdell and Berry (1990)
2	145	47	47.77	15	16	26	Bloomer and Hawkins (1989)
3	64	1	41.02	10	41	57.57	Brown *et al*. (1977)
4	175	10	52.77	21	7	42.98	Bryan *et al*. (1972)
5	162	---	---	57	---	---	Churikova *et al*. (2001)
6	175	59	52.62	38	49	14.51	Cole (1981)
7	121	21	4.19	18	35	47.06	Defant *et al*. (1991)
8	162	---	---	56	---	---	Dorendorf *et al*. (2000)
9	121	57	50.58	15	45	59.19	DuFrane *et al*. (2006)
10	174	57	25.3	21	22	37.82	Ewart and Bryan (1972)
11	172	---	---	28	---	---	Ewart *et al*. (1977)
12	173	30	2.53	52	5	49.4	Finney *et al*. (2008)
13	117	4	16.98	8	24	31.49	Foden and Varne (1980)
14	176	5	8.85	38	38	33.05	Gamble *et al*. (1995)
15	167	34	12.8	45	49	45.91	Haase *et al*. (2002)
16	145	2	21.06	4	4	29.4	Hegner and Smith (1992)
17	155	20	1.45	58	13	42.89	Hildreth *et al*. (2004)
18	140	5	29.61	38	10	14.97	Hirotani and Ban (2006)
19	162	---	---	54	---	---	Ishikawa *et al*. (2001)
20	159	26	24.29	54	2	51.98	Kepezhinskas *et al*. (1997)
21	140	4	49.81	37	10	53.22	Kimura and Yoshida (2006)
22	61	19	39.06	15	23	3.04	Lindsay *et al*. (2005)
23	121	57	50.58	16	45	59.19	McDermott *et al*. (2005)
24	174	12	1.94	52	11	46.01	Myers *et al*. (1985)
25	165	56	39.85	54	9	4.35	Romick *et al*. (1990)
26	176	4	32.98	38	41	38.75	Schmitz and Smith (2004)

Continues

Table S1 (Contd.). Longitude and latitude values of sample locations shown in the world map (Figure 1)*.

Serial No.	Longitude (E-W) (degree, minute, second)			Latitude (N-S) (degree, minute, second)			References
27	83	22	34.52	36	12	46.87	Schuth *et al*. (2009)
28	107	40	1.23	7	5	17.22	Sendjaja (2009)
29	142	---	---	34	---	---	Shukuno *et al*. (2006)
30	138	---	---	44	---	---	Shuto *et al*. (2006)
31	172	31	14.39	52	18	44.91	Singer *et al*. (1992)
32	0	47	42.52	60	44	44.24	Smellie (1983)
33	178	25	47.64	30	13	48.82	Smith *et al*. (2003)
34	93	6	24.11	20	40	45.19	Stephenson and Marshall (1984)
35	123	27	8.22	8	26	56.33	Stolz *et al*. (1990)
36	136	16	30.13	33	23	38.28	Tamura (1994)
37	143	---	---	30	---	---	Taylor and Nesbitt (1998)
38	109	53	11.71	1	55	34.75	Turner and Foden (2001)
39	61	31	43.82	16	10	26.37	Turner *et al*. (1996)
40	137	15	---	35	40	---	Ujike and Stix (2000)
41	145	36	41.07	16	37	25	Wade *et al*. (2005)
42	109	59	39.96	2	0	9.42	Wheller *et al*. (1987)
43	145	30	41	16	40	21	Woodhead (1988)
44	179	19	6.68	30	56	59.18	Wright *et al*. (2006)
45	25	23	43.79	36	24	3.54	Zellmer *et al*. (2000)
46	62	10	36.69	16	42	53.77	Zellmer *et al*. (2003)
47	154	49	54.39	47	56	55.85	Zhuravlev *et al*. (1987)
				Within-plate			
				(i) Continental rift (CR)			
1	125	---	---	45	---	---	Basu *et al*. (1991)
2	3	26	10.5	40	13	34.6	Benito *et al*. (1999)
3	44	---	---	39	4	41	Buket and Temel (1998)
4	42	26	25.37	16	48	59.02	Camp *et al*. (1991)
5	1	45	16.67	45	50	16.92	Chauvel and Jahn (1984)
6	43	9	25.42	11	32	55.3	Deniel *et al*. (1994)
7	7	38	35.16	50	41	12.65	Haase *et al*. (2004)
8	128	---	---	42	---	---	Hsu *et al*. (2000)
9	28	56	49.04	24	1	38.04	Kampunzu and Mohr (1991)
10	36	10	10.4	1	12	4.29	Le Roex *et al*. (2001)
11	36	13	45.45	1	8	56.9	MacDonald *et al*. (1995)
12	111	28	28.81	33	14	30.74	Moyer and Esperança (1989)
13	39	10	---	8	20	---	Peccerillo *et al*. (2003, 2007)
14	105	1	56.51	34	58	10.39	Perry *et al*. (1990)
15	106	44	13.23	35	36	46.46	Singer and Kudo (1986)

Continues

Table S1 (Contd.). Longitude and latitude values of sample locations shown in the world map (Figure 1)*.

Serial No.	Longitude (E-W) (degree, minute, second)			Latitude (N-S) (degree, minute, second)			References
				(ii) Within-plate granite (WPG)			
1	32	33	55.52	16	15	50.92	Harris *et al*. (1983)
2	8	32	26.59	9	51	21.19	Imeokparia (1982, 1983)
3	6	1	21.17	56	26	30.54	Walsh *et al*. (1979)
				Ocean-ridge granite (ORG)			
114	45	15	15.4	27	50	48.7	Aldiss (1981)
115	11	16	44.57	71	44	14.17	Engel and Fisher (1975)

* The longitude and latitude values were reported in only a few papers; therefore, most of the longitude and latitude values were inferred from the Google Earth.

Table S2. Number of samples in the training and testing sets of normally distributed discordant outlier-free database

Name*	Number	Training set	Testing set	Total
IA	1	277	25	302
CA	2	258	25	283
CR	3	219	25	244
COL	4	278	25	303
Sum	1–4	1032	100	1132

* IA = island arc; CA = continental arc; CR= continental rift; Col = collision; the numbers 1–4 are group numbers discussed in the text and used in other Tables.

Table S3. Mean and standard deviation of $(SiO_2)_{adj}$ and their log-transformed ratio variables for the four tectonic groups (IA, CA, CR, and Col) for discordant outlier-free samples of the training set

loge-transformed ratio variable	IA (1) (*n =277*)		CA (2) (*n = 258*)		CR (3) (*n =219*)		Col (4) (*n =278*)	
	$\bar{x}$	*s*	$\bar{x}$	*s*	$\bar{x}$	*s*	$\bar{x}$	*s*
$(SiO_2)_{adj}$	66.399	2.654	68.539	4.225	70.022	4.209	72.150	3.316
$\ln(TiO_2/SiO_2)_{adj}$	-4.661	0.285	-5.047	0.589	-5.095	0.599	-5.951	0.958
$\ln(Al2O_3/SiO_2)_{adj}$	-1.445	0.119	-1.487	0.146	-1.714	0.264	-1.569	0.110
$\ln(Fe2O_3/SiO_2)_{adj}$	-3.819	0.249	-4.252	0.577	-3.844	0.530	-4.999	0.730
$\ln(Feo/SiO_2)_{adj}$	-2.936	0.281	-3.438	0.649	-3.120	0.532	-4.275	0.766
$\ln(MnO/SiO_2)_{adj}$	-6.207	0.348	-6.558	0.439	-6.239	0.765	-7.588	0.806
$\ln(MgO/SiO_2)_{adj}$	-3.836	0.438	-4.424	0.899	-5.723	1.565	-5.495	1.217
$\ln(CaO/SiO_2)_{adj}$	-2.769	0.349	-3.188	0.697	-4.352	1.068	-4.064	0.837
$\ln(Na_2O/SiO_2)_{adj}$	-2.787	0.157	-2.796	0.171	-2.725	0.336	-2.933	0.151
$\ln(K_2O/SiO_2)_{adj}$	-3.7507	0.5269	-3.206	0.301	-2.785	0.193	-2.822	0.198
$\ln(P_2O_5/SiO_2)_{adj}$	-5.9795	0.4419	-6.363	0.809	-7.138	1.248	-6.705	0.884

$\bar{x}$ –mean; *s*–standard deviation.

Table S4. Test of equality of group means for the eleven elements log-transformed ratio variables in the training set (discordant outlier-free samples)

Element	Wilks' lambda	F-ratio	Significance
$\ln(TiO_2/SiO_2)_{adj}$	0.2383	9.8659	0.0000
$\ln(Al_2O_3/SiO_2)_{adj}$	0.2357	4.2601	0.0143
$\ln(Fe_2O_3/SiO_2)_{adj}$	0.2360	4.8275	0.0081
$\ln(FeO/SiO_2)_{adj}$	0.2345	1.5485	0.2131
$\ln(MnO/SiO_2)_{adj}$	0.2499	35.3349	0.0000
$\ln(MgO/SiO_2)_{adj}$	0.2355	3.8683	0.0212
$\ln(CaO/SiO_2)_{adj}$	0.2386	10.7547	0.0000
$\ln(Na_2O/SiO_2)_{adj}$	0.2351	2.9913	0.0506
$\ln(K_2O/SiO_2)_{adj}$	0.2753	90.6055	0.0000
$\ln(P_2O_5/SiO_2)_{adj}$	0.2401	13.8239	0.0000

Wilks' lambda (U-statistic) and univariate F-ratio with degree of freedom, df1= v1 = g-1 = 4-1 = 3 and df2 = v2 = n-g = 1032-4 = 1028, where g is the number of groups and n is total number of samples.

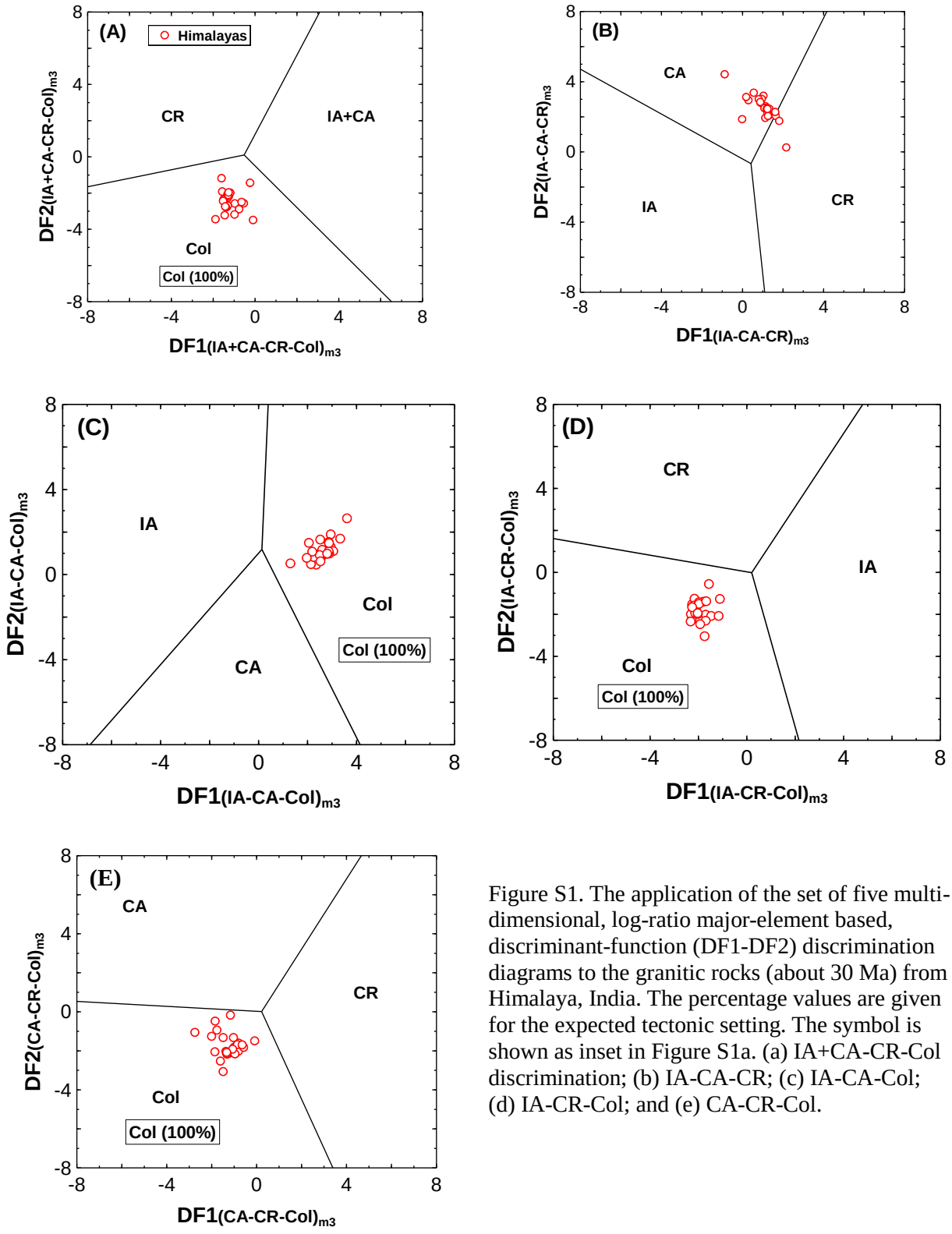

Figure S1. The application of the set of five multi-dimensional, log-ratio major-element based, discriminant-function (DF1-DF2) discrimination diagrams to the granitic rocks (about 30 Ma) from Himalaya, India. The percentage values are given for the expected tectonic setting. The symbol is shown as inset in Figure S1a. (a) IA+CA-CR-Col discrimination; (b) IA-CA-CR; (c) IA-CA-Col; (d) IA-CR-Col; and (e) CA-CR-Col.

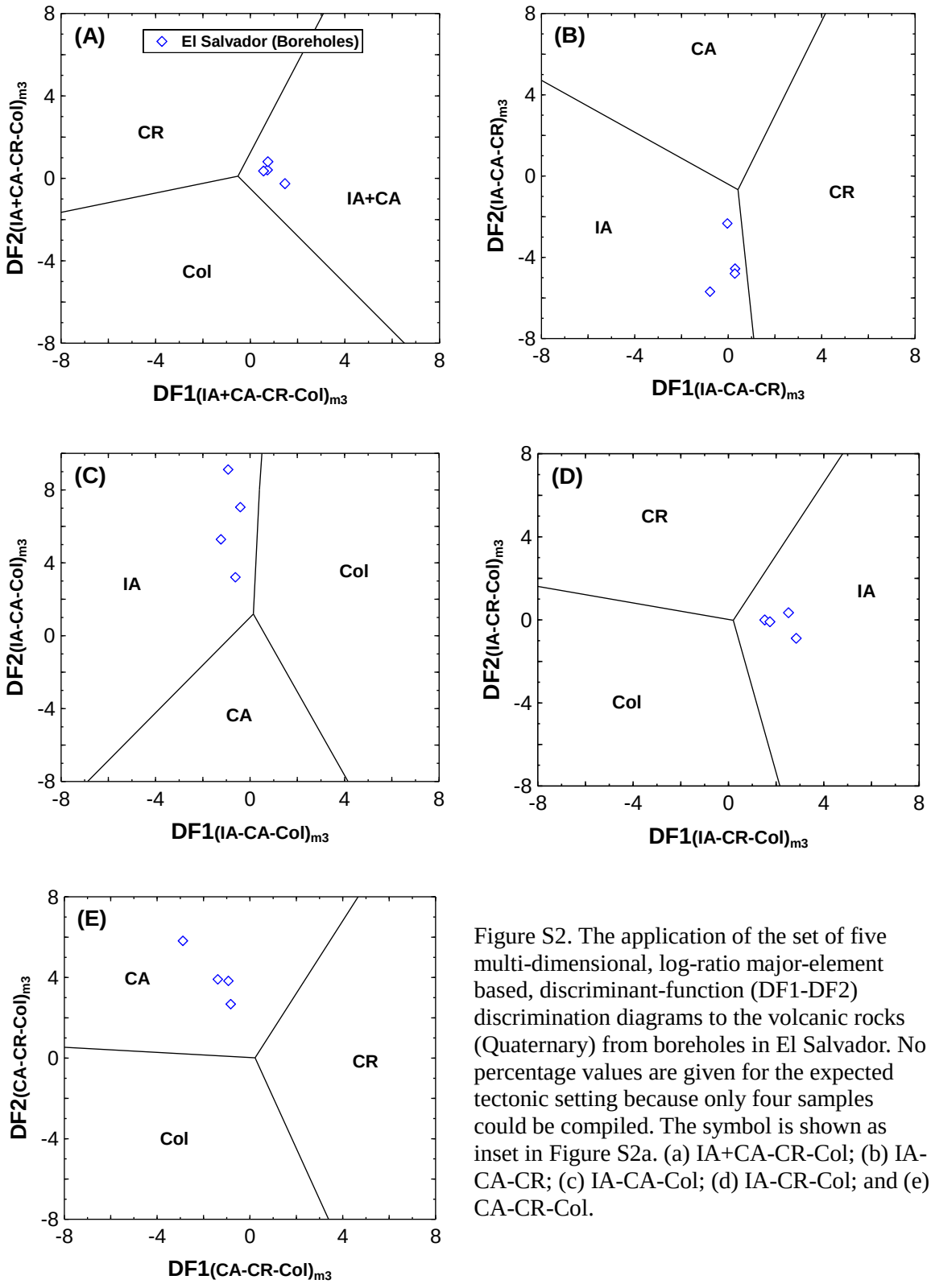

Figure S2. The application of the set of five multi-dimensional, log-ratio major-element based, discriminant-function (DF1-DF2) discrimination diagrams to the volcanic rocks (Quaternary) from boreholes in El Salvador. No percentage values are given for the expected tectonic setting because only four samples could be compiled. The symbol is shown as inset in Figure S2a. (a) IA+CA-CR-Col; (b) IA-CA-CR; (c) IA-CA-Col; (d) IA-CR-Col; and (e) CA-CR-Col.

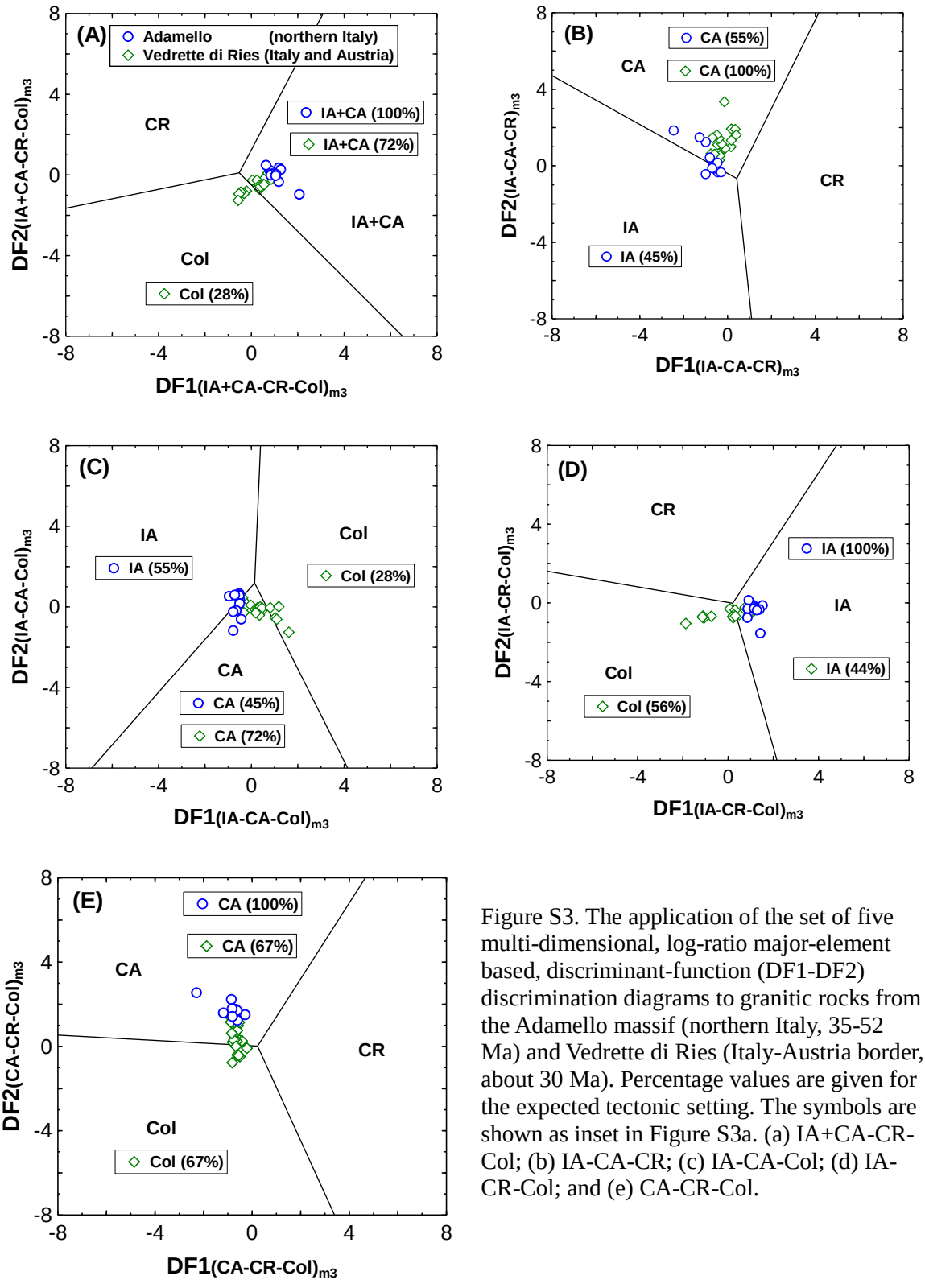

Figure S3. The application of the set of five multi-dimensional, log-ratio major-element based, discriminant-function (DF1-DF2) discrimination diagrams to granitic rocks from the Adamello massif (northern Italy, 35-52 Ma) and Vedrette di Ries (Italy-Austria border, about 30 Ma). Percentage values are given for the expected tectonic setting. The symbols are shown as inset in Figure S3a. (a) IA+CA-CR-Col; (b) IA-CA-CR; (c) IA-CA-Col; (d) IA-CR-Col; and (e) CA-CR-Col.

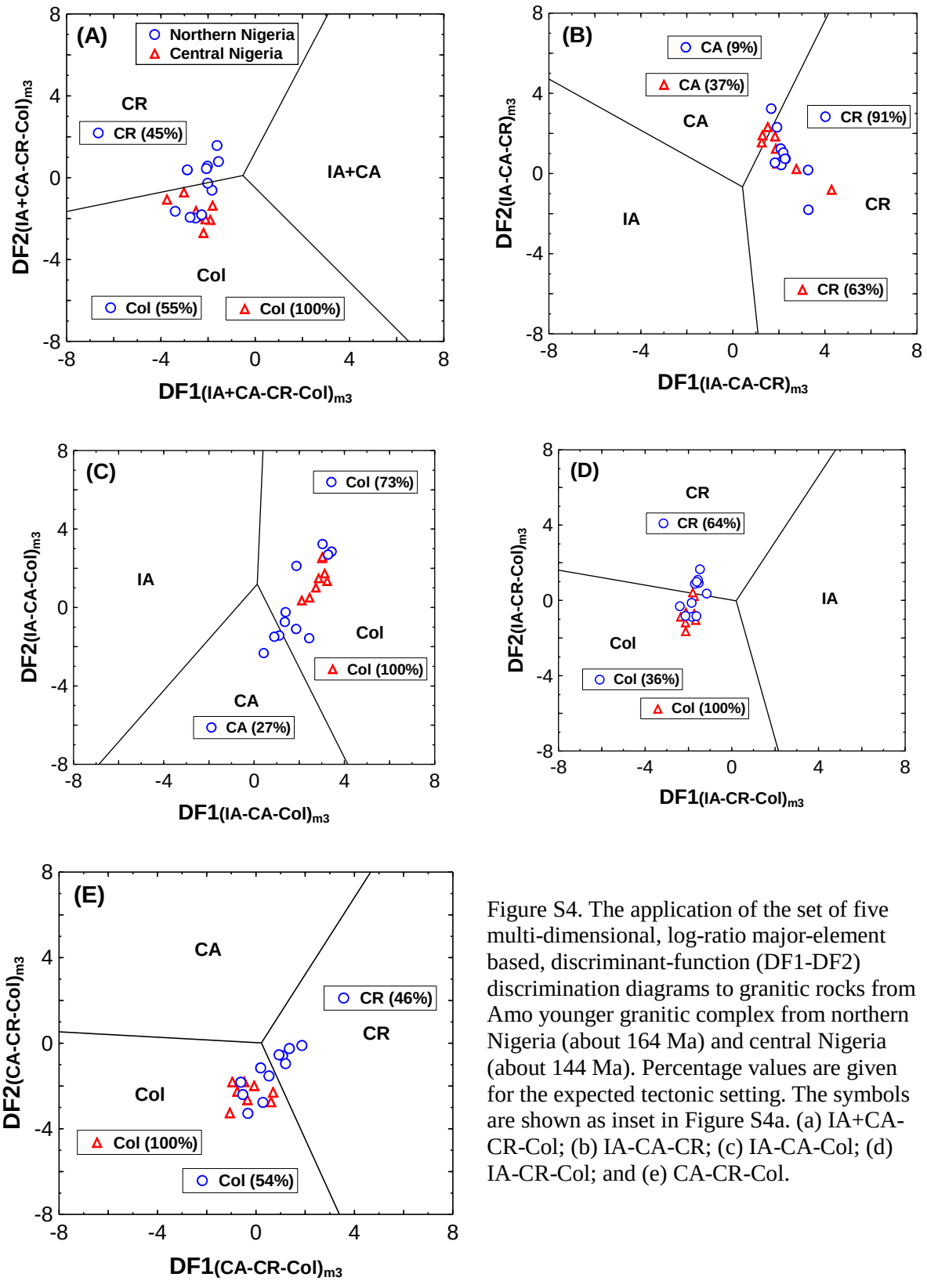

Figure S4. The application of the set of five multi-dimensional, log-ratio major-element based, discriminant-function (DF1-DF2) discrimination diagrams to granitic rocks from Amo younger granitic complex from northern Nigeria (about 164 Ma) and central Nigeria (about 144 Ma). Percentage values are given for the expected tectonic setting. The symbols are shown as inset in Figure S4a. (a) IA+CA-CR-Col; (b) IA-CA-CR; (c) IA-CA-Col; (d) IA-CR-Col; and (e) CA-CR-Col.

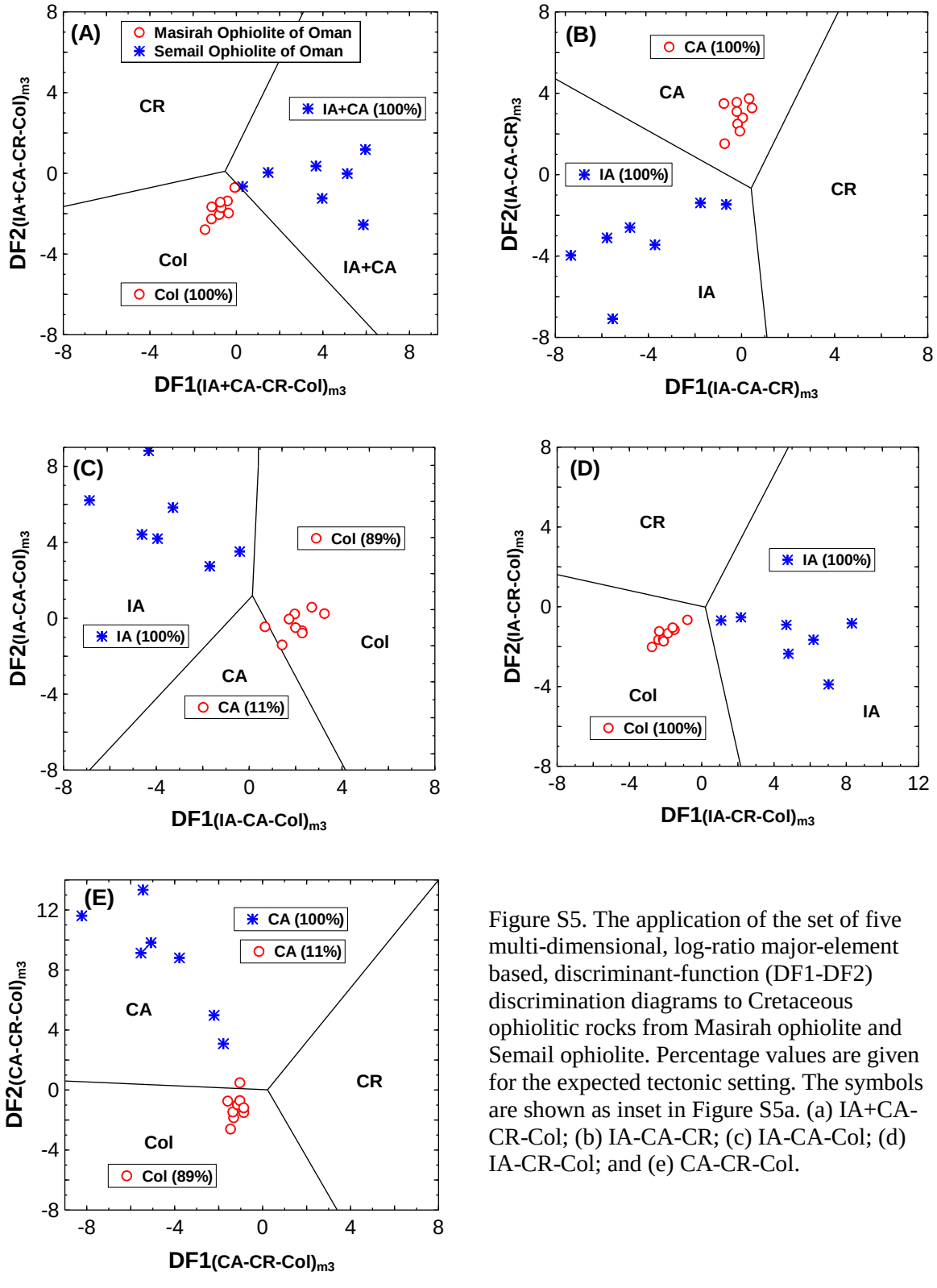

Figure S5. The application of the set of five multi-dimensional, log-ratio major-element based, discriminant-function (DF1-DF2) discrimination diagrams to Cretaceous ophiolitic rocks from Masirah ophiolite and Semail ophiolite. Percentage values are given for the expected tectonic setting. The symbols are shown as inset in Figure S5a. (a) IA+CA-CR-Col; (b) IA-CA-CR; (c) IA-CA-Col; (d) IA-CR-Col; and (e) CA-CR-Col.

Annexure II

ANNEXURE II (Page 189-200)

Verma S.P., Pandarinath, K., Verma, S.K., 2010. Statistically correct methodology for compositional data in new discriminant function tectonomagmatic diagrams and application to ophiolite origin: **Advance in Geosciences,** A 6-Volume Set (Set Editor-in-chief: Kenji Satake), Solid Earth, v. 26, p. 11-22, world Scientific Publishing Company.

Advances in Geosciences
Vol. 26: Solid Earth (2010)
Ed. Kenji Satake

STATISTICALLY CORRECT METHODOLOGY FOR COMPOSITIONAL DATA IN NEW DISCRIMINANT FUNCTION TECTONOMAGMATIC DIAGRAMS AND APPLICATION TO OPHIOLITE ORIGIN

SURENDRA P. VERMA* and KAILASA PANDARINATH
Departamento de Sistemas Energéticos, Centro de Investigación en Energía,
Universidad Nacional Autónoma de México,
Priv. Xochicalco s/no., Col. Centro,
Apartado Postal 34, Temixco, Mor. 62580, Mexico
**spv@cie.unam.mx*

SANJEET K. VERMA
Posgrado en Ingeniería, Centro de Investigación en Energía,
Universidad Nacional Autónoma de México,
Priv. Xochicalco s/no., Col. Centro,
Apartado Postal 34, Temixco, Mor. 62580, Mexico

In the lead presentation (invited talk) of Session SE05 (Frontiers in Geochemistry with Reference to Lithospheric Evolution and Metallogeny) of AOGS2010, we have highlighted the requirement of correct statistical treatment of geochemical data. In most diagrams used for interpreting compositional data, the basic statistical assumption of open space for all variables is violated. Among these graphic tools, discrimination diagrams have been in use for nearly 40 years to decipher tectonic setting. The newer set of five tectonomagmatic discrimination diagrams published in 2006 (based on major-elements) and two sets made available in 2008 and 2011 (both based on immobile elements) fulfill all statistical requirements for correct handling of compositional data, including the multivariate nature of compositional variables, representative sampling, and probability-based tectonic field boundaries. Additionally in the most recent proposal of 2011, samples having normally distributed, discordant-outlier free, log-ratio variables were used in linear discriminant analysis. In these three sets of five diagrams each, discrimination was successfully documented for four tectonic settings (island arc, continental rift, ocean-island, and mid-ocean ridge). The discrimination diagrams have been extensively evaluated for their performance by different workers. We exemplify these two sets of new diagrams (one set based on major-elements and the other on immobile elements) using ophiolites from Boso Peninsula, Japan. This example is included for illustration purposes only and is not meant for testing of these newer diagrams. Their evaluation and comparison with older, conventional bivariate or ternary diagrams have been reported in other papers.

1. Major Problems with Compositional Data Handling

Independent of the data quality, compositional data represent statistical samples drawn from a population characterized by a "closed" space that is limited to 0–1 or 0–100% values, viz., no component can exceed the "whole," being 1 for fractions or 100% for percentage units (Fig. 1). This is a serious limitation of compositional data, because they must plot totally within the shaded area in Fig. 1, the 100% values being reserved for a pure composition. Although we have illustrated only two components in a bivariate diagram (Fig. 1), similar reasoning is valid for a multi-component system. Thus, if we assume that compositions consist of n components and $(n-1)$ components, i.e., except one, are known, the unknown component is predictable, because it is the difference between the whole and the sum of the known components.

Problems of false correlations in compositional data were pointed out long ago in 1960 by Chayes,[1] among others. A simple consideration of SiO_2 (x-axis) and the sum of all the remaining components (y-axis) from different rock types reveal this problem, because, in this "extreme" example, both axes should sum up to 100%. For different magma types, the silica (SiO_2) content could vary as follows: 35–44% ultrabasic, 44–52% basic, 52–63% intermediate, and 63–100% felsic including pure quartz. Correspondingly, the sum of all remaining components in the respective

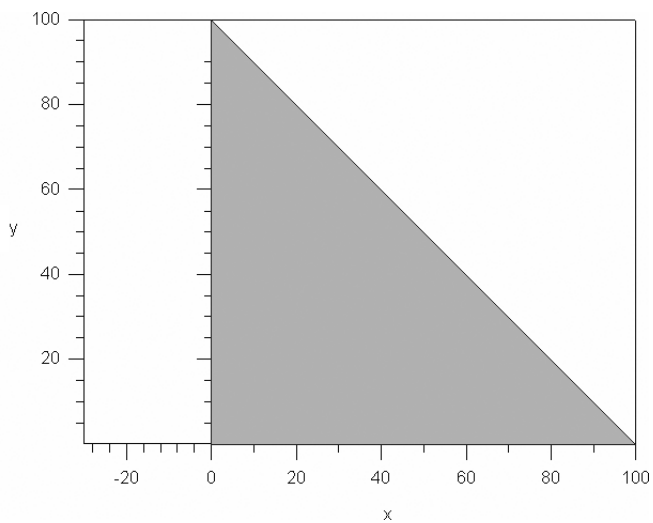

Fig. 1. Closed field for the bivariate ($x-y$) plot for compositional data (see shaded triangle).
Note: negative x-axis scale is added to show that no compositional data fall in this area.

magmas will vary in a complementary manner (65–56%, 56–48%, 48–37%, and 37–0% for ultrabasic, basic, intermediate, and felsic including pure quartz, respectively). In fact, no single component can exceed these latter values. Thus, negative correlations could be obtained from solely statistical considerations in the compositional space. When we are looking for correlations in such simple bivariate diagrams, it is quite possible to observe correlations that are simply due to the nature of closed compositional data and not due to some geological process or processes. In fact, Chayes[2] showed that both positive and negative correlations could be obtained in compositional data from statistical considerations alone and thus drew attention of geoscientists to such false correlations. Therefore, caution is required if we were to interpret geochemical data in diagrams based directly on compositional data.

Statistical methods to infer correlations of variables under study assume an "open" space for them, i.e., theoretically, the variables can take any value up to infinity, including negative values. Thus, most diagrams used in geochemical work for interpreting compositional data violate the basic statistical assumption of open space for all variables, although this violation may be of somewhat less concern for diagrams used simply for classification purposes.

Fortunately, an appropriate procedure for statistically correct handling of compositional data (based on log-ratio transformation to open the space theoretically to infinity in both positive and negative directions) has been available at least for the past 25 years through Aitchison's pioneering work.[3–5] Therefore, in compositional-data-based diagrams used in geosciences there is an urgent need to incorporate correct statistical treatment. Thus, many workers,[6–8] have pointed out problems with conventional handling of compositional data and have supported Aitchison's procedure[5] for this purpose.

2. Tectonomagmatic Discrimination Diagrams

Discrimination diagrams to decipher tectonic settings have been in use for nearly 40 years.[9–12] They seem to constitute one of the most frequently used procedures, if not the only one, to study older (Pre-Tertiary) terrenes where the actual tectonic setting is unknown as well as complex areas with imprints of multiple tectonic settings. For Precambrian and Archaean rocks, such as those in many parts of India, this problem is even worse. Undoubtedly in spite of their widespread use, most, if not all, bivariate and ternary diagrams

published in the literature are characterized by the above-mentioned defects of wrong statistical treatment; for details, see Refs. 12 and 13.

This problem of discrimination diagrams was recently (during 2004–2011) overcome jointly by researchers from India and Mexico who proposed new tectonomagmatic discrimination diagrams based on natural logarithm-transformation of appropriate element ratio variables and linear discriminant analysis (LDA). Specifically, one set of such diagrams proposed in 2004[14] is based on LDA of ratio variables of major-elements in basic and ultrabasic magmas, without log-transformation. The newer set of diagrams published in 2006 based on major-elements[15] and two sets made available in 2008[16] and 2011[17] based on relatively immobile elements comply with the above requirement of open space. In fact, these diagrams fulfill all other statistical requirements for correct handling of compositional data, including multivariate nature of compositional variables, representative sampling, and probability-based tectonic field boundaries. Additionally in the most recent proposal,[17] analytical data sets of the normally distributed, discordant-outlier free, log-ratio variables were achieved prior to LDA. This was done by using unpublished computer program DODESSYS (*S. P. Verma and L. Díaz-González, manuscript in preparation*). These "normally distributed" data were randomly divided into training and testing sets; the training set was used for LDA for proposing diagrams and the testing set for estimating success rates for discriminating different tectonic settings in these diagrams.

In these four sets of five diagrams for each set, the tectonomagmatic discrimination was successfully documented for four tectonic settings (island arc, continental rift, ocean-island, and mid-ocean ridge). It can be shown that five diagrams are required to objectively discriminate four tectonic settings. Owing to space limitations, we provide here details on only one set of five diagrams based on major-elements.[15]

To use these diagrams (Fig. 2), we must calculate the DF1 and DF2 functions (initially provided from LDA of training set data) for each of them. Thus, for the first diagram that discriminates ultrabasic and basic magmas from four tectonic settings of island arc (IAB), continental rift (CRB), ocean-island (OIB), and mid-ocean ridge (MORB), the DF1 and DF2 functions are calculated from the following equations:

$$\mathrm{DF1}_{(\mathrm{IAB-CRB-OIB-MORB})_{\mathrm{m2}}} = -4.6761 \times \ln(\mathrm{TiO_2/SiO_2})_{\mathrm{adj}}$$

$$
\begin{aligned}
&+ 2.5330 \times \ln(\mathrm{Al_2O_3/SiO_2})_{\mathrm{adj}} - 0.3884 \times \ln(\mathrm{Fe_2O_3/SiO_2})_{\mathrm{adj}} \\
&+ 3.9688 \times \ln(\mathrm{FeO/SiO_2})_{\mathrm{adj}} + 0.8980 \times \ln(\mathrm{MnO/SiO_2})_{\mathrm{adj}} \\
&- 0.5832 \times \ln(\mathrm{MgO/SiO_2})_{\mathrm{adj}} - 0.2896 \times \ln(\mathrm{CaO/SiO_2})_{\mathrm{adj}} \\
&- 0.2704 \times \ln(\mathrm{Na_2O/SiO_2})_{\mathrm{adj}} + 1.0810 \times \ln(\mathrm{K_2O/SiO_2})_{\mathrm{adj}} \\
&+ 0.1845 \times \ln(\mathrm{P_2O_5/SiO_2})_{\mathrm{adj}} + 1.5445, \qquad (1)
\end{aligned}
$$

$$
\begin{aligned}
&\mathrm{DF2}_{(\mathrm{IAB-CRB-OIB-MORB})_{\mathrm{m2}}} \\
&\quad = 0.6751 \times \ln(\mathrm{TiO_2/SiO_2})_{\mathrm{adj}} \\
&\qquad + 4.5895 \times \ln(\mathrm{Al_2O_3/SiO_2})_{\mathrm{adj}} + 2.0897 \times \ln(\mathrm{Fe_2O_3/SiO_2})_{\mathrm{adj}} \\
&\qquad + 0.8514 \times \ln(\mathrm{FeO/SiO_2})_{\mathrm{adj}} - 0.4334 \times \ln(\mathrm{MnO/SiO_2})_{\mathrm{adj}} \\
&\qquad + 1.4832 \times \ln(\mathrm{MgO/SiO_2})_{\mathrm{adj}} - 2.3627 \times \ln(\mathrm{CaO/SiO_2})_{\mathrm{adj}} \\
&\qquad - 1.6558 \times \ln(\mathrm{Na_2O/SiO_2})_{\mathrm{adj}} + 0.6757 \times \ln(\mathrm{K_2O/SiO_2})_{\mathrm{adj}} \\
&\qquad + 0.4130 \times \ln(\mathrm{P_2O_5/SiO_2})_{\mathrm{adj}} + 13.1639, \qquad (2)
\end{aligned}
$$

where the subscript "adj" refers to the adjusted data from SINCLAS.[21] Similar equations have to be used for the other four diagrams.[15] The discriminant functions are theoretically based on the multivariate technique of LDA applied to representative databases and establishment of probability-based boundaries in such diagrams. The reader is referred to the original papers[15–17] and the references cited therein.

The equations for the set of diagrams based on the elements La, Sm, Yb, Nb, and Th[16] are somewhat simpler than the above equations, i.e., they contain only four log-transformed ratio terms besides the constant term. Refer the original paper[16] for more details.

Finally, for the set of diagrams based on immobile elements TiO_2, Nb, V, Y, and Zr (Fig. 3), we recommend researchers to consult the original paper[17] that should be available for free download from the journal website. Here, we have reproduced the equations needed to use these diagrams.

For Fig. 3(a), the functions DF1 and DF2 are calculated as follows:

$$
\begin{aligned}
&\mathrm{DF1}_{(\mathrm{IAB-CRB+OIB-MORB})_{\mathrm{t2}}} \\
&\quad = -0.6611 \cdot \ln(\mathrm{Nb/TiO_2}) + 2.2926 \cdot \ln(\mathrm{V/TiO_2}) \\
&\qquad + 1.6774 \cdot \ln(\mathrm{Y/TiO_2}) + 1.0916 \cdot \ln(\mathrm{Zr/TiO_2}) + 21.3603, \qquad (3)
\end{aligned}
$$

$$\begin{aligned}\mathrm{DF2}_{(\mathrm{IAB-CRB+OIB-MORB})_{t2}} &= 0.4702\cdot\ln(\mathrm{Nb/TiO_2}) + 3.7649\cdot\ln(\mathrm{V/TiO_2}) \\ &\quad - 3.911\cdot\ln(\mathrm{Y/TiO_2}) + 2.2697\cdot\ln(\mathrm{Zr/TiO_2}) + 4.8487. \qquad (4)\end{aligned}$$

For Fig. 3(b), the functions DF1 and DF2 are as follows:

$$\begin{aligned}\mathrm{DF1}_{(\mathrm{IAB-CRB-OIB})_{t2}} &= -0.6146\cdot\ln(\mathrm{Nb/TiO_2}) + 2.3510\cdot\ln(\mathrm{V/TiO_2}) \\ &\quad + 1.6828\cdot\ln(\mathrm{Y/TiO_2}) + 1.1911\cdot\ln(\mathrm{Zr/TiO_2}) + 22.7253, \qquad (5)\end{aligned}$$

$$\begin{aligned}\mathrm{DF2}_{(\mathrm{IAB-CRB-OIB})_{t2}} &= 1.3765\cdot\ln(\mathrm{Nb/TiO_2}) - 0.9452\cdot\ln(\mathrm{V/TiO_2}) \\ &\quad + 4.0461\cdot\ln(\mathrm{Y/TiO_2}) - 2.0789\cdot\ln(\mathrm{Zr/TiO_2}) + 22.2450. \qquad (6)\end{aligned}$$

For Fig. 3(c), the functions DF1 and DF2 are as follows:

$$\begin{aligned}\mathrm{DF1}_{(\mathrm{IAB-CRB-MORB})_{t2}} &= -0.6624\cdot\ln(\mathrm{Nb/TiO_2}) + 2.4498\cdot\ln(\mathrm{V/TiO_2}) \\ &\quad + 1.2867\cdot\ln(\mathrm{Y/TiO_2}) + 1.0920\cdot\ln(\mathrm{Zr/TiO_2}) + 18.7466, \qquad (7)\end{aligned}$$

$$\begin{aligned}\mathrm{DF2}_{(\mathrm{IAB-CRB-MORB})_{t2}} &= 0.4938\cdot\ln(\mathrm{Nb/TiO_2}) + 3.4741\cdot\ln(\mathrm{V/TiO_2}) \\ &\quad - 3.8053\cdot\ln(\mathrm{Y/TiO_2}) + 2.0070\cdot\ln(\mathrm{Zr/TiO_2}) + 3.3163. \qquad (8)\end{aligned}$$

For Fig. 3(d), the functions DF1 and DF2 are as follows:

$$\begin{aligned}\mathrm{DF1}_{(\mathrm{IAB-OIB-MORB})_{t2}} &= -0.2646\cdot\ln(\mathrm{Nb/TiO_2}) + 2.0491\cdot\ln(\mathrm{V/TiO_2}) \\ &\quad + 3.4565\cdot\ln(\mathrm{Y/TiO_2}) + 0.8573\cdot\ln(\mathrm{Zr/TiO_2}) + 32.9472, \qquad (9)\end{aligned}$$

$$\begin{aligned}\mathrm{DF2}_{(\mathrm{IAB-OIB-MORB})_{t2}} &= 0.01874\cdot\ln(\mathrm{Nb/TiO_2}) + 4.0937\cdot\ln(\mathrm{V/TiO_2}) \\ &\quad - 4.8550\cdot\ln(\mathrm{Y/TiO_2}) + 2.9900\cdot\ln(\mathrm{Zr/TiO_2}) + 0.1995. \qquad (10)\end{aligned}$$

Finally, for Fig. 3(e), the functions DF1 and DF2 are as follows:

$$\begin{aligned}\mathrm{DF1}_{(\mathrm{CRB-OIB-MORB})_{t2}} &= -0.7829 \cdot \ln(\mathrm{Nb/TiO_2}) + 0.3379 \cdot \ln(\mathrm{V/TiO_2}) \\ &\quad + 3.3239 \cdot \ln(\mathrm{Y/TiO_2}) - 0.51232 \cdot \ln(\mathrm{Zr/TiO_2}) + 16.0941, \qquad (11)\end{aligned}$$

$$\begin{aligned}\mathrm{DF2}_{(\mathrm{CRB-OIB-MORB})_{t2}} &= 1.7478 \cdot \ln(\mathrm{Nb/TiO_2}) - 0.0421 \cdot \ln(\mathrm{V/TiO_2}) \\ &\quad + 3.5301 \cdot \ln(\mathrm{Y/TiO_2}) - 1.4503 \cdot \ln(\mathrm{Zr/TiO_2}) + 28.3592. \qquad (12)\end{aligned}$$

Again in terms of complexity, these equations contain four log-ratio terms besides the constant term,[17] and are similar to those for earlier set of diagrams based on La, Sm, Yb, Nb, and Th.[16] The advantage is that the newer equations[17] involve immobile elements that can be determined easily from X-ray fluorescence spectrometry.

2.1. *Application example*

The new and old discrimination diagrams have been extensively evaluated for their performance by different workers.[12,18,19] Therefore, it is unnecessary to deal with this aspect in the present work, especially because of the space limitations. Here, we apply these new diagrams to infer tectonic setting of just one suite of ophiolites from Japan and point out the success as well as limitations of this application.

Boso ophiolites were chosen because the potential readers of this paper (most of them being from Asia) are likely to be familiar with the geological and tectonic characteristics of these ophiolites. Nevertheless, we also note that this application is only for illustration purposes and is certainly not meant for testing these diagrams. The testing of diagrams is an important topic, which has already been covered in earlier papers.[12,18,19] For this application, data for all samples of ophiolitic rocks were compiled from Hirano *et al.*[20] Computer program SINCLAS[21] was used to ascertain the magma types. A total of 18 samples were classified as basic magma, one as ultrabasic, one as intermediate, and two as felsic. Nineteen samples (basic and ultrabasic) were plotted in the five diagrams proposed by Verma *et al.*[15] based on major-element log-transformed ratios (Fig. 2(a–e)). Similarly, these samples were also plotted (Fig. 3(a–e)) in the diagrams of Verma and Agrawal[17] based on immobile elements. We note that complete data

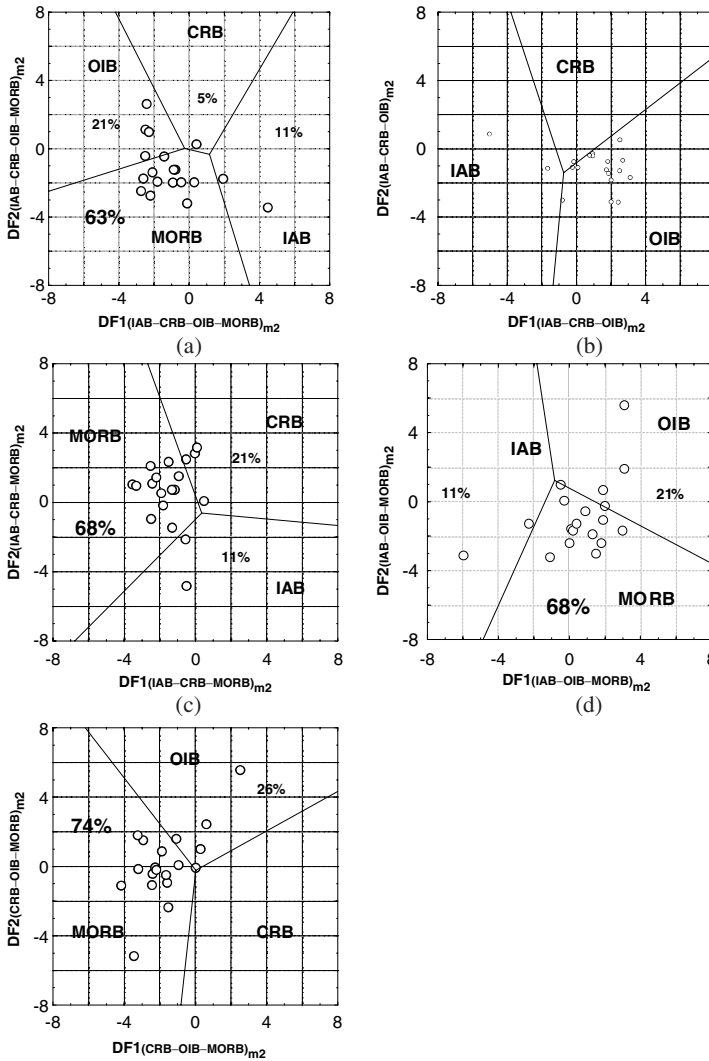

Fig. 2. Boso Peninsula ophiolite samples plotted in five discriminant-function-based diagram of Verma *et al.*[15] The subscript $_{m2}$ stands for the major-element-based diagrams of the second set. (a) Four field DF1–DF2 diagram for the discrimination of IAB, CRB, OIB, and MORB settings; (b) three field DF1–DF2 diagram for IAB, CRB, and OIB; (c) three field DF1–DF2 diagram for IAB, CRB, and MORB; (d) three field DF1–DF2 diagram for IAB, OIB, and MORB; and (e) three field DF1–DF2 diagram for CRB, OIB, and MORB.

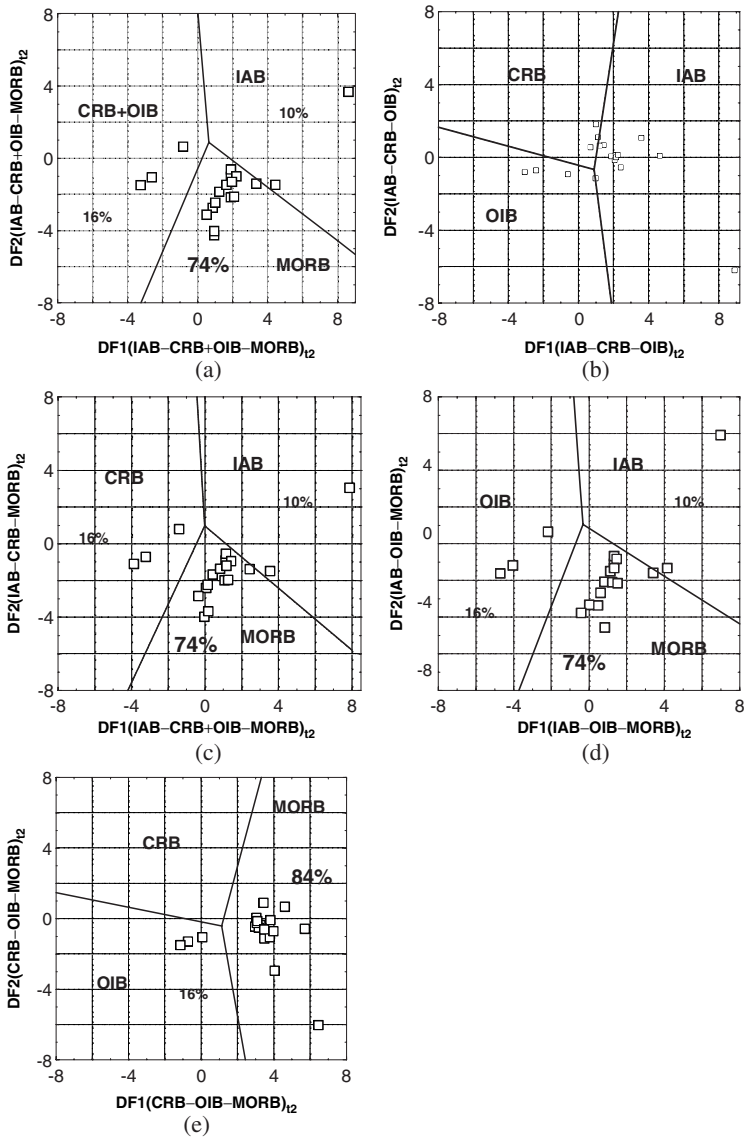

Fig. 3. Boso Peninsula ophiolite samples plotted in five discriminant-function-based diagram of Verma and Agrawal.[17] The subscript $_{t2}$ stands for the immobile, mostly trace-element-based diagrams of the second set. (a) Three field DF1–DF2 diagram for the discrimination of IAB, CRB+OIB, and MORB settings; (b) three field DF1–DF2 diagram for IAB, CRB, and OIB; (c) three field DF1–DF2 diagram for IAB, CRB, and MORB; (d) three field DF1–DF2 diagram for IAB, OIB, and MORB; and (e) three field DF1–DF2 diagram for CRB, OIB, and MORB.

on these samples were not available for the trace-element-based diagrams of Agrawal *et al.*[16] Therefore, these diagrams could not be used for this application.

Success rates calculated for each diagram (Figs. 2 and 3) are summarized in Table 1. Figure 2(a) shows that a large number of samples (12 out of 19) plot in the MORB field, which amounts to about 64% success rate (Table 1). Similarly, Fig. 3(a) also suggests MORB setting for these samples, because 14 out of 19 samples (74%, Table 1) plot in this field. The remaining samples (7 in Fig. 2(a) and 5 in Fig. 3(a)) plot in the other three fields (about 11% for IAB, 5% for CRB, and 21% for OIB, Fig. 2(a) and Table 1; 10% for IAB and 16% for CRB + OIB, Fig. 3(a), and Table 1). Both diagrams (Figs. 2(a) and 3(a)), nevertheless, suggest MORB setting for these samples. Because the remaining samples are scattered in different tectonic fields, no further inference about an alternate tectonic setting is indicated.

In the second set of diagrams (Figs. 2(b) and 3(b)) the expected MORB setting is missing, and, therefore, these diagrams should be considered inapplicable to this case study. We have indicated their results in Table 1 by an asterisk meaning inapplicable diagram (see legend of Table 1). In the absence of MORB setting, OIB setting seems to be indicated.

In all the remaining diagrams (Figs. 2(c–e) and 3(c–e)), the success rates for MORB setting are the highest (68–74% in Figs. 2(c–e) and 74–84% in Figs. 3(c–e); Table 1). Note that although both sets of diagrams (Figs. 2 and 3) provide consistent results, the success rates from the immobile-element-based diagrams[17] show somewhat higher values than the major-element-based procedure[15] (74–84% as compared with 64–74%, Table 1). Thus, MORB setting can be safely inferred for ophiolites from Boso Peninsula, Japan.

In this example, the results from both sets of diagrams are consistent. However, in the case of discrepancy in the results of applications to ophiolites or any other kind of rocks, the immobile-element-based diagrams[16,17] should be preferred as compared with the major-element-based diagrams.[15]

These new multi-dimensional discriminant-function-based diagrams have also been applied to complex tectonic setting in Mexico[19] and Turkey[12] as well as to older rocks.[22–24] Furthermore, the correct statistical methodology has also been applied to propose new discrimination diagrams for granitic or felsic magma[25] for discriminating four tectonic settings.

Table 1. Application of two sets of discrimination diagrams based on natural logarithm transformation of major-element ratio[15] and trace-element ratio[17] discriminant functions DF1–DF2, to ophiolitic rocks from Boso Peninsula, Japan (data from Ref. 20).

Figure no. (tectonic setting)	Total no. of samples (%)	Number of discriminated samples (%)				
			Within-plate			
		IAB	CRB + OIB	CRB	OIB	MORB
Figure 2(a) (IAB–CRB–OIB–MORB)$_{m2}$	19 (100)	2 (11)	—	1 (5)	4 (21)	**12 (64)**
Figure 3(a) (IAB–CRB + OIB–MORB)$_{t2}$	19 (100)	2 (10)	3 (16)	—	—	**14 (74)**
Figure 2(b)* (IAB–CRB–OIB)$_{m2}$	19 (100)	2 (11)	—	1 (5)	16 (84)	—
Figure 3(b)* (IAB-CRB–OIB)$_{t2}$	19 (100)	13 (68)	—	3 (16)	3 (16)	—
Figure 2(c) (IAB–CRB–MORB)$_{m2}$	19 (100)	2 (11)	—	4 (21)	—	**13 (68)**
Figure 3(c) (IAB–CRB–MORB)$_{t2}$	19 (100)	2 (10)	—	3 (16)	—	**14 (74)**
Figure 2(d) (IAB–OIB–MORB)$_{m2}$	19 (100)	2 (11)	—	—	4 (21)	**13 (68)**
Figure 3(d) (IAB–OIB–MORB)$_{t2}$	19 (100)	2 (10)	—	—	3 (16)	**14 (74)**
Figure 2(e) (CRB–OIB–MORB)$_{m2}$	19 (100)	—	—	0 (0)	5 (26)	**14 (74)**
Figure 3(e) (CRB–OIB–MORB)$_{t2}$	19 (100)	—	—	0 (0)	3 (16)	**16 (84)**

*Inapplicable results and diagrams for this application; boldface italic font shows the expected tectonic setting.

Acknowledgments

The authors are grateful to two anonymous reviewers and the editor for their comments on an earlier version of this paper, whose considerations improved our presentation.

References

1. F. Chayes, *J. Geophys. Res.* **65** (1960) 4185.
2. F. Chayes, *Ratio Correlation. A Manual for Students of Petrology and Geochemistry*, The University of Chicago Press, Chicago (1978) 99 p.
3. J. Aitchison, *Math. Geol.* **13** (1981) 175.
4. J. Aitchison, *Math. Geol.* **16** (1984) 617.
5. J. Aitchison, *The Statistical Analysis of Compositional Data* (Chapman and Hall, London, 1986) 416 p.
6. R. A. Reyment and E. Savazzi, *Aspects of Multivariate Statistical Analysis in Geology* (Elsevier, Amsterdam, 1999) 285 p.
7. J. J. Egozcue, V. Pawlowsky-Glahn, G. Mateu-Figueras and C. Barceló-Vidal, *Math. Geol.* **35** (2003) 279.
8. A. Buccianti, G. Mateau-Figueras and V. Pawlowsky-Glahn (Eds.), *Compositional Data Analysis in the Geosciences*: *From Theory to Practice* (Geological Society, London, 2006) 212 p.
9. J. A. Pearce and J. R. Cann, *Earth Planet. Sci. Lett.* **12** (1971) 339.
10. J. A. Pearce and J. R. Cann, *Earth Planet. Sci. Lett.* **19** (1973) 290.
11. H. R. Rollinson, *Using Geochemical Data*: *Evaluation, Presentation, Interpretation* (Longman Scientific Technical, Essex, 1993) 344 p.
12. S. P. Verma, *Turkish J. Earth Sci.* **19** (2010) 185.
13. S. Agrawal and S. P. Verma, *Geochim. Cosmochim. Acta* **71** (2007) 3388.
14. S. Agrawal, M. Guevara and S. P. Verma, *Int. Geol. Rev.* **46** (2004) 575.
15. S. P. Verma, M. Guevara and S. Agrawal, *J. Earth Syst. Sci.* **115** (2006) 485.
16. S. Agrawal, M. Guevara and S. P. Verma, *Int. Geol. Rev.* **50** (2008) 1057.
17. S. P. Verma and S. Agrawal, *Rev. Mex. Cienc. Geol.* **28** (2011) 24.
18. H. C. Sheth, *Terra Nova* **20** (2008) 229.
19. S. P. Verma, S. K. Verma, K. Pandarinath and M. A. Rivera-Gómez, *Pure Appl. Geophys.* (2011) in press.
20. N. Hirano, Y. Ogawa, K. Saito, T. Yoshida, H. Sato and H. Taniguchi. In *Ophiolites in Earth History*, Y. Dilek and P. T. Robinson (Eds). (Geological Society of London, 2003) 279.
21. S. P. Verma, I. S. Torres-Alvarado and Z. T. Sotelo-Rodríguez, *Comput. Geosci.* **28** (2002) 711.
22. J. Wiszniewska, E. Krzeminska and W. Dörr, *Gondwana Res.* **12** (2007) 268.
23. L. S. Shekhawat, M. K. Pandit and D. W. Joshi, *J. Earth Sys. Sci.* **116** (2007) 511.
24. A. Polat, P. W. U. Appel, B. Fryer, B. Windley, R. Frei, I. M. Samson and H. Huang, *Precam. Res.* **175** (2009) 87.
25. S. K. Verma, K. Pandarinath and S. P. Verma, *Int. Geol. Rev.* (2011) in press.

Annexure III

ANNEXURE III (Page 203-227)

Verma S.P., Verma, S.K., Pandarinath, K., Rivera-Gómez, M.A., 2011. Evaluation of recent tectonomagmatic discrimination diagrams and their application to the origin of basic magmas in southern Mexico and Central Americas: **Pure and Applied Geophysics,** v. 168, p. 1501-1525.

Pure Appl. Geophys. 168 (2011), 1501–1525

DOI 10.1007/s00024-010-0173-2

Pure and Applied Geophysics

Evaluation of Recent Tectonomagmatic Discrimination Diagrams and their Application to the Origin of Basic Magmas in Southern Mexico and Central America

Surendra P. Verma,[1] Sanjeet K. Verma,[2] Kailasa Pandarinath,[1] and María Abdelaly Rivera-Gómez[2]

Abstract—Discrimination diagrams to decipher tectonic settings have been in use for nearly 40 years. Although old diagrams have been extensively used, the recent ones based on discriminant functions of ratio variables, with or without log-transformation, proposed during 2004–2010 for the discrimination of four tectonic settings of island arc, continental rift, ocean-island and mid-ocean ridge, were newly evaluated to show their high success rates of 57.3–100% and 58.5–100% for major-element and immobile-element based diagrams, respectively. For the continental arc of the Andes evaluated for its similarity to island arc, these four sets of diagrams showed success rates of 62.1–83.8%. These four sets of five diagrams per set were therefore used to infer tectonic setting of the Mexican Volcanic Belt (MVB), Los Tuxtlas volcanic field (LTVF), and Central American Volcanic Arc (CAVA). Using this approach, the MVB, especially its western, central and eastern parts, and the LTVF of Southern Mexico show a dominantly continental rift setting and the CAVA shows an arc setting. The west-central part of the MVB is consistent with dual tectonics of arc and rift. These results confirm the application of an unusual mantle upwelling rift-model for the Mexican on-land volcanism, whereas the conventional plate tectonic subduction model seems to be applicable for the CAVA from Guatemala to north-western Costa Rica.

Key words: Mexico, Mexican Volcanic Belt, Los Tuxtlas volcanic field, subduction, rifting, geochemistry, tectonic setting.

1. Introduction

In plate tectonics theory, it is common to consider four main tectonic settings which are related to subduction processes (island arc and continental arc), extensional processes in continents (continental rift), special melting regimes in oceans (ocean-island), and extensional processes in oceans (mid-ocean ridge). (The number of tectonic settings can be higher, for example five if the subduction setting is divided into island and continental types, or more if other subdivisions are considered.) For nearly 40 years, discrimination diagrams have constituted a widely used complementary technique to other petrological and geochemical methods for interpreting compositional data and for inferring tectonic settings of older terrenes as well as of areas with complex (or multiple) tectonic settings (e.g., Pearce and Cann, 1971, 1973; Rollinson, 1993; Agrawal and Verma, 2007; Verma, 2010). Recently, Vermeesch (2007), Sheth (2008), and Verma (2010) have evaluated most existing discrimination diagrams.

The older bivariate and ternary discrimination diagrams are all plagued by erroneous treatment of compositional data (for correct statistical procedures, see Aitchison, 1986; Aitchison *et al*., 2000; Egozcue *et al*. 2003; Aitchison and Egozcue, 2005; Baxter *et al*., 2005; Egozcue and Pawlowsky-Glahn, 2005; Buccianti *et al*., 2006; Agrawal and Verma, 2007, Verma, 2010). Some of them, such as the Zr–Zr/Y bivariate diagram of Pearce and Norry (1979) and the $MgO–FeO^t–Al_2O_3$ ternary diagram of Pearce *et al*. (1977), show very low success rates. The "success rate" of a given diagram for a tectonic setting is a statistical parameter (see Verma, 2010) and is defined as the ratio, expressed as a percent, of the number of samples with correct tectonic discrimination and the total number of samples of that particular tectonic setting. For the evaluation of classification diagrams, the success rate is similarly defined as the correct

S. P. Verma was on sabbatical leave (April 2009–March 2010) at the División de Ciencias Básicas e Ingeniería, Universidad Autónoma Metropolitana-Iztapalapa, occupying the Chair (Cátedra) "Ronald Tunstall Ackroyd".

[1] Departamento de Sistemas Energéticos, Centro de Investigación en Energía, Universidad Nacional Autónoma de México, Priv. Xochicalco s/no., Col. Centro, 62580 Temixco, Morelos, Mexico. E-mail: spv@cie.unam.mx

[2] Posgrado en Ingeniería, Centro de Investigación en Energía, Universidad Nacional Autónoma de México, Priv. Xochicalco s/no., Col. Centro, 62580 Temixco, Morelos, Mexico.

rock classification for a given rock-type according to some accepted rock nomenclature (see VERMA *et al.*, 2010).

In other discrimination diagrams, e.g., the Zr–3Y–Ti/100 ternary diagram of PEARCE and CANN (1973), the Zr/4–Y–2Nb ternary diagram of MESCHEDE (1986), and the La/10-Nb/8-Y/15 ternary diagram of CABANIS and LECOLLE (1989), most samples plot in overlap regions of two tectonic settings. However, when success rates are greater, diagrams such as Ti/Y–Zr/Y by PEARCE and GALE (1977) and the Zr–3Y–Ti/100 ternary diagram of PEARCE and CANN (1973) then discriminate only two tectonic settings under the broad names of "within-plate" and "plate margin". For some other diagrams, such as the Nb/Y–Ti/Y bivariate diagram of PEARCE (1982), the Ti/1000–V bivariate diagram of SHERVAIS (1982), the Th–Ta–Hf/3 ternary diagram of Wood (1980), the $10MnO–10P_2O_5–TiO_2$ ternary diagram of MULLEN (1983), and the Zr/4–Y–2Nb ternary diagram of MESCHEDE (1986), although the success rates for some tectonic settings may be somewhat higher, they are certainly less than those for the old discriminant function based discrimination diagrams (viz., $Score_1$–$Score_2$ diagram of BUTLER and WORONOW, 1986 and F_1– F_2 and F_2–F_3 diagrams of PEARCE, 1976) as well as for the new DF1–DF2 (2004–2008) diagrams of AGRAWAL *et al.* (2004, 2008) and VERMA *et al.* (2006). Furthermore, the older discriminant function diagrams do not comply with all the recommendations for handling of compositional data (AITCHISON, 1986; AGRAWAL and VERMA, 2007), and are also not based on representative databases.

Therefore, it appears that the newer discriminant function diagrams proposed during 2004–2008 (AGRAWAL *et al.*, 2004, 2008; VERMA *et al.*, 2006) obtained from linear discriminant analysis (LDA) of representative databases for four tectonic settings (island arc, continental rift, ocean island, and mid-ocean ridge) and with probability-based tectonic field boundaries (AGRAWAL, 1999) work well with success rates up to about 99% (VERMA, 2010). Still newer discrimination diagrams based on all these new concepts, viz., representative database, correct statistical treatment of compositional data, multivariate techniques of LDA, probability-based field boundaries, and fulfillment of basic assumptions of normally distributed log-ratio transformed compositional variables, have also been proposed (VERMA and AGRAWAL, 2010) and are shown to perform with even higher success rates. The diagrams of AGRAWAL *et al.* (2004) and VERMA *et al.* (2006) are based on major-elements (the first with simple ratio variables and the second with log-transformation of ratio variables), whereas those of AGRAWAL *et al.* (2008) and VERMA and AGRAWAL (2010) use log-transformed ratios of immobile-elements (La, Sm, Yb, Nb, and Zr for the former and adjusted TiO_2, Nb, V, Y, and Zr for the latter).

Unfortunately, none of the existing diagrams to date is capable of successfully discriminating between the two very similar tectonic settings of island and continental arcs. Further, the continental arc setting was included in none of the four sets of the newer diagrams proposed during 2004–2010, which successfully discriminate four tectonic settings. In fact, AGRAWAL *et al.* (2004) noted that continental arc was missing from their diagrams and that this setting was initially included, but had to be set aside due to the significant similarities between major-element compositions of basic magmas from island and continental arcs. These authors further hypothesized that only highly differentiated rocks will give contrasting compositions for these two tectonic settings because different types of underlying crust might be involved in the genesis and evolution of magmas. To solve the problem for basic rocks, trace elements should be incorporated, although none of the more recent publications (AGRAWAL *et al.*, 2008; VERMA and AGRAWAL, 2010) has taken these recommendations into account. Therefore, there is still a worldwide interest in discriminating between island and continental arc settings, but given the similarities of basic magmas from these two tectonic settings, as documented by AGRAWAL *et al.* (2004) and VERMA *et al.* (2006), we should further test these newer diagrams for a typical continental arc setting of the Andes in South America before their application to the main aim of the present paper.

Figure 1 illustrates the schematic representation of the main volcanic areas of Southern Mexico and Central America, constituting the Mexican Volcanic Belt (MVB), Los Tuxtlas volcanic field (LTVF) and isolated centers, such as El Chichón volcano, which merge with the Central American Volcanic Arc (CAVA). Geochemical and radiogenic isotope data for volcanic rocks from Southern Mexico, mainly from the

central to eastern parts of the MVB and LTVF, were interpreted by Verma (2002, 2004) to demonstrate a lack of relationship with the subduction process, in spite of the ongoing subduction of the Cocos plate beneath the North American plate. Such a conclusion was also drawn by Verma (2006) for the LTVF. Verma (2002) also showed a text-book type case for volcanic centers of the CAVA, particularly from Guatemala to north-western Costa Rica (see also, Burbach *et al.*, 1984; Leeman *et al.*, 1994; Harry and Green, 1999; Patino *et al.*, 2000; Walker *et al.*, 2001).

Nevertheless, for the MVB and LTVF, there also exist conventional subduction-related models (e.g., Pardo and Suárez, 1995; Nelson *et al.*, 1995; Ferrari *et al.*, 2001; Gómez-Tuena *et al.*, 2007; Pérez-Campos *et al.*, 2008; and Pacheco and Singh, 2010) and other proposals such as plume-related origin (e.g., Márquez *et al.*, 1999a), which therefore make the tectonic setting of these provinces highly complex and controversial (e.g., Ferrari and Rosas-Elguera, 1999; Márquez *et al.*, 1999b; Sheth *et al.*, 2000; Torres-Alvardo *et al.*, 2002). More recently, Verma (2009) reviewed all the available geological, geochemical and geophysical evidence from the MVB, particularly for its central part, and concluded that this volcanic province should better be called the Mexican Volcanic Rift, because all the available data are more consistent with a rift rather than an arc.

These are some of the reasons that motivated us to explore more constraints for elucidating this problem of the Mexican Pacific and on-land volcanism, as well as to document the differences or similarities between the volcanism and tectonics of Southern Mexico and Central America (CAVA).

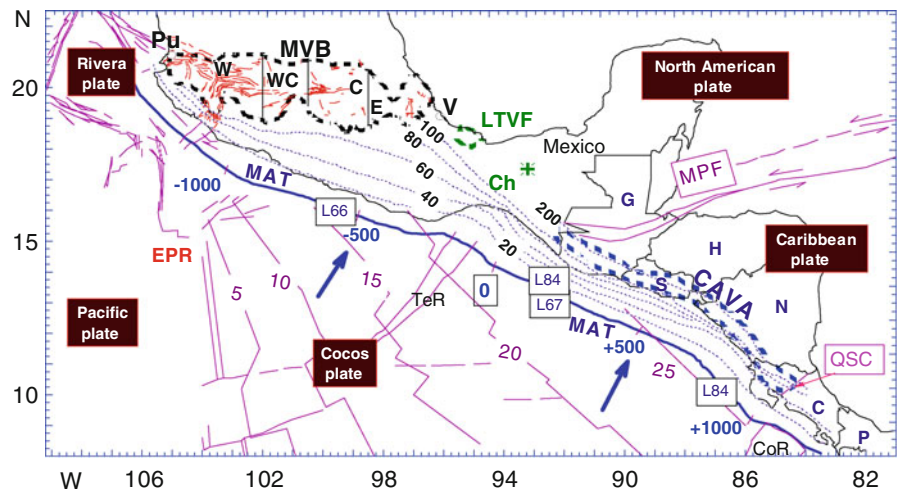

Figure 1

Simplified tectonic map of Southern Mexico and Central America (modified after Verma, 2002, 2006). The land–ocean boundary and the subdivision of land in countries are shown by *thick solid curves*. The on-land tectonic features (fractures and faults) in the Mexican Volcanic Belt (MVB) region are from the following sources: Negendank *et al.* (1985); Johnson and Harrison (1989a, b); Allan *et al.* (1991); Lyle and Ness (1991); and Suter *et al.* (1991, 1992, 1995a, b, 2001). Note the well-established triple junction in the western part of the MVB (Luhr *et al.*, 1985; Allan *et al.*, 1991). Rivera-Cocos plate diffuse boundaries are from Allan *et al.* (1991) and Bandy *et al.* (2000). *EPR* East Pacific Rise, *MAT* Middle America Trench, *LTVF* Los Tuxtlas Volcanic Field, *CAVA* Central American Volcanic Arc, *TeR* Tehuantepec Ridge, *CoR* Cocos Ridge, *MPF* Motagua-Polochic Fault, *QSC* Quesada Sharp Contortion, *Pu* Puerto Vallarta, *V* Veracruz, *Ch* El Chichón volcano, *G* Guatemala, *S* El Salvador, *H* Honduras; *N* Nicaragua, *C* Costa Rica, *P* Panamá. Legs L66, L67 and L84 are approximate Deep Sea Drilling Project Sites where drilling has recovered samples from the ocean floor. The numbers 5–25 in the Pacific Ocean give the approximate age of the ocean floor in Ma. The seismic depth contours marked 20–200 give the depth of the Benioff zone in km. Finally, the numbers 0, −500, −1,000, +500, and +1,000 are the distance in km for the transect used by Verma (2002) to understand the similarities and differences between Southern Mexico and Central America, as inferred along the Pacific coast (MAT). The abbreviations *W*, *WC*, *C*, and *E* within the MVB refer to the approximate subdivision of the MVB into western, west-central, central, and eastern parts, which was used in the presentation and interpretation of compiled geochemical data (see Tables 5, 6, 7, 8 for more details). L66, L67, and L84 refer to the Deep Sea Drilling Project Legs and Sites, from which subducting sediments and underlying basalt samples were recovered, whose geochemical data provided constraints on the on-land volcanism (see Verma, 2000a for more details)

Although the new discriminant function based discrimination diagrams for magmatic rocks have been tested by their respective authors using training sets by randomly dividing the databases into training and testing sets, and by Sheth (2008) using an independent database and by Verma (2010) using a much more extensive database, it would still be worthwhile to test them further using totally independent worldwide databases. If the diagrams perform satisfactorily for the discrimination of the four main tectonic settings and the continental arc of the Andes, we can then apply them to the study of fresh rocks from the subduction-related CAVA for further ascertaining the applicability of these new diagrams for a continental arc. Finally, we could determine the dominant tectonic setting(s) of controversial and complex volcanic areas of Southern Mexico (MVB and LTVF). Thus, a comprehensive database from the MVB and LTVF could be used to infer their tectonic settings from these diagrams provided, of course, they were also shown to work well for this purpose for the CAVA. The novelty of our approach lies in the multidimensional solution (note ten major-element ratios used by Agrawal *et al*., 2004 and Verma *et al*., 2006; and four immobile-element ratios by Agrawal *et al*., 2008 and Verma and Agrawal, 2010) and the use of correct statistical methodology (note log-transformation of element ratios using a common divisor in three of the four sets of diagrams; see also Agrawal and Verma, 2007 and Verma, 2010) offered by the newer sets of diagrams.

The highly complex equations used to construct these diagrams are not reproduced here to reduce journal space; they can be consulted in the original papers (Agrawal *et al*., 2004, 2008; Verma *et al*., 2006; Verma and Agrawal, 2010), or else in Verma (2010) or Verma and Rivera-Gómez (2010). Both of the latter papers can be freely downloaded from respective journal's website.

2. Databases

2.1. World Databases

For the statistical evaluation of the new discrimination diagrams, four extensive databases of basic and ultrabasic rocks of (1) island arc (IAB); (2) continental rift (CRB); (3) ocean-island (OIB); and (4) mid-ocean ridge (MORB), were separated from the combined database of all rock types. This was done from papers that were not included in any of the previous studies, in which the diagrams to be evaluated were proposed, i.e., not included in the databases used by Agrawal *et al.* (2004, 2008), Verma *et al*. (2006), and Verma and Agrawal (2010). Nevertheless, the same strict selection conditions as posed by these authors were maintained as follows: (a) age between late Miocene to Recent; (b) tectonic setting of the study area known explicitly without ambiguity; (c) rocks with adjusted silica $(SiO_2)_{adj} \leq 52\%$ after SINCLAS processing (Verma *et al*., 2002, 2003), i.e., after Fe-oxidation ratio adjustment (Middlemost, 1989) and on an anhydrous basis (Le Bas *et al*., 1986; Le Bas, 2000).

The island arc basic rocks (IAB) were compiled from the following areas and sources: Aleutian (Finney *et al*., 2008); Bicol and Bataan, Philippines (McDermott *et al*., 2005; DuFrane *et al*., 2006); Indonesia (Elburg and Kamenetsky, 2007; Sendjaja *et al*., 2009); Isu Bonin (Tamura *et al*., 2007); Lesser Antilles (Turner *et al*., 1996); Northern Honsu (Ohba *et al*., 2009); Solomon, SW Pacific (Schuth *et al*., 2009).

The continental rift basic rocks (CRB) were compiled from the following areas and sources: East Africa Rift system (Chakrabarti *et al*., 2009); Kenya Rift (Rogers *et al*., 2006; Macdonald *et al*., 2008); Main Ethiopian Rift (Peccerillo *et al*., 2007; Rooney *et al*., 2007; Ronga *et al*., 2009); and Mt. Etna, Italy (Ferlito *et al*., 2009).

The ocean-island basic rocks (OIB) were compiled from the following areas and sources: French Polynesia (Takamasa *et al*., 2009) and Hawaiian Islands (Xu *et al*., 2007; Dixon *et al*., 2008; Marske *et al*., 2008; Ireland *et al*., 2009).

The mid-ocean ridge basic rocks (MORB) were compiled from the following areas and sources: Arctic Mid-Ocean Ridge (Hellevang and Pedersen, 2008); Indian Ridge (Nakamura *et al*., 2007; Ray *et al*., 2007); and Mid-Atlantic Ridge (Debaille *et al*., 2006; Regelous *et al*., 2009).

Additionally, to further evaluate these diagrams for continental arc setting, the Andean data were compiled from the following sources listed according

to the publication year: López-Escobar *et al*. (1981, 1991, 1993), Deruelle (1982); Frey *et al*. (1984), Gerlach *et al*. (1988), Hickey-Vargas *et al*. (1989), Tormey *et al*. (1991), Vergara *et al*. (2004), and Bruni *et al*. (2008).

2.2. Central American Volcanic Arc Database

The CAVA database was an updated version of that used by Verma *et al*. (2006), except that the information from Carr's website was not included mainly to avoid repetition. The geochemical data for CAVA basic rocks reported from different countries were compiled as follows: Guatemala (Carr, 1984; Carr *et al*., 1990; Bardintzeff and Deniel, 1992; Walker *et al*., 2000); El Salvador (Carr, 1984; Carr *et al*., 1990; Agostini *et al*., 2006); Honduras (Patino *et al*., 1997; Walker *et al*., 2000); Nicaragua (Carr, 1984; Hazlett, 1987; Carr *et al*., 1990; Walker *et al*., 1990, 2001; La Femina *et al*., 2004); and NW Costa Rica (Reagan and Gill, 1989; Carr *et al*., 1990; Alvarado *et al*., 2006; Bolge *et al*., 2006; Ryder *et al*., 2006).

2.3. Mexican Databases

Databases were prepared for basic and ultrabasic rocks from the MVB and LTVF. The MVB database was an updated version of those used by Verma (2000a, 2002, 2004, 2009), Velasco-Tapia and Verma (2001), Torres-Alvarado *et al*. (2002), Verma and Hasenaka (2004), Verma *et al*. (2006), and Verma and Luhr (2010). Similarly, the LTVF database was updated from Verma (2006) and Verma *et al*. (2006).

Thus, the MVB data were compiled from the following sources listed according to the publication year: Williams (1950), Gunn and Mooser (1971), Negendank (1972), Robin (1976), Robin and Tournon (1978), Gastil *et al*. (1979), Pérez *et al*. (1979), Demant (1981), Luhr and Carmichael (1981, 1985), Verma and López (1982), Verma (1983, 2000a, 2001a, b, c, 2002, 2003), Allan and Carmichael (1984), Robin *et al*. (1984), Boudal (1985), Gilbert *et al*. (1985), Negendank *et al*. (1985), Allan (1986), Nelson (1986), Nelson and Livieres (1986), Cathelineau *et al*. (1987), Ferriz and Mahood (1987), Hasenaka and Carmichael (1987), Martin del Pozzo *et al*. (1987), Silva Mora (1988), Luhr *et al*. (1989), Martin del Pozzo (1989), Swinamer (1989), Verma and Nelson (1989a, b), Wallace and Carmichael (1989, 1992, 1999), Robin *et al*. (1990), Allan *et al*. (1991), Lange and Carmichael (1991), Hasenaka (1992), Righter and Carmichael (1992), Robin and Potrel (1993), Ferrari *et al*. (1994, 2000), Moore *et al*. (1994), Besch *et al*. (1995), Orozco-Esquivel (1995), Righter *et al*. (1995), Carmichael *et al*. (1996, 2006), Luhr (1997), Delgado *et al*. (1998), Blatter *et al*. (2001, 2007), Blatter and Hammersley, 2009), Righter and Rosas-Elguera (2001), Velasco-Tapia and Verma (2001), Chesley *et al*. (2002), García-Palomo *et al*. (2002), Siebert and Carrasco-Núñez (2002), Gómez-Tuena *et al*. (2003), Petrone *et al*. (2003), Siebe *et al*. (2004), Verma and Hasenaka (2004), Carrasco-Núñez *et al*. (2005), Lewis-Kenedi *et al*. (2005), Schaaf *et al*. (2005), Rossotti *et al*. (2006), Frey *et al*. (2007), Orozco-Esquivel *et al*. (2007), Torres-Alvarado *et al*. (2007), Arce *et al*. (2008), Maria and Luhr (2008), Meriggi *et al*. (2008), Straub *et al*. (2008), Vigouroux *et al*. (2008), Mori *et al*. (2009), Rodríguez *et al*. (2009), and Verma and Luhr (2010).

The LTVF database included data from the following sources: Nelson and Gonzalez-Caver (1992), Verma *et al*. (1993), Nelson *et al*. (1995), Verma (2006), and Espíndola *et al*. (2009).

3. Statistical Evaluation of Discriminant Function Discrimination Diagrams

We used five world databases to evaluate all four sets of new discrimination diagrams (Agrawal *et al*., 2004, 2008; Verma *et al*., 2006; Verma and Agrawal, 2010). For each set of diagrams, five different plots were prepared and the samples in different fields counted. Then, the success rate statistics were calculated and reported. In this way, 20 diagrams were thus obtained for the world data from each tectonic setting, amounting to a total of 100 diagrams for the five databases. To conserve space, these diagrams are not included here. The results are summarized in Tables 1, 2, 3 and 4.

Table 1

Statistical evaluation information of the set of five major-element based discriminant function DF1–DF2 discrimination diagrams (Agrawal et al., 2004) for basic rocks from island arc (IAB), continental rift (CRB), ocean-island (OIB) and mid-ocean ridge (MORB)

Tectonic setting (figure #)	Total # samples (%)	Number of discriminated samples (%)			
		IAB	CRB	OIB	MORB
IAB–CRB–OIB–MORB					
Island arc	64 (100)	***58*** (***90.6***)	0 (0.0)	0 (0.0)	6 (9.4)
Continental rift	110 (100)	15 (13.6)	***63*** (***57.3***)	17 (15.5)	15 (13.6)
Ocean-island	233 (100)	7 (3.0)	18 (7.7)	***200*** (***85.8***)	8 (3.5)
Mid-ocean ridge	71 (100)	2 (2.8)	0 (0.0)	0 (0.0)	***69*** (***97.2***)
Andes	57 (100)	***46*** (***80.7***)	11 (19.3)	0 (0.0)	0 (0.0)
IAB–CRB–OIB					
Island arc	64 (100)	***64*** (***100***)	0 (0.0)	0 (0.0)	–
Continental rift	110 (100)	21 (19.1)	***77*** (***70.0***)	12 (10.9)	–
Ocean-island	233 (100)	12 (5.2)	21 (9.0)	***200*** (***85.8***)	–
Andes	57 (100)	***46*** (***80.7***)	11 (19.3)	0 (0.0)	–
IAB–CRB–MORB					
Island arc	64 (100)	***59*** (***92.2***)	0 (0.0)	–	5 (7.8)
Continental rift	110 (100)	14 (12.7)	***83*** (***75.5***)	–	13 (11.8)
Mid-ocean ridge	71 (100)	2 (2.8)	0 (0.0)	–	***69*** (***97.2***)
Andes	57 (100)	***46*** (***80.7***)	10 (17.5)	–	1 (1.8)
IAB–OIB–MORB					
Island arc	64 (100)	***59*** (***92.2***)	–	0 (0.0)	5 (7.8)
Ocean-island	233 (100)	1(0.4)	–	***212*** (***91.0***)	20 (8.6)
Mid-ocean ridge	71 (100)	2 (2.8)	–	0 (0.0)	***69*** (***97.2***)
Andes	57 (100)	***44*** (***77.2***)	–	6 (10.5)	7 (12.3)
CRB–OIB–MORB					
Continental rift	110 (100)	–	***88*** (***80.0***)	8 (7.3)	14 (12.7)
Ocean-island	233 (100)	–	14 (6.0)	***205*** (***88.0***)	14 (6.0)
Mid-ocean ridge	71 (100)	–	0 (0.0)	0 (0.0)	***71*** (***100***)

Boldface italic font shows the correct (expected) tectonic setting. The results of inapplicable diagrams (diagrams from which the expected tectonic setting is absent for a given dataset) are not included in this table, e.g., Island arc is missing from the CRB–OIB–MORB combination (i.e., from the diagram that would correspond to this combination), and therefore, this setting is missing from the final part of table. Andean results are also not shown for this combination because it does not contain the expected IAB setting

The first set of major-element based discrimination diagrams (Table 1; Agrawal *et al.*, 2004) works well for all tectonic settings of island arc (success rates of 90.6–100%), continental rift (57.3–80.0%), ocean-island (85.8–91.0%), mid-ocean ridge (97.2–100%), and continental arc of the Andes evaluated for its similarity to island arc (77.2–80.7%). All success rates are statistically significant because they are $\gg$33.3% (being the simple "by chance" probability).

The second set of major-element based diagrams (Table 2; Verma *et al.*, 2006) using exactly the same samples as for the first set, were evaluated with the following success rates: island arc 96.9–100%, continental rift 70.0–96.4%, ocean-island 70.0–92.7%, mid-ocean ridge 97.2–100%, and the Andes evaluated for its similarity to island arc (73.7–82.5%).

The first set of immobile-element based diagrams (Table 3; Agrawal *et al.*, 2008) was also evaluated for IAB, CRB, OIB, and MORB (three settings at a time) settings using five world databases. The success rates from these databases of island arc, continental rift, ocean-island, mid-ocean ridge, and the Andes were, respectively, 71.7–84.9%, 66.7–100%, 69.7–83.5%, 96.6–98.3%, and identical values of 83.8%.

Finally, the second set of immobile-element based diagrams (Table 4; Verma and Agrawal, 2010) also complies with the requirement of normal distribution of the log-ratio variables used to construct these diagrams. This was achieved by the use of DODESYS software (Verma and Díaz-González, unpublished), which uses new precise and accurate critical values for discordancy tests (Barnett and Lewis, 1994;

Table 2

Statistical evaluation information of the set of five discrimination diagrams based on natural logarithm transformation of major-element ratios discriminant functions DF1–DF2 (Verma et al., 2006) for basic rocks from island arc (IAB), continental rift (CRB), ocean-island (OIB) and mid-ocean ridge (MORB)

Tectonic setting (figure #)	Total # samples (%)	Number of discriminated samples (%)			
		IAB	CRB	OIB	MORB
IAB–CRB–OIB–MORB					
Island arc	64 (100)	***64 (100)***	0 (0.0)	0 (0.0)	0 (0.0)
Continental rift	110 (100)	2 (1.8)	***87 (79.1)***	18 (16.4)	3 (2.7)
Ocean-island	233 (100)	1 (0.4)	38 (16.3)	***163 (70.0)***	30 (13.3)
Mid-ocean ridge	71 (100)	2 (2.8)	0 (0.0)	0 (0.0)	***69 (97.2)***
Andes	57 (100)	***45 (78.9)***	12 (21.1)	0 (0.0)	0 (0.0)
IAB–CRB–OIB					
Island arc	64 (100)	***64 (100)***	0 (0.0)	0(0.0)	–
Continental rift	110 (100)	0 (0.0)	***77 (70.0)***	33 (30.0)	–
Ocean-island	233 (100)	6 (2.6)	22 (9.4)	***205 (88.0)***	–
Andes	57 (100)	***42 (73.7)***	15 (26.3)	0 (0.0)	–
IAB–CRB–MORB					
Island arc	64 (100)	***64 (100)***	0 (0.0)	–	0 (0.0)
Continental rift	110 (100)	0 (0.0)	***106 (96.4)***	–	4 (3.6)
Mid-ocean ridge	71 (100)	2 (2.8)	0 (0.0)	–	***69 (97.2)***
Andes	57 (100)	***45 (78.9)***	12 (21.1)	–	0 (0.0)
IAB–OIB–MORB					
Island arc	64 (100)	***62 (96.9)***	–	2 (3.1)	0 (0.0)
Ocean-island	233 (100)	15 (6.4)	–	***216 (92.7)***	2 (0.9)
Mid-ocean ridge	71 (100)	2 (2.8)	–	0 (0.0)	***69 (97.2)***
Andes	57 (100)	***47 (82.5)***	–	8 (14.0)	2 (3.5)
CRB–OIB–MORB					
Continental rift	110 (100)	–	***81 (73.6)***	25 (22.7)	4 (3.6)
Ocean-island	233 (100)	–	30 (12.9)	***202 (86.7)***	1 (0.4)
Mid-ocean ridge	71 (100)	–	0 (0.0)	0 (0.0)	***71 (100)***

Boldface italic font shows the correct (expected) tectonic setting. The results of inapplicable diagrams (diagrams from which the expected tectonic setting is absent for a given dataset) are not included in this table, e.g., Island arc is missing from the CRB–OIB–MORB combination (i.e., from the diagram that would correspond to this combination), and therefore, this setting is missing from the final part of table. Andean results are also not shown for this combination because it does not contain the expected IAB setting

Verma and Quiroz-Ruiz, 2006a, b, 2008; Verma *et al.*, 2008). The success rates for the five world databases were as follows: island arc 92.6–100%, continental rift 58.5–100%, ocean-island identical values of 100%, mid-ocean ridge 83.1–100%, and the Andes 62.1–79.3%. We also calculated the success rates (not-tabulated) of these five entire databases before the application of DODESYS, i.e., without ascertaining that the log-transformed variables are normally distributed. A net gain of success rates was observed for the combined CRB + OIB (8.0%), OIB (16.7%) and MORB (5.4%) when discordant outlier-free data were used as compared to the entire dataset. On the contrary, a net loss was obtained for CRB (about 3.8%), IAB (about 0.1%), and the Andes (about 3.0%).

4. *Use of Discriminant Function based Discrimination Diagrams for Southern Mexico and Central America*

The results of the application of the four sets of new diagrams to basic rocks from Southern Mexico (MVB, arbitrarily divided into four parts: W–western, WC–west-central, C–central and E–eastern, and LTVF; see Fig. 1 for locations) and Central America (CAVA) are summarized in Tables 5, 6, 7 and 8. In these tables, success rates are calculated when the number of samples was at least 25 (an arbitrarily set limit), and the "inapplicable" results are also indicated. Although a total of 120 diagrams were prepared, we present only four sets of discrimination diagrams as follows: Agrawal *et al.* (2004) diagrams

Table 3

Statistical evaluation of the set of five discrimination diagrams based on natural logarithm transformation of trace-element ratios discriminant functions DF1–DF2 (Agrawal et al., 2008) for basic rocks from island arc (IAB), continental rift (CRB), ocean-island (OIB) and mid-ocean ridge (MORB)

Tectonic setting (figure #)	Total # samples (%)	Number of discriminated samples (%)				
		IAB	Within-plate			MORB
			CRB + OIB	CRB	OIB	
IAB–CRB–OIB–MORB						
Island arc	53 (100)	***45* (*84.9*)**	4 (7.5)	–	–	4 (7.5)
Continental rift	84 (100)	0 (0.0)	**84 (100)**	–	–	0 (0.0)
Ocean-island	109 (100)	0 (0.0)	**96 (88.1)**	–	–	13 (11.9)
Mid-ocean ridge	59 (100)	2 (3.4)	0 (0.0)	–	–	***57* (*96.6*)**
Andes	37 (100)	***31* (*83.8*)**	6 (26.2)	–	–	0 (0.0)
IAB–CRB–OIB						
Island arc	53 (100)	***38* (*71.7*)**	–	7 (13.2)	8 (15.1)	–
Continental rift	84 (100)	0 (0.0)	–	***74* (*88.1*)**	10 (11.9)	–
Ocean-island	109 (100)	0 (0.0)	–	33 (30.3)	***76* (*69.7*)**	–
Andes	37 (100)	***31* (*83.8*)**	–	5 (13.5)	1 (2.7)	–
IAB–CRB–MORB						
Island arc	53 (100)	***42* (*79.2*)**	–	7 (13.2)	–	4 (7.6)
Continental rift	84 (100)	0 (0.0)	–	***84* (*100*)**	–	0 (0.0)
Mid-ocean ridge	59 (100)	1 (1.7)	–	0 (0.0)	–	***58* (*98.3*)**
Andes	37 (100)	***31* (*83.8*)**	–	6 (16.2)	–	0 (0.0)
IAB–OIB–MORB						
Island arc	53 (100)	***41* (*77.4*)**	–	–	8 (15.1)	4 (7.5)
Ocean-island	109 (100)	0 (0.0)	–	–	***91* (*83.5*)**	18 (16.5)
Mid-ocean ridge	59 (100)	2 (3.4)	–	–	0 (0.0)	***57* (*96.6*)**
Andes	37 (100)	***31* (*83.8*)**	–	–	6 (16.2)	0 (0.0)
CRB–OIB–MORB						
Continental rift	84 (100)	–	–	***56* (*66.7*)**	28 (33.3)	0 (0.0)
Ocean-island	109 (100)	–	–	20 (18.3)	***78* (*71.6*)**	11 (10.1)
Mid-ocean ridge	59 (100)	–	–	1 (1.7)	0 (0.0)	***58* (*98.3*)**

Boldface italic font shows the correct (expected) tectonic setting. The results of inapplicable diagrams (diagrams from which the expected tectonic setting is absent for a given dataset) are not included in this table, e.g., Island arc is missing from the CRB–OIB–MORB combination (i.e., from the diagram that would correspond to this combination), and therefore, this setting is missing from the final part of table. Andean results are also not shown for this combination because it does not contain the expected IAB setting

for W-MVB and WC-MVB (Fig. 2); Verma *et al.* (2006) diagrams for C-MVB (Fig. 3); Agrawal *et al.* (2008) diagrams for E-MVB (Fig. 4); and Verma and Agrawal (2010) diagrams for LTVF and CAVA (Fig. 5).

We describe in detail only one set of diagrams (Fig. 2; Agrawal *et al.*, 2004) to illustrate their use for inferring the tectonic setting. The compiled W-MVB data (227 analyses, Table 5) plotted in Fig. 2a were counted to calculate success rates for all four tectonic settings of IAB, CRB, OIB, and MORB. The highest success rate obtained for CRB is about 78.9%, because 179 out of 227 samples plot in this field. For other tectonic settings, the success rates varied as follows: IAB 18.1% (41 out of 227 samples plot in this field), OIB 0.9% (2 out of 227 samples), and MORB 2.2% (5 out of 227 samples). These results show that for W-MVB the expected tectonic setting from the first four-field diagram (Fig. 2a) is a continental rift setting. However, the results are still not considered definitive, because all four remaining diagrams should be examined (Fig. 2b–e). Figures 2b and c confirm the results of Fig. 2a, because 177 and 174 samples, respectively (out of 227; with respective success rate of 78.0 and 76.7%, Table 5) plot in CRB on IAB-CRB-OIB and IAB-CRB-MORB plots. In Figure 2d, corresponding to IAB-OIB-MORB, the expected CRB field is missing. Therefore, this diagram (Fig. 2d) should be eliminated from any interpretations of W-MVB data, and the results

Table 4

Statistical evaluation of the set of five discrimination diagrams based on natural logarithm transformation of trace-element ratios discriminant functions DF1–DF2 (Verma and Agrawal, 2010) for basic rocks from island arc (IAB), continental rift (CRB), ocean-island (OIB) and mid-ocean ridge (MORB)

Tectonic setting (figure #)	Total # samples (%)	Number of discriminated samples (%)				
		IAB	Within-plate			MORB
			CRB + OIB	CRB	OIB	
IAB–CRB–OIB–MORB						
Island arc	27 (100)	***27*** (***100***)	0 (0.0)	–	–	0 (0.0)
Continental rift	65 (100)	0 (0.0)	***65*** (***100***)	–	–	0 (0.0)
Ocean-island	85 (100)	0 (0.0)	**85 (100)**	–	–	0 (0.0)
Mid-ocean ridge	65 (100)	10 (15.4)	0 (0.0)	–	–	***55*** (***84.6***)
Andes	29 (100)	***18*** (***62.1***)	6 (20.7)	–	–	5 (17.2)
IAB–CRB–OIB						
Island arc	27 (100)	***27*** (***100***)	–	0 (0.0)	0 (0.0)	–
Continental rift	65 (100)	0 (0.0)	–	***43*** (***66.2***)	22 (33.8)	–
Ocean-island	85 (100)	0 (0.0)	–	0 (0.0)	***85*** (***100***)	–
Andes	29 (100)	***23*** (***79.3***)	–	5 (17.2)	1 (3.4)	–
IAB–CRB–MORB						
Island arc	27 (100)	***27*** (***100***)	–	0 (0.0)	–	0 (0.0)
Continental rift	65 (100)	0 (0.0)	–	***65*** (***100***)	–	0 (0.0)
Mid-ocean ridge	65 (100)	8 (12.3)	–	0 (0.0)	–	***57*** (***87.7***)
Andes	29 (100)	***18*** (***62.1***)	–	6 (20.7)	–	5 (17.2)
IAB–OIB–MORB						
Island arc	27 (100)	***25*** (***92.6***)	–	–	0 (0.0)	2 (7.4)
Ocean-island	85 (100)	0 (0.0)	–	–	***85*** (***100***)	0 (0.0)
Mid-ocean ridge	65 (100)	11 (16.9)	–	–	0 (0.0)	***54*** (***83.1***)
Andes	29 (100)	***20*** (***69.0***)	–	–	6 (20.7)	3 (10.3)
CRB–OIB–MORB						
Continental rift	65 (100)	–	–	***38*** (***58.5***)	27 (41.5)	0 (0.0)
Ocean-island	85 (100)	–	–	0 (5.8)	***85*** (***100***)	0 (0.0)
Mid-ocean ridge	65 (100)	–	–	0 (0.0)	0 (0.0)	***65*** (***100***)

Boldface italic font shows the correct (expected) tectonic setting. The results of inapplicable diagrams (diagrams from which the expected tectonic setting is absent for a given dataset) are not included in this table, e.g., Island arc is missing from the CRB–OIB–MORB combination (i.e., from the diagram that would correspond to this combination), and therefore, this setting is missing from the final part of table. Andean results are also not shown for this combination because it does not contain the expected IAB setting

summarised in Table 5 ignored. The final diagram (Fig. 2e) for CRB-OIB-MORB further confirms the results of earlier diagrams (Fig. 2a–c) because 200 out of 227 samples (88.1%) plot in CRB field. Thus, for W-MVB consistent results are obtained from Fig. 2a–e.

For WC-MVB, on the other hand, this set of diagrams (Fig. 2a–e) does not provide a consistent result (Table 5). The samples plot in two distinct fields in Figs. 2a–c (IAB and CRB, with somewhat higher success rates for IAB; Table 5). Figures 2d and e do not have these two tectonic settings together, therefore high success rates are obtained for individual tectonic setting in these diagrams (61.0% for IAB in Fig. 2d and 53.7% for CRB in Fig. 2e). We may conclude that, for WC-MVB, a dual or transitional tectonic setting between arc and rift is being indicated.

Once the functioning of the set of five diagrams (Agrawal *et al.*, 2004) is fully understood from the above discussion (Fig. 2, Table 5), it will not be necessary to present in detail the functioning of other diagrams (Figs. 3, 4 5, Tables 6, 7, 8; Verma *et al.*, 2006; Agrawal *et al.* 2008; Verma and Agrawal, 2010), and it would suffice to simply point out the most important results. The following discussion is based on these diagrams (Figs. 3, 4, 5) as well as Tables 6, 7, 8. Therefore, we will not always explicitly refer to them, because the results are summarized in these tables.

Table 5

Application of the set of five major-element based discriminant function DF1–DF2 discrimination diagrams (Agrawal et al., 2004) for basic rocks from Southern Mexico and Central America

Tectonic setting (figure #)	Total # samples (%)	Number of discriminated samples (%)			
		IAB	CRB	OIB	MORB
IAB–CRB–OIB–MORB					
W-MVB (Fig. 2a)	227 (100)	41 (18.1)	***179* (*78.9*)**	2 (0.9)	5 (2.2)
WC-MVB (Fig. 2a)	82 (100)	***42* (*51.2*)**	**29 (35.4)**	0 (0.0)	11 (13.4)
C-MVB	79 (100)	6 (7.6)	***49* (*62.0*)**	2 (2.5)	22 (27.9)
E-MVB	197 (100)	23 (11.7)	***120* (*60.9*)**	1 (0.5)	53 (26.9)
LTVF	75 (100)	7 (9.3)	***62* (*82.7*)**	0 (0.0)	6 (8.0)
CAVA	119 (100)	***89* (*74.8*)**	2 (1.7)	0 (0.0)	28 (23.5)
IAB–CRB–OIB					
W-MVB (Fig. 2b)	227 (100)	48 (21.1)	***177* (*78.0*)**	2 (0.9)	–
WC-MVB (Fig. 2b)	82 (100)	***48* (*58.5*)**	**34 (41.5)**	0 (0.0)	–
C-MVB	79 (100)	11 (13.9)	***66* (*83.6*)**	2 (2.5)	–
E-MVB	197 (100)	33 (16.8)	***164* (*83.2*)**	0 (0.0)	–
LTVF	75 (100)	8 (10.7)	***67* (*89.3*)**	0 (0.0)	–
CAVA	119 (100)	***118* (*99.2*)**	1 (0.8)	0 (0.0)	–
IAB–CRB–MORB					
W-MVB (Fig. 2c)	227 (100)	46 (20.2)	***174* (*76.7*)**	–	7 (3.1)
WC-MVB (Fig. 2c)	82 (100)	***45* (*54.9*)**	23 (28.0)	–	14 (17.1)
C-MVB	79 (100)	9 (11.4)	***37* (*46.8*)**	–	**33 (41.8)**
E-MVB	197 (100)	23 (11.7)	***131* (*66.5*)**	–	43 (21.8)
LTVF	75 (100)	5 (6.7)	***67* (*89.3*)**	–	3 (4.0)
CAVA	119 (100)	***92* (*77.3*)**	2 (1.7)	–	25 (21.0)
IAB–OIB–MORB					
W-MVB (Fig. 2d)[a]	227 (100)	108 (47.6)	–	82 (36.1)	37 (16.3)
WC-MVB (Fig. 2d)	82 (100)	***50* (*61.0*)**	–	17 (20.7)	15 (18.3)
C-MVB[a]	79 (100)	19 (24.1)	–	11 (13.9)	49 (62.0)
E-MVB[a]	197 (100)	45 (22.8)	–	55 (27.9)	97 (49.2)
LTVF[a]	75 (100)	11 (14.7)	–	8 (10.6)	56 (74.7)
CAVA	119 (100)	***91* (*76.5*)**	–	1 (0.8)	27 (22.7)
CRB–OIB–MORB					
W-MVB (Fig. 2e)	227 (100)	–	***200* (*88.1*)**	2 (0.9)	25 (11.0)
WC-MVB (Fig. 2e)	82 (100)	–	***44* (*53.7*)**	0 (0.0)	**38 (46.3)**
C-MVB	79 (100)	–	***62* (*78.5*)**	1 (1.3)	16 (20.3)
E-MVB	197 (100)	–	***147* (*74.6*)**	2 (1.0)	48 (24.4)
LTVF	75 (100)	–	***66* (*88.0*)**	2 (2.7)	7 (9.3)
CAVA[a]	119 (100)	–	6 (5.0)	0 (0.0)	113 (95.0)

MVB Mexican Volcanic Belt, *W* western, *WC* west-central, *C* central, *E* eastern, *LTVF* Los Tuxtlas volcanic field, *CAVA* Central American Volcanic Arc

[a] Inapplicable results and diagrams; boldface italic font shows the expected tectonic setting; whenever this setting is followed by a significant (>33.3%) success rate for another setting, it is shown by simple boldface number for success rate

For W-MVB, a continental rift setting indicated by the first set of major-element based diagrams (Agrawal *et al*., 2004) is confirmed by the second set of major-element based diagrams (Verma *et al.*, 2006), with even greater success rates of 84.6–93.8% (Table 6). The first set of immobile trace-element based diagrams (Agrawal *et al*., 2008) indicates a dual arc and rift setting for the W-MVB, with success rates of 49.3 and 79.1% for arc and 59.7 and 68.7 for rift (Table 7). The other set of immobile element based diagrams (Verma and Agrawal, 2010) indicates an arc setting with success rates of 64.1–67.0% (Table 8). Thus, for the W-MVB it appears that both subduction (e.g., Bandy *et al*., 2000; Bandy and Hilde, 2000; Yang *et al*., 2009) and rifting (e.g., Luhr *et al*., 1985) processes play a significant role in controlling the magma compositions, although major-elements favor a rift setting. The transition between

Table 6

Application of the set of five discrimination diagrams based on natural logarithm transformation of major-element ratios discriminant functions DF1–DF2 (Verma et al., 2006) for basic rocks from Southern Mexico and Central America

Tectonic setting (figure #)	Total # samples (%)	Number of discriminated samples (%)			
		IAB	CRB	OIB	MORB
IAB–CRB–OIB–MORB					
W-MVB	227 (100)	22 (9.7)	***192* (*84.6*)**	9 (4.0)	4 (1.8)
WC-MVB	82 (100)	**35 (42.7)**	***42* (*51.2*)**	0 (0.0)	5 (6.1)
C-MVB (Fig. 3a)	79 (100)	7 (8.9)	***65* (*82.3*)**	1 (1.2)	6 (7.6)
E-MVB	197 (100)	25 (12.7)	***164* (*83.2*)**	5 (2.5)	3 (1.5)
LTVF	75 (100)	6 (8.0)	***69* (*92.0*)**	0 (0.0)	0 (0.0)
CAVA	119 (100)	***96* (*80.7*)**	4 (3.4)	0 (0.0)	19 (16.0)
IAB–CRB–OIB					
W-MVB	227 (100)	19 (8.4)	***201* (*88.5*)**	7 (3.1)	–
WC-MVB	82 (100)	22 (26.8)	***60* (*73.2*)**	0 (0.0)	–
C-MVB (Fig. 3b)	79 (100)	4 (5.1)	***73* (*92.4*)**	2 (2.5)	–
E-MVB	197 (100)	18 (9.1)	***177* (*89.8*)**	2 (1.0)	–
LTVF	75 (100)	8 (10.7)	***67* (*89.3*)**	0 (0.0)	–
CAVA	119 (100)	***91* (*76.5*)**	17 (14.3)	11 (9.2)	–
IAB–CRB–MORB					
W-MVB	227 (100)	17 (7.5)	***205* (*90.3*)**	–	5 (2.2)
WC-MVB	82 (100)	27 (32.9)	***48* (*58.5*)**	–	7 (8.5)
C-MVB (Fig. 3c)	79 (100)	4 (5.1)	***69* (*87.3*)**	–	6 (7.6)
E-MVB	197 (100)	19 (9.6)	***175* (*88.8*)**	–	3 (1.5)
LTVF	75 (100)	6 (8.0)	***69* (*92.0*)**	–	0 (0.0)
CAVA	119 (100)	***96* (*80.7*)**	5 (4.2)	–	18 (15.1)
IAB–OIB–MORB					
W-MVB[a]	227 (100)	72 (31.7)	–	115 (50.7)	40 (17.6)
WC-MVB	82 (100)	**59 (72.0)**	–	11 (13.4)	12 (14.6)
C-MVB (Fig. 3d)[a]	79 (100)	19 (24.0)	–	10 (12.7)	50 (63.3)
E-MVB[a]	197 (100)	44 (22.3)	–	81 (41.1)	72 (36.5)
LTVF[a]	75 (100)	26 (34.7)	–	42 (56.0)	7 (9.3)
CAVA	119 (100)	***98* (*82.4*)**	–	2 (1.7)	19 (16.0)
CRB–OIB–MORB					
W-MVB	227 (100)	–	***213* (*93.8*)**	9 (4.0)	5 (2.2)
WC-MVB	82 (100)	–	***70* (*85.4*)**	0 (0.0)	12 (14.6)
C-MVB (Fig. 3e)	79 (100)	–	***71* (*89.9*)**	1 (1.2)	7 (8.9)
E-MVB	197 (100)	–	***186* (*94.4*)**	5 (2.5)	6 (3.0)
LTVF	75 (100)	–	***74* (*98.7*)**	0 (0.0)	1 (1.3)
CAVA[a]	119 (100)	–	86 (72.3)	0 (0.0)	33 (27.7)

MVB Mexican Volcanic Belt, *W* western, *WC* west-central, *C* central, *E* eastern, *LTVF* Los Tuxtlas volcanic field, *CAVA* Central American Volcanic Arc

[a] Inapplicable results and diagrams; boldface italic font shows the expected tectonic setting; whenever this setting is followed by a significant (>33.3%) success rate for another setting, it is shown by simple boldface number for success rate

arc and rift settings and the significant role of both of them in the genesis of magmas in the W-MVB is being pointed out for the first time on the basis of these new discrimination diagrams, which may also imply the proximity of the termination of subduction of Rivera plate and the increasingly more significant rifting of the Jalisco block from on-land Mexico.

The contrasting behavior of major- and trace-element based diagrams may be related to higher analytical errors for trace-element determinations, such as Nb, Yb, Sm, La, and Y, as compared to those for the major-elements. For the evaluation of tectonic settings of fresh rocks, the major-element based diagrams (Figs. 2, 3, Tables 5, 6; Agrawal *et al.*, 2004; Verma *et al.*, 2006) should be preferred in comparison to the trace-element based diagrams (Figs. 4, 5, Tables 7, 8; Agrawal *et al.*, 2008; Verma and Agrawal, 2010).

Table 7

Application of the set of five discrimination diagrams based on natural logarithm transformation of trace-element ratios discriminant functions DF1–DF2 (Agrawal et al., 2008) for basic rocks from Southern Mexico and Central America

Tectonic setting (figure #)	Total # samples (%)	Number of discriminated samples (%)				
		IAB	Within-plate			MORB
			CRB + OIB	CRB	OIB	
IAB–CRB–OIB–MORB						
W-MVB	67 (100)	***33*** **(*49.3*)**	***33*** **(*49.3*)**	–	–	1 (1.5)
WC-MVB	34 (100)	***15*** **(*44.1*)**	7 (20.6)	–	–	**12 (35.3)**
C-MVB	12	0	***11***	–	–	1
E-MVB (Fig. 4a)	90 (100)	**7 (7.8)**	***71*** **(*78.9*)**	–	–	12 (13.3)
LTVF	19	6	***13***	–	–	0
CAVA	42 (100)	***22*** **(*52.4*)**	0 (0.0)	–	–	**20 (47.6)**
IAB–CRB–OIB						
W-MVB	67 (100)	***53*** **(*79.1*)**	–	7 (10.4)	7 (10.4)	–
WC-MVB	34 (100)	**12 (35.3)**	–	***18*** **(*52.9*)**	4 (11.8)	–
C-MVB	12	0	–	***11***	1	–
E-MVB (Fig. 4b)	90 (100)	18 (20.0)	–	***60*** **(*66.7*)**	12 (13.3)	–
LTVF	19	***16***	–	3	0	–
CAVA	42 (100)	***17*** **(*40.5*)**	–	14 (33.3)	11 (26.2)	–
IAB–CRB–MORB						
W-MVB	67 (100)	20 (29.9)	–	***46*** **(*68.7*)**	–	1 (1.5)
WC-MVB	34 (100)	***15*** **(*44.1*)**	–	8 (23.5)	–	11 (32.4)
C-MVB	12	0	–	***12***	–	0
E-MVB (Fig. 4c)	90 (100)	7 (7.8)	–	***71*** **(*78.9*)**	–	12 (13.3)
LTVF	19	4	–	***15***	–	0
CAVA	42 (100)	***22*** **(*52.4*)**	–	0 (0.0)	–	**20 (47.6)**
IAB–OIB–MORB						
W-MVB	67 (100)	19 (28.4)	–	–	**47 (70.1)**	1 (1.5)
WC-MVB	34 (100)	**15 (44.1)**	–	–	5 (14.7)	**14 (41.2)**
C-MVB[a]	12	0	–	–	4	8
E-MVB (Fig. 4d)[a]	90 (100)	8 (8.9)	–	–	68 (75.6)	14 (15.5)
LTVF[a]	19	6	–	–	13	0
CAVA	42 (100)	***22*** **(*52.4*)**	–	–	0 (0.0)	**20 (47.6)**
CRB–OIB–MORB						
W-MVB	67 (100)	–	–	***40*** **(*59.7*)**	22 (32.8)	5 (7.5)
WC-MVB	34 (100)	–	–	**12 (35.3)**	0 (0.0)	***22*** **(*64.7*)**
C-MVB	12	–	–	***11***	1	0
E-MVB (Fig. 4e)	90 (100)	–	–	***72*** **(*80.0*)**	3 (3.3)	15 (16.7)
LTVF	19	–	–	***19***	0	0
CAVA	42 (100)	–	–	1 (2.4)	0 (0.0)	**41 (97.6)**

MVB Mexican Volcanic Belt, *W* western; *WC* west-central; *C* central; *E* eastern; *LTVF* Los Tuxtlas volcanic field; *CAVA* Central American Volcanic Arc

[a] Inapplicable results and diagrams; boldface italic font shows the expected tectonic setting; whenever this setting is followed by a significant (>33.3%) success rate for another setting, it is shown by simple boldface number for success rate

For WC-MVB, the first set of major-element based diagrams (Table 5) indicates a dual arc and rift setting (51.2–61.0% for arc as compared to 35.4–53.7% for rift). The second set of major-element based diagrams, however, indicates a rift setting for the WC-MVB, with success rates from 51.2 to 85.4% (Table 6). Because this second set of diagrams is based on correct statistical treatment of compositional data (Aitchison, 1986; Agrawal and Verma, 2007; Verma, 2010), the results of this set should be considered more reliable. For WC-MVB the first set of immobile trace-element based diagrams also indicates a dual arc and rift setting although success rates for rift are somewhat greater (35.3–52.9% for

Table 8

Application of the set of five discrimination diagrams based on natural logarithm transformation of trace-element ratios discriminant functions DF1–DF2 (Verma and Agrawal, 2010) for basic rocks from Southern Mexico and Central America

Tectonic setting (figure #)	Total # samples (%)	Number of discriminated samples (%)				
		IAB	Within-plate			MORB
			CRB + OIB	CRB	OIB	
IAB–CRB–OIB–MORB						
W-MVB	103 (100)	***66* (*64.1*)**	27 (26.2)	–	–	10 (9.7)
WC-MVB	64 (100)	20 (31.2)	19 (29.7)	–	–	***25* (*39.1*)**
C-MVB	45 (100)	5 (11.1)	***20* (*44.4*)**	–	–	***20* (*44.4*)**
E-MVB	49 (100)	**2 (4.1)**	***30* (*61.2*)**	–	–	**17 (34.7)**
LTVF (Fig. 5a)	47 (100)	***22* (*46.8*)**	**17 (36.2)**	–	–	8 (17.0)
CAVA (Fig. 5a)	43 (100)	***29* (*67.4*)**	1 (2.3)	–	–	13 (30.3)
IAB–CRB–OIB						
W-MVB	103 (100)	***69* (*67.0*)**	–	27 (26.2)	7 (6.8)	–
WC-MVB	64 (100)	39 (60.9)	–	14 (21.9)	11 (17.2)	–
C-MVB	45 (100)	7 (15.6)	–	***31* (*68.9*)**	7 (15.6)	–
E-MVB	49 (100)	6 (12.2)	–	***32* (*65.3*)**	11 (22.4)	–
LTVF (Fig. 5b)	47 (100)	***23* (*48.9*)**	–	**17 (36.2)**	7 (14.9)	–
CAVA (Fig. 5b)	43 (100)	***38* (*88.4*)**	–	5 (11.6)	0 (0.0)	–
IAB–CRB–MORB						
W-MVB	103 (100)	***66* (*64.1*)**	–	29 (28.2)	–	8 (7.8)
WC-MVB	64 (100)	18 (28.1)	–	**22 (34.4)**	–	***24* (*37.5*)**
C-MVB	45 (100)	5 (11.1)	–	***23* (*51.1*)**	–	**17 (37.8)**
E-MVB	49 (100)	1 (2.0)	–	***34* (*69.4*)**	–	14 (28.6)
LTVF (Fig. 5c)	47 (100)	***19* (*40.4*)**	–	***19* (*40.4*)**	–	9 (19.1)
CAVA (Fig. 5c)	43 (100)	***29* (*67.4*)**	–	1 (2.3)	–	13 (30.2)
IAB–OIB–MORB						
W-MVB	103 (100)	***66* (*64.1*)**	–	–	25 (24.3)	12 (11.7)
WC-MVB	64 (100)	**22 (34.4)**	–	–	11 (17.2)	***31* (*48.4*)**
C-MVB	45 (100)	5 (11.1)	–	–	10 (22.2)	***30* (*66.7*)**
E-MVB	49 (100)	2 (4.1)	–	–	**20 (40.8)**	***27* (*55.1*)**
LTVF (Fig. 5d)	47 (100)	***26* (*55.3*)**	–	–	11 (23.4)	10 (21.3)
CAVA (Fig. 5d)	43 (100)	***27* (*62.8*)**	–	–	1 (2.3)	**15 (34.9)**
CRB–OIB–MORB						
W-MVB[a]	103 (100)	–	–	26 (25.2)	66 (64.1)	11 (10.7)
WC-MVB	64 (100)	–	–	20 (31.2)	13 (20.3)	***31* (*48.4*)**
C-MVB	45 (100)	–	–	***20* (*44.4*)**	8 (17.8)	**17 (37.8)**
E-MVB	49 (100)	–	–	***23* (*46.9*)**	14 (28.6)	12 (24.5)
LTVF (Fig. 5e)	47 (100)	–	–	***32* (*68.1*)**	8 (17.0)	7 (14.9)
CAVA (Fig. 5e)[a]	43 (100)	–	–	2 (4.7)	0 (0.0)	41 (95.3)

MVB Mexican Volcanic Belt, *W* western, *WC* west-central, *C* central, *E* eastern, *LTVF* Los Tuxtlas volcanic field, *CAVA* Central American Volcanic Arc

[a] Inapplicable results and diagrams; boldface italic font shows the expected tectonic setting; whenever this setting is followed by a significant (>33.3%) success rate for another setting, it is shown by simple boldface number for success rate

rift as compared to 35.3–44.1% for arc; Table 7). Finally, arc setting is indicated from the final set of immobile element based diagrams, with success rates of 34.4–60.9% (Table 8; 34.4% for rift in one diagram only). Thus, for WC-MVB also, both tectonics of arc and rift play significant role in the genesis of mafic magmas (Tables 5, 6, 7, 8).

For C-MVB, both sets of major-element based diagrams undoubtedly show a continental rift setting, with success rates of 46.8–83.6% for the first set (Table 5) and 82.3–92.4% for the second set of diagrams (Table 6); the latter set is shown to be statistically correct. For the first set of immobile element based diagrams, although the number of

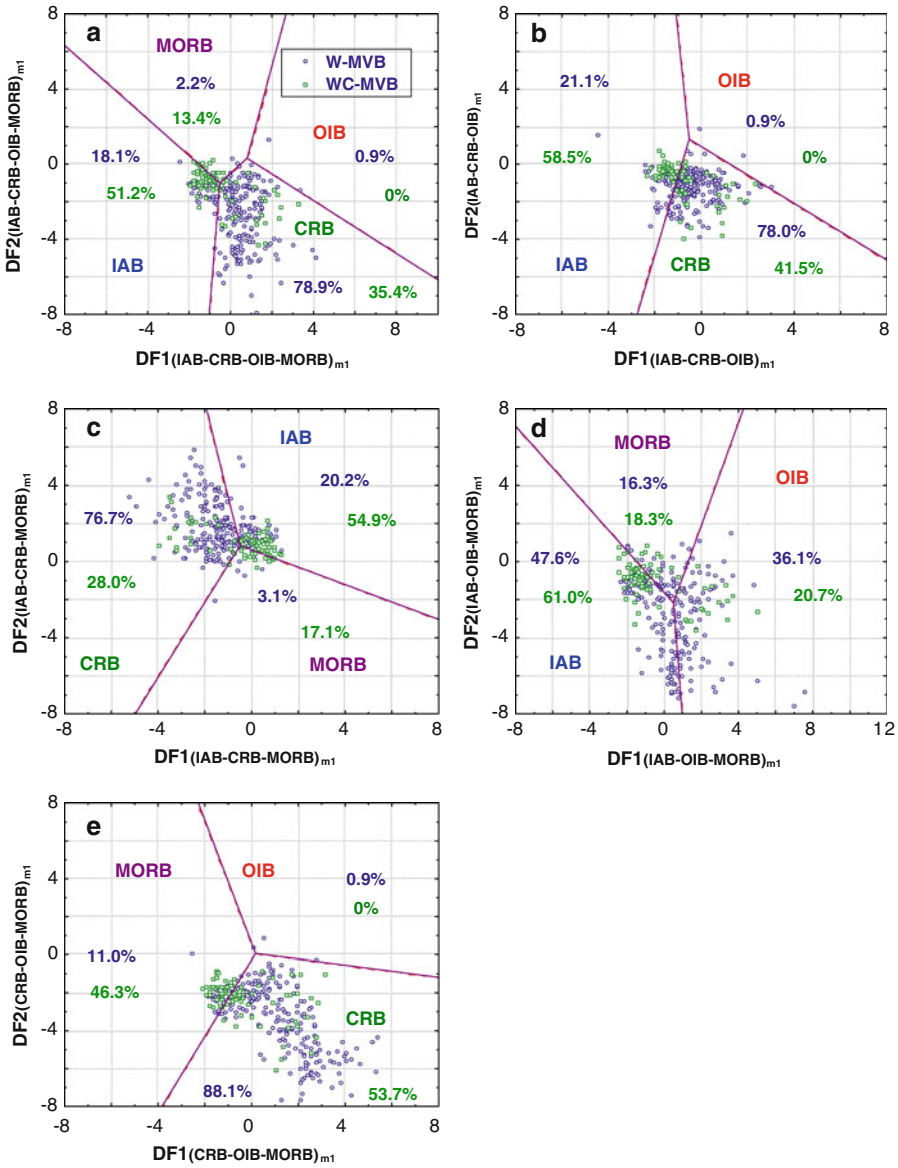

Figure 2

Application of the set of five major-element based discriminant function DF1–DF2 discrimination diagrams (see the subscript $_{m1}$ in all these diagrams; Agrawal *et al.*, 2004) for basic rocks from western Mexican Volcanic Belt (W-MVB) and west-central MVB (WC-MVB) compiled in this work. The percent values are given for each tectonic setting of island arc (IAB), continental rift (CRB), ocean-island (OIB), and mid-ocean ridge (MORB). The *symbols* are shown as inset in diagram (**a**). **a** Four tectonic settings IAB–CRB–OIB–MORB; **b** three tectonic settings IAB–CRB–OIB; **c** three tectonic settings IAB–CRB–MORB; **d** three tectonic settings IAB–OIB–MORB; and **e** three tectonic settings CRB–OIB–MORB

samples from the C-MVB is small (only 12 analyses; Table 7), the rift setting is more likely. Finally, from the second set of immobile element based diagrams a dual setting of rift and mid-ocean ridge (and not rift and arc) is inferred, with success rates for rift varying between 44.4 and 68.9% and for mid-ocean ridge between 37.8 and 66.7% (Table 8). No indications of arc setting are obtained, which is consistent with the absence of deep earthquakes beneath the C-MVB in spite of a very dense seismic network (Pacheco and Singh, 2010). These results would also be consistent with the recent suggestion by Verma (2009) that

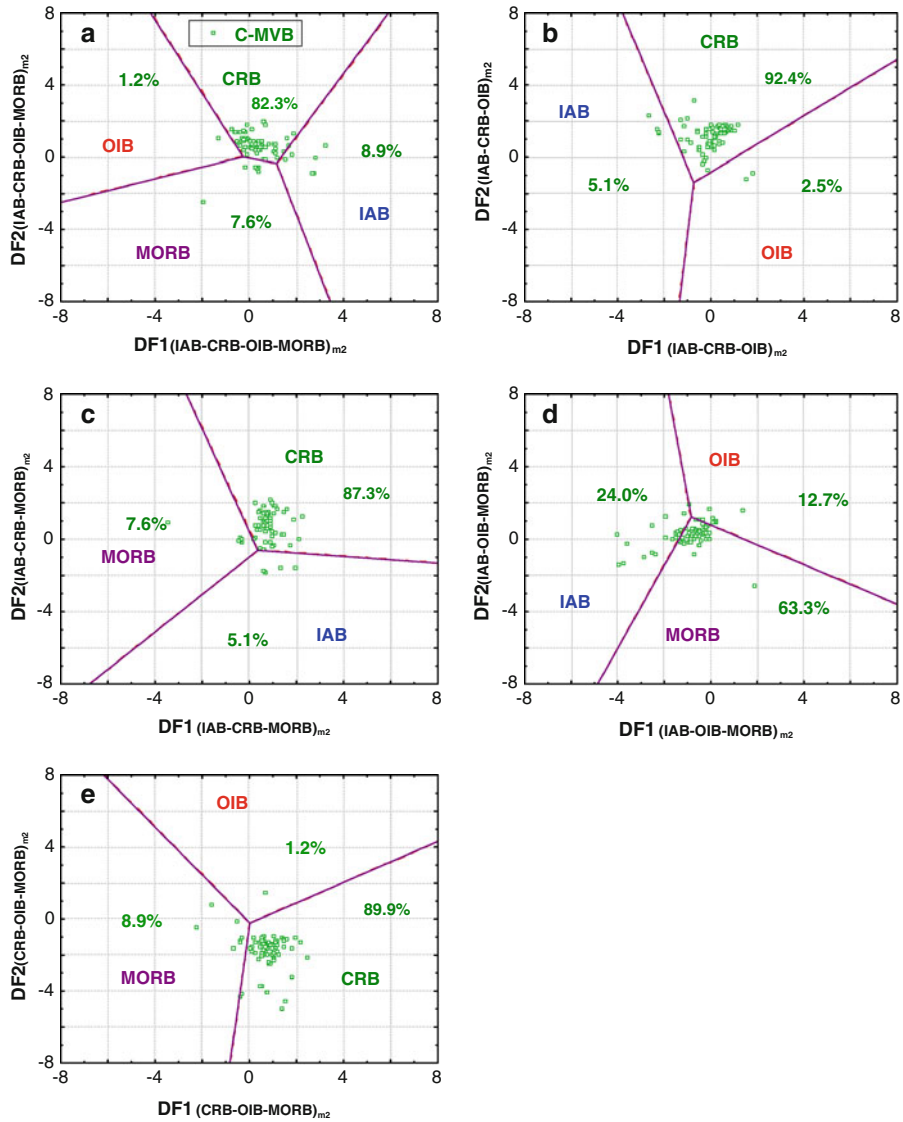

Figure 3

Application of the set of five major-element based discriminant function DF1–DF2 discrimination diagrams (see the subscript $_{m2}$ in all these diagrams; VERMA *et al*., 2006) for basic rocks from central Mexican Volcanic Belt (C-MVB) compiled in this work. The percent values are given for tectonic setting of island arc (IAB), continental rift (CRB), ocean-island (OIB), and mid-ocean ridge (MORB). The *symbols* are shown as inset in diagram (**a**). **a** Four tectonic settings IAB–CRB–OIB–MORB; **b** three tectonic settings IAB–CRB–OIB; **c** three tectonic settings IAB–CRB–MORB; **d** three tectonic settings IAB–OIB–MORB; and **e** three tectonic settings CRB–OIB–MORB

magmas in the C-MVB are the result of continental rifting rather than the subduction of the Cocos plate beneath Mexico. The duality of tectonic setting of rift with mid-ocean ridge, and not with arc, is an interesting result at this stage, which should be confirmed by later studies.

For the final part of the MVB–E-MVB, both sets of major-element based diagrams clearly show a continental rift setting, with very high success rates of 60.9–83.2% for the first set and even higher of 83.2–94.4% for the second set. Similarly, both sets of immobile-element based diagrams favor a rift setting for the E-MVB, with success rates varying between 66.7 and 80.0% for the first set and between 46.9 and 69.4% for the second.

For LTVF, both sets of major-element based diagrams clearly indicate a rift setting, with very high

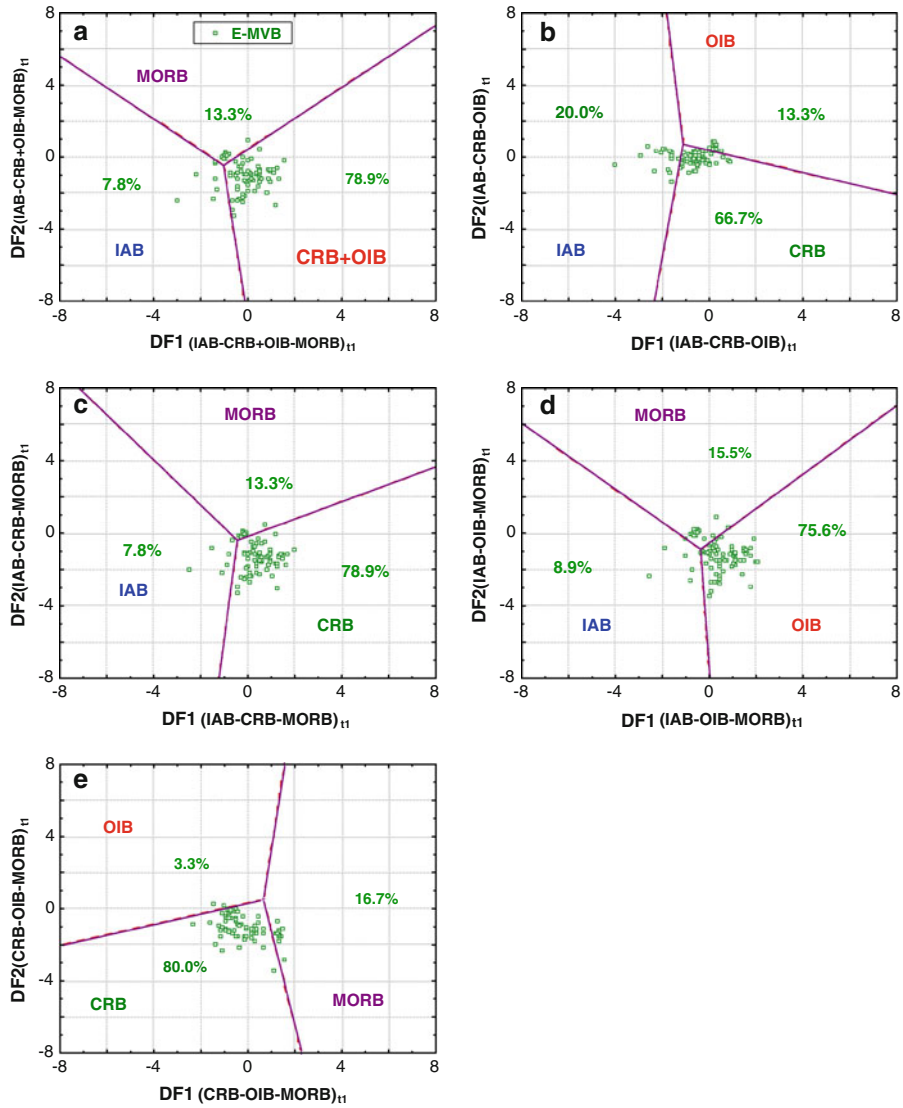

Figure 4

Application of the set of five major-element based discriminant function DF1–DF2 discrimination diagrams (see the subscript $_{t1}$ in all these diagrams; AGRAWAL *et al.*, 2008) for basic rocks from eastern Mexican Volcanic Belt (E-MVB) compiled in this work. The percent values are given for each tectonic setting of island arc (IAB), combined tectonic setting of continental rift and ocean-island (CRB + OIB), continental rift (CRB), ocean-island (OIB), and mid-ocean ridge (MORB). The *symbols* are shown as inset in diagram (**a**). **a** Three tectonic settings IAB–CRB + OIB–MORB; **b** three tectonic settings IAB–CRB–OIB; **c** three tectonic settings IAB–CRB–MORB; **d** three tectonic settings IAB–OIB–MORB; and **e** three tectonic settings CRB–OIB–MORB

success rates of 82.7–89.3 and 89.3–98.7% for the first and second sets, respectively (Tables 5, 6). For the first set of immobile-element diagrams, insufficient samples (only 19 analyses) were available in our database, but the indications are mostly in favor of a rift setting (Table 7). The final set of immobile-element based diagrams shows a dual setting of arc and rift, with success rates of 40.4–55.3% and 36.2–68.1%, respectively (Table 8). As stated above for W-MVB, the major-element based diagrams should be given higher weight when the results of these four sets of diagrams are mutually inconsistent, which would make the conclusion of a rift setting for the LTVF more likely.

For CAVA, both sets of major-element based diagrams clearly provide an arc setting, with high

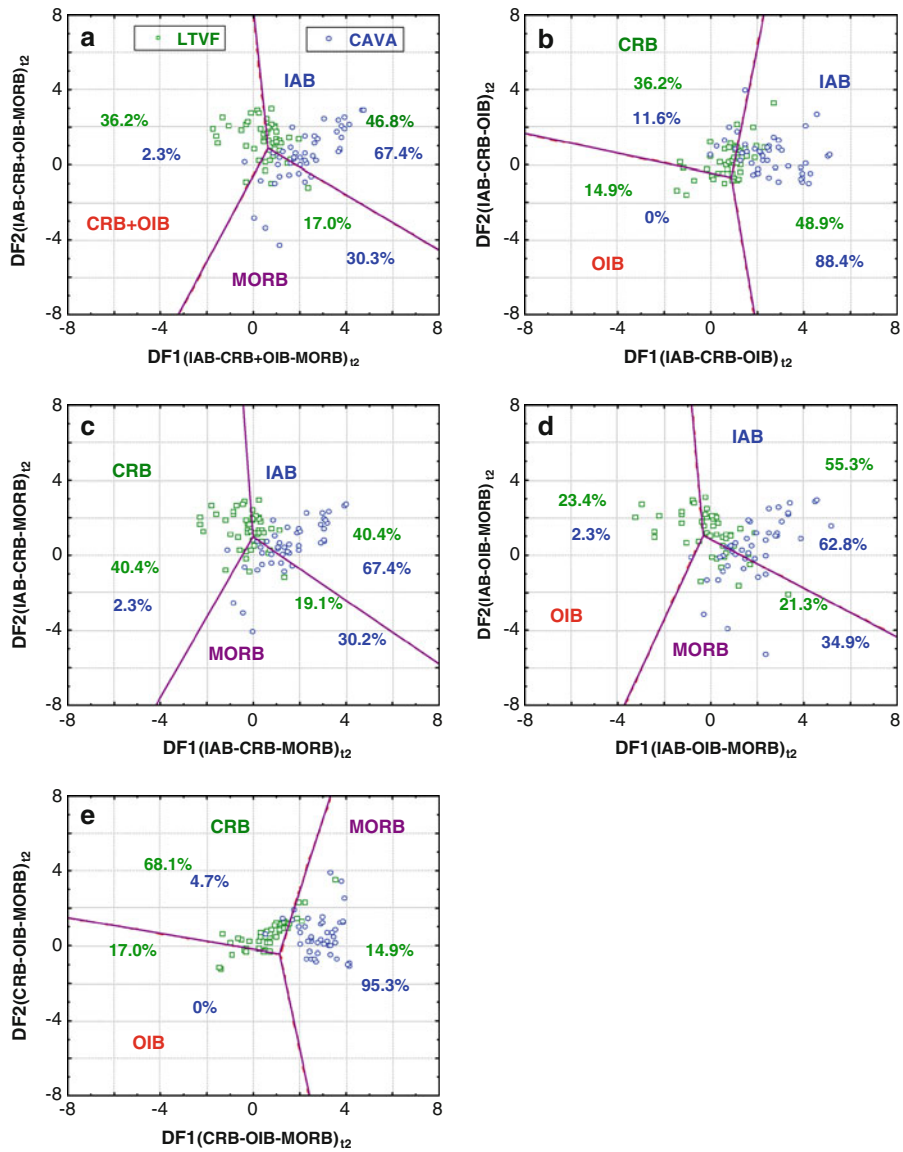

Figure 5

Application of the set of five major-element based discriminant function DF1–DF2 discrimination diagrams (see the subscript $_{t2}$ in all these diagrams; Verma and Agrawal, 2010) for basic rocks from Los Tuxtlas volcanic field (LTVF) and Central America Volcanic Arc (CAVA) compiled in this work. The percent values are given for each tectonic setting of island arc (IAB), combined tectonic setting of continental rift and ocean-island (CRB + OIB), continental rift (CRB), ocean-island (OIB), and mid-ocean ridge (MORB). The *symbols* are shown as inset in diagram (**a**). **a** Three tectonic settings IAB–CRB + OIB–MORB; **b** three tectonic settings IAB-CRB-OIB; **c** three tectonic settings IAB–CRB–MORB; **d** three tectonic settings IAB–OIB–MORB; and **e** three tectonic settings CRB–OIB–MORB

success rates of 74.8–99.2% (Table 5) and 76.5–82.4% (Table 6). The first set of immobile-element diagrams show a dual setting of arc and mid-ocean ridge (with no indications of a rift setting; Table 7) for this volcanic province, with high success rates for mid-ocean ridge (47.6–97.6%) compared to arc setting (40.5–52.4%). However, the other set of immobile-element based diagrams clearly indicates an arc setting for CAVA, with success rates of 62.8–88.4% (Table 8); the last diagram CRB-OIB-MORB should be considered as inapplicable because the expected arc (IAB) setting is absent from this case.

5. Final Considerations

All evaluations of the four tectonic settings of island arc, continental rift, ocean-island, and mid-ocean ridge in several studies (Agrawal *et al.*, 2004, 2008; Verma *et al*., 2006; Agrawal and Verma, 2007; Sheth, 2008; Verma, 2010; this work) have shown good functioning of these diagrams for samples from these four known tectonic settings. The continental arc of the Andes was also successfully evaluated for its similarities with island arc.

For their application to the MVB, LTVF, and CAVA, it is not clear why the major-elements, especially in the second set of statistically correct diagrams, clearly indicate a single tectonic setting, whereas the trace-elements, in some cases, favor a dual tectonic setting. Nevertheless, the single tectonic setting for both MVB and LTVF is shown to be a continental rift, and for CAVA an arc, which confirms the earlier conclusions by Verma (2002, 2004, 2006) from other constraints. The duality of tectonic settings in only a few (not all) diagrams was observed for W-MVB (arc–rift), WC-MVB (arc–rift) and LTVF (arc–rift), C-MVB (rift–mid-ocean ridge), and CAVA (arc–mid-ocean ridge). Do these volcanic areas represent a true transition between two main tectonic settings, or might some other factor explain them?

This question is clearly open for future work. One reason may be related to the data quality for trace-elements, especially Nb, Yb, Sm, La, and Y, involved in these trace-element-based diagrams. Therefore, for fresh rocks compiled from Southern Mexico and Central America, the conclusions from the major-element based diagrams could be given more weight as compared to the trace-element based ones. The other source of such discrepancies may be the fact that the diagrams are strictly applicable to an island arc instead of a continental arc setting.

Nevertheless, a continental rift setting (with less or negligible influence of the subduction process) and a mantle upwelling rift-model can be inferred for the MVB and LTVF, whereas an arc setting (subduction-related model) is confirmed for the CAVA.

Finally, the clear continental rift setting for both eastern and central parts of the MVB (E-MVB and C-MVB) as well as the dominance of this tectonic setting for both western and west-central parts (W-MVB and WC-MVB) indicate that this volcanic province could be called the Mexican Volcanic Rift, provided the dominance of the rift setting is also confirmed in future for intermediate and felsic magmas. Some indications, based on large ion lithophile, rare-earth, and high field strength elements, were recently documented by Verma (2009) for the C-MVB. For evaluating the tectonic significance from intermediate and felsic magmas, new discrimination diagrams will have to be proposed using correct statistical methodologies, as pointed out in the present work. A new computer program, TecD by Verma and Rivera-Gómez (2010), will be available for efficient use of these four sets of discriminant function diagrams for basic and ultrabasic magmas.

Acknowledgments

We are grateful to one of the guest editors, Bill Bandy, for extending an invitation to contribute to this special issue. Two of us (SKV and MARG) are grateful to Secretaría de Relaciones Exteriores and Conacyt, respectively, for fellowships towards respective Ph.D. and Master's studies. The first author (SPV) thanks the Universidad Autónoma Metropolitana for support during the development of this work. We are grateful to Samuele Agostini and an anonymous reviewer for helpful comments on an earlier version of this paper.

References

Agostini, S., Corti, G., Doglioni, C., Carminati, E., Innocenti, F., Tonarini, S., Manetti, P., Di Vincenzo, G., and Montanari, D. (2006), *Tectonic and magmatic evolution of the active volcanic front in El Salvador: insight into the Berlín and Ahuachapán geothermal areas*, Geothermics *35*, 368–408.

Agrawal, S. (1999), *Geochemical discrimination diagrams: a simple way of replacing eye-fitted boundaries with probability based classifier surfaces*, J. Geol. Soc. India *54*, 335–346.

Agrawal, S. Guevara, M., and Verma, S.P. (2004), *Discriminant analysis applied to establish major-element field boundaries for tectonic varieties of basic rocks*, Int. Geol. Rev. *46*, 575–594.

Agrawal, S. Guevara, M., and Verma, S.P. (2008), *Tectonic discrimination of basic and ultrabasic rocks through log-transformed ratios of immobile trace elements*, Int. Geol. Rev. *50*, 1057–1079.

AGRAWAL, S. and VERMA, S.P. (2007), *Comment on "Tectonic classification of basalts with classification trees" by Pieter Vermeesch (2006)*, Geochim. Cosmochim. Acta *71*, 3388–3390.

AITCHISON, J., The statistical analysis of compositional data. In: *The statistical analysis of compositional data* (Chapman and Hall, London and New York, pp. 416, 1986).

AITCHISON, J., BARCELÓ-VIDAL, C., MARTÍN-FERNÁNDEZ, J.A., and PAWLOWSKY-GLAHN, V. (2000), *Logratio analysis and compositional distance*, Math. Geol. *32*, 271–275.

AITCHISON, J. and EGOZCUE, J.J. (2005), *Compositional data analysis: where are we and where should we be heading?*, Math. Geol. *37*, 829–850.

ALLAN, J.F. (1986), *Geology of the northern Colima and Zacoalco grabens, southwest Mexico: Late Cenozoic rifting in the Mexican Volcanic Belt*, Geol. Soc. Am. Bull. *97*, 473–485.

ALLAN, J.F. and CARMICHAEL, I.S.E. (1984), *Lamprophyric lavas in the Colima graben, SW Mexico*, Contrib. Mineral. Petrol. *88*, 203–216.

ALLAN, J.F., NELSON, S.A., LUHR, J.F., CARMICHAEL, I.S.E., WOPAT, M., and WALLACE, P.J., Pliocene-Holocene rifting and associated volcanism in southwest Mexico: an exotic terrane in the making. In *The Gulf and Peninsular province of the Californias* (eds. DAUPHIN, J.P. and SIMONEIT, B.R.T.) (The American Association of Petroleum Geologists, Tulsa, Oklahoma, pp. 425–445, 1991).

ALVARADO, G.E., CARR, M.J., TURRIN, B.D., SCHNINCKE, H.-U., and HUDNUT, K.W., Recent volcanic history of Irazú volcano, Costa Rica: alternation and mixing of two magma batches, and pervasive mixing. In: *Volcanic hazards in Central America* (eds. ROSE, W.I., BLUTH, G.J.S., CARR, M.J., EWERT, J., PATINO, L.C., and VALLANCE, J.) (Geological Society of America, pp. 259–276, 2006).

ARCE, J.L., MACÍAS, R., GARCÍA PALOMO, A., CAPRA, L., MACÍAS, J.L., LAYER, P., and RUEDA, H. (2008), *Late Pleistocene flank collapse of Zempoala volcano (central Mexico) and the role of fault reactivation*, J. Volcanol. Geotherm. Res. *177*, 944–958.

BANDY, W.L. and HILDE, T.W.C., Morphology and recent history of the ridge propagator system located at 18°N, 106°W. In: *Cenozoic tectonics and volcanism of Mexico* (eds. Delgado-Granados, H., Aguirre-Díaz, G., and Stock, J.M.) (Geological Society of America, pp. 29–40, 2000).

BANDY, W.L., HILDE, T.W.C., and YAN, C.-Y., The Rivera-Cocos plate boundary: implications for Rivera-Cocos relative motion and plate fragmentation. In: *Cenozoic tectonics and volcanism of Mexico* (eds. DELGADO-GRANADOS, H., AGUIRRE-DÍAZ, G., and STOCK, J.M.) (Geological Society of America, pp. 1–28, 2000).

BARDINTZEFF, J.M. and DENIEL, C. (1992), *Magmatic evolution of Pacaya and Cerro Chiquito volcanological complex, Guatemala*, Bull. Volcanol. *54*, 267–283.

BARNETT, V. and LEWIS, T., *Outliers in statistical data* (Wiley, Chichester 1994).

BAXTER, M.J., BEARDAH, C.C., COOL, H.E.M., and JACKSON, C.M. (2005), *Compositional data analysis of some alkaline glasses*, Math. Geol. *37*, 183–196.

BESCH, T., VERMA, S.P., KRAMMER, U., NEGENDANK, J.F.W., TOBSCHALL, H.J., and EMMERMANN, R. (1995), *Assimilation of sialic crustal material by volcanics of the easternmost extension of the Trans-Mexican Volcanic Belt- Evidence from Sr and Nd isotopes*, Geofís. Int. *34*, 263–281.

BLATTER, D.L., CARMICHAEL, I.S.E., DEINO, A.L., and RENNE, P.R. (2001), *Neogene volcanism at the front of the central Mexican volcanic belt: basaltic andesites to dacites, with contemporaneous shoshonites and high-TiO_2 lava*, Geol. Soc. Am. Bull. *113*, 1324–1342.

BLATTER, D.L., FARMER, G.L., and CARMICHAEL, I.S.E. (2007), *A north-south transect across the Central Mexican Volcanic Belt at ~100°W: spatial distribution, petrological, geochemical, and isotopic characteristics of Quaternary volcanism*, J. Petrol. *48*, 901–950.

BLATTER, D.L. and HAMMERSLEY, L. (2009), *Impact of the Orozco Fracture Zone on the Central Mexican Volcanic Belt*, J. Volcanol. Geotherm. Res. (in press).

BOLGE, L.L., CARR, M.J., FEIGENSON, M.D., and ALVARADO, G.E. (2006), *Geochemical stratigraphy and magmatic evolution at Arenal volcano, Costa Rica*, J. Volcanol. Geotherm. Res. *157*, 34–48.

BOUDAL, C. (1985), Pétrologie d'un grand volcan andésitique mexicain: le Popocatepetl: Thèse de Doctorat, Univ. Clermont-Ferrand II, 140 p.

BRUNI, S., D'ORAZIO, M., HALLER, M.J., INNOCENTI, F., MANETTI, P., PÉCSKAY, Z., and TONARINI, S. (2008), *Time-evolution of magma sources in a continental back-arc setting: the Cenozoic basalts from Sierra de San bernardo (Patagonia, Chubut, Argentina)*, Geol. Mag. *145*, 714–732.

BUCCIANTI, A., MATEAU-FIGUERAS, G., and PAWLOWSKY-GLAHN, V., Compositional data analysis in the geosciences: from theory to practice (Geological Society Special Publication No. 262, London 2006).

BURBACH, G.V., FROHLICH, C., PENNINGTON, W.D., and MATUMOTO, T. (1984), *Seismicity and tectonics of the subducted Cocos plate*, J. Geophys. Res. *89*, 7719–7735.

BUTLER, J.C. and WORONOW, A. (1986), *Discrimination among tectonic settings using trace element abundances of basalts*, J. Geophys. Res. *91*, 10289–10300.

CABANIS, B. and LECOLLE, M. (1989), *Le diagramme La/10–Y/15–Nb/8: un outil pour la discrimination des séries volcaniques et la mise en évidence des processus de mélange et/ou de contamination crustale*, C.R. Acad. Sci. Paris, *309*, 2023–2029.

CARMICHAEL, I.S.E., FREY, H.M., LANGE, R.A., and HILL, C.M. (2006), *The Pleistocene cinder cones surrounding Volcán Colima, Mexico re-visited: eruption ages and volumes, oxidation states, and sulfur content*, Bull. Volcanol. *68*, 407–419.

CARMICHAEL, I.S.E., LANGE, R.A., and LUHR, J.F. (1996), *Quaternary minettes and associated volcanic rocks of Mascota, western Mexico: a consequence of plate extension above a subduction modified mantle wedge*, Contrib. Mineral. Petrol. *124*, 302–333.

CARR, M.J. (1984), *Symmetrical and segmented variation of physical and geochemical characteristics of the Central American volcanic front*, J. Volcanol. Geotherm. Res. *20*, 231–252.

CARR, M.J., FEIGENSON, M.D., and BENNETT, E.A. (1990), *Incompatible element and isotopic evidence for tectonic control of source mixing and melt extraction along the Central American arc*, Contrib. Mineral. Petrol. *105*, 369–380.

CARRASCO-NÚÑEZ, G., RIGHTER, K., CHESLEY, J., SIEBERT, L., and ARANDA-GÓMEZ, J.J. (2005), *Contemporaneous eruption of calc-alkaline and alkaline lavas in a continental arc (Eastern Mexican Volcanic Belt): chemically heterogeneous but isotopically homogeneous source*, Contrib. Mineral. Petrol. *150*, 423–440.

CATHELINEAU, M., OLIVER, R., and NIEVA, D. (1987), *Geochemistry of volcanic series of the Los Azufres geothermal field (Mexico)*, Geofís. Int. *26*, 273–290.

CHAKRABARTI, R., BASU, A.R., SANTO, A.P., TEDESCO, D., and VASELLI, O. (2009), *Isotopic and geochemical evidence for a*

hetrogeneous mantle plume origin of the Virunga volcanics, Western rift, East African Rift system, Chem. Geol. *259*, 273–289.

Chesley, J., Ruiz, J., Righter, K., Ferrari, L., and Gomez-Tuena, A. (2002), *Source contamination versus assimilation: an example from the Trans-Mexican Volcanic Arc*, Earth Planet. Sci. Lett. *195*, 211–221.

Debaille, V., Blichert-Toft, J., Agranier, A., Doucelance, R., Schiano, P., and Albarede, F. (2006), *Geochemical component relationship in MORB from the Mid-Atlantic Ridge, 22–35 N*, Earth Planet. Sci. Lett. *241*, 844–662.

Delgado, H., Molinero, R., Cervantes, P., Nieto-Obregón, J., Lozano-Santa Cruz, R., Macías-González, H.L., Mendoza-Rosales, C., and Silva-Romo, G. (1998), *Geology of Xitle volcano in southern Mexico City—a 2000-year-old monogenetic volcano in an urban area*, Rev. Mex. Cienc. Geol. *15*, 115–131.

Demant, A. (1981), L'axe néo-volcanique transmexicain, étude volcanologique et pétrographique, signification géodynamique *Faculté des Sciences et Techniques de St. Jérome* (Université de Droit, d'Economie et des Sciences d'Aix-Marseille).

Deruelle, B. (1982), *Petrology of the Plio-Quaternary volcanism of the south-central and meridional Andes*. J. Volcanol. Geotherm. Res. *14*, 77–124.

Dixon, J., Clague, D.A., Cousens, B., Monsalve, M.L., and Uhl, J. (2008), *Carbonatite and silicate melt metasomatism of the mantle surrounding the Hawaiian plume: Evidence from volatiles, trace elements, and radiogenic isotopes in rejuvenated-stage lavas from Niihau, Hawaii.*, G3 *9*, 1–34.

Dufrane, S.A., Asmerom, Y., Mukasa, S.B., Morris, J.D., and Dreyer, B.M. (2006), *Subduction and melting processes inferred from U-series, Sr-Nd-Pb isotope, and trace element data, Bicol and Bataan arcs, Philippines.*, Geochemical et Cosmochimica Acta *70*, 3401–3420.

Egozcue, J.J. and Pawlowsky-Glahn, V. (2005), *Groups of parts and their balances in compositional data analysis*, Math. Geol. *37*, 795–828.

Egozcue, J.J., Pawlowsky-Glahn, V., Mateu-Figueras, G., and Barceló-Vidal, C. (2003), *Isometric logratio transformations for compositional data analysis*, Math. Geol. *35*, 279–300.

Elburg, M.A. and Kamenetsky, V.S. (2007), *The origin of medium-K ankaramitic arc magmas from Lombok (Sunda arc, Indonesia): Mineral and melt inclusion evidence*, Chem. Geol. *240*, 260–279.

Espíndola, J.M., Zamora-Camacho, A., Godinez, M.L., Schaaf, P., and Rodríguez, S.R. (2009), *The 1793 eruption of San Martín Tuxtla volcano, Veracruz, Mexico*, J. Volcanol. Geotherm. Res. (in press).

Ferlito, C., Coltorti, M., Cristofolini, R., and Giacomoni, P.P. (2009), *The contemporaneous emission of low-K and high-K trachybasalts and the role of the NE Rift during the 2002 eruptive event, Mt. Etna, Italy*, Bull. Volcanol. *71*, 575–587.

Ferrari, L., Conticelli, S., Vaggelli, G., Petrone, C.M., and Manetti, P. (2000), *Late Miocene volcanism and intra-arc-tectonics during the early development of the Trans-Mexican Volcanic Belt*, Tectonophysics *318*, 161–185.

Ferrari, L., Garduño, V.H., Innocenti, F., Manetti, P., Pasquare, G., and Vaggelli, G. (1994), *A widespread mafic volcanic unit at the base of the Mexican Volcanic Belt between Guadalajara and Querétaro*, Geofís. Int. *33*, 107–123.

Ferrari, L., Petrone, C.M., and Francalanci, L. (2001), *Generation of oceanic-island basalt-type volcanism in the western Trans-Mexican volcanic belt by slab rollback, asthenosphere infiltration, and variable flux melting*, Geology *29*, 507–510.

Ferrari, L., Petrone, C.M., and Francalanci, L. (2002), *Reply: "Generation of oceanic-island basalt type volcanism in the western Trans-Mexican volcanic belt by slab rollback, asthenosphere infiltration, and variable flux melting"*, Geology *114*, 858–859.

Ferrari, L. and Rosas-Elguera, J. (1999), *Alkalic (ocean-island basalt type) and calc-alkaline volcanism in the Mexican volcanic belt: a case for plume-related magmatism and propagating rifting at an active margin? Comment and reply*, Geology *27*, 1055–1056.

Ferriz, H. and Mahood, G.A. (1987), *Strong compositional zonation in a silicic magmatic system: Los Humeros, Mexican Neovolcanic Belt*, J. Petrol. *28*, 171–209.

Finney, B., Turner, S., Hawkesworth, C., Larsen, J., Nye, C., George, R., Bindeman, I., and Eichelberger, J. (2008), *Magmatic differentiation at an Island -arc Caldera: Okmok Volcano, Aleutian Islands, Alaska*, J. Petrol. *49*, 857–884.

Frey, F.A., Gerlach, D.C., Hickey, R.L., Lopez-Escobar, L., And Munizaga-Villavicencio, F. (1984), *Petrogenesis of the Laguna del Maule volcanic complex, Chile (36°S)*, Contrib. Mineral. Petrol. *88*, 133–149.

Frey, H.M., Lange, R.A., Hall, C.M., Delgado-Granados, H., and Carmichael, I.S.E. (2007), *A Pliocene ignimbrite flare-up along the Tepic-Zacoalco rift: evidence for the initial stages of rifting between the Jalisco block (Mexico) and North America*, Geol. Soc. Am. Bull. *119*, 49–64.

García-Palomo, A., Macías, J.L., Tolson, G., Valdez, G., and Mora, J.C. (2002), *Volcanic stratigraphy and geological evolution of the Apan region, east-central sector of the Trans-Mexican volcanic belt*, Geofís. Int. *41*, 133–150.

Gastil, G., Krummenacher, D., and Minch, J. (1979), *The record of Cenozoic volcanism around the Gulf of California*, Geol. Soc. Am. Bull. *90*, 839–857.

Gerlach, D.C., Frey, F.A., Moreno-Roa, H., and Lopez-Escobar, L. (1988), *Recent volcanism in the Puyehue-Cordon Caulle region, southern Andes, Chile (40.5°S): petrogenesis of evolved lavas*, J. Petrol. *29*, 333–382.

Gilbert, C.M., Mahood, G.A., and Carmichel, I.S.E. (1985), *Volcanic stratigraphy of the Guadalajara area, Mexico*, Geofís. Int. *24*, 169–191.

Gómez-Tuena, A., Lagatta, A.B., Langmuir, C.H., Goldstein, S.L., Ortega-Gutiérrez, F., and Carrasco-Nuñez, G. (2003), *Temporal control of subduction magmatism in the eastern Trans-Mexican volcanic belt: mantle sources, slab contributions, and crustal contamination*, Geochem. Geophys, Geosyst. *4*, 8912. doi:10.1029/2003GC000524.

Gómez-Tuena, A., Langmuir, C.H., Goldstein, S.L., Straub, S.M., and Ortega-Gutiérrez, F. (2007), *Geochemical evidence for slab melting in the Trans-Mexican Volcanic Belt*, J. Petrol. *48*, 537–562.

Gunn, B.M. and Mooser, F. (1971), *Geochemistry of the volcanics of central Mexico*, Bull. Volcanol. *34*, 577–613.

Harry, D.L. and Green, N.L. (1999), *Slab dehydration and basalt petrogenesis in subduction systems involving very young oceanic lithosphere*, Chem. Geol. *160*, 309–333.

Hasenaka, T., *Chemical compositions of selected samples*. In *Subduction volcanism and tectonics of western Mexican Volcanic Belt. International Scientific Research Program (No. 03041014) Japan-Mexico Co-operative Research* (ed. Aoki, K.) (The

Faculty of Science, Tohoku University, Sendai, Japan, pp. 238–247, 1992).

HASENAKA, T. and CARMICHAEL, I.S.E. (1987), *The cinder cones of Michoacán-Guanajuato, Central Mexico: petrology and chemistry*, J. Petrol. *28*, 241–269.

HAZLETT, R.W. (1987), *Geology of San Cristobal volcanic complex, Nicaragua*, J. Volcanol. Geotherm. Res. *33*, 223–230.

HELLEVANG, B. and PEDERSEN, R.B. (2008), *Magma ascent and crustal accretion at ultraslow-spreading ridges: constraints from plagioclase ultraphyric basalts from the Arctic Mid-Ocean Ridge*, J. Petrol. *49*, 267–294.

HICKEY-VARGAS, R., MORENO ROA, H., LOPEZ ESCOBAR, L., AND FREY, F.A. (1989), *Geochemical variations in Andean basaltic and silicic lavas from the Villarrica-Lanin volcanic chain (39.5°S): an evaluation of source heterogeneity, fractional crystallization and crustal assimilation*, Contrib. Mineral. Petrol. *103*, 361–386.

IRELAND, T.J., WALKER, R.J., and GARCIA, M.O. (2009), *Highly siderophile elements and 187Os isotope systematics of Hawaiian picrites: Implications for parental melt composition and source heterogeneity*, Chem. Geol. *260*, 112–128.

JOHNSON, C.A. and HARRISON, C.G.A. (1989a), *Thematic mapper studies of volcanism and tectonism in central Mexico*, Adv. Space Res. *9*, 85–88.

JOHNSON, C.A. and HARRISON, C.G.A. (1989b), *Tectonics and volcanism in central Mexico: a Landsat thematic mapper perspective*, Remote Sens. Environ. *28*, 273–286.

LA FEMINA, P.C., CONNOR, C.B., HILL, B.E., STRAUCH, W., and SABALLOS, A. (2004), *Magma-tectonic interactions in Nicaragua: the 1999 seismic swarm and eruption of Cerro Negro volcano*, J. Volcanol. Geotherm. Res. *137*, 187–199.

LANGE, R.A. and CARMICHAEL, I.S.E. (1991), *A potassic volcanic front in western Mexico: the lamprophyric and related lavas of San Sabastian*, Geol. Soc. Am. Bull. *103*, 928–940.

LE BAS, M.J. (2000), *IUGS reclassification of the high-Mg and picritic volcanic rocks*, J. Petrol. *41*, 1467–1470.

LE BAS, M.J., LE MAITRE, R.W., STRECKEISEN, A., and ZANETTIN, B. (1986), *A chemical classification of volcanic rocks based on the total alkali-silica diagram*, J. Petrol. *27*, 745–750.

LEEMAN, W.P., CARR, M.J., and MORRIS, J.D. (1994), *Boron geochemistry of the Central American Volcanic Arc: Constraints on the genesis of subduction-related magmas*, Geochim. Cosmochim. Acta *58*, 149–168.

LEWIS-KENEDI, C.B., LANGE, R.A., HALL, C.M., and DELGADO GRANADOS, H. (2005), *The eruptive history of the Tequila volcanic field, western Mexico: ages, volumes, and relative proportions of lava types*, Bull. Volcanol. *67*, 391–414.

LÓPEZ-ESCOBAR, L., VERGARA, M., and FREY, F.A. (1981), *Petrology and geochemistry of lavas from Antuco volcano, a basaltic volcano of the southern Andes (37°25′)*, J. Volcanol. Geotherm. Res. *11*, 329–352.

LÓPEZ-ESCOBAR, L., TAGIRI, M., and VERGARA, M. (1991), *Geochemical features of southern Andes Quaternary volcanics between 41°5′ and 43°00′S.*, Geol. Soc. Am. Special Pap. *265*, 45–56.

LÓPEZ-ESCOBAR, L., KILIAN, R., KEMPTON, P.D., and TAGIRI, M. (1993), *Petrography and geochemistry of Quaternary rocks from the southern volcanic zone of the Andes between 41°30′ and 46°00′S, Chile*, Rev. Geol. Chile *20*, 33–35.

LUHR, J.F. (1997), *Extensional tectonics and the diverse primitive volcanic rocks in the western Mexican Volcanic Belt*, Can. Min. *35*, 473–500.

LUHR, J.F., ALLAN, J.F., CARMICHAEL, I.S.E., NELSON, S.A., and HASENAKA, T. (1989), *Primitive calc-alkaline and alkaline rock types from the western Mexican Volcanic Belt*, J. Geophys. Res. *94*, 4515–4530.

LUHR, J.F. and CARMICHAEL, I.S.E. (1981), *The Colima volcanic complex, Mexico: Part II. Late-Quaternary cinder cones*, Contrib. Mineral. Petrol. *76*, 127–147.

LUHR, J.F. and CARMICHAEL, I.S.E. (1985), *Jorullo Volcano, Michoacán, México (1759–1774): The earliest stages of fractionation in calc-alkaline magmas*, Contrib. Mineral. Petrol. *90*, 142–161.

LUHR, J.F., NELSON, S.A., ALLAN, J.F., and CARMICHAEL, I.S.E. (1985), *Active rifting in southwestern Mexico: Manifestations of an incipient eastward spreading-ridge jump*, Geology *13*, 54–57.

LYLE, M. and NESS, G.E., *The opening of the southern Gulf of California*. In *The Gulf and Peninsular province of the Californias* (eds. DAUPHIN, J.P. and SIMONEIT, B.R.T.) (The American Association of Petroleum Geologists, Tulsa, Oklahoma, pp. 403–423, 1991).

MACDONALD, R., BELKIN, H.E., FITTON, J.G., ROGERS, N.W., NEJBERT, K., TINDLE, A.G., and MARSHALL, A.S. (2008), *The role of fractional crystellization, magma mixing, crystal mush remobilization and volatile-melt interactions in the genesis of young basalt-peralkaline rhyolite suite, the Greater Olkaria Volcanic Complex, Kenya Rift Valley*, J. Petrol. *49*, 1515–1547.

MARIA, A.H. and LUHR, J.F. (2008), *Lamprophyres, basanites, and basalts of the western Mexican Volcanic Belt: volatile contents and a vein-wall rock melting relationship*, J. Petrol. *49*, 2123–2156.

MÁRQUEZ, A., OYARZUN, R., DOBLAS, M., and VERMA, S.P. (1999a), *Alkalic (ocean-island basalt type) and calc-alkalic volcanism in the Mexican Volcanic Belt: a case for plume-related magmatism and propagating rifting at an active margin?*, Geology *27*, 51–54.

MÁRQUEZ, A., OYARZUN, R., DOBLAS, M., and VERMA, S.P. (1999b), *Reply (to Comment by L. Ferrari and J. Rosas Elguera on "Alkalic (ocean basalt type) and calc-alkalic volcanism in the Mexican volcanic belt: a case of plume-related magmatism and propagating rift at an active margin?" Comment and Reply*, Geology *27*, 1055–1056.

MARSKE, J.P., GARCIA, M.O., PIETRUSZKA, A.J., RHODES, J.M., and NORMAN, M.D. (2008), *Geochemical variations during Kilauea's pu'u 'O'o eruption reveal a fine-scale mixture of mantle heterogeneities within the Hawaiian plume*, J. Petrol. *49*, 1297–1318.

MARTIN DEL POZZO, A.L., Geoquímica y paleomagnetismo de la Sierra Chichinautzin *Facultad de Ciencias* (U.N.A.M., Mexico, D.F., pp. 148, 1989).

MARTIN DEL POZZO, A.L., ROMERO, V.H., and RUIZ KITCHER, R.E. (1987), *Los flujos piroclásticos del volcán de Colima, México*, Geofís. Int. *26*, 291–307.

MCDERMOTT, F., DELFIN JR, F.G., DEFANT, M.J., TURNER, S., and MAURY, R. (2005), *The Petrogenesis of volcanics from Mt. Bulusan and Mt. Mayon in the Bicol arc, the Philippines*, Contrib. Mineral. Petrol. *150*, 652–670.

MERIGGI, L., MACÍAS, J.L., TOMMASINI, S., CAPRA, L., and CONTICELLI, S. (2008), *Heterogeneous magmas of the Quaternary Sierra Chichinautzin volcanic field (central Mexico): the role of an amphibole-bearing mantle and magmatic evolution processes*, Rev. Mex. Cienc. Geol. *25*, 197–216.

MESCHEDE, M. (1986), *A method of discriminating between different types of mid-ocean ridge basalts and continental tholeiites with the Nb–Zr–Y diagram*, Chem. Geol. *56*, 207–218.

MIDDLEMOST, E.A.K. (1989), *Iron oxidation ratios, norms and the classification of volcanic rocks*, Chem. Geol. *77*, 19–26.

MOORE, G., MARONE, C., CARMICHAEL, I.S.E., and RENNE, P. (1994), *Basaltic volcanism and extension near the intersection of the Sierra Madre volcanic province and the Mexican Volcanic Belt*, Geol. Soc. Am. Bull. *106*, 383–394.

MORI, L., GÓMEZ-TUENA, A., SCHAAF, P., GOLDSTEIN, S.J., PÉREZ-ARVIZU, O., and SOLÍS-PICHARDO, G. (2009), *Lithospheric removal as a trigger for flood basalt magmatism in the Trans-Mexican Volcanic Belt*, J. Petrol. *50*, 2157–2186.

MULLEN, E.D. (1983), *$MnO/TiO_2/P_2O_5$: a minor element discrimination for basaltic rocks of oceanic environments and its implications for petrogenesis*, Earth Planet. Sci. Lett. *62*, 53–62.

NAKAMURA, K., KATO, Y., TAMAKI, K., and ISHII, T. (2007), *Geochemistry of hydrothermally altered basaltic rocks from the Southwest Indian Ridge near Rodriguez Triple Junction*, Marine Geol. *239*, 125–141.

NEGENDANK, J.F.W. (1972), *Geochemical aspects of volcanic rocks of the Valley of Mexico*, Geofís. Int. *11*, 267–278.

NEGENDANK, J.F.W., EMMERMANN, R., KRAWCZYK, R., MOOSER, F., TOBSCHALL, H., and WERLE, D. (1985), *Geological and geochemical investigations on the eastern Trans Mexican Volcanic Belt*, Geofís. Int. *24*, 477–575.

NELSON, S.A. (1986), *Geologiá del Volcán Ceboruco, Nayrit, con una estimación de riesgos de erupciones futuras*, Rev. Inst. Geol. UNAM *6*, 243–258.

NELSON, S.A. and GONZALEZ-CAVER, E. (1992), *Geology and K-Ar dating of the Tuxtla volcanic field, Veracruz, Mexico*, Bull. Volcanol. *55*, 85–96.

NELSON, S.A., GONZALEZ-CAVER, E., and KYSER, T.K. (1995), *Constraints on the origin of alkaline and calc-alkaline magmas from the Tuxtla Volcanic Field, Veracruz, Mexico*, Contrib. Mineral. Petrol. *122*, 191–211.

NELSON, S.A. and LIVIERES, R.A. (1986), *Contemporaneous calc-alkaline and alkaline volcanism at Sanganguey volcano, Nayarit, Mexico*, Geol. Soc. Am. Bull. *97*, 798–808.

OHBA, T., MATSUOKA, K., KIMURA, Y., ISHIKAWA, H., and FUJIMAKI, H. (2009), *Deep crystallization differentiation of arc tholeiite basalt magmas from Northern Honshu Arc, Japan*, J. Petrol. *50*, 1025–1046.

OROZCO-ESQUIVEL, M.T., Zur Petrologie des Vulkangebietes von Palma-Sola, Mexiko. Ein Beispiel fuer den Uebergang von anorogenem zu orogenem Vulkanismus. *Institut für Petrographie und Geochemie* (Universitaet Karlsruhe, Karlsruhe, Germany, 167 p, 1995).

OROZCO-ESQUIVEL, T., PETRONE, C.M., FERRARI, L., TAGAMI, T., and MANETTI, P. (2007), *Geochemical and isotopic variability in lavas from the eastern Trans-Mexican Volcanic Belt: slab detachment in a subduction zone with varying dip*, Lithos *93*, 149–174.

PACHECO, J.F. and SINGH, S.K. (2010), *Seismicity and state of stress in Guerrero segment of the Mexican subduction zone*, J. Geophys. Res. *115*. doi:10.1029/2009JB006453.

PARDO, M. and SUÁREZ, G. (1995), *Shape of the subducted Rivera and Cocos plates in southern Mexico: Seismic and tectonic implications*, J. Geophys. Res. *100*, 12357–12373.

PATINO, L.C., CARR, M.J., and FEIGENSON, M.D. (1997), *Cross-arc geochemical variations in volcanic fields in Honduras C.A.: progressive changes in source with distance from the volcanic front*, Contrib. Mineral. Petrol. *129*, 341–351.

PATINO, L.C., CARR, M.J., and FEIGENSON, M.D. (2000), *Local and regional variations in Central American arc lavas controled by variations in subducted sediment input*, Contrib. Mineral. Petrol. *138*, 265–283.

PEARCE, J.A. (1976), *Statistical analysis of major element patterns in basalts*, J. Petrol. *17*, 15–43.

PEARCE, J.A., Trace element characteristics of lavas from destructive plate boundaries. In: *Andesites* (ed. Thorpe, R.S.) (Wiley, Chichester, pp. 525–548, 1982).

PEARCE, J.A. and CANN, J.R. (1971), *Ophiolite origin investigated by discriminant analysis using Ti, Zr and Y*, Earth Planet. Sci. Lett. *12*, 339–349.

PEARCE, J.A. and CANN, J.R. (1973), *Tectonic setting of basic volcanic rocks determined using trace element analyses*, Earth Planet. Sci. Lett. *19*, 290–300.

PEARCE, J.A. and GALE, G.H. (1977), *Identification of ore-deposition environment from trace-element geochemistry of associated igneous host rocks*, Geol. Soc. London Spec. Publ. *7*, 14–24.

PEARCE, J.A. and NORRY, M.J. (1979), *Petrogenetic implications of Ti, Zr, Y, and Nb variations in volcanic rocks*, Contrib. Mineral. Petrol. *69*, 33–47.

PEARCE, T.H., GORMAN, B.E., and BIRKETT, T.C. (1977), *The relationship between major element chemistry and tectonic environment of basic and intermediate volcanic rocks*, Earth Planet. Sci. Lett. *36*, 121–132.

PECCERILLO, A., DONATI, C., SANTO, A.P., ORLANDO, A., YIRGU, G., and AYALEW, D. (2007), *Petrogenesis of silicic peralkaline rocks in the Ethiopian Rift: geochemical evidence and volcanological implications*, J. Afr. Earth Sci. *48*, 161–173.

PÉREZ R., J., PAL, S., TERRELL, D.J., URRUTIA F., J., and LÓPEZ M., M. (1979), *Preliminary report on the analysis of some "in-house" geochemical reference samples from Mexico*, Geofís. Int. *18*, 197–209.

PÉREZ-CAMPOS, X., KIM, Y., HUSKER, A., DAVIS, P.M., CLAYTON, R.W., IGLESIAS, A., PACHECO, J.F., SINGH, S.K., MANEA, V.C., and GURNIS, M. (2008), *Horizontal subduction and truncation of the Cocos plate beneath central Mexico*, Geophys. Res. Lett. *35*, L18303.

PETRONE, C.M., FRANCALANCI, L., CARLSON, R.W., FERRARI, L., and CONTICELLI, S. (2003), *Unusual coexistence of subduction-related and intraplate-type magmatism: Sr, Nd and Pb isotope and trace element data from the magmatism of the San Pedro-Ceboruco graben (Nayarit, Mexico)*, Chem. Geol. *193*, 1–24.

RAY, D., IYER, S.D., BANEREJE, R., MISRA, S., and WIDDOWSON, M. (2007), *A petrogenetic model of basalts from the northern Central Indian Ridge: 3–11°S*, Acta Geol. Sinica *81*, 99–112.

REAGAN, M.K. and GILL, J.B. (1989), *Coexisting calcalkaline and high-niobium basalts from Turrialba volcano, Costa Rica: implications for residual titanates in arc magma sources*, J. Geophys. Res. *94*, 4619–4633.

REGELOUS, M., NIU, Y., ABOUCHAMI, W., and CASTILLO, P.R. (2009), *Shallow origin for South Atlantic Dupal anomaly from lower continental crust: geochemical evidence from the Mid-Atlantic Ridge at 26 S*, Lithos *112*, 57–72.

RIGHTER, K. and CARMICHAEL, I.S.E. (1992), *Hawaiite and related lavas in the Atenguillo graben, western Mexican Volcanic Belt*, Geol. Soc. Am. Bull. *104*, 1592–1607.

RIGHTER, K., CARMICHAEL, I.S.E., BECKER, T.A., and RENNE, P.R. (1995), *Pliocene-Quaternary volcanism and faulting at the intersection of the Gulf of California and the Mexican Volcanic Belt*, Geol. Soc. Am. Bull. *107*, 612–626.

Righter, K. and Rosas-Elguera, J. (2001), *Alkaline lavas in the volcanic front of the western Mexican Volcanic Belt: geology and petrology of the Ayutla and Tapalpa volcanic fields*, J. Petrol. *42*, 2333–2361.

Robin, C. (1976), *Présence simultanée de magmatismes de significations tectoniques opposées dans l'Est du Mexique*, Bull. Soc. Geol. Fr. *18*, 1637–1645.

Robin, C., Camus, G., Cantagrel, J.M., Gourgaud, A., Mossand, P., Vincent, P.M., Aubert, M., Dorel, J., and Murray, J.M. (1984), *Les volcanes de Colima (Mexique)*, Bull. P.I.R.P.S.E.V. *87*, 98 p.

Robin, C., Komorowski, J.-C., Boudal, C., and Mossand, P. (1990), *Mixed-magma pyroclastic surge deposits associated with debris avalanche deposits at Colima volcanoes, Mexico*, Bull. Volcanol. *52*, 391–403.

Robin, C. and Potrel, A. (1993), *Multi-stage magma mixing in the pre-caldera series of Fuego de Colima volcano*, Geofís. Int. *32*, 605–615.

Robin, C. and Tournon, J. (1978), *Spatial relations of andesitic and alkaline provinces of Mexico and Central America*, Can. J. Earth Sci. *15*, 1633–1641.

Rodríguez, S.R., Morales-Barrera, W., Layer, P., and González-Mercado, E. (2009), *A Quaternary monogenetic volcanic field in the Xalapa region, eastern Trans-Mexican Volcanic Belt: geology, distribution and morphology of the volcanic event*, J. Volcanol. Geotherm. Res. (in press).

Rogers, N.W., Thomas, L.E., Macdonald, R., Hawkesworth, C.J., and Mokadem, F. (2006), *238U-230Th disequilibrium in recent basalts and dynamic melting beneath the Kenya Rift*, Chem. Geol. *234*, 148–168.

Rollinson, H.R. (1993), *Using geochemical data: evaluation, presentation, interpretation* (Essex, Longman Scientific Technical).

Ronga, F., Lustrino, M., Marzoli, A., and Melluso, L. (2009), *Petrogenesis of a basalt-comendite-pantellerite rock suite: the Boseti Volcanic Complex (Main Ethiopian Rift)*, Miner. Petrol. doi:10.1007/s00710-009-0064-3.

Rooney, T., Furman, T., Bastow, I., Ayalew, D., and Yirgu, G. (2007), *Lithospheric modification during crustal extension in the Main Ethiopian Rift*, J. Geophys. Res. *112*, B10201. doi: 10.1029/2006JB004916.

Rossotti, A., Carrasco-Nuñez, G., Rosi, M., and Di Muro, A. (2006), *Eruptive dynamics of the "Citlaltépetl pumice" at Citlaltépetl volcano, eastern Mexico*, J. Volcanol. Geotherm. Res. *158*, 401–429.

Ryder, C.H., Gill, J.B., Tepley III, F., Ramos, F., and Reagan, M. (2006), *Closed- to open-system differentiation at Arenal volcano (1968–2003)*, J. Volcanol. Geotherm. Res. *157*, 75–93.

Schaaf, P., Stimac, J., Siebe, C., and Macías, J.L. (2005), *Geochemical evidence for mantle origin and crustal processes in volcanic rocks from Popocatépetl and surrounding monogenetic volcanoes, central Mexico*, J. Petrol. *46*, 1243–1282.

Schuth, S., Munker, C., Konig, S., Qopoto, C., Basi, S., Schonberg, D.G., and Ballhaus, C. (2009), *Petrogenesis of lavas along the Solomon Island Arc, SW Pacific: coupling of compositional variations and subduction zone geometry*, J. Petrol. *50*, 781–811.

Sendjaja, Y.A., Kimura, J., and Sunardi, E. (2009), *Across-arc geochemical variation of Quaternary lavas in West Java, Indonesia: Mass-balance elucidation using arc basalt simulator model*, Island Arc *18*, 201–224.

Shervais, J.W. (1982), *Ti-V plots and the petrogenesis of modern and ophiolitic lavas*, Earth Planet. Sci. Lett. *59*, 101–118.

Sheth, H.C. (2008), *Do major oxide tectonic discrimination diagrams work? Evaluating new log-ratio and discriminant-analysis-based diagrams with Indian Ocean mafic volcanics and Asian ophiolites*, Terra Nova *20*, 229–236.

Sheth, H.C., Torres-Alvarado, I.S., and Verma, S.P. (2000), *Beyond subduction and plumes: a unified tectonic-petrogenetic model for the Mexican Volcanic Belt*, Int. Geol. Rev. *42*, 1116–1132.

Siebe, C., Rodríguez-Lara, V., Schaaf, P., and Abrams, M. (2004), *Geochemistry, Sr-Nd isotope composition, and tectonic setting of Holocene Pelado, Guespalapa and Chichinautzin scoria cones, south of Mexico City*, J. Volcanol. Geotherm. Res. *130*, 197–226.

Siebert, L. and Carrasco-Núñez, G. (2002), *Late-Pleistocene to precolumbian behind-the-arc mafic volcanism in the eastern Mexican Volcanic Belt; implications for future hazards*, J. Volcanol. Geotherm. Res. *115*, 179–205.

Silva Mora, L. (1988), *Algunos aspectos de los basaltos y andesitas cuaternarias de Michoacán Oriental*, Rev. Inst. Geol. UNAM *7*, 89–96.

Straub, S.M., Lagatta, A.B., Pozzo, A.L.M., and Langmuir, C.H. (2008), *Evidence from high-Ni olivines for a hybridized peridotite/pyroxenite source for orogenic andesites from the central Mexican Volcanic Belt*, Geochem. Geophys. Geosys. *9*, 7 March 2008.

Suter, M., Aguirre, G., Siebe, C., Quintero, O., and Komorowski, J.C. (1991), Volcanism and active faulting in the central part of the Trans-Mexican Volcanic Belt, Mexico. In *Geological excursions in southern California and Mexico. Guidebook 1991 Annual Meeting Geological Society of America* (eds. Walawender, M.J. and Hanan, B.B.) (Geological Society of America, San Diego, pp. 224–243, 1991).

Suter, M., Quintero, O., and Johnson, C.A. (1992), *Active faults and state of stress in the central part of the Trans-Mexican Volcanic Belt, Mexico. 1. The Venta de Bravo fault*, J. Geophys. Res. *97*, 11983–11993.

Suter, M., Carrillo Martínez, M., López Martínez, M., And Farrar, E. (1995a), *The Aljibes half-graben—active extension at the boundary between the Trans-Mexican Volcanic Belt and the basin and range province, Mexico*, Geol. Soc. Am. Bull. *107*, 627–641.

Suter, M., Quintero-Legorreta., O., López-Martínez, M., Aguirre-Díaz, G., and Farrar, E. (1995b), *The Acambay graben: active intraarc extension in the Trans-Mexican Volcanic Belt, Mexico*, Tectonics *14*, 1245–1262.

Suter, M., López Martínez, M., Quintero Legorreta, O., And Carrillo Martínez, M. (2001), *Quaternary intra-arc extension in the central Trans-Mexican volcanic belt*, Geol. Soc. Am. Bull. *113*, 693–703.

Swinamer, R.T., The geomorphology, petrography, geochemistry and petrogenesis of the volcanic rocks in the Sierra del Chichinautzin, Mexico *Department of Geological Sciences* (Kingston, Queen's University, 212 p, 1989).

Takamasa, A., Nakai, S., Sahoo, Y., Hanyum, T., and Tatsumi, Y. (2009), *W isotope compositions of oceanic islands basalts from French Polynesia and their meaning for core-mantle interaction*, Chem. Geol. *260*, 37–46.

Tamura, Y., Tani, K., Chang, Q., Shukuno, H., Kawabata, H., Ishizuka, O., And Fiske, R.S. (2007), *Wet and dry basalt magma evolution at Torishima Volcano, Izu-Bonin Arc, Japan: the*

possible role of phengite in the downgoing slab, J. Petrol. *48*, 1999–2031.

TORMEY, D.R., HICKEY-VARGAS, R., FREY, F.A., and LÓPEZ-ESCOBAR, L., *Recent lavas from the Andean volcanic front (33 to 42°S); interpretations of along-arc compositional variations*. In *Andean magmatism and its tectonic setting, Geological Society of America Special Paper* (eds. HARMON, R.S. and RAPELA, C.W.) (Boulder, Colorado, Geological Society of America, pp. 57–77, 1991).

TORRES-ALVARADO, I.S., PANDARINATH, K., VERMA, S.P., and DULSKI, P. (2007), *Mineralogical and geochemical effects due to hydrothermal alteration in the Los Azufres geothermal field, Mexico*, Rev. Mex. Cienc. Geol. *24*, 15–24.

TORRES-ALVARADO, I.S., VERMA, S.P., and VELASCO-TAPIA, F. (2002), *Comment and reply to "Generation of oceanic-island basalt type volcanism in the western Trans-Mexican volcanic belt by slab rollback, asthenosphere infiltration, and variable flux melting"*, Geology *30*, 857–858.

TURNER, S., HAWKESWORTH, C.J., CALSTEREN, P.V., HEATH, E., MACDONALD, R., and BLACK, S. (1996), *U-series isotopes and destructive plate margin magma genesis in the Lesser Antilles*, Earth Planet. Sci. Lett. *142*, 191–207.

VELASCO-TAPIA, F. and VERMA, S.P. (2001), *First partial melting inversion model for a rift-related origin of the Sierra de Chichinautzin volcanic field, central Mexican Volcanic Belt*, Int. Geol. Rev. *43*, 788–817.

VERGARA, M., LÓPEZ-ESCOBAR, L., PALMA, J.L., HICKEY-VARGAS, R., and ROESCHMANN, C. (2004), *Late Tertiary volcanic episodes in the area of the city of Santiago de Chile: new geochronological and geochemical data*, J. South. Am. Earth. Sci. *17*, 227–238.

VERMA, S.P. (1983), *Magma genesis and chamber processes at Los Humeros caldera, Mexico—Nd and Sr isotope data*, Nature *301*, 52–55.

VERMA, S.P., *Geochemistry of the subducting Cocos plate and the origin of subduction-unrelated mafic volcanism at the volcanic front of the central Mexican Volcanic Belt*. In *Cenozoic tectonics and volcanism of Mexico* (eds. DELGADO-GRANADOS, H., AGUIRRE-DÍAZ, G., and STOCK, J.M.) (Geological Society of America, pp. 195–222, 2000a).

VERMA, S.P. (2000b), *Geochemical evidence for a lithospheric source for magmas from Los Humeros caldera, Puebla, Mexico*, Chem. Geol. *164*, 35–60.

VERMA, S.P. (2001a), *Geochemical evidence for a lithospheric source for magmas from Acoculco caldera, eastern Mexican Volcanic Belt*, Int. Geol. Rev. *43*, 31–51.

VERMA, S.P. (2001b), *Geochemical evidence for a rift-related origin of bimodal volcanism at Meseta Río San Juan, North-Central Mexican volcanic belt*, Int. Geol. Rev. *43*, 475–493.

VERMA, S.P. (2001c), *Geochemical and Sr–Nd–Pb isotopic evidence for a combined assimilation and fractional crystallisation process for volcanic rocks from the Huichapan caldera, Hidalgo, Mexico*, Lithos *56*, 141–164.

VERMA, S.P. (2002), *Absence of Cocos plate subduction-related basic volcanism in southern Mexico: a unique case on Earth?*, Geology *30*, 1095–1098.

VERMA, S.P. (2003), *Geochemical and Sr-Nd isotopic evidence for a rift-related origin of magmas in Tizayuca volcanic field, Central Mexican Volcanic Belt*, J. Geol. Soc. India *61*, 257–276.

VERMA, S.P. (2004), *Solely extension-related origin of the eastern to west-central Mexican Volcanic Belt (Mexico) from partial melting inversion model*, Curr. Sci. *86*, 713–719.

VERMA, S.P. (2006), *Extension related origin of magmas from a garnet-bearing source in the Los Tuxtlas volcanic field, Mexico*, Int. J. Earth Sci. *95*, 871–901.

VERMA, S.P. (2009), *Continental rift setting for the central part of the Mexican Volcanic Belt: a statistical approach*, Open Geol. J. *3*, 8–29.

VERMA, S.P. (2010), *Statistical evaluation of bivariate, ternary and discriminant function tectonomagmatic discrimination diagrams*, Turk. J. Earth Sci. *19*, 185–238.

VERMA, S.P. and AGRAWAL, S. (2010), *Discriminant function discrimination diagrams for basic and ultrabasic volcanic rocks through log-transformed ratios of high field strength elements and implications for petrogenetic processes*, Rev. Mex. Cienc. Geol. (in press).

VERMA, S.P. and HASENAKA, T. (2004), *Sr, Nd, and Pb isotopic and trace element geochemical contraints for a veined-mantle source of magmas in the Michoacán-Guanajuato volcanic field, west-central Mexican Volcanic Belt*, Geochem. J. *38*, 43–65.

VERMA, S.P. and LOPEZ M., (1982), *Geochemistry of Los Humeros caldera, Puebla, Mexico*, Bull. Volcanol. *45*, 63–79.

VERMA, S.P. and LUHR, J.F. (2010), *Sr, Nd, and Pb isotopic evidence for the origin and evolution of the Cántaro-Colima Volcanic Chain, Western Mexican Volcanic Belt*, J. Volcanol. Geotherm. Res. (submitted).

VERMA, S.P. and NELSON, S.A. (1989a), *Isotopic and trace element constraints on the origin and evolution of alkaline and calc-alkaline magmas in the northwestern Mexican Volcanic Belt*, J. Geophys. Res. *94*, 4531–4544.

VERMA, S.P. and NELSON, S.E. (1989b), *Correction to "Isotopic and trace element constraints on the origin and evolution of alkaline and calc-alkaline magmas in the northwestern Mexican Volcanic Belt" by Surendra P. Verma and Stephen A. Nelson*, J. Geophys. Res. *94*, 7679–7681.

VERMA, S.P. and QUIROZ-RUIZ, A. (2006a), *Critical values for six Dixon tests for outliers in normal samples up to sizes 100, and applications in science and engineering*, Rev. Mex. Cienc. Geol. *23*, 133–161.

VERMA, S.P. and QUIROZ-RUIZ, A. (2006b), *Critical values for 22 discordancy test variants for outliers in normal samples up to sizes 100, and applications in science and engineering*, Rev. Mex. Cienc. Geol. *23*, 302–319.

VERMA, S.P. and QUIROZ-RUIZ, A. (2008), *Critical values for 33 discordancy test variants for outliers in normal samples for very large sizes of 1,000 to 30,000*, Rev. Mex. Cienc. Geol. *25*, 369–381.

VERMA, S.P. and RIVERA-GÓMEZ, M.A. (2010), *TecD: A new computer program for tectonomagmatic discrimination from discriminant function diagrams for basic and ultrabasic magmas*, Rev. Mex. Cienc. Geol. (submitted).

VERMA, S.P., SALAZAR-V., A., NEGENDANK, J.F.W., MILÁN, M., NAVARRO-L., I., and BESCH, T. (1993), *Características petrográficas y geoquímicas de elementos mayores del campo volcánico de Los Tuxtlas, Veracruz, México*, Geofís. Int. *32*, 237–248.

VERMA, S.P., TORRES-ALVARADO, I.S., and SOTELO-RODRÍGUEZ, Z.T. (2002), *SINCLAS: standard igneous norm and volcanic rock classification system*, Comput. Geosci. *28*, 711–715.

VERMA, S.P., TORRES-ALVARADO, I.S., and VELASCO-TAPIA, F. (2003), *A revised CIPW norm*, Schweiz. Miner. Petrog. Mitteil. *83*, 197–216.

VERMA, S.P., GUEVARA, M., and AGRAWAL, S. (2006), *Discriminating four tectonic settings: five new geochemical diagrams for basic and ultrabasic volcanic rocks based on log-ratio transformation of major-element data*, J. Earth Syst. Sci. *115*, 485–528.

VERMA, S.P., QUIROZ-RUIZ, A., and DÍAZ-GONZÁLEZ, L. (2008), *Critical values for 33 discordancy test variants for outliers in normal samples up to sizes 1000, and applications in quality control in Earth Sciences*, Rev. Mex. Cienc. Geol. *25*, 82–96.

VERMA, S.P., RODRÍGUEZ-RÍOS, R., and GONZÀLEZ-RAMÌREZ, R. (2010), *Statistical evaluation of classification diagrams for altered igneous rocks*, Turk. J. Earth Sci. *19*, 239–265.

VERMEESCH, P. (2007), *Tectonic discrimination diagrams revisited*, G3 *7*. doi:10.1029/2005GC001092.

VIGOUROUX, N., WALLACE, P.J., AND KENT, A.J.R. (2008), *Volatiles in high-K magmas from the western Trans-Mexican volcanic belt: evidence for fluid fluxing and extreme enrichment of the mantle wedge by subduction processes*, J. Petrol. *49*, 1589–1618.

WALKER, J.A., CARR, M.J., FEIGENSON, M.D., and KALAMARIDES, R.I. (1990), *The petrogenetic significance of interstratified high- and low-Ti basalts in central Nicaragua*, J. Petrol. *31*, 1141–1164.

WALKER, J.A., PATINO, L.C., CAMERON, B.I., and CARR, M.J. (2000), *Petrogenetic insights provided by compositional transects across the Central American arc: southeastern Guatemala and Honduras*, J. Geophys. Res. *105*, 18949–18963.

WALKER, J.A., PATINO, L.C., CARR, M.J., AND FEIGENSON, M.D. (2001), *Slab control over HFSE depletions in central Nicaragua*, Earth Planet. Sci. Lett. *192*, 533–543.

WALLACE, P. and CARMICHAEL, I.S.E. (1989), *Minette lavas and associated leucitites from the western front of the Mexican Volcanic Belt: petrology, chemistry and origin*, Contrib. Mineral. Petrol. *103*, 470–492.

WALLACE, P. and CARMICHAEL, I.S.E. (1992), *Alkaline and calc-alkaline lavas near Los Volcanes, Jalisco, Mexico: geochemical diversity and its significance in volcanic arcs*, Contrib. Mineral. Petrol. *111*, 423–439.

WALLACE, P.J. and CARMICHAEL, I.S.E. (1999), *Quaternary volcanism near the Valley of Mexico: implications for subduction zone magmatism and the effects of crustal thickness variations on primitive magma compositions*, Contrib. Mineral. Petrol. *135*, 291–314.

WILLIAMS, H. (1950), *Volcanoes of the Parícutin region, Mexico*, U.S. Geol. Surv. Bull. *965-B*, 1–279.

WOOD, D.A. (1980), *The application of a Th-Hf-Ta diagram to problems of tectonomagmatic classification and to establishing the nature of crustal contamination of basaltic lavas of the British Tertiary volcanic province*, Earth Planet. Sci. Lett. *50*, 11–30.

XU, G., FREY, F.A., CLAGUE, D.A., ABOUCHAMI, W., BLICHERT-TOFT, J., COUSENS, B., AND WEISLER, M. (2007), *Geochemical characteristics of West Molokai shield- and postshield-stage lavas: Constraints on Hawaiian plume models*, G3 *8*, 1–40.

YANG, T., GRAND, S.P., WILSON, D.S., GUZMAN-SPEZIALE, M., GOMEZ-GONZALEZ, J.M., DOMINGUEZ-REYES, T., AND NI, J. (2009), *Seismic structure beneath the Rivera subduction zone from finite-frequency seismic tomography*, J. Geophys. Res. *114*, doi: 10.1029/2008JB005830.

(Received February 15, 2010, revised May 11, 2010, accepted May 25, 2010, Published online June 22, 2010)

ANNEXURE IV

Pandarinath, K., Verma, S.K., 2012. Application of four sets of tectonomagmatic discriminant function based diagrams to basic rocks from northwest Mexico: **Journal of Iberian Geology, in press**.

.

Application of four sets of tectonomagmatic discriminant function based diagrams to basic rocks from northwest Mexico

Aplicación de cuatro conjuntos de los diagramas tectonomagmáticos basados en funciones discriminantes a las rocas básicas del noroeste de México

Kailasa Pandarinath[a*] and Sanjeet K. Verma[b]

[a]*Departamento de Sistemas Energéticos, Centro de Investigación en Energía, Universidad Nacional Autónoma de México, Priv. Xochicalco s/no., Col. Centro, Apartado Postal 34, Temixco, Mor. 62580, MEXICO. pk@cie.unam.mx*

[b]*Doctorate student, Posgrado en Ingeniería, Centro de Investigación en Energía, Universidad Nacional Autónoma de México, Priv. Xochicalco s/no., Col. Centro, Apartado Postal 34, Temixco, Mor. 62580, MEXICO.*

* *Corresponding author*

Received: 02/05/11 / Accepted 13/12/11

Abstract

Discrimination diagrams are being widely used for the past four decades to infer the tectonomagmatic affiliation of the older rocks. There are several major- and trace-element composition based bivariate, ternary and multi-element discriminant function used diagrams in the literature. Recent evaluation of the performance of these diagrams indicates that four sets of recent discriminant function based diagrams, in which the tectonic boundaries are determined based on probability estimates for four tectonic settings of island arc, continental rift, ocean-island and mid-ocean ridge, have shown very high success rates. In this work, we have created an extensive geochemical database for on-land and off-shore basic rocks of northwest Mexico and applied these four sets of recent and highly successful tectonomagmatic discriminant function based diagrams to infer their tectonomagmatic origin. Each of these four sets of diagrams (two for major and two for trace elements) contained five diagrams. All the four sets of diagrams confirm the dominant continental rift setting for on-land basic rocks of <13 Ma age, with success rates of 71%-93% and 58%-90% for major-element and trace-element based diagrams, respectively. For the on-land basic rocks of >13 Ma age, major-element based diagrams indicated dominant rift setting (high success rates of 62-92%) and less-dominant arc setting (low but significant success rates of 23-54%). However, the trace-element based discrimination diagrams indicated the dominant arc setting (success rates of 31-100%) and less-dominant rift setting (significant success rates of 0-77%). This shows the dual (arc and rift) or transition of tectonic setting from arc to rift for these rocks. All the four sets of discrimination diagrams indicate MORB setting (success rates 90%-98% and 100% for major-

element and trace-element based diagrams, respectively) for off-shore rocks (dominantly from DSDP drilled sites in the Gulf of California and some dredged rock samples from the Gulf of California) with very high success rates. All the inferred tectonic settings from these four sets of new discrimination diagrams in general are in conformity with those reported in the literature based on other methods. The results show that these discrimination diagrams may successfully discriminate the original tectonic setting of comparatively younger and older on-shore rocks as well as sea-water altered deep-sea rocks and dredged material.

Keywords: Basic rocks, geochemistry, tectonic setting, arc, rifting, discrimination diagrams, Mexico.

Resumen

Diagramas de discriminación tectonomagmáticas están siendo ampliamente utilizado en los últimos cuatro decenios para inferir la afiliación tectonomagmáticos de las rocas más antiguas. Hay varios de diagramas en la literatura basado de la composición de los elementos mayores y trazas utiliza bivariante, ternarios y la función de discriminante de multi-elementos. Evaluación reciente de la rendimiento de estas diagramas indica que los últimos cuatro conjuntos de diagramas tectonomagmáticos, en los que límites tectónicos se determina con base en estimaciones de probabilidades de cuatro configuraciones tectónicas de la isla arco, ruptura continental, las islas del océano y la cordillera en medio del océano, han demostrado tasas de éxito muy alto. En este trabajo, hemos creado una amplia base de datos geoquímicos de rocas básicas de la tierra y costa afuera del noroeste de México y aplicado estos diagramas recientes basado de la función discriminante para deducir su origen

tectonomagmáticos. Cada uno de estos cuatro conjuntos de diagramas (dos de los elementos mejores y dos de los trazas) contenía cinco diagramas. Todos los cuatro tipos de diagramas confirman la dominante configuración del ruptura continental para las rocas de la tierra de <13 años Ma edad, con tasas de éxito de 71%-93% y 58%-90% para las diagramas de elementos mejores y trazas, respectivamente. Para las rocas básicas de la tierra de > 13 años Ma edad, los diagramas de los elementos mejores indica configuración tectónica dominante de ruptura (altas tasas de éxito de 62-92%) y configuración tectónica menos-dominante de arco (tasas de éxito menor pero significativa de 23-54%). Sin embargo, los diagramas de discriminación basadas de los elementos trazas indica la configuración dominante de arco (tasas de éxito de 31-100%) y configuración tectónica menos-dominante de ruptura (tasas de éxito significativos de 0-77%). Esto demuestra el doble (de arco o ruptura) o la transición de ambiente tectónico de arco a ruptura para estas rocas. Todos los cuatro tipos de diagramas de discriminación indican la configuración de MORB (las tasas de éxito del 90% -98% y 100% para los elementos mejores y trazas, respectivamente) para las racas de costa afuera (predominantemente de los sitios de DSDP perforados en el Golfo de California y algunas muestras de rocas de dragado del Golfo de California) con tasas de éxito muy alto. Todos los configuraciones tectónicos inferidos a partir de estos cuatro conjuntos de diagramas nuevas de discriminación, en general, están en conformidad con los reportados en la literatura sobre la base de otros métodos. Los resultados muestran que estos diagramas de discriminación puede discriminar correctamente la configuración original de la tectónica de comparativamente más joven y más antiguas rocas de la tierra, así como de las rocas más profundas de mar alteradas por el agua del mar y los materiales de dragado.

Palabras clave: Rocas básicas, geoquímica, ambiente tectónico, arco, ruptura continental, diagramas de discriminación, México.

1. Introduction

Tectonomagmatic discrimination diagrams are being widely used to infer the original tectonic setting of volcanic rocks (e.g., Pearce *et al*., 1977; Rollinson, 1993; Verma, 2010). These diagrams are developed on two major basic assumptions: (1) concentrations of the characteristic chemical elements being used in the discriminate diagrams show large variations in the rocks of different tectonic settings; and (2) these characteristic chemical elements of the rocks are immobile from the period of rock formation to the present.

There are several major- and trace-element composition based diagrams for geochemical tectonic discrimination in the literature, which may be grouped to: (1) bivariate diagrams (Pearce and Gale, 1977; Pearce and Norry, 1979; Shervais, 1982; Pearce, 1982); (2) ternary diagrams (Pearce and Cann, 1973; Pearce *et al*., 1977; Wood, 1980; Mullen, 1983; Meschede, 1986; Cabanis and Lecolle, 1989); (3) discriminant function based diagrams (Butler and Woronow, 1986; Pearce, 1976; Agrawal *et al*., 2004); and (4) multi-element discriminant function diagrams based on log-transformed ratios (Verma *et al*., 2006; Agrawal *et al*., 2008; Verma and Agrawal, 2011). All these discrimination diagrams have been developed based on a geochemical database of the volcanic rocks from known tectonic environments. In majority of the above mentioned diagrams the tectonic discrimination boundaries were drawn by eye, i.e., were based on visual appearance of the clustering of data points of known tectonic settings, except a few recent ones (Agrawal *et al*., 2004; Verma *et al*., 2006; Agrawal *et al*., 2008; Verma and Agrawal, 2011), in which the tectonic boundaries

are determined based on probability estimates. Agrawal (1999) and Agrawal and Verma (2007) were already criticized the use of eye for drawing tectonic field boundaries.

Recently, there are extensive evaluations of existing diagrams, which indicated the variable success rates in discriminating the tectonic settings (Vermeesch, 2006; Verma *et al*., 2006; Vermeesch, 2007; Sheth, 2008; Verma, 2010; Verma *et al*., 2011). Verma (2011) has recently documented serious statistical problems with both bivariate and ternary diagrams. Sheth (2008) evaluated some of the diagrams (Verma *et al*., 2006; Vermeesch, 2006) with data of ocean-island, arc and mid-ocean ridge lavas from the Indian Ocean and reported that the log-ratio transformation and linear discriminant analysis appear to be powerful methods in tectonomagmatic discrimination studies. Verma (2010) evaluated a large number of bivariate, ternary and multi-dimensional diagrams and inferred that the newer diagrams proposed during 2004-2011 provide more reliable results. Similarly, Verma *et al.* (2012) have successfully applied these multi-element based discriminant diagrams for basic rocks of Southern Mexico and Central America for inferring their tectonomagmatic origin.

In this article, we have evaluated the more recent and highly successful multi-element discriminant function diagrams with simple elemental ratio variables (Agrawal *et al*., 2004) and based on log-transformed ratios (Verma *et al*., 2006; Agrawal *et al*., 2008; Verma and Agrawal, 2011) with an application to the basic rocks of on-land and off-shore of northwest Mexico.

2. Tectonic framework of the study area

The late Cenezoic tectonic framework of northwestern Mexico has been discussed in detail by several researchers (for example, Rogers et al., 1985; Saunders *et al*., 1987; Luhr *et al*., 1995; Calmus *et al*., 2003) and hence, only a brief discussion is provided here. The west coast of northwestern Mexico has been a convergent plate boundary since mid-Cretaceous. The eastward subduction of oceanic lithosphere beneath western North America continued from Cretaceous to about 29 Ma (Mammerickx and Klitgord, 1982). Towards the western part of northwestern Mexico, subduction related magmatism is represented by batholitic granitoids between 90 and 40 Ma (McDowell *et al*., 1997 and 2001), whereas towards the east of the Baja California peninsula, a continuous subduction related magmatism during Eocene-Oligocene (between 38 and 23 Ma) has generated important inland magmatism along the Sierra Madre Occidental belt (McDowell and Keizer, 1977; Stock and Lee, 1994; Benoit *et al*., 2002). Afterwards, during the Lower Miocene, the volcanic front shifted towards the west, forming the magmatic arc (the Comondú arc) all along the Baja California Peninsula. This volcanic belt had a longer activity between 24 and 12 Ma in southern Baja California compared to northern Baja California where Miocene (21 to 16 Ma) volcanism constituted several volcanic fields. The subduction in this region ended at 12.9 Ma (Mammerickx and Klitgord, 1982; Calmus *et al*., 2003). Afterwards, transform boundary was developed between Pacific and North America plates parallel to the Pacific margin of Baja California (Spencer and Normark, 1979). Consequently, the tectonic setting has changed from subduction to rifting along the western margin of North America in Late-Cenozoic time (Grijalva-Noriega and Roldán-Quintana, 1998).

3. Methodology

We have prepared a database by compiling geochemical data of basic rocks of northwest Mexico from the published articles. For this purpose, we considered the basic rocks of on-land (Baja California, Baja California Sur and Sonora states of Mexico) and the off-shore (mainly from the DSDP sites of Gulf of California, and a few from Alarcon Rise and dredged rocks from three sites near the mouth of the Gulf of California and close to the East Pacific Rise) regions of northwest Mexico (Fig. 1). The geochemical data from the above mentioned regions were obtained from the published articles that were not included in any of the previous studies, in which the diagrams to be applied were proposed, i.e., not included in the databases used by Agrawal *et al*. (2004, 2008), Verma *et al*. (2006), and Verma and Agrawal (2011).

The literature sources for on-land geochemical data were as follows: Saunders *et al*. (1987); Luhr *et al*. (1995); Aguillón-Robles *et al*. (2001); Benoit *et al*. (2002); Calmus *et al*. (2003); Solano *et al*. (2005); Bellon *et al*. (2006); Pallares *et al*. (2007); Vidal-Solano *et al*. (2008); Till *et al*. (2009) ; Housh *et al*. (2010) ; Calmus *et al*. (2011). The literature sources for the off-shore geochemical data were as follows: Lopez *et al*. (1978); Jochum and Verma (1996); Castillo *et al*. (2002); Flower *et al*. (2007); Perfit *et al*. (2007); Saunders (2007); Saunders *et al*. (2007); Zolotarev and Margolin (2007); Morrison and Thompson (2007).

Based on the geochemical data, rock types were determined using SINCLAS computer program (Verma *et al*. 2002, 2003), with the Middlemost (1989) option for Fe-oxidation adjustment. This program requires the complete chemical analyses, involving 10 major elements (with total Fe as Fe_2O_3 or FeO), be available for the rock. Only basic rock types

having $(SiO_2)_{adj}$ < 52% (Le Bas *et al*. 1986) as inferred from the SINCLAS software were considered for this study. With this condition, we have left with the chemical data for only 102 basic rocks from on-shore region. Number of samples (n) from the specific areas (Fig. 1) are as follows: Hermosillo (n=2), San Borja volcanic field (n=8), La Purísima volcanic field (n=2), Santa Clara volcanic field (n=6), San Ignacio volcanic field (n=1), San Quintín volcanic field (n=36), Isla Tortuga (n=1), Jaraguay volcanic field (n=1), Sierra El Aguaje (n=6), Isla Isabel (n=10), Guaymas Basin (n=2), San Carlos-Santa Catarina (n=6), Pinacate Area, Sonora (n=4), Sierra Libre (n=2), Coastal Sonora (n=2), Comondú Formation (n=1), Sierra Madre Occidental (n=3), Sierra Santa Ursula (n=2), Suaqui Grande (n=2) and Sahuaripa (n=5). Similarly, we have chemical data for 612 basic rocks from the offshore region (Fig. 1). These offshore chemical data are from the rocks of: DSDP site 482 (n=176), DSDP site 483 (n=132), DSDP site 485 (n=93), DSDP site 474 (n=76), DSDP site 475 (n=11), DSDP site 477 (n=33), DSDP site 478 (n=50), DSDP site 481 (n=4), Alarcon Rise lava from Gulf of California (n=29), Mouth of the Gulf of California (n=4; dredged rocks from the mouth of the Gulf of California; including 8 subdivided parts of three of these dredged rocks) and other deep-sea samples (Seamount, Basin stations etc; n=4). Natural log-transformed ratios for major elements were calculated as follows: $\ln(TiO_2/SiO_2)_{adj}$, $\ln(Al_2O_3/SiO_2)_{adj}$, $\ln(Fe_2O_3/SiO_2)_{adj}$, $\ln(FeO/SiO_2)_{adj}$, $\ln(MnO/SiO_2)_{adj}$, $\ln(MgO/SiO_2)_{adj}$, $\ln(CaO/SiO_2)_{adj}$, $\ln(Na_2O/SiO_2)_{adj}$, $\ln(K_2O/SiO_2)_{adj}$, and $\ln(P_2O_5/SiO_2)_{adj}$, in which $(SiO_2)_{adj}$ was used as the common denominator.

In general, ~13 Ma BP is considered as the end of subduction along the northwestern Mexico (Mammerickx and Klitgord, 1982; Calmus *et al*., 2003). We have grouped our on-land basic rock samples in rocks of >13 Ma ages (as of subduction-arc magmatism) and <13 Ma (as

of rift magmatism) to identify their diverse tectonic settings. The diagrams of Agrawal *et al*. (2004) and Verma *et al*. (2006) are based on major-elements (the first with simple ratio variables and the second with log-transformation of ratio variables), whereas those of Agrawal *et al*. (2008) and Verma and Agrawal (2011) use log-transformed ratios of immobile-elements (La, Sm, Yb, Nb, and Zr for the former and adjusted TiO_2, Nb, V, Y, and Zr for the latter). In all the above-mentioned four new discriminant function based tectonomagmatic diagrams, there is no differentiation between the continental and oceanic arc settings, and the entire arc setting is represented by island arc setting (IAB). Based on the availability of the required chemical data in the above mentioned literature for the application of these four sets of recent tectonomagmatic discriminant function based diagrams for basic rocks, we obtained the final number of samples for each diagram as follows: (1) 89, 13, and 611 rock samples for on-land basic rocks of younger age (<13 Ma), on-land basic rocks of older age (>13 Ma) and off-shore rocks (including 3 sea-floor dredged rocks), respectively, for the major-elemental concentrations based discrimination diagrams of Agrawal *et al*. (2004) and Verma *et al*. (2006); (2) 80, 13, and 8 rock samples for on-land basic rocks of younger age (<13 Ma), on-land basic rocks of older age (>13 Ma) and sea-floor dredged rocks (different parts of three rock samples), respectively, for the immobile trace-elemental concentrations based discrimination diagram of Agrawal *et al*. (2008); and finally, (3) 68, 1, and 78 rock samples for on-land basic rocks of younger age (<13 Ma), on-land basic rocks of older age (>13 Ma) and off-shore rocks, respectively, for the immobile trace-element concentrations based discrimination diagram of Verma and Agrawal (2011). In the literature, chemical data for basic rocks are limited in comparison to acidic rocks. Chemical data for the older (>13 Ma age) basic rocks are further lacking as compared to the basic rocks of <13 Ma age. Among the

compiled chemical data for on-land basic rocks, only one rock sample of >13 Ma age contained the necessary immobile trace elements data to plot in the diagram of Verma and Agrawal (2011) which shows the dearth of trace element chemical data for the rocks of this region.

4. Results and Discussion

The compiled geochemical data of on-land and off-shore basic rocks of northwest Mexico are plotted in all four sets of new discrimination diagrams (Agrawal *et al*., 2004, 2008; Verma *et al*., 2006; Verma and Agrawal, 2011) to infer the tectonomagmatic origin of these rocks. For each set of diagrams, five different plots were prepared, which provided a total of 20 diagrams. The samples in different tectonic setting fields are counted and their percentage range in each tectonic setting was calculated (wherever number of samples >8) and reported (Figs. 2-5; Tables 1-4). We discuss below only the dominant tectonic settings inferred by these diagrams for each group of rocks. All the indicated dominant tectonic setting are statistically significant because they are >>33.3% (being the simple "by chance" probability). The results are summarized in Tables 1-4. The results were fully consistent with those resulting from the application of computer program TecD (Verma and Rivera-Gómez, 2011).

4.1. Tectonomagmatic origin of on-shore basic rocks of northwest Mexico

Two sets of major-element (Agrawal *et al*., 2004, Fig. 2, Table 1; Verma *et al*., 2006, Fig.3, Table 2) and two sets of immobile trace-element Agrawal *et al*. (2008; Fig. 4; Table 3;

Verma and Agrawal, 2011; Fig. 5; Table 4)) based discrimination diagrams were applied for discrimination of IAB, CRB, OIB, and MORB tectonic settings.

Out of the five diagrams in each of the two sets of major-element based diagrams, the first diagram contains four tectonic settings and other four diagrams with three settings at a time. The first set of major-element based discrimination diagrams of Agrawal *et al*. (2004; Fig. 2; Table 1) indicated the tectonic setting of continental rift (success rates of 71%-86%) for on-land basic rocks of <13 Ma age. Whereas for on-land basic rocks of >13 Ma age, these diagrams indicated the tectonic setting of continental rift with high success rates (62%-92%) and island arc setting with low but significant success rates (23%-38%).

When we used exactly the same samples as for the first set, the second set of major-element based diagrams of Verma *et al*. (2006; Fig.3; Table 2) also revealed the dominant continental rift setting with high success rates (80%-93%) for on-land basic rocks of <13 Ma age. For on-land basic rocks of >13 Ma age, similar to the first set of diagrams, these second set of major-element based diagrams indicated the tectonic setting of continental rift with high success rates (77%-92%) and island arc setting with low but significant success rates (15%-54%).

The first set of immobile trace element based diagrams of Agrawal *et al*. (2008; Fig. 4; Table 3) was also applied for IAB, CRB, OIB, and MORB (all five diagrams contains three tectonic settings at a time). The indicated tectonic settings are: (1) the dominant continental rift setting (success rates of 58%-80%) for on-land basic rocks of <13 Ma age; (2) continental rift tectonic setting with high success rates (38%-77%) and island arc with low but significant success rates (31%-38%) for on-land basic rocks of >13 Ma age; (3) when there is no CRB

setting in the diagram (Fig. 4a), the on-land basic rocks of <13 Ma age have plotted in the combined tectonic field settings of CRB+OIB with a high success rate of 80%; and (4) when there is no IAB setting in the diagram (Fig. 4d; filled circles), the on-land basic rocks of >13 Ma age have dominantly (success rate of 77%) plotted in the tectonic field of CRB.

Finally, the second set of immobile-element based diagrams of Verma and Agrawal (2011; Fig. 5; Table 4) was also applied for IAB, CRB, OIB, and MORB (three settings at a time in all the five diagrams). These immobile-element based diagrams of Verma and Agrawal (2011; Fig. 5; Table 4) complies the requirement of normal distribution of the log-ratio variables. This was achieved by identification and elimination of outlier data points by using the software DODESSYS (Verma and Dìaz-González, 2011), which allows the application of the multiple-test method initially proposed by Verma (1997) and uses new precise and accurate critical values for discordancy tests (Barnett and Lewis, 1994; Verma and Quiroz-Ruiz, 2006a, 2006b, 2008; Verma *et al*., 2008). The indicated tectonic settings are as follows: continental rift setting (66%-90%) for on-land basic rocks of <13 Ma age and island-arc setting for the only one on-land basic rock sample of >13 Ma age.

The observed tectonomagmatic settings by the new discriminant function based tectonomagmatic settings for younger (<13 Ma age) and older (>13 Ma age) on-land basic rocks are generally in concordance with those reported in the literature. The two sets of major-element (success rates of 71%-86%, Agrawal *et al*., 2004; success rates of 80%-93%, Verma *et al*., 2006) and two sets of trace-element (success rates of 58%-80%, Agrawal *et al*., 2008; success rates of 66%-90%, Verma and Agrawal, 2011) based discrimination diagrams confirm the dominant continental rift setting (CRB; Tables 1-4; Figs. 2-5) for on-land basic rocks of

<13 Ma age. This is in agreement with that of the literature. The subduction of oceanic (Pacific) lithosphere beneath western North America continued from Cretaceous and ended at 12.9 Ma (Mammerickx and Klitgord, 1982; Calmus *et al*., 2003). After this period, during Late-Cenozoic, transform boundary is developed between Pacific and North America plates parallel to the Pacific margin of Baja California (Spencer and Normark, 1979) which resulted in change of the tectonic setting from subduction to rifting along the western margin of North America (Grijalva-Noriega and Roldán-Quintana, 1998).

For the on-land basic rocks of >13 Ma age: (1) the major-element based diagrams of Agrawal *et al*. (2004; Table 1; Fig. 2) and Verma *et al*. (2006; Table 2; Fig. 3) indicated continental rift setting with high success rates (62%-92% and 77%-92% respectively) and island arc setting with low but significant success rates (23%-38% and 15%-54% respectively); and (2) the trace-element based discrimination diagrams of Agrawal *et al*. (2008; Table 3; Fig. 4) and Verma and Agrawal (2011; Table 4; Fig. 5) have not indicated any clear dominant tectonic settings between island arc-continental rift. In both of these two sets of the trace-element based diagrams (Agrawal *et al*., 2008; Verma and Agrawal, 2011) only two out of five diagrams in each set where both IAB and CRB fields are available (Table 3 and 4; Fig. 4 and 5). In the diagrams of Agrawal *et al*. (2008), one diagram indicated a dominant CRB setting (success rates of CRB and IAB are 69% and 31%, respectively) and another diagram indicated combined CRB-IAB setting (equal success rates of 38.5% for both CRB and IAB; Table 3 and Fig. 4). Whereas, the only one rock sample, which has the necessary trace-element data to be plotted in the diagrams of Verma and Agrawal (2011), has plotted in the field of IAB in both the diagrams (success rate of 100%; Table 4 and Fig. 5). The observed not so clear dominant tectonic setting between IAB and CRB for the on-land

basic rocks of >13 Ma age by the two sets of immobile trace-element based discrimination diagrams and low but statistically significant success rates for IAB by two sets of major-element based diagrams may suggest the dual (arc and rift) or transition of tectonic setting from arc to rift during this period.

However, in the compiled data base of the present study, only 13 and one on-land basic rocks of >13 Ma age consists the necessary immobile trace-element data for application of trace element based discrimination diagrams of Agrawal *et al*. (2008) and Verma and Agrawal (2011), respectively. This clearly indicates the dearth of trace element data for the basic rocks of >13 Ma age, in particularly, for any meaningful application of the diagram of Verma and Agrawal (2011).

Among the 13 older on-land basic rocks (>13 Ma), nine rocks belongs to Southern Sonora (19-28 Ma; Till *et al*., 2009), three rocks (27-45 Ma age; Albrecht and Goldstein, 2000) belongs to Sierra Madre Occidental, northwestern Mexico and the one rock (20.06 Ma age; Pallares *et al*., 2007) belongs to Comondú Formation (from Cataviña; Pallares *et al*., 2007). It is reported that the Sierra Madre Occidental and Comondú arc were formed as the result of the subduction of oceanic lithosphere beneath western North America during Eocene-Oligocene and Lower Miocene respectively (McDowell and Keizer, 1977; Stock and Lee, 1994; Benoit *et al*., 2002). Recently, Till *et al*. (2009) have reported that mafic volcanic rocks erupted in southern Sonora from 27 to 8 Ma have continental arc signature and appear to be derived from the metasomatized sub-arc mantle below Sonora. They were also of the opinion that the geochemistry of the rocks of Sonora is not consistent with the predictions of petrotectonic models and contrasts with central and southern Baja. The chemical data reported

for basic rocks in the article of Till *et al.* (2009) was already included in the database of this work. As discussed above, all the four recent tectonic discriminate diagrams for basic rocks (Agrawal et al., 2004; Verma et al., 2006; Agrawal et al., 2008; Verma and Agrawal, 2011) have indicated the dominant continental rift setting (CRB) and transition of tectonic setting from arc to rift (or dual, arc and rift) for rocks of <13 Ma and >13 Ma age, respectively. For further clarity, we have applied the new discriminant-function-based multi-dimensional diagrams for acid (Verma et al., 2012) and intermediate rocks (Verma and Verma, un published) reported in Till *et al.* (2009). The tectonic discriminant diagrams for both acid and intermediate rocks have indicated a dominant rift setting. This is in consistent to the observed dominant rift setting by the four sets of discriminate diagrams for basic rocks, discussed above, although Till *et al*. (2009) proposed an arc setting.

4.2. Tectonomagmatic origin of off-shore basic rocks of northwest Mexico

The first set of major-element based discrimination diagrams of Agrawal *et al*. (2004; Fig. 2; Table 1) have indicated the tectonic setting of MORB (success rates of 90%-97%) for the off-shore rocks off northwest Mexico. When there is no MORB setting in the diagram (Fig. 2b), the samples occupied OIB (47%) and IAB (37%) settings.

When we used exactly the same samples as for the first set, the second set of major-element based diagrams of Verma *et al*. (2006; Fig.3; Table 2) also indicated the MORB setting (88%-98%). When there is no tectonic setting of MORB in the diagram (Fig. 3b), 93% of these rock samples occupied OIB setting.

Because the required chemical data for all five trace elements (La, Sm, Nb, Yb and Th) were not available for any of the off-shore rocks, the first set of immobile-element based diagrams of Agrawal *et al*. (2008; Fig. 4; Table 3) could not be applied for these rocks.

Finally, the second set of immobile-element based diagrams of Verma and Agrawal (2011; Fig. 5; Table 4) indicated MORB tectonic setting (100%) for these off-shore rocks. When MORB setting is missing from a diagram (Fig. 5b), all these off-shore rock samples occupied IAB setting.

Thus, two sets of major-element based discrimination diagrams of Agrawal *et al*. (2004) and Verma *et al*. (2006; Figs. 2-3; Tables 1-2) and the immobile-trace element based diagrams of Verma *et al*. (2011; Fig. 5; Table 4) indicated the tectonic setting of MORB for off-shore basement rocks of DSDP drilled core locations in the Gulf of California.

We have included in the present database the whole-rock chemical data of three rocks dredged from the locations close to the East Pacific Rise near the mouth of the Gulf of California (Lopez *et al*., 1978; Jochum and Verma, 1996). Lopez *et al*. (1978) have reported that these rocks are geochemically similar to other samples from the East Pacific Rise and surrounding seamounts, and are characterized by sea-water alteration effects. The available whole-rock chemical data of these rocks allowed us to apply only major-element based diagrams (Agrawal *et al*., 2004; Verma *et al*., 2006). All the three rock samples dredged from the sea-floor near the mouth of the Gulf of California occupied the field of MORB setting in these major element based diagrams (Figures 2-3; Tables 1-2). Earlier, Lopez *et al*. (1978) have reported that these samples are clustered in the field of ocean floor basalts in the discrimination diagrams of Pearce and Cann (1973) and Pearce (1975). We have also included

in the present work, the detailed chemical analysis of the individually sampled three parts (the inner less altered "core", the outer more altered "margin" and "glass" from the outer part) of each of these three dredged rocks (Jochum and Verma, 1996). The available geochemical data for these three parts of each of three dredged rocks allowed us to apply only the set of immobile element based diagrams of Agrawal *et al*. (2008). These diagrams indicated a MORB setting for inner less altered "core" and outer altered "margin" parts, and combined island-arc and MORB settings for altered "glass" parts of these three rocks.

Thus, all diagrams – the two sets of new major-element (Agrawal *et al*., 2004; Verma *et al*., 2006) and two sets of trace-element (Agrawal *et al*., 2008; Verma and Agrawal, 2011) based discrimination diagrams – confirm the MORB setting for off-shore rocks. Majority of these off-shore rocks are the basement rocks from the DSDP drilled locations. Concentrations of geochemical elements will be effected by sea-water alteration at these great depths of the oceans as observed in the dredged rocks from the locations close to the East Pacific Rise near the mouth of the Gulf of California (Lopez *et al*., 1978; Jochum and Verma, 1996). In spite of sea-water alteration effects in geochemistry of these three dredged rocks (Lopez *et al*., 1978; Jochum and Verma, 1996), the new tectonomagmatic discrimination diagrams are able to identify their tectonomagmatic origin as MORB. These results show that these four sets of new tectonomagmatic discrimination diagrams may successfully discriminate the original tectonic setting of deep-sea basement rocks and dredged material in spite the possibility of sea-water alteration effects in their geochemical concentrations.

5. Conclusions

The recent discriminant function based discrimination diagrams (Agrawal *et al*., 2004) along with the log-transformed ratios of chemical variables (Verma *et al*., 2006; Agrawal *et al*., 2008; Verma and Agrawal, 2011), in which the tectonic boundaries are determined based on probability estimates, are more powerful and have shown very high success rates in finding the tectonomagmatic origin of on-shore and offshore basic rocks of northwest Mexico. These diagrams have indicated: (1) the dominant continental rift setting for on-land basic rocks of <13 Ma age; (2) the dual tectonic settings of continental rift and arc (or transition of tectonic setting from arc to rift) for on-land basic rocks of >13 Ma age; and (3) MORB setting for off-shore rocks. All these inferred tectonic settings are generally in conformity with those reported in the literature. This work suggests that these new diagrams prepared by relevant statistical methodologies can be successfully applied to infer the tectonic setting of fresh as well as altered basic rocks.

Acknowledgements

We wish to thank Dr. Mike de Villiers, Prof. Salil Agrawal and an anonymous reviewer for providing the valuable comments in improving the earlier version of the manuscript. Similarly, we are grateful to Dr. Surendra P. Verma for his suggestions in improving the chemical database used in this work.

References:

Agrawal, S. (1999): Geochemical discrimination diagrams: a simple way of replacing eye-fitted boundaries with probability based classifier surfaces. *Journal of the Geological Society of India*, 54: 335-346.

Agrawal, S., Verma, S.P. (2007): Comment on "Tectonic classification of basalts with classification trees" by Pieter Vermeesch (2006). *Geochimica et Cosmochimica Acta*, 71: 3388-3390.

Agrawal, S., Guevara, M., Verma, S.P. (2004): Discriminant analysis applied to establish major-element field boundaries for tectonic varieties of basic rocks. *International Geology Review*, 46: 575-594.

Agrawal, S., Guevara, M., Verma, S.P. (2008): Tectonic discrimination of basic and ultrabasic rocks through log-transformed ratios of immobile trace elements. *International Geology Review*, 50: 1057-1079.

Aguillón-Robles, A., Calmus, T., Benoit, M., Bellon , H., Maury, R.C., Cotten, J., J., B., Michaud, F. (2001): Late Miocene adakites and Nb-enriched basalts from Vizcaino Peninsula, Mexico: Indicators of East Pacific Rise subduction below southern Baja California? *Geology*, 29: 531-534.

Albrecht, A., Goldstein, S.L. (2000): Effects of basement composition and age on silicic magmas across an accreted terrane-Precambrian crust boundary, Sierra Madre Occidental, Mexico. *Journal of South American Earth Sciences*, 13: 255-273.

Barnett, V., Lewis, T. (1994): *Outliers in statistical data* (Third Edition). John Wiley & Sons, Chichester: 584 p.

Bellon, H., Aguillón-Robles, A., Calmus, T., Maury, R.C., J., B., Cotten, J. (2006): La Purisima volcanic field, Baja California Sur (Mexico): Miocene to Quaternary volcanism related to subduction and opening of an asthenospheric window. *Journal of Volcanology and Geothermal Research*, 152: 253-272.

Benoit, M., Robles, A.A., Calmus, T., Maury, R.C., Bellon , H., Cotten, J., J., B., Michaud, F. (2002): Geochemical Diversity of Late Miocene Volcanism in Southern Baja California, México: Implication of Mantle and Crustal Sources during the Opening of an Asthenospheric Window. *Journal of Geology*, 110: 627-648.

Butler, J.C., Woronow, A. (1986): Discrimination among tectonic settings using trace element abundances of basalts. *Journal of Geophysical Research*, 91: 10289-10300.

Cabanis, B., Lecolle, M. (1989): Le diagramme La/10-Y/15-Nb/8: un outil pour la discrimination des séries volcaniques et la mise en évidence des processus de mélange et/ou de contamination crustale. *C.R. Acad. Sci. Paris*, 309: 2023-2029.

Calmus, T., Aguillón-Robles, A., Maury, R.C., Bellon , H., Benoit, M., Cotten, J., Bourgois, J., Michaud, F. (2003): Spatial and temporal evolution of basalts and magnesian andesites ("Bajaites") from Baja California, Mexico: the role of slab melts. *Lithos*, 66: 77-105.

Calmus, T., Pallares, C., Maury, R.C., Robles, A.A., Bellon, H., Benoit, M., Michaud, F. (2011): Volcanic Markers of the Post-Subduction Evolution of Baja California and Sonora, Mexico: Slab Tearing Versus Lithospheric Rupture of the Gulf of California. *Pure and Applied Geophysics*, 168: 1303-1330.

Castillo, P.R., Hawkins, J.W., Lonsdale, P.F., Hilton, D.R., Shaw, A.M. (2002): Petrology of Alarcon Rise lavas, Gulf of California: Nascent intracontinental ocean crust. *Journal of Geophysical Research*, 107: 2222.

Flower, M.F.J., Pritchard, R.G., Schmincke, H.-U., Robinson, P.T. (2007): Geochemistry of Basalts: Deep Sea Drilling Project Sites 482, 483, and 485 near the Tamayo Fracture Zone, Gulf of California. *Deep Sea Drilling Project*, 65: 559-578.

Fornari, D.J., Saunders, A.D., Perfit, M.R. (2007): Major-Element Chemistry of Basaltic Glasses Recovered during Deep Sea Drilling Project Leg 64. *Deep Sea Drilling Project*, 64: 643-648.

Grijalva-N., F.J., Roldán-Q., J. (1998): An Overview of the Cenozoic tectonic and magmatic evolution of Sonora, Northwestern Mexico. *Revista Mexicana de Ciencias Geológicas*, 15: 145-156.

Housh, T.B., Aranda-Gómez, J.J., Luhr, J.F. (2010): Isla Isabel (Nayarit, México): Quaternary alkalic basalts with mantle xenoliths erupted in the mouth of the Gulf of California. *Journal of Volcanology and Geothermal Research*, 197: 85-107.

Jochum, K.P., Verma, S.P. (1996): Extreme enrichment of Sb, Tl and other trace elements in altered MORB. *Chemical Geology*, 130: 289-299.

Le Bas, M.J., Le Maitre, R.W., Streckeisen, A., Zanettin, B. (1986): A chemical classification of volcanic rocks based on the total alkali-silica diagram. *Journal of Petrology*, 27: 745-750.

Lopez M., M., Perez R., J., Urrutia F., J., Pal, S., Terrell, D.J. (1978): Geochemistry and petrology of some volcanic rocks dredged from the Gulf of California. *Geochemical Journal*, 12: 127-132.

Luhr, J.F., Aranda-Gómez, J.J., Housh, T.B. (1995): San Quintín volcanic field, Baja California Norte, México: geology, petrology, and geochemistry. *Journal of Geophysical Research*, 100: 10353-10380.

Mammerickx, J., Klitgord, K.D. (1982): Northern East Pacific Rise: evolution from 25 m.y. B.P. to the Present. *Journal of Geophysical Research*, 87: 6751-6759.

McDowell, F.W., Keizer, R.P. (1977): Timing of mid-tertiary volcanism in the Sierra Madre Occidental between Durango City and Mazatlan, Mexico. *Geological Society of America Bulletin*, 88: 1479-1487.

McDowell, F.W., Roldán-Q., J., Amaya-M., R. (1997): Interrelationship of sedimentary and volcanic deposits associated with Tertiary extension in Sonora, Mexico. *Geological Society of America Bulletin*, 109: 1349-1360.

Meschede, M. (1986): A method of discriminating between different types of mid-ocean ridge basalts and continental tholeiites with the Nb-Zr-Y diagram. *Chemical Geology*, 56: 207-218.

Middlemost, E.A.K. (1989): Iron oxidation ratios, norms and the classification of volcanic rocks. *Chemical Geology*, 77: 19-26.

Morrison, M.A., Thompson, R.N. (2007): Alteration of Basalt: Deep Sea Drilling Project Legs 64 and 65. *Deep Sea Drilling Project*, 65: 643-660.

Mullen, E.D. (1983): $MnO/TiO_2/P_2O_5$: a minor element discrimination for basaltic rocks of oceanic environments and its implications for petrogenesis. *Earth and Planetary Science Letters*, 62: 53-62.

Pallares, C., Maury, R.C., Bellon, H., Royer, J.-Y., Calmus, T., Aguillón-Robles, A., Cotten, J., Benoit, M., Michaud, F., Bourgois, J. (2007): Slab-tearing following ridge-trench collision: evidence from Miocene volcanism in Baja California, Mexico. *Journal of Volcanology and Geothermal Research*, 161: 95-117.

Pearce, J.A. (1975): Basalt geochemistry used to investigate past tectonic environments on Cyprus. *Tectonophysics*, 25: 41-67.

Pearce, J.A. (1976): Statistical analysis of major element patterns in basalts. *Journal of Petrology*, 17: 15-43.

Pearce, J.A. (1982), Trace element characteristics of lavas from destructive plate boundaries. in *Andesites*. R.S. Thorpe, Ed. Chichester: John Wiley & Sons.

Pearce, J.A., Cann, J.R. (1973): Tectonic setting of basic volcanic rocks determined using trace element analyses. *Earth and Planetary Science Letters*, 19: 290-300.

Pearce, J.A., Gale, G.H. (1977): Identification of ore-deposition environment from trace-element geochemistry of associated igneous host rocks. *Geological Society of London Special Publication*, 7: 14-24.

Pearce, J.A., Norry, M.J. (1979): Petrogenetic implications of Ti, Zr, Y, and Nb variations in volcanic rocks. *Contributions to Mineralogy and Petrology*, 69: 33-47.

Pearce, T.H., Gorman, B.E., Birkett, T.C. (1977): The relationship between major element chemistry and tectonic environment of basic and intermediate volcanic rocks. *Earth and Planetary Science Letters*, 36: 121-132.

Perfit, M.R., Saunders, A.D., Fornari, D.J. (2007): Phase Chemistry, Fractional Crystallization, and Magma Mixing in Basalts from the Gulf of California, Deep Sea Drilling Project Leg 64. *Deep Sea Drilling Project*, 64: 649-666.

Rogers, G., Saunders, A.D., Terrell, D.J., Verma, S.P., Marriner, G.F. (1985): Geochemistry of Holocene volcanic rocks associated with ridge subduction in Baja California, Mexico. *Nature*, 315: 389-392.

Rollinson, H.R. (1993): Using geochemical data: evaluation, presentation, interpretation. Longman Scientific Technical, Essex: 344 p.

Saunders, A.D. (2007): Geochemistry of Basalts Recovered from the Gulf of California during Leg 65 of the Deep Sea Drilling Project. *Deep Sea Drilling Project*, 65.

Saunders, A.D., Fornari, D.J., Joron, J.-L., Tarney, T., M., T. (2007): Geochemistry of Basic Igneous Rocks, Gulf of California, Deep Sea Drilling Project Leg 64. *Deep Sea Drilling Project*, 64: 595-642.

Saunders, A.D., Rogers, G., Marriner, G.F., Terrell, D.J., Verma, S.P. (1987): Geochemistry of Cenozoic volcanic rocks, Baja California, Mexico: implications for the petrogenesis of post-subduction magmas. *Journal of Volcanology and Geothermal Research*, 32: 223-245.

Shervais, J.W. (1982): Ti-V plots and the petrogenesis of modern and ophiolitic lavas. *Earth and Planetary Science Letters*, 59: 101-118.

Sheth, H.C. (2008): Do major oxide tectonic discrimination diagrams work? Evaluating new log-ratio and discriminant-analysis-based diagrams with Indian Ocean mafic volcanics and Asian ophiolites. *Terra Nova*, 20: 229-236.

Solano, V.J., Moreno, F.A.P., Iriondo, A., Demant, A., Cochemé, J.-J. (2005): Middle Miocene peralkaline ignimbrites in the Hermosillo region (Sonora, Mexico): Geodynamic implications. *Geomaterials (Petrology)*, 337: 1421-1430.

Spencer, J.E., Normark, R. (1979): Tosco-Abreojos fault zone: A Neogene transform plate boundary within the Pacific margin of southern Baja California, Mexico. *Geology*, 7: 554-557.

Stock, J.M., Lee, J. (1994): Do microplates in subduction zones leave a geological record? *Tectonics*, 13: 1472-1487.

Till, C.B., Gans, P.B., Spera, F.J., MacMillan, I., Blair, K.D. (2009): Perils of petrotectonic modeling: A review from southern Sononra, Mexico. J*ournal of Volcanology and Geothermal Research*, 186: 160-68.

Verma, S.K., Pandarinath, K., Verma, S.P. (2012): Statistical evaluation of tectonomagmatic discrimination diagrams for granitic rocks and proposal of new discriminant-function-based multi-dimensional diagrams for acid rocks. *International Geology Review*, 54: 325-347.

Verma, S.P. (1997): Sixteen statistical tests for outlier detection and rejection in evaluation of International Geochemical Reference Materials: example of microgabbro PM-S. *Geostandards Newsletter. The Journal of Geostandards and Geoanalysis*, 21: 59-75.

Verma, S.P. (2000): Geochemistry of the subducting Cocos plate and the origin of subduction-unrelated mafic volcanism at the volcanic front of the central Mexican Volcanic Belt. in Cenozoic tectonics and volcanism of Mexico. H. Delgado-Granados, Aguirre-Díaz, G., Stock, J.M., Eds., *Geological Society of America Special paper*, 334: 195-222.

Verma, S.P. (2010): Statistical evaluation of bivariate, ternary and discriminant function tectonomagmatic discrimination diagrams. *Turkish Journal of Earth Sciences*, 19: 185-238.

Verma, S.P. (2011): Geochemometrics. Santoyo, E., Torres-Alvarado, I.S., Pandarinath, K. (editors) Special Section on XX Congreso Nacional de Geoquímica, *Revista Mexicana de Ciencias Geológicas* (in press).

Verma, S.P., Agrawal, S. (2011): New tectonic discrimination diagrams for basic and ultrabasic volcanic rocks through log-transformed ratios of high field strength elements and implications for petrogenetic processes. *Revista Mexicana de Ciencias Geológicas*, 28: 24-44.

Verma, S.P., Díaz-González, L. (2011): Application of discordant outlier detection and separation system (DODESSYS) in geosciences. *International Geology Review*, submitted.

Verma, S.P., Rivera-Gómez, M.A. (2011): Application of TecD (A new computer program for tectonomagmatic discrimination from discriminant function diagrams for basic and ultrabasic magmas) to basic rocks from cratonic areas. In: Monograph on Geochemistry in Mexico, Verma, S.P., Pandarinath, K. (editors). *Journal of Iberian Geology* (submitted).

Verma, S.P., Guevara, M., Agrawal, S. (2006): Discriminating four tectonic settings: five new geochemical diagrams for basic and ultrabasic volcanic rocks based on log-ratio transformation of major-element data. *Journal of Earth System Science*, 115: 485-528.

Verma, S.P., Quiroz-Ruiz, A. (2006): Critical values for 22 discordancy test variants for outliers in normal samples up to sizes 100, and applications in science and engineering. *Revista Mexicana de Ciencias Geológicas*, 23: 302-319.

Verma, S.P., Quiroz-Ruiz, A. (2008): Critical values for 33 discordancy test variants for outliers in normal samples for very large sizes of 1,000 to 30,000. *Revista Mexicana de Ciencias Geológicas*, 25: 369-381.

Verma, S.P., Quiroz-Ruiz, A. (2006): Critical values for six Dixon tests for outliers in normal samples up to sizes 100, and applications in science and engineering. *Revista Mexicana de Ciencias Geológicas*, 23: 133-161.

Verma, S.P., Quiroz-Ruiz, A., Díaz-González, L. (2008): Critical values for 33 discordancy test variants for outliers in normal samples up to sizes 1000, and applications in quality control in Earth Sciences. *Revista Mexicana de Ciencias Geológicas*, 25: 82-96.

Verma, S.P., Rodríguez-Ríos, R., González-Ramírez, R. (2010): Statistical evaluation of classification diagrams for altered igneous rocks. *Turkish Journal of Earth Sciences*, 19: 239-265.

Verma, S.P., Torres-Alvarado, I.S., Sotelo-Rodríguez, Z.T. (2002): SINCLAS: standard igneous norm and volcanic rock classification system. *Computers & Geosciences*, 28: 711-715.

Verma, S.P., Torres-Alvarado, I.S., Velasco-Tapia, F. (2003): A revised CIPW norm. *Schweizerische Mineralogische und Petrographische Mitteilungen*, 83: 197-216.

Verma, S.P., Verma, S.K., Pandarinath, K., Rivera-Gómez, M.A. (2011): Evaluation of recent tectonomagmatic discrimnation diagrams and their application to the origin of basic magmas in Southern Mexico and Central America. *Pure and Applied Geophysics*, 168, 1501-1525.

Vermeesch, P. (2007): Tectonic discrimination diagrams revisited. *Geochemistry Geophysics Geosystems*, 7, Q06017, doi:10.1029/2005GC001092..

Vermeesch, P. (2006): Tectonic discrimination of basalts with classification trees. *Geochimica et Cosmochimica Acta*, 70: 1839-1848.

Vidal-Solano, J.R., Demant, A., Moreno, F.A.P., H., L., Ortega-Rivera, M.A., Lee, J.K.W. (2008): Insights into the tectonomagmatic evolution of NW Mexico: Geochronology and

geochemistry of the Miocene volcanic rocks from the Pinacate area, Sonora. *GSA Bulletin*, 120: 691-708.

Wood, D.A. (1980): The application of a Th-Hf-Ta diagram to problems of tectonomagmatic classification and to establishing the nature of crustal contamination of basaltic lavas of the British Tertiary volcanic province. *Earth and Planetary Science Letters*, 50: 11-30.

Zolotarev, B.P., Margolin, E.M. (2007): Geochemistry and Rare-Earth Element Abundances of Basalts from Sites 482, 483, and 485 in the Gulf of California. *Deep Sea Drilling Project*, 65: 579-590.

Captions to the Figures

Leyendas de las figuras

Fig. 1. Schematic map showing the locations of the basic rock samples used in this study. The open and filled circles represent the on-shore basic rocks of <13 Ma and >13 Ma ages, respectively. The open squares represent off-shore basic rocks.

Fig. 1. Mapa de esquemática mostrando la ubicación de las muestras de rocas básicas utilizadas en este estudio. Los círculos abiertos y llenados representados a las rocas básicas de la tierra de <13 Ma y de >13 Ma años edad, respectivamente. Los cuadrados abiertos representan a las rocas básicas de fuera de la costa.

Fig. 2. Application of the major-element discriminant function based discrimination diagrams of Agrawal *et al*. (2004) for basic rocks from northwestern Mexico.

Fig. 2. Aplicación de las diagramas discriminantes basado de los elementos mayores y de la función discriminación de Agrawal *et al*. (2004) para rocas básicas del noroeste de México.

Fig. 3. Application of the major-element discriminant function based discrimination diagrams of Verma *et al*. (2006) for basic rocks from northwestern Mexico.

Fig. 3. Aplicación de las diagramas discriminantes basado de los elementos mayores y de la función discriminación de Verma *et al*. (2006) para rocas básicas del noroeste de México.

Fig. 4. Application of the trace-element discriminant function based discrimination diagrams of Agrawal *et al*. (2008) for basic rocks from northwestern Mexico.

Fig. 4. Aplicación de las diagramas discriminantes basado de los elementos trazas y de la función discriminación de Agrawal *et al*. (2008) para rocas básicas del noroeste de México.

Fig. 5. Application of the trace-element discriminant function based discrimination diagrams of Verma and Agrawal (2011) for basic rocks from northwestern Mexico. The samples marked with red color are outliers.

Fig. 5. Aplicación de las diagramas discriminantes basado de los elementos trazas y de la función discriminación de Verma y Agrawal (2011) para rocas básicas del noroeste de México. Las muestras marcadas con el color rojo son los valores desviados.

Table 1. Information on tectonomagmatic origin obtained from the set of five discriminant function based discrimination diagrams of Agrawal *et al*. (2004) for on-land and off-shore basic rocks of northwest Mexico

Tabla 1. Información sobre el origen tectonomagmáticas obtenidas a partir del conjunto de las cinco diagramas de discriminación basado del función discriminante de Agrawal *et al*. (2004) para las rocas básicas provenido de la tierra y afuera de costa del noroeste de México

Locality	Discrimination function discrimination diagram	Total number of samples	Number of discriminated samples (%)			
			IAB (1)	CRB (2)	OIB (3)	MORB (4)
On-land basic rocks (<13 Ma)	1-2-3-4	89	0 (0)	***63 (71)***	4 (4)	22 (25)
	1-2-3	89	13 (15)	***75 (84)***	1 (1)	---
	1-2-4	89	2 (2)	***67 (75)***	---	20 (23)
	1-3-4	89	3 (3)	---	***50 (56)***	***36 (41)***
	2-3-4	89	---	***76 (86)***	3 (3)	10 (11)
On-land basic rocks (>13 Ma)	1-2-3-4	13	3 (23)	***10 (77)***	0	0
	1-2-3	13	4 (31)	***9 (69)***	0	---
	1-2-4	13	***5 (38)***	***8 (62)***	---	0
	1-3-4	13	***5 (38.5)***	---	***5 (38.5)***	3 (23)
	2-3-4	13	---	***12 (92)***	0	1 (8)
Off-shore rocks	1-2-3-4	608	4 (1)	9 (1)	46 (8)	***549 (90)***
	1-2-3	608	*227 (37)*	98 (16)	***283 (47)***	---
	1-2-4	608	2 (0.3)	17 (2.8)	---	***589 (96.9)***
	1-3-4	608	5 (1)	---	38 (6)	***565 (93)***
	2-3-4	608	---	6 (1)	51 (8)	***551 (91)***
Sea-floor dredged material	1-2-3-4	3	0	0	0	***3***
	1-2-3	3	***3***	0	0	---
	1-2-4	3	0	0	---	***3***
	1-3-4	3	0	---	0	***3***
	2-3-4	3	---	0	0	***3***

Table 2. Information on tectonomagmatic origin obtained from the set of five discriminant function based discrimination diagrams of Verma *et al*. (2006) for on-land and off-shore basic rocks of northwest Mexico

Tabla 2. Información sobre el origen tectonomagmáticas obtenidas a partir del conjunto de las cinco diagramas de discriminación basado del función discriminante de Verma *et al*. (2006) para las rocas básicas provenido de la tierra y fuera de costa del noroeste de México

Locality	Discrimination function discrimination diagram	Total number of samples	Number of discriminated samples (%)			
			IAB (1)	CRB (2)	OIB (3)	MORB (4)
On-land basic rocks (<13 Ma)	1-2-3-4	89	1 (1)	***71 (80)***	11 (12)	6 (7)
	1-2-3	89	1 (1)	***83 (93)***	5 (6)	---
	1-2-4	89	1 (1)	***81 (91)***	---	7 (8)
	1-3-4	89	9 (10)	---	***52 (58)***	28 (32)
	2-3-4	89	---	***80 (90)***	2 (2)	7 (8)
On-land basic rocks (>13 Ma)	1-2-3-4	13	3 (23)	***10 (77)***	0	0
	1-2-3	13	2 (15)	***11 (85)***	0	---
	1-2-4	13	2 (15)	***11 (85)***	---	0
	1-3-4	13	***7 (54)***	---	3 (23)	3 (23)
	2-3-4	13	---	***12 (92)***	0	1 (8)
Off-shore rocks	1-2-3-4	608	4 (0.7)	2 (0.3)	15 (2.5)	***587 (96.5)***
	1-2-3	608	5 (1)	37 (6)	***566 (93)***	---
	1-2-4	608	5 (1)	4 (1)	---	***599 (98)***
	1-3-4	608	4 (1)	---	61 (10)	***543 (89)***
	2-3-4	608	---	4 (1)	20 (3)	***584 (96)***
Sea-floor dredged material	1-2-3-4	3	0	0	0	***3***
	1-2-3	3	1	1	1	---
	1-2-4	3	1	0	---	***2***
	1-3-4	3	0	---	0	***3***
	2-3-4	3	---	0	0	***3***

Table 3. Information on tectonomagmatic origin obtained from the set of five discriminant function based discrimination diagrams of Agrawal *et al*. (2008) for on-land and off-shore basic rocks of northwest Mexico

Tabla 3. Información sobre el origen tectonomagmáticas obtenidas a partir del conjunto de las cinco diagramas de discriminación basado del función discriminante de Agrawal *et al*. (2008) para las rocas básicas provenido de la tierra y fuera de costa del noroeste de México

Locality	Discrimination function discrimination diagram	Total number of samples	Number of discriminated samples (%)				
			IAB (1)	CRB (2)	CRB (2) + OIB (3)	OIB (3)	MORB (4)
On-land basic rocks (<13 Ma)	1-2+3-4	80	12 (15)	---	***64 (80)***	---	4 (5)
	1-2-3	80	14 (17)	***46 (58)***	---	20 (25)	---
	1-2-4	80	12 (15)	***64 (80)***	---	---	4 (5)
	1-3-4	80	11 (14)	---	---	***61 (76)***	8 (10)
	2-3-4	80	---	***52 (65)***	---	21 (26)	7 (9)
On-land basic rocks (>13 Ma)	1-2+3-4	13	4 (31)	---	***9 (69)***	---	0
	1-2-3	13	***5 (38.5)***	***5 (38.5)***	---	3 (23)	---
	1-2-4	13	4 (31)	***9 (69)***	---	---	0
	1-3-4	13	4 (31)	---	---	***8 (61)***	1 (8)
	2-3-4	13	---	***10 (77)***	---	2 (15)	1 (8)
Altered glass	1-2-3-4	2	***1***	---	0	---	***1***
	1-2-3	2	***1***	0	---	***1***	---
	1-2-4	2	***1***	0	---	---	***1***
	1-3-4	2	***1***	---	---	0	***1***
	2-3-4	2	---	0	---	0	***2***
Margin	1-2+3-4	3	1	---	0	---	***2***
	1-2-3	3	1	0	---	***2***	---
	1-2-4	3	1	0	---	---	***2***
	1-3-4	3	1	---	---	0	***2***
	2-3-4	3	---	0	---	0	***3***
Core samples	1-2+3-4	3	0	---	0	0	***3***
	1-2-3	3	0	0	---	***3***	---
	1-2-4	3	0	0	---	---	***3***
	1-3-4	3	0	---	---	0	***3***
	2-3-4	3	---	0	---	0	***3***

Table 4. Information on tectonomagmatic origin obtained from the set of five discriminant function based discrimination diagrams of Verma and Agrawal (2011) for on-land and off-shore basic rocks of northwest Mexico

Tabla 4. Información sobre el origen tectonomagmáticas obtenidas a partir del conjunto de las cinco diagramas de discriminación basado del función discriminante de Verma y Agrawal (2011) para las rocas básicas provenido de la tierra y fuera de costa del noroeste de México

Locality	Discrimination function discrimination diagram	Total number of samples	Number of discriminated samples (%)				
			IAB (1)	CRB (2)	CRB (2) + OIB (3)	OIB (3)	MORB (4)
On-land basic rocks (<13 Ma)	1-2+3-4	68	3 (4)	---	***60 (89)***	---	5 (7)
	1-2-3	68	6 (9)	***45 (66)***	---	17 (25)	---
	1-2-4	68	3 (4)	***61 (90)***	---	---	4 (6)
	1-3-4	68	3 (4)	---	---	***52 (77)***	13 (19)
	2-3-4	68	---	***45 (66)***	---	18 (27)	5 (7)
On-land basic rocks (>13 Ma)	1-2+3-4	1	***1***	---	0	---	0
	1-2-3	1	***1***	0	---	0	---
	1-2-4	1	***1***	0	---	---	0
	1-3-4	1	***1***	---	---	0	0
	2-3-4	1	---	0	---	0	***1***
Off-shore rocks	1-2-3-4	78	0 (0)	---	0 (0)	---	***78 (100)***
	1-2-3	78	***75 (96)***	3 (4)	---	0 (0)	---
	1-2-4	78	0 (0)	0 (0)	---	---	***78 (100)***
	1-3-4	78	0 (0)	---	---	0 (0)	***78 (100)***
	2-3-4	78	---	0 (0)	---	0 (0)	***78 (100)***

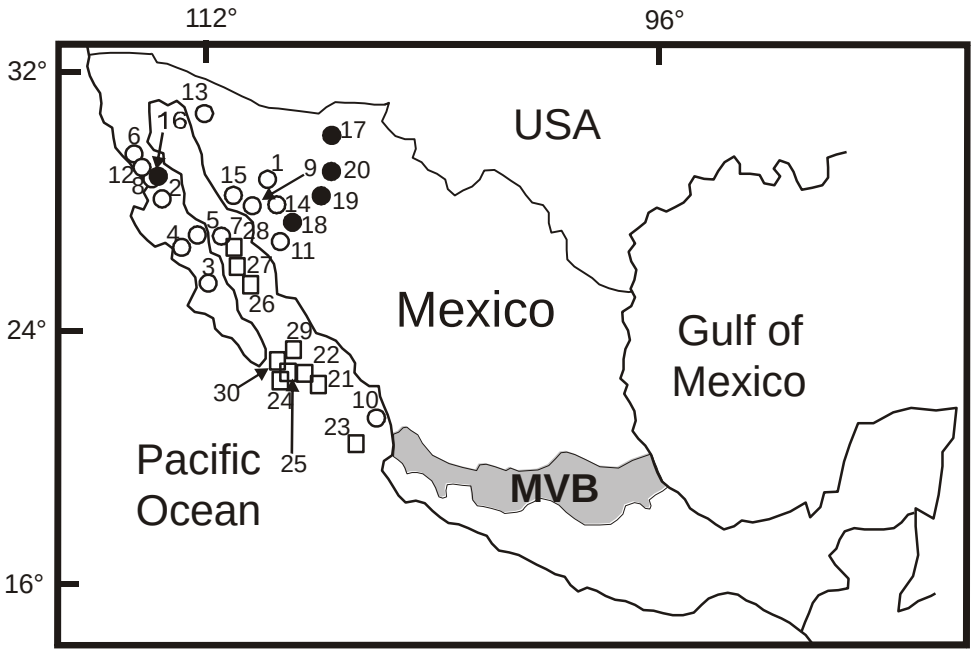

1. Hermosillo (n=2)
2. San Borja vol. field (n=8)
3. La Purisima vol. field (n=2)
4. Santa Clara vol. field (n=6)
5. San Ignacio vol. field (n=1)
6. San Quintin vol. field (n=36)
7. Isla Tortuga (n=1)
8. Jaraguay vol. field (n=1)
9. Sierra El Aguaje (n=6)
10. Isla Isabel (n=10)
11. Guaymas Basin (n=2)
12. San Carlos-Santa Catarina (n=6)
13. Pinacate Area,Sonora (n=4)
14. Sierra Libre (n=2)
15. Coastal Sonora (n=2)
16. Comondú Formation (n=1)
17. Sierra Madre Occidental (n=3)
18. Sierra Santa Ursula (n=2)
19. Suaqui Grande (n=2)
20. Sahuaripa (n=5)
21. DSDP site 482 (n=176)
22. DSDP site 483 (n=132)
23. DSDP site 485 (n=93)
24. DSDP site 474 (n=76)
25. DSDP site 475 (n=12)
26. DSDP site 477 (n=34)
27. DSDP site 478 (n=50)
28. DSDP site 481 (n=5)
29. Alarcon Rise (n=29)
30. Mouth of the Gulf of California (n=4)

Fig. 1

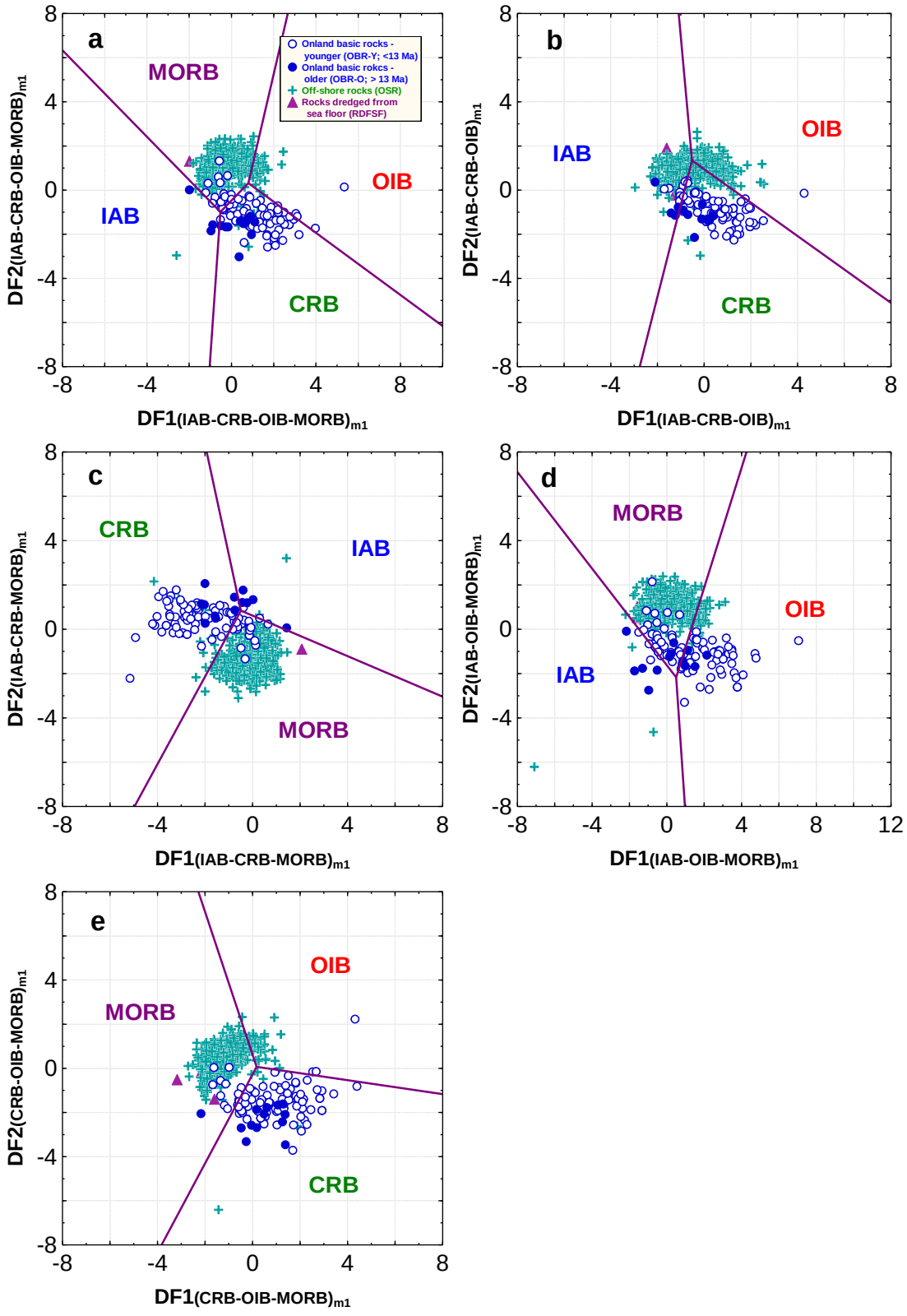
a
MORB
OIB
IAB
CRB
Onland basic rocks - younger (OBR-Y; <13 Ma)
Onland basic rokcs - older (OBR-O; > 13 Ma)
Off-shore rocks (OSR)
Rocks dredged frrom sea floor (RDFSF)
DF2(IAB-CRB-OIB-MORB)m1
DF1(IAB-CRB-OIB-MORB)m1
b
IAB
OIB
CRB
DF2(IAB-CRB-OIB)m1
DF1(IAB-CRB-OIB)m1
c
CRB
IAB
MORB
DF2(IAB-CRB-MORB)m1
DF1(IAB-CRB-MORB)m1
d
MORB
OIB
IAB
DF2(IAB-OIB-MORB)m1
DF1(IAB-OIB-MORB)m1
e
OIB
MORB
CRB
DF2(CRB-OIB-MORB)m1
DF1(CRB-OIB-MORB)m1

Fig. 2

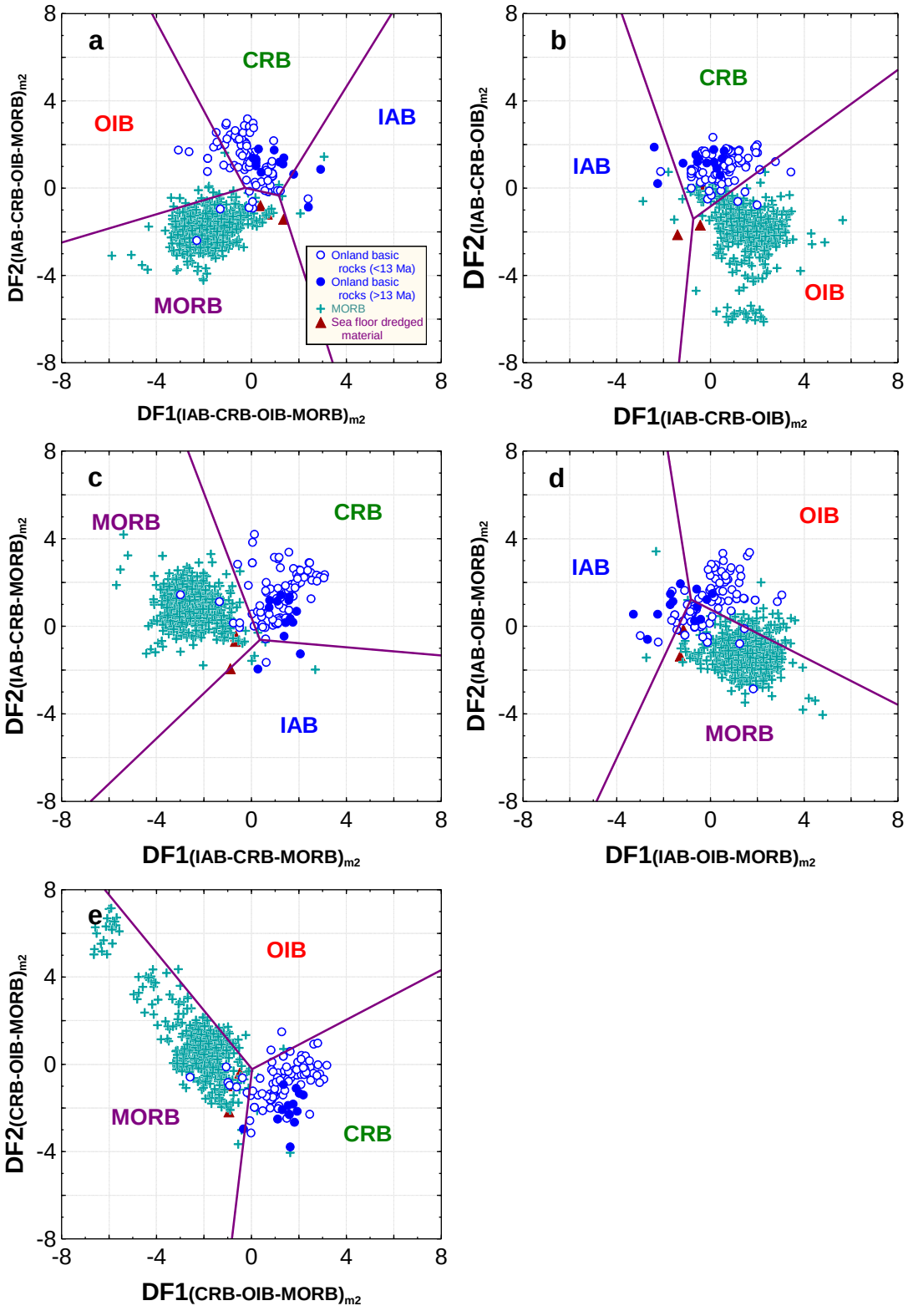
a
CRB
OIB
IAB
MORB
Onland basic rocks (<13 Ma)
Onland basic rocks (>13 Ma)
MORB
Sea floor dredged material
DF2(IAB-CRB-OIB-MORB)m2
DF1(IAB-CRB-OIB-MORB)m2
b
CRB
IAB
OIB
DF2(IAB-CRB-OIB)m2
DF1(IAB-CRB-OIB)m2
c
MORB
CRB
IAB
DF2(IAB-CRB-MORB)m2
DF1(IAB-CRB-MORB)m2
d
OIB
IAB
MORB
DF2(IAB-OIB-MORB)m2
DF1(IAB-OIB-MORB)m2
e
OIB
MORB
CRB
DF2(CRB-OIB-MORB)m2
DF1(CRB-OIB-MORB)m2

Fig. 3

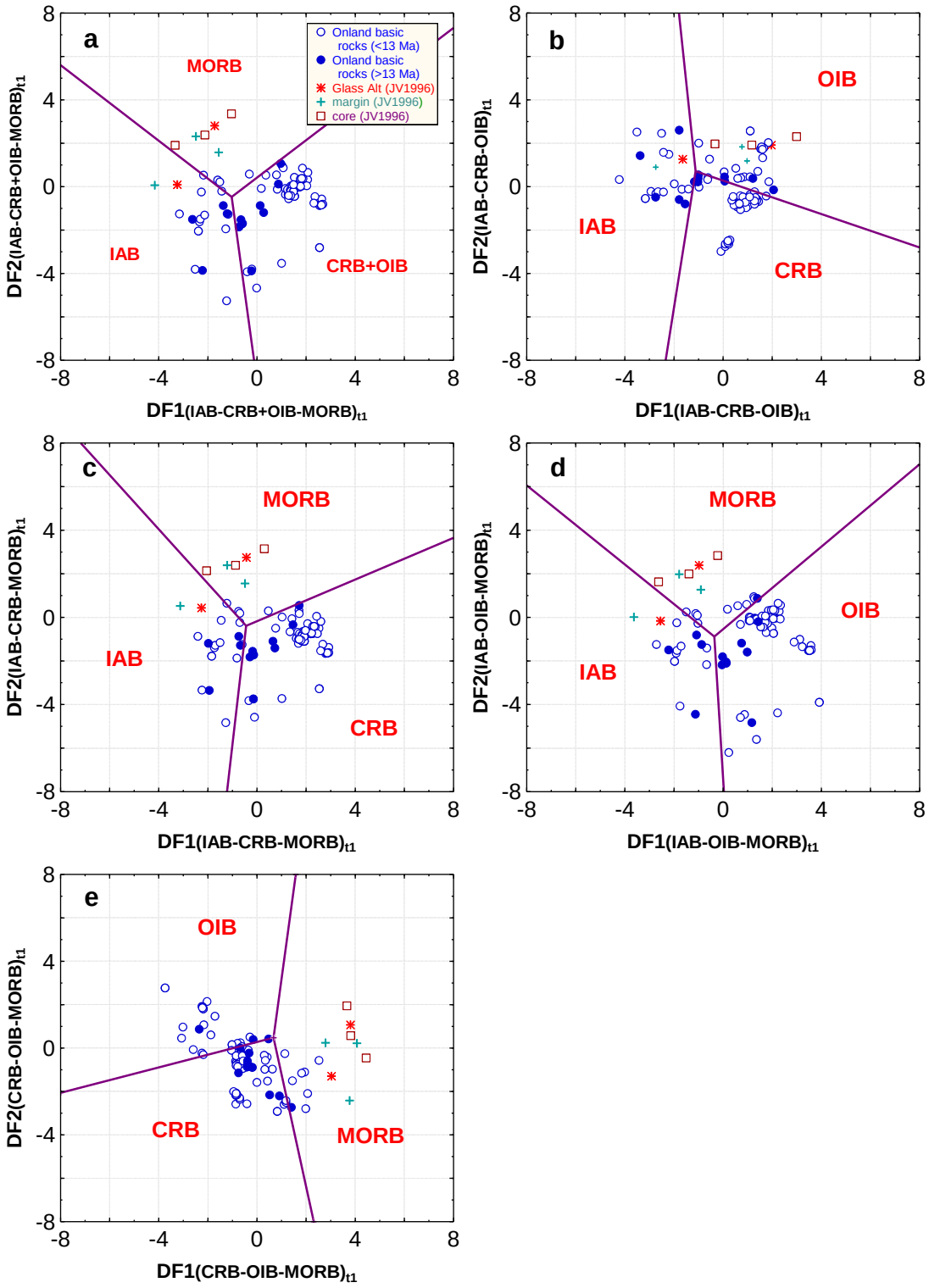
a
MORB
IAB
CRB+OIB
Onland basic rocks (<13 Ma)
Onland basic rocks (>13 Ma)
Glass Alt (JV1996)
margin (JV1996)
core (JV1996)
DF2(IAB-CRB+OIB-MORB)t1
DF1(IAB-CRB+OIB-MORB)t1
b
OIB
IAB
CRB
DF2(IAB-CRB-OIB)t1
DF1(IAB-CRB-OIB)t1
c
MORB
IAB
CRB
DF2(IAB-CRB-MORB)t1
DF1(IAB-CRB-MORB)t1
d
MORB
OIB
IAB
DF2(IAB-OIB-MORB)t1
DF1(IAB-OIB-MORB)t1
e
OIB
CRB
MORB
DF2(CRB-OIB-MORB)t1
DF1(CRB-OIB-MORB)t1

Fig. 4

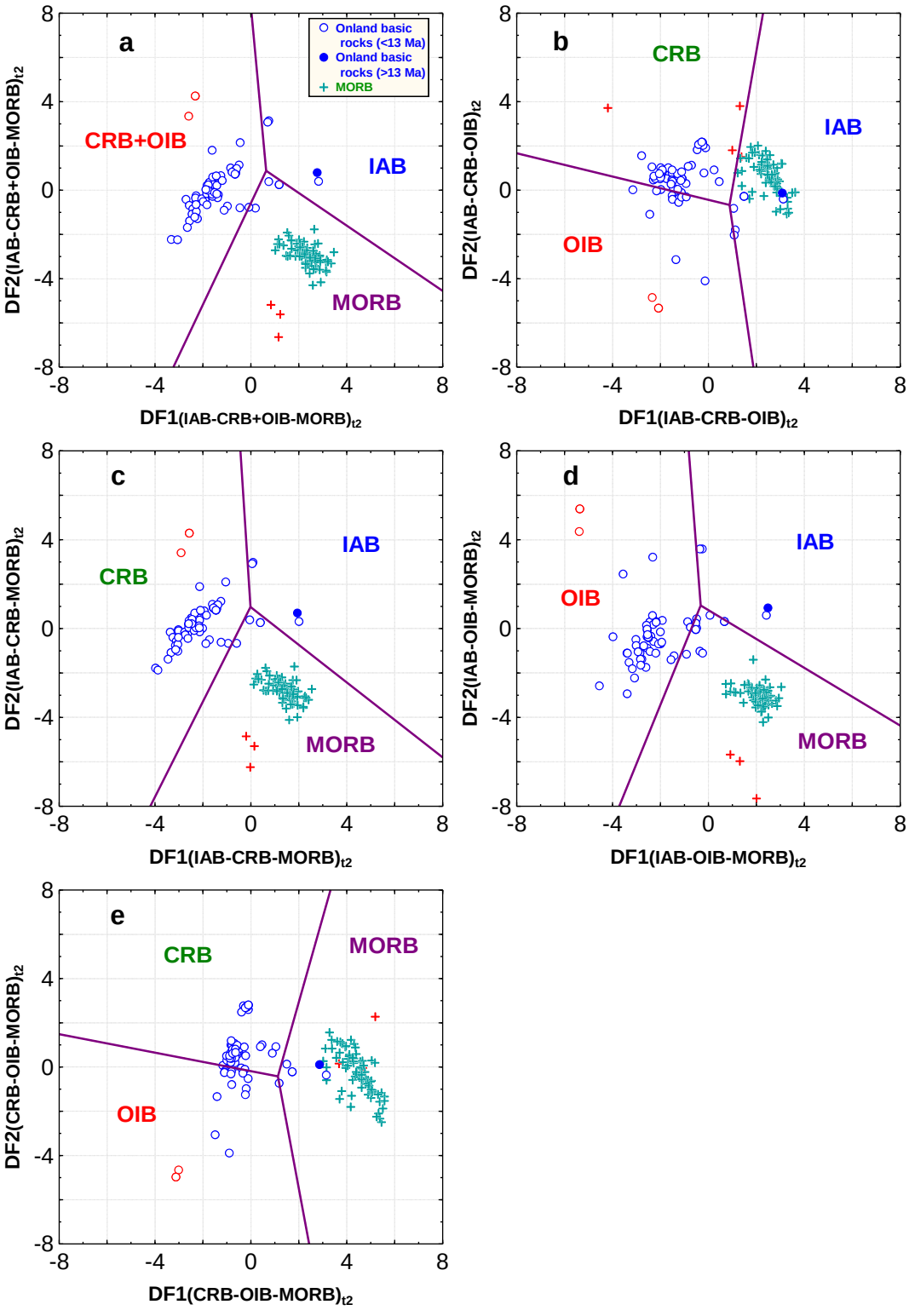
a
Onland basic rocks (<13 Ma)
Onland basic rocks (>13 Ma)
MORB
CRB+OIB
IAB
MORB
DF2(IAB-CRB+OIB-MORB)t2
DF1(IAB-CRB+OIB-MORB)t2
b
CRB
IAB
OIB
DF2(IAB-CRB-OIB)t2
DF1(IAB-CRB-OIB)t2
c
IAB
CRB
MORB
DF2(IAB-CRB-MORB)t2
DF1(IAB-CRB-MORB)t2
d
IAB
OIB
MORB
DF2(IAB-OIB-MORB)t2
DF1(IAB-OIB-MORB)t2
e
CRB
MORB
OIB
DF2(CRB-OIB-MORB)t2
DF1(CRB-OIB-MORB)t2

Fig. 5

Annexure V

ANNEXURE V

Verma, S.P., Verma, S.K., 2012. The First Fifteen Probability-Based Multi-Dimensional Tectonic Discrimination Diagrams for Intermediate Magmas and their Robustness against Post-Emplacement Compositional Changes and Petrogenetic Processes: **Turkish Journal of Earth Sciences, submitted**.

.

The First Fifteen Probability-Based Multi-Dimensional Tectonic Discrimination Diagrams for Intermediate Magmas and their Robustness against Post-Emplacement Compositional Changes and Petrogenetic Processes

SURENDRA P. VERMA[1,*] & SANJEET K. VERMA[2]

[1] Departamento de Sistemas Energéticos, Centro de Investigación en Energía, Universidad Nacional Autónoma de México, Temixco, Mor. 62580, Mexico

[2]posgrado en Ingeniería, Centro de Investigación en Energía, Universidad Nacional Autónoma de México, Temixco, Mor. 62580, Mexico

* Corresponding author. Email: spv@cie.unam.mx

Running title: DISCRIMINATION DIAGRAMS FOR INTERMEDIATE MAGMAS

Manuscript submitted to: **Turkish Journal of Earth Sciences**, April 12, 2012

Abstract: Although for ultrabasic and basic magmas a plethora of tectonomagmatic diagrams have been used, with the exception of one bivariate diagram for refined tectonic setting of orogenic andesites, none is available for highly abundant intermediate magma. We present three sets of discrimination diagrams obtained from the correct statistical methodology of $\log_e$-ratio transformation and linear discriminant analysis. All major element $\log_e$-ratio variables in 3664 samples, only immobile major and trace element $\log_e$-ratio variables in 1858 samples, and immobile trace element $\log_e$-ratio variables in 1512 samples were used. These diagrams with probability-based tectonic field boundaries and high success rates (about 69%−96%, 63%−100%, and 64%−100%, respectively, for diagrams based on all major-elements, immobile major and trace elements, and immobile trace elements) were first tested for fresh and highly altered rocks. The expected tectonic setting was indicated from our diagrams. The probability based decisions and total percent probability estimates can fully replace the actual plotting of samples in diagrams. The probability calculations were then used for tectonic discrimination of seven case studies of Archean to Proterozoic rocks. An island arc setting was indicated for the Wawa greenstone belt (Canada) implying the existence of plate tectonic processes during the Late Archean, for western Tasmania (Australia) during the Cambrian, and for Chichijima Island (Bonin Islands, Japan) during the Eocene. Similarly, an arc setting (indecisive island or continental type) was obtained for south-central Sweden during the Paleoproterozoic and for Adola (southern Ethiopia) during the Neoproterozoic. A within-plate setting was inferred for the Neoproterozoic Malani igneous complex, Rajasthan, India and a collision setting was indicated for the Alps (France-Italy-Switzerland) during the Late Carboniferous. Modeling of likely as well as extreme processes indicates that these diagrams are robust against post-emplacement compositional changes caused by analytical errors, element mobility, Fe-oxidation, alteration, and petrogenetic processes.

Key Words: arc, collision, natural logarithm transformation of element ratios, tectonomagmatic discrimination, within-plate tectonic setting

Annexure VI

ANNEXURE VI (Page 273-296)

Verma, S.K., Verma, S.P., 2012. Identification of plate tectonic processes in the Archean from multi-dimensional discrimination diagrams and probability calculations. **International Geology Review, in press,** DOI: 10.1080/00206814.2012.693246, ISSN 0020-6814 print/ISSN 1938-2839 online.

.

CE: JF CE QA: AS

International Geology Review
Vol. 00, No. 00, Xxxx 2012, 1–24

Taylor & Francis
Taylor & Francis Group

Identification of Archaean plate tectonic processes from multidimensional discrimination diagrams and probability calculations

Sanjeet K. Verma[a] and Surendra P. Verma[b]*

[a]*Centro de Investigación en Energía, Universidad Nacional Autónoma de México, Temixco, Morelos 62580, Mexico;* [b]*Departamento de Sistemas Energéticos, Centro de Investigación en Energía, Universidad Nacional Autónoma de México, Temixco, Morelos 62580, Mexico*

(*Accepted 9 May 2012*)

We applied our group's previously published multidimensional diagrams in 2006–2008 and corresponding probability estimates in 2011–2012 to geochemical data for Archaean rocks compiled from cratons in Australia, South Africa, Brazil, Canada, and India. Tectonic processes similar to present-day plate tectonics evidently were active at least since the Palaeoarchaean (about 3570 million years). This seems to be true in spite of a presumably hotter Earth at that time. For the eastern part of the Pilbara craton (Australia), a Palaeoarchaean (3570–3450 million years) and Mesoarchaean (2900 million years) continental arc settings apparently evolved to a collision (Col) setting during the Neoarchaean (2600 million years). We infer an island arc (IA) environment for Kambalda (Australia) during the Neoarchaean (2700 million years). For the Barberton belt (South Africa), a transition from a mid-ocean ridge regime during the older part of the Palaeoarchaean (3470 million years) to an IA setting during the younger part (3300–3260 million years) is likely. We inferred an arc environment for the São Francisco craton (Brazil) and the Rio Maria terrane (Brazil) during the Mesoarchaean (3085–2983 million years and 2870 million years, respectively), whereas a within-plate setting is clearly indicated for the Carajás metallogenic province (Brazil) during the Neoarchaean (2740–2700 million years). We also recognize an IA regime for the Mesoarchaean (3000 million years) North Caribou and Neoarchaean (2700 million years) Abitibi greenstone belts (Canada), and for the Gadwal greenstone belt (India) during the Neoarchaean (2700–2500 million years). A Col setting was inferred for the Archaean sanukitoid suite (Canada) and the Kolar suture zone (India) during the Neoarchaean (2700–2660 million years and 2630–2520 million years, respectively).

Keywords: Archaean rocks; collision; continental arc; island arc; log-ratio transformation; mid-ocean ridge setting; Archaean plate tectonics; tectonic settings

Introduction

There seems to be no consensus on how far back in time tectonic processes similar to the modern plate tectonics have been operative in the Earth (e.g. Condie and Pease 2008; Ernst 2009; McCall 2010; Van Kranendonk 2010; Korsch *et al*. 2011). Although some authors (e.g. Stern 2008; Hamilton 2011) agree that this may certainly be true for the Proterozoic, its validity during the Archaean, albeit controversial, has been proposed by numerous workers (e.g. Kerrich and Polat 2006; Condie and Kröner 2008; Foley 2008; Pease *et al*. 2008; Polat *et al*. 2008; Shirey *et al*. 2008; Furnes *et al*. 2009; Manikyamba and Kerrich 2012). New evidence could, therefore, better constrain the answers to this vital question.

Recently (during 2006–2011), three sets of diagrams (five in each set) based on log-ratio transformation and linear discriminant analysis have been proposed to discriminate four tectonic settings of arc [no distinction between island arc (IA) and continental arc (CA)], continental rift (CR), ocean island (OI), and mid-ocean ridge (MOR) for basic or ultrabasic magma (Verma *et al*. 2006, based on major elements; Agrawal *et al*. 2008, based on immobile trace elements; and Verma and Agrawal 2011, based on immobile high-field strength elements). For basic and ultrabasic rocks, a computer program TecD (Verma and Rivera-Gómez 2012) should prove useful for an efficient application of all four sets of multidimensional discrimination diagrams (Agrawal *et al*. 2004, 2008; Verma *et al*. 2006; Verma and Agrawal 2011). Even more recently (during 2012), four sets of multidimensional diagrams (five diagrams for each set) were similarly proposed for discriminating four tectonic settings of IA, CA, within plate (only CR for acid magma, but combined CR and OI for intermediate magma), and collision (Col) for acid magma (Verma *et al*. 2012, based on major elements) and intermediate magma (Verma and Verma 2012, based on major elements,

*Corresponding author. Email: spv@cie.unam.mx

ISSN 0020-6814 print/ISSN 1938-2839 online

http://dx.doi.org/10.1080/00206814.2012.693246
http://www.tandfonline.com

immobile major and trace elements, and immobile trace elements). Besides the original authors, these diagrams have been tested and used by Sheth (2008), Verma (2010), Verma *et al*. (2011), Pandarinath and Verma (2012), and Verma (2012), among others.

The diagrams allow the visualization of geochemical data of 5 immobile elements to 11 major element variables in two dimensions. The discrimination boundaries were based on an objective criterion of equal probabilities for the two or three tectonic fields being separated in different parts of the diagrams (Agrawal 1999). For the newer diagrams (for basic and ultrabasic magmas by Verma and Agrawal 2011; acid magma by Verma *et al*. 2012; and intermediate magma by Verma and Verma 2012), the authors also reported the methodology for the calculation of probability-based discrimination boundaries. Such probability calculations for individual samples can, in fact, replace the actual plotting of samples in diagrams as recently illustrated by Verma (2012).

Polat *et al*. (2011a), among others, have pointed out similarities as well as differences of element ratios between the Archaean and Cenozoic ultrabasic and basic rocks. Nevertheless, the evaluation of the geochemical characteristics in multidimensional diagrams has been seldom reported for Archaean rocks. Bailie *et al*. (2010) used just one of the five multidimensional diagrams of Agrawal *et al*. (2008) for Archaean basic rocks from South Africa to indicate an arc setting. Polat *et al*. (2009a, 2009b, 2011a) used only two of the five diagrams of Agrawal *et al*. (2008) to infer an arc or a MORB to arc transitional setting for Archaean rocks from Greenland. In a review article on Eoarchaean to Mesoarchaean rocks from Greenland, Polat *et al*. (2011b), on the other hand, employed all five diagrams of Agrawal *et al*. (2008) to show a transitional MOR to arc tectonic setting. Verma and Verma (2012), on the other hand, compiled the data for the Neoarchaean Wawa greenstone belt (Canada) from Polat *et al*. (1999) and Polat (2009) and used all 15 discrimination diagrams for intermediate magma to infer an IA setting for these Archaean rocks. Similarly, Verma and Díaz-González (2012) used two complete sets of multidimensional diagrams (Verma and Agrawal 2011; Verma *et al*. 2012) to understand the probable tectonic setting of the Archaean to Proterozoic basic and acid rocks from several areas.

The multidimensional diagrams allow us to achieve a probability-based quantitative comparison of geochemical data in many dimensions, whereas so far, with the exception of the few studies mentioned above, only qualitative comparisons have been attempted mostly in element ratios, i.e. only two or at most four compositional variables are compared at a time. Thus, there is an ample scope to resort to multidimensional diagrams for understanding plate tectonic processes during the Archaean.

We report the use of new multidimensional diagrams and probability estimates to geochemical data of Archaean rocks from cratons in Australia, South Africa, Brazil, Canada, and India and infer that tectonic processes similar to the present-day plate tectonics might have been active at least since the Palaeoarchaean (about 3570 million years). This seems to be true in spite of the presumably hotter Earth during that time (e.g. Foley 2008; van Hunen and van den Berg 2008; van Kranendonk 2010; Polat *et al*. 2011b).

Data base and procedures

We compiled age and geochemical data for Archaean rocks from Australia, South Africa, Brazil, Canada, and India (Table 1). The ages range from Palaeoarchaean (3570–3450 million years) to Neoarchaean (2600 million years) for the eastern part of the Pilbara craton (Australia); Palaeoarchaean (3470–3260 million years) for the Barberton belt (South Africa); Mesoarchaean (3085–2870 million years) for the São Francisco craton (Brazil) and Rio Maria terrane (Brazil) to Neoarchaean (about 2740–2700 million years) for the Carajás metallogenic province (Brazil); Mesoarchaean (3000 million years) for the North Caribou greenstone belt (Canada) to Neoarchaean (2700–2660 million years) for the Abitibi greenstone belt (Canada) and Archaean sanukitoid suite (Canada); and Neoarchaean (2700–2520 million years) for the Gadwal greenstone belt of the Dharwar craton (India) and Kolar suture zone of the Kolar schist belt (India). For the subdivision of the Archaean, we followed the scheme proposed by the International Commission on Stratigraphy (Gradstein *et al*. 2004).

The total numbers of rock samples from each area grouped according to their ages are also presented in Table 1. All major element data were processed in SINCLAS computer program (Verma *et al*. 2002) under the Middlemost (1989) option for Fe-oxidation subdivision. The rocks were separated into acid, intermediate, and basic or ultrabasic varieties (Le Bas *et al*. 1986) and the data were used in the respective discrimination diagrams for acid (Verma *et al*. 2012), intermediate (Verma and Verma 2012), and basic or ultrabasic (Verma *et al*. 2006; Agrawal *et al*. 2008; Verma and Agrawal 2011) magmas. The log-transformed ratios were also tested by DODESSYS computer program (Verma and Díaz-González 2012) for the identification and separation of discordant outlier observations. For the newer diagrams proposed during 2011–2012, this procedure was adopted for all diagrams.

SINCLAS, DODESSYS, and TecD computer programs are therefore recommended as important tools for the use of these newer diagrams. Posterior probabilities were estimated for each diagram of the newer sets (Verma and Agrawal 2011; Verma *et al*. 2012; Verma and Verma 2012) and interpreted following Verma (2012).

Results and discussion

The results of discrimination diagrams and probability calculations are summarized in Table 2 for acid rocks, Table 3

Table 1. Synthesis of Archaean bulk-rock chemical data base.

AQ11

Number of case study and its name	Country	Approximate location		Number of samples*	Age and rock type		Reference(s)
		Longitude (°)	Latitude (°)		Epoch (age in million years)	Rock type	
1a. Pilbara craton	Australia	120 E	21.3 S	29 (25A, 4I)	Palaeoarchaean (3570–3450)	Granitoid (pluton and gneiss)	Jahn *et al*. (1981) and Bickle *et al*. (1983)
1b. Pilbara craton	Australia	120 E	21.2 S	7 (7A)	Mesoarchaean (2900)	Older plutonic rock	Jahn *et al*. (1981)
1c. Pilbara craton	Australia	120 E	21.2 S	3 (3A)	Neoarchaean (2600)	Post-tectonic adamellite	Jahn *et al*. (1981)
2. Kambalda	Australia	121.64 E	31.19 S	35 (1A, 17I, 17B)	Neoarchaean (2700)	Komatiite, basalt	Arndt and Jenner (1986)
3a. Barberton belt	South Africa	30.57 E	25.33 S	11 (1I, 10B)	Palaeoarchaean (3470)	Komatiite	Lahaye *et al*. (1995)
3b. Barberton belt	South Africa	30.57 E	25.33 S	10 (8I, 2B)	Palaeoarchaean (3300–3260)	Komatiite	Lahaye *et al*. (1995)
4. São Francisco craton	Brazil	39.48 W	9.80 S	12 (8A, 4I)	Mesoarchaean (3085–2983)	TTG, orthogranulite	Oliveira *et al*. (2010)
5. Rio Maria terrane	Brazil	50.03 W	7.32 S	12 (12A)	Mesoarchaean (2870)	Granodiorite, intermediate rock	Oliveira *et al*. (2009)
6. Carajás metallogenic province	Brazil	49.58 W	6.10 S	28 (28A)	Neoarchaean (2740–2700)	Granodiorite, granite	Barros *et al.* (2009) and Sardinha *et al.* (2006)
7. North Caribou greenstone belt	Canada	90.38 W	52.61 N	29 (6A, 7I, 16B)	Mesoarchaean (3000)	Komatiite, volcanic	Hollings and Kerrich (1999)
8. Abitibi greenstone belt	Canada	81.0 W	48.5 N	30 (7I 19B + 4U)	Neoarchaean (2700)	Boninite, tholeiite	Lahaye *et al*. (1995) and Kerrich *et al*. (1998)
9. Archaean sanukitoid suite	Canada	89.04 W	48.64 N	16 (10A, 6I)	Neoarchaean (2700–2660)	Diorite, granite	Stevenson *et al*. (1999)
10. Gadwal greenstone belt	India	77.8 E	18.23 N	21 (21B)	Neoarchaean (2700–2500)	Boninite, tholeiite	Manikyamba *et al*. (2005)
11. Kolar suture zone	India	78.00 E	13.00 N	7 (6A, 1I)	Neoarchaean (2630–2520)	Gneiss, granite	Krogstad *et al*. (1995)

Note: A, acid rock; I, intermediate rock; B, basic rock; U, ultrabasic rock; TTG, tonalite-tondhjemite-granodiorite.

Table 2. Application of the set of five discriminant function-based multidimensional discrimination diagrams (Verma *et al*. 2012) to Archaean acid rocks through probability calculations.

Locality (Country) (Epoch)	Tectonic diagram	Total number of samples	Number of discriminated samples [$\bar{x} \pm s$ of probability values] (range of probability values for samples)				
			IA + CA	IA	CA	CR	Col
Pilbara craton (Australia) (Palaeoarchaean)	IA+ CA–CR–Col	25	20 [0.804 ± 0.132] (0.5611 − 0.9553)	–	–	1 (0.5785)	4 [0.822 ± 0.267] (0.4241 − 0.9965)
	IA–CA–CR	25	–	6 [0.757 ± 0.143] (0.5406 − 0.8938)	17[0.691 ± 0.151] (0.4994 − 0.9984)	2 [0.950 ± 0.068] (0.9016 − 0.9984)	–
	IA–CA–Col	25	–	10 [0.645 ± 0.200] (0.3753 − 0.9068)	10 [0.585 ± 0.088] (0.4684 − 0.7448)	–	5 [0.858 ± 0.191] (0.5430 − 1.0000)
	IA–CR–Col*	25	–	17 [0.866 ± 0.087] (0.5775 − 0.9999)	–	1 (0.5413)	7 [0.773 ± 0.196] (0.5177 − 0.9999)
	CA–CR–Col	25	–	–	20 [0.920 ± 0.105] (0.5966 − 0.9999)	1 (0.5945)	4 [0.788 ± 0.227] (0.4528 − 0.9487)
1a. Pilbara craton (Australia)	**{Σn} {Σprob} [%prob]**	**{125}**	**{20} {16.0801} [–]**	**{33} {25.7007} [33.2%]**	**{47} {35.9898} [46.5%]**	**{5} {3.6144} [3.7%]**	**{20} {16.1438} [16.6%]**
Pilbara craton (Australia) (Mesoarchaean)	IA + CA–CR–Col	7	5 [0.898 ± 0.117] (0.6946 − 0.9874)	–	–	0	2 [0.735 ± 0.252] (0.5566 − 0.9136)
	IA–CA–CR	7	–	3 [0.789 ± 0.065] (0.7346 − 0.8613)	4 [0.778 ± 0.112] (0.6487 − 0.9119)	0	–
	IA–CA–Col	7	–	3 [0.797 ± 0.093] (0.7293 − 0.9032)	3 [0.608 ± 0.017] (0.5930 − 0.6272)	–	1 (0.8789)
	IA–CR–Col	7	–	5 [0.922 ± 0.151] (0.6521 − 0.9982)	–	0	2 [0.848 ± 0.131] (0.7552 − 0.9400)
	CA–CR–Col	7	–	–	6 [0.912 ± 0.158] (0.5963 − 0.9997)	0	1 (0.8559)
1b. Pilbara craton (Australia)	**{Σn} {Σprob} [%prob]**	**{35}**	**{5} {4.4922} [–]**	**{11} {9.3684} [39.4%]**	**{13} {10.4105} [43.8%]**	**{2} {1.4702} [5.0%]**	**{4} {3.3000} [11.8%]**
Pilbara craton (Australia) (Neoarchaean)	IA + CA–CR–Col	3	0	–	–	0	3 [0.852 ± 0.051] (0.7931 − 0.8903)
	IA–CA–CR*	3	–	0	3 [0.920 ± 0.070] (0.8399 − 0.9650)	0	–
	IA–CA–Col	3	–	0	1 (0.5375)	–	2 [0.780 ± 0.068] (0.7323 − 0.8279)
	IA–CR–Col	3	–	0	–	0	3 [0.916 ± 0.037] (0.8890 − 0.9587)
	CA–CR–Col	3	–	–	0	0	3 [0.784 ± 0.031] (0.7625 − 0.8195)

1c. Pilbara craton (Australia)	**{Σn} {Σprob} [%prob]**	**{15}**	**{0} {0} [–]**	**{0} {0} [0%]**	**{4} {0.5375} [5.3%]**	**{0} {0} [0%]**	**{11} {9.6242} [94.7%]**
São Francisco craton (Brazil)	IA + CA–CR–Col	8	7 [0.879 ± 0.126] (0.6187 − 0.9919)	–	–	0	1 (0.8784)
	IA–CA–CR	8	–	6 [0.741 ± 0.0120] (0.6224 − 0.9620)	2 [0.620 ± 0.200] (0.4789 − 0.7612)	0	–
	IA–CA–Col	8	–	7 [0.723 ± 0.180] (0.4052 − 0.9786)	0	–	1 (0.5745)
	IA–CR–Col	8	–	7 [0.924 ± 0.186] (0.5022 − 0.9999)	–	0	1 (0.8124)
	CA–CR–Col*	8	–	–	8 [0.949 ± 0.111] (0.6752 − 0.9999)	0	0
4. São Francisco craton (Brazil)	**{Σn} {Σprob} [%prob]**	**{40}**	**{7} {6.1523} [–]**	**{20} {15.9727} [60.4%]**	**{10} {8.8293} [33.4%]**	**{0} {0} [%]**	**{3} {2.0654} [6.2%]**
Rio Maria terrane (Brazil)	IA + CA–CR–Col	12	8 [0.687 ± 0.122] (0.5085 − 0.8706)	–	–	0	4 [0.550 ± 0.105] (0.4588 − 0.6962)
	IA–CA–CR	12	–	0	12 [0.691 ± 0.076] (0.6081 − 0.8308)	0	–
	IA–CA–Col	12	–	0	11 [0.682 ± 0.048] (0.6251 − 0.7675)	–	1 (0.4729)
	IA–CR–Col*	12	–	6 [0.795 ± 0.160] (0.5389 − 0.9482)	–	0	6 [0.530 ± 0.119] (0.3840 − 0.7289)
	CA–CR–Col	12	–	–	7 [0.565 ± 0.126] (0.4486 − 0.8054)	0	5 [0.576 ± 0.092] (0.4912 − 0.7176)
5. Rio Maria terrane (Brazil)	**{Σn} {Σprob} [%prob]**	**{60}**	**{8} {5.4970} [–]**	**{6} {4.7672} [15.0%]**	**{30} {19.7521} [62.5%]**	**{0} {0} [0%]**	**{16} {8.7113} [22.5%]**
Carajás metallogenic province (Brazil)	IA + CA–CR–Col	28	3 [0.722 ± 0.150] (0.5488 − 0.8139)	–	–	25 [0.753 ± 0.279] (0.0797 − 0.9831)	0
	IA–CA–CR	28	–	3 [0.700 ± 0.032] (0.6651 − 0.7274)	0	25 [0.906 ± 0.134] (0.5768 − 0.9979)	–
	IA–CA–Col*	28	–	3 [0.687 ± 0.024] (0.6720 − 0.7148)	6 [0.608 ± 0.086] (0.5179 − 0.7661)	–	19 [0.783 ± 0.183] (0.4954 − 0.9874)
	IA–CR–Col	28	–	3 [0.825 ± 0.160] (0.6721 − 0.9909)	–	20 [0.886 ± 0.090] (0.6449 − 0.9714)	5 [0.658 ± 0.119] (0.5455 − 0.8025)
	CA–CR–Col	28	–	–	3 [0.973 ± 0.031] (0.9374 − 0.9950)	19 [0.857 ± 0.084] (0.6650, 0.9479)	6 [0.643 ± 0.105] (0.4623 − 0.7429)
6. Carajás metallogenic province (Brazil)	**{Σn} {Σprob} [%prob]**	**{140}**	**{3} {2.1654} [–]**	**{9} {6.6351} [6.8%]**	**{9} {6.5681} [6.8%]**	**{89} {75.4646} [66.9%]**	**{30} {22.0280} [19.5%]**
North Caribou greenstone belt (Canada)	IA + CA–CR–Col	6	4 [0.762 ± 0.168] (0.5189 − 0.9249)	–	–	0	1 (0.6727)
	IA–CA–CR	6	–	2[0.596 ± 0.167] (0.5920,0.6005)	4 [0.575 ± 0.167] (0.4054 − 0.8027)	1 (0.7324)	–

(*Continued*)

Table 2. (Continued).

Locality (Country) (Epoch)	Tectonic diagram	Total number of samples	Number of discriminated samples [$\bar{x} \pm s$ of probability values] (range of probability values for samples)				
			IA + CA	IA	CA	CR	Col
	IA–CA–Col	6	–	2[0.625 ± 0.108] (0.5482 – 0.7013)	1 (0.4982)	–	3 [0.655 ± 0.231] (0.4926 – 0.9185)
	IA–CR–Col*	6	–	3 [0.821 ± 0.223] (0.5640 – 0.9695)	–	0	3 [0.742 ± 0.130] (0.6215 – 0.8799)
	CA–CR–Col	6	–	–	6 [0.900 ± 0.138] (0.6600 – 0.9970)	0	0
7. North Caribou greenstone belt (Canada)	**{Σn} {Σprob} [%prob]**	**{30}**	**{4} {3.8098} [–]**	**{7} {4.9046} [28.1%]**	**{11} {8.1966} [47.0%]**	**{1} {0.7324} [3.3%]**	**{7} {4.8618} [21.6%]**
Archaean sanukitoid suite (Canada)	IA + CA–CR–Col	10	2 [0.702 ± 0.088] (0.6397, 0.7639)	–	–	0	8 [0.690 ± 0.097] (0.5619 – 0.8241)
	IA–CA–CR*	10	–	0	10 [0.744 ± 0.125] (0.5720 – 0.9305)	0	–
	IA–CA–Col	10	–	0	6 [0.637 ± 0.105] (0.4949 – 0.7635)	–	4 [0.529 ± 0.033] (0.4959 – 0.5756)
	IA–CR–Col	10	–	2 [0.584 ± 0.068] (0.5366, 0.6324)	–	0	8 [0.782 ± 0.101] (0.6319–0.9387)
	CA–CR–Col	10	–	–	2 [0.714 ± 0.284] (0.5129, 0.9151)	0	8 [0.685 ± 0.054] (0.5920 – 0.7489)
9. Archaean sanukitoid suite (Canada)	**{Σn} {Σprob} [%prob]**	**{50}**	**{2} {1.4036} [–]**	**{2} {1.1690} [3.7%]**	**{18} {12.6839} [40.3%]**	**{0} {0} [0%]**	**{28} {19.3787} [60.0%]**
Kolar suture zone (India)	IA + CA–CR–Col	6	1 (0.9882)	–	–	0	5 [0.786 ± 0.149] (0.6170 – 0.9739)
	IA–CA–CR*	6	–	1 (0.9946)	5 [0.791 ± 0.171] (0.5798 – 0.9408)	0	–
	IA–CA–Col	6	–	1 (0.9995)	0	–	5 [0.635 ± 0.243] (0.4361 – 0.9542)
	IA–CR–Col	6	–	2 [0.772 ± 0.322] (0.5451 – 0.9999)	–	0	4 [0.937 ± 0.049] (0.8649 – 0.9671)
	CA–CR–Col	6	–	–	3 [0.837 ± 0.241] (0.5602, 1.0000)	0	3 [0.801 ± 0.145] (0.6475 – 0.9352)
11. Kolar suture zone (India)	**{Σn} {Σprob} [%prob]**	**{30}**	**{1} {0.9882} [–]**	**{4} {3.5391} [16.0%]**	**{8} {6.4654} [29.3%]**	**{0} {0} [0%]**	**{17} {13.2542} [54.7%]**

Notes: IA, island arc; CA, continental arc; CR, continental rift; Col, collision; $\bar{x} \pm s$, mean ± 1SD of the probability estimates for all samples discriminated in a given tectonic setting; these are reported in [], and the second set of values are also included in [] when the single-outlier type discordancy tests identified one or more probability values as discordant; ∗ denotes inapplicable diagram identified whenever it is clearly established; the final row gives a synthesis of results as **{Σn} {Σprob} [%prob]**, where **{Σn}** the total number of samples or data points plotting in all five diagrams are reported in the column of total number of samples, whereas the sum of samples plotting in a given tectonic field are reported in the respective tectonic field column; **{Σprob}** the sum of probability values for all samples plotting in a given tectonic field are reported in the respective tectonic field column; and **[%prob]** the total probability of a given tectonic setting expressed in percent after assigning the probability of IA + CA to IA and CA (using weighing factors explained in the text).

Table 3. Application of three sets of five each (15) discriminant function-based multidimensional discrimination diagrams (Verma and Verma 2012) to Archaean intermediate rocks through probability calculations.

Locality (Country) (Epoch)	Figure type	Total number of samples	Number of discriminated samples				
			Arc			Within-plate CR + OI [$\bar{x} \pm s$] [p_{CR+OI}]	Collision Col [$\bar{x} \pm s$] [p_{Col}]
			IA + CA [$\bar{x} \pm s$] (p_{IA+CA})	IA [$\bar{x} \pm s$] [p_{IA}]	CA [$\bar{x} \pm s$] [p_{CA}]		
Pilbara craton (Australia) (Palaeoarchaean)	IA + CA–CR + OI–Col	4	3 [0.614 ± 0.104] (0.4942 − 0.6782)	–	–	1 (0.9688)	0
	IA–CA–CR + OI	4	–	0	3 [0.590 ± 0.076] (0.5034 − 0.6437)	1 (0.5081))	–
	IA + CA–Col	4	–	1 (0.6047)	3 [0.692 ± 0.268] (0.5018 − 0.9982)	–	0
	IA–CR + OI–Col*	4	–	2 [0.572 ± 0.052] (0.5354, 0.6089)	–	1 (0.8756)	1 (0.4904)
	CA–CR + OI–Col	4	–	–	3 [0.684 ± 0.008] (0.6791 − 0.6938)	1 (0.5559)	0
1a. Pilbara craton (Australia) All major element-based diagrams	**{Σn} {Σprob} [%prob]**	**{20}**	**{3} {1.8420} [–]**	**{3} {1.7490} [16.8%]**	**{9} {5.8973} [56.8%]**	**{4} {2.9085} [22.6%]**	**{1} {0.6143} [3.8%]**
Kambalda (Australia)	IA + CA–CR + OI–Col	17	16 [0.966 ± 0.062] (0.8051 − 1.0000)	–	–	0	1 (0.8623)
	IA–CA–CR + OI	17	–	13 [0.867 ± 0.125] (0.5275 − 0.9987)	4 [0.690 ± 0.195] (0.5355 − 0.9473)	0	–
	IA + CA–Col	17	–	17 [0.841 ± 0.192] (0.1943 − 0.9744)	0	–	0
	IA–CR + OI–Col	17	–	17 [0.976 ± 0.044] (0.8441 − 1.0000)	–	0	0
	CA–CR + OI–Col*	17	–	–	15 [0.9678 ± 0.045] (0.8629 − 0.9999)	0	2 [0.798 ± 0.1255] (0.8629 − 0.9999)
2. Kambalda (Australia) All major element-based diagrams	**{Σn} {Σprob} [%prob]**	**{85}**	**{16} {15.4577} [–]**	**{47} {42.1583} [68.8%]**	**{19} {17.2774} [28.3%]**	**{0} {0} [0%]**	**{3} {2.2793} [2.9%]**
Kambalda (Australia)	IA + CA–CR + OI–Col	6	6 [0.837 ± 0.107] (0.7020 − 0.9397)	–	–	0	0
	IA–CA–CR + OI	6	–	6 [0.854 ± 0.054] (0.7711 − 0.9233)	0	0	–

(*Continued*)

Table 3. (Continued).

Locality (Country) (Epoch)	Figure type	Total number of samples	Number of discriminated samples				
			Arc			Within-plate CR + OI $[\bar{x} \pm s]$ $[p_{CR+OI}]$	Collision Col $[\bar{x} \pm s]$ $[p_{Col}]$
			IA + CA $[\bar{x} \pm s]$ (p_{IA+CA})	IA $[\bar{x} \pm s]$ $[p_{IA}]$	CA $[\bar{x} \pm s]$ $[p_{CA}]$		
	IA + CA–Col	6	–	6 [0.807 ± 0.054] (0.7122 – 0.8703)	0	–	0
	IA–CR + OI–Col	6	–	6 [0.8861 ± 0.088] (0.7165 – 0.9361)	–	0	0
	CA–CR + OI–Col*	6	–	–	5 [0.7292 ± 0.179] (0.5111 – 0.9511)	0	1 (0.5330)
2. Kambalda (Australia) All immobile major and trace element-based diagrams	**{Σn} {Σprob} [%prob]**	**{30}**	**{6} {5.0241} [–]**	**{18} {15.1274} [78.8%]**	**{5} {3.6461} [19.0%]**	**{0} {0} [0%]**	**{1} {0.5330} [2.2%]**
Barberton belt (South Africa)	IA + CA–CR + OI–Col	8	8 [0.991 ± 0.010] (0.9752 – 0.9998)	–	–	0	0
	IA–CA–CR + OI	8	–	8 [0.823 ± 0.196] (0.5632 – 0.9947)	0	0	–
	IA + CA–Col	8	–	8 [0.947 ± 0.063] (0.8595 – 0.9983)	0	–	0
	IA–CR + OI–Col*	8	–	8 [0.989 ± 0.014] (0.9629 – 0.9998)	–	0	0
	2–3 + 4–5	8	–	–	8 [0.809 ± 0.193] (0.5628 – 0.9985)	0	0
3b. Barberton belt (South Africa) All major element-based diagrams	**{Σn} {Σprob} [%prob]**	**{40}**	**{8} {7.9311} [–]**	**{24} {22.0716} [77.3%]**	**{8} {6.4752} [22.7%]**	**{0} {0} [0%]**	**{0} {0}[0%]**
Barberton belt (South Africa)	IA + CA–CR + OI–Col	8	8 [0.943 ± 0.043] (0.8881 – 0.9927)	–	–	0	0
	IA–CA–CR + OI	8	–	6 [0.748 ± 0.189] (0.5068 – 0.9403)	2 [0.566 ± 0.022] (0.5509 – 0.5813)	0	–
	IA + CA–Col	8	–	4 [0.821 ± 0.105] (0.6714 – 0.9003)	4 [0.599 ± 0.057] (0.5268 – 0.6445)	–	0
	IA–CR + OI–Col	8	–	8 [0.929 ± 0.060] (0.8429 – 0.9957)	–	0	0
	CA–CR + OI–Col*	8	–	–	8 [0.944 ± 0.042] (0.8697 – 0.9888)	0	0

3b. Barberton belt (South Africa) All immobile trace element-based diagrams	**{Σn} {Σprob} [%prob]**	**{40}**	**{8} {7.5425} [–]**	**{18} {15.2016} [57.8%]**	**{14} {11.0831} [42.2%]**	**{0} {0} [0%]**	**{0} {0} [0%]**
North Caribou greenstone belt (Canada)	IA + CA–CR + OI–Col	7	7 [0.958 ± 0.048] (0.8686 − 0.9973)	–	–	0	0
	IA–CA–CR + OI	7	–	7 [0.921 ± 0.100] (0.7148 − 1.0000)	0	0	–
	IA + CA–Col	7	–	7 [0.954 ± 0.054] (0.8537 − 1.0000)	0	–	0
	IA–CR + OI–Col	7	–	7 [0.836 ± 0.204] (0.4237 − 0.9606)	–	0	0
	2–3 + 4–5*	7	–	–	6 [0.836 ± 0.204] (0.4237 − 0.9606)	0	1 (0.5229)
7. North Caribou greenstone belt (Canada) All major element-based diagrams	**{Σn} {Σprob} [%prob]**	**{35}**	**{7} {6.7032} [–]**	**{21} {19.8929} [78.6%]**	**{6} {5.0169} [19.8%]**	**{0} {0} [0%]**	**{1} {0.5229} [1.6%]**
North Caribou greenstone belt (Canada)	IA + CA–CR + OI–Col	7	6 [0.828 ± 0.180] (0.5244 − 0.9967)	–	–	0	1 (0.5229)
	IA–CA–CR + OI	7	–	7 [0.803 ± 0.086] (0.6607 − 0.9188)	0	0	–
	IA + CA–Col	7	–	6 [0.740 ± 0.137] (0.5867 − 0.9140)	0	–	1 (0.7760)
	IA–CR + OI–Col	7	–	6 [0.837 ± 0.160] (0.5574 − 0.9958)	–	0	1 (0.8427)
	CA–CR + OI–Col*	7	–	–	6 [0.629 ± 0.286] (0.1720 − 0.9980)	0	1 (0.9886)
7. North Caribou greenstone belt (Canada) All immobile major and trace element-based diagrams	**{Σn} {Σprob} [%prob]**	**{35}**	**{6} {5.0462} [–]**	**{19} {15.0831} [69.7%]**	**{6} {3.7765} [17.5%]**	**{0} {0} [0%]**	**{4} {3.5137} [12.8%]**
North Caribou greenstone belt (Canada)	IA + CA–CR + OI–Col	7	6 [0.850 ± 0.134] (0.6692 − 0.9739)	–	–	0	1 (0.8142)
	IA–CA–CR + OI	7	–	6 [0.779 ± 0.231] (0.4082 − 0.9777)	1 (0.4606)	0	–

(*Continued*)

Table 3. (Continued).

Locality (Country) (Epoch)	Figure type	Total number of samples	Number of discriminated samples				
			Arc			Within-plate CR + OI [$\bar{x} \pm s$] [p_{CR+OI}]	Collision Col [$\bar{x} \pm s$] [p_{Col}]
			IA + CA [$\bar{x} \pm s$] (p_{IA+CA})	IA [$\bar{x} \pm s$] [p_{IA}]	CA [$\bar{x} \pm s$] [p_{CA}]		
	IA + CA–Col	7	–	5 [0.824 ± 0.200] (0.4737 – 0.9757)	1 (0.4187)	–	1 (0.7759)
	IA–CR + OI–Col	7	–	6 [0.8725 ± 0.158] (0.6400 – 0.9894)	–	0	1 (0.7743)
	CA–CR + OI–Col*	7	–	–	6 [0.743 ± 0.147] (0.5797 – 0.9656)	0	1 (0.8325)
7. North Caribou greenstone belt (Canada) All immobile trace element-based diagrams	**{Σn} {Σprob} [%prob]**	**{35}**	**{6} {5.0998} [–]**	**{17} {14.0306} [64.1%]**	**{8} {5.3376} [24.4%]**	**{0} {0} [0%]**	**{4} {3.1970} [11.5%]**
Abitibi greenstone belt (Canada)	IA + CA–CR + OI–Col	7	7[0.998 ± 0.003] (0.9908 – 1.0000)	–	–	0	0
	IA–CA–CR + OI	7	–	5 [0.923 ± 0.094] (0.7586 – 0.9929)	2 [0.992 ± 0.004] (0.9892 – 0.9948)	0	–
	IA + CA–Col	7	–	5 [0.966 ± 0.034] (0.9079 – 0.9933)	2 [0.940 ± 0.015] (0.9300 – 0.9506)	–	1 (0.5629)
	IA–CR + OI–Col	7	–	7 [0.999 ± 0.002] (0.9959 – 1.0000)	–	0	0
	CA–CR + OI–Col*	7	–	–	7 [0.998 ± 0.003] (0.9919 – 1.0000)	0	0
8. Abitibi greenstone belt (Canada) All major element-based diagrams	**{Σn} {Σprob} [%prob]**	**{35}**	**{7} {6.9874} [–]**	**{17} {16.4418} [60.2%]**	**{11} {10.8501} [39.8%]**	**{0} {0} [0%]**	**{0} {0} [0%]**
Abitibi greenstone belt (Canada)	IA + CA–CR + OI–Col	7	7 [0.971 ± 0.012] (0.9549 – 0.9916)	–	–	0	0
	IA–CA–CR + OI	7	–	7 [0.922 ± 0.047] (0.8508–0.9768)	0	0	–
	IA + CA–Col	7	–	7 [0.913 ± 0.048] (0.8413 – 0.9718)	0	–	0
	IA–CR + OI–Col	7	–	7 [0.976 ± 0.009] (0.9606 – 0.9909)	–	0	0
	CA–CR + OI–Col*	7	–	–	7 [0.857 ± 0.102] (0.6933 – 0.9684)	0	0

8. Abitibi greenstone belt (Canada) All immobile major and trace element-based diagrams	**{Σn} {Σprob} [%prob]**	**{35}**	**{7} {6.7967} [–]**	**{21} {19.6770} [76.6%]**	**{7} {5.9987} [23.4%]**	**{0} {0} [0%]**	**{0} {0} [0%]**
Abitibi greenstone belt (Canada)	IA + CA–CR + OI–Col	7	7 [1.000 ± 0.000] (0.9998 − 1.0000)	–	–	0	1 (0.5229)
	IA–CA–CR + OI	7	–	7 [0.979 ± 0.016] (0.9578 − 0.9967)	0	0	–
	IA + CA–Col	7	–	7 [0.968 ± 0.023] (0.9410 − 0.9952)	0	–	0
	IA–CR + OI–Col	7	–	7 [1.000 ± 0.000] (0.9998 − 1.0000)	–	0	0
	CA–CR + OI–Col*	7	–	–	7 [1.000 ± 0.000] (0.9991 − 0.9999)	0	0
8. Abitibi greenstone belt (Canada) All immobile trace element-based diagrams	**{Σn} {Σprob} [%prob]**	**{35}**	**{7} {6.9994} [–]**	**{21} {20.6272} [74.7%]**	**{7} {6.9969} [25.3%]**	**{0} {0} [0%]**	**{0} {0} [0%]**
Archaean sanukitoid suite (Canada)	IA + CA–CR + OI–Col	6	0	–	–	1 (0.4575)	5 [0.841 ± 0.172] (0.6272 − 0.9883)
	IA–CA–CR + OI*	6	–	0	4 [0.743 ± 0.120] (0.6300 − 0.4408)	2 [0.500 ± 0.083] (0.4408, 0.5588)	–
	IA + CA–Col	6	–	0	3 [0.675 ± 0.124] (0.5374 − 0.7784)	–	3 [0.794 ± 0.232] (0.5274 − 0.9508)
	IA–CR + OI–Col	6	–	0	–	1 (0.5205)	5 [0.886 ± 0.125] (0.7341 − 0.9948)
	CA–CR + OI–Col	6	–	–	2 [0.482 ± 0.058] (0.4409, 0.5230)	0	4 [0.876 ± 0.082] (0.7558 − 0.9320)
9. Archaean sanukitoid suite (Canada) All major element-based diagrams	**{Σn} {Σprob} [%prob]**	**{30}**	**{0} {0} [–]**	**{0} {0} [0%]**	**{9} {5.9591} [26.5%]**	**{4} {1.9776} [8.8%]**	**{17} {14.5173} [64.7%]**
Archaean sanukitoid suite (Canada)	IA + CA–CR + OI–Col	6	1 (0.6623)	–	–	2 [0.850 ± 0.103] (0.7769 − 0.9222)	3 [0.668 ± 0.284] (0.4867 − 0.9952)

(*Continued*)

Table 3. (Continued).

Locality (Country) (Epoch)	Figure type	Total number of samples	Number of discriminated samples				
			Arc			Within-plate CR + OI [$\bar{x} \pm s$] [p_{CR+OI}]	Collision Col [$\bar{x} \pm s$] [p_{Col}]
			IA + CA [$\bar{x} \pm s$] (p_{IA+CA})	IA [$\bar{x} \pm s$] [p_{IA}]	CA [$\bar{x} \pm s$] [p_{CA}]		
	IA–CA–CR + OI	6	–	0	6 [0.763 ± 0.182] (0.5289 – 0.9555)	0	–
	IA + CA–Col	6	–	0	5 [0.820 ± 0.137] (0.6301 – 0.9848)	–	1 (0.9884)
	IA–CR + OI–Col*	6	–	1 (0.5282)	–	2 [0.929 ± 0.072] (0.8782, 0.9800)	3 [0.765 ± 0.200] (0.6293 – 0.9951)
	CA–CR + OI–Col	6	–	–	4 [0.767 ± 0.156] (0.6042 – 0.9096)	1 (0.5253)	1 (0.9958)
9. Archaean sanukitoid suite (Canada) All immobile major and trace element-based diagrams	**Σn} {Σprob} [%prob]**	**{30}**	**{1} {0.6623} [–]**	**{1} {0.5282} [2.4%]**	**{15} {11.7404} [53.1%]**	**{5} {4.0827} [17.5%]**	**{8} {6.2831} [27.0%]**
Archaean sanukitoid suite (Canada)	IA + CA–CR + OI–Col	6	0	–	–		6 [0.999 ± 0.002] (0.6272 – 0.9883)
	IA–CA–CR + OI*	6	–	0	3 [0.818 ± 0.250] (0.5287 – 0.9677)	3 [0.783 ± 0.110] (0.7166 – 0.9094)	–
	IA + CA–Col	6	–	0	0	–	6 [0.982 ± 0.044] (0.8915 – 1.0000)
	IA–CR + OI–Col	6	–	0	–	0	6 [0.999 ± 0.001] (0.9974 – 1.0000)
	CA–CR + OI–Col	6	–	–	0	0	6 [0.990 ± 0.024] (0.9422 – 0.9999)
9. Archaean sanukitoid suite (Canada) All immobile trace element-based diagrams	**{Σn} {Σprob} [%prob]**	**{30}**	**{0} {0} [–]**	**{0} {0} [0%]**	**{3} {2.4526} [8.6%]**	**{3} {2.3475} [8.2%]**	**{24} {23.8244} [83.2%]**

Note: For more explanation, see footnote of Table 2; see also Verma (2012).

for intermediate rocks, and Tables 4–6 for basic or ultrabasic rocks. The results from solely probability calculations are presented in Tables 1–4, whereas those based on actual plotting of samples in diagrams (Figures 1 and 2) and calculation of percent success (% success) are included in Tables 5 and 6. The results are included in tables for all those cases for which three or more samples with complete data set were available in our data base; otherwise for one or two samples, the results are simply mentioned in the text.

Pilbara craton (Australia)

This three-part case study for the Pilbara craton is subdivided according to the age of rocks (case study 1a for Palaeoarchaean, 1b for Mesoarchaean, and 1c for Neoarchaean). We describe in detail the application of discrimination diagrams and probability calculations for the first part (1a) of this first case study (see the first set of results in Table 2); all other results are simply pointed out and briefly discussed.

For this case study (1a), geochemical data were available for 29 samples of Palaeoarchaean rocks, of which 25 proved to be acid magma and 4 intermediate magma (Table 1). The data for acid rocks (25 samples; Table 2) were used for probability calculations corresponding to the first of the five multidimensional diagrams of Verma *et al*. (2012) that discriminates three tectonic settings of IA + CA together, CR, and Col (see the first row IA + CA–CR–Col of results in Table 2). Twenty out of 25 samples would plot in the IA + CA field, 1 in the CR, and 4 in the Col field. In fact, instead of actually plotting the samples in the IA + CA–CR–Col diagram, we estimated the respective probabilities of each sample for the three tectonic fields being discriminated from the method outlined by Verma (2012).

In any diagram, each sample will have the total probability of 1, which is subdivided into three probability values corresponding to each of the tectonic fields being discriminated (IA + CA, CR, and Col; see figure 5A in Verma *et al*. 2012). A sample will plot in the field for which it has the highest probability. A tectonic field boundary is characterized by two equal probability values of 0.5000 for the two fields it separates. At the triple point where all three tectonic fields meet, the probability for each field would also be equal, being about 0.3333. When a sample plots within a tectonic field, its probability for that field would increase rapidly as the sample moves away from the tectonic field boundary into that particular field. In other words, the sample would have a probability value for that particular tectonic field >0.5000 or >0.3333, depending on the region where it actually plots, whether away from the triple point or close to it, respectively. The highest probability values for samples belonging to a given field were used to calculate the statistics (mean $\pm$ 1SD,) and the range of probability values for that field. This information is included next to the number of samples in Table 2.

Coming back to our first example of the Pilbara craton, 20 samples (out of 25) showed the highest probability of 0.804 ± 0.132 (range of 0.5611–0.9553) for the combined IA + CA field, only one sample indicated the highest probability of 0.5785 for the CR field, and four samples had the highest probability of 0.822 ± 0.267 (range of 0.4241–0.9965) for the Col setting (Table 2). Note that this diagram contains only the combined IA + CA field, the separate IA and CA fields being absent. This procedure was repeated for the other four diagrams of Verma *et al*. (2012), all of which discriminate three (out of four) tectonic settings at a time (Table 2). The combined IA + CA field is missing from all of them.

The synthesis row highlighted in bold face (see the row identified by **1a. Pilbara craton (Australia)** in Table 2) presents the sum of the samples **{Σn}** plotting in a given field, the sum of the highest probability values for the respective samples **{Σprob}**, and the total percent probability estimate **[%prob]** for each of the four tectonic settings being discriminated (IA, CA, CR, and Col), although **{Σn}** and **{Σprob}** data are also included for the combined IA + CA field. The method of calculation of [%prob] is explained in detail by Verma (2012). Thus, out of the total of 125 samples corresponding to all five diagrams 20 samples plotted in the IA + CA fields (**{Σn} = 20**) and had the total probability of 16.0801 (**{Σprob}** = 16.0801). Similarly, for the IA, CA, CR, and Col fields, total numbers of samples were 33, 47, 5, and 20, respectively, with total probability values of about 25.7007, 35.9898, 3.6144, and 16.1438, respectively. The total probability of 16.0801 for IA + CA had to be assigned proportionately to the total probability of IA and CA fields. Thus, the total percent probability values for the IA, CA, CR, and Col were about 33.2%, 46.5%, 3.7%, and 16.6%, respectively. Because this total percent probability value was the highest for the CA field (46.5%), a CA setting is indicated from the interpretation of all five diagrams (Table 2) for the Pilbara craton during the Palaeoarchaean. Note that the 'by-chance' total percent probability for any of the four fields (IA, CA, CR, or Col) would be 25% only. The actual total percent probability values of 46.5% and 33.2% for both the CA and IA fields are significantly greater than this value; this is particularly true for the CA field (CA 46.5% > IA 33.2% > by-chance 25%). Consequently, if a CA setting were inferred for the Pilbara craton during the Palaeoarchaean, the diagram (IA–CR–Col), from which the CA field is absent, can be declared as the inapplicable diagram according to the convention used by the original authors (Verma *et al*. 2012); this is indicated by an asterisk (*) in Table 2.

The four Palaeoarchaean intermediate rock samples from the Pilbara craton (Table 1) also indicated a CA setting with a total percent probability of 56.8% for this tectonic field (case study 1a in Table 3).

For the second part of the first case study (1b) for the Pilbara craton during the Mesoarchaean, only seven

Table 4. Application of the set of five discriminant function-based multidimensional discrimination diagrams (Verma and Agrawal 2011) to Archaean basic and ultrabasic rocks through probability calculations.

			Number of discriminated samples [$\bar{x} \pm s$ of probability values] (range of probability values for samples)				
Locality	Tectonic diagram	Total number of samples	IAB	CRB + OIB	CRB	OIB	MORB
Kambalda (Australia)	IAB–CRB + OIB–MORB	5	5 [0.984 ± 0.012] (0.9712 − 0.9977)	0	–	–	0
	IAB–CRB–OIB	5	5 [1.000 ± 0.000] (1.0000 − 1.0000)	–	0	0	–
	IAB–CRB–MORB	5	5 [1.000 ± 0.000] (1.0000 − 1.0000)	–	0	–	0
	IAB–OIB–MORB	5	5 [1.000 ± 0.000] (1.0000 − 1.0000)	–	–	0	0
	CRB–OIB–MORB*	5	–	–	0	0	5 [0.792 ± 0.025] (0.7552 − 0.8237)
1. Kambalda (Australia)	**{Σn} {Σprob} [%prob]**	**{25}**	**{20} {19.9195} [83.4%]**	**{0} {0} [–]**	**{0} {0} [0%]**	**{0} {0} [0%]**	**{5} {3.9587} [16.6%]**
North Caribou greenstone belt (Canada)	IAB–CRB + OIB–MORB	16	16 [0.973 ± 0.040] (0.8519 − 0.9999)	0	–	–	0
	IAB–CRB–OIB	16	16 [1.000 ± 0.000] (0.9994 − 1.0000)	–	0	0	–
	IAB–CRB–MORB	16	16 [0.998 ± 0.003] (0.9840 − 1.0000)	–	0	–	0
	IAB–OIB–MORB	16	16 [0.994 ± 0.018] (0.9308 − 1.0000)	–	–	0	0
	CRB–OIB–MORB*	16	–	–	0	0	16 [0.806 ± 0.062] (0.6018 − 0.8827)
2. North Caribou greenstone belt (Canada)	**{Σn} {Σprob} [%prob]**	**{80}**	**{64} {63.4371} [83.1%]**	**{0} {0} [–]**	**{0} {0} [0%]**	**{0} {0} [0%]**	**{16} {12.8952}[16.9%]**
Abitibi greenstone belt (Canada)	IAB–CRB + OIB–MORB	14	12 [0.996 ± 0.010] (0.9672 − 0.9999)	0	–	–	2 [0.827 ± 0.168] (0.7088 − 0.9461)
	IAB–CRB–OIB	14	14 [0.998 ± 0.005] (0.9834 − 1.0000)	–	0	0	–

	IAB–CRB–MORB	14	14 [0.978 ± 0.062] (0.7824 − 1.0000)	–	0	–	0
	IAB–OIB–MORB	14	12 [0.999 ± 0.001] (0.9951 − 1.0000)	–	–	0	2 [0.861 ± 0.067] (0.8131 − 0.9086)
	CRB–OIB–MORB*	14	–	–	7 [0.834 ± 0.153] (0.5383 − 0.9691)	0	7 [0.794 ± 0.144] (0.6212 − 0.9654)
3. Abitibi greenstone belt (Canada)	**{Σn} {Σprob} [%prob]**	**{70}**	**{52} {51.6041} [77.7%]**	**{0} {0} [–]**	**{7} {5.8364} [8.8%]**	**{0} {0} [0%]**	**{11} {8.9329} [13.5%]**
Gadwal greenstone belt (India)	IAB–CRB + OIB–MORB	21	7 [0.883 ± 0.074] (0.7486 − 0.9669)	0	–	–	14 [0.846 ± 0.187] (0.5091 − 0.9996)
	IAB–CRB–OIB	21	20 [1.000 ± 0.000] (0.9999–1.0000)	–	0	1 (0.9450)	–
	IAB–CRB–MORB	21	19 [0.952 ± 0.100] (0.6780 − 1.0000)	–	0	–	2 [0.998 ± 0.002] (0.9969, 0.9992)
	IAB–OIB–MORB	21	20 [0.980 ± 0.088] (0.6069 − 1.0000)	–	–	0	1(0.9177)
	CRB–OIB–MORB*	21	–	–	16 [0.906 ± 0.102] (0.5978 − 0.9779)	0	5 [0.817 ± 0.184] (0.5100 − 1.0000)
10. Gadwal greenstone belt (India)	**{Σn} {Σprob} [%prob]**	**{105}**	**{66} {63.8725} [65.1%]**	**{0} {0} [–]**	**{16} {14.4896} [14.8%]**	**{1} {0.9450} [0.9%]**	**{22} {18.8506} [19.2%]**

Note: For more explanation, see footnote of Table 2.

AQ12 Table 5. Application of the set of five discriminant function-based multidimensional discrimination diagrams (Agrawal *et al*. 2008) to Archaean basic and ultrabasic rocks.

Locality	Tectonic diagram	Total number of samples	Number of discriminated samples [$\bar{x} \pm s$ of probability values] (range of probability values for samples)				
			IAB	CRB + OIB	CRB	OIB	MORB
Barberton belt (South Africa)	IAB–CRB + OIB–MORB	7	0	0	–	–	7
	IAB–CRB–OIB*	7	0	–	0	7	–
	IAB–CRB–MORB	7	0	–	0	–	7
	IAB–OIB–MORB	7	0	–	–	0	7
	CRB–OIB–MORB	7	–	–	0	0	7
3a. Barberton belt (South Africa)	**{Σn} [%success]**	**{35}**	**{0} [0%]**	**{0} [–]**	**{0} [0%]**	**{7} [20%]**	**{28} [80%]**
North Caribou greenstone belt (Canada)	IAB–CRB + OIB–MORB	16	8	0	–	–	8
	IAB–CRB–OIB	16	9	–	3	4	–
	IAB–CRB–MORB	16	8	–	0	–	8
	IAB–OIB–MORB	16	8	–	–	0	8
	CRB–OIB–MORB	16	–	–	0	0	16
7. North Caribou greenstone belt (Canada)	**{Σn} [%success]**	**{80}**	**{33} [41%]**	**{0} [–]**	**{3} [4%]**	**{4} [5%]**	**{40} [50%]**
Abitibi greenstone belt (Canada)	IAB–CRB + OIB–MORB	19	0	0	–	–	19
	IAB–CRB–OIB*	19	0	–	11	8	–
	IAB–CRB–MORB	19	0	–	0	–	19
	IAB–OIB–MORB	19	0	–	–	0	19
	CRB–OIB–MORB	19	–	–	0	0	19
8. Abitibi greenstone belt (Canada)	**{Σn} [%success]**	**{95}**	**{0} [0%]**	**{0} [–]**	**{11} [12%]**	**{8} [8%]**	**{76} [80%]**
Gadwal greenstone belt (India)	IAB–CRB + OIB–MORB	21	20	0	–	–	1
	IAB–CRB–OIB	21	20	–	0	1	–
	IAB–CRB–MORB	21	20	–	0	–	1
	IAB–OIB–MORB	21	20	–	–	0	1
	CRB–OIB–MORB*	21	–	–	0	0	21
10. Gadwal greenstone belt (India)	**{Σn} [%success]**	**{105}**	**{80} [76%]**	**{0} [–]**	**{0} [0%]**	**{1} [1%]**	**{24} [23%]**

samples of acid rocks were available (Table 1). These samples clearly showed a subduction-related setting (Table 2), but the distinction between the CA and IA settings was not so clear (the total percent probability of 43.8% for the CA setting was only slightly greater than 39.4% for the IA).

For the final part of this case study (1c) for the Neoarchaean, only three samples of acid rocks (Table 1) were available, which clearly showed a Col setting (Table 2), with a very high total percent probability of 94.7%.

Thus, for the Pilbara craton, the tectonic setting of CA during the Palaeoarchaean to Mesoarchaean may have changed to Col during the Neoarchaean. The original authors (Jahn *et al*. 1981) did not comment on the actual tectonic setting for the Pilbara craton, although they discussed that these rocks were presumably derived from basaltic sources. Bickle *et al*. (1983), on the other hand, pointed out the similarities of the REE patterns of the Pilbara rocks with modern IA and CA. In spite of such geochemical similarities, these authors refrained from inferring a tectonic setting for these Archaean rocks because of some other geochemical differences between the Archaean rocks and the modern Andean-type magmatism.

Kambalda (Australia)

Thirty-five Neoarchaean rock samples from Kambalda consisted of 1 acid, 17 intermediate, and 17 basic magma (Table 1). The sample of acid rock indicated an IA setting with a very high probability approaching 1 (results are not shown in Table 2). Seventeen samples of intermediate rocks (Table 3) showed an IA setting in two sets of diagrams of Verma and Verma (2012). The total percent probability values for IA in these major element-based and immobile major and trace element-based diagrams were very high (about 68.8% and 78.8%, respectively).

For the immobile major and trace element-based diagrams for basic or ultrabasic rocks (Verma and Agrawal 2011), only five samples (out of 17) had complete data

Table 6. Application of the set of five discriminant function-based multidimensional discrimination diagrams (Verma *et al*. 2006) to Archaean basic and ultrabasic rocks.

Locality	Tectonic diagram	Total number of samples	Number of discriminated samples [$\bar{x} \pm s$ of probability values] (range of probability values for samples)			
			IAB	CRB	OIB	MORB
Kambalda (Australia)	IAB–CRB–OIB–MORB	17	15	0	0	2
	IAB–CRB–OIB	17	15	1	1	–
	IAB–CRB–MORB	17	13	0	–	4
	IAB–OIB–MORB	17	16	–	1	0
	CRB–OIB–MORB*	17	–	5	4	8
2. Kambalda	**{Σn} [%success]**	**{85}**	**{59} [70%]**	**{6} [7%]**	**{6} [7%]**	**{14} [16%]**
Barberton belt (South Africa)	IAB–CRB–OIB–MORB	5	0	5	0	0
	IAB–CRB–OIB	5	0	0	5	–
	IAB–CRB–MORB	5	0	0	–	5
	IAB–OIB–MORB	5	0	–	5	0
	CRB–OIB–MORB	5	–	0	5	0
3a. Barberton belt (South Africa)	**{Σn} [%success]**	**{25}**	**{0} [0%]**	**{5} [20%]**	**{15} [60%]**	**{5} [20%]**
North Caribou greenstone belt (Canada)	IAB–CRB–OIB–MORB	15	14	0	0	1
	IAB–CRB–OIB	15	14	1	0	–
	IAB–CRB–MORB	15	13	0	–	2
	IAB–OIB–MORB	15	14	–	0	1
	CRB–OIB–MORB*	15	–	1	3	11
7. NorthCaribou greenstone belt (Canada)	**{Σn} [%success]**	**{75}**	**{55} [73%]**	**{2} [3%]**	**{3} [4%]**	**{15} [20%]**
Abitibi greenstone belt (Canada)	IAB–CRB–OIB–MORB	14	10	2	0	2
	IAB–CRB–OIB	14	13	1	0	–
	IAB–CRB–MORB	14	12	0	–	2
	IAB–OIB–MORB	14	11	–	3	0
	CRB–OIB–MORB*	14	–	5	5	4
8. Abitibi greenstone belt (Canada)	**{Σn} [%success]**	**{70}**	**{46} [67%]**	**{8} [11%]**	**{8} [11%]**	**{8} [11%]**
Gadwal greenstone belt (India)	IAB–CRB–OIB–MORB	7	7	0	0	0
	IAB–CRB–OIB	7	7	0	0	–
	IAB–CRB–MORB	7	7	0	–	0
	IAB–OIB–MORB	7	7	–	0	0
	CRB–OIB–MORB*	7	–	5	0	2
10. Gadwal greenstone belt (India)	**{Σn} [%success]**	**{35}**	**{28} [80%]**	**{5} [14%]**	**{0} [0%]**	**{2} [6%]**

set, all of which plotted well inside the arc field (see probability values of 0.9712–1.0000; Table 4). The corresponding total percent probability was also very high (83.4%, Table 4). For the other set of immobile element-based diagrams (Agrawal *et al*. 2008), complete data were not available for any sample (note Table 5 does not include Kambalda). Finally, 17 samples in the major element-based diagrams for basic or ultrabasic rocks (Verma *et al*. 2006) also indicated an IA setting with very high percent success (% success of about 70%, Table 6; note the probability calculation procedure for individual samples is not available for this set of diagrams).

Thus, all sets of diagrams applied to this area consistently showed an IA setting for Kambalda during the Neoarchaean. The original authors (Arndt and Jenner 1986) did not mention anything about the probable tectonic setting of their samples.

Barberton belt (South Africa)

For the third case study (3a and 3b, Table 1), 9 samples of intermediate rocks and 12 samples of basic rocks were complied from this area. Although both sets of rocks are Palaeoarchaean, 11 samples (1 intermediate and 10 basic) are somewhat older (about 3470 million years) than the remaining 10 samples (8 intermediate and 2 basic, 3300–3260 million years).

Out of 10 basic rock samples of the older group (3a, Table 1), no sample had complete data set for the immobile element-based diagrams of Verma and Agrawal (2011). Seven of these samples did have complete data for the diagrams of Agrawal *et al*. (2008), which clearly showed a MOR setting for them (Figure 1, Table 5). For the major element-based diagrams of Verma *et al*. (2006) only 5 of these 10 samples had complete major element data (for five samples, Na_2O concentration data were missing). These

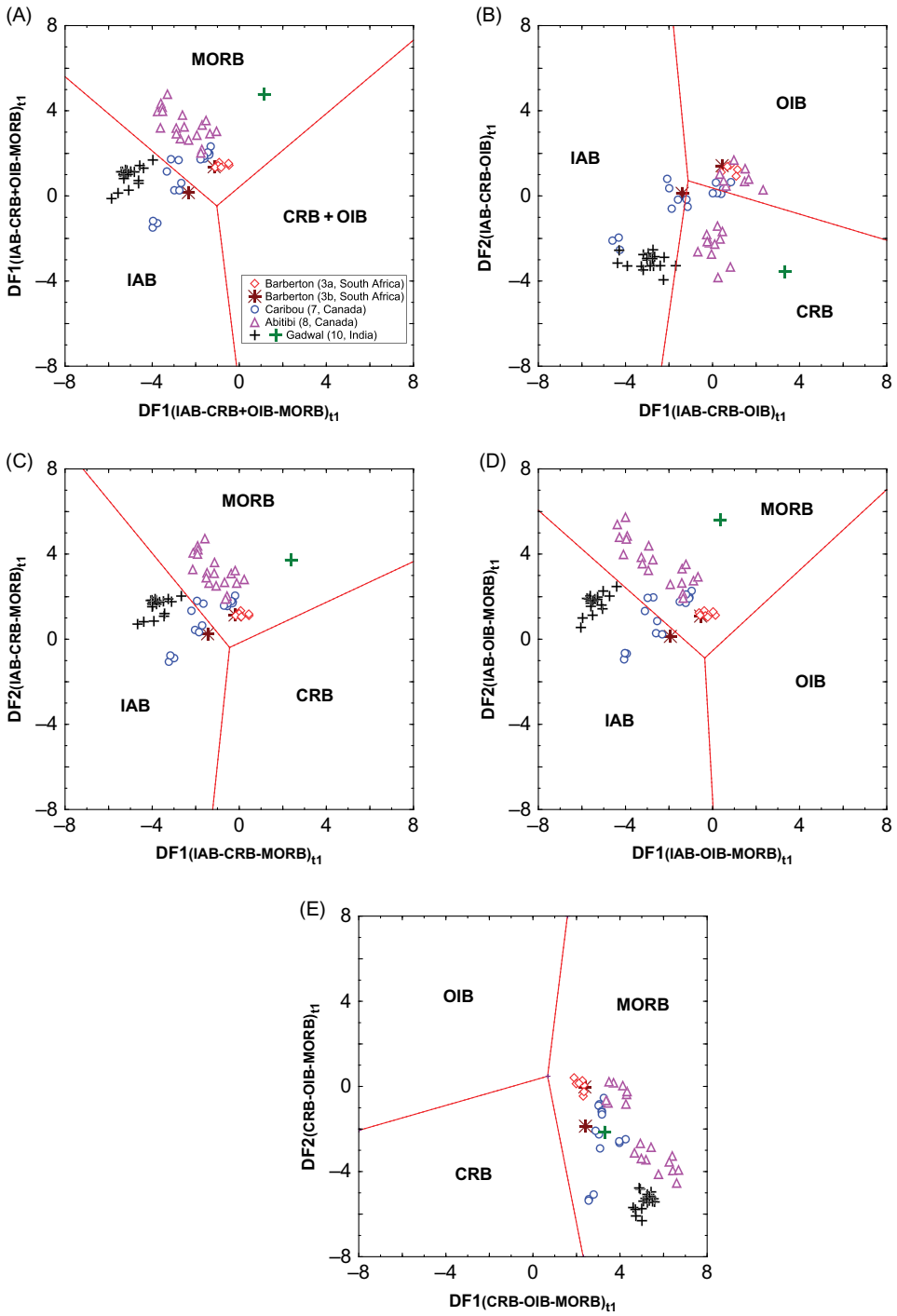

Figure 1. Application of the set of five immobile trace element-based discriminant function DF1–DF2 discrimination diagrams (see the subscript t1 in all these diagrams; Agrawal *et al*. 2008) for basic rocks from Barberton (South Africa), Caribou (Canada), Abitibi (Canada), and Gadwal (India). The numbers of samples for tectonic setting of island arc (IAB), combined tectonic setting of continental rift and ocean island (CRB + OIB), continental rift (CRB), ocean island (OIB), and mid-ocean ridge (MORB) are given in Table 5. The %success values are also included in Table 5. The symbols are shown as inset in (A), in which the numbers before the country names refer to the case study numbers in Table 1. Note for the Gadwal area, the symbol in green refers to a discordant outlier. (A) Three tectonic settings IAB–CRB + OIB–MORB; (B) three tectonic settings IAB–CRB–OIB; (C) three tectonic settings IAB–CRB–MORB; (D) three tectonic settings IAB–OIB–MORB; and (E) three tectonic settings CRB–OIB–MORB.

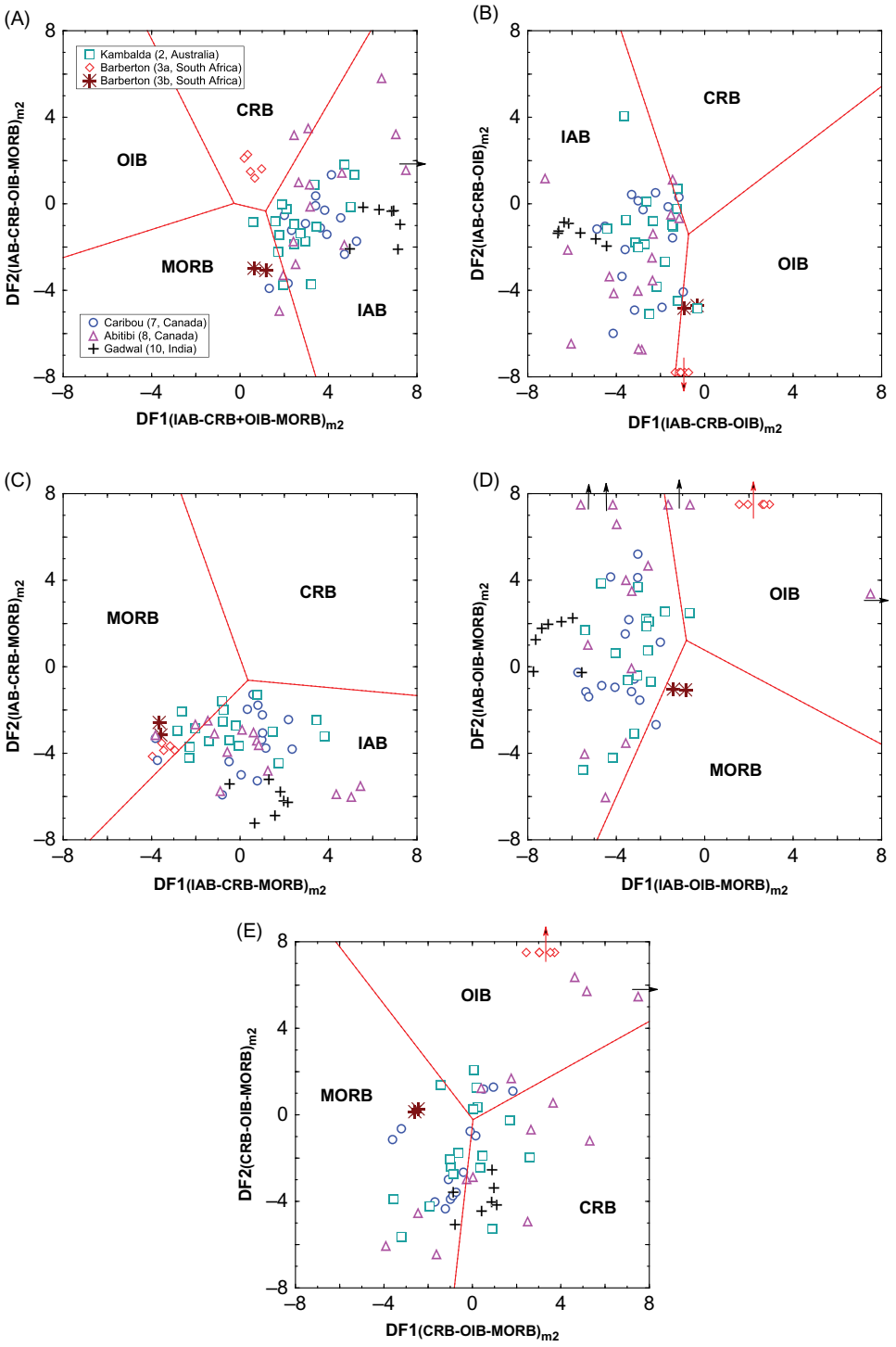

Figure 2. Application of the set of five major element-based discriminant function DF1–DF2 discrimination diagrams (see the subscript m2 in all these diagrams; Verma *et al*. 2006) for basic rocks from Kambalda (Australia), Barberton (South Africa), Caribou (Canada), Abitibi (Canada), and Gadwal (India). The total number of samples and %success values are given in Table 6 for tectonic setting of island arc (IAB), continental rift (CRB), ocean island (OIB), and mid-ocean ridge (MORB). The symbols are shown as inset in (A), in which the numbers before the country names refer to the case study numbers in Table 1. The arrows in diagrams (A), (B), (D), and (E) indicate that the data plot outside the diagrams. (A) Four tectonic settings IAB–CRB–OIB–MORB; (B) three tectonic settings IAB–CRB–OIB; (C) three tectonic settings IAB–CRB–MORB; (D) three tectonic settings IAB–OIB–MORB; and (E) three tectonic settings CRB–OIB–MORB.

five samples, at first instance, indicated an OI basalt setting (Table 6). However, for three major elements Na_2O, K_2O, and P_2O_5, the data reported to only one significant digit (0.01–0.05%) seem to be of poor quality, most of which were very likely close to the respective detection limits. These data are, therefore, likely characterized by extremely large analytical errors. This may be the reason why these samples plotted even outside the plot area in most of these diagrams (Figures 2B, D, and E). Therefore, we should not seriously consider these results (Figure 2, Table 6). Finally, a single intermediate rock sample from the older group (3a, Table 1) with complete data for two of the three sets of diagrams of Verma and Verma (2012), indicated an IA setting. Note that the MOR setting inferred from the basic rock samples is missing from this set of diagrams.

The eight intermediate rock samples from the younger group (3b, Table 1) had complete data set for two of the three sets of diagrams of Verma and Verma (2012). Both sets of diagrams consistently indicated an IA setting for these samples with high total percent probability values of 77.3% for all major element-based diagrams and 57.8% for immobile trace element-based diagrams (Table 3). The remaining probability of 22.7% and 42.2%, respectively, was for the CA setting. Therefore, a subduction-related setting, most likely an IA setting, seems to be confirmed for the Barberton belt for the relatively younger group of Palaeoarchaean intermediate rocks (3b in Tables 1 and 3). The two samples of basic rocks (3b, Table 1) plotted mostly in the IA and MOR fields in the major element-based diagrams (Figure 2), but indicated a MOR setting in the immobile element-based diagrams (Figure 1). Poor quality of at least two major elements (K_2O and P_2O_5) may have caused the discrepancy in the major element-based diagrams.

The original authors (Lahaye *et al*. 1995) did not comment on the probable tectonic setting for their rocks from the Barberton belt. Nevertheless, our results indicate a MOR setting for the older group (3470 million years) and an IA setting for the younger group (3300–3260 million years). Thus, a transition from a MOR to an IA setting could be inferred for the Barberton belt during the period 3470 to 3260 million years.

São Francisco craton (Brazil)

For the fourth case study, eight samples of acid and four of intermediate rocks were compiled (Table 1). The acid rock samples showed an IA setting with a high total percent probability of 60.4% (Table 2). Only two (out of four) intermediate rock samples had complete data for the second set of diagrams based on major and trace elements (Verma and Verma 2012), which did not indicate any consistent result (results of only two samples were not included in Table 3). For the third set of diagrams based on immobile trace elements, no sample had complete data set.

In summary, the multidimensional diagrams for acid and intermediate magmas can be interpreted to show an arc setting for the São Francisco craton during the Mesoarchaean, which is consistent with the conclusion of the original authors (Oliveira *et al*. 2010).

Rio Maria terrane (Brazil)

Twelve samples of acid rocks from the Bannach area of the Rio Maria terrane (Oliveira *et al*. 2009) indicated a CA setting with a high total percent probability of 62.5% (Table 2). Two samples of intermediate rocks from the same area showed a Col setting in two sets of diagrams of Verma and Verma (2012). Oliveira *et al*. (2009) also presented data for other areas of the Rio Maria terrane from the literature sources. These and other geochemical data should, in future, be considered along with the age constraints, to better understand the tectonic inferences from multidimensional diagrams. These authors (Oliveira *et al*. 2009) did not discuss about the tectonic setting of Rio Maria. Nevertheless, a subduction-related setting has been proposed for this area during the Mesoarchaean (Leite *et al*. 2004; Oliveira *et al*. 2011). Our results for acid rocks are consistent with this proposal.

Carajás metallogenic province (Brazil)

All samples compiled from this province proved to be acid rocks. These 28 samples of the Neoarchaean acid rocks indicated a within-plate setting with a high total percent probability of 66.9% (Table 2). Both papers, from which the data were compiled (Barros *et al*. 2009; Sardinha *et al*. 2006), also indicated a within-plate setting for the study area.

North Caribou greenstone belt (Canada)

Out of 29 samples of the Mesoarchaean compiled from this belt, 6 samples proved to be acid, 7 intermediate, and 16 basic rocks. The acid rock samples indicated a CA setting with the total percent probability of about 47.0% (Table 2); for the IA setting this probability value (28.1%) was considerably lower and close to the by-chance probability value (25%). All three sets of diagrams for intermediate magma showed an IA setting for North Caribou with very high percent probability values of 64.1–78.6% (Table 3).

Eleven (out of 16) basic rock samples had complete data set for the immobile element-based diagrams of Verma and Agrawal (2011). This set of diagrams showed an arc setting with a very high total percent probability of 83.1% (Table 4). A transitional MOR to arc setting (%success of about 50–41%, Table 5) was instead indicated from Agrawal *et al*. (2008) diagrams. Nevertheless, 15 basic rock samples with complete data set clearly showed an arc

setting for this area in the major element-based diagrams of Verma *et al*. (2006), because a high %success of about 73% (Table 6) was obtained for this tectonic setting.

Our results of an IA setting are consistent with the original authors (Hollings and Kerrich 1999), who also hypothesized an arc setting for this area.

Abitibi greenstone belt (Canada)

Out of 30 Neoarchaean rock samples compiled from this area, 7 proved to be intermediate, 19 basic, and 4 ultrabasic (Table 1). Seven intermediate rock samples indicated an IA setting in all three sets of diagrams (%prob of 60.2–76.6%, Table 3). Eleven (out of 19) basic and four ultrabasic rock samples had complete data for the immobile element-based diagrams of Verma and Agrawal (2011). They indicated an IA setting with a high total percent probability of 77.7% (Table 4). For the diagrams of Agrawal *et al*. (2008), 15 basic and 4 ultrabasic rock samples with complete dataset showed instead a MOR setting with a high total percent probability of 80% (Figure 1, Table 5). It is not clear at present why these diagrams do not indicate an arc setting. The major element-based diagrams of Verma *et al*. (2006) indicated an arc setting for 10 basic and 4 ultrabasic rocks (high %success of about 67%, Table 6, Figure 2). Although Lahaye *et al*. (1995) did not mention the probable tectonic setting for their samples, an arc setting would be consistent with Kerrich *et al*. (1998).

Archaean sanukitoid suite (Canada)

For the ninth case study, 10 samples of acid and 6 of intermediate rocks were compiled (Table 1). The acid rock samples showed a Col setting with a high total percent probability of 60.0% (Table 2). The same setting (Col) was also indicated for intermediate rock samples from major element-based and immobile trace element-based diagrams, with high total percent probability values ([%prob] of 64.7% and 83.2%, respectively, Table 3). However, the set of diagrams based on immobile major and trace elements (Verma and Verma 2012) indicated a CA setting, with a somewhat lower total percent probability value of 53.1% (Table 3).

In summary, the multidimensional diagrams for acid and intermediate magmas can be interpreted to show a Col setting for these Neoarchaean rocks from Canada. The original authors (Stevenson *et al*. 1999) argued for a more complex scenario for their rocks and stated that their emplacement may have post-dated the subduction or Col event in the western Superior Province.

Gadwal greenstone belt (India)

Twenty-one Neoarchaean basic rock samples were compiled from this area (Table 1). The immobile element-based diagrams of Verma and Agrawal (2011) showed an arc setting with a high total percent probability of 65.1% (Table 4). An arc setting (%success of about 76%, Table 5) was also indicated from Agrawal *et al*. (2008) diagrams. Seven basic rock samples with complete data set (out of 21, K_2O data were missing for 14 samples) clearly showed an arc setting for this area in the major element-based diagrams of Verma *et al*. (2006), because a very high %success of about 80% (Table 6) was obtained for this tectonic setting.

Our results of an IA setting are consistent with the original authors (Manikyamba *et al*. 2005), who also hypothesized a subduction-related setting for this area.

Kolar suture zone (India)

Out of seven Neoarchaean rock samples compiled from this area (six acid and one intermediate, Table 1), six acid rock samples from the Kolar suture zone indicated a Col setting, with a total percent probability value of 54.7% (Table 2). One intermediate rock sample from this area also showed a Col setting. Thus, a Col setting is indicated for this suture zone. However, according to Krogstad *et al*. (1995), a subduction-related setting is likely for this area, although the arguments for the validity of this tectonic setting were not clearly presented by these authors.

Additional remarks

The use of SINCLAS computer program (Verma *et al*. 2002) is mandatory, because this program allows an objective separation of the igneous rock samples from a given area into acid, intermediate, and basic or ultrabasic varieties. Thus, suitable sets of diagrams can be chosen for the application. Besides, TecD computer program (Verma and Rivera-Gómez 2012) facilitates the application of the diagrams for basic and ultrabasic magmas.

When DODESSYS computer program (Verma and Díaz-González 2012) was used to identify discordant outliers, the discordant observations in some cases plotted in a different tectonic field than the remaining bulk of observations. As an example, one sample (identified as a discordant outlier from DODESSYS) from the Gadwal greenstone belt (Manikyamba *et al*. 2005) consistently plotted away from the remaining samples in Figure 1. Examining the original paper (Manikyamba *et al*. 2005), we noticed that this particular sample (G16) had a very high Nb concentration (6.26 $\mu g\ g^{-1}$) as compared to all other samples (range of Nb concentration of 0.31–1.41 $\mu g\ g^{-1}$), but sample G16 did not show significant differences for any other elements, not even for any other high-field strength elements. Therefore, it is very likely that this Nb concentration value may be due to a typographical error in the original data table (Manikyamba *et al*. 2005); alternatively, some analytical problems may explain this discrepancy.

From the above discussion, a generally good functioning of the multidimensional diagrams for Archaean rocks can be inferred. Similar conclusions of good functioning of multidimensional diagrams were reached from studies for basic and ultrabasic (Verma *et al*. 2006; Agrawal *et al*. 2008; Verma 2010; Verma and Agrawal 2011), as well as acid (Verma *et al*. 2012) and intermediate magmas (Verma and Verma 2012). Possible reasons for such a good functioning of discrimination diagrams are explained by Verma (2012).

In this study, only major element-based diagrams were available for acid magmas, although for other magma varieties, all kinds of diagrams based on all major elements or immobile elements could be used. Still newer diagrams for acid magmas based on immobile elements (currently under preparation by Verma and colleagues) can be used in future to confirm or rectify the results of acid diagrams. The probability-based approach would certainly reinforce such geological applications.

To promote a more efficient use of these new multidimensional diagrams and probability calculations (Verma *et al*. 2012; Verma and Verma 2012), an updated version of TecD (Verma and Rivera-Gómez 2012) is currently being written, which will allow data input from an Excel or Statistica spreadsheet. In the mean time, potential users can send the authors their data (in Excel) for processing them in Statistica software. Thus, anybody interested in multidimensional diagrams can use this innovative probability-based methodology.

Conclusions

Applications of new multidimensional diagrams (proposed by our group during 2006–2012), based on natural logarithms of element ratios and linear discriminant analysis, to Archaean igneous rocks from Australia, South Africa, Brazil, Canada, and India have been successfully documented. Probability calculations have been shown to successfully replace the newer diagrams proposed during 2011–2012. Therefore, such probability-based methods, proposed and used by Verma (2012) and also practiced in this study, are likely to open new ways of interpreting geochemical data.

Acknowledgements

The first author (SKV) expresses cordial gratitude to the Secretaría de Relaciones Exteriores (Mexico) and Ministry of Human Resource Development (India) for his doctorate fellowship.

References

Agrawal, S., 1999, Geochemical discrimination diagrams: A simple way of replacing eye-fitted boundaries with probability based classifier surfaces: Journal of the Geological Society of India, v. 54, p. 335–346.

Agrawal, S., Guevara, M., and Verma, S.P., 2004, Discriminant analysis applied to establish major-element field boundaries for tectonic varieties of basic rocks: International Geology Review, v. 46, p. 575–594.

Agrawal, S., Guevara, M., and Verma, S.P., 2008, Tectonic discrimination of basic and ultrabasic rocks through log-transformed ratios of immobile trace elements: International Geology Review, v. 50, p. 1057–1079.

Arndt, N.T., and Jenner, G.A., 1986, Crustally contaminated komatiites and basalts from Kambalda, western Australia: Chemical Geology, v. 56, p. 229–255.

Bailie, R., Gutzmer, J., and Rajesh, H.M., 2010, Lithogeochemistry as a tracer of the tectonic setting, lateral integrity and mineralization of a highly metamorphosed Mesoproterozoic volcanic arc sequence on the eastern margin of the Namaqua Province, South Africa: Lithos, v. 119, p. 345–362.

Barros, C.E.M., 2009, Structure, petrology, geochemistry and zircon U/Pb and Pb/Pb geochronology of the synkinematic Archean (2.7 Ga) A-type granites from the Carajás metallogenic province, northern Brazil: Canadian Mineralogist, v. 47, p. 1423–1440.

Bickle, M.J., Bettenay, L.F., Barley, M.E., Chapman, H.J., Groves, D.I., Campbell, H.I., and De Laeter, J.R., 1983, A 3500 Ma plutonic and volcanic calc-alkaline province in the Archaean East Pilbara block: Contributions to Mineralogy and Petrology, v. 84, p. 25–35.

Condie, K.C., and Kröner, A., 2008, When did plate tectonics begin? Evidence from the geologic record, *in* Condie, K.C., and Pease, V., eds., When did plate tectonics begin on planet Earth?: Geological Society of America Special Paper 440, p. 281–294.

Condie, K.C., and Pease, V., 2008, Preface, *in* Condie, K.C., and Pease, V., eds., When did plate tectonics begin on planet Earth?: Geological Society of America Special Paper 440, p. v–viii.

Ernst, W.G., 2009, Archean plate tectonics, rise of Proterozoic supercontinentality and onset of regional, episodic stagnant-lid behavior: Gondwana Research, v. 15, p. 243–253.

Foley, S., 2008, A trace element perspective on Archean crust formation and on the presence or absence of Archean subduction, *in* Condie, K.C., and Pease, V., eds., When did plate tectonics begin on planet Earth?: Geological Society of America Special Paper 440, p. 31–50.

Furnes, H., Rosing, M., Dilek, Y., and de Wit, M., 2009, Isua supracrustal belt (Greenland) – A vestige of a 3.8 Ga suprasubduction zone ophiolite, and the implications for Archean geology: Lithos, v. 113, p. 115–132.

Gradstein, F.M., Ogg, J.G., Smith, A.G., Bleeker, W., and Lourens, L.J., 2004, A new Geologic Time Scale, with special reference to Precambrian and Neogene: Episodes, v. 27, p. 84–100.

Hamilton, W.B., 2011, Plate tectonics began in Neoproterozoic time, and plumes from deep mantle have never operated: Lithos, v. 123, p. 1–20.

Hollings, P., and Kerrich, R., 1999, Trace element systematics of ultramafic and mafic volcanic rocks from the 3 Ga North Caribou greenstone belt, northwestern Superior Province: Precambrian Research, v. 93, p. 257–279.

Jahn, B.-M., Glikson, A.Y., Peucat, J.J., and Hickman, A.H., 1981, REE geochemistry and isotopic data of Archean silicic volcanics and granitoids from the Pilbara Block, Western Australia: Implications for the early crustal evolution: Geochimica et Cosmochimica Acta, v. 45, p. 1633–1652.

Kerrich, R., and Polat, A., 2006, Archean greenstone-tonalite duality: Thermochemical mantle convection models or plate

tectonics in the early earth global dynamics: Tectonophysics, v. 415, p. 141–165.

Kerrich, R., Wyman, D., Fan, J., and Bleeker, W., 1998, Boninite series: Low Ti-tholeiite associations from the 2.7 Ga Abitibi greenstone belt: Earth and Planetary Science Letters, v. 164, p. 303–316.

Korsch, R.J., Kositcin, N., and Champion, D.C., 2011, Australian island arcs through time: Geodynamic implications for the Archean and Proterozoic: Gondwana Research, v. 19, p. 716–734.

Krogstad, E.J., Hanson, G.N., and Rajamani, V., 1995, Sources of continental magmatism adjacent to the late Archean Kolar Suture Zone, south India: Distinct isotopic and elemental signatures of two late Archean magmatic series: Contributions to Mineralogy and Petrology, v. 122, p. 159–173.

Lahaye, Y., Arndt, N., Byerly, G., Chauvel, C., Fourcade, S., and Gruau, G., 1995, The influence of alteration on the trace-element and Nd isotopic compositions of komatiites: Chemical Geology, v. 126, p. 43–64.

Le Bas, M.J., Le Maitre, R.W., Streckeisen, A., and Zanettin, B., 1986, A chemical classification of volcanic rocks based on the total alkali-silica diagram: Journal of Petrology, v. 27, p. 745–750.

Leite, A.A.S., Dall'Agnol, R., Macambira, M.J.B., and Althoff, F.J., 2004, Geologia e geocronologia dos granitóides arqueanos da região de Xinguara-Pa E Suas implicações na evolução do terreno granito-greenstone de Rio Raria, cráton Amazônico: Revista Brasileira de Geociências, v. 34, p. 447–458.

Manikyamba, C., and Kerrich, R., 2012, Eastern Dharwar Craton, India: Continental lithosphere growth by accretion of diverse plume and arc terranes: Geoscience Frontiers, v. 3, p. 225–240.

Manikyamba, C., Naqvi, S.M., Rao, D.V.S., Mohan, M.R., Khanna, T.C., Rao, T.G., and Reddy, G.L.N., 2005, Boninites from the Neoarchaean Gadwal greenstone belt, Estern Dharwar Craton, India: Implications for Archaean subduction processes: Earth and Planetary Science Letters, v. 230, p. 65–83.

McCall, G.J.H., 2010, New paradigm for the early Earth: Did plate tectonics as we know it not operate until the end of the Archean: Australian Journal of Earth Sciences, v. 57, p. 349–355.

Middlemost, E.A.K., 1989, Iron oxidation ratios, norms and the classification of volcanic rocks: Chemical Geology, v. 77, p. 19–26.

Oliveira, E.P., McNaughton, N.J., and Armstrong, R., 2010, Mesoarchaean to Palaeoproterozoic growth of the northern segment of the Itabuna_Salvador_Curaçá orogen, São Francisco craton, Brazil: Geological Society of America, v. 338, p. 263–286.

Oliveira, M.A., Dall'Agnol, R., and Almeida, J.A.C., 2011, Petrology of the Mesoarchean Rio Maria suite and the discrimination of sanukitoid series: Lithos, v. 127, p. 192–209.

Oliveira, M.A., Dall'Agnol, R., Althoff, F.J., and Leite, A.A.S., 2009, Mesoarchean sanukitoid rocks of the Rio Maria Granite-Greenstone Terrane, Amazonian craton, Brazil: Journal of South American Earth Sciences, v. 27, p. 146–160.

AQ6

Pandarinath, K., and Verma, S.K., 2012, Application of four sets of tectonomagmatic discriminant function based diagrams to basic rocks from northwest Mexico: Journal of Iberian Geology (in press).

Pease, V., Percival, J., Smithies, H., Stevens, G., and Van Kranendonk, M., 2008, When did plate tectonics begin? Evidence from the orogenic record, *in* Condie, K.C., and Pease, V., eds., When did plate tectonics begin on planet Earth?: Geological Society of America Special Paper 440, p. 199–228.

Polat, A., 2009, The geochemistry of Neoarchean (ca. 2700 Ma) tholeiitic basalts, transitional to alkaline basalts, and gabbros, Wawa Subprovince, Canada: Implications for petrogenetic and geodynamic processes: Precambrian Research, v. 168, p. 83–105.

Polat, A., Appel, P.W.U., Fryer, B., Windley, B., Frei, R., Samson, I.M., and Huang, H., 2009a, Trace element systematics on the Neoarchean Fiskenæsset anorthosite complex and associated meta-volcanic rocks, SW Greenland: Evidence for a magmatic origin: Precambrian Research, v. 175, p. 87–115.

Polat, A., Appel, P.W.U., and Fryer, B.J., 2011b, An overview of the geochemistry of Eoarchean to Mesoarchean ultramafic to mafic volcanic rocks, SW Greenland: Implications for mantle depletion and petrogenetic processes at subduction zones in the early Earth: Gondwana Research, v., 20, p. 255–283.

Polat, A., Frei, R., Appel, P.W.U., Fryer, B., Dilek, Y., and Ordóñez-Calderón, J.C., 2008, An overview of the lithological and geochemical characteristics of Mesoarchean (ca. 3075 Ma) Ivisaartoq greenstone belt, southern West Greenland, *in* Condie, K.C., and Pease, V., eds., When did plate tectonics begin on planet Earth?: Geological Society of America Special Paper 440, p. 51–76.

Polat, A., Frei, R., Fryer, B., and Appel, P.W.U., 2009b, The origin of geochemical trends and Eoarchean (ca. 3700 Ma) zircons in Mesoarchean (ca. 3075 Ma) ocelli-hosting pillow basalts, Ivisaartog greenstone belt, SW Greenland: Evidence for crustal contamination versus crustal recycling: Chemical Geology, v. 268, p. 248–271.

Polat, A., Fryer, B.J., Appel, P.W.U., Kalvig, P., Kerrich, R., Dilek, Y., and Yang, Z., 2011a, Geochemistry of anorthositic differentiated sills in the Archean (~2970 Ma) Fiskenæsset Complex, SW Greenland: Implications for parental magma compositions, geodynamic setting, and secular heat flow in arcs: Lithos, v. 123, p. 50–72.

Polat, A., Kerrich, R., and Wyman, D.A., 1999, Geochemical diversity in oceanic komatiites and basalts from the late Archean Wawa greenstone belts, Superior Province, Canada: Trace element and Nd isotope evidence for a heterogeneous mantle: Precambrian Research, v. 94, p. 139–173.

Sardinha, A.S., Barros, C.E.M., and Krymsky, R., 2006, Geology, geochemistry, and U–Pb geochronology of the Archean (2.74 Ga) Serra do Rabo granite stocks, Carajás Metallogenetic Province, northern Brazil: Journal of South American Earth Sciences, v. 20, p. 327–329.

Sheth, H.C., 2008, Do major oxide tectonic discrimination diagrams work?: Evaluating new log-ratio and discriminant-analysis-based diagrams with Indian Ocean mafic volcanics and Asian ophiolites: Terra Nova, v. 20, p. 229–236.

Shirey, S.B., Kamber, B.S., Whitehouse, M.J., Mueller, P.A., and Basu, A.R., 2008, A review of the isotopic and trace element evidence for mantle and crustal processes in the Hadean and Archean: Implications for the onset of plate tectonic subduction, *in* Condie, K.C., and Pease, V., eds., When did plate tectonics begin on planet Earth?: Geological Society of America Special Paper 440, p. 1–30.

Stern, R.J., 2008, Modern-style plate tectonics began in Neoproterozoic time: An alternative interpretation of Earth's tectonic history, *in* Condie, K.C., and Pease, V., eds., When did plate tectonics begin on planet Earth?: Geological Society of America Special Paper 440, p. 265–280.

Stevenson, R., Henry, P., and Gariépy, C., 1999, Assimilation–fractional crystallization origin of Archean sanukitoid suites:

Western Superior Province, Canada: Precambrian Research, v. 96, p. 83–99.

van Hunen, J., and van den Berg, A.P., 2008, Plate tectonic on the early Earth: Limitations imposed by strength and buoyancy of subducted lithosphere: Lithos, v. 103, p. 217–235.

Van Kranendonk, M.J., 2010, Two types of Archean continental crust: Plume and plate tectonics on early earth: American Journal of Science, v. 310, p. 1187–1209.

Verma, S.K., Pandarinath, K., and Verma, S.P., 2012, Statistical evaluation of tectonomagmatic discrimination diagrams for granitic rocks and proposal of new discriminant-function-based multi-dimensional diagrams for acid rocks: International Geology Review, v. 54, p. 325–347.

Verma, S.P., 2010, Statistical evaluation of bivariate, ternary and discriminant function tectonomagmatic discrimination diagrams: Turkish Journal of Earth Sciences, v. 19, p. 185–238.

Verma, S.P., 2012, Application of multi-dimensional discrimination diagrams and probability calculations to acid rocks from Portugal and Spain: Comunicações Geológicas, v. 99 (in press).

Verma, S.P., and Agrawal, S., 2011, New tectonic discrimination diagrams for basic and ultrabasic volcanic rocks through log-transformed ratios of high field strength elements and implications for petrogenetic processes: Revista Mexicana de Ciencias Geológicas, v. 28, p. 24–44.

Verma, S.P., and Díaz-González, L., 2012, Application of the discordant outlier detection and separation system in the geosciences: International Geology Review, v. 54, p. 593–614.

Verma, S.P., Guevara, M., and Agrawal, S., 2006, Discriminating four tectonic settings: Five new geochemical diagrams for basic and ultrabasic volcanic rocks based on log-ratio transformation of major-element data: Journal of Earth System Science, v. 115, p. 485–528.

Verma, S.P., and Rivera-Gómez, M.A., 2012, New computer program TecD for tectonomagmatic discrimination from discriminant function diagrams for basic and ultrabasic magmas and its application to ancient rocks: Journal of Iberian Geology (in press).

Verma, S.P., Torres-Alvarado, I.S., and Sotelo-Rodríguez, Z.T., 2002, SINCLAS: Standard igneous norm and volcanic rock classification system: Computers & Geosciences, v. 28, p. 711–715.

Verma, S.P., and Verma, S.K., 2012, The first fifteen probability-based multi-dimensional discrimination diagrams for intermediate magmas and their robustness against post-emplacement compositional changes and petrogenetic processes: Turkish Journal of Earth Sciences (in press).

Verma, S.P., Verma, S.K., Pandarinath, K., and Rivera-Gómez, M.A., 2011, Evaluation of recent tectonomagmatic discrimination diagrams and their application to the origin of basic magmas in Southern Mexico and Central America: Pure and Applied Geophysics, v. 168, p. 1501–1525.